The Time and Length Scales of Magma Mixing: The Natural Laboratory of Volcán Quizapu, Chile

Philipp Ruprecht

A dissertation
submitted in partial fulfillment of the
requirements for the degree of

Doctor of Philosophy

University of Washington

2009

Program Authorized to Offer Degree:
Earth and Space Sciences

University of Washington
Graduate School

This is to certify that I have examined this copy of a doctoral dissertation by

Philipp Ruprecht

and have found that it is complete and satisfactory in all respects,
and that any and all revisions required by the final
examining committee have been made.

Chair of the Supervisory Committee:

_____

George W. Bergantz

Reading Committee:

_____

George W. Bergantz

_____

Kari M. Cooper

_____

Olivier Bachmann

Date: _____

In presenting this dissertation in partial fulfillment of the requirements for the doctoral degree at the University of Washington, I agree that the Library shall make its copies freely available for inspection. I further agree that extensive copying of the dissertation is allowable only for scholarly purposes, consistent with "fair use" as prescribed in the U.S. Copyright Law. Requests for copying or reproduction of this dissertation may be referred to ProQuest Information and Learning, 300 North Zeeb Road, Ann Arbor, MI 48106-1346, 1-800-521-0600, to whom the author has granted "the right to reproduce and sell (a) copies of the manuscript in microform and/or (b) printed copies of the manuscript made from microform."

Signature_____

Date_____

University of Washington

Abstract

The Time and Length Scales of Magma Mixing: The Natural Laboratory of Volcán Quizapu, Chile

Philipp Ruprecht

Chair of the Supervisory Committee:
Professor George W. Bergantz
Department of Earth and Space Sciences

Injection of magma from the lower crust and mantle into pre-existing shallow crustal magma reservoirs is major control on the eruptive behavior of the volcanoes and the diversity of volcanic rocks found on the Earth surface. The first section of this study examines magma mixing caused by gas-driven overturn and the response of dispersed crystals in recharge and residing magma. Large-scale redistribution of crystals during a single overturn is predicted, resulting in crystal-melt chemical disequilibria. Furthermore, it is predicted that the overturn time scale is (1) short compared to the response time scale of crystallization and (2) similar to the response time scale of dissolution.

The second part of this work focuses on the process of magma mixing in the natural system of Volcán Quizapu and its historic eruptions of 1846/47 and 1932. In contrast, to most arc magma system, the 1846/47 eruption of Volcán Quizapu exhibits a simple mixing relationship between andesite recharge and residing dacite magma. Comparing and contrasting this eruption with the homogeneous dacite from the 1932 eruption provides a catalog of the magma mixing signatures that develop on the whole rock and crystal scales during a single mixing event. Moreover, the temperature evolution in the shallow dacite magma system is investigated using multiple geo-thermometers. It is shown that heat

transfer of sensible and latent heat due to crystallization in the hot recharge magma during the magma mixing results in a late-stage reheating of the dacite magmas and their eruptions as effusive lava rather explosive pumice.

The final chapter of this work explores the time scales magma storage in the shallow crust at Volcán Quizapu using the ^{226}Ra-^{230}Th age dating as well as the time scale that is associated with the recharge, mixing, and eruption in 1846/47 using Magnesium diffusion in plagioclase. A four-component mixture model is developed to decipher ^{226}Ra-^{230}Th age information from bulk mineral separates. It is shown that single mixing events alter the long-term record for crystal storage and that the time scales of recharge, mixing, and eruption are on the order days to weeks for the 1846/47 eruption of Volcán Quizapu.

TABLE OF CONTENTS

LIST OF FIGURES

LIST OF TABLES

ACKNOWLEDGEMENTS

I would like to express my gratitude to my graduate advisors Professor George W. Bergantz and Professor Kari M. Cooper for their intellectual encouragement and support. They challenged me throughout my graduate career, while always guiding me with much appreciated suggestions, questions and discussions through the academic program. I would like to thank my committee members Olivier Bachmann and Bob Breidenthal for their stimulating discussions about magma chamber dynamics and the size of "Mama Bear". The project would have not been possible without the appreciated support from Mike Dungan, Wes Hildreth, Bruce Nelson, Adam Kent, Erik Klemetti, Scott Kuehner, and Pablo Salas in the field and in the lab. I wish to thank my fellow graduate students, especially those in the Physical Petrology and Isotope Geochemistry Group including Joe Dufek, Theresa Kayzar, Tenley Banik, Charles Plummer, Glen Wallace, and James Loetterle for a memorable time at the University of Washington. Finally, I would like to thank my family (Jutta, Gerhard, and Felix Ruprecht) and Janina Klaus for their motivation, patience and support.

DEDICATION

Diese Dissertation möchte ich meiner Familie widmen – meiner Mutter für ihre Gabe mir zu zeigen, dass man durch Uneigenützigkeit die Welt ein wenig verbessern kann, meinem Vater, der mich gelehrt hat, dass man nach vorne schauen muss, um weiterzukommen und meinem Bruder, mit dem ich in spielerischen Wettkämpfen gelernt habe über mein Limit hinaus zu gehen.

- Chapter 1 -

Introduction

Magma mixing has been recognized for many decades as one of the major processes that produce the diversity of igneous rocks observed on the Earth surface [*Wilcox*, 1999]. The physical mingling and mixing of distinct magma batches has been identified in all tectonic settings [e.g., *Rhodes et al.*, 1979; *Eichelberger*, 1980; *Bacon and Metz*, 1984; *Sinton and Dettrick*, 1992; *Bindeman and Valley*, 2002; *Troll and Schmincke*, 2002]. While oceanic hotspot and mid-ocean ridge magmas often conceal the presence of magma mixing as a result of a small compositional range in the magmas, arc magmas vary over a wide range of magma compositions and provide macroscopic evidence for magma mixing. In many arc magmas the physical interaction of distinct magma batches is expressed by the presence of magmatic inclusion – the juxtaposition of distinct magma types as a result of incomplete magma mixing [e.g., *Eichelberger*, 1980; *Hildreth and Drake*, 1992; *Feeley and Dungan*, 1996; *Murphy et al.*, 1998; *Clynne*, 1999; *Coombs et al.*, 2003; *Bacon and Lanphere*, 2006; *Browne et al.*, 2006]. Moreover, microscopic evidence in the crystal record demonstrates that magma mixing is ubiquitous in arc magmas even where macroscopic evidence is missing [e.g., *Anderson*, 1976; *Humphreys et al.* 2006; *Ruprecht and Wörner*, 2007].

Mixed arc magmas frequently show evidence for the involvement of chemically distinct magmas, including evolved magmas generated by fractional crystallization or crustal melting, mafic magmas derived from the mantle, and assimilated crustal rocks during the ascent from the mantle to the surface. Various degrees of interaction between these magmas result in complex textural (non-linear crystal size distributions and glomerocrysts) and geochemical (trace element and

isotopic) characteristics [e.g., *Singer et al.*, 1995; *Davidson and Tepley*, 1997; *Tepley et al.*, 1999; *Ginibre et al.*, 2002; *Charlier et al.,* 2007; *Morgan et al.*, 2007; *Salisbury et al.*, 2008; *Humphreys et al.*, 2009]. This complexity often obscures individual processes of magma-magma interaction [e.g., *Clynne*, 1999; *Wallace and Bergantz*, 2005], and hence limits our ability to unravel the signature that an individual episode of magma mixing can leave in the crystal record of magma system. However, understanding the impact individual mixing events may have on the eruptive behavior of volcanoes and the heat and volatile budget in the magma system has been a long-standing interest in volcanology and petrology [*Sparks*, 1977]. This work examines the role of the crystal cargo that is redistributed during physical mingling and mixing and how it provides information on the mixing process itself (i.e. time scales of mixing and degree of crystal dispersal) as well as how it records the state of (i.e. heat budget, composition time) and crystal residence in a shallow magma chamber.

The mixing of vesiculated recharge magma and residing magma is thought to be one of the major mechanism for density inversion and initiation of magma mixing [*Eichelberger* et al., 1980]. Previous studies have used analog and numerical techniques to explore the bulk magma redistribution during overturn and mixing [e.g., *Oldenburg et al.*, 1989; *Bergantz and Ni*, 1999; *Jellinek and Kerr*; 1999; *Longo et al.*, 2006]. In Chapter 2 of this work a numerical approach that integrates a multiphase continuum model with a crystal-tracking algorithm is developed to examine the emergence of new heterogeneous crystal populations and the development of crystal-melt disequilibrium conditions. The crystals are active tracers that potentially respond to body and surface forces. However, the vigor of the overturn and the size of the crystals in the simulations results in strong one-way coupling between crystals and melt. The model enables the comparison of overturn, crystallization, and dissolution time scales. This work demonstrates that crystals are redistributed efficiently in a single overturn event and that the process of

redistribution is not recorded in the crystal record as crystallization time scales are much longer than overturn time scales. Crystals record variable post-mixing conditions in the magmatic system, as gradients in intensive variables are commonly developed for instantaneous and step-wise density inversions [*Oldenburg et al.*, 1989]. Thus, complex crystal populations develop within a single overturn event.

Most natural systems in magmatic arcs that show magma mixing on the micro- and macroscopic scale display the mixing of multiple end-members. Resulting mixing signatures are complex and impede the examination of a single overturn event in a natural environment [*Tepley et al.*, 1999]. Few arc magmas show simple mixing relationships between two chemically distinct magmas. The historic eruptions of Volcán Quizapu in the Southern Andean Volcanic zone provide a natural system that can be studied to examine binary mixing between vesiculated recharge magma and evolved dacite magma [*Hildreth and Drake*, 1992]. End-members of the binary mixture are preserved in andesitic inclusions of the effusive eruption in 1846/47 and in homogeneous dacite from the ensuing plinian eruption in 1932. Chapter 3 summarizes the features on the micro- and macro scale that define the overall simple binary mixing of hot mafic magma with cold dacite magma in the shallow crustal plumbing system. A holistic approach that integrates textural data, geochemical data, and geothermometry from the equilibrium assemblages of the individual end-members allows an examination of the physical mechanisms of magma mixing and subsequent eruption. Similar to other arc systems it is demonstrated that the mixing process itself may have been temporarily dominated by solid-liquid disaggregation of chilled mafic inclusions that are dispersed during the overturn [*Humphreys et al.*, 2009]. Furthermore, it is highlighted that a single mixing event creates a range in chemical composition with distinct macroscopic features preserved in mixed magmas (macroscopic homogeneity vs. heterogeneity). Geo-thermometry of the different mixed magmas reveals that reheating is comprehensive in the residing dacite magma. Such reheating is only present in the effusive eruption

of 1846/47, while dacite magma that erupted explosively in 1932 is cold. It is suggested that the shift in pre-eruptive temperatures as a result of mafic recharge and magma mixing influenced the eruptive behavior at Volcán Quizapu. This contrasts with existing models that comprehensive reheating may be a result of decompression crystallization in the conduit [*Blundy et al.*, 2006] and that mafic recharge is the trigger of explosive eruptions [*Sparks*, 1977].

To further constrain the connection between mafic recharge, magma mixing, and eruption, it has been shown that elemental diffusion in crystals that are displaced into chemical disequilibrium during magma mixing provide estimates for the time scales of crystal storage and magma mixing [*Gerlach and Grove*, 1982; *Zellmer et al.*, 1999; *Costa et al.*, 2003; *Morgan et al.*, 2004; *Costa and Dungan*, 2005]. It should be noted that crystal storage time scales obtained from elemental diffusion in crystals are conceptually different from crystal storage time scales obtained by uranium-series dating techniques [*Reid et al.*, 1997; *Cooper et al.*, 2001; *Cooper and Reid*, 2003; *Turner et al.*, 2003]. While both techniques provide residence times of crystals in the shallow crust, uranium-series dating constrains an average absolute age of a crystal population. In contrast, elemental diffusion records the residence times associated with the last event of chemical disequilibrium, which may have occurred long after initial crystal growth. In the case of magma mixing, elemental diffusion can be used to constrain the integrated time of recharge, magma mixing, and eruption, which has ranged in previous studies between days and years. The low concentration of uranium-series nuclides in plagioclase requires the use of bulk mineral separates to obtain absolute residence age with the ^{226}Ra-^{230}Th system [*Cooper et al.*, 2001]. As mixed magmas inevitably contain mixed crystal populations, uncorrected residence ages are mixed ages of distinct crystal populations. In Chapter 4 a four-component mixing model of two plagioclase types and two types of contaminating glass is developed to deconvolve the age information obtained from bulk mineral separate ^{226}Ra-^{230}Th dating. Recharge and residing

magmas are characterized by distinct crystal residence ages suggesting distinct crystallization regimes for ascending mafic recharge magmas and stored cooling evolved magmas. The overall residence ages are distinct from the residence times of crystals within the mixed magma. Modeling of magnesium diffusion in plagioclase [*Costa et al.*, 2003] results in short residence time scales of days to weeks for mixing and eruption. Such short time scales are different from most diffusion studies, but confirm results from *Gerlach and Grove* [1982].

Chapters 2 to 4 have been written for publication as separate manuscripts for Geochemistry, Geophysics, Geosystems (G^3), Geological Society of America Bulletin and Earth Planetary Science Letters, respectively. Chapter 2 was written with co-authors Prof. George Bergantz and Josef Dufek. Modified versions of Chapters 3 and 4 will be submitted with co-authors Prof. George Bergantz, Prof. Kari Cooper, and Wes Hildreth.

- Chapter 2 -

Modeling of Gas-Driven Magmatic Overturn: Tracking of Phenocryst Dispersal and Gathering During Magma Mixing

2.1 Introduction

The chemical and textural characteristics of crystals [*Singer et al*., 1995, *Zellmer et al*., 2003; *Ginibre et al.*, 2004; *Humphreys et al.*, 2006; *Morgan et al.*, 2007; *Davidson et al.*, 2007; *Ruprecht and Wörner*, 2007] suggest complex magmatic histories for many volcanic centers [*Davidson and Tepley*, 1997; *Bachmann et al*., 2002; *Vazquez and Reid*, 2004]. Such case studies have shown that this heterogeneity in the crystals emerges from the in situ mixing of magmatic additions in the shallow crust [*Knesel et al*., 1999; *Tepley et al*., 2000*; Couch et al*., 2001; *Coombs and Gardner*, 2004] and/or during eruption [*Cioni et al.*, 1995].

A quantitative understanding of the emergence of crystal-scale heterogeneity has still to be developed. The chemical and textural information recorded in a crystal is a competition between the rate at which the crystal travels through regions of distinct chemical potential, and the rate at which the crystal can respond to those changes through crystallization or dissolution. *Wallace and Bergantz* [2005] have developed a method to identify groups of crystals that have shared some common residence history. However, their approach did not allow one to connect specific rates and paths of crystal transport with the rates at which crystals can respond t o changes. Our objective is to exemplify the styles and scales of crystal dispersal and gathering t o understand t he controls and consequences of magma chamber dynamics as expressed in the crystal cargo.

All physical processes that promote efficient large-scale mixing require advective mass flux, which is a mechanism for both stretching (which reduces diffusive length scales) and redistribution. Gravitational instabilities provide one of the primary mechanisms for mixing in systems with unstable stratification arising from thermal, compositional, or phase segregation driven buoyancy [*Jellinek et al.*, 1999]. One example is Rayleigh-Taylor instabilities such as dripping dense crystal layers [*Marsh*, 1988; *Bergantz and Ni*, 1999], superposition of silicic and/or cold magma over mafic and/or hot magma [*Oldenburg et al.*, 1989; *Snyder and Tait*, 1996; *Folch and Martí*, 1998; *Snyder*, 2000; *Bergantz and Breidenthal*, 2001; *Couch et al.*, 2001] or the injection of replenishing magma [*Jellinek et al.*, 1999; *Jellinek and Kerr*, 1999; *Phillips and Woods*, 2001; *Longo et al.*, 2006].

All these models resolve some features of the large-scale or averaged behavior of the mixing process such as the bulk changes of temperature or redistribution of a gas bubble fraction. Multiphase continuum models can calculate mass and energy fluxes, and this is an essential first step in illuminating how distinct regions of temperature or composition of a magma system emerge, mix and decay. However, the progressive, transient paths of individual crystals and the local conditions that are recorded on the crystal-scale cannot be resolved with these methods alone. The emergence and evolution of different crystal populations can only be deduced by combining ‘smart crystals’, which are Lagrangian tracers, with the temporally changing conditions for the magma chamber. These tracers are like flight recorders in the way they can probe for information at the crystal scale, and are also fully coupled physically to the flow, and so they are not simple passive tracers. This approach has been used extensively in engineering problems [e.g., *Derksen*, 2003], in which particles are dynamically responding to the local body and surface forces, and are not just tracers following the motion.

Our aim is to investigate how much diversity in individual crystal zoning and crystal populations can arise from a simple kinematic template: one cycle of overturn associated with degassing from a vesiculated mafic magma that has intruded into a more silicic layer. To do this we examine the trajectory of neighboring crystal pairs after a cycle of overturn and how their transport produces regions of homogeneity and heterogeneity in a crystal population. Mixing associated with volatile exsolution from a recharging magma has been suggested as a potentially important process [*Eichelberger*, 1980]. The physical nature of such gas-driven mixing and overturn has been investigated with analog [*Phillips and Woods*, 2001], analytical [*Bergantz and Breidenthal*, 2001], and numerical techniques [*Longo et al.*, 2006].

2.2 Physical Model of Magma Mixing and Crystal Tracking

Our objective is to explore the transport and zoning of crystals in a single episode of magma chamber overturn. Our numerical model describes the compositional mixing/hybridization caused by a gas-rich magma underlying a bubble-free magma, a condition suggested to arise in nature [e.g., *Eichelberger*, 1980; *Pallister et al.*, 1992; *Nakamura*, 1995]. This is a useful end-member for magma chamber overturn because it is likely one of the fastest, naturally occurring instabilities with respect to instability growth and overturn completion due to the large density variations between the gas bubbles and the magma. In our simulations we begin with a fixed bubble volume fraction in the bubble-bearing magma, which is intrinsically unstable. Hence we do not attempt to model the complex and poorly understood paths to progressive vesiculation. Natural recharge events will likely have a range of mass flux and exsolved bubble-volume fraction. Our aim is not to model any particular recharge event but to explore the dynamics associated with a geologically reasonable, but end-member set of conditions.

All simulations were performed under isothermal conditions because we assume that the time-scale of advection of enthalpy by the overturning process is

much faster than any other heat transfer process. Thus, we ignore processes such as secondary nucleation and additional gas exsolution. We simplify the natural system by assuming an identical solid and liquid composition for the bubble-free and the bubble-bearing magmas. Thus, viscosity variations arising from temperature and compositional dependence, phase transitions and bubble coalescence are ignored. In our model viscosity differences only emerge from the varying content in bubbles. In natural systems these viscosity variations may alter the kinematic template significantly and further studies including those complexities will be necessary. However, to be able to assess the individual effects of viscosity and initial density contrast we need to consider these effects separately to make progress in understanding the dynamics of magma-magma interaction on the bulk and the crystal scale. Thus, we have focused on a simple but geologically significant end-member.

To resolve the complex multiphase character of natural magmas, we have divided the system into two parts each of which resolves different scales. The first and largest scale is calculated with a multiphase finite-volume approach [*Patankar*, 1980; *Gidaspow*, 1994] for a carrier phase (silicate melt plus "background" crystals) and a dispersed phase (bubbles). We assume t hat t he "background" crystals are passively advected by the melt [*Aref*, 1990], thus treating the carrier phase as a virtual single phase whose properties can be calculated using mixture theory [*Burgisser et al.*, 2005]. We subsequently refer to this melt and crystal mixture as the magma phase. For sufficiently small crystal volume fractions, melt and magma viscosities are of similar order of magnitude (Table 2.1). Hence, the crystals have little effect on the kinematic template established by the fluid motion. We employ a form of the MFIX [*Syamlal et al.*, 1993] multiphase fluid code that we have modified for magma conditions. *Dufek and Bergantz* [2005, 2007] used a similar approach to investigate flow dynamics in a magmatic conduit and in a pyroclastic flow. The simulation tracks the volume fractions of the silicate melt-crystal mixture and the gas bubbles in a magmatic system that is 200 m wide and 100 m high.

Different aspect ratios were not considered here. Varying aspect ratios can have a significant effect on the mixing dynamics, which is discussed as part of the overall mixing dynamics below. The width of the model was chosen to ensure that the boundaries are not affecting the flow and the width is greater than several wavelengths of the examined Rayleigh-Taylor type instabilities that dominate the most active period of the flow.

For all multiphase fluid dynamics simulations the initial conditions are a 60 m thick bubble-free magma overlying a 40 m thick bubble-bearing magma. The physical properties are given in Table 2.1. Six simulations were performed, where the only difference was the bubble volume fraction, $\varepsilon_{bubbles}$ of, the lower bubble-rich layer. The lowest bubble volume fraction was 0.02 and the highest was 0.4.

The boundaries of the system are subject to no-slip for the bottom and top wall and free-slip conditions for the sidewalls. Thus, the velocities for all phases approach zero on the horizontal boundaries, while the velocity gradients approach zero on the sidewalls:

$$v_{bottom} = v_{top} = 0, \tag{2.1}$$

$$\left(\frac{dv}{dx}\right)_{east} = \left(\frac{dv}{dx}\right)_{west} = 0. \tag{2.2}$$

These conditions are appropriate for a magma system that is sill-like and may continue horizontally.

Table 2.1 Physical Properties and Model Parameters Used in the Simulations.

Description	Parameter	Value
Melt viscosity	μ_{magma}	10^4 Pa s [a]
Particle density	$\rho_{particle}$	2800 kg m^{-3}
Melt density	ρ_{melt}	2400 kg m^{-3}
Bubble density	$\rho_{bubbles}$	600 kg m^{-3} [b]
Bubble-bearing layer thickness	h	40 m
Bubble diameter	$\phi_{bubbles}$	10^{-3} m
Particle diameter	$\phi_{particle}$	10^{-3} m
Bubble volume fraction	$\varepsilon_{bubbles}$	0.02, 0.05, 0.1, 0.2, 0.3, 0.4
Critical bubble volume fraction	ε_{cp}	0.5
Cell resolution (vertical and horizontal)		0.4 m

[a] resembles most intermediate to silicic melts [*Scaillet et al.*, 1998]. Following Equation 2.3 and a volume balance between crystals and melt, we can calculate the effective melt viscosities. For common crystal volume fractions of 0 to 0.25 in arc magmas the effective melt viscosity remains of the same order and ranges from 7.4 to10 x 10^4 Pa s.

[b] Similar bubble density taken as for Pinatubo dacite [*Gerlach et al.*, 1996].

Bubbles are modeled as rigid spheres implying that bubble surface tension exceeds viscous stresses from fluid motion. Analog conduit experiments performed by *Namiki and Manga* [2006] demonstrated that even under conditions of high magmatic viscosity and high shear rates, like volcanic conduits during an eruption, bubbles maintain their spherical shape.

The within-phase bubble viscosity $\mu_{bubbles}$, which is the drag of the bubbles by the other bubbles, is modeled using the relationship by [*Beckermann and Viskanta*, 1993],

$$\mu_{bubbles} = \mu_{magma}\left(1 - \frac{\varepsilon_{bubbles}}{\varepsilon_{cp}}\right)^{-2.5\varepsilon_{cp}}, \tag{2.3}$$

where ε_{cp} is the closed packing bubble volume fraction and μ_{magma} the dynamic melt viscosity.

Once the dynamics of the overturn have been solved (as shown in Figure 2.1), the so-called smart crystals, or crystal recorders are imbedded in the flow. In this step 20,000 crystals are randomly seeded throughout the magma system and their progress is tracked. The motion of the particles is calculated using the particle motion model of *Burgisser et al.* [2005]. The Bassinet-Boussinesq-Oseen (BBO) equation describes the force-balance for spherical particles [*Maxey and Riley*, 1983]. For most applications only the drag and body forces are of importance [*Burgisser et al.*, 2005]. In this case the horizontal and vertical component of the acceleration for each crystal can be calculated from the local melt velocity field, respectively, by:

$$\frac{dv_i}{dt} = \frac{f}{\tau_v}(u_i - v_i)\left(\frac{2\rho_p}{2\rho_p + \rho_f}\right), \tag{2.4a}$$

$$\frac{dv_i}{dt} = \frac{f}{\tau_v}(u_i - v_i)\left(\frac{2\rho_p}{2\rho_p + \rho_f}\right) + g\left(\frac{2\rho_p - 2\rho_f}{2\rho_p + \rho_f}\right), \tag{2.4b}$$

where v_i and u_i are the crystal and melt phase velocities, respectively, and g, ρ_p and $\rho_f$are the acceleration due to gravity, crystal density and melt density, respectively. The magma velocity from the multiphase fluid model is used to approximate the melt phase velocity. As noted earlier, for sufficiently small crystal volume fractions this approximation is valid, because crystal-crystal interaction is limited [*Burgisser et al.*, 2005]. Following *Burgisser et al.* [2005] the drag coefficient f and the particle response time τ_v are defined as:

$$f = 1 + 0.15\,\mathrm{Re}_p^{0.687} + \frac{0.0175}{\left(1 + 42500\,\mathrm{Re}_p^{-1.16}\right)}, \tag{2.5}$$

$$\tau_v = \frac{(\rho_p - \rho_f)\phi^2}{18\mu}, \tag{2.6}$$

with Re_P, ϕ and μ being the particle Reynolds number, particle diameter and the dynamic viscosity, respectively.

The particle Reynolds number Re_P, which describes the kinematics of the flow regime of a melt around a particle, is given as:

$$\mathrm{Re}_p = \frac{U_T \phi}{\upsilon}, \tag{2.7}$$

where U_T is a reference velocity taken here as the terminal fall velocity and υ is the kinematic viscosity.

We only track one size of crystals (1 mm) in our tracer calculations. In a scaling study on igneous processes *Burgisser et al.* [2005] showed that for conditions in a magma chamber with high melt viscosity and small particle size, the crystal response time is much shorter than the timescale of fluid motion. Hence, crystals closely follow the fluid flow. The particle response time, despite its quadratic dependence on crystal size (Equation 2.6), is on the order of nanoseconds. Thus, a single crystal size is sufficient to track any crystal paths during the overturn.

Equations 2.4 through 2.7 provide the framework to determine the trajectory of each crystal within the developing flow. The velocity field of the melt at the position of the crystal is interpolated based on the calculated velocity values at the control volume interfaces. In the present model 20,000 Lagrangian particles distributed randomly over the entire magma chamber were followed for the simulation with $\varepsilon_{bubbles} = 0.1$ and $\varepsilon_{bubbles} = 0.3$, respectively (Figure 2.1). Crystal motions are calculated until the major overturn has cease and the average crystal velocities are less than 0.08 mm s^{-1}.

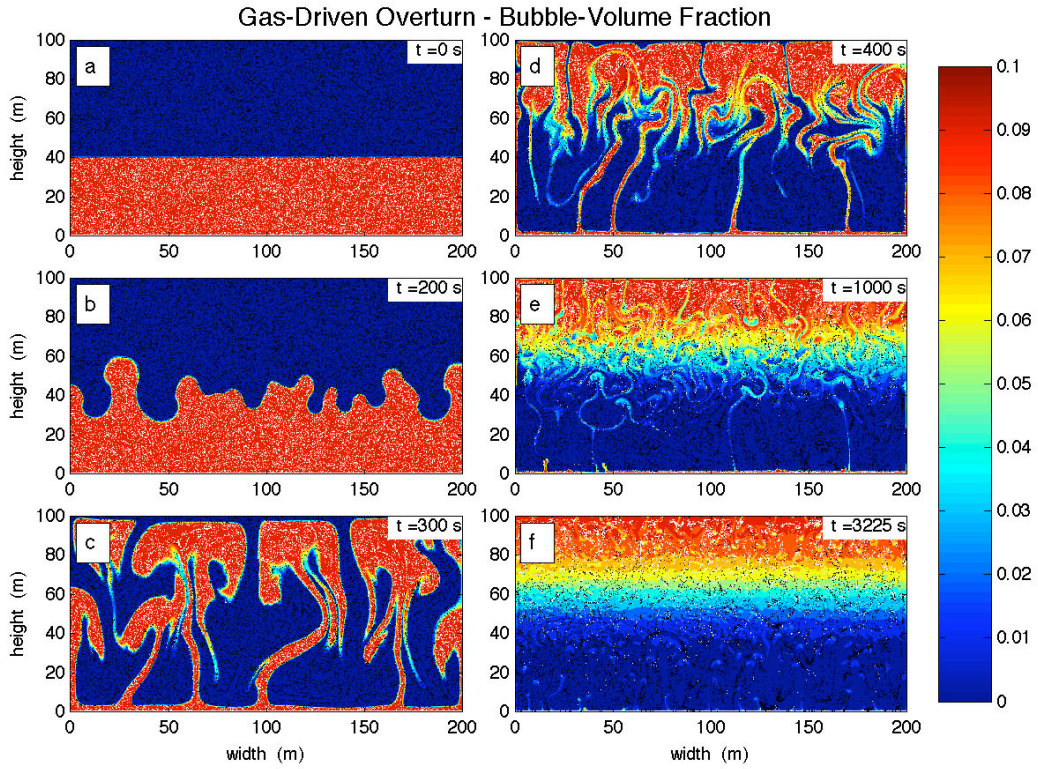

Figure 2.1 Snapshots of gas-driven overturn. Different stages in the overturn of a lower, bubble-rich layer for an initial $\varepsilon_{bubbles} = 0.1$. Colors indicate $\varepsilon_{bubbles}$. White and black Lagrangian crystals refer to initially bound to the bubble-rich and bubble-poor layers, respectively. Symbols are bigger than the crystal diameter of 1mm. Initial conditions are a 60 m thick bubble poor layer overlying a 40 m bubble-bearing layer. East and west boundaries are free-slip, while top and bottom boundaries are non-slip. Physical properties are given in Table 2.1. The transient overturn is showing different generations of plumes rising through the chamber until ~1000 s. The simulation is terminated after 3225 s. A stable stratified system has developed and average crystal velocities are smaller than 0.08 mm s^{-1}. Appendix A1 and A2 show snapshots of the entire simulation. Appendix A1 omits displaying the 'smart' crystals to improve the visibility of the dynamics in the multiphase simulation. A complete video of these two simulations can be found in *Ruprecht et al.* [2008].

2.3 Results: Overall Mixing Dynamics

Given our initial conditions where there is a density gradient that is opposite to the pressure gradient, a Rayleigh-Taylor (R-T) instability forms. The governing parameters describing the evolution of an R-T instability are the Atwood number A [*Ramaprabhu and Andrews*, 2004], and the viscosity ratio μ_l/μ_u of the lower layer ml and the upper layer μ_u, respectively [*Ramberg*, 1981; Table 2.2]. The viscosity ratio is required because the Reynolds numbers are not high enough to ensure that the motion is fully turbulent with a loss of memory of initial conditions. Hence, the flow is not self-similar. The Atwood number describes the dimensionless density ratio of the two layers where

$$A = \frac{(\rho_u - \rho_l)}{(\rho_u + \rho_l)}, \tag{2.8}$$

and ρ_u and ρ_l refer to the density of the upper and lower layers, respectively. Much work has focused on systems with large values of A [e.g., *Youngs*, 1984]. In contrast, a more recent study by *Linden and Redondo* [1991] employed an experimental approach to investigate a Rayleigh-Taylor instability in a system with low values of A, which are similar to values of A found in shallow magmatic systems. In our study A ranges from 2×10^{-3} to 1.8×10^{-1}.

Following *Chandrasekhar* [1961] and given A and the average kinematic viscosity of the system υ we can predict the characteristic wavelength λ_m of the main plumes generated from the R-T instability using,

$$\lambda_m = 4\pi\left(\frac{\upsilon^2}{gA}\right)^{1/3}, \tag{2.9}$$

$$\upsilon = \frac{\left(\mu_{melt} + \varepsilon_{bubbles}\mu_{bubbles} + \left(1 - \varepsilon_{bubbles}\right)\mu_{melt}\right)}{\left(\rho_{melt} + \varepsilon_{bubbles}\rho_{bubbles} + \left(1 - \varepsilon_{bubbles}\right)\rho_{melt}\right)}. \quad (2.10)$$

The energy and timescale of the over-turning motion is directly related to $\varepsilon_{bubbles}$. Hence we considered six different bubble volume fractions ranging from 0.02 to 0.40. The observed timescales decrease for increasing $\varepsilon_{bubbles}$ with the exception of the simulation with the largest bubble volume fraction. In the case of $\varepsilon_{bubbles}$ = 0.4 the timescale is increasing, because the initial instability contains so much potential energy that the system overshoots. The viscosity is not capable of damping the overturn significantly and after the main overturn has ceased small waves are traveling through the system, keeping the average crystal velocities above our termination criterion for the simulation. The wavelength also has a minimum for $\varepsilon_{bubbles}$ between 0.2 and 0.3 after which the kinematic viscosity increases dramatically. Therefore, the characteristic wavelength of the overturning motion increases again for large-bubble volume fractions. The maximum system-wide Reynolds number (Re) for each simulation varies from 15 to 364, respectively (Table 2.2). It is calculated on the basis of the velocity approximation $v_{instability}$ for particle-laden blobs [*Nitsche and Batchelor*, 1997] and the diameter L of the largest plume that crosses a plane at 45 m height [*Nitsche and Batchelor*, 1997]:

$$\mathrm{Re} = \frac{v_{instability} L}{\upsilon_{magma}}, \quad (2.11)$$

$$v_{instability} = \frac{\left(\rho_{instability} - \rho_{magma}\right) g L^2}{3\mu_{magma}} \frac{\mu_{magma} + \mu_{instability}}{\mu_{magma} + \frac{3}{2}\mu_{instability}}, \quad (2.12)$$

where $\rho_{instability}$ and $\mu_{instability}$ are the mean density and viscosity of the particle-laden blobs. Here, we consider the bubbles as a separate dispersed phase of the magma, while crystals and melt are combined together as the virtual single phase. Although differing by up to one order of magnitude for the lowest bubble volume fractions from the expected values presented in the previous section, Re numbers still fall into the regime of transitional flow: not fully turbulent but unsteady. All the simulations produced a fast overturn: less than 3 hours (Table 2.2), with a complex dynamic template composed of an incomplete spectrum of eddy sizes in this transitional flow regime.

Changing the aspect ratio or the volume of bubble-bearing magma has an immediate effect on the Reynolds number of the system, thus affecting the overturn timescale. Increasing the height of the magma system would increase the transient overturn timescale.

Table 2.2 Atwood Number *A*, Density Ratio, Viscosity Ratio, Reynolds Number *Re*, Overturn Timescale, and Wavelength.

$\varepsilon_{bubbles}$	A	ρ_l/ρ_u	μ_l/μ_u	Re [a]	Re [b]	$t_{overturn}$ [c] [hr]	λ_m [d] [m]
0.02	0.008	0.985	1.001	92	15	2.13	77.9
0.05	0.019	0.963	1.007	146	52	1.60	57.7
0.10	0.039	0.925	1.032	206	104	1.13	46.5
0.20	0.081	0.850	1.179	291	364	0.83	39.2
0.30	0.127	0.775	1.643	356	344	0.80	39.5
0.40	0.176	0.700	3.591	412	355	0.99	52.6

[a] Predicted values after *Linden and Redondo* [1991].

[b] Observed *Re* number for simulation, calculated from *Nitsche and Batchelor* [1997].

[c] Time until average velocity of 'smart' crystals is smaller than 0.08 mm/s.

[d] Predicted wavelengths after *Linden and Redondo* [1991].

Figure 2.1 shows a typical simulation throughout a cycle of overturn. *Youngs* [1984] described the mixing process in the fully turbulent regime by three evolutionary stages. Although turbulent conditions are not likely to occur in silicic magmatic systems, the same growth stages could be recognized. A complete set of snapshots of this simulation can be found in the Appendix A1. Initially, the instability grows exponentially until the characteristic wavelength λ_m emerges. Results for predicted λ_m ranging from 39.2 m and 77.9 m (Table 2.2) are in good agreement with our initial condition requiring the generation of multiple plumes in the 200 m wide system. Observed wavelengths are of similar order. This length scale dominates the second evolutionary stage, in which those plumes rise undisturbed to about $\lambda_m/2$. Subsequently, the plume head grows in width by entrainment and the associated vortical circulation influences the neighboring plumes causing their internal structure to become increasingly more complex. In addition, local Kelvin-Helmholtz instabilities develop along the interface of the rising plume. These instabilities generate eddies between the upward moving lighter melt-bubble mixture and the downward moving magma. All these interactions temporally and spatially cause stretching and translation.

Once the bubble-rich plumes reach the top, they spread out and create a layer of bubble-rich magma. While the main plumes move upward through the system, a second wave of smaller plumes with a range of length scales emerges from the remaining bottom layer. Plume generation continues until the initial bubble-rich layer at the bottom is consumed. Similar behavior was described by *Bergantz and Ni* [1999].

The process of convective overturn creates a gradually stratified magma chamber overlying bubble free magma. The first wave of plumes produces the largest eddies and is most efficient in mixing in magma of the overlying bubble-free layer. They entrain and deform large volumes of the overlying magma that get

stretched and redistributed by subsequent smaller plumes. This stirring associated with stretching and redistribution leads to local homogeneity in the progress toward a gradual vertical stratification. Finally, this gradual stratified layer becomes increasingly concentrated in bubbles at the top, while the bubbles continue to rise separately or in small bubble trains. We do not observe an increase in bubble volume fraction within the top layer beyond its initial volume fraction. As mention earlier, our model ignores bubble coalescence, which results in a maximum rise speed of the bubbles equal to the terminal rise velocity of 10^{-1} mm/s for the 1 mm large bubbles. This limits the vertical accumulation of bubbles over the short timescale of this transient overturn.

Figure 2.2 represents the temporal evolution shown in Figure 2.1 in a more compact form. One can recognize the temporal evolution from instability growth, the subsequent dynamic mixing by overturn, to the final stratification. The two end-member simulations are shown in Figure 2.2. In the small Re case ($\varepsilon_{bubbles} = 0.02$) multiple pulses of plume generation are shown within the time series of horizontally averaged $\varepsilon_{bubbles}$. In the high Re case ($\varepsilon_{bubbles} = 0.4$) several plume generation events are also present, but occur at a higher frequency and are therefore not as well defined by the horizontal averaging used in Figure 2.2. Additionally, for small bulk Re numbers (i.e., small bubble volume fractions) the zone of stratification is smaller than for large Re numbers (Figure 2.2). In the high Re case more of the bubble free magma is dragged into the vortices of the plumes, thus more efficiently mixed into the bubbles-bearing magma. *Bergantz and Ni* [1999] presented similar results on the sedimentation of dripping crystal-bearing plumes in viscous fluids. It was confirmed that for high-viscosity fluids (low Re) the mixing efficiency was much smaller than for low-viscosity fluids (high Re).

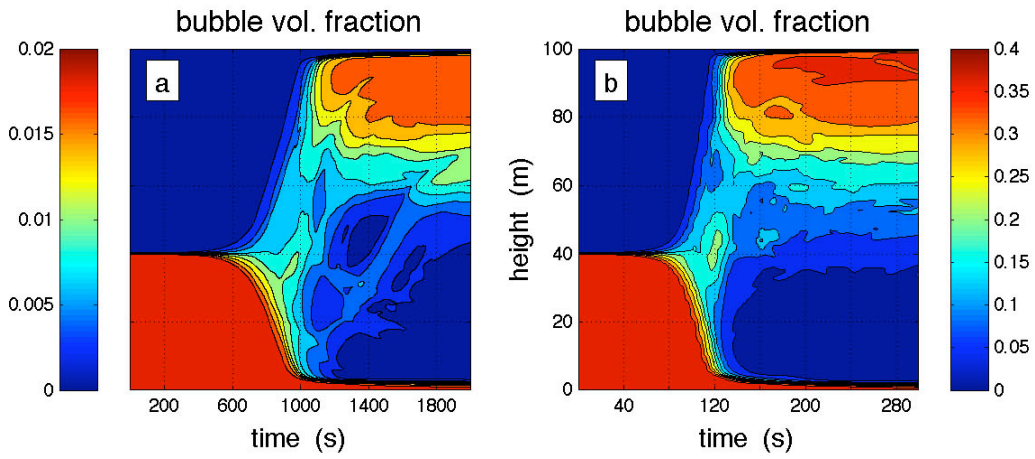

Figure 2.2 Horizontally-averaged bubble volume fraction evolution as a function of time. The overturn is characterized by three stages: a build-up of the instability, the transient and chaotic upward-transport of the bubble-bearing magma, and the damping of the overturning motion that creates a stratified magmatic system. (a) Low *Re* number case for bubble volume fraction of 0.02. The transient mixing dynamics occur on a timescale of 10^3 s. (b) High *Re* number case for bubble volume fraction of 0.4. The transient mixing dynamics occur on a timescale of 10^2 s. Note the different time axes for the two time series. Appendix A1 shows how Figure 2.2 is generated from Figure 2.1.

The overturning process produces mixing of the bubble-free and the bubble-bearing layers. Several approaches have been used to quantify the efficiency of the mixing, such as various statistical measures of the progressive change of the concentration field during the mixing process [*Oldenburg et al.*, 1989], changes in the interface length [*Ottino*, 1990] and the change in potential energy of the system [*Linden and Redondo*, 1991]. We adopt a slightly modified version of this latter approach [*Jellinek et al.*, 1999]. The mixing efficiency, E, is an expression for the vertical stratification, or gradient, of a mixed quantity at the end of overturn [*Linden and Redondo*, 1991]:

$$E = \frac{\left(P_f - P_{\min}\right)}{\left(P_{\max} - P_{\min}\right)}, \tag{2.13}$$

$$P_f = \int_0^H g\left(\rho_{melt} - \rho(z)\right) z dz, \tag{2.14}$$

where P_f is the integrated potential energy of the stratified system. P_{min} and P_{max} correspond to no mixing where the two layers exchange position without mixing, and complete mixing, where the mixture composition is the same everywhere. Mixing efficiency is generally low for this fixed volume system, resulting in a stratified system. The simulation with the highest bubble volume fraction reaches a mixing efficiency of 0.45. Low mixing efficiencies for the magmas imply an equally low mixing efficiency for crystals that are dispersed in the flow, since for a fast overturn process and small crystal diameters, crystals will have a Stokes number [*Burgisser et al.*, 2005] much less than unity and so simply follow the flow. However, since there is some mixing present, it is of interest on which length scales the crystal gathering and dispersal is observed.

2.4 Linking the Dynamics of Crystal Gathering and Dispersal to Geological Observations

Crystal gathering and dispersal is a function of the strain associated with the redistribution and stretching during the mixing process [*Kellogg and Turcotte*, 1990]. During strain accumulation for a 2-dimensional system a circle with radius a_0 is deformed into an ellipse with a long and a short axis of length a_i, where i refers to the two perpendicular directions. Similarly to a circle, we can compare the distance between two points that are initially separated by the distance a_0. In mantle mixing studies [*Kellogg and Turcotte*, 1990; *Ferrachat and Ricard*, 1998; *Coltice and Schmalzl*, 2006] the change of a_i with respect to a_0 for these two points has been

used to investigate the mantle flow dynamics. The change of a_i is commonly expressed as the Lyapunov exponent σ_i:

$$\sigma_i = \lim_{\substack{t\to\infty \\ a_0\to 0}} \frac{1}{t} \ln\left(\frac{a_i}{a_0}\right). \tag{2.15}$$

A system is chaotic and mixing is efficient on the local scale if one Lyapunov exponent is positive [*Ferrachat and Ricard*, 1998]. In contrast, Lyapunov exponents equal to zero indicate regular mixing.

The tracked crystals in the simulations are tracers of individual particles and act owing to their low Stokes numbers simultaneously as tracers of small volumes of magma. Thus, we can use the advected crystals to estimate the strain a_i/a_0 and the Lyapunov exponent by choosing particle pairs for which a_0 is sufficiently small. By calculating the distance a_0 between all ~2.0 x 10^8 crystal-crystal pairs ((n(n-1))/2 for n = 20,000 crystals) for their initial location, we can select those crystal-crystal pairs that are closer to each other than an arbitrarily chosen cutoff distance. We call this cutoff distance the Maximum Crystal-Crystal Distance (MCCD) (Figure 2.3). Following Equation 2.15 the MCCD needs to be as small as possible to determine σ for the local scale. Hence, the limiting factor is statistical significance for the number of pairs that fall within this distance.

The selection criterion for the statistical analysis of a crystal-crystal pair therefore is

$$a_0 \leq MCCD. \tag{2.16}$$

Figure 2.4 shows the time series of the Lyapunov exponent for the simulations with varying bubble-volume fraction and for a MCCD of 2 m. For the gas-driven overturn with variable bubble-volume fraction the Lyapunov exponents are positive, but several orders of magnitude smaller than σ for mantle mixing studies [*Coltice and Schmalzl*, 2006], which may be as high as 10^5. Values for σ in Figure 2.4 are only minimum estimates, because our calculations ignore the possibility of folding. The vorticity that the crystal pair experiences needs to be considered for an exact calculation of the maximum Lyapunov exponent [*Wolf et al.*, 1985]. We ignore this effect, because the tracking of folding is computationally expensive and because we argue below that a modified version of the Lyapunov exponent is a better measure to characterize the mixing dynamics of gas-driven overturn.

On the basis of the estimates for *Re* we know that gas-driven overturn is chaotic for the presented range in bubble-volume fractions. However, Figure 2.4 shows that σ_{max} asymptotically approaches zero with time, which indicates regular mixing. This disagreement stems from the fact that transient flows have a finite strain a_i/a_0.

Once the potential energy of the initial instability is dissipated a_i remains constant, thus σ_i intrinsically has to approach zero asymptotically. Even so, the calculated Re at peak strain rates yields a chaotic mixing regime. While for statistically steady but time-dependent f lows, as observed in mantle dynamics, a Lyapunov exponent can be calculated following Equation 2.15, transient flows, which dominate crustal magma processes, cannot be characterized very well with the conventional Lyapunov exponent. Therefore, we favor estimating the strain over the use of the Lyapunov exponent in the gas-driven overturn to characterize the dynamic behavior.

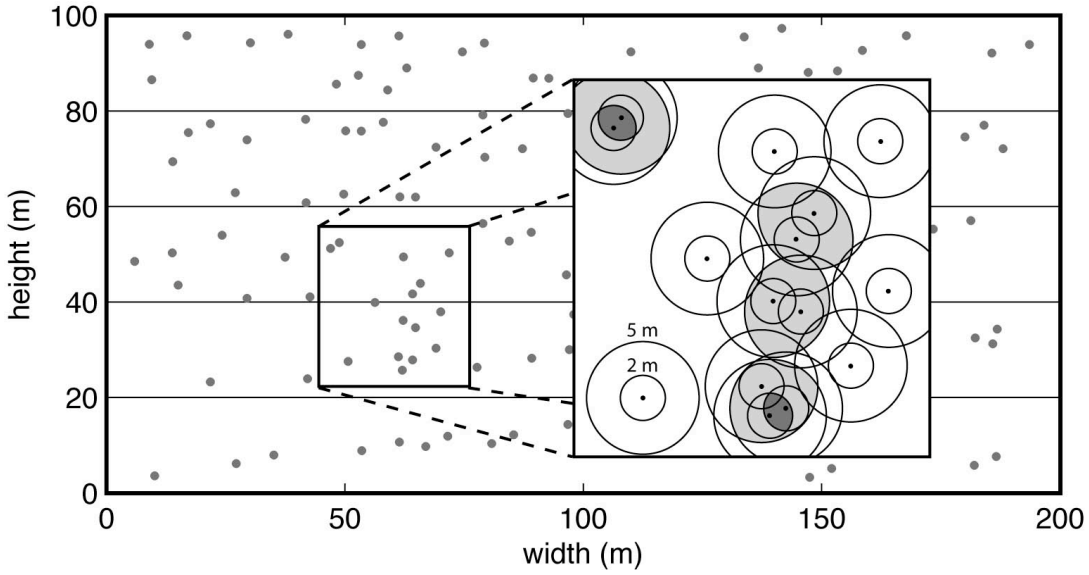

Figure 2.3 Technique for investigating crystal dispersal and gathering. For each 'smart crystal' the distance to all other crystals was calculated and only crystal pairs closer to each other than the Maximum Crystal-Crystal Distance (MCCD) were chosen for the prior-after overturn comparison. The insert represents a subset of crystal locations after the overturn. The circles around each crystal represent the 2 m and 5 m MCCD, respectively. In this example, the particle pairs falling in the dark gray and light gray areas are chosen for a comparison of their location prior to and after the overturn for the 2 m and 5 case. Thus, only a subset of the $n(n-1)/2$ crystal pairs are used for the analysis. We select those pairs for the entire volume as well as 20 m thick layers.

The strain for adjacent particles enables us to connect the process of gas-driven overturn directly to petrologic observations. Petrological analysis is typically based on small-sized samples, and one objective is to understand how compositional and textural heterogeneity at that scale reflects a distinct set of dynamic processes at much larger scales. Thus, one must resolve crystal paths through all scales of the flow. By comparing adjacent crystals on the basis of their spacing prior to the onset of a dynamic process such as mixing, and their final spacing after the process has finished, we can estimate the average dispersal and gathering for a given crystal-crystal pair, which is equal to the local strain. This in turn gives an estimate of the volume that is sampled in a single thin section during a single overturn. While

commonly the strain is calculated on the basis of initially adjacent particles, we calculated the strain from crystal pairs that are close to each other AFTER the overturn event. Thus, we can use the simulations to understand natural examples, in which we can only image the final stage. As discussed in section 2, we define the end of the transient signal as the time when the average crystal motion has fallen below 0.08 mm s^{-1}. Therefore, the accumulated strain that we compare for the different simulations is defined as

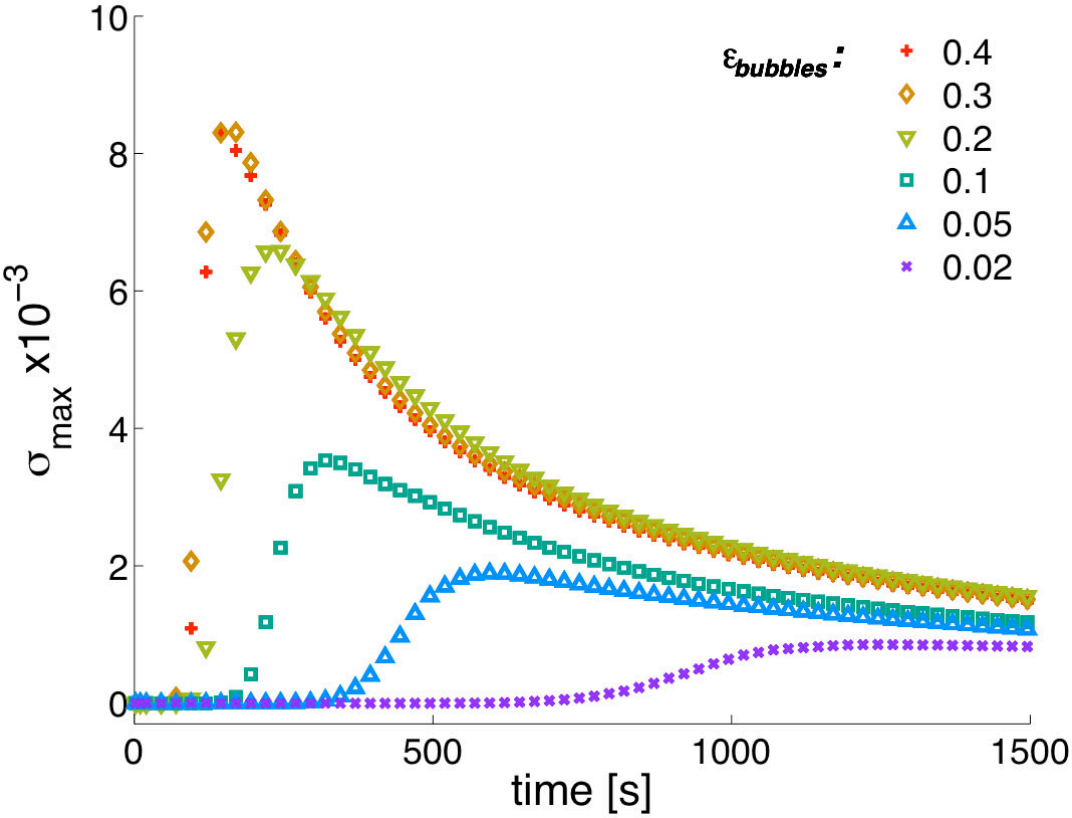

Figure 2.4 Time series for the maximum Lyapunov exponent σ for a_0 = 2 m. A positive σ indicates chaotic mixing during the transient gas-driven overturn. Once that transient signal decays, σ also asymptotically approaches zero. For further discussion, see text.

$$strain = \frac{a_0}{a_{final}}, \tag{2.17}$$

$$a_{final} \leq MCCD. \tag{2.18}$$

Note the different selection criterion compared to Equation 2.16 that is commonly used to calculate the Lyapunov exponent. This strain calculated from the crystal-crystal pairs is a measure for the gathering strength of the flow and compares the original volume that is tapped during the mixing. For a_0/a_{final} equal to one no differential movement between the crystals has occurred, while a value larger than

Ideally, the MCCD should be 3 cm, the scale of a thin section. However, given 20,000 randomly distributed tracer crystals over the entire system restricts this approach to larger MCCDs, to ensure statistical significance. A MCCD of 10 cm reduces the population size to ~1 x 104 crystal-crystal pairs. We have chosen seven different MCCDs with 0.1 m, 0.2 m, 0.5 m, 1 m, 2 m, 5 m, and 10 m, respectively. The population size for the largest MCCD (10 m) increases to ~6 x 10^6 crystal-crystal pairs.

To exemplify the process described above, we apply these concepts of strain accumulation and crystal-crystal pair homogeneity to four cases of our simulation runs, thus combining the information from the bulk multiphase model and the crystal-tracking algorithm (Figure 2.5). The runs with a bubble volume fraction of 0.1 and 0.3 correspond to the low and high Re numbers in our simulations, respectively. In Figure 2.5 we compare these runs f or a small (0.1 m), and an intermediate (1 m) MCCD, respectively. Larger MCCDs have limited value for the connection of modeling data with thin section scale observations. In all four cases

over 95% of the crystal-crystal pairs have a a_0/a_{final} greater than one. For the average particle (median) this gathering range varies over one log unit from $10^{1.5}$ to $10^{2.5}$ of their final distance. Thus, most crystals with a $a_{final} \leq$ MCCD are between 30 to 300 times further apart of each other before the mixing.

Comparing the CFDs in Figure 2.5 for the low and the high *Re* case in more detail reveals a weaker strain accumulation for low *Re*. This behavior is observed for large and small MCCDs. The difference in the median of the CFD between high and low *Re* case for both MCCDs is ~0.15 log units, respectively. Additionally, the strain accumulation increases, for a smaller MCCD. Besides the shift to larger medians for small MCCDs, we also observe a decrease in the slope of the CFDs. For small MCCD the distribution gets very broad, indicating that the crystals experience very different gathering length scales. The largest heterogeneity in gathering length scales occurs for low *Re* and small MCCD.

We have also analyzed these crystal-crystal pairs of the two different simulations ($\varepsilon_{bubbles} = 0.1$; $\varepsilon_{bubbles} = 0.3$) for varying horizontal behavior of particles for the smallest MCCD (0.1 m) case (Figure 2.6). The crystal-crystal pairs are divided into five horizontal layers of 20 m each. Not all layers are shown; instead Figure 2.6 shows an envelope that is composed of the CFDs of all five horizontal layers. As expected, the range of gathering displayed by this envelope varies around the average value for the entire crystal population. For the low *Re* case this range is much larger (~0.6 log units) than the range observed in the high *Re* case (~0.2 log units). This discrepancy stems mainly from the initially bottom layer in the low Re case, which shows a significantly smaller length scale in gathering. Thus, while the kinematic behavior for the uppermost 80 m is very uniform with fairly small scatter around the average value, the lowermost bubble-bearing magma shows a different kinematic behavior. The lowermost 20 m stay more coherent over the course of the overturn then the rest of the magma and are less vigorously mixed.

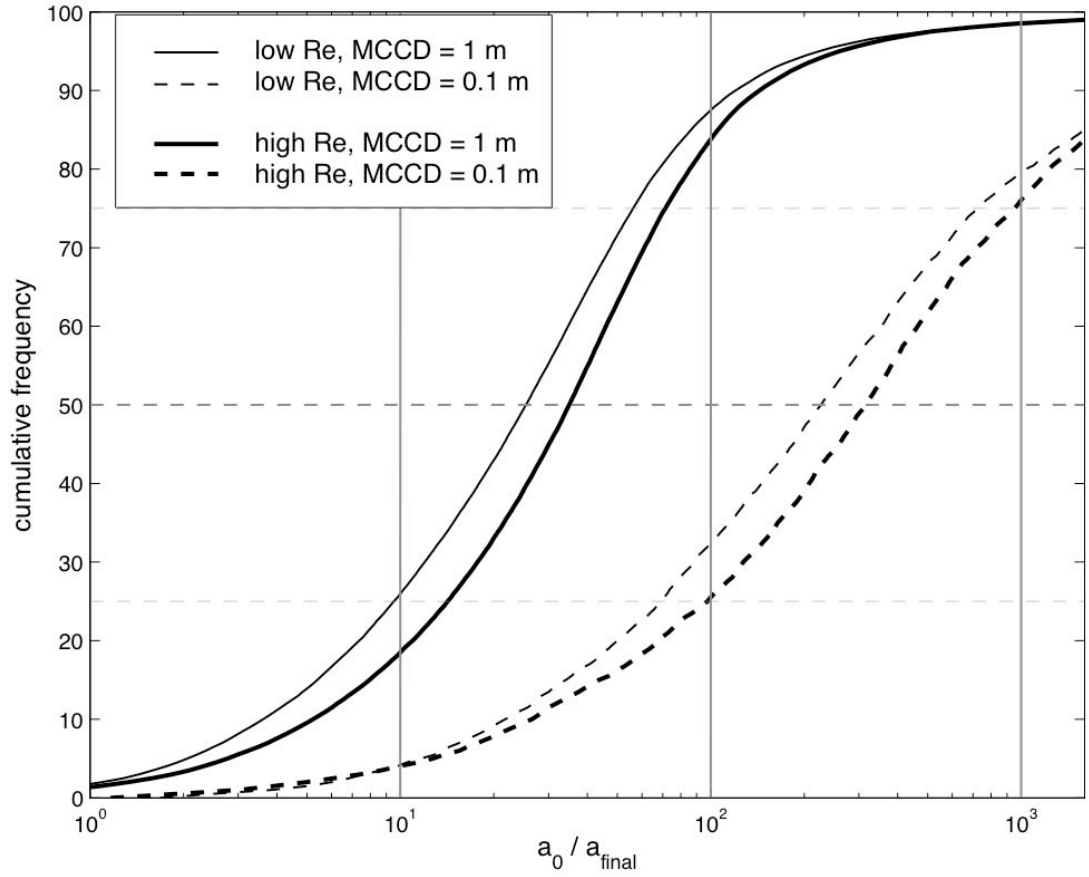

Figure 2.5 Cumulative Frequency Distribution (CFD) curves for populations of particle pairs within threshold proximity after the mixing event. High and low Re cases refer to $\varepsilon_{bubbles}$ = 0.3 and $\varepsilon_{bubbles}$ = 0.01, respectively.

While the results for 20,000 randomly distributed 'smart' crystals show an unambiguous trend of heterogeneous behavior on the bulk and the crystal scale, they were only applied to two of the six simulated $\varepsilon_{bubbles}$. The remaining simulations with different $\varepsilon_{bubbles}$ are also analyzed for the relative crystal-crystal pair motion. However, we have reduced the number of tracked crystals to n = 5000, hence minimizing computational time.

These simulations decrease the number of crystal-crystal pairs that can be analyzed by a factor of ~$1/4^2$ (($n(n$-1))/2 = 1.25 x 10^7). This requires an increase in the MCCD to the meter scale. In fact, for an MCCD of 1 m we generate only ~3 x 10^3 crystal-crystal pairs for the statistical analysis. For an MCCD of 10 m we have more than one order of magnitude less crystal-crystal pairs available (~4 x 10^5) compared to the simulations with 20,000 crystals. Thus, for these lower resolution simulations we do not reach a length scale that is similar to the length scale of a thin section. However, in light of the high-resolution simulations with 20,000 'smart' crystals, these additional simulations expand our understanding for the simulations with the lowest and highest *Re* numbers, respectively.

Instead of presenting the results from the additional simulations with 5000 'smart' crystals in separate cumulative frequency diagrams, we summarize all simulations by their strain accumulation and their particle population homogeneity (Figure 2.7). At high Re mixing events are characterized by smaller particle population heterogeneity and stronger strain accumulation. Comparing the large MCCD (10 m) with the small MCCD (0.1 m) of crystal gathering as a function of changing Re number reveals a shift from small variations in strain accumulation and large changes in particle population homogeneity to mainly strain accumulation dominated behavior. The simulations with 5000 'smart' crystals follow the trend of the high-resolution simulations. They also support that simulations with large $\varepsilon_{bubbles}$ (0.2, 0.3, and 0.4) are very similar to each other. This is in good agreement with the observed *Re* numbers (Table 2.2) that identify a very similar mixing behavior on the bulk scale. The simulations with low $\varepsilon_{bubbles}$ are more variable in their strain accumulation and particle population homogeneity.

Figure 2.7 also enables us to assess the statistical robustness for the small MCCD cases. The results from the high-resolution simulations with 20,000 'smart' crystals have very similar values for the strain accumulation and the particle

population homogeneity as the simulations with 5000 ‘smart’ crystals. The smallest chosen MCCD (1 m) for the smaller number of ‘smart’ crystals starts to diverge from the results of the high-resolution simulations. Thus, any smaller MCCD would not be statistically robust.

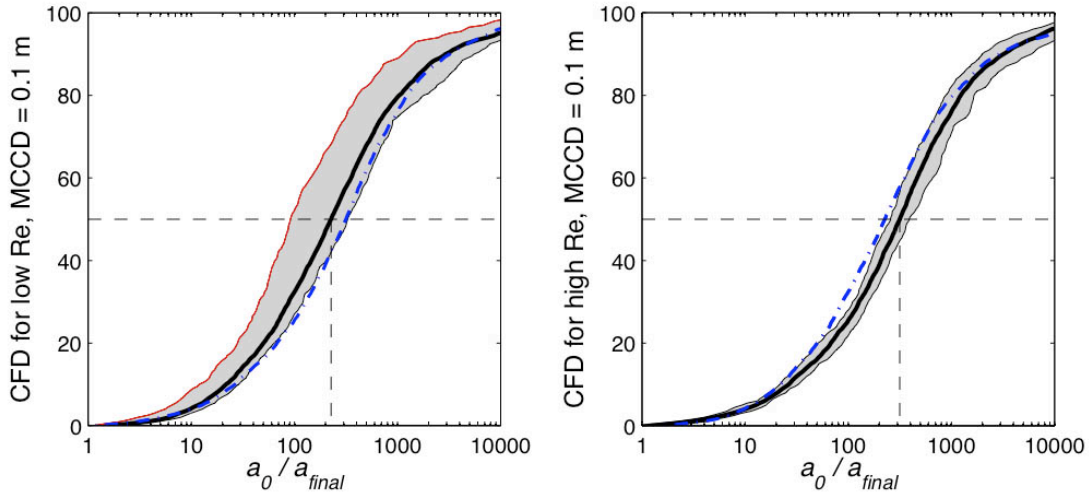

Figure 2.6 Cumulative Frequency Distribution (CFD) curves for high-resolution simulations with 20,000 ‘smart’ particles. The low Re case ($\varepsilon_{bubbles}$ = 0.10) on the left is compared with the high Re case ($\varepsilon_{bubbles}$ = 0.30) on the right. The black line represents the CFD for the entire population; the blue dashed line is the opposite case for comparison. The gray field outlines the variability of CFDs for different horizontal regions in the simulation. The low *Re* case is composed of much more variability; in particular the lowermost layer (red outline) shows smaller amounts of strain accumulation.

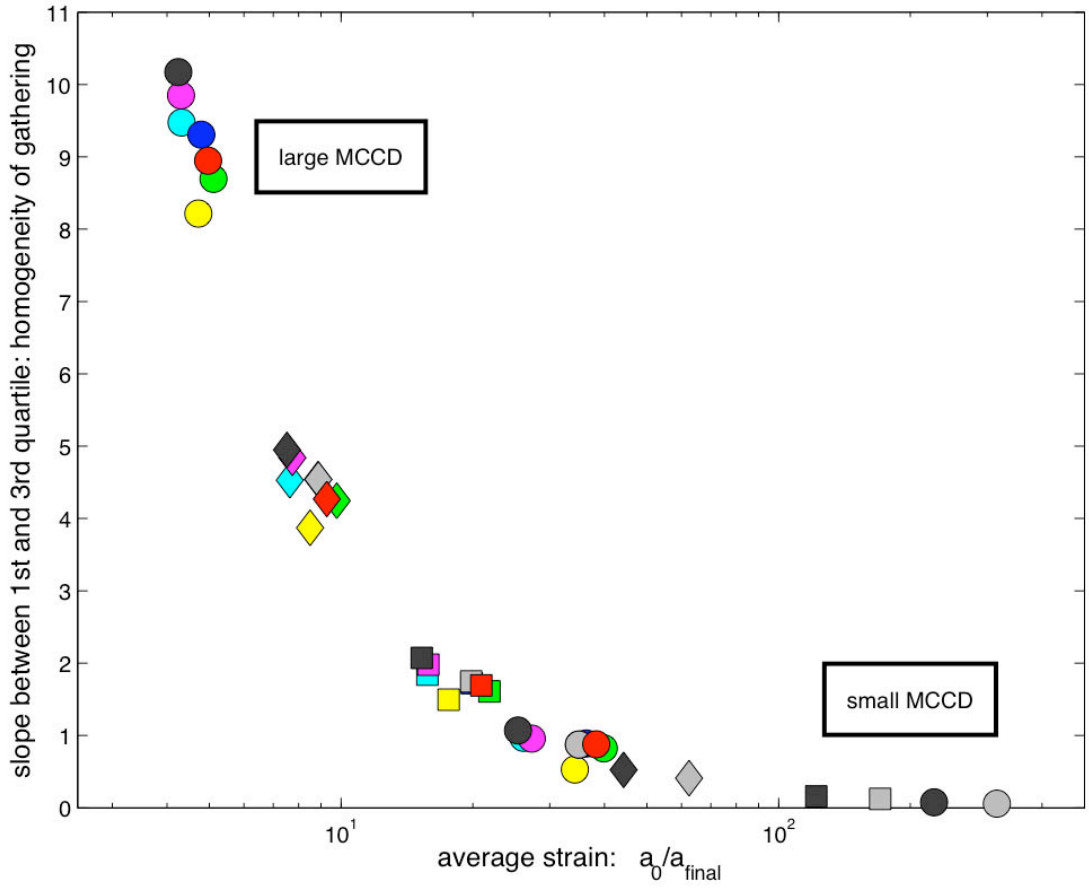

Figure 2.7 All population CFDs are represented with their median and a slope calculated using the first and third quartile. $\varepsilon_{bubbles}$: 0.02 (yellow), 0.05 (cyan), 0.10 (magenta), 0.20 (green), 0.30 (blue), 0.40 (red). MCCD: 10 m (circles), 5 m (diamonds), 2 m (squares), 1 m (circles), 0.5 m (diamonds), 0.2 m (squares), 0.1 m (circles). Grey symbols are runs with 20,000 particles, where $\varepsilon_{bubbles}$: 0.10 (dark), 0.30 (light). All other CFDs were calculated for 5000 'smart' particles.

2.5 Discussion

2.5.1 Length Scale of Crystal Gathering in Thin Section

The results from the coupled multiphase-particle tracking simulations show that in a single overturn, most crystals that end up in the same small-scale volume are gathered over tens of meters during one overturn. A significant proportion (~20%) of the crystal cargo may have originated from a distance of 100 m or more from each other. Therefore, a single mixing event is capable of juxtaposing crystals

that originated from spatially distinct regions of the chamber, and with completely different histories (compositional zoning, textures, etc.). Thus, heterogeneous populations with chemical variations and kinked crystal size distributions are common [*Morgan et al.*, 2007].

Our methodology is also applicable to a closed-system, in which heat transfer occurs through the walls. *Singer et al.* [1995] employed the dynamic template of quasi-steady overturn as proposed by *Marsh* [1988, 1989]. Our simulations with the lowest bubble-volume fraction might be an appropriate proxy for this case. For $\varepsilon_{bubbles}$ of 0.05 and 0.10, density differences between the two layers are 3.7% and 7.5%, respectively. The dynamic viscosity varies by 0.7% and 3.2%, respectively (Table 2.2). These are reasonable for the sluggish closed-system processes. Even at these low bubble volume fractions, chaotic mixing dominates and we expect the crystal cargo to be heterogeneous. This chaotic behavior limits the extent of repeated zoning patterns in crystals experiencing cyclical magma overturn in a closed system.

2.5.2 Damköhler Numbers for Crystal Growth and Dissolution

Crystals that are transferred to a different chemical environment by convective motion may react to those changes in chemical potential by dissolution or crystallization. However, the record of this transport may be incompletely preserved in the crystals. How much of this data is recorded is a competition between the reaction and transport timescales. For example, at the fastest transport rates, during the ascent in a conduit, it has been shown that the crystal recorder is too slow to record the transient changes [*Kerr*, 1995]. To understand fully the interplay between crystal response time and transport time requires a kinetic model for crystal nucleation, crystal growth and/or resorption. Our knowledge of nucleation, crystallization and resorption under magmatic conditions is limited [*Hersum and Marsh*, 2007]. Several authors [*Dowty*, 1980; *Cashman*, 1990; *Larsen*, 2005] have compiled existing experimental data on nucleation and growth kinetics and data on

crystal growth inferred from crystal zoning studies. These compilations include results from simple binary systems, e.g., growth kinetics in the system of albite-anorthite solid solution, as well as from multi-component systems resembling closer natural magma compositions. *Larsen* [2005] reports a range for crystal growth rates G from 10^{-1} mm s^{-1} to 10^{-11} mm s^{-1}. The largest growth rates have only been observed in very simplified systems. Therefore, we focus furthermore on the growth rates G for multi-component compositions that range from 10^{-6} mm s^{-1} to 10^{-11} mm s^{-1}.

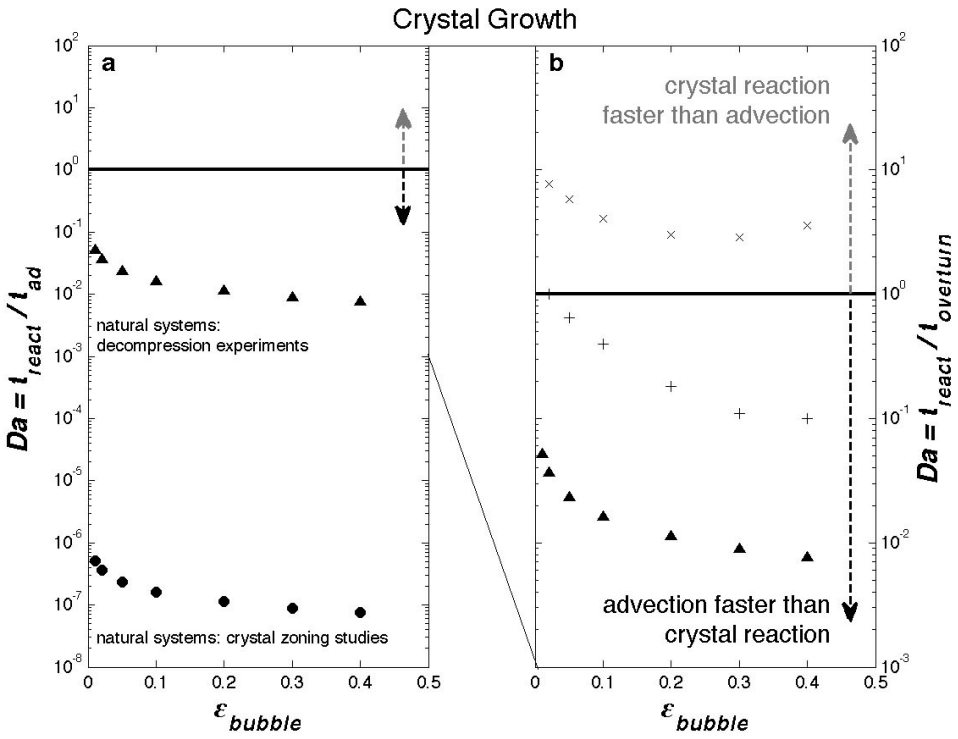

Figure 2.8 Damköhler number *Da* for crystal growth plotted vs. bubble volume fraction ($\varepsilon_{bubbles}$). For $Da << 1$ advection is faster than crystal growth. (a) *Da* numbers using the theoretical advection time scale after *Linden and Redondo* [1991] compared to two different growth rates G of 10^{-6} mm s^{-1}(Δ), and 10^{-11} mm s^{-1}(O), respectively. (b) *Da* numbers for the numerically derived advection timescale and reaction timescale from decompression experiments. The advection timescale presented in Table 2.2 (X) combines the initiation of the instability, the overturn, and the damping after overturn until average crystal movement has decrease below 0.08 mm s^{-1}. Considering only the transient overturn (+) reduces the *Da* numbers by an order of magnitude. (Δ) as in Figure 2.8a.

Recent results from decompression experiments on the 1991 Pinatubo dacite [*Hammer and Rutherford*, 2002], on a synthetic composition of the 1996 andesitic Montserrat dome [*Couch et al.*, 2003], and on a synthetic haplogranitic composition [*Couch*, 2003] suggest maximum plagioclase growth rates G on the order of 10^{-6} mm s^{-1}. Crystallization decompression-induced degassing is viewed as one of the fastest crystallization mechanisms. Therefore, these growth rates constitute a lower time limit on noticeable plagioclase growth.

The competition between the reaction timescale t_{react}, i.e., crystallization or dissolution, and the transport timescale t_{ad}, i.e., advection, can be compared by defining a Damköhler number Da,

$$Da = \frac{t_{ad}}{t_{react}}, \tag{2.19a}$$

$$Da = \frac{t_{overturn}}{t_{react}}, \tag{2.19b}$$

$$t_{ad} = \left(\frac{H}{gA}\right)^{1/2}, \tag{2.20}$$

$t_{overturn}$ = timescale obtained from multiphase simulations, (2.21)

$$t_{react} = \frac{d}{G}, \tag{2.22}$$

where t_{ad} is the theoretically derived advection timescale by *Linden and Redondo* [1991] and $t_{overturn}$ is the numerically derived advection time scale obtained from the overall duration of each of our simulations (Table 2.2). This timescale $t_{overturn}$ is the total time of instability growth, overturn and damping after the overturn has ceased. The theoretical advection time scale t_{ad} is a measure for the time it takes for the mixing region to extend throughout the fluid. The reaction timescale t_{react} is

estimated by the growth rate G and a resolvable length scale d of crystal overgrowth (d = 1μm) using an electron microprobe [*Ginibre et al.*, 2002a]. For $Da << 1$ the advective transport is much faster than significant crystal growth.

On the basis of the growth rate G in natural systems and the theoretically derived advection timescale tad we calculate $Da << 1$ (Figure 2.8a). The Da number ranges over one order of magnitude for a given crystal growth rate. The lowest estimates of crystal growth rates ($G = 10^{-11}$ mm s^{-1}) that are inferred from crystal zoning studies result in $Da < 10^{-6}$. Decompression and degassing-induced crystallization as assumed for our multiphase simulations shows $Da < 10^{-1}$. Even for the most sluggish case with the largest advection timescale and the fastest growth rates we find the $t_{ad} << t_{react}$ ($Da \approx 0.04$).

Considering $t_{overturn}$ as advection timescale causes Da numbers to be significantly larger (Figure 2.8b). Let us only focus on the case for crystal growth rates induced from decompression experiments ($G = 10^{-6}$ mm s^{-1}), since these conditions are most reflective of our multiphase simulations for gas-driven overturn. If we choose $t_{overturn}$ as defined earlier, the time until average crystal motions has slowed down to 0.08 mm s^{-1}, we consistently observe $Da > 1$. However, this advection timescale is a maximum timescale by including the initial growth of the instability, the transient overturn, and the final waning of the mixing process. A better measure for the advection time scale is the transient overturn itself, since this is the time when extreme variations in chemical potential exist. The duration of the transient stage of the overturn is on the order of 10^2 to 10^3 s (Figure 2.2). This advection timescale is still more than one order of magnitude larger than t_{ad} obtained from linear theory. The resulting Da number ranges from 10^{-1} to 1 for large and small $\varepsilon_{bubbles}$, respectively. Thus, under this assumption the advection and the reaction time scale are of similar order for small density differences (i.e. $A \approx 0$) between the bubble-free and the bubble-bearing magma.

In summary, we find that for magma overturn due to large density differences (i.e. $\varepsilon_{bubbles} \geq 0.2$) existing crystals record only their initial and final disequilibrium environment. They may not record the short-lived extremes in intensive variables that drive mixing or overturn. Once the transient overturn has ceased, bubbles and crystal may settle to their neutral buoyancy level. During the settling crystals may record the change in chemical potential associated with the observed stratification. For a natural system, in which bubble-rich andesite recharge mixes with a more evolved magma, crystals would potentially be normally zoned.

For very sluggish system with small density differences crystal growth and magma mixing are of similar order of magnitude. In this case crystal growth is not negligible during the overturning process. In contrast to crystal growth, crystal dissolution may, even for large $\varepsilon_{bubbles}$, more faithfully keep pace during the transient part of the gas-driven overturn (Figure 2.9). Dissolution rates G_{Dis} for natural melt compositions based on experimental data [*Donaldson*, 1985; *Zhang et al.*, 1989] and dissolution models [*Liang*, 2000, 2003] are on the order of 10^{-4} to 10^{-6} mm s^{-1}. Thus, analogous to the discussion about crystal growth during gas-driven overturn we calculate $Da \geq 1$.

The effects on the *Da* number caused by processes that may slow down the dissolution process can only be discussed qualitatively. Parameters that influence the dissolution rate are the dissolution mechanism, melt viscosity and melt composition [*Shaw*, 2006]. In particular, the dissolution mechanism, which is a competition between interface-controlled and diffusion-controlled dissolution, has strong effects on the dissolution kinetics. While interface-controlled growth may complicate the dissolution kinetics [*Shaw*, 2006], it has been reported that for highly viscous melts dissolution is generally diffusion-controlled [*Jackson and Mills*, 1997]. Therefore, we will focus our discussion on diffusion-controlled dissolution. A complete

discussion on dissolution rates and dissolution mechanisms can be found in the review by *Edwards and Russell* [1996] as well as in the paper by *Shaw* [2006].

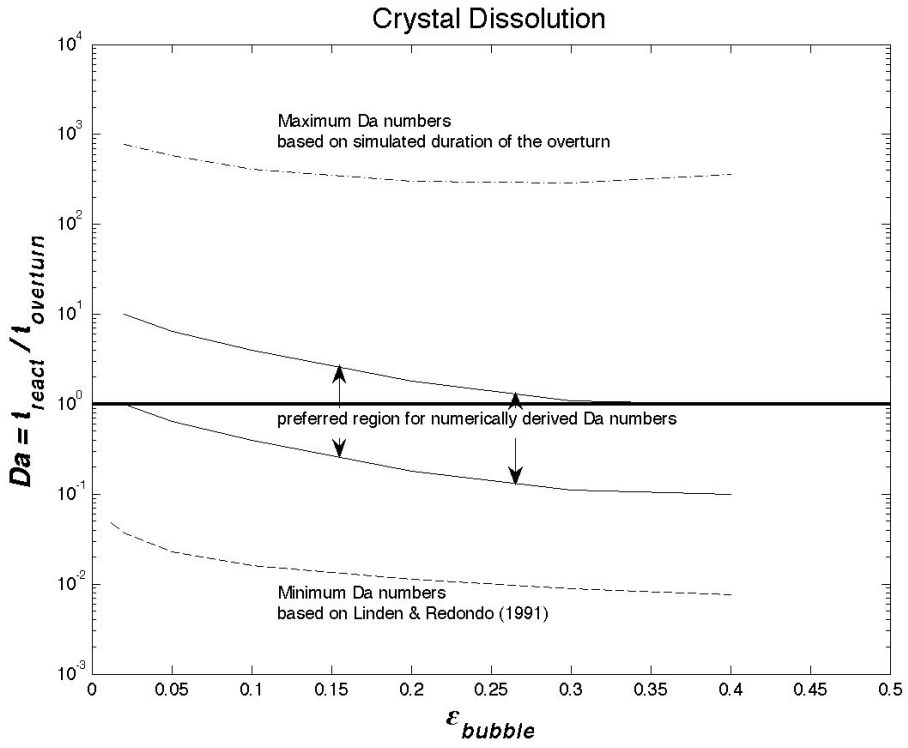

Figure 2.9 Damköhler number *Da* for crystal dissolution plotted versus bubble volume fraction ($\varepsilon_{bubbles}$). For $Da > 1$, crystal dissolution is taking place during magmatic overturn. The preferred region of *Da* numbers (solid lines) is ≥ 1 for all $\varepsilon_{bubbles}$, indicating a tight competition between dissolution and advection. It is calculated for advection timescale obtained from the transient overturn stage and dissolution rates G_{Dis} from 10^{-5} mm s^{-1} to 10^{-6} mm s^{-1}. Minimum estimates (dashed lines) for *Da* are based on slow dissolution rates (10^{-6} mm s^{-1}) and as well as t_{ad}. Maximum estimates (dashed-dotted lines) for *Da* are calculated for the fastest dissolution (10^{-4} mm s^{-1}) and the overturn time scale from Table 2.2.

Diffusion-controlled dissolution results in a time-dependent dissolution rate [*Zhang et al.*, 1989] and the progress of a dissolution front d_{dis} can be estimated by [*Liang*, 2000, 2003]:

$$d_{dis} = 2\alpha\left(D_1 t\right)^{1/2}, \tag{2.23}$$

where α and D_1 are the dimensionless diffusion parameter and the diffusion coefficient of component 1 in the liquid, respectively. Dissolution calculations are generally performed for α = -0.4 [*Liang*, 2003] and D_1 between 10^{-11} m^2 s^{-1} and 10^{-14} m^2 s^{-1} [D_1 taken from *Watson*, 1994].

A more detailed examination of the diffusion processes [*Zhang et al.*, 1989, *Liang*, 2003] shows that the dominating dissolution rates are close to the lower limit ($G_{Dis} = 10^{-6}$ mm s^{-1}) of the reported range. The dissolution rate limiting parameters are the diffusion coefficient for the components of the crystal and the nonlinear behavior of Equation 23 ($d_{dis} \sim t^{1/2}$). Following *Liang* [2003] the dissolution process is limited by the slowest diffusing component in a multi-component system, thus small diffusion coefficients ($D_1 = 10^{-14}$ m^2 s^{-1}) have the largest impact on the dissolution kinetics. Additionally, considering the dissolution rate over time we observe the highest dissolution rates only in the first few seconds of dissolution. This short time interval is insufficient to significantly dissolve the crystal. Within 10^2 s the overall dissolution rate falls off by a factor of $10^{1.5}$. Thus, the effective dissolution rate for processes on the order of 10^2 s to 10^3 s, which we investigate in our multiphase simulations, is probably on the order of 10^{-5} mm s^{-1} to 10^{-6} mm s^{-1} and $Da \approx 1$ (Figure 2.9).

These results for the *Da* number indicate that crystal resorption will be limited to the crystal edges; anhedral to subhedral crystal textures will dominate the

crystal cargo. These results are in good agreement with results on convective crystal dissolution by *Kerr* [1995] for convective motion in a magmatic dyke. Complete dissolution of crystals is unlikely. Instead, partial dissolution will occur because of the similar order of magnitude for advection and dissolution.

2.5.3 Crystallization and Dissolution During Temperature-Driven Convection

While gas-driven convection is characterized by a tight competition between advection and crystal reaction rates, advection timescales for temperature-driven convection are much slower. This causes crystal reaction rates to be orders of magnitude faster than advection rates. Our model for gas-driven convection assumes an instantaneous density inversion, which causes fast convection even for small $\varepsilon_{bubbles}$ and *Da* close to 1. Temperature-driven convection typically assumes a Rayleigh-Bénard convection cell [*Marsh*, 1988]. There may be heating from below due to underplating magma, but generally the magma system is governed by the conductive cooling through the roof and the sidewalls.

Adopting the dynamic template of *Marsh* [1988] for temperature-driven convection results in large *Da* numbers between 10^1 and 10^6. An advective timescale t_{ad} of several years can be estimated for this dynamic template using Equation 2.18 of *Marsh* [1988]:

$$U = \frac{K}{H} Nu^2, \tag{2.24}$$

$$t_{ad} = \frac{H}{U}, \tag{2.25}$$

where U, K, and Nu are the velocity, thermal diffusivity and the Nusselt number, respectively (For common rock material: $K = 10^{-6}$ m^2 s^{-1}). The Nusselt number relates the total heat transfer Q_{total} through the roof and the sidewalls to the heat transfer for conduction Q_{cond} alone:

$$Nu = \frac{Q_{total}}{Q_{cond}}. \tag{2.26}$$

Following *Marsh* [1988] we assume a maximum $Nu = 2$, since the roof and sidewalls may be insulated by a solidification front that grows inward toward the center of the magma chamber. The reaction timescale is the same as in Equation 2.22 and varies for the range of observed growth rates in natural systems. As previously noted the fastest growth rates are typically observed in decompression experiments [*Hammer and Rutherford*, 2002; *Couch et al*., 2003].

Thus, the sluggish overturn due to temperature gradients is accompanied by slow growth rates between 10^{-8} mm s^{-1} and 10^{-11} mm s^{-1} [*Singer et al.*, 1995; *Davidson and Tepley*, 1997]. The slow removal of heat through the walls may reduce the effective undercooling that drives crystallization and subsequently crystallization itself is slowed down as well. Nonetheless, even for these slow growth rates we observe $Da >> 1$. Thus, crystallization kinetics is fast enough to record various chemical conditions that may persist in the sluggish behaving magma chamber.

While there is sufficient time for the crystal to record changes in chemical potential during purely temperature-related effects, there is also potentially enough time for complete crystal dissolution. Following the diffusion-controlled dissolution model of Equation 2.23 we estimate a complete dissolution within days for millimeter-sized crystals. This would suggest that temperature-driven convection

could completely erase the crystal record. However, to answer ultimately the question if dissolution is complete under such conditions we have to consider the simultaneous change in chemical potential. Extensive phenocryst dissolution will drive the system quickly to smaller degrees of undersaturation. Therefore, we expect that not the complete crystal is dissolved. Instead, small anhedral crystals may survive and record a strong dissolution surface between the remaining core and a significantly different newly growing mantle or rim as seen typically in arc magmas [e.g., *Ruprecht and Wörner*, 2007].

Eruption triggering recharge events may subsequently gather chemically distinct crystal populations and without extensive modification of the crystal cargo transport this crystal assemblage to the surface [*Spera*, 1984; *Trial et al.*, 1992].

2.6 Conclusion

Crystal-chemical and textural data from igneous systems reveal complex open-system behavior and internal circulation [e.g., *Singer et al.*, 1995; *Zellmer et al.*, 2003; *Ginibre et al.*, 2004]. Our results from a simple overturn model with viscosities applicable to intermediate and silicic systems [*Scaillet et al.*, 1998] show that this heterogeneity can even arise from a single overturning event. Multiple overturn events can lead to repeated gathering and dispersal of crystals and can obscure the apparent signature of crystals spatially residing together in a thin section (2.7 cm). Crystal-isotope-stratigraphy [*Davidson and Tepley*, 1997; *Davidson et al.*, 2007] has shown that arc magmas frequently gather crystals from isotopically very distinct environments. Gas-driven overturn is a very efficient process to facilitate the juxtaposition of crystal with distinct isotopic signature. On the basis of our calculations such a population of crystals is gathered over meters to tens of meters within a single overturn. Therefore, the common path of a pair of crystals is probably very limited as has also been observed by *Wallace and Bergantz* [2005]. Systems with small density variations between the two mixing magmas have the largest

potential for significant common path lengths between crystal-crystal pairs. However, even for those small *Re* cases we find this behavior only for a minor proportions of all crystal pairs.

The common result from our multiphase mixing simulations (Figures 2.1 and 2.2) is not a homogeneous, but rather a stratified magma body with a maximum in $\varepsilon_{bubbles}$ on top and a continuous decrease in $\varepsilon_{bubbles}$ toward the bottom. Gradients are inevitable during a single overturn and mixing of the two instantaneously superimposed magmas is inefficient. This is due to the chaotic, not turbulent, flow regime for compositionally intermediate magmas. These heterogeneous environments of temperature and chemical gradients can persist over timescales much longer than the gathering timescale for gas-driven overturn, which is on the order of minutes to hours. These results are consistent with other fluid dynamic studies that predict final stratification in case of an instantaneous R-T instability [*Linden and Redondo*, 1991; *Jellinek et al.*, 1999]. We do not observe homogeneity neither on the bulk nor on the crystal scale. Crystals follow closely the fluid flow during gas-driven overturn. Therefore, the stratification in bubble-volume fraction after the overturn reflects also a stratification of crystal-origin. Crystals initially dispersed in the bubble-bearing magma are mixed into the bubble-free magma with similar proportions as is the bubble-bearing magma. A model that includes bubble coalescence may produce larger extents of differential movement between melt, crystals and bubbles of the recharging magma. However, the nonlinear processes of bubble coalescence, additional gas exsolution and secondary nucleation probably further increase the complex assembly of different crystal populations during the overturn.

Considering the competition of crystal reaction rates with the advection rates during the overturn, we find that gas-driven advection is typically faster than crystal growth but of similar order in case of crystal dissolution. Thus, the crystals will not

be able to record the actual mixing process with all its extremes in chemical potential. *Da* numbers less than 1 for crystal growth suggest that they will record only the stages prior-to, and following, the mixing event. In cases where dissolution is the response to the changes in chemical potential older stages of crystal growth may be erased. These conditions may vary from crystal to crystal and eventually may be sampled on the length scale of a thin section. Basically, any mixing will create a complex crystal population mixture even though the cause may be a simple low Re overturn. We investigated the most simplified system possible. Assuming mixing of chemically and/ or physically different magma batches would constitute a much more complex initial condition. Such complex starting scenarios must inheritably increase even further complexity observed within the crystal population.

For overturning processes that invoke longer timescales such as temperature-driven overturn the crystal cargo may record even more complex information, since crystallization rates, and therefore response through crystal growth to the changing environment may be faster than physical mixing rates [*Singer et al.*, 1995]. The resulting zonation record is likely to be more comprehensive and may include transient physical mixing processes.

- Chapter 3 -

Volcán Quizapu – Revisited: The eruptions of 1846/47 and 1932

3.1 Introduction

Volcán Quizapu is the location of two of the largest historic eruptions in the entire Andean cordillera [*Domeyko and Tocornal*, 1849; *Hildreth and Drake*, 1992]. In the winter of 1846/47 a fissure eruption produced silicic lavas that covered about 50 km^2 (Figure 3.1). In 1932 a second eruption, plinian in nature, dispersed ash and lapilli across large parts of the South American continent. The geology of the area was first described by *Domeyko and Tocornal* [1849], when the area was visited after the effusive eruption in 1846/47. More recently, the petrologic and volcanologic work of *Hildreth and Drake* [1992] on the two eruptions led to the recognition of Volcán Quizapu as an example for the effusive-explosive transition in silicic magmatic systems.

Excellent preservation and exposure at Volcán Quizapu provide excellent conditions to compare and contrast the 1846/47 and 1932 eruptions, which have contrasting eruption styles. The dry climate in these latitudes (35 –36 ˚S) of the Andes preserved the deposits formed during the plinian eruption in 1932, while still providing access to most of the eruptive sequence of 1932 in small drainage systems coming off the surrounding mountains. Simultaneously, the 1932 pumice deposits partially cover the lava flows of the 1846/47 eruption, thus allowing good access to the entire flow field.

Many arc magmatic systems transition between effusive and explosive behavior as well as between mafic and silicic magma compositions [e.g., *Hildreth and Fierstein*, 2000; *Bacon and Lanphere*, 2006]. The transition from effusive to explosive eruption behavior is foremost dependent on magma composition [*Papale et al.*, 1998]. Furthermore, pre-eruptive magma gas content and syn-eruptive degassing are proposed as the additional controls for switching between eruptive styles [*Eichelberger and Westrich*, 1981; *Eichelberger et al.*, 1986; *Jaupart and Allegre*, 1991; *Papale et al.*, 1998]. The diversity in magma compositions is driven by various differentiation processes in the crust, such as (1) fractional crystallization [e.g., *Bowen*, 1928; *Brophy*, 1991; *Bachmann and Bergantz*, 2004], (2) assimilation of supra-crustal material [e.g., *DePaolo*, 1981], and (3) mixing of magmas with distinct compositions [e.g., *Eichelberger*, 1980]. Natural magmatic systems are typically complex and evolve over time through an intricate interplay of the various processes. These two compositionally simple eruptions at Volcán Quizapu present a rare opportunity for a natural example to isolate a single aspect of magma evolution - late-stage magma mixing- from the other magma chamber processes.

In many arc systems magma mixing has been proposed to occur as a solid-liquid disaggregation mechanism [e.g., *Bacon and Metz*, 1984; *Feeley and Dungan*, 1996], while volatile exsolution provides the necessary density reduction [*Eichelberger*, 1980]. The simple system of Volcán Quizapu provides snapshots of the different stages of magma mixing during solid-liquid disaggregation – (1) mingling and (2) complete hybridization. Documenting how the crystal cargo is chemically and physically affected during the evolution of the disaggregation provides further inside for which post-mixing textures are unique to solid-liquid mixing.

At Volcán Quizapu we investigate how late-stage magma mixing can account for the compositionally diverse magmas and how magma mixing may

condition the eruptive behavior of gas-charged potentially explosive silicic magma. Despite the contrasting eruptive behavior, the most evolved magmas from the 1846/47 and 1932 eruptions of Volcán Quizapu match each other closely in terms of whole rock composition, crystal and water content [*Hildreth and Drake*, 1992]. Eruptive behavior may be influenced by mafic recharge [*Sparks*, 1977], evidence of which is present in both eruptions from Volcán Quizapu. While the 1846/47 eruption is characterized by extensive physical mixing as a consequence of mafic-silicic magma interaction, 1932 magmas show little mingling and hybridization. Thus, by comparing and contrasting these two eruptions we can investigate the various ways in which complexity on the crystal and magma scale emerges by simple late-stage magma mixing.

We employ geochemical, petrologic and textural information from the phenocryst phases of the two eruptions to decipher the effects of magmatic recharge and subsequent mixing. In particular, we have identified distinct crystal populations, and their dispersal during open system processes. By documenting the spatial and temporal distribution of phenocryst populations during a simple magma mixing event we can identify which prograde conditions may be recorded and which may be lost as a consequence magma mixing.

3.2 Volcán Quizapu – Geologic Overview

Volcán Quizapu is part of a large cluster of volcanic vents dominated by the stratovolcanoes Descabezado Grande and Cerro Azul, situated in the Southern Andean Volcanic Zone [Figure 3.1; *Hildreth and Drake*, 1992]. Volcán Quizapu itself is a small volcanic cone on the northern flank of Cerro Azul. The eruptive history of Volcán Quizapu constitutes only two historic eruptions, in 1846/47 CE (common era) and in 1932 CE. Prior to the onset of volcanic activity at Volcán Quizapu, silicic magmas were mainly erupted from Descabezado Grande and Cerro Azul. The two eruptions at Quizapu crater are the two largest historic eruptions in the

Chilean Andes, each producing about 5 km^3 of erupted magma. Despite the significant removal of magma no collapse features have been recognized.

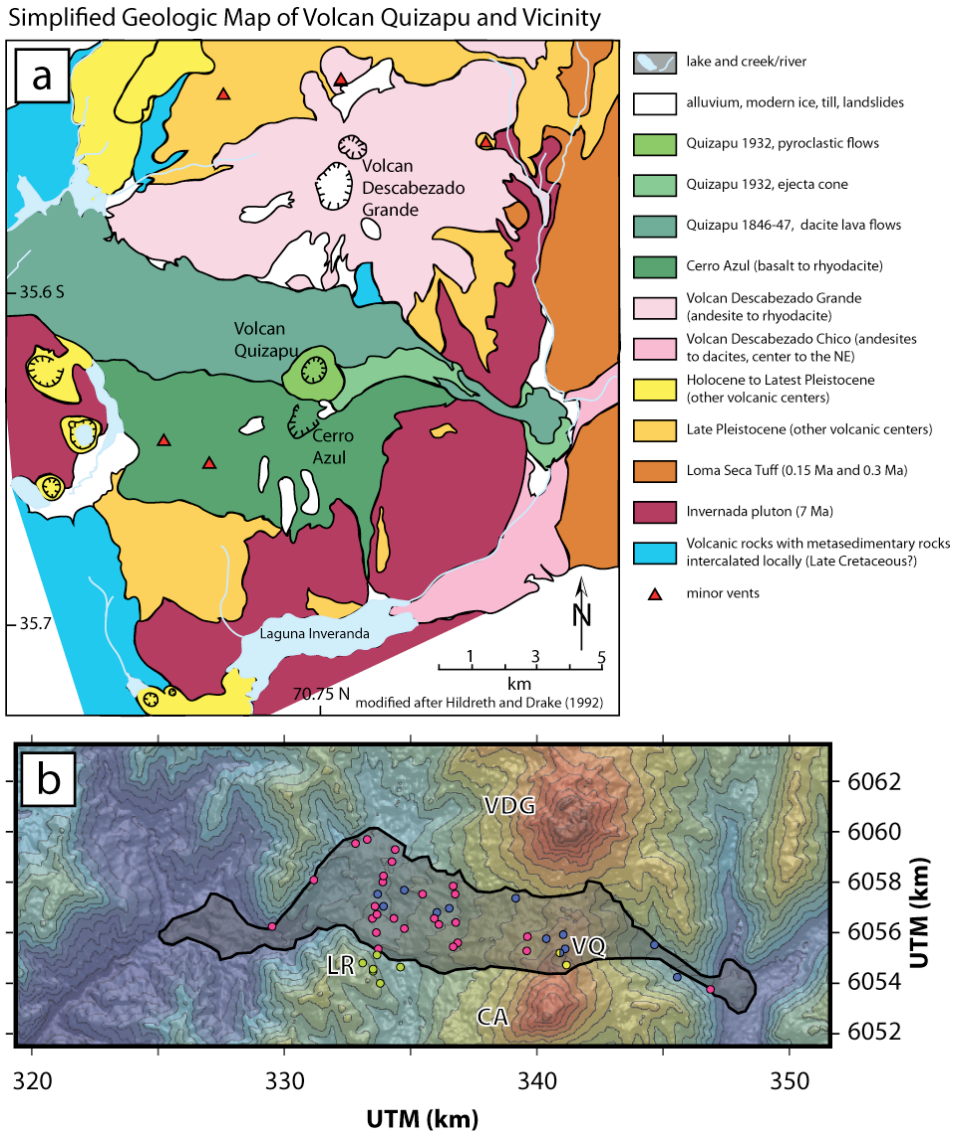

Figure 3.1 Overview of the Geology and Topography of the Area around Volcán Quizapu. a) Simplified geologic map of Quizapu and its vicinity. Note the extensive coverage of the area by cinder cones, maars, and minor vents. b) Shaded relief map with the flow field of the 1846/47 eruption outlined. VQ-: Volcán Quizapu; CA: Cerro Azul; LR: La Resolana; VDG: Volcán Descabezado Grande. The shaded relief map was rendered from ASTER satellite image (https://wist.echo.nasa.gov/api/). Sample locations are displayed (red: eruption of 1846/47; blue: eruption of 1932, green: mafic magmas from peripheral cones and from Quizapu deposits).

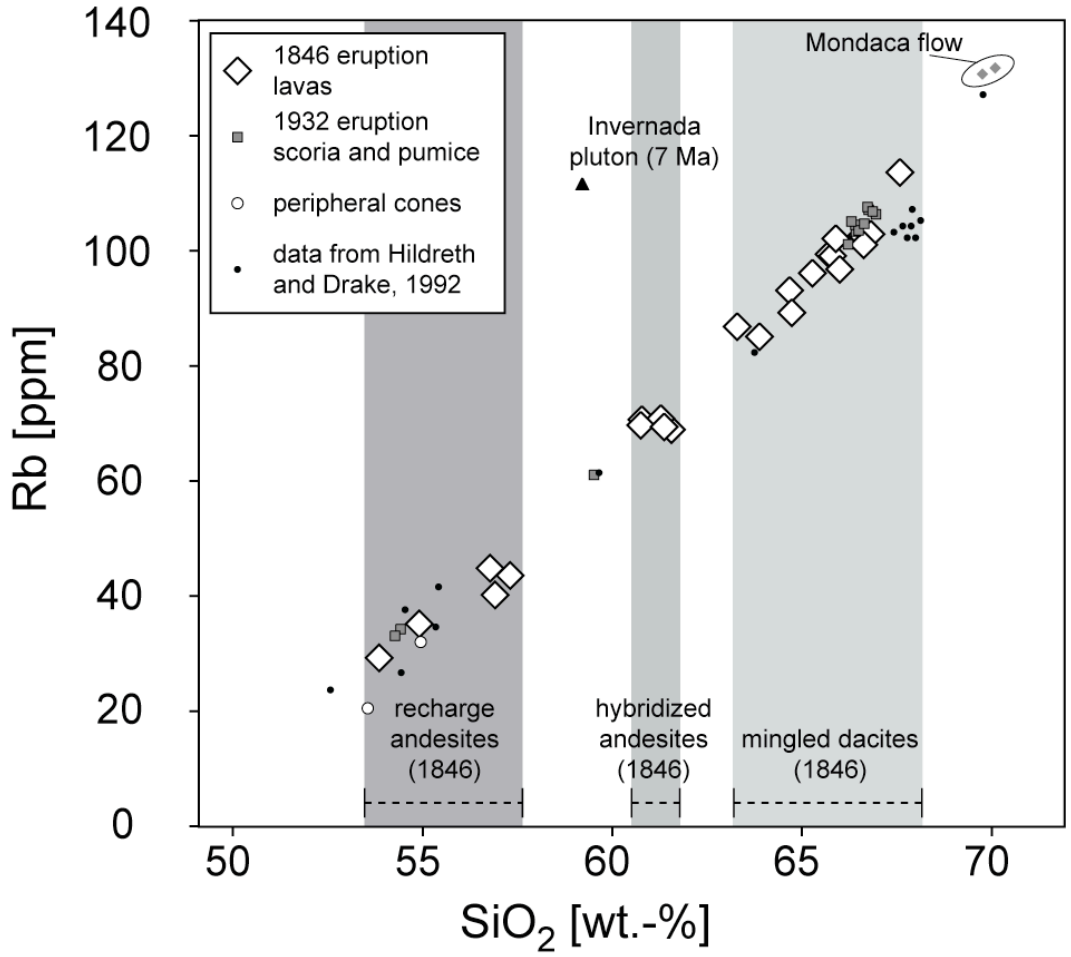

Figure 3.2 Binary Mixing Array in Rb-SiO_2 space for Samples in the Vicinity of Quizapu. Note, the data from Hildreth et al. (1992) are normalized to 100% and therefore plot to higher SiO_2 values. The mixing array between mafic and silicic end-members for regional erupted products from the vicinity of Quizapu suggest limited involvement of the Invernada pluton in the petrogenesis of the volcanics. The Mondaca Flow is another young lava flow in the vicinity of Quizapu. The eruption probably occurred around 1760 CE (pers. comm., J.A. Naranjo).

The recent volcanism in the Quizapu area is bimodal by volume with many mafic cinder cone vents and larger cinder stratocones contrasting with the mainly dacitic character of the volumetrically larger volcanic centers. Towards the East and the North the silicic character of the volcanic cluster continues with the large Calabozos Caldera and the Mondaca lava flow. The Calabozos Caldera erupted more than 1000 km^3 of rhyodacite to dacite magma in at least two caldera-forming

eruptions during the last 300 kyrs [*Hildreth et al.*, 1984; *Grunder and Mahood*, 1988]. The rhyodacitic Mondaca lava flow fills in the Lontué valley just North of Descabezado Grande. Based on historic accounts it erupted in ~1760 CE [pers. comm. J.A. Naranjo]. Small volume, mafic centers are ubiquitous throughout the area in the form of cinder cones, stratocones and maars [*Hildreth and Drake*, 1992].

Hildreth and Drake [1992] presented whole rock data for 31 samples of the two Quizapu eruptions. We sampled and analyzed 40 additional whole rock samples of the Quizapu eruptions, the peripheral cones and the Mondaca Flow (Figure 3.2; Table 3.1). Figure 3.2 shows that basaltic andesite and dacite for samples from the 1846/47 eruption at Quizapu fall along a mixing array in SiO_2 versus Rb compositional space. This binary mixing array is seen for most trace elements with the exception of the most compatible elements Ni and Cr. Lavas of the 1846 eruption can be divided into three groups; (1) andesite recharge magmas present as mafic inclusions with varying SiO_2 content of up to 57 wt.%, (2) hybridized magmas with similar SiO_2 contents of ~ 61 wt.%, and (3) mingled dacites with varying degrees of recharge magma interaction and SiO_2 content between 63 and 68 wt.%. Figure 3.2 also shows that in contrast to the restricted compositional range of mingled dacites (67-68 wt. % SiO_2) reported by *Hildreth and Drake* (1992], the new results and additional unpublished data (W. Hildreth, pers. commun.) show large variations (7 wt.% SiO_2) across the flow field. In contrast to the compositionally zoned effusive 1846 eruption, the plinian 1932 eruption was much more compositionally homogeneous. Most of the volumetrically small contribution of the andesite magmas in the 1932 eruption was erupted as initial and terminal scoria.

Table 3.1 Whole rock major and trace element compositions1

	1846/47 hybridized andesites					1846/47 mingled dacite			
Sample	VQ-06-02	VQ-06-09	VQ-06-10	VQ-06-15	VQ-06-16	VQ-06-04D	VQ-06-06	VQ-06-08D	VQ-06-11
SiO_2	61.37	61.56	60.78	61.28	60.75	64.67	65.89	67.59	65.71
TiO_2	0.71	0.71	0.72	0.71	0.69	0.59	0.56	0.53	0.56
Al_2O_3	16.71	16.71	16.44	16.40	16.35	15.80	15.62	15.17	15.52
FeO*	5.08	5.00	4.93	4.79	4.82	3.61	3.09	3.07	3.19
MnO	0.11	0.11	0.11	0.11	0.11	0.09	0.09	0.08	0.09
MgO	2.52	2.40	2.51	2.39	2.33	1.34	0.95	1.08	0.99
CaO	5.18	5.11	4.69	4.53	4.89	3.15	2.48	2.06	2.50
Na_2O	4.48	4.54	4.56	4.63	4.49	4.95	5.17	5.18	5.10
K_2O	2.30	2.34	2.37	2.44	2.34	2.98	3.19	3.61	3.18
P_2O_5	0.18	0.18	0.18	0.17	0.17	0.15	0.15	0.10	0.15
Total	98.64	98.65	97.28	97.44	96.94	97.34	97.19	98.48	96.99
Ni	31	36	38	53	34	19	12	26	17
Cr	67	69	66	113	64	34	18	45	26
Sc	17	16	14	13	16	11	9	11	9
V	125	123	108	102	115	66	44	34	44
Ba	468	479	487	498	475	576	608	652	605
Rb	70	69	71	71	70	94	103	114	100
Sr	468	461	399	385	442	325	282	185	275
Zr	184	187	194	196	186	238	255	291	252
Y	20	22	22	21	20	24	24	29	24
Nb	5	7	7	8	7	7	8	8	8
Ga	20	19	20	19	20	19	19	18	18
Cu	46	39	27	30	41	19	10	15	12
Zn	68	69	68	69	65	63	61	64	60
Pb	14	14	14	14	13	17	20	20	16
La	18	15	17	22	20	18	22	27	23
Ce	40	41	41	39	40	47	52	58	41
Th	6	5	5	5	5	9	11	11	8
Nd	20	21	22	19	19	23	24	26	20

Table 3.1 continued

1846/47 mingled dacite (continued)

Sample	VQ-06-12	VQ-06-14	VQ-06-22D	VQ-06-24D	VQ-06-26D	VQ-07-35	VQ-07-36	VQ-07-39	VQ-07-44D
SiO_2	66.58	65.80	63.29	65.27	63.88	66.82	66.63	65.99	64.73
TiO_2	0.57	0.56	0.64	0.60	0.64	0.57	0.57	0.60	0.63
Al_2O_3	15.66	15.49	16.00	15.83	16.07	15.73	15.80	15.93	15.96
FeO*	3.14	3.09	3.96	3.59	4.08	3.16	3.23	3.51	3.94
MnO	0.09	0.09	0.10	0.09	0.10	0.09	0.09	0.10	0.10
MgO	0.95	0.95	1.70	1.31	1.70	0.96	0.97	1.12	1.54
CaO	2.54	2.43	3.57	3.08	3.83	2.53	2.63	2.90	3.51
Na_2O	5.17	5.12	4.85	5.00	4.85	5.20	5.16	5.12	4.94
K_2O	3.24	3.20	2.77	3.03	2.78	3.24	3.20	3.07	2.91
P_2O_5	0.15	0.15	0.16	0.15	0.16	0.15	0.15	0.17	0.16
Total	98.10	96.88	97.04	97.96	98.08	98.46	98.41	98.51	98.40
Ni	4	13	29	20	8	5	8	8	7
Cr	12	19	48	33	22	9	18	17	19
Sc	9	8	11	10	11	9	8	8	12
V	44	43	79	62	82	43	46	56	74
Ba	611	613	543	578	545	619	617	599	561
Rb	103	100	87	97	86	104	102	98	90
Sr	278	271	342	316	361	277	294	314	340
Zr	255	253	222	243	222	257	247	239	231
Y	24	24	23	25	24	25	24	24	24
Nb	7	8	7	8	6	7	7	6	6
Ga	18	19	19	19	17	17	18	19	18
Cu	12	9	18	16	28	16	15	14	25
Zn	63	62	64	62	64	64	61	67	66
Pb	15	17	16	17	14	17	16	16	14
La	25	26	21	25	20	23	24	25	24
Ce	52	48	46	54	39	52	56	47	46
Th	12	8	9	10	10	11	10	12	10
Nd	25	24	23	25	21	23	25	23	21

Table 3.1 continued

	1846/47 mafic recharge andesites					1932 dacite			
Sample	VQ-06-04A	VQ-06-22A	VQ-06-24A	VQ-06-26A	VQ-07-44A	VQ-06-17	VQ-06-20	VQ-06-21	VQ-06-23
SiO_2	54.92	53.85	56.78	57.32	56.92	66.30	66.74	66.85	66.64
TiO_2	0.81	1.00	0.79	0.80	0.81	0.53	0.53	0.55	0.54
Al_2O_3	17.53	17.95	17.14	17.30	17.29	15.46	15.51	15.64	15.60
FeO*	6.78	7.61	6.39	6.27	6.53	2.94	2.88	3.04	2.96
MnO	0.13	0.13	0.13	0.12	0.12	0.09	0.09	0.09	0.09
MgO	4.08	4.76	3.56	3.60	3.75	0.87	0.85	0.93	0.88
CaO	7.85	7.95	7.05	7.21	7.37	2.30	2.28	2.40	2.34
Na_2O	3.77	3.81	3.98	3.97	3.89	5.16	5.15	5.14	5.19
K_2O	1.38	1.19	1.65	1.68	1.58	3.25	3.30	3.29	3.26
P_2O_5	0.18	0.21	0.19	0.19	0.19	0.14	0.14	0.14	0.14
Total	97.42	98.47	97.66	98.46	98.45	97.04	97.45	98.07	97.64
Ni	23	48	21	13	15	13	10	10	8
Cr	56	71	45	42	42	13	10	12	6
Sc	25	22	22	22	23	8	8	9	7
V	201	205	183	174	181	37	37	39	36
Ba	318	315	358	359	348	612	618	612	621
Rb	36	30	45	44	41	106	108	108	105
Sr	654	573	603	591	606	269	265	274	272
Zr	106	114	126	128	121	254	256	252	255
Y	17	18	19	18	19	25	24	24	24
Nb	3	5	5	4	3	7	8	8	7
Ga	20	19	20	18	18	18	20	17	19
Cu	49	48	62	67	52	7	11	15	12
Zn	77	78	72	71	76	60	59	61	61
Pb	9	9	12	8	9	19	19	19	20
La	13	12	15	17	17	24	24	25	24
Ce	31	29	29	37	31	48	52	52	49
Th	4	3	4	4	5	12	11	11	12
Nd	18	15	16	18	18	23	24	25	24

Table 3.1 continued

	1932 dacite (continued)						1932 andesites and mingled pumice		
Sample	VQ-06-31	VQ-07-37A	VQ-07-37C	VQ-07-37D	VQ-07-40	VQ-07-41	VQ-06-18	VQ-07-37B	VQ-07-42
SiO_2	66.22	66.50	66.76	66.41	66.94	66.42	54.27	59.52	54.42
TiO_2	0.57	0.54	0.53	0.54	0.52	0.55	0.97	0.79	0.97
Al_2O_3	15.60	15.47	15.38	15.50	15.45	15.71	17.91	16.94	17.91
FeO*	3.14	2.97	2.90	2.94	2.87	3.09	7.21	5.54	7.14
MnO	0.09	0.09	0.09	0.09	0.08	0.09	0.13	0.11	0.13
MgO	0.91	0.87	0.84	0.86	0.81	0.93	4.77	2.99	4.72
CaO	2.47	2.38	2.28	2.36	2.27	2.53	8.03	5.53	8.02
Na_2O	5.13	5.13	5.15	5.15	5.15	5.15	3.75	4.41	3.77
K_2O	3.21	3.27	3.33	3.28	3.34	3.22	1.29	2.11	1.33
P_2O_5	0.15	0.14	0.14	0.14	0.13	0.14	0.21	0.19	0.21
Total	97.47	97.36	97.37	97.26	97.58	97.83	98.53	98.12	98.61
Ni	5	5	7	4	5	5	67	21	38
Cr	11	11	15	8	10	12	110	36	63
Sc	8	8	7	7	7	8	23	16	24
V	41	40	37	36	36	43	201	131	194
Ba	616	617	624	620	617	609	322	455	326
Rb	102	104	108	105	107	104	34	62	35
Sr	278	265	256	266	258	283	587	445	577
Zr	252	256	258	255	257	247	117	173	117
Y	25	25	24	24	26	25	17	21	18
Nb	6	7	6	6	7	6	6	5	4
Ga	18	18	17	18	16	17	19	19	18
Cu	9	12	20	12	12	9	59	40	82
Zn	62	61	60	60	61	62	75	73	74
Pb	17	17	18	17	18	17	9	12	7
La	22	24	25	24	26	22	15	19	13
Ce	50	52	57	50	47	49	29	40	33
Th	12	12	13	12	12	12	3	8	4
Nd	25	23	26	23	23	25	17	21	19

Table 3.1 continued

	Peripheral cones		**Mondaca Lava Flow**		**Invernada pluton**
Sample	HOR-06-01	RES-06-01	MO-07-01	MO-07-02	TI-06-01
SiO_2	53.55	54.94	69.75	70.10	59.21
TiO_2	0.81	0.89	0.37	0.38	0.92
Al_2O_3	17.42	17.38	14.53	14.52	16.60
FeO*	7.48	7.13	2.06	2.08	5.97
MnO	0.14	0.13	0.06	0.06	0.10
MgO	5.55	5.10	0.44	0.46	3.04
CaO	9.46	7.85	1.31	1.36	5.31
Na_2O	3.30	3.84	4.99	5.01	3.89
K_2O	0.98	1.37	3.97	3.98	2.90
P_2O_5	0.17	0.21	0.04	0.07	0.22
Total	98.86	98.85	97.52	98.02	98.17
Ni	32	43	4	4	25
Cr	109	84	9	9	41
Sc	31	24	6	6	16
V	241	198	17	17	137
Ba	251	339	648	644	525
Rb	21	32	132	133	112
Sr	668	660	143	144	401
Zr	69	109	268	274	430
Y	15	17	25	26	26
Nb	2	5	8	8	8
Ga	18	18	17	18	16
Cu	98	73	7	9	31
Zn	73	75	51	50	64
Pb	7	8	21	20	12
La	8	16	24	21	26
Ce	22	32	48	54	47
Th	2	4	16	14	14
Nd	12	16	21	24	25

[1] analyses performed at Washington State University

The mixing array in Figure 3.2 also includes other regional volcanic rocks from the peripheral mafic cones (Los Hornitos and La Resolana), the Mondaca flow, and the plinian eruption of 1932 CE at Quizapu. A single sample of the local 7 Ma old La Invernada pluton that is extensively exposed at the base of Cerro Azul is compositionally very different from the mixing array, and its high Rb concentration suggest that it has only minimal contributions in the shallow crust to the generation of the recent volcanic rocks in the Quizapu area.

In summary, Volcán Quizapu is an ideal location to study late-stage magma mixing processes because of its two similar erupted magmas and yet distinct eruptive styles. In contrast to many other arc systems the eruption ages are known and the two distinct eruptions are separated by an extended period of quiescence [*Hildreth and Drake*, 1992, and references therein] ensuring independent triggering mechanisms. In contrast, other systems often lack well-defined age constraints (year of eruption) of two sequential and contrasting eruptions or are characterized of long continuous sequences of changing eruptive styles [e.g., Pinatubo: *Pallister et al.*, 1992].

3.3 Analytical Methods

Whole rock analyses were performed at the GeoAnalytical Laboratory at Washington State University following the procedure of *Johnson et al.* [1999]. Mingled samples were carefully crushed to 1 cm, and andesitic inclusions (> 5 mm) in the dacite end-member were removed prior XRF whole rock compositions of the dacite end-member. The andesite end member composition was estimated by analyzing separates of andesite inclusions.

Quantitative mineral analyses as well as image acquisitions of textural and compositional maps were performed at the University of Washington using a JEOL 733 4-wavelength dispersive spectrometer microprobe. Quantitative analyses were performed at 15 kV and 10 to 15 nA with a focused (Fe-Ti oxides, pyroxenes,

olivines) or defocused beam (amphibole; 3 μm; plagioclase: 5 μm), respectively. Counting times for most phases and elements were 40 s on peak and 20 s on the background. Sodium mobility was not observed when Na was measured first. Minor elements in plagioclase required longer counting times, such as Sr (40-120 s), Ba (40-200 s), Fe (90-150 s), Mg (50-300 s). Counting times were shorter for general mineral characterization and longer for higher count rates in mineral traverses. Rim analyses with apparent high Fe concentration probably reflect secondary fluorescence [*Longhi et al.*, 1976; *Sugawara*, 2001] and are not used in this study. Semi-quantitative maps of selected thin sections were obtained at 15 kV and 15 to 40 nA. Long counting times (0.5-2 ms on each pixel) at high spatial resolution (4-10 μm/pixel) provide the means to distinguish between different phases as well as between sodic and calcic plagioclase as a consequence of varying mean atomic number.

LA-ICP-MS analyses on selected plagioclase crystals were conducted at Oregon State University using a NewWave DUV on 193 nm ArF Eximer Laser. Ablation was carried out in a He atmosphere and ablated material was analyzed using a VG PQ ExCell quadrupole ICP-MS. Laser spots for plagioclase crystals were either 50 or 80 μm. Spot analyses were conducted on the same locations as preceding microprobe analyses. Calcium measured by electron microprobe was used as internal standard. The analytical conditions and procedures are further described in detail in *Kent et al.* [2004, 2007].

Crystal size distributions (CSD) were obtained on 13 thin sections. Crystal size data was evaluated with the CSD software provided by *Higgins* [2000] and crystal aspect ratios were approximated using the method described in *Morgan and Jerram* [2006].

3.4 Compositional and Textural Characteristics of the Quizapu Magmas

Based on the crystal-chemical and textural context three main types of magmatic crystals can be commonly distinguished [e.g., *Bacon and Lowenstern*, 2005; *Charlier et al.*, 2005]: (1) phenocrysts *sensu stricto* are large crystals that are co-genetic with the melt that they are erupting with, (2) antecrysts (term introduced by Wes Hildreth at the "Longevity and Dynamics of Rhyolitic Magma Systems" Penrose Conference, 2001) grew in a similar liquid as they are residing in at the time of eruption and therefore are crystals that can be recycled in the magma chamber, and (3) xenocrysts are truly foreign to the melt and may originate from assimilated wall-rocks. Phenocrysts *sensu lato* are all crystals that reside in the magma and exceed tens to hundreds of μm in size. In the following we use the terminology *sensu lato* unless otherwise noted.

Plagioclase

Plagioclase is the volumetrically dominant phenocryst phase in the Quizapu magmas. Most samples have a phenocryst plagioclase mode between 10 vol.% and 15 vol.%. Only VQ-08D, a volumetrically minor flow lobe in the interior of the flow field, is much more crystal poor with a plagioclase mode of 3.3 vol.% (Table 3.2). Hybrid andesites consistently contain ~14 vol.% of plagioclase.

Plagioclase phenocrysts are divided into six plagioclase types based on textures and chemical composition (Figure 3.3a-p, Table 3.3). Only three of these types are volumetrically significant (types I, III, and IV) in magmas of Quizapu. Type I is the major phenocryst phase in the dacite magmas with low An content (An_{25}-An_{40}). Anhedral to subhedral varieties of type I are predominant in lavas from 1846/47, while euhedral type I phenocrysts are characteristic of the 1932 dacite. Type I phenocrysts (Figure 3.3a-d; Type Ia) show weak patchy zoning and rare melt inclusions in the core associated with large resorption features. These resorption

Table 3.2 Plagioclase Phenocryst Mode for Selected Samples from Quizapu

Sample	Plagioclase phenocryst mode	SiO_2 [wt.%]
1846/47		
Hybrid andesite		
VQ-02	14.9	61.4
VQ-09	14.0	61.6
VQ-10	13.5	60.8
VQ-15	13.7	61.3
Mingled dacite		
VQ-04D	11.6-14.4	64.7
VQ-06	11.6	65.9
VQ-08D	3.3	67.6
VQ-11	14.6	65.7
VQ-14	14.9	65.8
VQ-22D	10.9 (71% so[$];29% ca[$])	63.3
VQ-24D	12.8	65.3
Andesitic inclusion		
VQ-22A	13.98 (100% ca[$])	53.9
1932		
Glassy dacite		
VQ-17	11.0	61.3

[$] so: sodic plagioclase (<An56.5); ca: calcic plagioclase (>An56.5), see text for further explanation

features are only found in lavas from the 1846/47 eruption. Type Ib, only found in lavas from 1846/47, (Figure 3.3e and f) is subhedral to anhedral and fully interspersed with melt inclusions and melt channels. The few crystals of type Ib that were observed occurred in both dacite and andesite end members of the 1846/47 lavas. Type Ic (Figure 3.3g and h) is texturally very similar to type Ia, although it contains a more calcic core (> An_{45}). The cores show a sharp transition from calcic cores to the typical dacite plagioclase phenocryst compositions (~An_{35}). They often

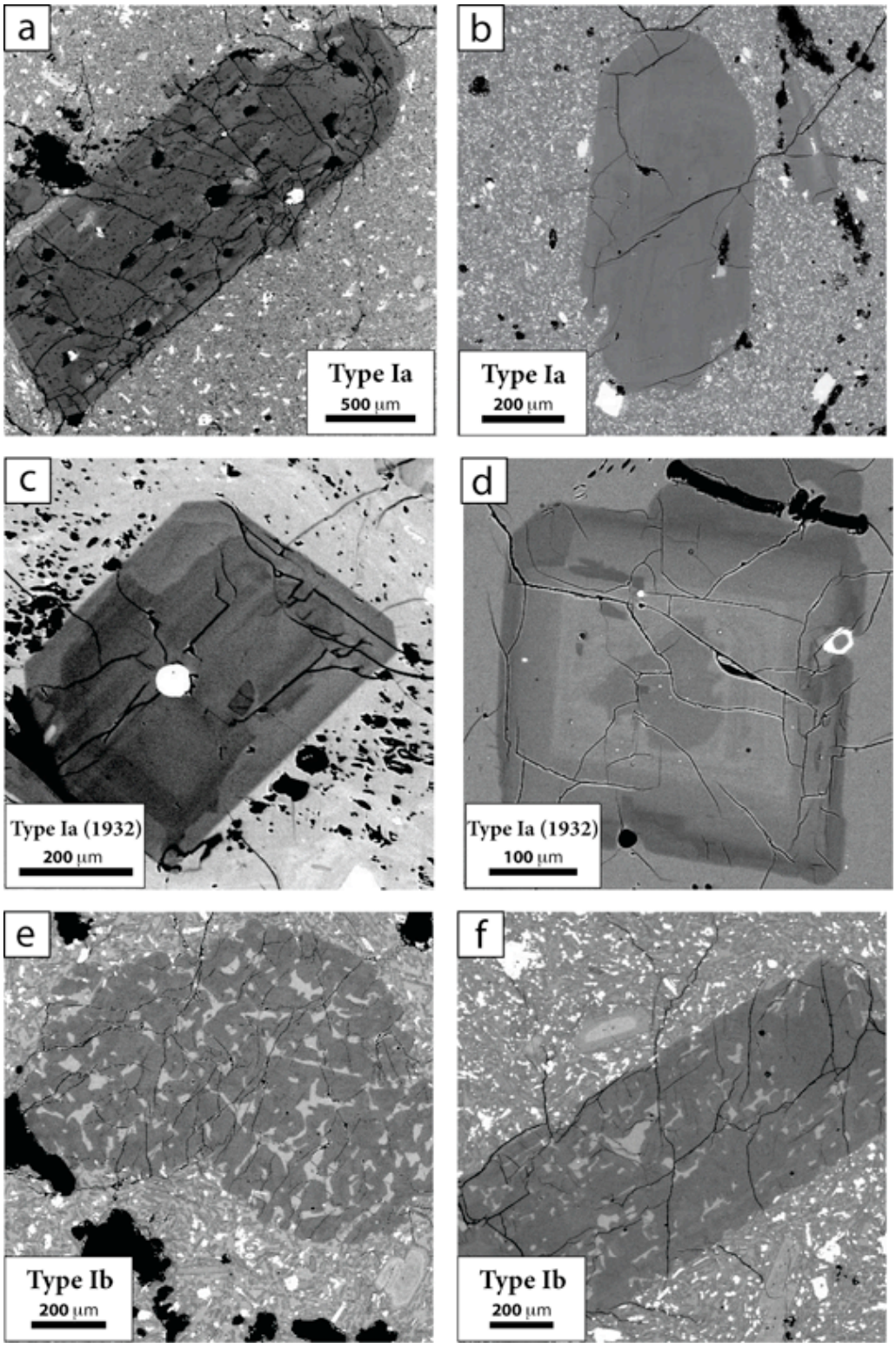

Figure 3.3 Caption on the next page.

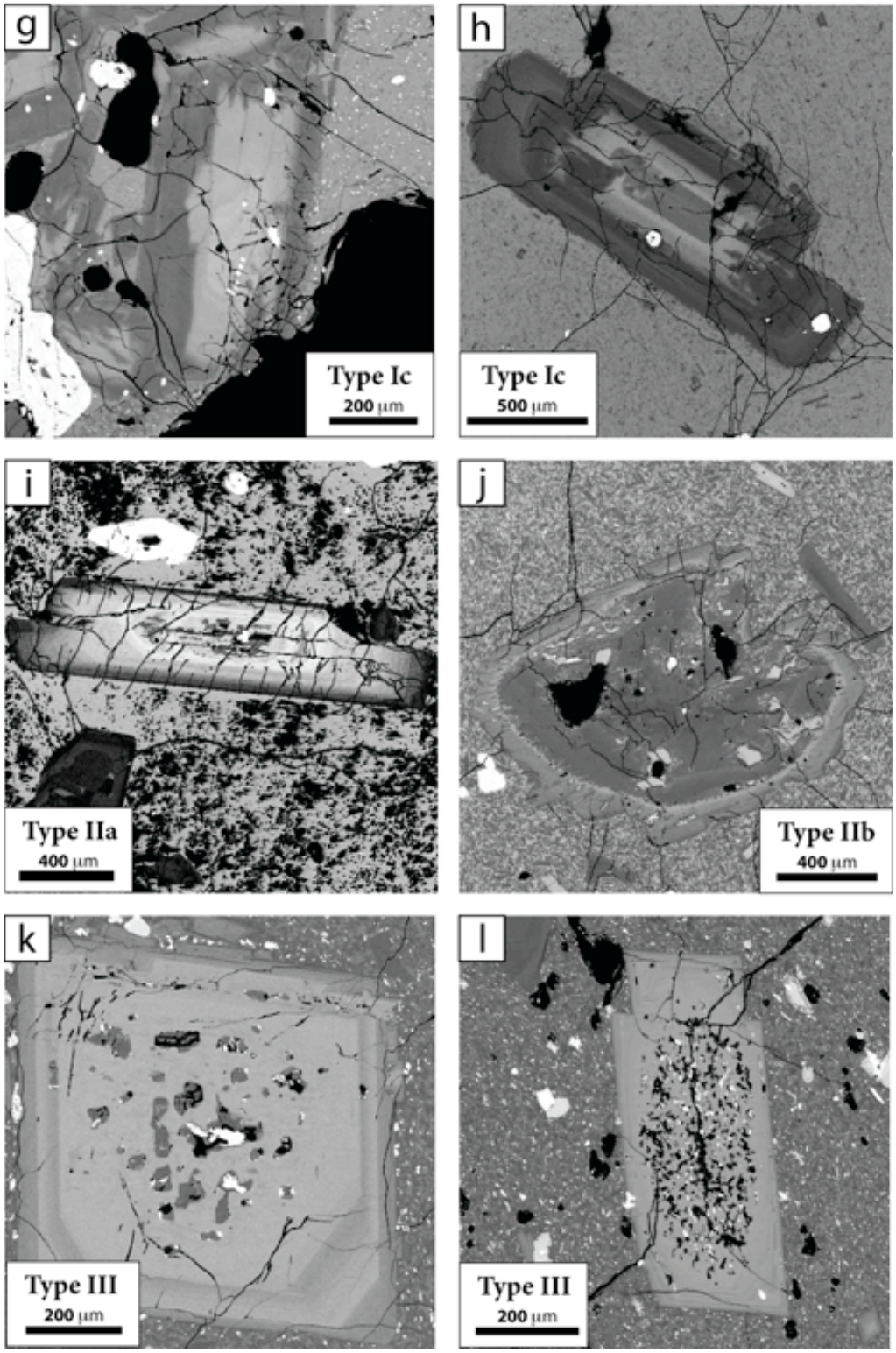

Figure 3.3 Caption on the next page.

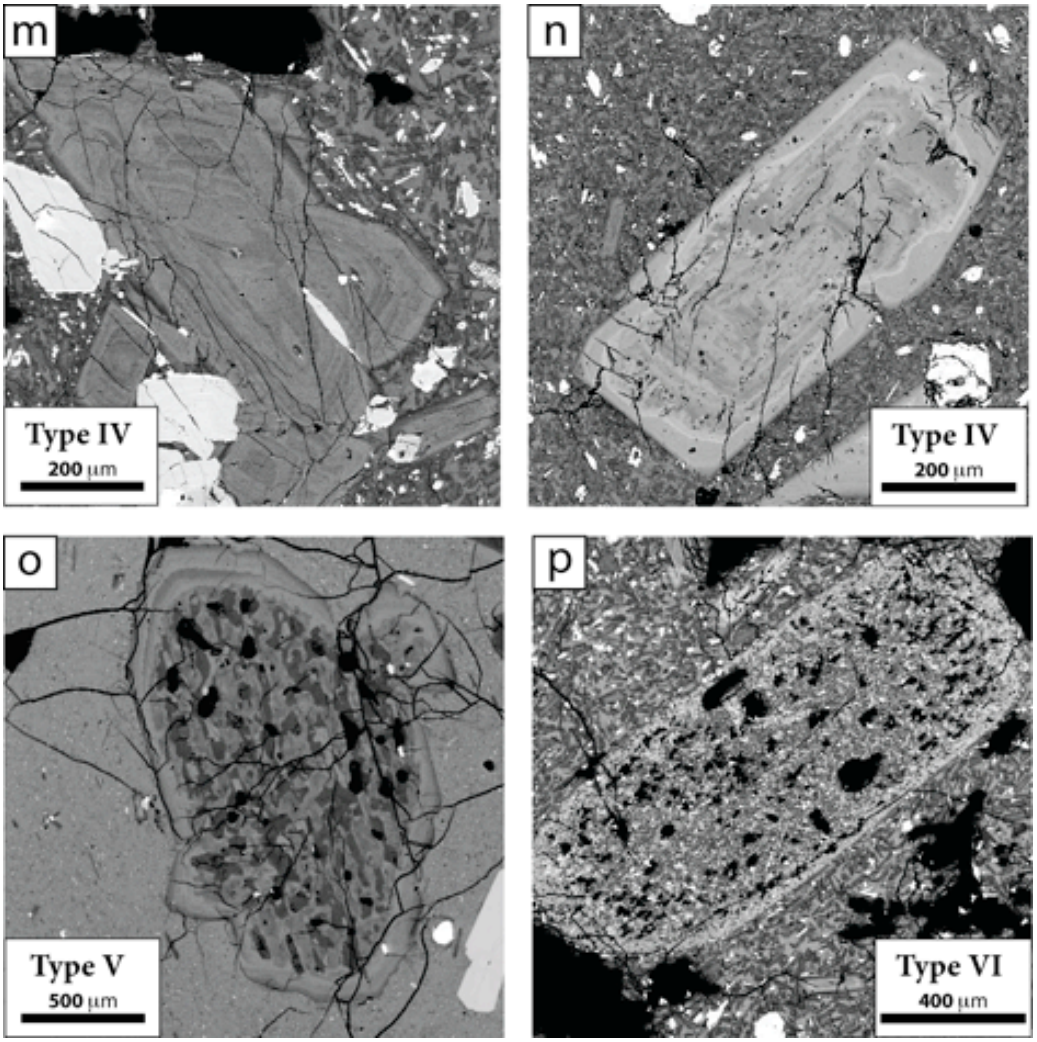

Figure 3.3 Plagioclase Types in Magmas from the two Historic Eruptions of Quizapu. Type I is the most common type in dacites from the Quizapu. Type II can be found mainly in 1932 dacites. Type III and IV are high An plagioclase crystals derived from andesite recharge magmas. Type V and VI are rarely found in magmas from Quizapu.

occur within glomerocrysts (Figure 3.3e) with pyroxenes and Fe-Ti oxides. Despite some similarities between type Ic and IIa, type IIa (Figure 3.3i) are distinct from Ic by their gradual normal zoning from a calcic (~An_{60}) core to rims that are in equilibrium with the dacite magma. In larger crystals, these high An cores may represent overgrowth mantles over low An content cores. This transition occurs in a zone of resorption-regrowth (exposed in Figure 3.3i in the center of the crystal).

Table 3.3 Plagioclase Types in Magmas from Volcán Quizapu

Type	Characteristics
Ia	most common type I of phenocryst in dacite end member: low An content (An30 - An45), often embayed, weak patchy zoning, melt inclusions common
Ib	rare type I crystals in dacite end member: low constant An content (An30-An45), strongly resorbed with extensive melt channels
Ic	antecrysts found in the dacite end-member: mostly in crystal agglomerations, typically subhedral with more An rich core (>An60) and sodic rim (An30-An45)
IIa	Normal zoned phenocrysts (An30-An60): Cores sometimes patchy zoned with low An (An30) or slightly sieve-textured
IIb	rare dacite-derived crystals: low An core (An30-An45) with patchy zones and melt inclusions overgrown by a resorption-regrowth zone (after large resorption, zoning 2, normal zoned towards the rim)
III	common as large phenocryst in andesite recharge magmas: large melt inclusions and resorption features in the core, mantle homogenous at >~An70, normal zoning at the outermost rim An
IV	common as intermediate-sized phenocrysts in andesite recharge magmas: low-amplitude, low frequency oscillatory zoning around An70
V	dacite-derived plagioclase: coarsely sieve-textured core overgrown by pronounced normal zoned mantles/rims
VI	extensively sieve-textured plagioclase, with very small rim of high An overgrowth

Type IIb (Figure 3.3j) are extreme cases of large low An cores with overgrowth mantles of higher An content. The low An cores that dominates the crystal growth history of type IIb resembles strongly type Ia phenocrysts. In a few cases, the high An portions of these type II phenocrysts are entirely sieve-textured. Type III (Figure 3.3k and l) plagioclase crystals are euhedral and calcic (An_{70}-An_{85}) and except for the core and the outermost rim show very little internal zoning. Cores contain melt inclusions and areas of extensive resorption. The 10 to 20 μm thick rims are sodic (An_{40}) and very similar in composition to groundmass crystals. This type is

ubiquitous in lavas from the 1846/47 eruption. Type III is found mostly as single crystals in the glass or groundmass matrix; occasionally these crystals are associated with glomerocrysts. Type III is a common type of phenocryst in mafic recharge magmas. The other phenocryst-type is Type IV (Figure 3.3m and n), which are euhedral, calcic in composition (An_{60}-An_{70}), and show low-amplitude, high frequency oscillatory zoning. Only minor resorption surfaces are developed in type IV crystals. Type III and IV are often mutually exclusive in the different andesite inclusions. Type V (Figure 3.3o) crystals are similar to type IIb with the exception that crystal cores show extensive signs of resorption in the form of melt inclusions and melt channels. Multiple normal-zoned overgrowth rims (An_{45}-An_{55}) may occur for type V. Type VI (Figure 3.3p) shows the most pronounced disequilibrium textures. Almost the entire crystal is sieve-textured. Only a small more calcic rim is developed.

Figure 3.4 shows the range in An content that can be found in lavas from the 1846/47 eruption. Generally, plagioclase crystals range in An content from An_{18} to An_{90} (Plagioclase compositions in Appendix B1). Three modes are present, which correspond to the voluminous significant plagioclase types I, III, and IV. The transitional compositions in between types I and IV are dominated by type II and V crystals. The hybridized andesites contain the entire range of plagioclase compositions; crystals in VQ-02 vary from An_{18} to An_{89}. The andesitic and dacitic end-members, e.g., VQ-22A and VQ-06, are volumetrically mostly restricted to type III and IV and type I, respectively. Thus, type III and IV are referred to in the following as andesite-derived plagioclase, while type I plagioclase is identified as dacite-derived. The plagioclase phenocryst population of 1932 dacite is also dominated by type I and to lesser extent by type II phenocrysts. Andesite-derived plagioclase phenocrysts are almost absent in the dacite magma of 1932. However, analyses of plagioclase in terminal scoria magma from the 1932 eruption provide

evidence that the recharge magma in 1932 contained similar phenocrysts as the 1846/47 recharge magmas.

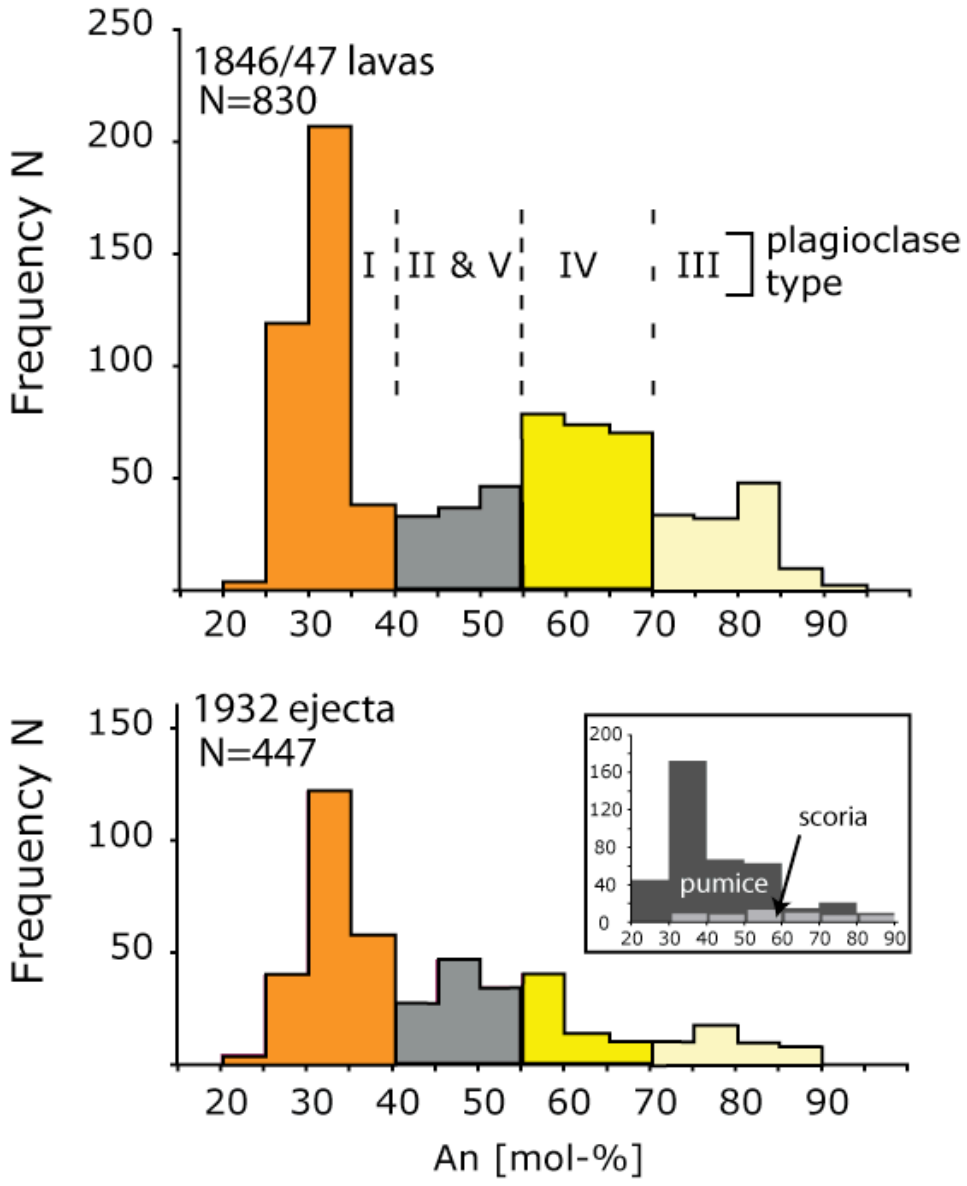

Figure 3.4 Histogram of Plagioclase Microprobe Analyses for Quizapu. Quantitative microprobe analyses showing the distinct peak for dacite-derived plagioclase (orange) and a broader distribution for andesite-derived plagioclase (yellow). Insert: Plagioclase data for scoria and pumice. Most high An plagioclase analyses are from mafic scoria in 1932. The dacite pumice contains rare plagioclase with high An content (>An60).

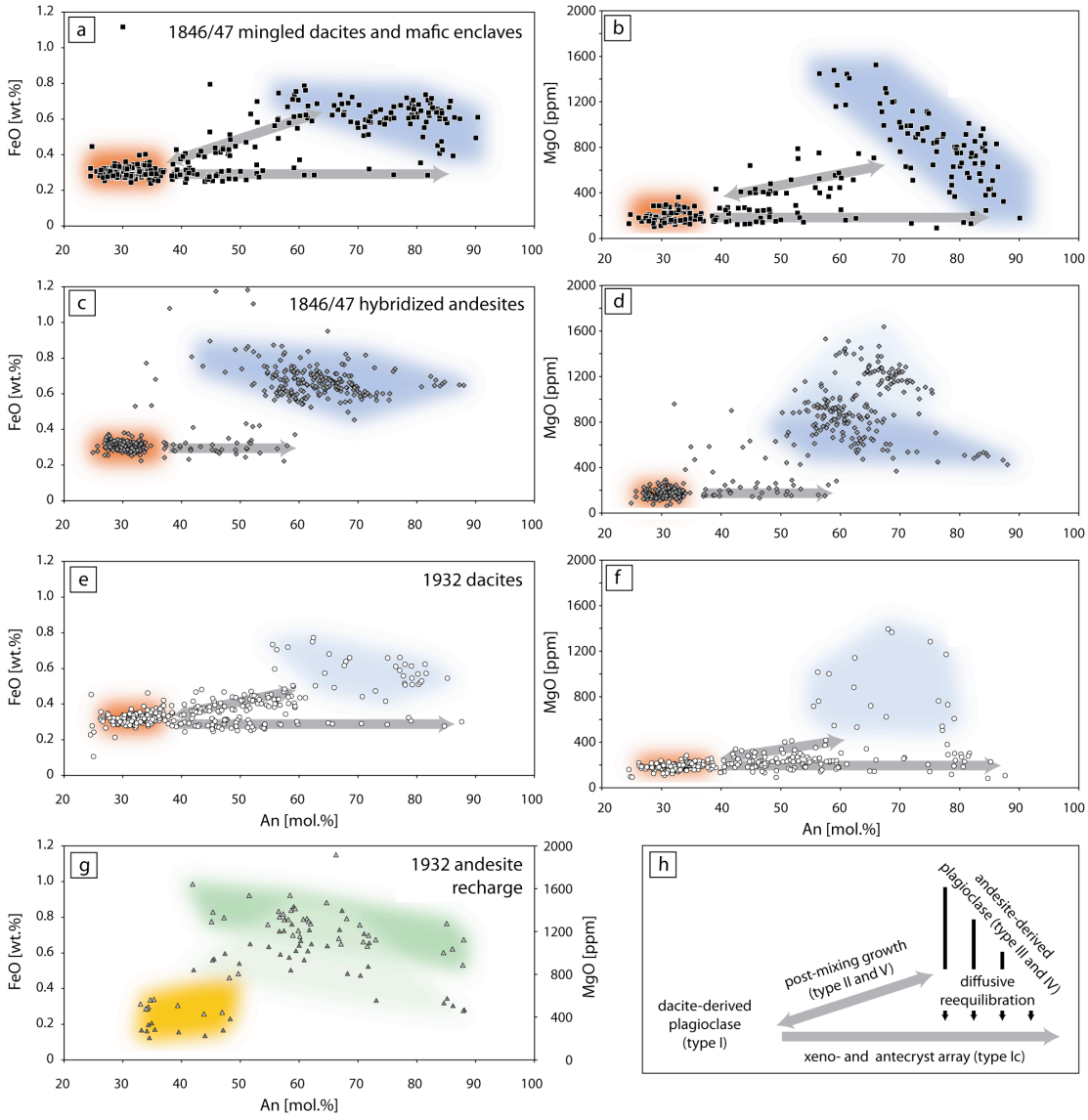

Figure 3.5 Fe and Mg versus An in Plagioclase from Quizapu. Dacite-derived and andesite-derived plagioclases are distinct in Fe and Mg concentrations. Plagioclase phenocrysts are from 1846/47 mingled dacites (black squares), hybridized andesites (grey squares), 1932 dacites (white circles) and 1932 recharge andesite (grey diamonds). Plagioclase compositional data in Appendix B1.

The use of Fe and Mg in plagioclase has been shown to be very valuable in distinguishing among compositionally different magma inputs [*Hattori and Sato*, 1996; *Ginibre et al.*, 2002b; *Ruprecht and Wörner*, 2007; *Humphreys et al.*, 2009]. The minor element compositions provide further evidence for distinguishing andesite and dacite-derived plagioclase phenocrysts for the magmatic system of Quizapu (Figure 3.5a-h). Textural types show distinct chemical signatures (Figure 3.5h). In general, dacite-derived plagioclase is low of Fe (0.2-0.4 wt.%) and Mg (100-400 ppm), while andesite-derived plagioclase has high concentrations in Fe (up to 1.0 wt.%) and Mg (up to 1600 ppm). The dacite-derived plagioclase contains little Fe and Mg, consistent with equilibrium partitioning between plagioclase and dacite magma [*Bindemann et al.*, 1998]. In contrast, high Fe and Mg concentrations in andesite-derived plagioclase are consistent with growth from a mafic magma. In particular, Mg shows strong correlation with An content, which is consistent with low partition coefficients for Mg in anorthite [*Bindemann et al.*, 1998]. Diffusion may affect Fe and Mg concentrations in andesite-derived plagioclase that is found in dacite-magma [e.g., *Costa et al.*, 2003]. The antecrysts and xenocrysts that have low Fe (< 0.4 wt.%) and Mg (< 200 ppm) concentrations despite their An contents are in equilibrium with the mixed host magma due to complete diffusive re-equilibration. Type II and V phenocrysts show textural characteristics of magma mixing (normal zoning, resorption-regrowth features) that is supported by geochemical constraints. These phenocrysts predominantly fall on an array that connects the dacite- and andesite-derived plagioclase compositions, suggesting growth from hybrid magma. However, these phenocrysts are rare in the hybrid magmas (Figure 3.5c and d) studied and therefore cannot represent previous major magma hybridization events in the main magma reservoir. Thus, other zones of hybridization must exist in the subvolcanic plumbing system. While hybridized magmas of 1846/47 lack post-mixing growth plagioclase (type II and V), we observe two distinct groups of andesite derived-plagioclase phenocrysts in two different hybrid andesites. These two plagioclase groups are only evident in their Mg concentrations. Plagioclase from

pumice samples of the 1932 eruption contain all four groups of phenocrysts, however, only few crystals make up the field of andesite-derived plagioclase (Figure 3.5e and f). By volume, the crystals within the magma are dominated by dacite-derived plagioclase, post-mixing growth plagioclase, and antecrysts that are part of glomerocrysts or that have been dispersed by magma chamber dynamics. Phenocrysts in 1932 scoria have similar compositions to recharge magmas from 1846/47. Most plagioclase crystals have high Fe (up to 1 wt.%) and high Mg (up to 1600 ppm). The few crystals that are sodic have minor-element characteristics consistent with being dacite-derived (Figure 3.5g).

Trace-element compositions of plagioclase phenocrysts from the 1846/47 and 1932 eruptions were measured on grain mounts via LA-ICPMS (Figure 3.6, Plagioclase trace element compositions in Appendices B7 and B8). Thus, textural correlation is not possible. Nonetheless, trace elements show distinct concentrations for the andesite- and the dacite-derived plagioclase component, consistent with growth from very distinct magmas. A few andesite-derived plagioclase crystals from the 1932 ejecta show various degrees of diffusive equilibration with the more evolved liquid of the dacite. We observe consistent diffusive element behavior with respect to the different diffusivities ($D_{Mg} < D_{Pb} \approx D_{Fe} < D_{Sr} < D_{Ba} < D_{La}$) for most plagioclase crystals that show altered trace element concentration [*Cherniak*, 1995; *Giletti and Shanahan*, 1997; *Cherniak*, 2002; *Costa el al.*, 2003; *Cherniak* 2003]. Actual time scales of re-equilibration for these plagioclase crystals cannot be calculated due to the missing textural context and the analysis of crystal fragments. However, the observed patterns of the various elements indicate that with improved sensitivity and spatial resolution of LA-ICPMS we may be able use large sets of elements of where each element may be sensitive to a single intensive variable (X, T, pH_2O) with distinct diffusion coefficients. By combining these elements with major element zonation we may be able uniquely distinguish among different physical processes in the future.

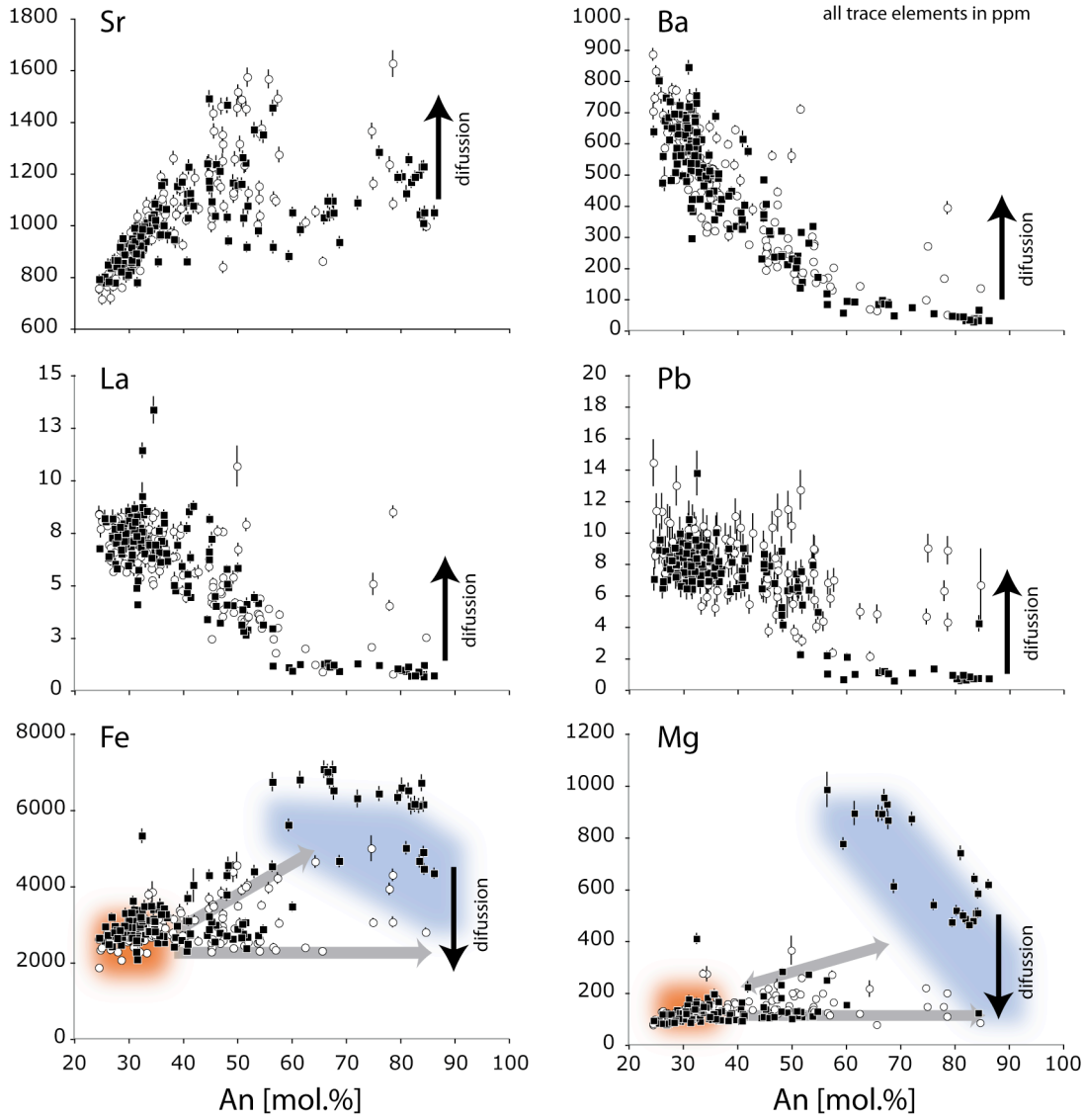

Figure 3.6 Trace Element Concentrations in Plagioclase from Quizapu. Plagioclase phenocrysts are from the 1846/47 (black squares) and the 1932 eruption (white circles). Plagioclase trace element compositional data in Appendices B7 and B8.

Microlites are intermediate to sodic in compositions ranging from (An_{30} to An_{60}). Microlite compositions have not been analyzed quantitatively, but a grayscale-comparison with adjacent phenocrysts provides qualitative constraints for microlite compositions. Microlite abundance increases from absent in dacite ejecta from the 1932 eruption, to abundant in mingled dacites in the 1846/47 lavas ubiquitous in hybridized andesites.

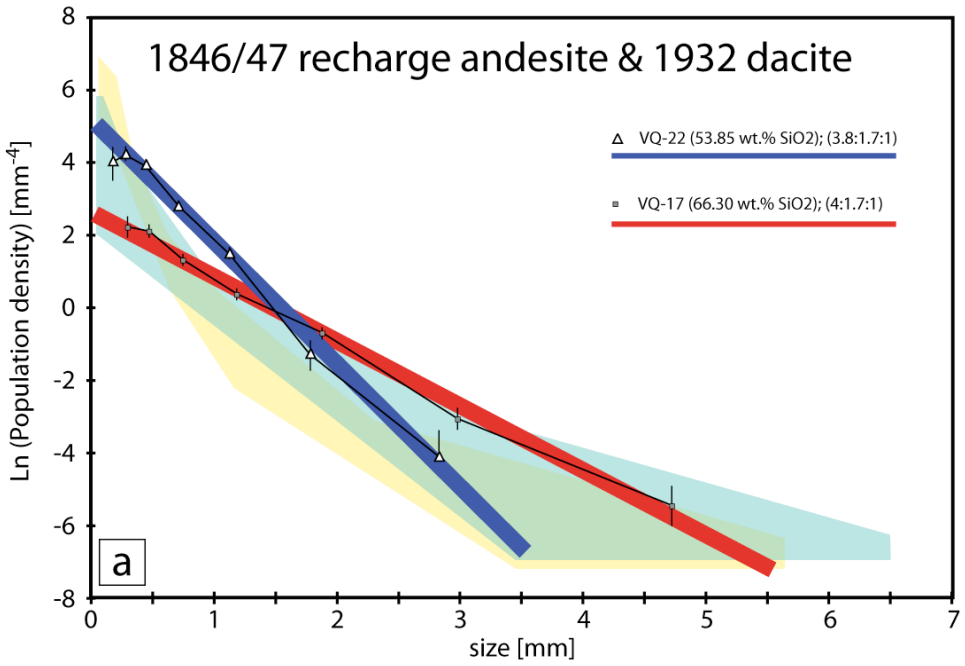

Figure 3.7 Crystal Size Distribution (CSD) for Magmas from Volcán Quizapu. a) Only two samples show CSDs suggesting continuous growth of a single population. b) Mingled dacites from the 1846/47 eruption have concave-up CSD, predominantly as a result of the addition of microlites. c) Hybridized show strongly curved CSDs as a result of the hybridization process.

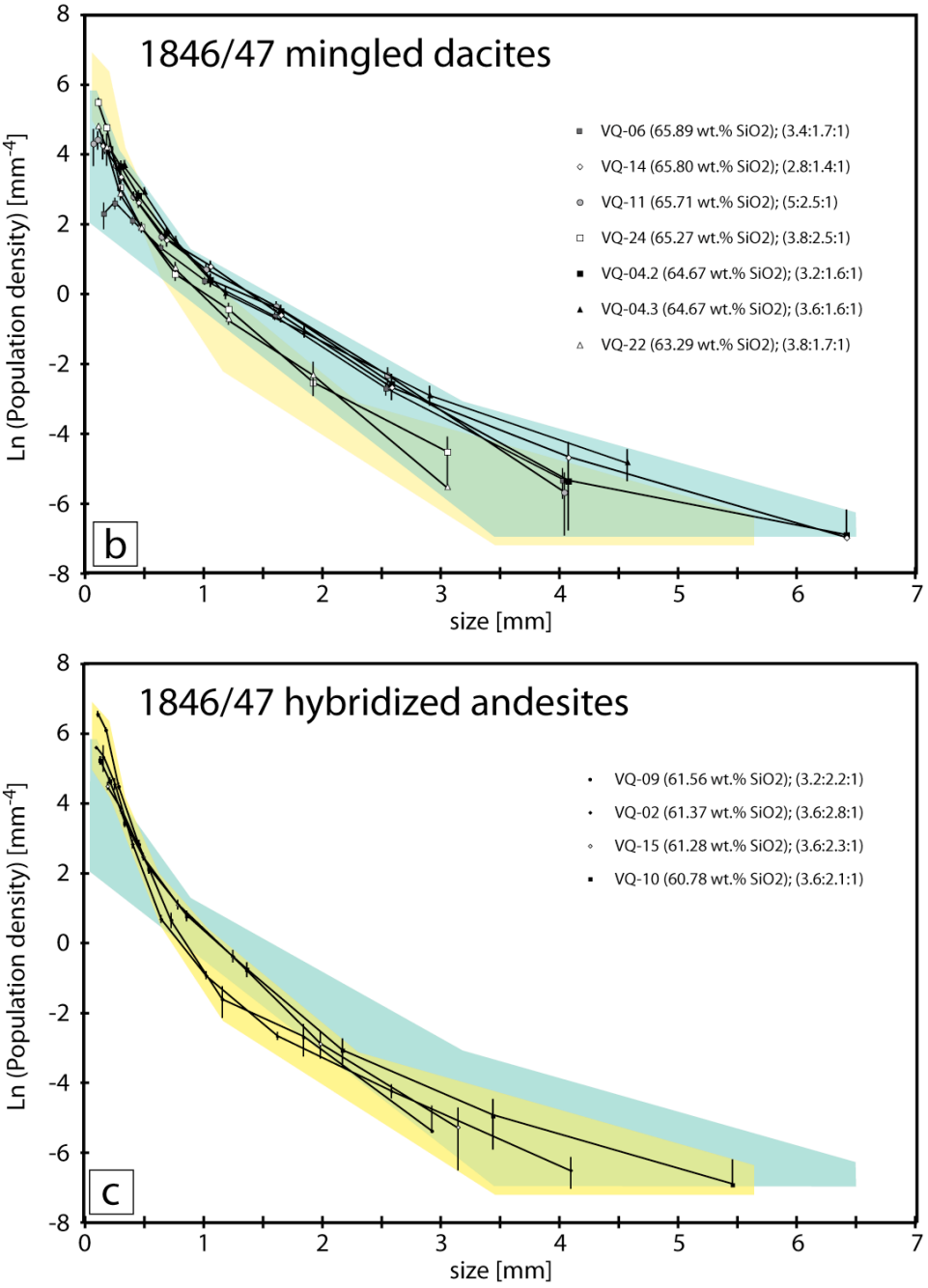

Figure 3.7 continued.

We analyzed the crystal size distributions (CSD) of plagioclase in mingled dacites, hybridized andesites and andesite inclusions from the 1846/47 as well from a dense dacite from 1932 to further characterize the plagioclase populations found at

Quizapu (Figure 3.7). CSDs provide a means to identify distinct crystal populations and quantify overall crystal volume fractions [e.g., *Cashman and Marsh*, 1988; *Higgins*, 2000; *Salisbury et al.*, 2008]. We have produced CSDs for only phenocrysts and microphenocrysts, which provide the long-term information for the evolution of the crystal cargo. According to *Marsh* [1998] individual crystal populations that are characterized by relatively constant nucleation and growth rates over the evolution of a magma systems follow a linear relationship on a log-linear plot of population density and crystal size. Large crystal sizes are more prone to uncertainties due to their smaller number density.

Only two samples that we analyzed followed the linear behavior expected in the case of continuous growth of a single crystal population, an andesite inclusion from the 1846/47 eruption and a dense dacite from 1932 deposits. Crystals from the andesite inclusion are on average smaller and have higher population densities to account for similar crystallinities in andesites and dacites. Other samples from 1846/47 lavas show a concave-up CSD pattern indicating higher population densities for smaller crystals (Figure 3.7). CSDs for mingled dacites from the 1846/47 lavas are mostly linear for large crystal sizes (> 1 mm). For very large crystal sizes (> 4 mm) this linearity breaks down, however, such large crystals are rarely seen in thin sections and counting errors become significant. The smaller size fractions (< 1 mm) show higher population densities, which is consistent with the addition of andesite-derived plagioclase due to mingling and mixing. Hybridized andesites show very pronounced concave-up CSD pattern. Dacite- and andesite-derived plagioclase populations contribute with equally to the plagioclase CSDs for the hybridized andesites.

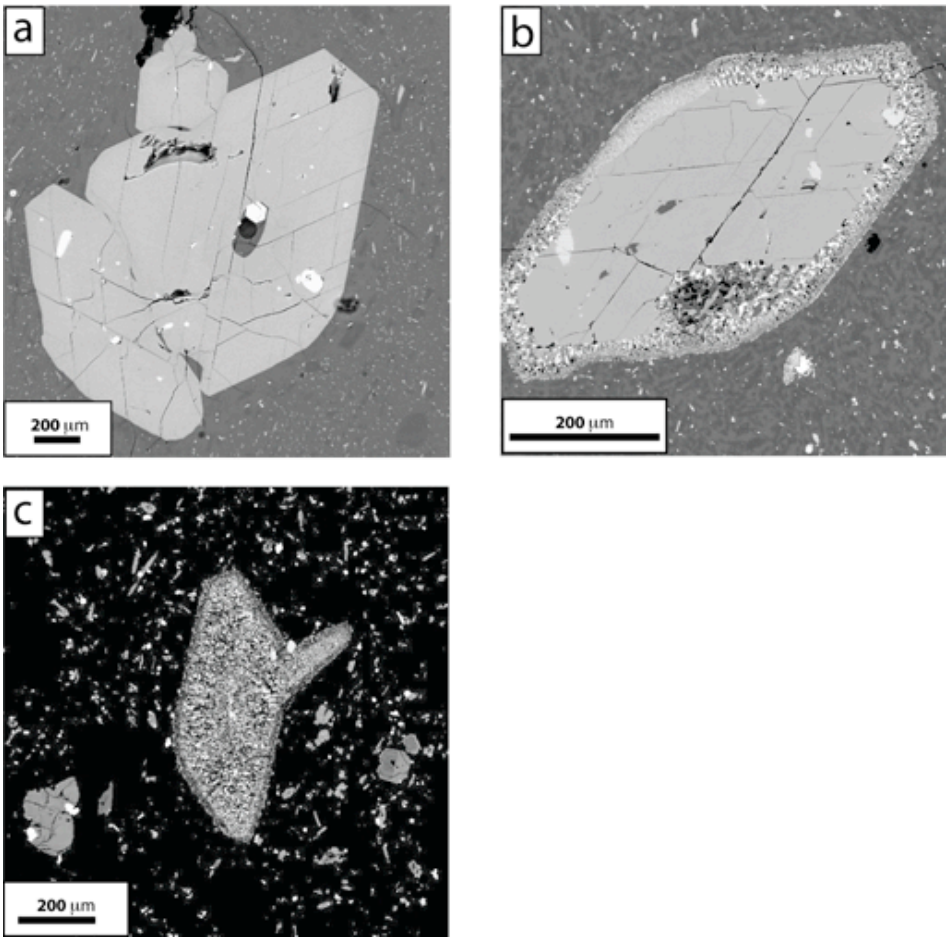

Figure 3.8 Backscattered-electron Images of Amphiboles in Magmas from Quizapu: Recrystallization rims. a) Euhedral amphibole in lavas from the 1846/47 eruption; b) decomposition rim on euhedral amphibole from a 1846/47 lava. Decomposition products are plagioclase, titanomagnetite, and clinopyroxene, c) decomposed amphibole remnants from a hybridized andesite.

Amphibole

Amphibole is ubiquitous in dacites from Quizapu [*Hildreth and Drake*, 1992]. Most amphiboles in lavas and plinian dacites are pristine and euhedral (Figure 3.8a). Some flow lobes of the 1846/47 eruption contain amphibole with up to 50 µm thick decomposition rims composed of plagioclase, titanomagnetite and clinopyroxene (Figure 3.8b). The interior parts of the decomposition rims are relatively coarse-grained with 5 to 10 µm large crystals. The exterior parts of the rims are fine-grained with crystal sizes of less than 5 µm. Hybridized andesites

contain entirely decomposed amphibole remnants (Figure 3.8c). They also show fine-grained outermost rims, while the interior is coarse-grained.

A total of 317 amphibole analyses from 29 crystals provide calcic amphibole compositions (Figure 3.9, Amphibole compositions in Appendix B2 [*Leake et al.*, 1997]) with Ca ranging from 1.63 to 1.84 apfu (atoms per formula unit). Amphiboles vary from edenite to magnesiohastingsite and pargasite with a total range for Si of ~ 0.6 apfu. Edenitic amphiboles are euhedral phenocrysts in the dacite magmas of the 1846/47 and 1932 eruptions (Figure 3.10). In contrast to the edenites, pargasites and magnesiohastingsites are found either as older cores in edenite mantles or as subhedral glomerocrysts intergrown with plagioclase, Fe-Ti oxides, and apatite. The cores and glomerocrysts are mainly pargasitic in the 1932 ejecta, while similar cores and glomerocrysts in 1846/47 lavas are magnesiohastingsite with more ferric iron than octahedral-coordinated aluminum (Figures 3.9 and 3.10).

Compositional variations are mostly accommodated by simple ferrous iron and magnesium exchange as well as by the temperature sensitive edenite exchange

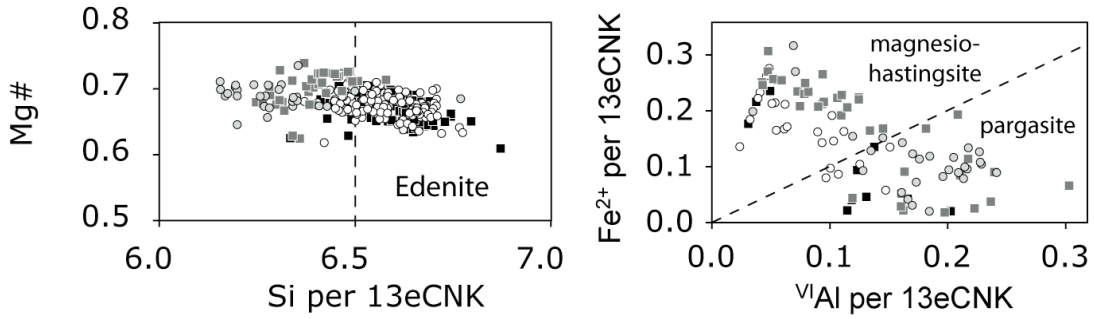

Figure 3.9 Amphibole Compositions in magmas from Quizapu. Most amphiboles are edenite (black squares and white circles as in Figure 3.6). Old cores and amphiboles that are associated with glomerocrysts are less silica-rich and are magnesiohasting-sites and pargasites (grey squares, 1846/47; grey circles, 1932). Amphibole compositional data in Appendix B2.

($^{T}Si + {}^{A}\square = {}^{T}Al + {}^{A}(Na+K)$) similar to other magmatic systems [*Bachmann and Dungan*, 2002] (Figure 3.11). The two amphibole populations in the magmas from Quizapu, (1) edenite and (2) magnesiohastingsite and pargasite, are distinct with respect to the Ti-Tschermak exchange ($^{T}Si + {}^{M1\text{-}M3}Mn = {}^{T}Al + {}^{M1\text{-}M3}Ti$). While the edenites show a good correlation ($R^2 = 0.67$) between ^{T}Al and $^{M1\text{-}M3}Ti$ (~40% accommodation of the variations in ^{T}Al), magnesiohastingsites and pargasites show a weak correlation ($R^2 = 0.27$) along the Ti-Tschermark exchange. The remaining variation in ^{T}Al is accommodated by the "plagioclase exchange" ($^{T}Si + {}^{M4}Na = {}^{T}Al + {}^{M4}Ca$).

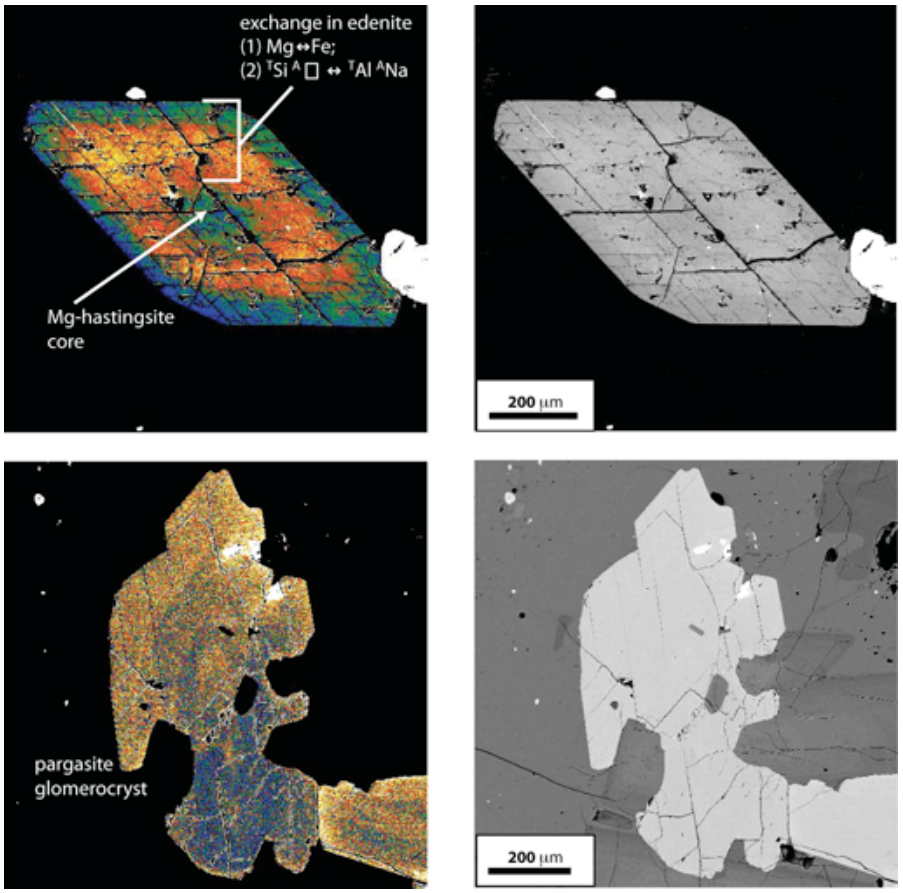

Figure 3.10 Backscattered-electron Images of Amphiboles in Magmas from Quizapu: Zonation patterns. Top: Euhedral edenite phenocryst with magnesio-hastingsite core, bottom: pargasitic glomerocrysts intergrown with plagioclase.

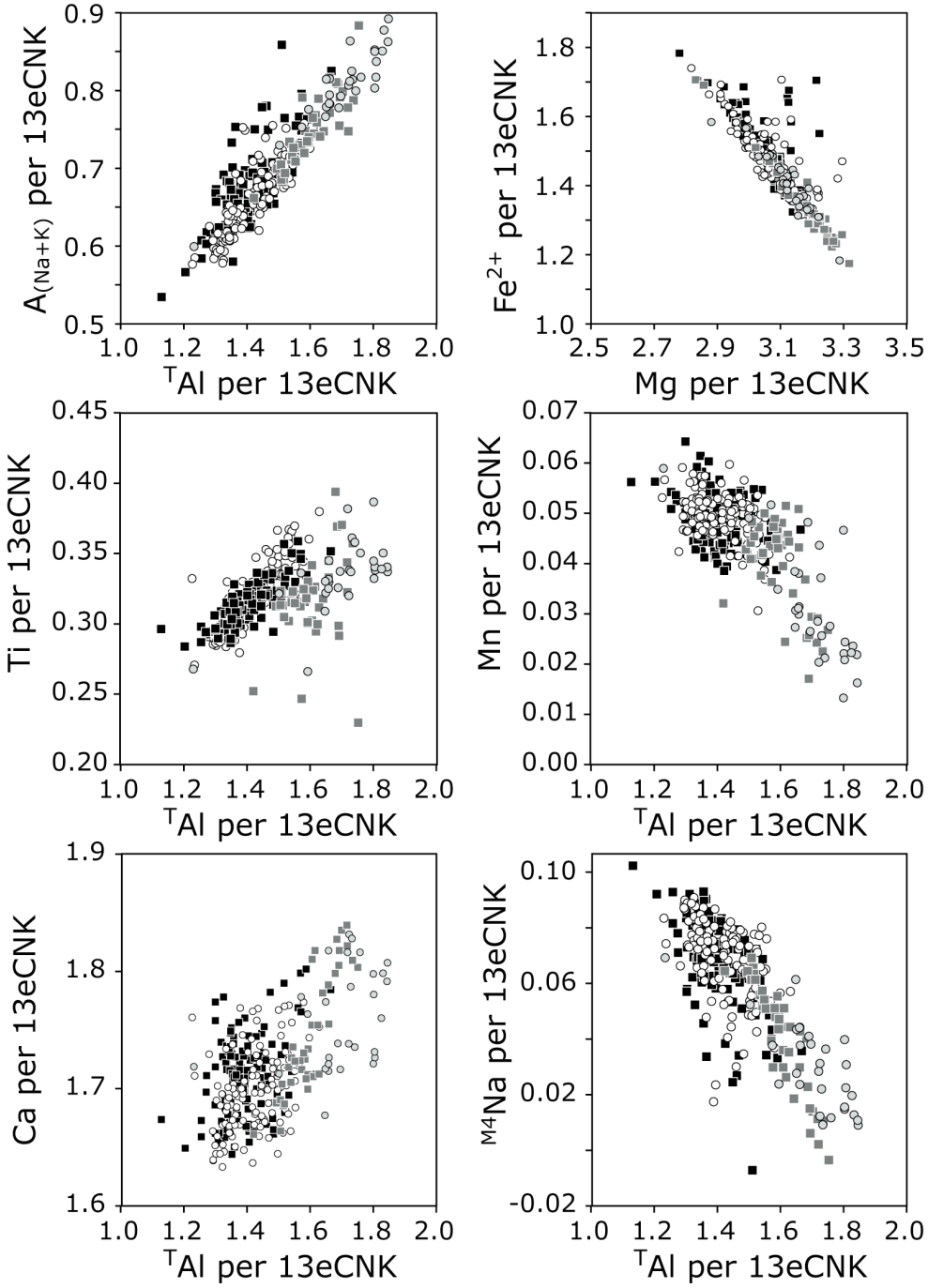

Figure 3.11 Temperature-dependent Exchange and Mg-Fe Exchange in Amphibole. Edenite exchange takes up most of the compositional variation. To minor extent Ti-Tschermak and plagioclase exchange contribute to the variations found in amphiboles form Quizapu. Magnesiohastingsites and pargasites follow the same edenite exchange trend. They differ considerably for the Ti-Tschermak and plagioclase exchange. Symbols as in Figure 3.9.

Pyroxene, olivine and accessory phases

Dacite magmas of Quizapu contain mostly orthopyroxene, while clinopyroxene is found predominantly as phenocryst phase of the recharge magmas. Orthopyroxenes in the mingled dacites are frequently anhedral suggesting late-stage resorption. We have found a similar compositional range as that reported by *Hildreth and Drake* [1992] (Figure 3.12, Pyroxene compositions in Appendix B4), where orthopyroxenes are similar between the two dacites from 1846/47 (En_{65-77}) and 1932 ($En_{66-72.5}$). Orthopyroxenes in andesite inclusions have slightly lower Mg numbers for orthopyroxenes than those in the dacite ($En_{62.5-71}$). Pyroxene compositions in the hybridized andesites cover the entire range (En_{63-77}) spanned by dacites and recharge andesites. With the exception of crystals in one andesite recharge magma, most orthopyroxenes have low Ca concentrations of Wo_{2-3}. Pigeonite microlites have been analyzed in an andesite inclusion of 1846/47 recharge magma, suggesting late growth at shallow depth and high temperatures [*Longhi and Bertka*, 1996]. Ca content varies in these pigeonites between Wo_{6-23}. Augites have been only analyzed in lavas from 1846/47. Their compositions vary around an average of $En_{44}Fs_{14}Wo_{42}$. No systematic difference exists between recharge magmas and dacite magma.

Olivines are phenocryst phases in the mafic recharge magmas. They occur also as xenocrysts in mingled dacites from the 1846/47 lavas and in dacites from the 1932 plinian ejecta. In the dacite magmas the olivines are normally zoned, which has been used by *Costa and Chakraborty* [2004] to infer time scales of magma mixing. The compositions of olivine are more mafic in the 1846/47 lavas at ~ Fo_{76} compared to ~ Fo_{70} in samples from the 1932 dacite (Olivine compositions in Appendix B5). Apatite, titanomagnetite, ilmenite and sulphides are ubiquitous in the dacites of Quizapu. They occur as phenocryst phases as well as mineral inclusions in plagioclase and amphibole. Zircon has not been reported previously [*Hildreth and Drake*, 1992]. We have found zircon (< 50 μm) in three different thin sections of the mingled dacites from the 1846/47 eruption. They are typically associated with

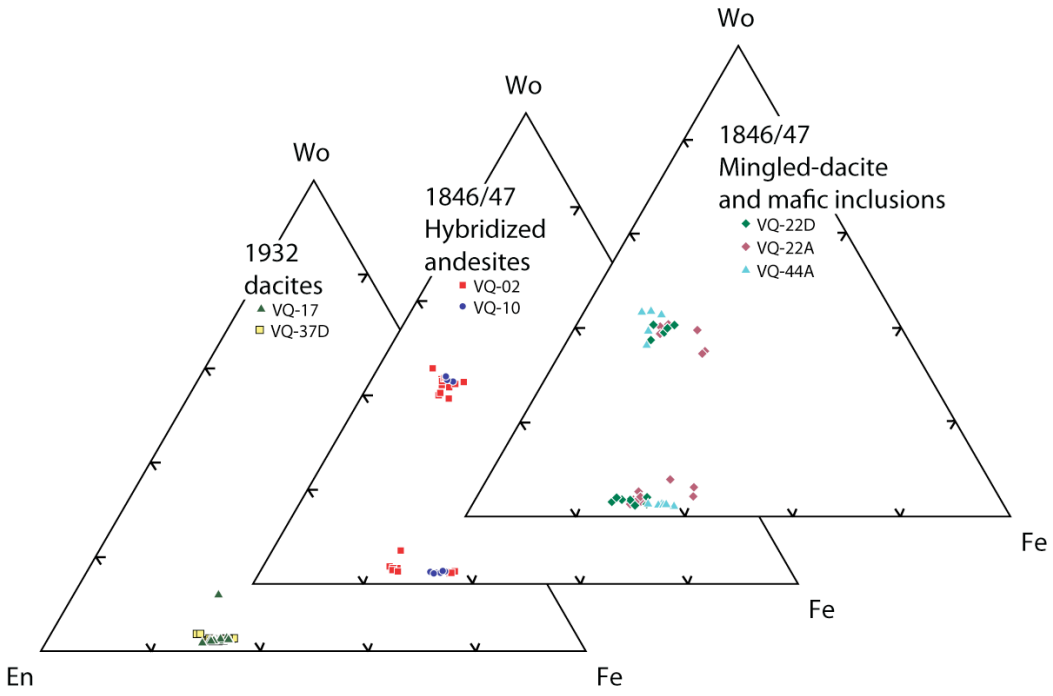

Figure 3.12 Ternary Pyroxene Diagram. Clinopyroxene is rare in dacites from Quizapu. Pyroxene compositional data in Appendix B4

magnetite and amphibole crystal clots. Quartz has been only observed in plagioclase grain mounts without textural context. The overall lack of significant fractions of quartz in the dacites suggests high temperatures and high water content of the dacites [*Whitney*, 1988].

3.5 Pre-eruptive Magmatic Temperatures

The mineral assemblage observed at Quizapu enables us to calculate pre-eruptive magmatic temperatures using various phenocryst-pair equilibrium geothermometers: Fe-Ti oxide thermometry [*Ghiorso and Evans*, 2008] and amphibole-plagioclase thermometry [*Holland and Blundy*, 1994] provide time-temperature information for dacite magmas that resided in shallow crustal chamber, while the two-pyroxene thermometer [*Putirka*, 2008] in conjunction with the Fe-Ti oxide thermometer provides similar results on the time-temperature path for andesite

recharge magmas. Since Fe-Ti oxides can be used for both dacite and andesite end-members, we will discuss them together at the end of this section.

Plagioclase-amphibole equilibrium temperatures are calculated for all 317 amphibole analyses using the temperature model B of *Holland and Blundy* [1994], which is appropriate for phenocryst assemblages lacking quartz. Figure 3.13 shows the histogram of the temperature calculations for the two eruptions from 1846/47 and 1932. Temperatures for the two eruptions are indistinguishable from each other at approximately 845 ± 35 ˚C, assuming a plagioclase composition of An_{33}. The calculated temperatures are at the low end of the temperature estimates by *Hildreth and Drake* [1992] using Fe-Ti oxides. Uncertainties on the equilibrium An content in plagioclase results in an uncertainty of about 30 ˚C.

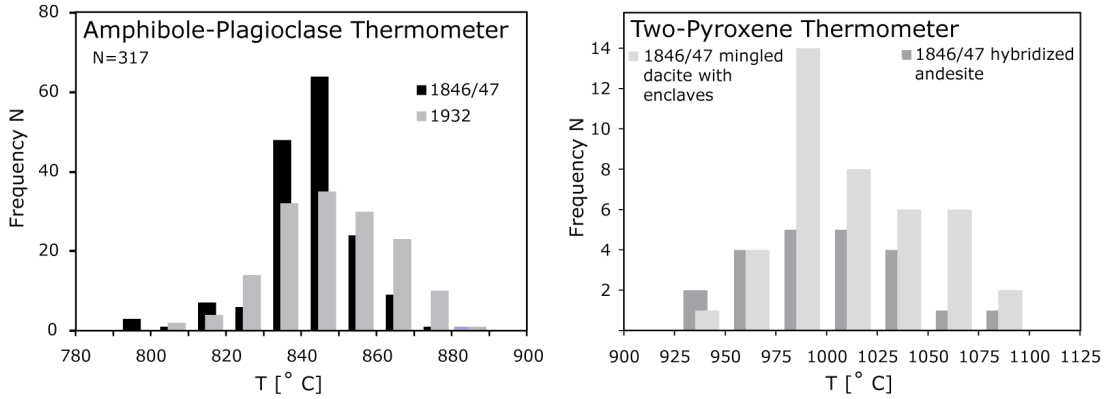

Figure 3.13 Amphibole-Plagioclase Thermometer and Two-Pyroxene Thermometer. The Amphibole-plagioclase thermometer applied to 317 amphibole analyses in the dacites of 1846/47 and 1932 magmas gives a normal temperature distribution with an average dacite storage temperature of 845 ± 35 ˚C. The two-pyroxene thermometer has been applied to mingled dacites and hybridized andesites of the 1846/47 eruption. The pairs that are in chemical equilibrium show much higher temperatures than the temperatures obtained from the amphibole-plagioclase thermometer with an average of 1010 ± 40 ˚C as they record andesite temperatures and subsequent partial re-equilibration during the magma mixing.

Dacitic to rhyodacitic calc-alkaline magmas typically have only small amounts of clinopyroxene present, thus limiting the use of two-pyroxene thermometry. The lack of clinopyroxene in the dacite end-member of Quizapu is similar to other magmatic systems [Mt St. Helens: *Rutherford* 1985; *Rutherford and Hill*, 1993; Mt Unzen: *Holtz et al.*, 2005; San Pedro: *Costa et al.*, 2004; Soufriere Hills: *Rutherford and Devine*, 2003]. As has been interpreted for those other magmatic systems, the Quizapu dacite may be too cold and too wet for amphibole and clinopyroxene to coexist.

The two-pyroxene thermometry [*Putirka*, 2008] provides an alternative to the amphibole-plagioclase geothermometer for the recharge magma. In contrast to the cold dacite end-member, temperatures in the andesitic recharge magma may be potentially beyond the amphibole stability. We analyzed pyroxene pairs in a mingled dacite and one andesite inclusion as well as in a hybridized andesite (Figure 3.13). Any pair that we used for temperature estimates was checked for equilibrium using the Fe-Mg exchange between clinopyroxene and orthopyroxene [*Putirka*, 2008]. Other samples in which pyroxenes where also analyzed do not contain clinopyroxene and orthopyroxene in chemical equilibrium. For the hybridized andesite a total of 23 pairs from eight clinopyroxene crystals and six orthopyroxene crystals yield a temperature range of 938-1094 ˚C (Figure 3.13). The lack of adjacent pairs causes this spread and provides only a general estimate for the magmatic temperatures of the andesite recharge and potentially for the hybridized andesite in which some of the pyroxene crystals may have partially re-equilibrated by diffusion [e.g., *Dimanov and Sautter*, 2000; *Morgan et al.*, 2004]. Overall temperature estimates from two-pyroxene equilibria for the hybridized andesite average to 1007 ± 50 ˚C. Within the mingled dacite a total of 41 pairs from ten clinopyroxene crystals and 16 orthopyroxene crystals that were not touching are in chemical equilibrium. They are dispersed in the andesite inclusion as well as in the dacite magma. Clinopyroxene crystals are small (<100 μm) and may have partially equilibrated with the dacite

magma. Temperature estimates for the 41 pyroxene pairs range from 928-1085 ˚C and yield an average of 1012 ± 35 ˚C.

Fe-Ti oxide geothermometry has been applied to the dacites and andesites erupted at Quizapu (Figure 3.14a, Fe-Ti oxide compositions in Appendix B3) and the results add substantial new temperature information to the already existing data from *Hildreth and Drake* [1992]. We have been able to obtain equilibrium pairs for most lithologies of the 1846/47 and the 1932 eruption. A tight cluster of nine oxide-pairs from two dacite samples yields temperature estimates of 866-885˚C for the plinian eruption in 1932. These temperature estimates are consistent with the reported two-oxide temperatures of *Hildreth and Drake* [1992].

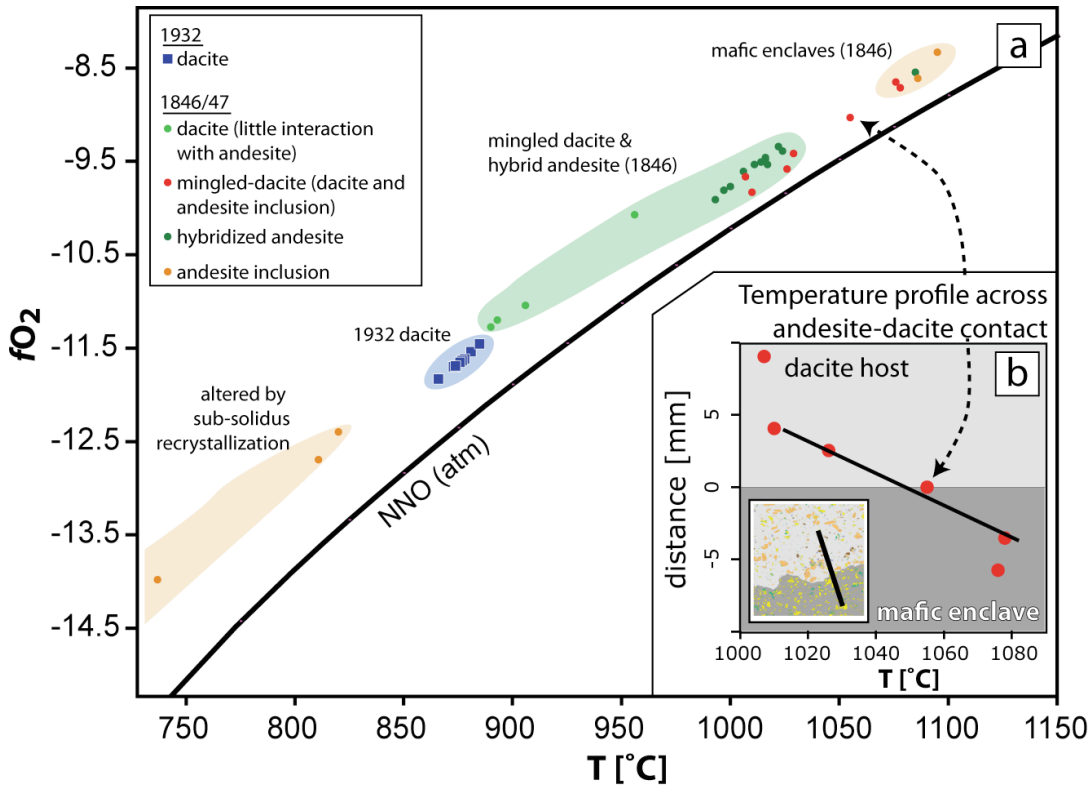

Figure 3.14 Fe-Ti Oxide Geothermometry. a) Oxygen Fugacity versus Temperature from Fe-Ti oxide Pairs. b) Fine scaled temperature variations across a contact between an andesite inclusion and the dacite host magma. insert: gray-scale interpreted BSE map from Figure 4.2 with the location of the transect (black line) along Fe-Ti oxide pairs have been measured.

We observe elevated temperatures and a much wider range in temperatures (890-956˚C) from four pairs for the dacite-end member of the 1846/47 eruption compared to the 1932 dacite. Mingled dacites and hybridized andesites of the 1846/47 eruption have similar Fe-Ti oxide and two-pyroxene temperatures. With the exception of one Fe-Ti oxide pair that yields a magmatic temperature of 1085 ˚C, eleven pairs from the hybridized andesite yield temperatures of 993-1024 ˚C. Seven titanomagnetite-ilmenite pairs in a mingled dacite were analyzed across the inclusion-dacite interface along a 1-cm long transect (red data points in Figures 3.14a and b). Temperatures of these pairs range from 1007-1078 ˚C, where highest temperatures are observed in the inclusion and the lowest temperatures are found away from the inclusion (Figure 3.14b). A second inclusion from a different sample gives similar temperatures results to the former inclusion (two pairs: 1086 ˚C and 1095 ˚C). However, three additional pairs in the second inclusion yield temperatures between 737-820 ˚C. This sample contains abundant exsolution lamellae providing evidence that some of these Fe-Ti oxides may have been intermittently subsolidus [*Von Gruenewaldt*, 1985].

By applying a series of different geothermometers to the magmatic system of Quizapu we can delineate a time-temperature evolution. Fe-Ti oxides thermometry records the late-stage (days to months prior to eruption) temperature distribution of the magmatic system [*Freer and Hauptman*, 1978; *Venezky and Rutherford*, 1999]. Pyroxene Mg-Fe interdiffusion re-equilibrates the crystal pairs on the order of months to hundreds of years [e.g., *Dimanov and Sautter*, 2000; *Morgan et al.*, 2004] and provides, thus, information about the long-term storage temperature for the recharge magmas. However, the presence of pigeonite indicates that some pyroxenes grew late immediately prior to eruption and suggesting that the two-pyroxene thermometer does not reliably record the long-term temperature evolution of the recharge magmas. In contrast, complementary amphibole-plagioclase thermometry reliably records the long-term temperature of the dacite magma. Re-equilibration by

diffusion in amphibole is very slow due to the coupled exchange of multiple elements. There is a lack of experimental data on elemental diffusion in amphibole, but metamorphic rocks that experience long time scale temperature path show sluggish elemental diffusion in amphibole [*Garcia-Casco*, 2002]. Figure 3.15 shows a time-temperature path for the magmas of the two eruptions based on the time scale of re-equilibration. While evolved magmas of the 1846/47 eruption experienced a late-stage heating from the recharge andesite, the 1932 dacite remained relatively cold at about 870 ˚C.

Pre-eruptive water contents can be estimated using the hygrometer of *Lange et al.* [2009]. Assuming average glass (glass compositions in Appendix B6) and plagioclase compositions from microprobe analyses together with temperature estimates from the amphibole-plagioclase geothermometer we estimate dacite water contents of 4-6 wt.%. The water contents of the 1846/47 and 1932 eruptions are indistinguishable from each other, which is consistent with the lack of significant amounts of quartz [*Whitney*, 1988].

Oxygen fugacity

Lavas from the 1846/47 eruption vary much more in the oxygen fugacities compared to their very tightly clustered dacites from 1932 (Figure 3.14). Oxygen fugacity has been calculated using the calibration of *Ghiorso and Evans* [2008]. Oxygen fugacity (fO_2) ranges in dacites from the plinian eruption from NNO +0.67 to NNO +0.71. Mingled dacites from the 1846/47 eruption have oxygen fugacities varying between NNO +0.74 and NNO +0.85. Hybridized andesites and mafic recharge magmas are more reduced with oxygen fugacities ranging from NNO +0.24 to NNO +0.53. The Fe-Ti oxide pairs that yield low temperatures and are affected by subsolidus alteration are the most oxidized samples with NNO +0.94 to NNO +1.34.

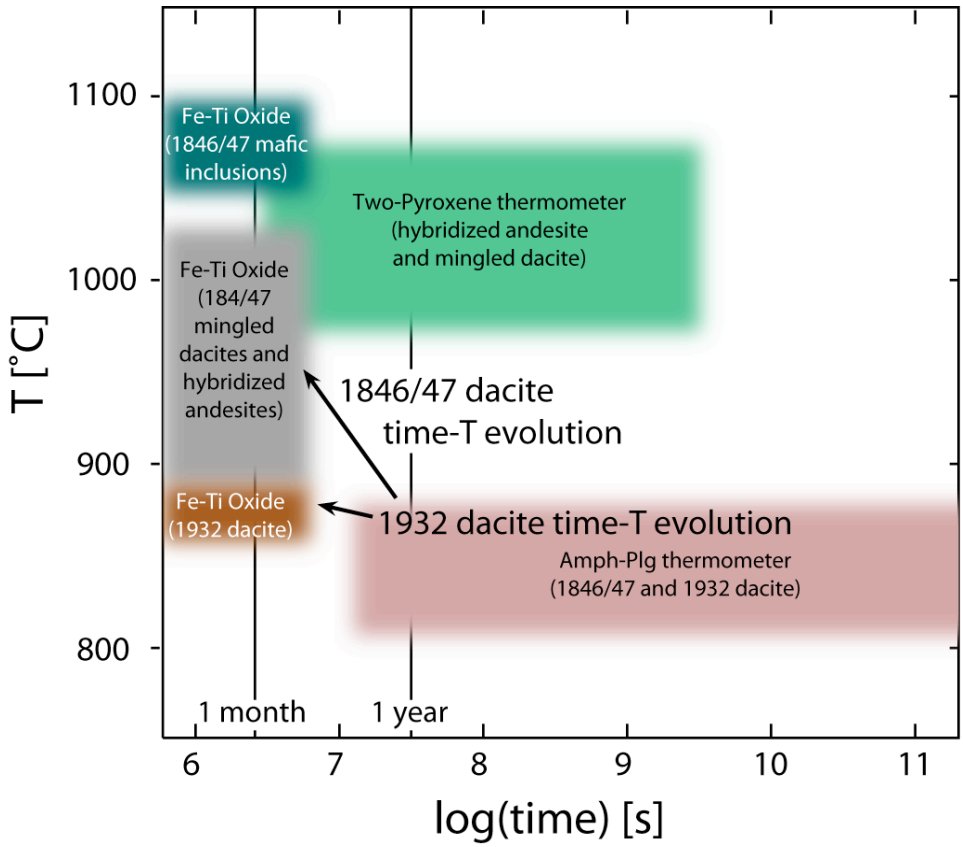

Figure 3.15 Conceptual Time-Temperature Evolution of Magmas from the Historic Quizapu Eruptions.

3.6 Building Blocks of the Quizapu Magmas

Thin section scale back-scattered electron maps provide an overview of the textural units found in the magmas in the two eruptions of Quizapu (Plates I-VI). The textural types closely follow the classification for the 1846/47 lavas into recharge magma/andesite inclusions, hybridized andesites and mingled dacite magmas based on the whole rock composition (Figure 3.2). Combining the thin-section scale textural information with the previously describe compositional variations allows us to deconvolve the building blocks that constitute the magma system of Quizapu.

Hybridized andesites from 1846/47 lavas are composed of a physically complete mixture of dacite and mafic andesite. Based on whole rock composition the ratio of dacite to andesite is about 3 to 2 (Plate I). Phenocrysts from the different end-members are evenly dispersed throughout the magma. The smaller phenocrysts, microphenocrysts and microlites are mostly of andesitic origin as evidenced by the CSDs and consistent with other studies that suggest microlite transfer during magma mixing [*Humphreys et al.*, 2009]. Andesite-derived plagioclase is in chemical disequilibrium with the hybrid magma, but it may respond to the cooling and depressurization with rim growth (~10 μm) thus adjusting to the new X-T conditions [*Ruprecht*, 2009; Chapter 4]. Olivines adjust to the new conditions either through diffusive re-equilibration [*Costa and Dungan*, 2005] or through growth as documented by the formation of normal zoned rims. In contrast, the late-stage pre-eruptive temperature increase and shift to a more mafic melt composition causes the dacite phenocrysts to be removed far from chemical equilibrium. This is seen in the resorption features in plagioclase and in the decomposition reaction of amphibole. The resorption of the dacitic phenocrysts results in a loss of the smaller size fractions and size reduction of the bigger phenocrysts as is seen by the overall shift of the CSDs in hybrid andesites to lower population densities for larger crystals. As a consequence, the hybridized andesites obtain a porphyritic texture [e.g., *Feeley and Dungan*, 1996], in which the large dacitic phenocrysts are dispersed in a magma that otherwise is dominated by the smaller crystals from the andesite.

In comparison to the hybridized andesites, mingled dacites from the 1846/47 eruption (Plate II to IV) maintain mostly their dacite character and texturally more closely resemble the 1932 dacites. Glomerocrysts provide evidence for the evolution of the dacite from a mush [*Bachmann and Bergantz*, 2004]. However, the high temperatures (~ 850 ˚C) of the dacites at Quizapu that are far from the eutectic (~ 700 ˚C; *Whitney*, 1988) require large lenses of magma of much lower crystallinity. In addition to the macroscopically visible andesite inclusions, small inclusions (< 5

mm) comprised of clots of mafic crystals and microlites are dispersed throughout the dacite and provide evidence for incomplete hybridization in the mingled dacites. The mingled dacites provide a snapshot for the process of mechanical disaggregation and slow incorporation as is proposed in many magmatic systems [e.g., *Bacon and Metz*, 1984; *Feeley and Dungan*, 1996; *Tepley et al.*, 1999]. The well-characterized end-members in this system therefore allow deconvolution of the mixing process. Similar to those in the hybridized andesites, dacitic phenocrysts also experienced elevated temperatures and disequilibrium conditions that resulted in crystal phenocryst dissolution.

Despite the compositional similarity among andesite inclusions (Figure 3.2), we find texturally distinct types of inclusions (Plate II to IV). They differ predominantly in their phenocryst content. Some inclusions contain large euhedral calcic plagioclase with strongly resorbed cores, while others contain plagioclase showing little evidence of disequilibrium. The andesite inclusions that contain resorbed plagioclase cores also contain rare sodic plagioclase that suggests that the small variation in whole rock composition (54 wt.% SiO_2 vs. 57 wt.%) may in fact be the result of small amounts of dacite magma mixing into andesite magma.

The crystal cargo of magma from the 1932 eruption is dominated by dacitic euhedral phenocrysts contrasting the complex textural and compositional variations from the 1846/47 lavas. Old glomerocrysts that have diffusively equilibrated with respect to their trace element compositions are present. Microlites are absent in these magmas further supporting the idea that microlites are transferred from andesite recharge magma into the dacite in the 1846/47 eruption. Similar observations have been made at Soufriere Hills [*Humphreys et al.*, 2009].

3.7 Discussion

3.7.1 Magma Mixing and the Generation of A Spectrum of Magma Compositions

Magma mixing is among other mechanisms (e.g., fractional crystallization) an important factor in contributing to the compositional diversity in arc magmas [e.g., *Gardner et al.*, 1995, *Eichelberger et al.*, 2000]. This diversity manifests itself on the crystal and on the whole rock scale. The 1846/47 eruption provides information on how much diversity can be attained by a single mixing episode. Compared to many other arc systems [e.g., *Clynne et al.*, 1999; *Tepley et al.*, 1999] the crystal-scale diversity of the 1846/47 eruption is quite restricted, where a few distinct crystal populations can be characterized. With additional mixing events the crystal-scale diversity may result in more and more complex crystal cargo. In contrast, the whole-rock diversity of mafic andesites, hybridized silicic andesites, and dacites is already established in a single mixing episode. Simple numerical mixing models support the distinct evolution of large-scale and crystal-scale diversity [*Ruprecht et al.*, 2008]. Thus, only the crystal record preserves a semi-quantitative record of increasing magma complexity over time.

3.7.2 Magma Homogeneity at Volcán Quizapu

Homogeneity on the crystal scale and the whole rock scale of the dacite magma system prior to magma mixing requires that the system was either born as a simple homogenous magma system or that there is an effective mechanism to restore homogeneity after open-system behavior. Magma stirring is the most effective processes to attain homogeneity, however many studies have shown that in crustal magma chambers, in which transient recharge or crystal dense rich-plumes initiate overturn and stirring, magma mixing is potentially incomplete and gradients in composition, temperature or other intensive variables develop [e.g., *Bergantz and Ni*, 1999; *Jellinek and Kerr*, 1999; *Huber et al.*, 2009]. More effective proposed

homogenization mechanisms such as melt compaction of a crystal mush [*Brophy*, 1991; *Bachmann and Bergantz*, 2004] or "mushification" and latent heat buffering near the eutectic [*Huber et al.*, 2009] require large crystal fractions. While mushification near the eutecitc is unlikely to produce the dacite magmas at Quizapu due to the high temperatures recorded in amphiboles, dacite melt extraction from an overall andesitic mush can explain many features observed in the dacite magma [*Brophy*, 1991; *Bachmann and Bergantz*, 2004].

An andesite mush in which interstitial dacite melt is extracted by mush compaction [*Bachmann and Bergantz*, 2004] is envisioned to form the bulk of the eruptible part of the Quizapu magma chamber. Andesitic mush that is stored in the crust has a dacitic melt composition and requires andesite magma temperatures of less than 900˚C at 65% crystallinity [*Murphy et al.*, 2000]. A rigid mush may develop at even higher temperatures and lower crystallinity [*Marsh*, 1989]. Within this dacite liquid new sodic plagioclase and amphibole grew at slightly lower temperatures (~850˚C) with little record of andesite-derived cores. The low crystallinity (~20%) in the dacite supports dacite melt extraction from a crystal mush and subsequent crystal growth of distinct dacite-derived crystals. The occasional presence of glomerocrysts and type Ic plagioclase crystals may reflect that some minor portions of the andesite mush were incorporated in the dacite magma during compaction. The andesite mush provides the heat to maintain a long-lived dacite magma chamber at ~850˚C. The overall longevity of the dacite magma system is unknown, but Ra-Th plagioclase separate ages suggest at least thousands of years of dacite magma chamber existence [*Ruprecht*, 2009; Chapter 4]. Continuous recharge of the andesite mush may have stabilized the architecture of the Quizapu system and established a warmer lower part of hotter (>1000˚C) andesite magma. Some mafic recharge may have breached the andesite mush that physically separated cold dacite from hotter andesite. Once hot andesite magma interacted with dacite magma, mingling and mixing occurred on various length scales to form most of the erupted

mingled dacite and hybridized andesite of the 1846/47 eruption. The chilling of the andesite against the dacite resulted in andesite magma vesiculation and buoyant rise of the mingled and mixed magmas. While these magmas erupted in the 1846/47 eruption, mainly homogenous dacite magma overlying the remaining andesite mush was left behind. This may explain why the following eruption in 1932 was volumetrically dominated by homogenous dacite. The model of dacite magma mixing with hot recharge and andesite mush magma also provides an explanation for the variability of andesite-derived crystals (type III and IV), where some may derive from the andesite mush and are less mafic and others are derived from the decompressing recharge magma that may result in sieve-textured plagioclase [*Nelson and Montana*, 1992]. Similar models of recharge and magma dynamics have been proposed elsewhere [*Kayzar et al.*, 2009].

3.7.3 Magma Mixing During Solid-Liquid Disaggregation of Andesite Inclusions and the Implications for Deciphering Post-Mixing Records

Microlite growth has been shown to occur during the final stages of magma ascent in the volcanic conduit [*Geschwind and Rutherford*, 1995; *Hammer and Rutherford*, 2002]. However, as seen in mingled dacites from Quizapu and other examples [e.g., *Feeley and Dungan*, 1996; *Humphreys et al.*, 2009] hybridization during magma mixing and mingling may result in the presence of lots of microlites in the dacite magma that is independent of late-stage decompression and eruption. Andesite inclusions are filled with microlites as a consequence of the chilling of andesite recharge against cold dacite magma. In the case of Quizapu up to 70 % of the recharge magma is composed of microlites. While decompression will further enhance microlite growth, a large fraction of the microlites is already present in the magma plumbing system during the solid-liquid disaggregation. The observation of apparent reheating as a consequence of decompression and crystallization proposed for arc andesite volcanoes [*Blundy et al.*, 2006] may in fact represent the

hybridization process at depth independent of the magma ascent. *Blundy et al.* [2006] argue that the correlated increase in temperature, and crystallinity with decreasing pH_2O is directly a consequence of crystal growth during magma ascent and not a result of magma mixing. The samples examined by *Blundy et al.* [2006] lack macroscopic evidence of magma mixing. In the case of Quizapu magma mixing is documented on the macro- and micro scale. While phenocryst crystallinities in mingled dacites and hybridized andesite remain similar at ~ 20 %, the solid-liquid disaggregation mechanism of the inclusions, results in the same observations presented by *Blundy et al.* [2006]. Overall crystallinities (phenocrysts + microlites) in the mixed dacites will increase due to magma mixing and the addition of microlite-rich recharge magma. Temperature also increases significantly during mingling and mixing. Though magma chamber pH2O has not determined for magmas of Quizapu, the low H2O solubility in andesites compared to amphibole-bearing dacites suggest that with ongoing magma mixing the pH2O of the mixed magmas would decrease by mass balance. Therefore, magma mixing is likely to result in the same characteristic observed effects as the decompression-reheating model by *Blundy et al.* [2006]. If hybridization is complete and macroscopic evidence for magma mixing is missing, low pH2O, high crystallinity at high temperatures can erroneously be interpreted purely as a conduit reheating process during decompression.

3.7.4 Reheating During Magma Mixing and Implications for Effusive Eruptive Behavior of Silicic Water-rich Magmas

Mafic hot recharge magmas provide large amounts of energy to reheat silicic andesite and dacite magmas in the shallow crustal magma chambers. Similar to Quizapu, andesite inclusions are present in many arc magma systems [*Murphy et al.*, 1998; *Costa and Singer*, 2002; *Holtz et al.*; 2005; *Zellmer et al.*, 2007] demonstrating that late-stage mingling and mixing is an ubiquitous process in arc magmas. Magma systems, for which extensive temperature information exists for the distinct magmas,

show large temperature differences (~100-200˚C) between cold host magmas and hot recharge magma (e.g., Montserrat [*Murphy et al.*, 1998]; Unzen [*Holtz et al.*, 2005]). Reheating is typically observed in the host dacite magmas. Such a reheating would have a strong effect on the viscosity of the dacite magma [e.g., *Hess and Dingwell*, 1996; *Giordano et al.*, 2008] and on the dissipation of frictional stresses in the conduit.

The simple system of Quizapu with its two eruptions of contrasting eruptive behavior provides evidence that the reheating of the dacite magma drives the system into effusive eruptive behavior. A similar temperature increase may lead also in other arc systems to a reduced explosive potential. Although higher magma crystallinities and as a consequence higher magma viscosities characterize these systems, the reheating from the recharge magma may offset partially the higher viscosity due to higher crystallinity. Furthermore, as shown in the previous section and by *Humphreys et al.* [2009] microlites can be substantially derived from recharge magmas and may only subordinately result from decompression nucleation and growth. Thus, dacite magmas that are crystal-rich once they reach the surface may initially have had much lower crystallinity and thus lower viscosity and thus may have facilitated passive degassing early in the ascent history. Moreover, even though magma viscosity is higher for magmas with high crystallinity, bubble movement through the melt is alleviated due to the lower melt viscosity as a result of reheating.

3.8 Conclusions

The lavas from the 1846/47 eruption of Volcán Quizapu contain petrologic evidence for mixing of cold dacite magma residing in the subvolcanic plumbing system with hot andesitic recharge magma. During this magma mixing the andesite magma gets chilled resulting in enhanced microlite growth and the formation of rigid andesitic inclusions. Parts of the mafic andesite completely mix with the host dacite magmas to form macroscopically homogenous porphyritic hybridized andesites. The

1846/47 dacites are hybridized with the mafic andesite to various degrees, indicated by the presence of andesite-derived plagioclase and olivine crystals in the dacite magma. The simple overturn as a result of andesitic recharge produces a large spectrum of magma compositions (Figure 3.2). The partial mixing present in the dacite magmas is a result of solid-liquid disaggregation of the andesite inclusions. During magma mixing and ascent the andesite inclusions are slowly eroded as dacite magma shears off the exterior of the andesite inclusions. In contrast to the 1846/47 lavas, the erupted deposits of the 1932 plinian eruption provide evidence for a predominantly dacitic eruption. There is only small interaction with mafic recharge magma in the bulk of the dacite.

The mixing of mafic magma into the dacite is accompanied with a significant reheating event by the about 200 ˚C hotter recharge andesite mixed into the cold dacite (~845 ˚C). Multiple mineral-mineral equilibrium thermometers indicate that post-mixing magmas reach temperatures of ~1000 ˚C (Figure 3.15). The heating of the dacite and simultaneously cooling of the recharge magma affects the crystal-cargo as well as the eruptive style of the dacite eruption of 1846/47 at Quizapu. Dacite-derived crystals respond by partial dissolution, while andesite-derived crystals experience extensive undercooling, which results in microlite- and rim growth. As a consequence, porphyritic textures and strongly curved CSDs are developed. At Volcán Quizapu, the evidence that reheating occurs during magma mixing further underlines that late-stage reheating may not be a result of decompression induced crystallization and latent heat release during the final ascent in the conduit. Increase in temperature and crystallinity may in fact be both caused by the recharging andesites. The reheating of the dacite also leads to a reduction of the melt viscosity in the dacite. This viscosity reduction and the ensuing reduction of frictional stresses in the conduit may be responsible for the effusive eruptive behavior in 1846/47. The late-stage pre-eruptive magma temperature of the 1932

eruption remained cold, thus causing an explosive eruption triggered by only subordinate recharge magmas.

Results of this study indicate that the dacites from Volcán Quizapu reflect the eruptible magma that is residing in the subvolcanic plumbing system, opposing models that envision a shallow crustal andesitic magma chamber recharged by ascending dacite magma [*Eichelberger and Izbekov*, 2000; *Maksimov*, 2008]. The high temperatures observed in mafic recharge magmas indicate a deep origin of the andesites, which otherwise at more shallow levels would quickly cool. Moreover, the reheating of the dacite from the andesite and the reduction in viscosity of the dacite may alleviate magma ascent and passive-degassing in the dacite. As a consequence the water-rich dacite at Quizapu erupted effusively.

Plate I

1846/47 Hybridized andesite (60.5-62 wt.% SiO2)

VQ-10 (60.78 wt.% SiO2)

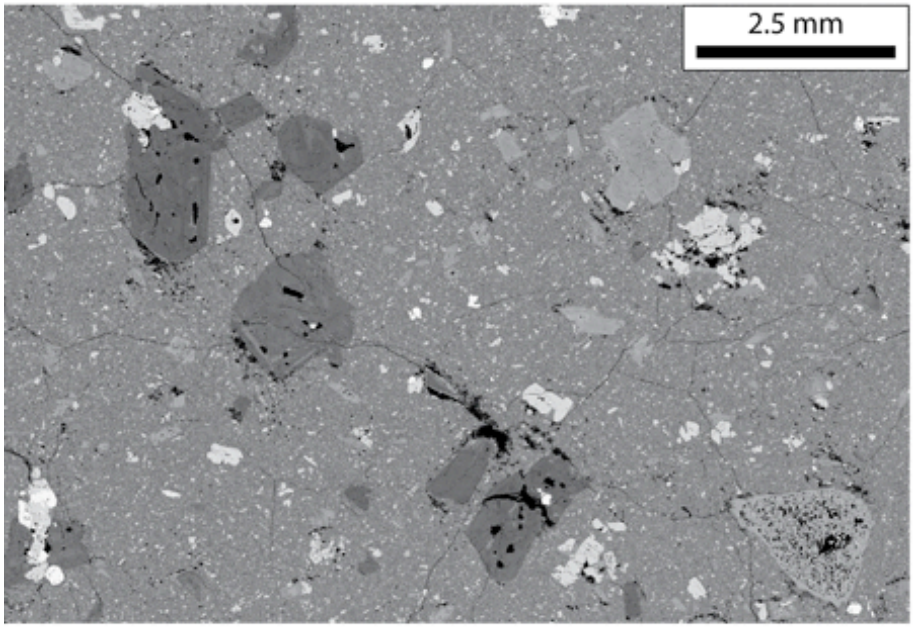

VQ-02 (61.37 wt.% SiO2)

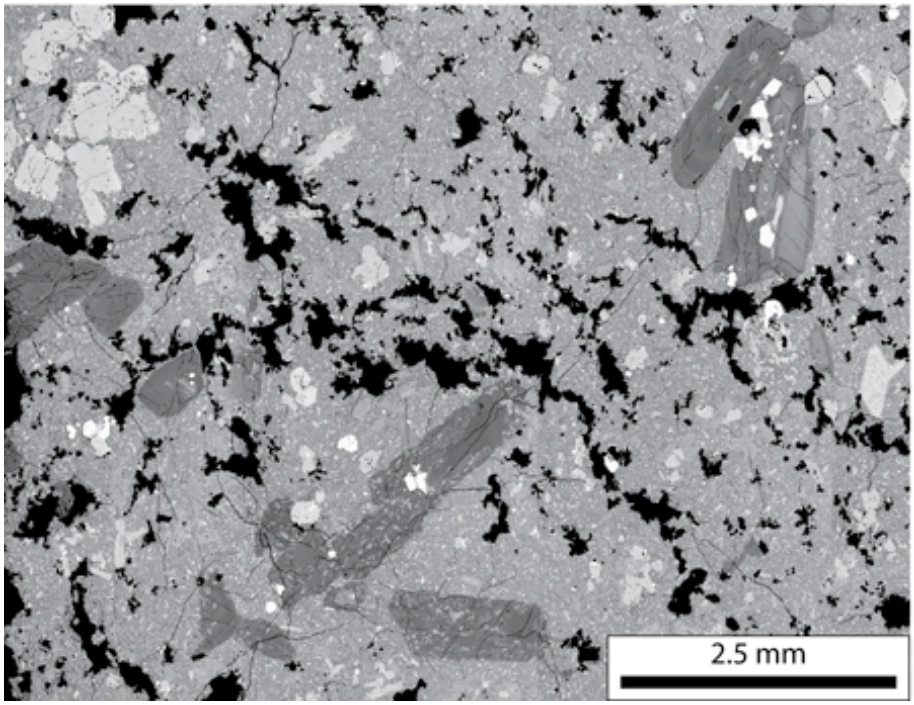

Plate II

1846/47 Mingled dacite (63-68 wt.% SiO2) and mafic enclaves (54-57 wt.% SiO2)

VQ-22 (63.29 and 53.85 wt.% SiO2)

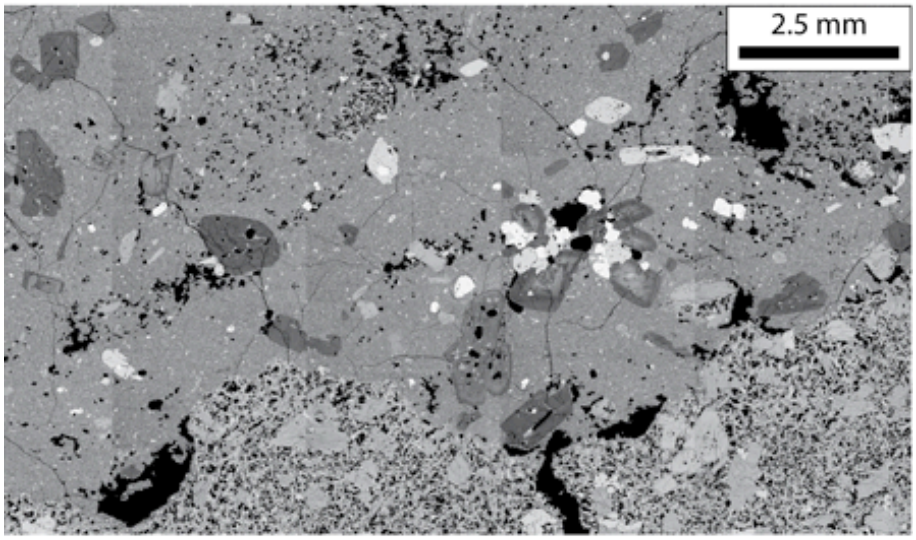

VQ-44 (64.73 and 56.91 wt.% SiO2)

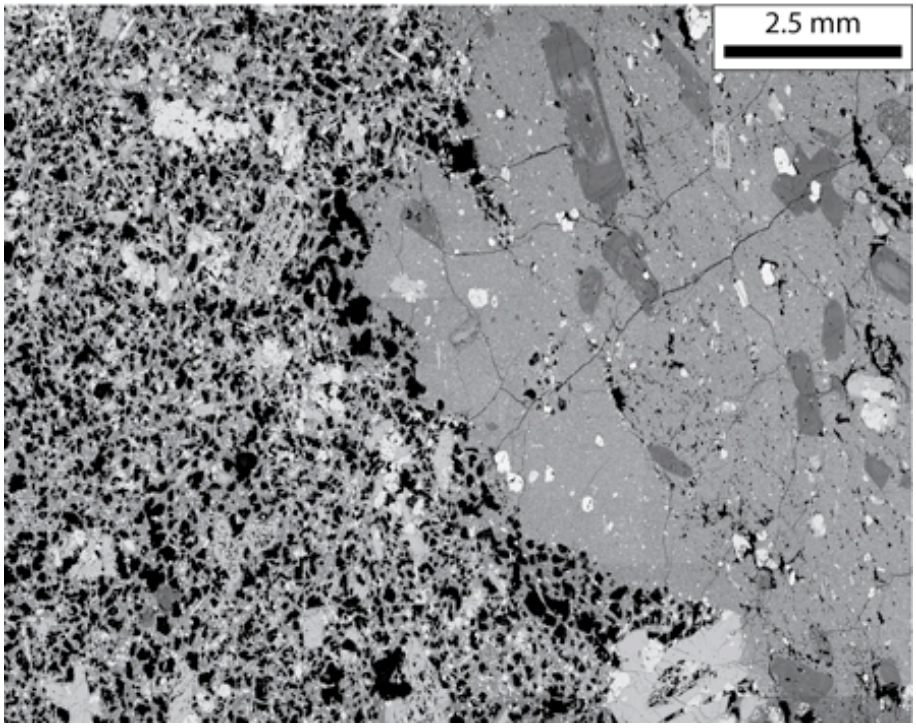

Plate III

1846/47 Mingled dacite (63-68 wt.% SiO2)

VQ-11 (65.71 wt.% SiO2)

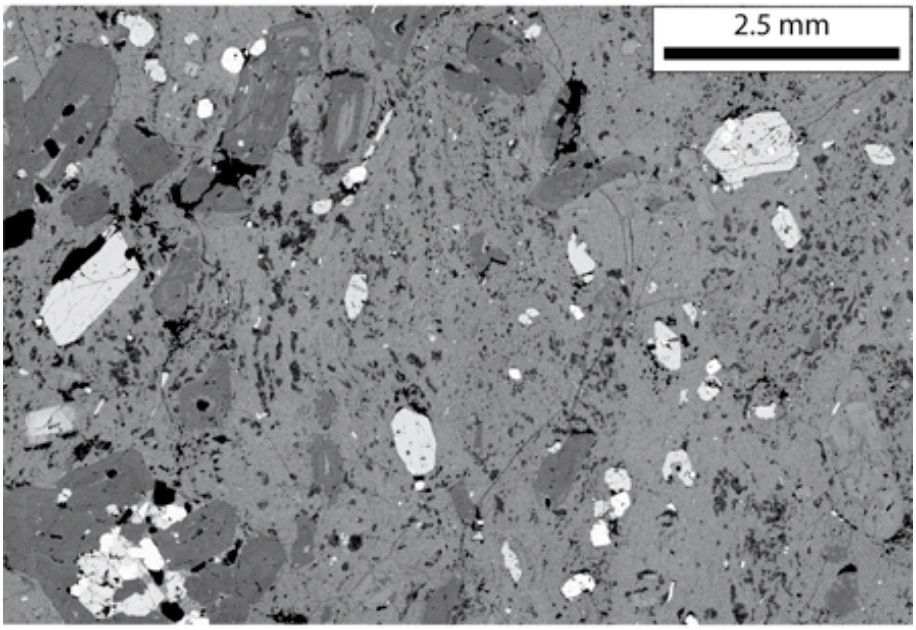

VQ-06 (65.89 wt.% SiO2)

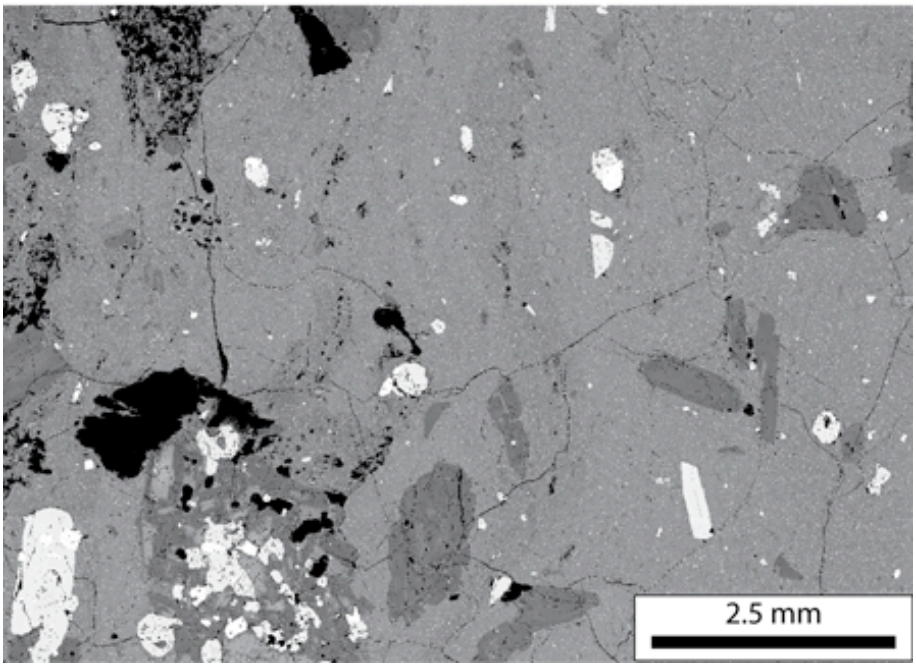

Plate IV

1846/47 Mingled dacite (63-68 wt.% SiO2)

VQ-24 (65.27 and 56.78 wt.% SiO2)

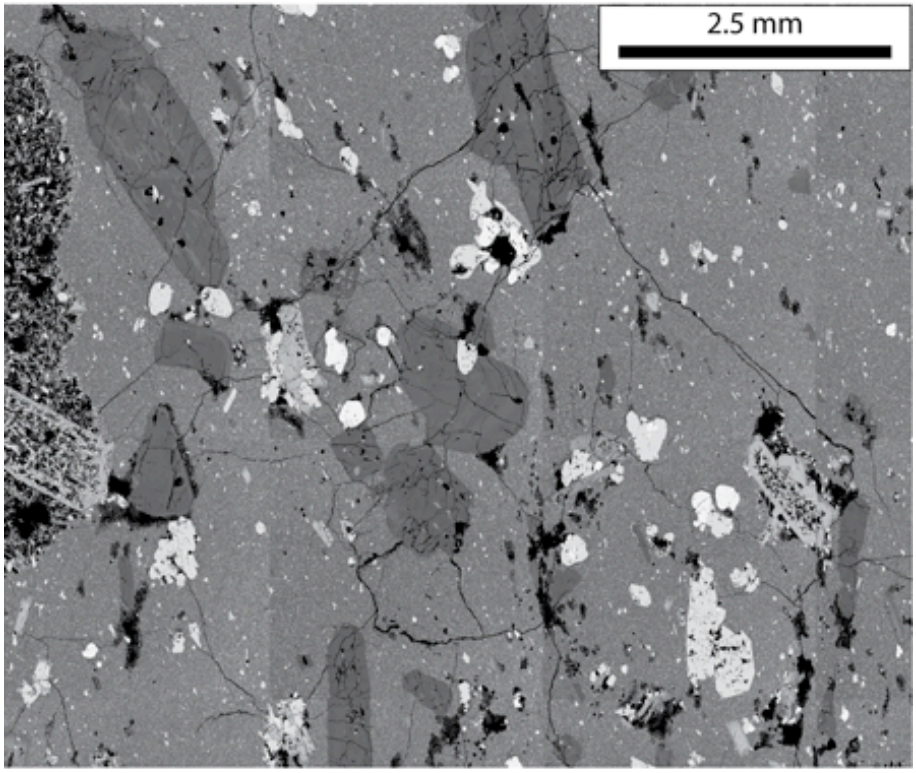

VQ-14 (65.80 wt.% SiO2)

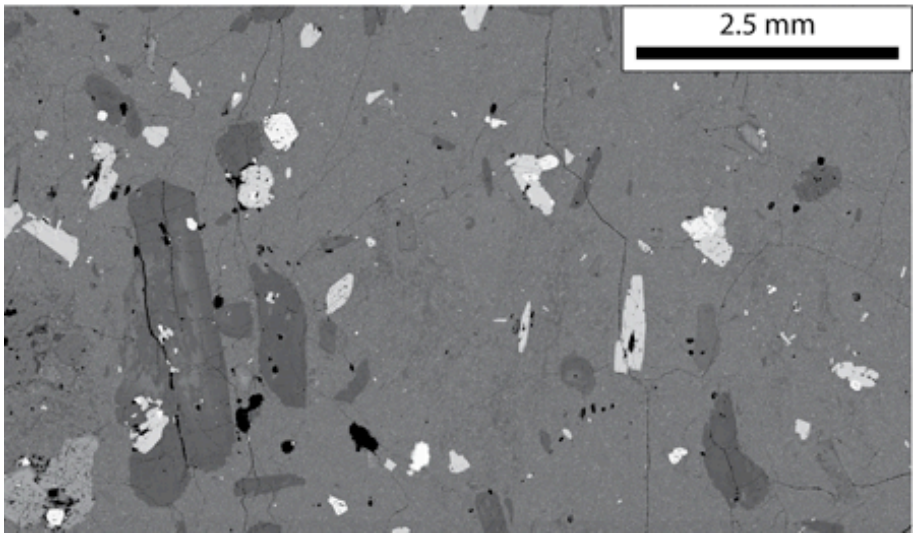

Plate V

1932 dacite (66-68 wt.% SiO2)

VQ-17 (66.30 wt.% SiO2)

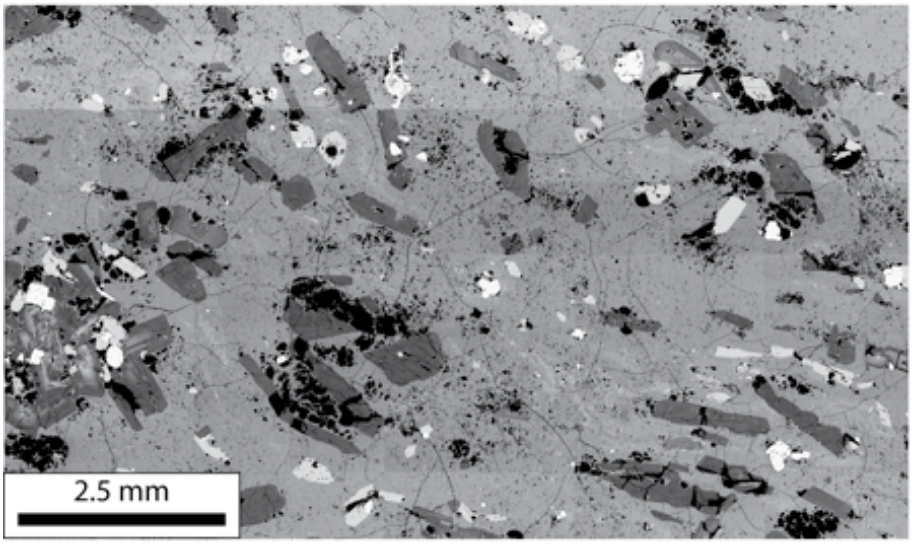

Q-6 (68.12 wt.% SiO2)

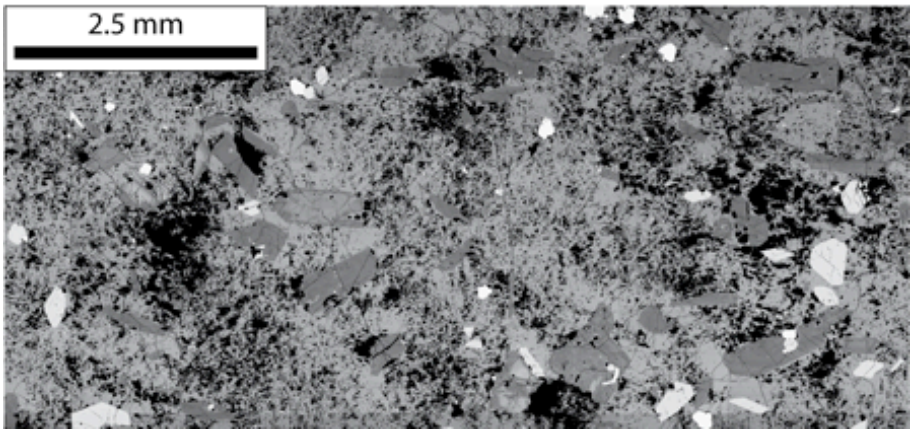

Plate VI

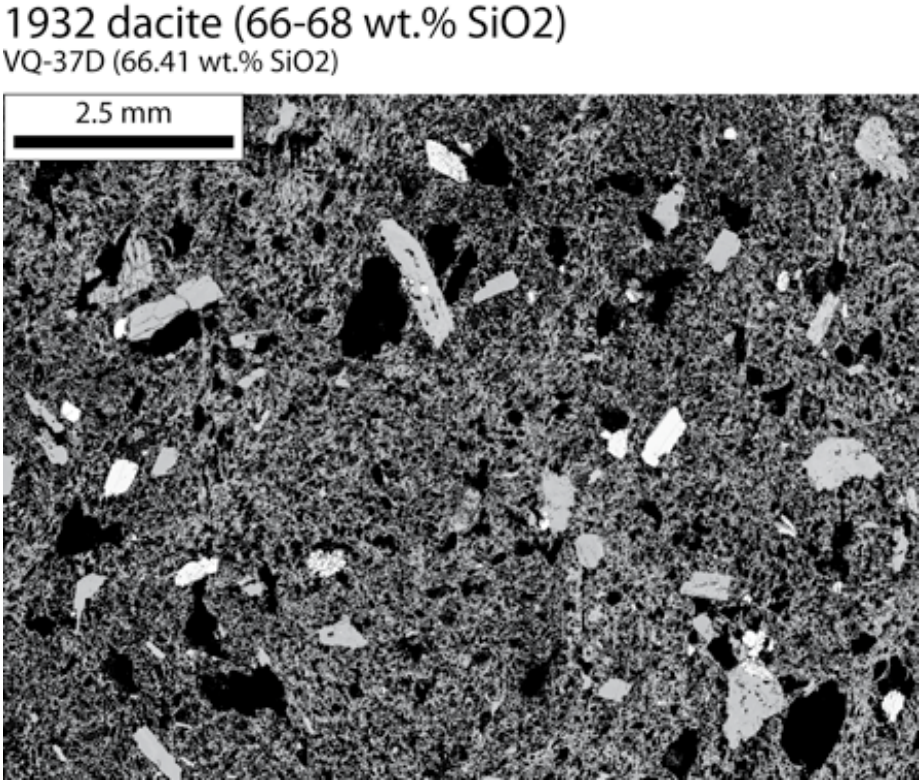

- Chapter 4 -

Crystal Residence Times in Mixed Magmas from Volcán Quizapu – Reconciling Different Geochronometers

4.1 Introduction

Continental arc magmas frequently contain macro- and microscopic evidence for magma mixing [e.g., *Hildreth and Drake*, 1992; *Clynne*, 1999; *Costa and Singer*, 2002; *Coombs et al.*, 2003; *Bacon and Lanphere*, 2006; *Browne et al.*, 2006]. The time scales of crystallization and crystal storage as well as recharge and magma mixing are essential for our understanding of the evolution of long-lived shallow crustal magma systems [e.g., *Reid*, 2003; *Cooper and Reid*, 2008] and the monitoring of volcanic hazards [e.g., *Sparks*, 1977; *Costa and Dungan*, 2005]. Recharge magmas are transient disruptions of the chemical and energetic balance that modify the crystal record linked with crystallization and crystal storage, and provide new heat to keep the magmatic system above its solidus.

Understanding the temporal relationship of phenocryst growth, magma recharge, mixing, and eruption requires chronometers that provide absolute and relative age constraints on the different magmas in the shallow crustal system. The uranium-238 decay series provides us with a unique tool to investigate the time scales of crystallization and residence in the magmatic system in an absolute sense [*Condomines et al.*, 2003; *Reid*, 2003; *Cooper and Reid*, 2008], while elemental diffusion can be exploited to extract time information from transient magma chamber processes that is independent of the absolute age of a crystal [e.g., magma mixing; *Zellmer et al*., 1999; *Costa et al*., 2003; *Morgan et al*., 2004]. With respect to the uranium-series dating technique, the ^{238}U-^{230}Th and the ^{226}Ra-^{230}Th parent-daughter

pairs in particular have half-lives that are comparable to timescales of magma storage, and have been shown to provide absolute age constraints on the crystallization of major and accessory phases in magmatic systems [see recent review by *Cooper and Reid*, 2008]. ^{238}U-^{230}Th mineral isochron ages can be applied to systems as old as a few 100 kyrs [e.g., *Condomines et al*., 2003], therefore enabling studies of long-term evolution of a volcanic center [e.g., *Jicha et al*., 2005, 2007, 2009]. However, the ^{238}U-^{230}Th mineral isochron dating technique typically cannot resolve absolute ages better than several thousands of years. In the case of very young eruptions, the ^{226}Ra-^{230}Th system can be applied and can resolve time scales as short as hundreds of years. Thus, ^{226}Ra-^{230}Th dating is often much more powerful in distinguishing the temporal relations of crystal growth, residence, and eruption, where an individual transient processes like magma recharge is studied. Furthermore, for a scenario of an individual magma recharge event, elemental diffusion modeling can resolve the timing of the recharge with respect to the eruption [e.g., *Costa et al*., 2003]. Elements incorporated in the major magmatic phases span a large range of diffusion rates, and therefore provide access to a large range of time scales [*Cherniak*, 2003]. Choosing an element with the appropriate rate of diffusion allows us to match the time scale of magmatic processes. Mg, Sr, and Ba diffusion in plagioclase have been used frequently to understand magmatic processes [*Costa et al.*, 2003; *Zellmer et al.*, 2003]. While Sr and Ba access long time scales (years to centuries) of magmatic processes, the fast diffusion of Mg in plagioclase at magmatic temperatures enables us to investigate the time scales of magma recharge that may occur within days to years.

We present ^{238}U-^{230}Th and ^{226}Ra-^{230}Th crystal ages for samples of the two historic eruptions of Volcán Quizapu (1846/47 and 1932) in the Chilean Andes [*Domeyko and Tocornal*, 1849; *Hildreth and Drake*, 1992]. The 1846/47 eruption is characterized by magma recharge and the formation of andesite inclusions dispersed in many flow lobes of the largely dacitic effusive eruption. We analyzed plagioclase

mineral separates for ^{238}U-^{230}Th and ^{226}Ra-^{230}Th from several units of both historic eruptions. In the case of the 1846/47 eruption we investigate magmas that showed micro- and macroscopic evidence for dacite-andesite interaction. In addition to U-series crystal residence ages, we also present time scales from Mg diffusion in plagioclase in a hybridized andesite from the 1846/47 eruption. The second eruption in 1932 of Volcán Quizapu shows little andesite-dacite interaction. Instead, we can use the eruptive products of this eruption as an analog for the unmodified dacite end-member of the 1846/47 eruption to investigate how magma mixing may alter the time scales of crystallization and crystal storage.

4.2 Time Scales of Magma Chamber Evolution

The decay of uranium-238 to its intermediate nuclides and to its final daughter product lead-206 has been used in various dating techniques to understand subvolcanic plumbing systems. Recently, uranium-series age dating has been mainly applied to determine the crystal residence in magmatic systems [e.g., *Pyle et al.*, 1988; *Bourdon et al.*, 1994; *Reid et al*., 1997; *Zellmer et al.*, 2000; *Cooper et al*., 2001; *Cooper and Reid*, 2003; *Jicha et al.,* 2005*; Turner et al*., 2003; *Tepley et al.*, 2006; *Bachmann et al*., 2007; *Simon et al*., 2008]. Many studies have shown that the obtained crystal residence ages have to be interpreted in the light of complex crystal populations containing phenocrysts, antecrysts, and xenocrysts [e.g., *Heath et al*., 1998; *Cooper and Reid*, 2003; *Reagan et al*., 2006; *Tepley et al*., 2006; *Cooper and Reid*, 2008]. In particular, studies using the uranium-series decay chain have shed light on the prolonged evolution of magmatic systems [*Reid et al.*, 1997; *Simon et al.*, 2008]. During eruptive periods a volcanic system can tap magmas recently emplaced in the shallow crust, remnant magma from previous episodes of magmatic activity within the same system (i.e., antecrysts) and/or recycled crustal material (xenocrysts). While the long-lived parent-daughter pairs within the decay chain (^{238}U-^{230}Th and U-Pb) are valuable in characterizing the longevity and overall evolution of a magmatic system, they lack the resolving power to investigate the

time scales associated with individual magmatic processes, such as degassing or magma mixing. The shorter-lived parent-daughter pairs (e.g., ^{226}Ra-^{230}Th and ^{226}Ra-^{210}Pb) have been successfully applied to understanding actively degassing magmatic systems [*Gauthier et al.*, 1999; *Kayzar et al*., 2009] as well as to quantifying time scales of crystal growth and storage [*Volpe and Hammond*, 1991; *Pietruszka et al*., 2001; *Cooper and Reid*, 2003; *Turner et al*., 2003].

While most studies have investigated the evolution of a magmatic system over multiple eruptions, this study focuses on deconvolving time scale information from different flow units with distinct textural and chemical signatures within a single eruption. This approach provides an opportunity to investigate the homogeneity of the crystal residence age population within a single eruption. A larger goal of this approach is to compare ages of crystals in the dacite and andesite end-members in order to understand the pre-mixing history of different magmas in the system. Moreover, comparing crystal residence ages of the 1846/47 and 1932 eruptions allows us to examine how crystal populations have changed in the intervening time.

As noted earlier, elemental diffusion age dating provides time scale information for processes that alter the chemical environment in which the crystals are stored. Such changes may occur either as crystals themselves are redistributed within the magmatic system or as the surrounding melt changes bulk composition as a result of crystallization, mixing, or assimilation. Diffusion ages have been successfully applied in identifying remobilization of older antecrystic material and determining the time scale of storage of such remobilized material [e.g., *Zellmer et al*., 2003; *Morgan and Blake*, 2006]. Furthermore, magma mixing time scales have been derived from elemental diffusion in olivine, pyroxene, plagioclase, and Fe-Ti oxides [e.g., *Nakamura*, 1995; *Venezky and Rutherford*, 1999; *Costa et al*., 2003; *Morgan et al*., 2004; *Costa and Dungan*, 2005].

4.3 Analytical Methods

Plagioclase, glass, and groundmass separates were initially purified using magnetic separation. Plagioclase separation was performed for selected samples on multiple size fractions (75-125 μm, 125-250 μm, and 250-500 μm). Pure plagioclase separates were generated using large magnetic fields and very shallow angles of separation. Two samples were obtained as separates from W. Hildreth (Q-4, Q-6). A third sample (Q-34) obtained from Hildreth was separated at the University of Washington, but not sieved to extract different size fractions. Visual estimates of glass contamination using a binocular microscope are less than ~ 1% and have been confirmed through back-scattered electron (BSE) imaging of grain mounts. Thus, an additional purification by handpicking was not required after inspection with the binocular microscope. Small amounts of contamination by quartz (<1 vol. %) have been observed in grain mounts using BSE imaging and energy-dispersive x-ray analyses. After magnetic separation of plagioclase, glass, and groundmass, separates were cleaned by ultrasonication in acetone, water, and dilute HCl and rinsed multiple times with de-ionized water. The procedures for sample digestion, U, Th, Ra, and Ba purification and analysis by multi-collector inductively-coupled plasma mass spectrometry (MC-ICPMS) are described in detail in *Cooper and Donnelly* [2008]. In short, ~1-3 g of plagioclase and glass separates as well as whole rock powder were dissolved by microwave acid digestion with hydrofluoric and nitric acids followed by evaporation with boric acid. Dissolved samples were stored in hydrochloric, saturated boric, and trace hydrofluoric acid. Two small aliquots of the sample solutions equivalent to 3-25 mg and 10-250 mg of rock or mineral were analyzed for (1) Ba concentrations and (2) U and Th concentrations, respectively, using isotope dilution. Another small aliquot (10-50 mg) of the plagioclase samples was analyzed for trace elements using a quadrupole ICP-MS at University of California, Davis. The remaining (and largest) aliquot was used for Ra concentration measurements using isotope dilution and U–Th isotopic composition measurements. A combination of Eichrom TRU™ resin and anion and cation exchange resin was used to purify the

elements of interest. Prior to column chemistry isotope dilution aliquots were spiked and equilibrated with ^{135}Ba, ^{233}U, ^{229}Th, and ^{228}Ra, respectively. Isotope measurements were performed at the University of Washington and the University of California, Davis, on NuPlasma MC-ICP-MS instruments at each institution. Data accuracy and reproducibility was monitored by analysis of several rock standards (BCR-2, TML, W-2, BHVO-2) over the course of the study. Uncertainties (including in-run standard error and uncertainties in spike calibration measurements) were <0.5% for Th, U, and Ba concentration measurements by isotope dilution. Uncertainties on Ra concentrations are given in Table 4.1. Reproducibility was assessed by replicate measurements of rock standards and solution standards, and was better than 1% for all concentration measurements and for U and Th isotopic composition measurements. Total-process blanks for Ra, Th, U, and Ba were monitored, and were corrected for during calculations of concentrations from the isotope dilution measurements, although they were negligible compared to the sample size.

4.4 Volcán Quizapu – Geological Background

Crustal magma chambers evolve over time by crystallization, crystal storage and fractionation as well as by recharge of (typically mafic) magmas that lead to magma mixing [*Davidson et al.*, 2007]. These processes create complex crystal populations in most arc magmas, for which it is often difficult to decipher meaningful time scales associated with crystallization, storage, and recharge. Unless we can account for the different crystal components of a magmatic system, the mixed ages of bulk mineral separates can be difficult to interpret. In particular, interpretations based on bulk crystal separates to understand the time scales of magmatic processes can be rendered erroneous in the case of complex crystal populations. Therefore, a petrologically simple magmatic system [e.g., *Cooper et al.*, 2001] is required to quantify the time scales of crystallization and storage of individual crystal populations. In more complex cases obtained information from

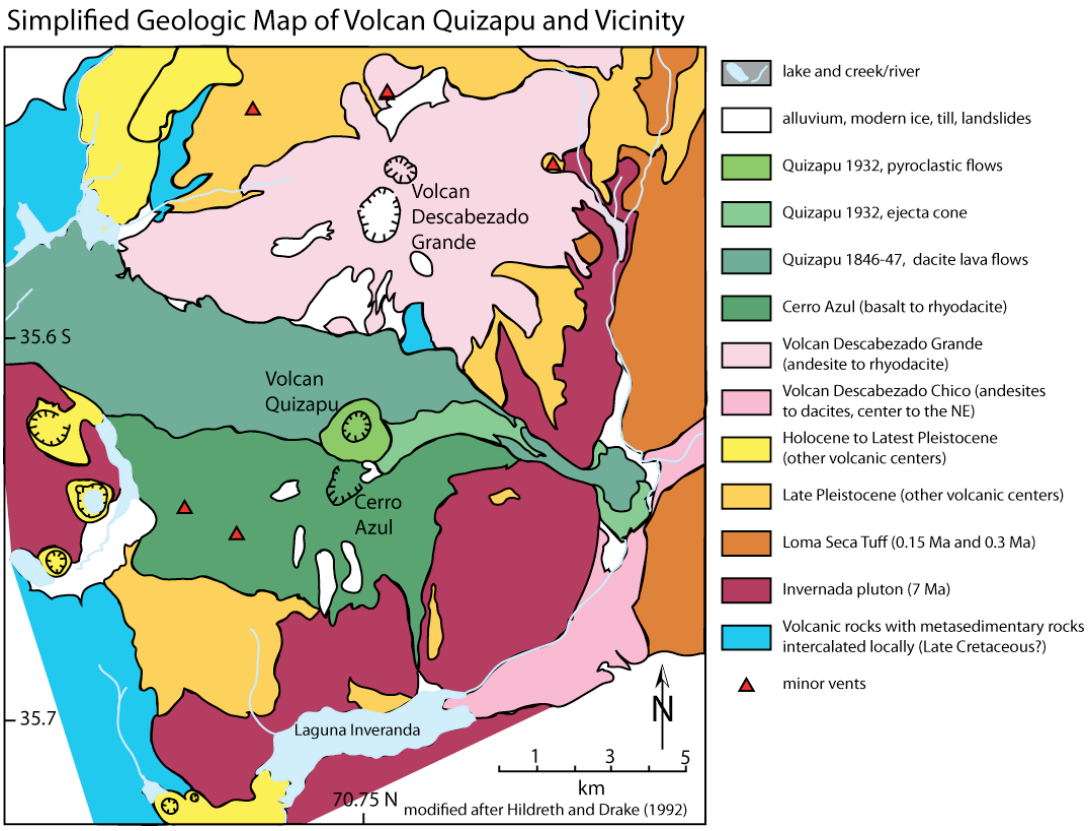

Figure 4.1 Simplified geologic map. Sample for this study were taken from the lavas of the 1846/47 eruption and fall deposits of the 1932 Plinian eruption.

U-series age dating may provide only qualitative information about the time scales and storage of crystal populations.

In contrast to most arc volcanoes, Volcán Quizapu displays a simple shallow crustal history of magma storage and recharge [*Hildreth and Drake*, 1992; Figure 4.1]. Quizapu is a prime location to study the timing of crystallization, crystal storage, and magma mixing due to the excellent age control of the two historic eruptions (1846/47 and 1932). Both eruptions are significant in volume having each erupted 4-5 km^3 of mainly dacite magma. This dacite magma, which constitutes the bulk of the erupted material, shows a simple crystal cargo [*Ruprecht*, 2009; Chapter

3]. Simultaneously, Quizapu eruptions are characterized by mafic recharge magmas that are associated with magma mixing prior to eruption. In the 1846/47 eruption, mafic recharge and subsequent magma mixing and mingling produced a series of hybridized andesites and mingled dacites with various proportions of andesite recharge magma. Mingling refers to the stage of magma-magma interaction when distinct magma batches are still macroscopically distinguishable by textural or color differences and the presence of sharp gradients between these different magmas. In contrary, we refer to mixing when the magma-magma interaction has progressed to the point where the macroscopic evidence of two distinct magma batches has been erased as a result of continuous stirring and redistribution. The 1932 eruption shows little physical mixing between mafic recharge magma and dacite host magma. The crystal components of the recharge magma are chemically distinct from the dacite-derived crystals, and thus can be tracked whenever occurring in mingled and mixed magmas of the historic Quizapu eruptions [*Ruprecht*, 2009; Chapter 3].

4.5 Distinguishing Crystal Populations at Quizapu: Mingled Dacite VQ-22 – A Simple Case for Magma Mixing

In the following, we use crystal-chemical and textural information similar to that presented by *Salisbury et al*. [2008] to identify different crystal populations in a mixed magma of Volcán Quizapu. By applying the criteria obtained in this characterization to all magmas from Quizapu we can quantify the proportions of various different crystal populations. As noted earlier, this is crucial when interpreting bulk mineral separate data of complex crystal populations.

The mingled dacite VQ-22 is used to evaluate the mixing processes in the 1846 eruption of Quizapu. Moreover, it constitutes our type sample to deconvolve the magma mixing and derive pure end-member compositions, since it is exceptionally well preserved and reflects a simple binary mixing between dacitic and mafic end members. VQ-22 shows macroscopic, microscopic and geochemical

evidence for incomplete hybridization and mingling. In this sample, magma mixing is manifested by the presence of light colored, vesiculated andesite inclusions (VQ-22A) that are macroscopically distinct from the surrounding dark colored, glassy porphyritic dacite (VQ-22D) (Figure 4.2a). The inclusions are dispersed throughout the dacite magma. While macroscopically the dacite suggests limited interaction with the andesite in the form of discrete, sharply bounded andesite inclusions [*Ruprecht*, 2009; Chapter 3], microscopic and chemical information reveals that magma mixing has advanced beyond mingling of dacite and andesite magma, and dacite hybridization is already in progress.

Textural and crystal-chemical information from VQ-22 provides evidence for a heterogeneous phenocryst assemblage in the dacite magma. In contrast, the phenocryst assemblage in the andesite inclusion is compositionally and texturally simple [Figure 4.2b-e]. A detailed description of the distinct plagioclase types that are found in the two historic eruptions of Volcán Quizapu is presented elsewhere [*Ruprecht*, 2009; Chapter 3].

Here, we use a back-scattered electron (BSE) map of a contact between an andesite inclusion and the dacite magma to illustrate the distinct chemical and textural characteristics of crystals within the dacite and andesite end-members. Firstly, the two major plagioclase populations in VQ-22, andesite- and dacite-derived plagioclase, can be distinguished by their anorthite (An) content, where low-An plagioclase, consistent with chemical equilibrium with a dacitic liquid, is interpreted as derived from the dacite, whereas high-An plagioclase is interpreted as derived from the andesite [*Ruprecht*, 2009; Chapter 3]. Dacite-derived plagioclase (low An, highlighted in orange in Figure 4.2c) is only found in the dacite end member, while andesite-derived plagioclase (high An, highlighted in yellow in Figure 4.2c) occurs in both the dacite and the andesite magma. Secondly, crystal-size distributions (CSD) for the two populations further reflect (Figure 4.2d) the distinct dacite- and andesite-

derived plagioclase populations present in VQ-22. Both populations have straight CSDs suggesting simple but distinct nucleation events for each population [*Marsh*, 1998]. The steeper CSD curves with smaller maximum crystal sizes for the andesite-derived plagioclase phenocrysts reflect the presence of more numerous smaller andesite-derived phenocrysts compared to dacite-derived plagioclase. In addition, CSDs for andesite-derived plagioclase populations in the inclusions and in the dacite end-member are parallel to each other. This suggests no significant crystallization or dissolution of these phenocrysts after the mixing event led to the entrainment of andesite-derived plagioclase crystals into the dacite end-member. A detailed description of CSDs in magmas from Quizapu can be found in [*Ruprecht*, 2009; Chapter 3]. Thirdly, dacite- and andesite-derived plagioclase phenocrysts are also distinct in trace element compositions. Figure 4.2e shows Mg concentrations for plagioclase from VQ-22 and other selected samples with An content ranging over 60 mol.%. Dacite-derived plagioclase ($< An_{56.5}$) has low Mg concentrations consistent with equilibrium growth for typical dacite magma temperatures and melt compositions. Equilibrium concentrations are calculated using a linear partitioning relationship as quantified by *Bindeman et al.* [1998]. In contrast, andesite-derived plagioclase ($> An_{56.5}$) has much higher Mg concentrations, suggesting an origin from more mafic, hotter magmas. Finally, mass balance calculations of whole rock compositions of the andesite and the mixed dacite end member (Figure 4.2f) provide a test to check for consistency of a simple mixing history of andesite and dacite magma for VQ-22. We assume that the dacite component of VQ-22 is a mixture of the recharge magma and the evolved dacite magma (compositionally similar to VQ-06). Both the andesite and the dacite end member were initially homogeneous on the crystal and whole rock scale. As a consequence of the mixing, a mixed dacite with two distinct phenocryst populations is formed, while the andesite remains homogeneous. We calculate a best-fit composition of the dacite component of VQ-22 using 19.7 vol.% of the andesite recharge magma and 80.3 vol.% of VQ-06. The minimum of the root-mean squares of the deviation between measured and

calculated major elements of the dacite component of VQ-22 is used as the measure for the goodness of fit. Calculated major element concentrations of the dacite component of VQ-22 match the measured concentrations within 1.1 % with the exception of TiO_2, which matches within 2.7 %. The calculated volume of andesite contribution to the dacite component of VQ-22 is consistent with the observed crystal volume fractions in VQ-22 of approximately 23 vol.% (3.1 vol.% of andesite-derived plagioclase in VQ-22D vs. 13.4 vol.% in VQ-22A). The discrepancy of 3.3 vol.% between the volume estimate from the major element mass balance calculation and the estimate from the crystal record could be due to minor andesite addition present even in the sample used to estimate the dacite end-member (VQ-06). VQ-06 also contains a small fraction (less than 7 vol.%) of andesite-derived plagioclase. Except for Ni and Cr, trace elements are also consistent with this simple mixing history. The Ni and Cr concentrations are more than 30 % lower in the calculated mingled dacite compared to VQ-22D and may stem from small variations in volume fractions of mafic accessory phases.

Combining plagioclase major and trace element compositions, plagioclase textures, and whole rock mass balance information provides evidence for simple mixing of andesite recharge and dacite host magma. While the evidence has only been shown here in detail for VQ-22, other samples show very similar geochemical and textural characteristics suggesting that all samples from Quizapu can be compared in a model of simple magma mixing. Following the observations from VQ-22 we use $An_{56.5}$ as our criterion to distinguish between andesite-derived and dacite-derived plagioclase in all other samples. In particular, this is important for the interpretation of model crystal residence ages from U-series disequilibria. Bulk mineral separate analyses require a careful characterization of the crystal cargo in a thin section to ensure meaningful interpretations of the results from the mineral separates. In addition to the characterization of crystal populations in the thin section

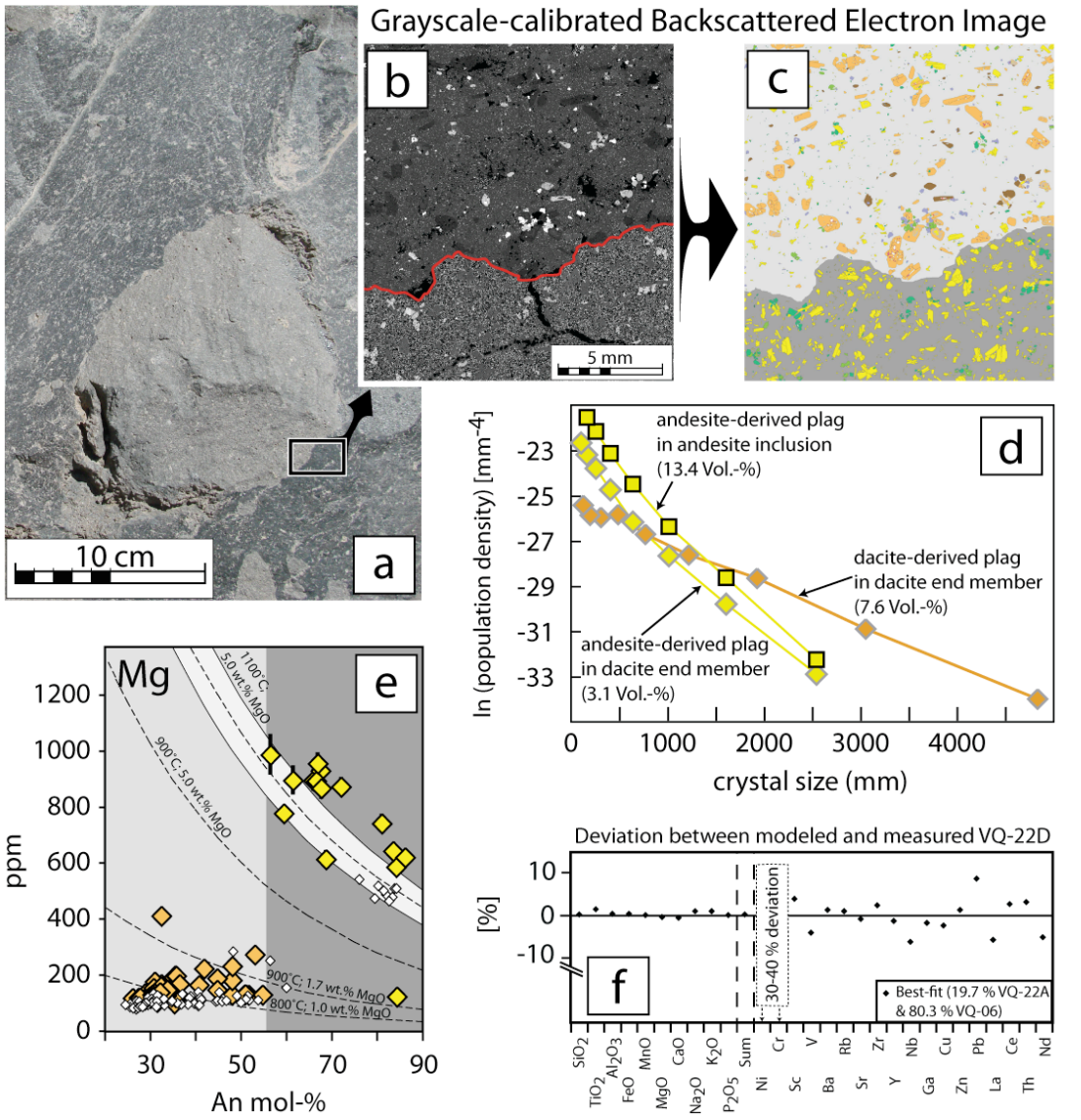

Figure 4.2 Simple Magma Mixing Documented in Various Textural and Chemical Signatures for Sample VQ-22. a) Field picture of an andesite inclusion in dacite magma. b) Electron microprobe backscattered electron (BSE) map of a contact between andesite inclusion and dacite magma. The contacts shown in a) and b) are from different andesite inclusions. c) Grayscale-interpreted version of the BSE map, show the andesite-derived plagioclase in yellow and the dacite-derived plagioclase in orange. d) Crystal-size distribution for the two different plagioclase populations. e) Mg concentrations in the two different populations. Symbols as follows: yellow = andesite-derived of VQ-22; orange = dacite-derived of VQ-22; white = unspecified measurements from other samples. f) Whole rock mass balance between the andesite recharge magma VQ-22A and a dacite end-member (VQ-06) to model the bulk composition of the dacite component of VQ-22. See text for further explanation.

we also characterize grain mounts of the mineral separates using the same criterion for andesite- and dacite-derived plagioclase to be able to account for preferential separation of the different plagioclase types during the preparation of the mineral separate. Further details can be found in Appendix C1.

4.6 Samples Selected for U-series and Diffusion Modeling

U-series dating of mineral separates allows us to assess the timing of crystallization and crystal storage in the dacite and andesite magmas of Quizapu. We obtained U-series data for whole rock, glass, and plagioclase separates on samples of an andesite inclusion (VQ-22A), a hybridized andesite (VQ-02), and a mingled dacite (VQ-22D) of the 1846/47 eruption. In addition, we measured U-series concentrations and isotopic compositions for mineral separates and glasses for five dacites from 1932 and for two mingled dacites from 1846/47 as well as an additional sample containing andesite inclusions. Five other samples from the 1846/47 and 1932 eruptions were selected for whole rock U-series isotope analysis (Table 4.1).

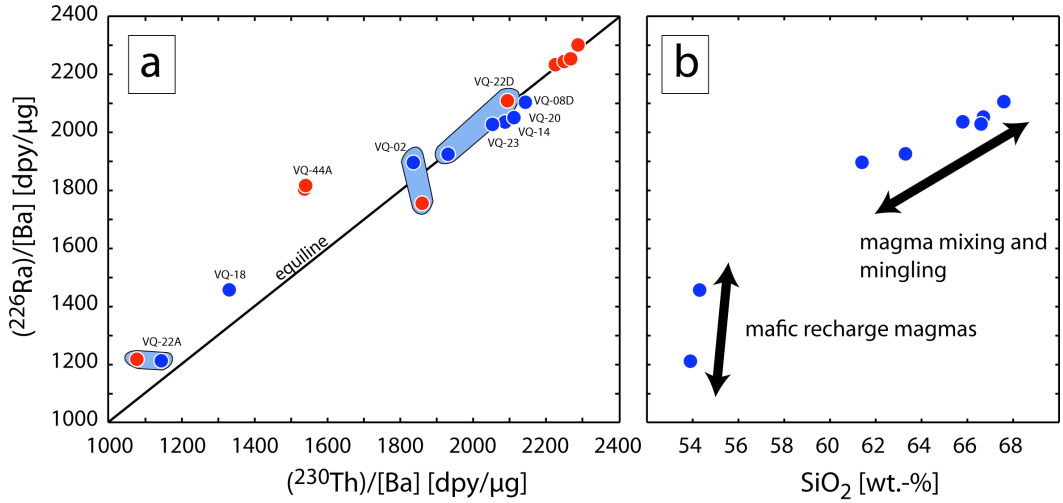

Figure 4.3 ^{226}Ra-^{230}Th-Ba composition for Whole Rocks and Glasses from Volcán Quizapu. a) ^{226}Ra-^{230}Th equiline diagram for whole rocks (blue) and glass (red). The two eruptions of1846/47 and 1932 are not distinguished. b) ^{226}Ra-Ba ratio as a function of SiO_2 content.

While U-series mineral separate age dating provides us with an absolute age estimate of crystal storage, elemental diffusion as a consequence of chemical disequilibrium between glass and crystal due to redistribution of crystals during magma mixing has the potential to assess the timing of the mixing event and the subsequent eruption of the magma. We selected the hybridized magma (VQ-02) for an elemental diffusion study. Based on its textures (i.e. amphibole breakdown, complete hybridization) it is most like to reflect the magma in which crystals experienced disequilibrium conditions the longest. Thus, diffusion profiles should be the most advanced.

4.7 Uranium-Series Results

We report new ^{238}U-^{230}Th-^{226}Ra isotope and trace element compositions for samples from the 1846/47 eruption of Volcán Quizapu (Table 4.1). In addition, results for andesite-and dacite-derived plagioclase separates presented in Table 4.2 are also given after correction for contamination by glass and dacite- and andesite-derived plagioclase, respectively. The reported values are calculated average concentrations based on the mass balance calculations. All whole rock, glass, and groundmass samples have either small ^{230}Th excesses or are within error of secular equilibrium, with $(^{230}Th)/(^{238}U)$ ranging from 0.99 to 1.03. Most plagioclase separates are within error of secular equilibrium with respect to $(^{230}Th)/(^{238}U)$. Four samples show small ^{230}Th excesses of 2%, while five separates show slightly larger ^{238}U excesses of 3-6 %. Th/U concentration ratios in plagioclase separates range from 2.5 to 3.7. The two plagioclase size fractions (125-250 μm and 250-500 μm) from the dacite end-member of VQ-22D have the lowest Th/U ratios (3.3 and 2.5, respectively). The smallest size fraction (75-125 um) of the hybridized andesite (VQ-02) also has a low Th/U ratio of 3.0. Whole rock, groundmass, and glass separates have a much more restricted range in Th/U of 3.6 to 3.8 compared to plagioclase separates.

Most of the glasses and whole rocks from dacites of the two Quizapu eruptions have (^{226}Ra)/(^{230}Th) activity ratios within error of secular equilibrium. Activity ratios range from 0.97 to 1.01 with an average 2-sigma error of 1.3 % (Figure 4.3a). The three samples that have small ^{230}Th excesses (VQ-08D, VQ-14, VQ-20) are from both Quizapu eruptions. In contrast to the dacites, which are all close to secular equilibrium, most whole rock, glass and groundmass samples for the hybridized andesite (VQ-02) and the mafic recharge magmas (VQ-22A, VQ-44A, VQ-18) show ^{226}Ra excess with (^{226}Ra)/(^{230}Th) activity ratios ranging from 1.03 to 1.18. The glass separate of VQ-02 is the only separate of this group of samples that shows ^{230}Th excess with a (^{226}Ra)/(^{230}Th) activity ratio of 0.94. Uncorrected plagioclase separates all have (^{226}Ra)/(^{230}Th) > 1 (up to 3.4 for the 75-125 μm size fraction of VQ-02).

Comparing ^{226}Ra activities normalized to Ba for the whole rocks shows a mixing array between low (^{226}Ra)/[Ba] ratios of the mafic recharge magmas and high (^{226}Ra)/[Ba] ratios of the dacite magma. The mixing array is consistent with the simple mixing model presented earlier (Figure 4.3b).

Table 4.1 Measured U-Th-Ra-Ba Concentrations and Isotope Compositions

Sample	Lab[§]	Eruption	U (ppm)	Th (ppm)	Th/U	Ra (fg/g)	2se (%)	Ba (ppm)	(238U)/ (232Th)	(230Th)/ (232Th)	2se (%)	(230Th)/ (238U)	(234U)/ (238U)	(226Ra)/ (230Th)	(230Th) [dpm/g]	(226Ra) [dpm/g]	(230Th)/ Ba [dpy/mg]	(226Ra)/ Ba [dpy/µg]
Mingled dacite																		
VQ-22D glass	UCD	1846/47	3.20	11.64	3.63	1081.0	0.9	591.1	0.837	0.831	0.23	0.992	1.000	1.008	2.353	2.372	2094	2111
VQ-22D-250 plg	UCD	1846/47	0.06	0.20	3.34	58.2	1.6	496.5	0.911	0.907	0.29	0.996	1.016	2.860	0.045	0.128	47	135
VQ-22D-500 plg	UCD	1846/47	0.16	0.40	2.51	88.3	3.3	518.9	1.211	1.196	0.15	0.987	1.006	1.684	0.115	0.194	117	197
VQ-22D wr	UCD	1846/47	2.72	9.98	3.67	930.6	1.2	557.7	0.828	0.843	0.25	1.018	1.009	0.998	2.047	2.042	1931	1926
Andesite inclusions																		
VQ-22A gm	UCD	1846/47	0.89	3.34	3.76	339.4	0.9	322.0	0.809	0.813	0.19	1.004	0.999	1.129	0.660	0.745	1078	1217
VQ-22A-250 plg[a]	UCD	1846/47	0.04	0.14	3.69	33.1	1.6	175.0	0.825	0.822	0.34	0.997	1.004	2.564	0.028	0.073	85	218
VQ-22A wr	UCD	1846/47	0.90	3.39	3.77	330.2	1.2	314.6	0.806	0.831	0.29	1.031	1.005	1.058	0.685	0.725	1145	1212
VQ-44A-M gm	UCD	1846/47	1.38	4.98	3.60	554.2	0.9	354.3	0.845	0.855	0.28	1.013	0.996	1.174	1.036	1.216	1538	1805
VQ-44A-NM gm	UCD	1846/47	1.40	5.05	3.62	561.5	0.9	356.7	0.841	0.849	0.16	1.009	0.998	1.179	1.045	1.232	1541	1817
VQ-44A-250 plg[a]	UCD	1846/47	0.08	0.25	3.36	53.0	1.4	482.0	0.906	0.859	0.28	0.948	0.988	2.193	0.053	0.116	58	127
Hybridized andesite																		
VQ-02 glass	UCD	1846/47	2.71	9.86	3.63	859.7	1.0	565.1	0.838	0.833	0.21	0.994	1.000	0.944	1.998	1.887	1860	1756
VQ-02-125 plg	UCD	1846/47	0.04	0.13	3.00	47.2	1.5	563.9	1.016	0.966	0.70	0.951	1.008	3.393	0.030	0.103	28	97
VQ-02-250 plg	UCD	1846/47	0.04	0.13	3.58	40.8	1.6	568.0	0.850	0.826	0.73	0.972	1.004	3.352	0.027	0.090	25	83
VQ-02-500 plg	UCD	1846/47	0.05	0.16	3.46	37.8	1.2	569.8	0.880	0.840	0.29	0.955	1.005	2.589	0.032	0.083	30	77
VQ-02 wr	UCD	1846/47	2.20	8.02	3.65	780.4	1.3	474.9	0.835	0.849	0.31	1.017	1.005	1.033	1.658	1.712	1836	1896
Dacite (no macroscopic inclusions)																		
Q-34 glass	UW	1846/47	3.88	14.37	3.70	1336.0	1.3	690.0	0.823	0.835	0.25	1.015	1.007	1.004	2.920	2.932	2226	2235
Q-34 plg	UW	1846/47	0.07	0.25	3.67	43.8	10.1	588.0	0.830	0.843	0.32	1.016	1.006	1.905	0.050	0.096	45	86
VQ-06 glass	UCD	1846/47	3.59	13.06	3.63	712.5	0.7	668.3	0.838	0.831	0.15	0.992	1.004	0.592	2.641	1.564	2079	1231
VQ-06-250 plg	UCD	1846/47	0.06	0.22	3.62	47.2	1.0	566.1	0.841	0.854	0.16	1.015	1.002	2.245	0.046	0.104	43	96
Q-2 glass	UW	1932	4.46	16.50	3.70	1508.5	1.1	699.6	0.822	0.836	0.39	1.018	1.009	0.985	3.360	3.310	2526	2489
Q-2 plg	UW	1932	0.32	1.16	3.70	164.1	1.5	520.2	0.823	0.838	0.32	1.019	1.009	1.515	0.238	0.360	240	364
Q-6 glass	UW	1932	4.07	14.80	3.64	1373.6	1.3	705.6	0.836	0.838	0.29	1.002	1.008	0.999	3.019	3.014	2250	2247
Q-6 plg	UW	1932	0.13	0.49	3.67	88.1	1.3	531.2	0.828	0.829	0.25	1.001	1.009	1.962	0.099	0.193	98	191

Table 4.1 continued.

Sample	Lab[§]	Eruption	U (ppm)	Th (ppm)	Th/U	Ra (fg/g)		Ba (ppm)	(238U)/ (232Th)	(230Th)/ (232Th)		(230Th)/ (238U)	(234U)/ (238U)	(226Ra)/ (230Th)	(230Th) [dpm/g]	(226Ra) [dpm/g]	(230)/ Ba [dpy/mg]	(226)/ Ba [dpy/µg]
Q-4 plg	UW	1932	0.33	1.11	3.41	154.2	1.4	521.7	0.892	0.839	0.26	0.941	1.007	1.493	0.227	0.338	228	341
Q-4HF plg[b]	UW	1932	0.31	1.15	3.69	150.2	2.1	507.6	0.825	0.842	0.37	1.020	1.006	1.402	0.235	0.330	244	341
VQ-17 glass	UCD	1932	4.02	14.63	3.64	1359.7	1.0	681.2	0.837	0.832	0.27	0.994	1.000	1.007	2.962	2.984	2287	2304
VQ-17-250 plg	UCD	1932	0.10	0.35	3.66	75.0	1.3	509.5	0.833	0.840	0.16	1.008	1.003	2.280	0.072	0.165	74	170
VQ-37D glass	UCD	1932	3.85	14.23	3.69	1316.8	0.9	673.9	0.824	0.839	0.29	1.019	1.004	0.995	2.906	2.890	2268	2255
VQ-37D-250 plg	UCD	1932	0.39	1.44	3.64	187.6	1.5	524.6	0.835	0.838	0.18	1.004	1.002	1.404	0.293	0.412	294	413
VQ-37D-500 plg	UCD	1932	0.24	0.89	3.63	130.9	1.2	553.8	0.838	0.840	0.22	1.003	1.004	1.587	0.181	0.287	172	273
Other whole rock dacite																		
VQ-08D wr	UCD/UW	1846/47	3.60	13.14	3.66	1209.5	1.1	663.0	0.832	0.844	0.23	1.014	1.006	0.983	2.701	2.654	2143	2106
VQ-14 wr	UCD/UW	1846/47	3.28	12.05	3.67	1101.3	1.3	624.1	0.829	0.844	0.29	1.018	1.004	0.976	2.477	2.417	2087	2037
VQ-20 wr	UCD/UW	1932	3.33	12.18	3.66	1117.41	1.2	628.3	0.832	0.851	0.46	1.022	1.006	0.972	2.523	2.452	2112	2053
VQ-23 wr	UCD/UW	1932	3.27	11.98	3.66	1112.15	1.4	632.8	0.831	0.847	0.33	1.019	1.003	0.988	2.470	2.441	2053	2029
Other whole rock andesite																		
VQ-18 wr	UCD/UW	1932	1.08	4.01	3.71	404.9	1.2	320.8	0.820	0.831	0.44	1.014	1.003	1.094	0.812	0.889	1331	1457
Solution Standards - University of Washington																		
WUN (N=5)										0.802								
IRMM-035 (N=2)										2.103								
OU (N=1)										1.122								
Solution Standards - University of California, Davis																		
WUN (N=9)										0.800								
IRMM-035 (N=7)										2.112								
IRMM-036 (N=1)										0.555								

[§]Laboratory in which most of the analyses where performed: UCD: University of California, Davis; UW: University of Washington. Sample labeled UCD/UW: Th isotopic compositions obtained at UW, other analyses at UCD. Column chemistry performed by various personnel.

[a] Ba isotope dilution measurements repeated

[b] Ra column chemistry repeated on the sample because of problems in the first run

Table 4.2 Average Corrected U-Th-Ra-Ba Concentrations and Isotope Compositions for Plagioclase Separates[1]

Sample	Eruption	U (ppm)	Th (ppm)	Th/U	Ra (fg/g)	Ba (ppm)	(238U)/ (232Th)	(230Th)/ (232Th)	(230Th)/ (238U)	(226Ra)/ (230Th)	(230Th) [dpm/g]	(226Ra) [dpm/g]	(230Th)/ Ba [dpy/mg]	(226Ra)/ Ba [dpy/µg]
Mingled dacite														
VQ-22D-250 plg[a]	1846/47	0.07	0.24	3.38	62.0	503.8	0.998	0.898	0.900	2.615	0.052	0.136	54	142
VQ-22D-500 plg	1846/47	0.14	0.31	2.26	81.9	530.9	0.970	11.033	11.790	2.152	0.099	0.180	97	178
Andesite inclusions														
VQ-22A-250 plg	1846/47	0.08	0.29	3.83	37.1	174.0	1.007	0.794	0.788	1.564	0.056	0.082	169	245
VQ-44A-250 plg[a]	1846/47													
Hybridized andesite														
VQ-02-125 plg	1846/47	0.08	0.26	3.30	59.9	578.2	0.979	0.903	0.922	2.289	0.058	0.132	52	120
VQ-02-250 plg	1846/47	0.06	0.21	3.62	47.9	574.6	0.927	0.816	0.888	6.723	0.042	0.105	38	96
VQ-02-500 plg	1846/47	0.09	0.32	3.58	52.7	573.7	0.976	0.838	0.860	2.024	0.065	0.116	60	106
Dacite (no macroscopic inclusions)														
Q-34 plg	1846/47	0.12	0.43	3.68	60.7	589.3	1.015	0.840	0.827	1.583	0.088	0.133	78	119
VQ-06-250 plg	1846/47	0.07	0.26	3.62	49.6	571.5	1.020	0.859	0.842	2.531	0.055	0.109	50	100
Q-2 plg	1932	0.31	1.16	3.70	163.7	520.2	1.019	0.839	0.823	1.552	0.237	0.359	239	363
Q-6 plg	1932	0.06	0.24	3.71	66.2	534.4	1.000	0.802	0.802	5.741	0.048	0.145	47	143
Q-4 plg	1932	0.12	0.34	2.95	86.9	518.2	0.695	0.852	1.385	5.677	0.071	0.191	71	193
Q-4HF plg	1932	0.11	0.42	3.78	85.5	499.3	1.066	0.852	0.800	2.320	0.087	0.188	92	197
VQ-17-250 plg	1932	0.10	0.35	3.65	74.9	512.5	1.033	0.853	0.826	4.292	0.071	0.164	73	168
VQ-37D-250 plg	1932	0.31	1.12	3.63	160.6	525.7	0.998	0.838	0.840	1.564	0.229	0.353	229	352
VQ-37D-500 plg	1932	0.09	0.31	3.51	79.6	549.8	0.863	0.858	1.034	9.515	0.063	0.175	60	167

[1] Note: Samples Q-2 plg and Q-34 plg compositions are identical to Table 4.1, because they have not been characterized via grain mounts

[a] Four-component model calculations result in negative Th, U, and Ra concentrations that are not reported here. This sample has been characterized to be contamiated by >80% with dacite-derived plagioclase based on semi-quantitive crystal separate microprobe characterization

4.8 Discussion

4.8.1 Impurities in Mineral Separates

In this study we present ^{226}Ra-^{230}Th model ages between plagioclase and glass separates. In order to accurately calculate crystal ages, plagioclase separates must be corrected for mineral and glass impurities in the separates and for small differences in chemical behavior between Ra and Ba [*Cooper et al*. 2001; *Cooper and Reid*, 2003]. The ^{226}Ra-^{230}Th system does not have a long-lived or stable Ra isotope that can be used as a normalizing isotope, while, e.g., results in the ^{238}U-^{230}Th system can be normalized to the long-lived ^{232}Th isotope and thus allow deconvolving of radioactive decay and chemical behavior. In replacement for a stable Ra isotope, Ba is commonly used as proxy for the chemical behavior of Ra [*Reagan et al*., 1992; *Volpe and Hammond*, 1991].

The potential contaminants of plagioclase separates that could significantly change Ra-Th-Ba systematics are glass, zircon, and apatite. In addition, plagioclase separates of Quizapu are composed of andesite- and dacite-derived plagioclase. Grain mounts of the mineral separates contain subordinate quartz, which has a diluting effect for U-series radionuclide concentrations in the mineral separates. However, we observe mostly less than 1 vol.% of quartz in the grain mounts, causing a negligible dilution effect. Zircon and apatite have not been observed in the grain mounts despite their strong contrast in back-scattered electron images. Moreover, zircon and apatite are significantly smaller than the observed quartz grains. Thus, if present at similar volume fractions compared to quartz, number densities of zircons and apatite would have to be much larger, thus we expect << 1 vol.% of zircon and apatite to be present in the mineral separates. Additionally, based on simple mass balance calculations of uranium and zirconium in the mineral separates, we can estimate the maximum volume fraction of zircon in the plagioclase separates. U concentrations in the plagioclase separates are generally less than 300 ppb (Table 4.1). Contamination of the mineral separates with 0.1 % zircon inclusions (assuming

a U concentration of 300 ppm) would already lead to > 300 ppb U. Zirconium concentrations even further restrict the presence of zircon in the mineral separates. We measure < 35 ppm Zr in the mineral separates, which results in < 0.01 % of zircon contamination, if all Zr is derived from zircon. Hence, even small volumes of mineral inclusions would be recognizable.

In contrast to zircon and apatite, adhering glass has been observed in the plagioclase grain mounts. To account for the glass as well as the distinct plagioclase populations we have quantified the fractions of dacite- and andesite-derived plagioclase (Appendix C1). The fraction of glass contamination, though it can be estimated from the grain mounts, is better quantified using trace element concentrations. The differences in trace-element concentrations between different plagioclase populations and between plagioclase and glass lend themselves to rigorous mass balance calculations of the contributions of adhering glass and the different plagioclase end-members observed in erupted products from Volcán Quizapu to the bulk mineral separates. In Appendix C1 we give the estimated fractions of andesite- and dacite-derived plagioclase for each grain mount based on the $An_{56.5}$-criterion. We assume that the grain mount characterization is representative of the plagioclase populations in the mineral separates used for U-series chemistry. To account for glass impurities the plagioclase separates were analyzed by ICP-MS. Despite a large data set of 32 elements, only Y and Sr lend themselves as useful tracers for glass contamination. Other elements are either not well known for the pure components of glass, andesite-, and dacite-derived plagioclase or are not suitable because of their similar concentration in dacite-derived plagioclase (low An) and complementary glass. Y and Sr have similar concentrations in andesite- and dacite-derived plagioclase, but are significantly different in glasses of the same sample. Here, only Y is used to estimate glass contamination in plagioclase separates, due to its highly incompatible behavior in plagioclase in comparison to Sr.

4.8.2 Mass Balance for Mineral Separates

We have developed a four-component mixing model to account for contributions from dacite and andesite glass as well as dacite- and andesite derived plagioclase in the mineral separates. Taking into account four components is of particular importance for the andesite inclusions (VQ-22A and VQ-44A), which contain large proportions (>30 %) of dacite-derived plagioclase and glass. We use the following set of equations to constrain the concentrations C in our plagioclase separate from the andesite end-member VQ-22A (Equation 4.1) and dacite end-member VQ-22D (Equation 4.2):

$$C_{mixA} = \left[C_{glA} \frac{f_{AnA}}{f_{AnA} + f_{AbA}} + C_{glD} \frac{f_{AbA}}{f_{AnA} + f_{AbA}} \right] f_{glA} + C_{An} f_{AnA} + C_{Ab} f_{AbA} \tag{4.1}$$

$$C_{mixD} = \left[C_{glA} \frac{f_{AnD}}{f_{AnD} + f_{AbD}} + C_{glD} \frac{f_{AbD}}{f_{AnD} + f_{AbD}} \right] f_{glD} + C_{An} f_{AnD} + C_{Ab} f_{AbD} \tag{4.2}$$

where C_{mix}, C_{gl}, C_{An}, and C_{Ab} are referring to the measured concentration in our separate, the measured concentration in our glass or groundmass separate, the concentration of each element in our pure andesite-derived plagioclase population, and the concentration of each element in our pure dacite-derived plagioclase population, respectively. The volume fractions of the glass or groundmass, the andesite-derived plagioclase, and dacite-derived plagioclase are f_{gl}, f_{An}, and f_{Ab}, respectively. The two unknowns in Equations 4.1 and 4.2 are C_{An} and C_{Ab}.

As constitutive equations for the four-component mixing model, we assume (1) a known ratio of andesite- and dacite-derived plagioclase in our mineral separates ($EPMA_{mix}$) that is derived from grayscale-interpreted BSE map of grain mounts for each plagioclase separate (Figure C1 in Appendix C1), and (2) no contribution from other phases to the observed concentrations in our separates:

$$\frac{f_{AnA}}{f_{AbA}} = EPMA_{mixA} \tag{4.3}$$

$$\frac{f_{AnD}}{f_{AbD}} = EPMA_{mixD} \tag{4.4}$$

$$f_{AnA} + f_{AbA} + f_{glA} = 1 \tag{4.5}$$

$$f_{AnD} + f_{AbD} + f_{glD} = 1 \tag{4.6}$$

The uncertainty in the volume fractions of the different components in each mineral separate dominate the uncertainties in the calculation of the concentrations in the pure andesite- and dacite-derived plagioclase. We assume a conservative 2%-error.

The four-component model is applied to the 125-250 μm size fractions of VQ-22A and VQ-22D. It provides the best estimate for the composition of the pure end-member plagioclase, because crystal populations have been extensively characterized and, as discussed earlier, the data are consistent with a simple binary mixing model. In the case of dacite plagioclase separates the composition of andesite-derived plagioclase is assumed to be that of pure andesite-derived plagioclase end member of VQ-22A (125-250 μm size fraction). For the other andesite inclusion (VQ-44A) we assume that the dacite-derived plagioclase has the composition of the pure dacite-derived plagioclase end member from VQ-22D (125-250 μm size fraction).

4.8.3 Model ages: Crystal Residence Times

The calculations of the absolute ages of the bulk crystal population are affected by the different chemical behaviors of Ra and Ba. In most major mineral phases (e.g., plagioclase and pyroxene), Ra is predicted to be more incompatible than Ba during equilibrium crystallization due to the slightly larger ionic radius of Ra compared to Ba [e.g., *Blundy and Wood*, 1994; *Wood and Blundy*, 1997; *Blundy and Wood*, 2003]. This effect needs to be accounted for in order to calculate accurate ^{230}Th-^{226}Ra crystal ages [*Cooper et al*., 2001]. Here, the elastic-strain model of *Blundy and Wood* [1994, 2003] is used to account for Ra-Ba fractionation. Recently, *Fabbrizio et al*. [2009] have presented experimentally determined Ra partitioning data for plagioclase, which predict somewhat lower Ra concentrations compared to the elastic-strain model. Such different Ra-Ba behavior in plagioclase results in younger crystal residence ages. Nonetheless, ratios of Ra to Ba are affected less than absolute values of the partition coefficients. Furthermore, relative age differences, which are of more importance for this study, are subordinately affected. We calculate model crystal model ages for contamination-corrected plagioclase concentrations, assuming equilibrium crystal growth (i.e., equilibrium Ra-Ba fractionation) between plagioclase and host glass from Volcán Quizapu. A detailed derivation of the method to calculate (^{226}Ra)/[Ba] model ages can be found in *Cooper and Reid* [2008].

The partitioning of Ra and Ba into plagioclase is a function of crystallization temperature and plagioclase composition [*Blundy and Wood*, 2003]. We apply temperature estimates from Chapter 3 [*Ruprecht*, 2009] to our model calculations. The reported pre-eruptive dacite temperatures are 845±35 ˚C for the dacite end-member using the amphibole-plagioclase thermometer. In our calculations we extend this range to higher temperatures (825-900 ˚C) assuming that magma temperatures may have been hotter at the time of crystallization. Pre-eruptive temperatures for the andesite end-member have been determined to be ~ 1080 ˚C. We assume a conservative range of temperatures for the andesite recharge of 1000-1200˚C. The

mean plagioclase composition is estimated from microprobe quantitative analyses and BSE maps. Residence ages are calculated for a range of An_{30}-An_{50} and An_{60}-An_{85} for dacite-derived and andesite-derived plagioclase end-member compositions, respectively, corresponding to the majority pf plagioclase analyses of the grain mounts and thin sections.

Figure 4.4 shows that all analyzed dacite-derived plagioclase separates have (^{226}Ra)/[Ba] consistent with equilibrium growth from the host glass. Ages for all separates are on the order of thousands of years. Most ages have an uncertainty of ~ 1500 yrs. These relatively conservative uncertainties reflect mainly the combination of uncertainties in the volume of contaminant in the separates, the measurement uncertainty, and uncertainties in the conditions of crystallization (i.e., temperature) in the pure-plagioclase separates. Melts in equilibrium with the plagioclase crystals show (^{226}Ra)/[Ba] variations of ~ 1000 dpy/µg for a given sample, based on all of these uncertainties combined. Uncertainties in the determination of the isotope composition of the complementary glass translate only into an age uncertainty on the order of hundreds of years. Two of three samples for which multiple size fractions have been analyzed (VQ-02 and VQ-37D) show younger ages in smaller size fractions. This suggests that plagioclase fragmentation during the separation process is limited, in which case the size-age relationship can be used to determine long-term growth rates that integrate over multiple events of growth and dissolution.

The glass compositions in mingled and mixed magmas of the 1846/47 eruption are a function of SiO_2 (Figure 4.3b). The more mafic, mixed magmas have lower (^{226}Ra)/[Ba] ratios than the evolved magmas. The most evolved magmas are compositionally similar to the glass separates from the 1932 eruption indicating - in addition to textural and other geochemical characteristics [*Ruprecht*, 2009; Chapter 3] - that the residing magmas were homogenous, evolved dacites, in which the dacite-derived crystals grew. Therefore, crystal residence model ages for the mixed

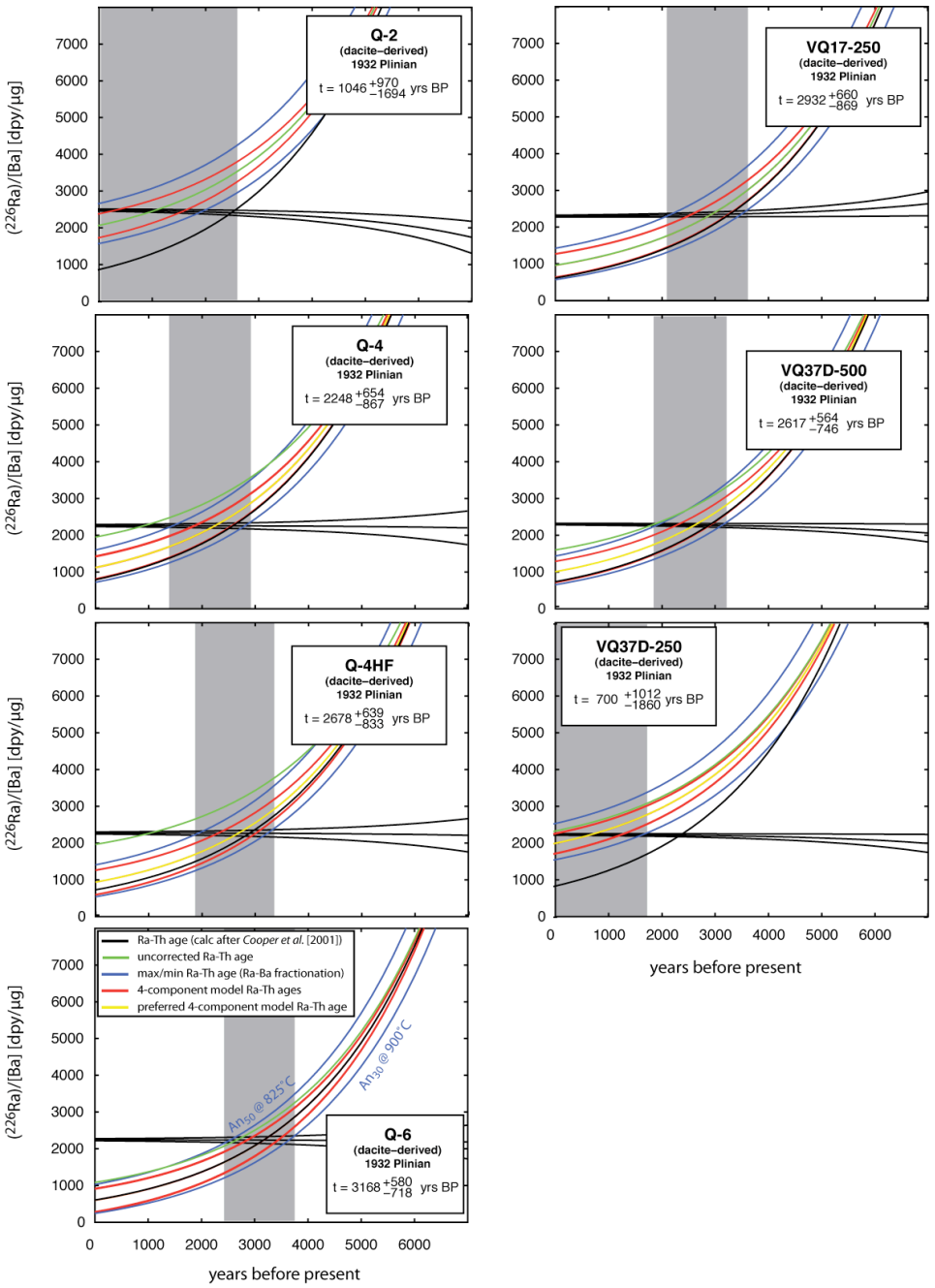

Figure 4.4 Ra-Ba Evolution Diagrams. Dacite-derived plagioclase from the 1846/47 and 1932 eruption. Sample Q4-HF is the same sample as Q-4, but the plagioclase separate was treated with weak HF to test if adhering glass can be dissolved prior to sample digestion. This sample experienced analytical difficulties during element separation. Isotope composition was not affected as confirmed by the same composition between Q-4 and Q4-HF. We assume a 2 %-error for the grain mount estimates of dacite- and andesite derived plagioclase and the glass estimates.

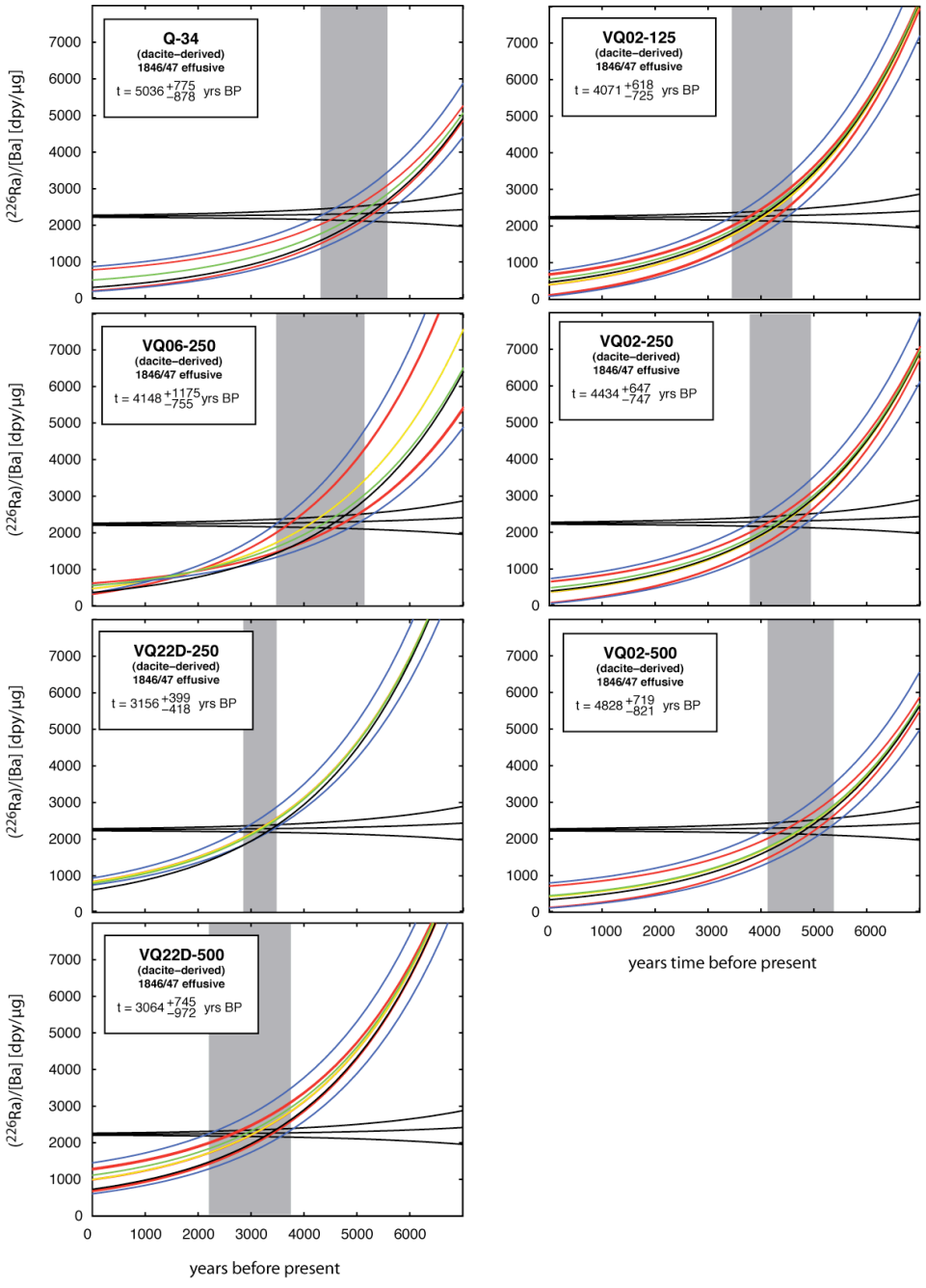

Figure 4.4 continued.

and mingled samples of the 1846/47 eruption are calculated by using the dacite end-member isotope glass composition (Q-34). This assumption is reasonable, since the plagioclase separates of these samples are mostly composed of dacite-derived crystals (Appendix C1). The host glass separates to each sample have Ra/Ba that has been modified by mixing with mafic magma, and thus would produce erroneous crystal residence model ages.

4.8.4 Age Populations for Dacite-Derived Plagioclase Crystals From the 1846/47 and the 1932 Eruption

Figure 4.5 shows a comparison of the crystal residence model ages of the dacite-derived plagioclase for both eruptions of Volcán Quizapu. The mean square of weighted deviates [MSWD; *McIntyre et al*., 1966] calculated for all ages for the crystal separates from both of the Quizapu eruptions (1.80, n = 14) is slightly higher than would be consistent with a simple, single age population. Overall, we observe older ages of 3861 ± 251 yrs BP (MSWD = 1.38; n = 7) in the effusive eruption of 1846/47 that are characterized by extensive magma mixing compared to the Plinian eruption of 1932. Considering the smaller number of samples, the MSWD calculated for these data are consistent with a simple age population. The plagioclase separates for the younger, plinian eruption of 1932 give mean crystal residence age of 2572 ± 301 yrs BP (MSWD = 0.71; n = 7). The low MSWD suggests an overestimation of the error. For both eruptions we allow for a conservative wide range of crystallization temperatures and average anorthite compositions, which are the two variables that have the largest effect on the error calculations, in addition to the uncertainties in the isotope composition of the plagioclase separates. Thus, a smaller range in temperatures and crystal compositions may be statistically justified.

The shift in average age between dacite-derived plagioclase in the 1846/47 and 1932 eruptions could be a result of (1) reheating of the 1846/47 magma and subsequent plagioclase dissolution, which would disproportionately affect the

youngest crystallization, (2) new growth of plagioclase rims during the repose time of 86 years in between the two eruptions on the 1846/47 plagioclase crystals, (3) a magma chamber zoned in crystal residence, (4) two distinct magmatic systems, or (5) age bias produced during the mineral separation process. The fifth option cannot be ruled out completely, since plagioclase separates from the 1932 magmas are from pumice samples and therefore crystal fragments are better preserved during the separation procedure, which may lead to preferential incorporation of young rim portions of crystal fragments. However, below we provide a geologically viable explanation for the younger plagioclase residence ages in 1932 magmas.

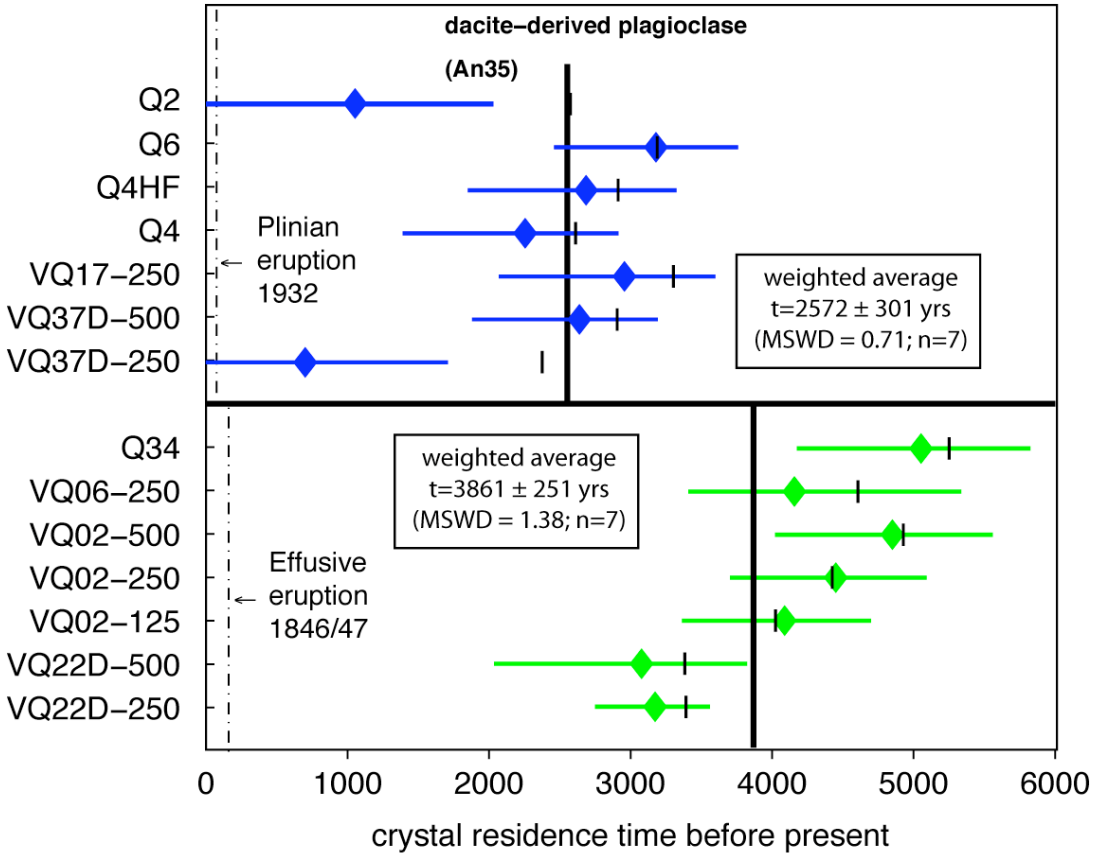

Figure 4.5 Age Comparison For Quizapu Dacite-Derived Plagioclase Crystals. Shown is the age range calculated using the 4-component mixing model (green and blue symbols and error bars) and the crystal model age taking only glass contamination into account (black bars) as described in *Cooper et al.* [2001].

Quizapu dacites from the 1846/47 and 1932 eruptions are almost identical in crystal and bulk rock compositions, with similar phenocryst modes and volatile abundances [*Hildreth and Drake*, 1992; *Ruprecht*, 2009; Chapter 3]. The main difference observed between dacites from the two eruptions is their pre-eruptive temperature conditions [*Ruprecht*, 2009; Chapter 3]. Therefore, we do not observe evidence for a zoned magma chamber in most intensive and extensive variables at Quizapu. It also appears rather unlikely that two independent magma chambers of probably more than 5 km^3 of compositionally identical dacite were residing in the shallow crust [*Eichelberger et al*., 2006]. Therefore, new growth on plagioclase from the 1932 eruption or dissolution of plagioclase from the 1846/47 eruption are the most likely geologically relevant explanations for the shift in crystal residence age.

The large temperature pulse associated with magma recharge prior to the 1846/47 eruption [*Ruprecht*, 2009; Chapter 3] provides sufficient heat energy to account for plagioclase dissolution by raising the temperature throughout the 1846/47 magma by at least 30˚C (most silicic end-member). During the dissolution the outermost youngest part of the dacite-derived plagioclase crystals would be resorbed. Sodic plagioclase that experiences mafic recharge and consequently increased temperatures has been shown to extensively dissolve [*Tsuchiyama*, 1985]. By melting the youngest parts of the plagioclase crystals the ^{226}Ra-^{230}Th plagioclase model ages would be biased towards older cores. An alternative to the dissolution of plagioclase is that plagioclase crystals in the 1932 eruption may have continued to grow during the repose time of 86 years and thus lowered the average crystal age. Crystals in the 1932 eruptive products potentially did not experience a melting event, since they did not undergo as much reheating as the 1846/47 eruption. By knowing the Ra compositions in the melt and the crystal separates from Quizapu samples we can calculate that 250 to 500 μm large crystals from the 1846/47 would need to grow 20 to 40 μm wide zero-age rims to shift the crystal residence age by 1000 yrs. Such a rim can be easily resolved by microprobe imaging, if a dissolution surface has

developed. Such consistently thin rims are not found in plagioclase phenocrysts, instead we observe melting in the form of subhedral to anhedral crystals [*Ruprecht*, 2009; Chapter 3] and potential melting of several μm for crystals from the 1846/47 eruption, which can also account for older ages observed in the early lavas. If only dissolution as a response to reheating was responsible for the shift in ^{226}Ra-^{230}Th plagioclase-melt model ages, mineral separate ages from sample that experienced the least amount of reheating as a result of magma recharge (i.e., the most silicic magmas) of the 1846/47 eruption should yield similar ages to the mineral separate ages of the 1932 eruption, which do not show evidence for major reheating. Instead, we observe that the most silicic samples of the 1846/47 eruption (VQ-06 and Q-34) have the oldest crystal residence ages. The most silicic magmas erupted towards the end of the eruption in 1846/47, which lasted more than a month. Thus, these magmas potentially experienced elevated temperatures as result of magma recharge over a longer duration than the hybridized andesites (VQ-02) and extensively mingled dacites (VQ-22). This extended exposure to higher temperatures may be responsible for the most extensive young crystal rim resorption in the most silicic samples.

4.8.5 Andesite-Derived Plagioclase Residence Times

The large contribution from dacite-derived plagioclase crystals to the andesite-derived plagioclase separate s renders the derivation of crystal model ages using the 226Ra-230Th disequilibrium difficult (Figure 4.6). Based on backscattered-electron maps of grain mounts, the andesitic sample VQ-44A is strongly contaminated by dacite-derived plagioclase (> 80 vol.%), which has a large effect on the uncertainty of the corrected andesite-derived separate. A dacite-derived plagioclase -uncorrected crystal model age can be calculated (~1567 yrs BP). A crystal residence model age for the andesite-derived plagioclase is obtained only from the andesite inclusion VQ-22A. The plagioclase-uncorrected determined residence ages of 3348 yrs BP calculated assuming only glass as a contaminant (after *Cooper et al.* [2001]) is a maximum age estimate, since it does not take into account

the large fraction (>30 vol. %) of old dacite-derived plagioclase that has been identified by electron microprobe in grain mounts of this mineral separate. In the usual bulk crystal model age calculation [*Cooper et al.*, 2001], plagioclase is assumed to dominantly reflect one composition (supported in that case by microprobe analyses) and therefore large concentrations of incompatible elements are assumed to reflect predominantly glass or groundmass contamination. However, in the case of the Quizapu andesitic inclusion plagioclase separate, sodic plagioclase can account for most of the observed incompatible element concentrations. Attributing the incompatible element concentrations to glass or to old dacite-derived plagioclase has opposite effects during the mass balance corrections. While correcting for groundmass with a high (^{226}Ra)/[Ba] ratio would lead to older age estimates, dacite-derived plagioclase contamination with a low (^{226}Ra)/[Ba] results in

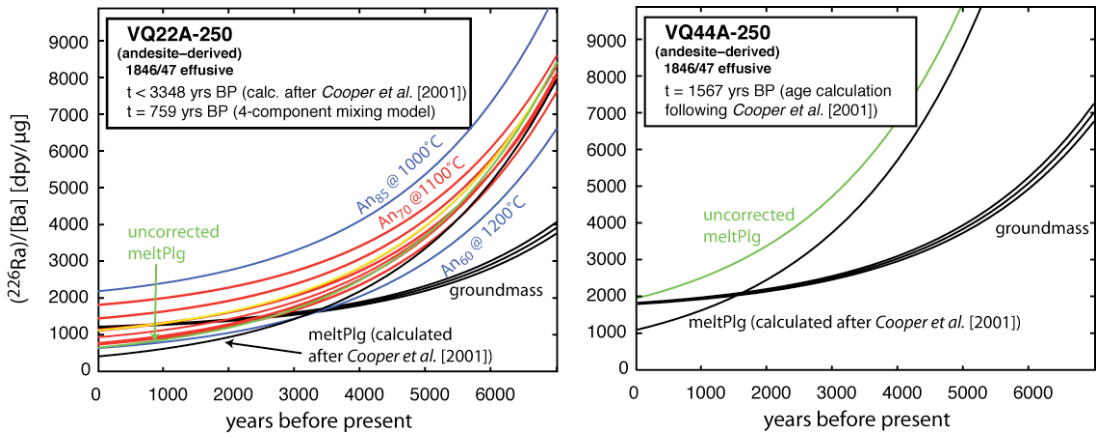

Figure 4.6 Evolution Diagrams for Andesite-Derived Plagioclase. The large contribution of dacite-derived plagioclase to the mineral separates of the andesite inclusions result in complex mass balance calculations and only broad estimates for the crystal model ages. VQ-44A-250 has more than 80 % dacite-derived crystal contamination, therefore the model curves for the 4-component model are not shown. Ba concentrations in the plagioclase separate of VQ-22A and VQ-44A were reanalyzed from a different plagioclase separate to confirm high (^{226}Ra)/[Ba]. Line colors as in Figure 4.4.

an age shift towards younger crystal residence ages. The error envelope for the mineral separate of VQ-22A expands to high (^{226}Ra)/[Ba] in the Ra-Ba fractionation corrected mineral separates (Figure 4.6). This would be in equilibrium with a melt that at present has a higher (^{226}Ra)/[Ba] (~ 2200 dpy/µg) than the measured Quizapu dacite glasses or the observed ratio in the andesitic groundmass (~1200 dpy/µg).

To ensure that groundmass and andesite-derived plagioclase are in chemical equilibrium we consider textural and geochemical evidence. The phenocrysts in the andesite inclusions are euhedral in shape suggesting that their co-genetic melt was chemically similar to the melt they resided in during the eruption [*Ruprecht*, 2009; Chapter 3]. In contrast to the more evolved rocks at Volcán Quizapu, the more mafic compositions are characterized by low (^{226}Ra)/[Ba] suggesting that mafic magmas in this volcanic system have low (^{226}Ra)/[Ba] (Figure 4.3b). We further examine if the effect of non-equilibrium crystallization could be responsible for potentially high (^{226}Ra)/[Ba] in the andesite-derived plagioclase. To address the possibility of non-equilibrium growth for the andesite inclusions we turn to stable elements that have slow diffusion coefficients. In particular, Sr and Ba as slow diffusing [*Cherniak and Watson*, 1994; *Cherniak*, 2002] and relatively abundant trace elements in plagioclase have the potential to identify non-equilibrium behavior. Growth entrapment as a result of slow diffusion during fast crystal growth potentially can result in higher (^{226}Ra)/[Ba] ratios than assumed under equilibrium growth [*Watson and Liang*, 1995; *Watson*, 1996; *Cooper and Reid*, 2003]. In case of observed growth entrapment for Sr and Ba, an even larger effect for growth entrapment of Ra is expected, due to its large ionic radius, which results in smaller diffusion coefficients for Ra than Sr and Ba [*Cooper and Reid*, 2003]. We have only a few reliable Ba data for the andesite-derived plagioclase crystals from LA-ICPMS. This data set for VQ-22A and VQ-44A (n = 23) provides insight about the crystallization behavior of Ba and Sr (Figure 4.7). The Sr data for VQ-22A and VQ-44A are consistent with equilibrium growth along a fractional crystallization trend assuming partition coefficients from *Blundy*

and Wood [1991]. Ba shows larger deviations from a simple fractional crystallization trend. However, the more calcic plagioclase crystals are also consistent with fractional crystallization. The more sodic crystals show lower Ba concentrations than is expected for fractional crystallization. Nonetheless, the Ba data of the most sodic plagioclase is inconsistent with significant growth entrapment crystallization, since they are displaced in the wrong direction to lower Ba concentrations. The fractional crystallization trend is based on modeling Ba and Sr whole rock concentration s during fractional crystallization starting with a liquid like that erupted from the peripheral cones, which are crystal-poor with almost no plagioclase, as well as glass estimates for andesite inclusions from the 1846/47 eruption. Ba in the groundmass of the andesite inclusions was measured accurately via isotope dilution for the U-series age dating. Sr in the groundmass of the andesite inclusions is estimated based on mass balancing from the whole rock composition.

In the case of the andesitic inclusion the uncertainty of the fractions of dacite- and andesite-derived plagioclase is potentially larger. Therefore, it seems to be that the grain mounts lead to an overestimation of dacite-derived plagioclase. The grain mounts in this study were prepared from remnants of the mineral separates after dissolution for U-series analyses. Obtaining a large enough mineral separate for U-series analyses was difficult for VQ-22A and VQ-44A due to the small size of andesite inclusions (< 5 cm) and a limited sample volume. Therefore, only a small fraction that potentially was smaller in size than the average separate was left over for grain mount studies. This is likely to have affected the grain mount for VQ-22A and VQ-44A more than other separates, because in these cases sufficient volume remained to take a representative sample for the grain mount characterization. The samples of andesite-derived plagioclase, though not fully conclusive, show the potential effect of different plagioclase populations on the calculated crystal residence age. The bulk crystal model age that accounts for glass contamination provides a maximum age for the andesite-derived plagioclase. However, the

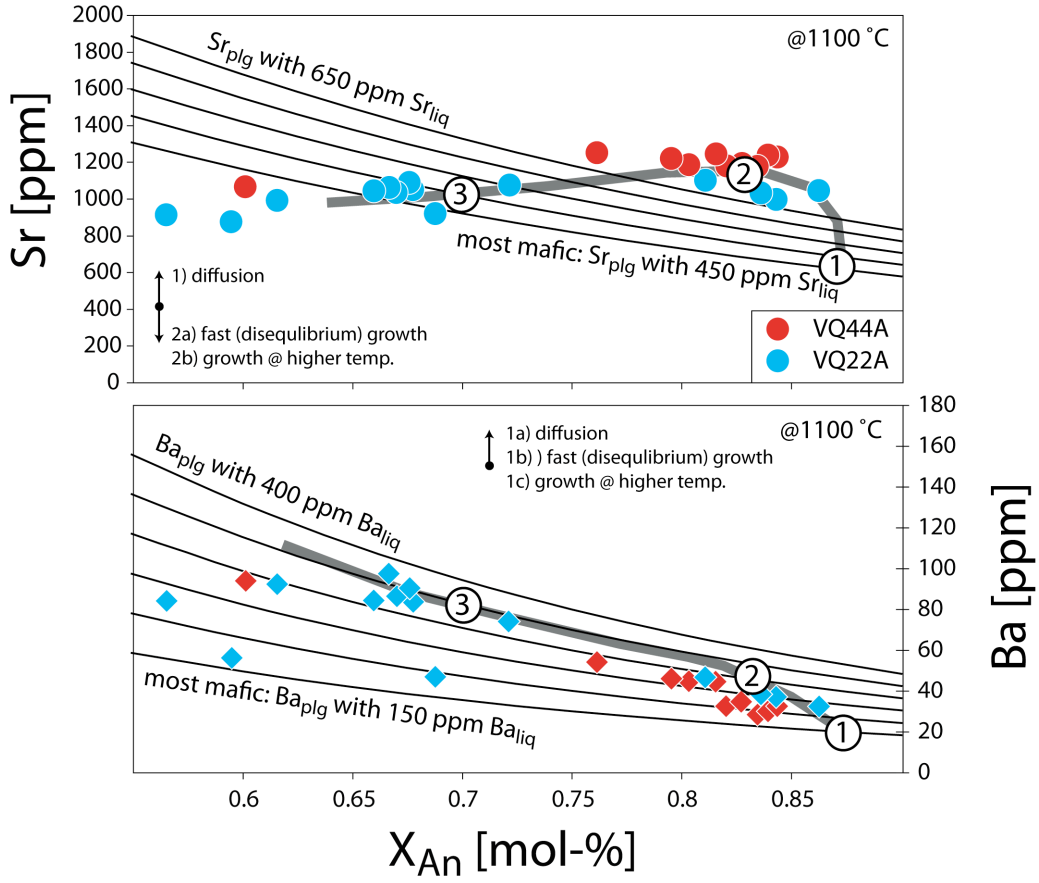

Figure 4.7 LA-ICPMS Data on Andesite-Derived Plagioclase from two Andesite Inclusions. Fractional crystallization accounts for the variation observed in these plagioclase crystals. (1) most mafic crystal poor magma from a peripheral cone; (2) more evolved mafic crystal poor magma from a peripheral cone; (3) groundmass composition for the andesite inclusion VQ-22A (Ba) and mass balance calculated Sr concentration from whole rock composition of VQ-22A.

presence of old dacite-derived plagioclase in plagioclase separates of the andesite inclusions may substantially lower the crystal age and therefore inferred residence time for crystals of mafic recharge magmas.

Independent of the exact crystal residence age for the andesite inclusion we see a distinct temporal relationship for crystal residence in the dacite magma that resides in the shallow magma system and the andesite recharge magma that ascent

from deeper crustal levels, where the maximum age of crystallization of the andesite-derived plagioclase is potentially younger than the age of the dacite-derived plagioclase. This suggests that dacite magma system has been active over thousands of years, while the ascending andesite may be overall crystal poor along its way through the crust by analogy to the crystal-poor peripheral magmas. Significant crystallization in the recharge andesite may occur late in its history, just prior to the interaction with the dacite magma. Furthermore, we see evidence for resorption in the long-lived dacite magma chamber as a consequence of hot mafic recharge. ^{226}Ra-^{230}Th ages would likely be affected by the resorption, since the youngest parts of the crystal are lost. This suggests that ^{226}Ra-^{230}Th crystal model ages may in general be biased toward old growth due to the combination of fluctuating growth and resorption as well as radioactive decay.

4.9 Time Scale of Magma Mixing – Mg in Plagioclase

Elemental diffusion between crystals and glass can be used to delineate the timing of hybridization and magma mingling that is recognized on the micro- and macro scale [e.g., *Zellmer et al.*, 2003; *Costa et al*., 2003]. Most mixing processes may disperse phenocrysts throughout the entire volume participating in the mixing event [e.g., *Jellinek and Kerr*, 1999; *Ruprecht et al*., 2008]. For buoyancy-driven mixing processes in magma chambers the chaotic dispersal is time-dependent with a short pulse of extensive mixing occurring over minutes to hours. Crystals are quickly redistributed with respect to their local chemical environment. The time scale of dispersal is typically much shorter than the time scale of the crystal response by growth or dissolution [*Ruprecht et al*., 2008]. Therefore, crystals may be displaced effectively instantaneously into a melt with which they are in chemical disequilibrium. To attain new chemical equilibrium crystals can (1) shield off the sections of the crystal in disequilibrium by new growth zones that are in chemical equilibrium, (2) partially or fully resorb crystals in chemical disequilibrium, or (3) diffusively exchange components between melt and crystal until chemical

equilibrium is reached. In the following, a combination of modeling the diffusive equilibration and estimating the time of post-mixing crystal growth is used to constrain the timing of recharge, mixing, and subsequent eruption of the 1846/47 lavas.

We use a one-dimensional diffusion finite-difference model following *Costa et al.* [2003] for Mg to estimate a minimum residence time for the andesite-derived plagioclase in the dacite magma:

$$\frac{\partial C_{\mathrm{Mg}}}{\partial \mathrm{t}} = \left(D_{\mathrm{Mg}} \frac{\partial^2 C_{\mathrm{Mg}}}{\partial x^2} + \frac{\partial C_{\mathrm{Mg}}}{\partial x} \frac{\partial D_{\mathrm{Mg}}}{\partial \mathrm{x}}\right) - \frac{A}{\mathrm{RT}} \left(D_{\mathrm{Mg}} \frac{\partial C_{\mathrm{Mg}}}{\partial x} \frac{\partial X_{\mathrm{An}}}{\partial x} + C_{\mathrm{Mg}} \frac{\partial D_{\mathrm{Mg}}}{\partial x} \frac{\partial X_{\mathrm{An}}}{\partial x} + D_{\mathrm{Mg}} C_{\mathrm{Mg}} \frac{\partial^2 X_{\mathrm{An}}}{\partial x^2} \right), \tag{4.7}$$

with the concentration of Mg in the crystal C_{Mg}, the linear factor of *Bindeman et al.* [1998] for Mg partitioning in plagioclase A, the ideal gas constant R, the storage temperature at which diffusion occurs T, and the An zonation pattern of the crystal X_{An}. *Costa et al.* [2003] have shown that one-dimensional models typically overestimate residence times. However, we use the diffusion model to get first order information about the time scale between magma mixing and eruption, therefore a maximum time is still useful. The model does not account for crystal dissolution or growth after crystals have been displaced into an environment of chemical disequilibrium. Diffusion time scales are extended if fast growth occurs. The effects of crystal growth on the diffusion time scales is assessed using the growth-entrapment model of *Watson and Liang* [1995] and *Watson* [1996] with the growth Peclet number Pe:

$$Pe = Vl/D_{Mg}. \tag{4.8}$$

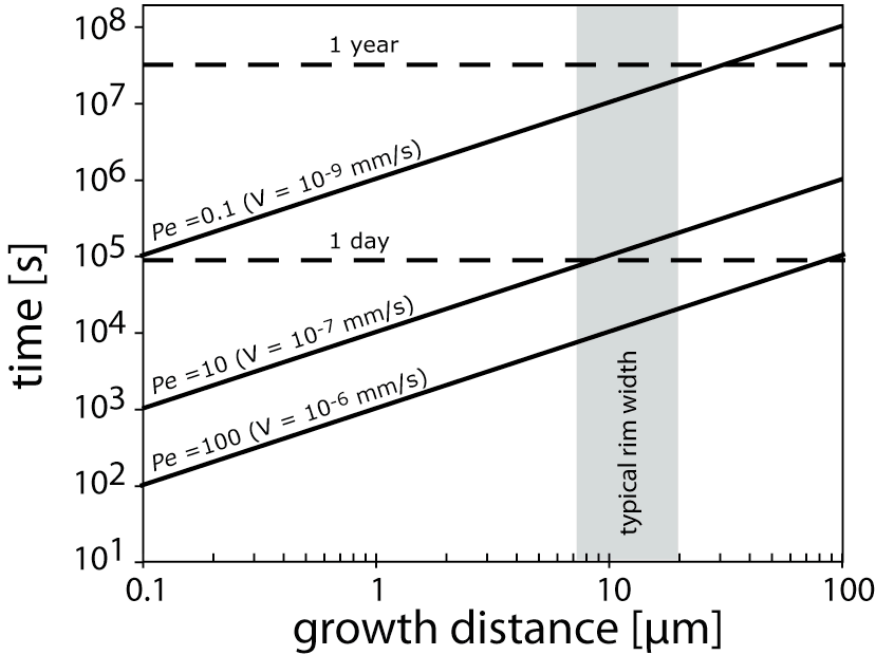

Figure 4.8 Time versus Growth Distance for Different Peclet Numbers. A constant diffusion coefficient of 10-4 $\mu m^2/s$ is assumed.

Here, V, l, and D_{Mg} are the linear growth rate, the half-thickness of the enriched boundary layer, and the diffusion coefficient of Mg, respectively. For Pe = 0.1 growth entrapment is measurable and for Pe = 10 growth entrapment is significant [*Watson*, 1996]. Minimum diffusion coefficients of Mg plagioclase in the hybridized andesites (An_{70} at 1050˚C) are on the order of 10^{-4} $\mu m^2/s$ [*Costa et al.*, 2003]. Given maximum growth rim thicknesses (~10 μm), (Figure 4.8) shows that growth entrapment may be active in the andesite-derived plagioclase from the hybridized andesites only within one year after the mixing of andesite and dacite. Longer time scales require either slower growth, which would results in unaffected diffusion time scales, or growth rim thicknesses larger than what is observed for andesite-derived plagioclase. Therefore, we can provide maximum residence times for the andesite-derived plagioclase crystals in the hybridized magma, where in the case of fast growth diffusion may be limited and the thickness of the growth rims provides the maximum residence time. For slower growth we obtain a maximum residence time through the elemental diffusion modeling.

Table 4.3 Diffusion Time Scales and Pre-[a] and Post-Mixing[b] Storage Conditions

		pre-mixing		post-mixing	
	time [days]	MgO [wt.%]	T [˚C]	MgO [wt.%]	T [˚C]
Andesite-derived plagioclase crystals in hybridized andesite					
Plg27-Line1	11.6				
Plg27-Line2	4.2	3.5	1075		
Plg27-Line3	6.0				
Plg33-Line1	20.1	2.8	1100		
Plg33-Line2	1.6				
Plg35-Line1	5.1	4.1	1050	2.5	1050
Plg35-Line2	5.6				
Dacite-derived plagioclase crystals in hybridized andesite					
Plg3-Line1	< 0.06	0.66	850		
Plg3-Line2	< 0.06	0.66	850		
Plg22-Line1	< 0.06	0.66	850		

[a] Mg concentration and storage temperatures were approximated by a least-quares fitting routine of the initial Mg concentration profile to the measured data in the center of the crystals. Note: The range in initial Mg concentrations is negatively correlated with pre-mixing temperature

[b] Mg concentration and storage temperatures were approximated from plagioclase rim concentration and Fe-Ti oxide geothermometry, respectively.

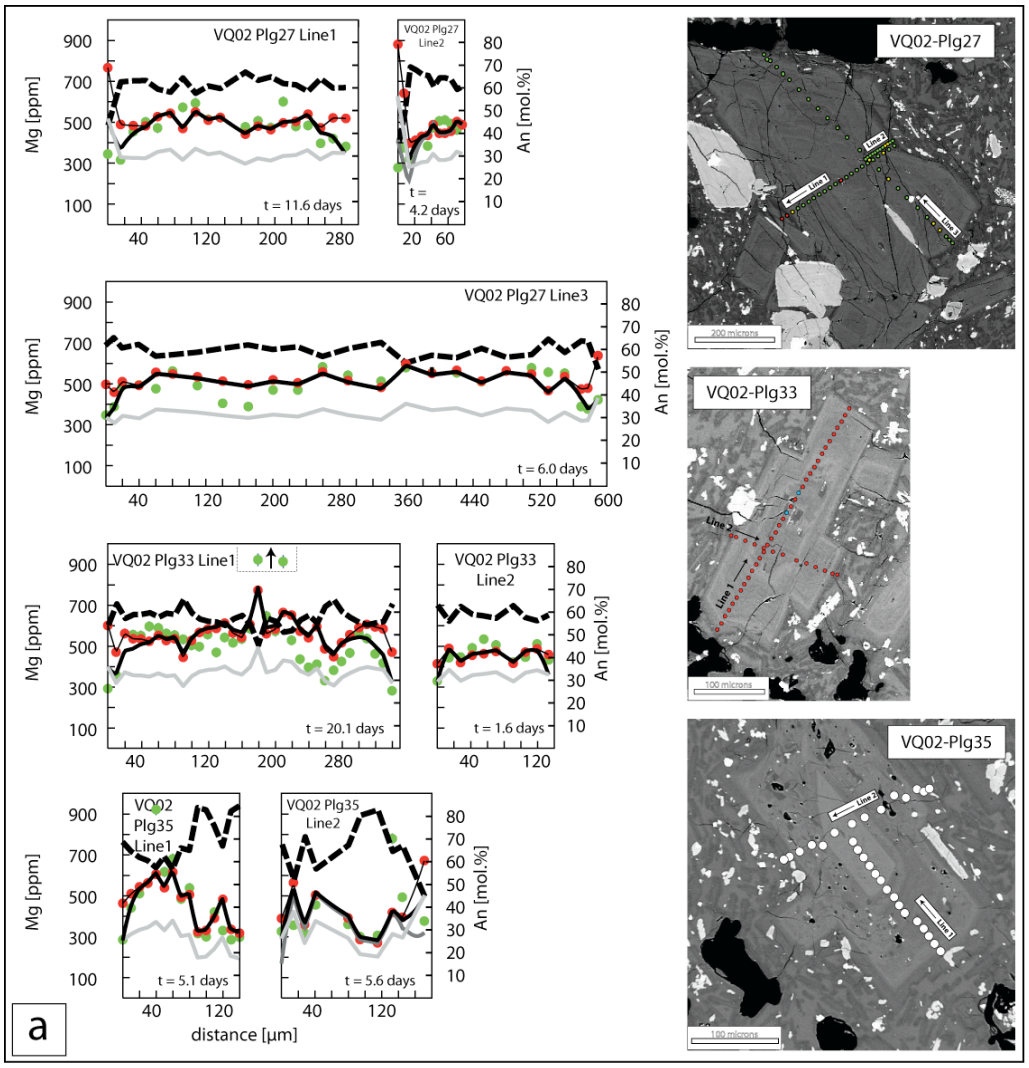

Figure 4.9 Diffusion Profiles for Plagioclase Crystals from a Hybridized Andesite of Quizapu. a) Andesite-derived plagioclase from the hybridized andesite VQ-02. Time scales of magma storage after mixing range between 2 and 20 days. The time scales are maximum estimates, since the model is one-dimensional. Two lines show clear effects of two-dimensional diffusion (VQ-02-Plg27-Line 3, VQ-02-Plg33-Line 1) suggesting shorter diffusion time scales than calculated. b) Diffusion profiles for dacite-derived plagioclase in the hybridized andesite VQ-02. Calculated diffusion time scales are short, since dissolution is dominating. Prior to diffusion andesite-derived plagioclase crystals were stored in a melt with 3-4 wt.% MgO at approximately 1100 ˚C. The dacite-derived crystals were stored in a melt with less than 1 wt.% MgO at approximately 850 ˚C prior to mixing and the onset of diffusion. We assume that magnesium diffusion occurred in the hybridized andesite at 1050 ˚C containing 2.5 wt.% MgO in the melt. For initial conditions and boundary conditions see Table 4.3.

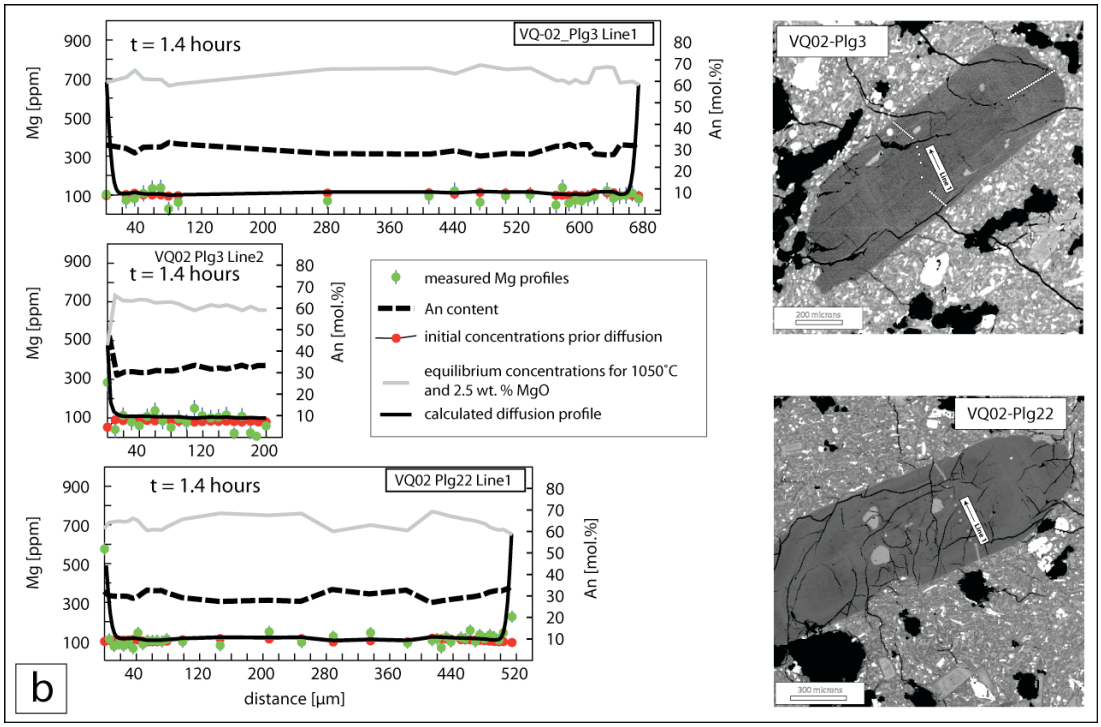

Figure 4.9 continued.

The diffusion model is applied to the hybridized andesite (VQ-02), since the extensive mixing with complete hybridization suggests that these magmas record the longest interaction between dacite and andesite. They provide a maximum time scale associated with the recharge and magma-mixing event. In contrast, andesite-derived plagioclase crystals that are found in mingled dacites of the 1846/47 eruption (e.g., VQ-22) may have spent less time in the dacite magma as reflected by the incomplete mixing. In particular, we focus on the andesite-derived plagioclase crystals that are dispersed throughout the hybridized melt for which we obtained Mg profiles by electron microprobe (Figure 4.9a).

High Mg concentrations in the andesite-derived plagioclase crystals from core to rim indicate chemical equilibrium with an andesite magma containing 3-4

wt.% MgO (i.e. the recharge magma) in the melt at storage temperatures of around 1100˚C (Figure 4.9a). This indicates that even the interior parts of the andesite-derived plagioclase had equilibrated with the andesite recharge magma. The hybridized andesite contains 2.5 wt.% MgO, which is chosen as melt composition and presents a maximum Mg concentration in the glass. Diffusion time scales as a result are also maximum residence time scales. Within the hybridized magma in which diffusion started pre-eruptive storage temperatures of 1050 ˚C have been obtained from Fe-Ti geothermometry [*Ruprecht*, 2009; Chapter 3]. Some of the crystals show small overgrowth rims of more sodic compositions reflecting this change in melt composition. Diffusion exchange is restricted to a narrow zone of about 40 μm close to the rim. The small degree of re-equilibration results in only small deviations of the time scale estimates from a one-dimensional diffusive model compared to more accurate two- or three-dimensional models [*Costa et al*., 2003]. Nonetheless, the one-dimensional model provides maximum time scales for crystal residence times. Diffusion time scales that do not take crystal overgrowth into account provide a residence time for the andesite-derived plagioclase crystals in the newly formed hybridized andesite of 2-20 days (Table 4.3). Fast overgrowth cannot be ruled out, but would on its own require short mixing time scales of days to weeks. This indicates that the events of recharge, mixing, and eruption were probably days to weeks apart of each other. *Gerlach and Grove* [1982] have proposed similar very short succession of mixing and eruption based on olivine zonation.

Dacite-derived plagioclase crystals have also the potential to record the mixing time scale in the hybridized andesite as they find themselves in more mafic glass at higher temperatures than they equilibrated with in the dacite. However, they show no significant diffusive equilibration on the rims as they are actively resorbed in the hot and more mafic hybridized magma. Sodic plagioclase crystals show flat Mg profiles through the entire crystal. Elevated concentrations suggesting diffusive re-equilibration are only observed for rim analyses (Figure 4.9b). This suggests that

dissolution Peclet number *Pe* is larger than 10, therefore that dissolution rates are larger than diffusion rates.

4.10 Conclusions

Shallow crustal magmatic systems are typically assembled over tens of thousands of years [*Reid et al.*, 1997; *Jicha et al.*, 2005] with longer time scales for more evolved magmas. The time scales of crystal storage for Volcán Quizapu reveal predominantly shorter crystal residence time scales for both residing dacite magmas and mafic recharge magmas, on the order of 1000s of yrs (or potentially less, in the case of the andesite). Recharge and residing magma show crystal residence times of similar order. However, results for the mafic magma can only reveal a maximum time scale for plagioclase crystal storage in the mafic magma. Overall we conclude that while crystal residence in the dacite magma was relatively prolonged for 3000-4000 yrs, the mafic recharge magma is characterized by very short crystal residence times and growth that only briefly preceded the ascent and magma interaction with the host dacite magma. This time scale is independent of the transfer time of mafic magma from the mantle wedge to the shallow crustal magma plumbing system. It has been shown that mafic arc magmas may be stored over long time scales in the crust [*Jicha et al.*, 2005] and that lower crustal assimilation and melting processes may alleviate the time restriction imposed by the presence of Ra excess [*Dufek and Cooper*, 2005].

Following results of this work, it is stressed that the interpretation of model bulk separate crystal ages requires careful characterization of the analyzed mineral separate in thin section and in the grain mounts. Mixed crystal populations may have significant effects on the calculated crystal residence times. In the case of the mafic recharge magmas, mineral separates have significant contamination (>10 %) from the dacite plagioclase population, while the plagioclase populations in the thin section of andesite inclusions are much more homogeneous. As other contaminants

such as glass have been corrected for in previous studies [*Cooper et al.*, 2001], it is noted that contamination by different plagioclase population is often more cryptic and therefore difficult to deconvolve. Hence, meaningful model crystal ages can only be obtained from relatively simple systems, which either have single crystal populations or, as in the case of Quizapu, contain different populations that can be identified through geochemical tracers and then corrected for.

While pre-mixing time scales of magma evolution in the shallow crustal magma chamber of Quizapu indicate a slow evolution and rather stagnant conditions in the dacite magma chamber, the transient mixing event shifted the shallow plumbing system into a dynamic environment that developed disequilibrium conditions on the crystal scale. Such disequilibrium conditions have been shown to provide time scale information for magma mixing and subsequent eruption [*Costa et al.*, 2003]. Using Magnesium diffusion in plagioclase reveals that the mixing event at Volcán Quizapu was quickly followed by eruption of the 1846/47 lavas. The time scale of days to weeks suggests that there is a direct connection between the mixing event and the triggering of the eruption. This time scale is most sensitive to temperature estimates for the conditions of diffusive equilibration. Previous studies have estimated conservative temperature estimates for the diffusive equilibration. At Volcán Quizapu independent temperature estimates provide evidence that the reheating as a result of hot andesite recharge and mixing was pervasive for large parts of the dacite magma.

- Chapter 5 -

Final Remarks and Future Directions

As shown throughout the previous chapters of this work, magma mixing is affecting the evolution of subvolcanic plumbing systems on multiple length and time scales. It is responsible for some of the diversity of igneous rocks found on the Earth surface. In particular, magma mixing is the main process that juxtaposes magmas that took on their unique characters in distinct levels of the magmatic mantle-to-surface column, and creates a complexity in the crystal cargo of intermediate to silicic magmas. Such complexity is found throughout the rock record, and systems that follow a closed-system liquid line of descend, which moves magma compositions only towards more evolved compositions, are the exception [*Eichelberger et al.*, 2006]. Although fractional crystallization is the major process that creates the range of magmas observed on Earth, the complexity on the crystal-scale is a result of intermittent periods of magma mixing. Nonetheless, to unravel the complexity of the crystal cargo in mixed magmas requires a dynamic framework that predicts characteristic mixing features on the micro- and macro scale that develop during mixing. In this work, individual aspects of magmatic processes were considered separately and were finally combined to construct and interpret such a framework.

This work has shown that complex crystal populations in a stored magma body can emerge even during a single overturn event, where the complexity is only weakly dependent on the magnitude of potential energy that is released during gas-driven overturn. Multiple overturns eventually results in heterogeneity on the crystal scale, which may obscure the common history of components in the magma. On the bulk scale, stratification has been recognized to be rather the rule than the exception

in mixed viscous fluids [*Oldenburg et al.*, 1989] as a result of the chaotic -not turbulent- flow regime for compositionally intermediate magmas. The arising heterogeneity during magma mixing is thus expressed on both the bulk and on the crystal scale. In the case of gas-driven overturn, time scales of crystal dissolution and magma overturn can be on a similar order of magnitude. This suggests that the loss of information of previous magmatic processes initiates quickly after magma mixing commences. In contrast, crystallization time scales may be too long to record short episodes of dynamic overturn. While melts are hybridized during magma evolution and loose unambiguous memory of the individual magmatic processes over time, crystals retain that memory in the zoning pattern. However, the stored record may be incomplete due to delayed crystallization or record deletion during crystal dissolution. This work examines the time scale of crustal response (via crystallization or dissolution) and shows that a tight competition may exits between changes in chemical potential as a result of magma mixing and the crystal response. Future research should further quantify the relation between time scales of magmatic processes and the crystal response to improve our understanding of what kind of information is stored in the crystal record and which information is inevitably lost as crystals lag behind the dynamic processes in the crust. Moreover, future models should consider phase transitions and the progressive growth of density instabilities. Such models will provide an improved understanding of the time and length scales of magma mixing. As is shown in arc magmatic systems, a solid-liquid disaggregation mechanism may dominate magma mixing in crustal magma chambers. Such mixing is expected to have strong influence on the time and length scales of magma mixing.

To some extent we understand how volcanic expressions (passive degassing, caldera collapse, edifice deformation, effusive and explosive behavior) on the Earth surfaces can be explained by subsurface magmatic processes. However, connecting surface and crustal processes requires further research. One avenue will be the improved understanding of the time scales of magmatic processes that may be

unique for individual physical and chemical processes in the subvolcanic plumbing system. Volcán Quizapu is an ideal system to identify the time scales of magma mixing and storage in intermediate-sized evolved arc systems. As shown also for many other such arc systems, volcanic unrest may be related to transient processes in the upper crustal magma chamber and may not be related to the overall long-term cooling and evolution of the crustal magma chamber.

Though experimental and numerical models can provide a catalog of signatures that are unique to magmatic processes in general and magma mixing in particular, careful selection of natural magmatic systems that can inform us about individual magmatic processes will further improve our understanding of the subvolcanic plumbing system. Volcán Quizapu is such a simple system that has been documented to display a binary mixing between hot vesiculated mafic magmas and cold residing dacite magma. Extensive textural and geochemical characterization enables the identification of the distinct components (mafic and dacitic phenocrysts as well as subordinate antecrysts) that are redistributed during a single mixing event. A record of magma-magma interaction on all scales can be compiled by documenting the variability in a single eruption and comparing the two magmas that record the pre-mixing state. Such records provide the natural parallel to numerical and analog experiments, which can be matched against and mutually inform each other in future studies. Such catalogs are developed for the major magmatic processes (i.e. melting, crystallization, assimilation and mixing), which are now understood on their fundamental thermodynamic and kinematic level. This knowledge combined with petrographic and petrologic tools known for a few decades enables the development of a unifying process-related concept of magma evolution in the crust. Even though natural systems may show unlimited levels of complexity, the underlying fundamental processes repeat themselves over and over again. Therefore, the complexity observed in natural systems is mostly driven by (1) the varying boundary conditions imposed in the various tectonic setting found on

Earth and (2) the variable combination of melting, mixing, crystallization, and assimilation when magmas are assembled on their way from the mantle through the crust to the Earth surface.

BIBLIOGRAPHY

Anderson, A. (1976), Magma mixing: petrological process and volcanological tool, *Journal of Volcanology and Geothermal Research*, *1*, 3-33.

Aref, H. (1990), Chaotic Advection of Fluid Particles, *Philosophical Transactions: Physical Sciences and Engineering*, *333*, 273-288.

Bachmann, O., M. A. Dungan, and P. W. Lipman (2002), The Fish Canyon Magma Body, San Juan Volcanic Field, Colorado: Rejuvenation and Eruption of an Upper-Crustal Batholith, *Journal of Petrology*, *43*, 1469-1503.

Bachmann, O., and M. A. Dungan (2002), Temperature-induced Al-zoning in hornblendes of the Fish Canyon magma, Colorado, *American Mineralogist*, *87*, 1062-1076.

Bachmann, O., and G. W. Bergantz (2004), On the Origin of Crystal-poor Rhyolites: Extracted from Batholitic Crystal Mushes, *Journal of Petrology*, *45*, 1565-1582.

Bachmann, O., B.L.A. Charlier, and J. B. Lowenstern (2007), Zircon crystallization and recycling in the magma chamber of the rhyolitic Kos Plateau Tuff (Aegean Arc), *Geology*, *35*, 73-76.

Bacon, C. R., and J. Metz (1984), Magmatic inclusions in rhyolites, contaminated basalts, and compositional zonation beneath the Coso volcanic field, California, *Contributions to Mineraolgy and Petrology*, *85*, 346-365, doi: 10.1007/BF01150292.

Bacon, C. R., and J. B. Lowenstern (2005), Late Pleistocene granodiorite source for recycled zircon and phenocrysts in rhyodacite lava at Crater Lake, Oregon, *Earth and Planetary Science Letters*, *233*, 277-293, doi: 10.1016/j.epsl.2005.02.012.

Bacon, C. R., and M. A. Lanphere (2006), Eruptive history and geochronology of Mount Mazama and the Crater Lake region, Oregon, *Geological Society of America Bulletin*, *118*, 1331-1359, doi: 10.1130/B25906.1.

Beckermann, C., and R. Viskanta (1993), Mathematical modeling of transport phenomena during alloy solidification, *Applied Mechanics Reviews*, *46*, 1-27.

Bergantz, G. W., and J. Ni (1999), A numerical study of sedimentation by dripping instabilities in viscous fluids, *International Journal of Multiphase Flow*, *25*, 307 - 320.

Bergantz, G. W., and R. E. Breidenthal (2001), Non-stationary entrainment and tunneling eruptions: A dynamic link between eruption processes and magma mixing, *Geophysical Research Letters*, *28*, 3075 - 3078.

Bindeman, I. N., A. M. Davis, and M. J. Drake (1998), Ion microprobe study of plagioclase-basalt partition experiments at natural concentration levels of trace elements, *Geochemica Cosmochemica Acta*, *62*, 1175-1193.

Bindeman, I. N., and J. W. Valley (2002), Oxygen isotope study of the Long Valley magmaz system, California: isotope thermometry and convection in large silicic magma bodies, *Contributions to Mineralogy and Petrology*, *144*, 185-205.

Blundy J.D., and B. J. Wood (1991), Crystal-chemical controls on the partitioning of Sr and Ba between plagioclase feldspar, silicate melts, and hydrothermal solutions, *Geochemica Cosmochemica Acta*, *55*, 193-209.

Blundy J., and B. Wood (1994), Prediction of crystal-melt partition coefficients from elastic moduli, *Nature*, *372*, 452-454.

Blundy J., and B. Wood (2003), Mineral-melt partitioning of uranium, thorium and their daughters, *Reviews in Mineralogy and Geochemistry*, *52*, 59-123.

Blundy, J., K. Cashman, and M. Humphreys (2006), Magma heating by decompression-driven crystallization beneath andesite volcanoes, *Nature*, *443*, 76-80.

Bourdon, B., A. Zindler, and G. Wörner (1994), Evolution of the Laacher See magma chamber: Evidence from SIMS and TIMS measurements of U-Th disequilibria in minerals and glasses. *Earth and Planetary Science Letters*, 126, 75-90.

Bowen, N. L. (1928), The evolution of the igneous rocks, 334 pp., Princeton University.

Brophy, J. G. (1991), Compositional gaps, critical crystallinity, and fractional crystallization in orogenic (calc-alkaline) magmatic systems, *Contributions to Mineralogy and Petrology*, *109*, 173-182, doi: 10.1007/BF00306477.

Browne B.L., J. Eichelberger, L. C. Patino, T. A. Vogel, J. Dehn, K. Uto, and H. Hoshizumi (2006), Generation of Porphyritic and Equigranular Mafic

Enclaves During Magma Recharge Events at Unzen Volcano, Japan, *Journal of Petrology*, *47*, 301-328.

Burgisser, A., G. W. Bergantz, and R. E. Breidenthal (2005), Addressing complexity in laboratory experiments: the scaling of dilute multiphase flows in magmatic systems, *Journal of Volcanology and Geothermal Research*, *141*, 245 - 265.

Cashman, K. V., and B. D. Marsh (1988), Crystal size distribution (CSD) in rocks and the kinetics and dynamics of crystallization; II. Makaopuhi lava lake. *Contributions to Mineralogy and Petrology*, *99*, 292-305.

Cashman, K. V. (1990), Textural constraints on the kinetics of crystallization of igneous rocks, in *Modern methods of igneous petrology, understanding magmatic processes*, *Reviews in Mineralogy*, 24, 259-314.

Chandrasekhar, S. (1961), *Hydrodynamic and Hydromagnetic Stability*, 654 pp., Oxford Univ.Press, London.

Charlier, B. L. A., C. J. N. Wilson, J. B. Lowenstern, S. Blake, P. W. van Calsteren, and J. P. Davidson (2005), Magma Generation at a Large, Hyperactive Silicic Volcano (Taupo, New Zealand) Revealed by U-Th and U-Pb Systematics in Zircons, *Journal of Petrology*, *46*, 3-32, doi: 10.1093/petrology/egh060.

Cherniak, D. J. (1995), Diffusion of lead in plagioclase and K-feldspar: an investigation using Rutherford Backscattering and Resonant Nuclear Reaction Analysis, *Contributions to Mineralogy and Petrology*, *120*, 358-371, doi: 10.1007/BF00306513.

Cherniak, D. J. (2002), Ba diffusion in feldspar, *Geochimica et Cosmochimica Acta*,

66, 1641-1650.

Cherniak, D. J. (2003), REE diffusion in feldspar, *Chemical Geology*, *193*, 25-41.

Cherniak, D., and E. Watson (1994), A study of strontium diffusion in plagioclase using Rutherford backscattering spectroscopy, *Geochimica et Cosmochimica Acta*, *58*, 5179-5190.

Cioni, R., L. Civetta, P. Marianelli, N. Metrich, R. Santacroce, and A. Sbrana (1995), Compositional Layering and Syn-eruptive Mixing of a Periodically Refilled Shallow Magma Chamber: the AD 79 Plinian Eruption of Vesuvius, *Journal of Petrology*, *36*, 739-776.

Clynne, M. (1999), A complex magma mixing origin for rocks erupted in 1915, Lassen Peak, California, *Journal of Petrology*, *40*, 105-132.

Coltice, N., and J. Schmalzl (2006), Mixing times in the mantle of the early Earth derived from 2-D and 3-D numerical simulations of convection, *Geophysical Research Letters*, *33*, L23304, doi:10.1029/2006GL027707.

Condomines, M., P. Gauthier, and O. Sigmarsson (2003), Timescales of magma chamber processes and dating of young volcanic rocks, *Reviews in Mineralogy and Geochemistry*, *52*, 125-174.

Coombs, M. L., J. C. Eichelberger and M. J. Rutherford (2003), Experimental and textural constraints on mafic enclave formation in volcanic rocks, *Journal of Volcanology and Geothermal Research*, *119*, 125-144.

Coombs, M. L., and J. E. Gardner (2004), Reaction rim growth in silicic melts: Implications for magma mixing, *American Mineralogist*, *89*, 748-459.

Cooper, K. M., M. R. Reid, M. T. Murrell, and D. A. Clague (2001), Crystal and magma residence at Kilauea Volcano, Hawaii: 230Th-226Ra dating of the 1955 east rift eruption, *Earth and Planetary Science Letters*, *184*, 703-718.

Cooper, K. M., and M. R. Reid (2003), Re-examination of crystal ages in recent Mount St. Helens lavas: implications for magma reservoir processes, *Earth and Planetary Science Letters*, *213*, 149-167.

Cooper, K. M., and C. T. Donnelly (2008), 238U-230Th-226Ra disequilibria in dacite and plagioclase from the 2004-2005 eruption of Mount St. Helens. In: Sherrod, D. R., W. E. Scott, and P. H. Stauffer, A Volcano Rekindled: The Renewed Eruption of Mount St. Helens, 2004-2006, *U. S. Geological Survey Professional Paper*, *1750*, 827-845.

Cooper, K. M., and M. R. Reid (2008), Uranium-series Crystal Ages, *Reviews in Mineralogy and Geochemistry*, *69*, 479-544.

Costa, F., and B. Singer (2002), Evolution of holocene Dacite and Compositionally Zoned Magma, Volcan San Pedro, Southern Volcanic Zone, Chile, *Journal of Petrology*, *43*, 1571-1593.

Costa, F., S. Chakraborty, and R. Dohmen (2003), Diffusion coupling between trace and major elements and a model for calculation of magma residence times using plagioclase, *Geochimica et Cosmochimica Acta*, *67*, 2189-2200.

Costa, F., and S. Chakraborty (2004), Decadal time gaps between mafic intrusion and silicic eruption obtained from chemical zoning in olivine, *Earth and Planetary Science Letters*, *227*, 517-530.

Costa, F., B. Scaillet, and M. Pichavant (2004), Petrological and experimental constraints on the pre-eruption conditions of Holocene dacite from Volcan San Pedro (36 degrees S, Chilean Andes) and the importance of sulphur in silicic subduction-related magmas, *Journal of Petrology*, *45*, 855-881, doi: 10.1093/petrology/egg114.

Costa F., and M. A. Dungan (2005), Short time scales of magmatic assimilation from diffusion modeling of multiple elements in olivine, *Geology*, *33*, 837-840.

Couch, S., R. S. J. Sparks, and M. R. Carroll (2001), Mineral disequilibrium in lavas explained by convective self-mixing in open magma chambers, *Nature*, *411*, 1037-1039.

Couch, S., R. S. J. Sparks, and M. R. Carroll (2003), The Kinetics of Degassing-Induced Crystallization at Soufriere Hills Volcano, Montserrat, *Journal of Petrology*, *44*, 1477-1502.

Couch, S. (2003), Experimental investigation of crystallization kinetics in a haplogranite system, *American Mineralogist*, *88*, 1471-1485.

Davidson, J. P. and F. J. Tepley III (1997), Recharge in Volcanic Systems: Evidence from Isotope Profiles of Phenocrysts, *Science*, *275*, 826-829.

Davidson, J. P., D. J. Morgan, B. L. A. Charlier, R. Harlou, and J. Hora (2007), Tracing magmatic processes and timescales through mineral- scale isotopic data, *Annual Reviews of Earth and Planetary Sciences*, *35*, 273-311.

Derksen, J. J. (2003), Numerical Simulation of Solids Suspension in a Stirred Tank, *AIChE Journal*, *49*, 2700-2714.

DePaolo, D. J. (1981), Trace element and isotopic effects of combined wallrock assimilation and fractional crystallization. *Earth Planetary Science Letters*, *53*, 189-202.

Dimanov, A., and V. Sautter (2000), "Average" interdiffusion of (Fe,Mn)-Mg in natural diopside, *European Journal of Mineralogy*, *12*, 749-760.

Domeyko, I., and J. Tocornal (1849), Facultad de Medicina I de Ciencias Fisicas i Matemáticas session del 11 de setiembre de 1849: Viajes a las Cordilleras de Talca i de Chillian, Segunda Parte, [Santiago: s.n.].

Donaldson, C. H. (1985), The rates of dissolution of olivine, plagioclase, and quartz in a basalt melt, *Mineralogical Magazine*, *49*, 683-693.

Dowty, E. (1980), Crystal Growth and Nucleation Theory and the Numerical Simulation of Igneous Crystallization, in *Physics of Magmatic Processes*, edited by R. B. Hargraves, 420-485, Princeton Univ. Press, Princeton.

Dufek, J., and G. W. Bergantz (2005), Transient two-dimensional dynamics in the upper conduit of a rhyolitic eruption: A comparison of closure models for the granular stress, *Journal of Volcanology and Geothermal Research*, *143*, 113-132.

Dufek, J., and K. M. Cooper (2005), $^{226}Ra/^{230}Th$ excess generated in the lower crust: Implications for magma transport and storage time scales, *Geology*, *33*, 833-836.

Dufek, J., and G. W. Bergantz (2007), Dynamics and deposits generated by the Kos Plateau Tuff eruption: controls of basal particle loss on pyroclastic flow

transport, *Geochemistry Geophysics Geosyst*ems, *8*, Q12007, doi:10.1029/2007GC001741.

Edwards, B. R., and J. K. Russell (1996), A review and analysis of silicate mineral dissolution experiments in natural silicate melts, *Chemical Geology*, *130*, 233-245.

Eichelberger, J. C. (1980), Vesiculation of mafic magma during replenishment of silicic magma reservoirs, *Nature*, *288*, 446-450.

Eichelberger, J. C., and H. R. Westrich (1981), Magmatic Volatives in Explosive Rhyolitic Eruptions, *Geophysical Research Letters*, *8*, 757-760.

Eichelberger, J. C., C. R. Carrigan, H. R. Westrich, and R. H. Price (1986), Non-explosive silicic volcanism, *Nature*, *323*, 598-602.

Eichelberger, J. C., and P. E. Izbekov (2000) Eruption of andesite triggered by dyke injection: contrasting cases at Karymsky Volcano, Kamchatka and Mt Katmai, Alaska, *Royal Society of London Philosophical Transactions*, *A358*, 1465-1485.

Eichelberger, J. C., P. E. Izbekov, and B. L. Browne (2006), Bulk chemical trends at arc volcanoes are not liquid lines of descent, *Lithos*, *87*, 135-154.

Fabbrizzio, A., M. W. Schmidt, D. Günther, and J. Eikenberg (2009), Experimental determination of Ra mineral/melt partitioning for feldspars and ^{226}Ra-disequilibrium crystallization ages of plagioclase and alkali-feldspars, *Earth and Planetary Science Letters*, *280*, 137-148.

Feeley, T. C., and M. D.. Dungan (1996), Compositional and Dynamic Controls on mafic-silicic magma Interactions at Continental Arc Volcanoes: Evidence from Cordón El Guadal, Tatara-San Pedro Complex, Chile, *Journal of Petrology*, *37*, 1547-1577.

Ferrachat, S., and Y. Ricard (1998), Regular vs. chaotic mantle mixing, *Earth and Planetary Science Letters*, *155*, 75-86.

Folch, A., and J. Martí (1998), The generation of overpressure in felsic magma chambers by replenishment, *Earth and Planetary Science Letters*, *163*, 301-314.

Freer, R., and Z. Hauptman (1978), Experimental study of magnetite-titanomagnetite interdiffusion, *Physics of the Earth and Planetary Interiors*, *16*, 223-231.

García-Casco, A., R. L. Torres-Roldán, G. Millán, P. Monié, and J. Schneider (2002), Oscillatory zoning in eclogitic garnet and amphibole, Northern Serpentinite Melange, Cuba: a record of tectonic instability during subduction?, *Journal of Metamorphic Geology*, *20*, 581-598, doi: 10.1046/j.1525-1314.2002.00390.x.

Gardner, J., S. Carey, M. J. Rutherford, and H. Sigurdsson (1995), Petrologic diversity in Mount St. Helens dacites during the last 4,000 years – implications for magma mixing, *Contributions to Mineralogy and Petrology*, *119*, 224-238.

Gauthier, P. J., and M. Condomines (1999) ^{210}Pb-^{226}Ra radioactive disequilibria in recent lavas and radon degassing: inferences on the magma chamber

dynamics at Stromboli and Merapi volcanoes. *Earth and Planetary Science Letters*, *172*, 111–126.

Gerlach, D., and T. Grove (1982) Petrology of Medicine Lake Highland volcanics: Characterization of endmembers of magma mixing, *Contributions to Mineralogy and Petrology*, *80*, 147-159.

Gerlach, T. M., H. R. Westrich, and R. B., Symonds (1996), Preeruption Vapor in Magma of the Climactic Mount Pinatubo Eruption: Source of the Giant Stratospheric Sulfur Dioxide Cloud, in *Fire and Mud: Eruptions and Lahars of Mount Pinatubo, Philippines*, edited by C. G. Newhall and R. S. Punongbayan, 415-433, Washington Univ. Press, Seattle.

Geschwind, C., and M. J. Rutherford (1995) Crystallization of microlites during magma ascent: the fluid mechanics of 1980–1986 eruptions at Mount St Helens, *Bulletin of Volcanology*, *57*, 356-370.

Ghiorso, M. S., and B. W. Evans (2008), Thermodynamics of Rhombohedral Oxide Solid Solutions and a Revision of the Fe-Ti Two-Oxide Geothermometer and Oxygen-Barometer, *American Journal of Science*, *308*, 957-1039, doi: 10.2475/09.2008.01.

Gidaspow, D. (1994), *Multiphase flow and fluidization: continuum and kinetic theory descriptions*, 467 pp., Academic Press, Boston.

Giletti, B. J., and T. M. Shanahan (1997), Alkali diffusion in plagioclase feldspar, *Chemical Geology*, *139*, 3-20.

Ginibre, C., A. Kronz, and G. Wörner (2002a), High-resolution quantitative imaging of plagioclase composition using accumulated backscattered electron images: new constraints on oscillatory zoning, *Contributions to Mineralogy and* Petrology, *142*, 436-448.

Ginibre, C., G. Wörner, and A. Kronz (2002b), Minor- and trace-element zoning in plagioclase: implications for magma chamber processes at Parinacota Volcano, northern Chile, *Contributions to Mineralogy and Petrology*, *143*, 300-315.

Ginibre, C., G. Wörner, and A. Kronz (2004), Structure and Dynamics of the Laacher See Magma Chamber (Eifel, Germany) from Major and Trace Element Zoning in Sanidine: a Cathodoluminescence and Electron Microprobe Study, *Journal of Petrology*, *45*, 2197-2223.

Giordano, D., J. K. Russell, and D. B. Dingwell (2008) Viscosity of magmatic liquids: A model, *Earth and Planetary Science Letters*, *271*, 123-134.

Grunder, A. L., and G. A. Mahood (1988), Physical and Chemical Models of Zoned Silicic Magmas: The Loma Seca Tuff and Calabozos Caldera, Southern Andes, *Journal of Petrology*, *29*, 831-867, doi: 10.1093/petrology/29.4.831.

Heath, E., R. Macdonald, H. E. Belkin, C. J. Hawkesworth, and H. Sigurdsson (1998), Magmagenesis at Soufriere Volcano, St. Vincent, Lesser Antilles arc, *Journal of Petrology*, *39*, 1721-1764.

Hess, K., and D. Dingwell (1996) Viscosities of hydrous leucogranitic melts: A non-Arrhenian model, *American Mineralogist*, *81*, 1297-1300.

Higgins, M. D. (2000), Measurement of crystal size distributions, *American Mineralogist*, *85*, 1105-1116.

Hammer, J., and M. J. Rutherford (2002), An experimental study of the kinetics of decompression-induced crystallization in silicic melt, *Journal of Geophysical Research*, *107*, 148-227.

Hersum, T., and B. Marsh (2007), Igneous textures: On the kinetics behind the words, *Elements*, *3*, 247-252.

Hildreth, W., and R. E. Drake (1992), Volcán Quizapu, Chilean Andes, *Bulletin of Volcanology*, *54*, 93-125.

Hildreth, W., and J. Fierstein (2000), Katmai volcanic cluster and the great eruption of 1912, *Geological Society of America Bulletin*, *112*, 1594-1620.

Holland, T., and J. Blundy (1994), Non-ideal interactions in calcic amphiboles and their bearing on amphibole-plagioclase thermometry, *Contributions to Mineralogy and Petrology*, *116*, 433-447, doi: 10.1007/BF00310910.

Holtz, F., H. Sato, J. Lewis, H. Behrens, and S. Nakada (2005), Experimental petrology of the 1991-1995 Unzen dacite, Japan. Part I: Phase relations, phase composition and pre-eruptive conditions, *Journal of Petrology*, *46*, 319-337, doi: 10.1093/petrology/egh077.

Huber, C., O. Bachmann, M. Manga (2009) Homogenization processes in silicic magma chambers by stirring and mushification (latent heat buffering). *Earth and Planetary Science Letters*, *283*, 38-47.

Humphreys, M. C. S., J. D. Blundy, and R. S. J. Sparks (2006), Magma evolution and open-system processes at Shiveluch Volcano: Insights from phenocryst zoning, *Journal of Petrology*, *47*, 2303-2334.

Humphreys, M., T. Christopher, and V. Hards (2009), Microlite transfer by disaggregation of mafic inclusions following magma mixing at Soufrière Hills volcano, Montserrat, *Contributions to Mineralogy and Petrology*, *157*, 609-624, doi: 10.1007/s00410-008-0356-3.

Jackson, M. J., and B. Mills (1997), Dissolution of quartz in vitrified ceramic materials, *Journal of Material Sciences*, *32*, 5295–5304.

Jaupart, C., and C. J. Allegre (1991), Gas content, eruption rate and instabilities of eruption regime in silicic volcanoes, *Earth and Planetary Science Letters*, *102*, 413-429, doi: 10.1016/0012-821X(91)90032-D.

Jellinek, A. M., R. C. Kerr, R. W. Griffiths (1999), Mixing and compositional stratification produced by natural convection: 1. Experiments and their application to Earth's core and mantle, *Journal of Geophysical Research*, *104*, 7183-7201.

Jellinek, A. M., and R. C. Kerr (1999), Mixing and compositional stratification produced by natural convection: 2. Applications to the differentiation of basaltic and silicic magma chambers and komatiite lava flows, *Journal of Geophysical Research*, *104*, 7203-7218.

Jicha, B. R., B. S. Singer, B. L. Beard, and C. M. Johnson (2005), Contrasting timescales of crustallization and magma storage beneathe the Aleutian Island arc, *Earth and Planetary Science Letters*, *236*, 195-210.

Jicha, B. R., B. S. Singer, B. L. Beard, C. M. Johnson, H. Moreno-Roa, and J. A. Naranjo (2007) Rapid magma ascent and generation of ^{230}Th excesses in the lower crust at Puyehue-Cordón Caulle, Southern Volcanic Zone, Chile, *Earth and Planetary Science Letters*, *255*, 229-242.

Jicha, B. R., C. M. Johnson, W. Hildreth, B. L. Beard, G. L. Hart, S. B. Shirey, B. S. and Singer (2009) Discriminating assimilants and decoupling deep- vs. shallow-level crystal records at Mount Adams using ^{238}U/^{230}Th disequilibria and Os isotopes, *Earth and Planetary Science Letters*, *277*, 38-49.

Johnson, D. M., P. R. Hooper, and R. M. Conrey (1999), XRF analysis of rocks and minerals for major and trace elements on a single low dilution Li-tetraborate fused bead, *Advances in X-ray Analysis*, 41, 843-867.

Kayzar, T. M, K. M. Cooper , M. K. Reagan, and A. J. R. Kent (2009), Gas transport model for the magmatic system at Mount Pinatubo, Philippines: Insights from (^{210}Pb)/(^{226}Ra), *Journal of Volcanology and Geothermal Research*, *181*, 124-140.

Kellogg, L. H., and D. L. Turcotte (1990), Mixing and the distribution of heterogeneities in a chaotically convecting mantle, *Journal Geophysical Research*, *95*, 421-432, doi:10.1029/JB095iB01p00421.

Kent, A. J. R., E. M. Stolper, D. Francis, J. Woodhead, R. Frei, J. Eiler (2004), Mantle heterogeneity during the formation of the North Atlantic Igneous Province: Constraints from trace element and Sr-Nd-Os-O isotope systematics of Baffin Island picrites, *Geochemistry Geophysics Geosystems*, *5*, Q11004, doi: 10.1029/2004GC000743.

Kent A. J. R., J. Blundy, K. Cashman, K. M. Cooper, C. Donnelly, J. S. Pallister, M. Reagan, M. C. Rowe, C. R. Thornber (2007), Vapor transfer prior to the October 2004 eruption of Mount St. Helens, Washington, *Geology*, *35*, 231-234.

Kerr, R.C. (1995) Convective Crystal Dissolution, *Contrib. Min. Pet.*, *121*, 237-246.

Knesel, K. M., J. P. Davidson, and W. A. Duffield (1999), Evolution of Silicic Magma through Assimilation and Subsequent Recharge: Evidence from Sr Isotopes in Sanidine Phenocrysts, Taylor Creek Rhyolite, NM, *Journal of Petrology*, *40*, 773-786.

Lange, R. A., H. M. Frey, and J. Hector (2009), A thermodynamic model for the plagioclase-liquid hygrometer/thermometer, *American Mineralogist*, *94*, 494-506.

Larsen, J. F. (2005), Experimental study of plagioclase rim growth around anorthite seed crystals in rhyodacitic melt, *American Mineralogist*, *90*, 417-427.

Leake, B. E., A. R. Woolley, C. E. S. Arps, W. D. Birch, M. C. Gilbert, J. D. Grice, F. C. Hawthorne, A. Kato, H. J. Kisch, V. G. Krivovichev, K. Linthout, J. Laird, J. A. Mandarino, W.V. Maresch, E. H. Nickel, N. M. S. Rock, J. C.

Schumacher, D. C. Smith, N. C. N. Stephenson, L. Ungaretti, E. J. W. Whittaker, G Youzhi (1997) Nomenclature of amphiboles; report of the subcommittee on amphiboles of the International Mineralogical Association, Commission on New Minerals and Mineral Names, *Canadian Mineralogist*, *35*, 219-246.

Liang, Y. (2000), Dissolution in molten silicates: Effects of solid motion, *Geochimica et Cosmochimica Acta*, *64*, 1617-1627.

Liang, Y. (2003), Kinetics of crystal-melt reaction in partially molten silicates: 1. Grain scale processes, *Geochemistry Geophysics Geosystems*, *4*, 1045, doi: 10.1029/2002GC000375.

Linden, P.F. and J. M. Redondo (1991), Molecular mixing in Rayleigh-Taylor instability. Part I: Global mixing. *Physics of Fluids A: Fluid Dynamics*, *3*, 1269-1277.

Longhi J., D. Walker, and J. F. Hays (1976), Fe and Mg in plagioclase, *Lunar Science Conference Proceedings 7th*, *1*, 1281-1300.

Longhi, J., and C. M. Bertka (1996), Graphical analysis of pigeonite-augite liquidus equilibria, *American Mineralogist*, *81*, 685-695.

Longo, A., M. Vassalli, P. Papale, and M. Barsanti (2006) Numerical simulation of convection and mixing in magma chambers replenished with CO2-rich magma. *Geophysical Research Letters*, *33*, L21305, doi:10.1029/2006GL027760.

Maksimov, A. (2008) A physicochemical model for deep degassing of water-rich magma, *Journal of Volcanology and Seismology*, *2*, 356-263.

Marsh, B. D. (1988), Crystal capture, sorting, and retention in convecting magma, *Geological Society of America Bulletin*, *100*, 1720-1737.

Marsh, B. D. (1989), On convective style and vigor in sheet-like magma chambers, *Journal of Petrology*, *30*, 479-530.

Marsh, B. D. (1998), On the interpretation of Crystal Size Distributions in Magmatic Systems, *Journal of Petrology*, *39*, 553-599.

Maxey, M. R., and J. J. Riley (1983), Equation of motion for a small rigid sphere in a nonuniform flow, *Physics of Fluids*, *26*, 883-889.

McIntyre, G. A., C. Brooks, W. Compston, and A. Turek (1966),The statistical assessment of Rb-Sr isochrons, *Journal of Geophysical Research*, *71*, 5459-5468.

Morgan, D. J., S. Blake, N. W. Rogers, B. DeVivo, G. Rolandi, R. Macdonald, and C. J. Hawkesworth (2004), Time scales of crystal residence and magma chamber volume from modeling of diffusion profiles in phenocrysts: Vesuvius 1944, *Earth and Planetary Science Letters*, *222*, 933-946.

Morgan, D. J., and D. A. Jerram (2006), On estimating crystal shape for crystal size distribution analysis, *Journal of Volcanology and Geothermal Research*, *154*, 1-7.

Morgan, D. J., D. A. Jerram, D. G. Chertkoff, J. P. Davidson, D. G. Pearson, A. Kronz, and G. M. Nowell (2007), Combining CSD and isotopic

microanalysis: Magma supply and mixing processes at Stromboli Volcano, Aeolian Islands, Italy, *Earth and Planetary Science Letters*, *260*, 419-431.

Morgan, D., and S. Blake (2006), Magmatic residence times of zoned phenocrysts: introduction and application of the binary element diffusion modelling (BEDM) technique. *Contributions to Mineralogy and Petrology*, *151*, 58-70.

Murphy, M. D., R. S. J. Sparks, J. Barclay, M. R. Carroll, and T. S. Brewer (2000) Remobilization of Andesite Magma by Intrusion of Mafic Magma at the Soufriere Hills Volcano, Montserrat, West Indies, *Journal of Petrology*, *41*, 21-42(2000).

Murphy, M. D., R. S. J. Sparks, J. Barclay, M. R. Carroll, A. M. Lejeune, T. S. Brewer, R. Macdonald, S. Black, and S. Young (1998), The role of magma mixing in triggering the current eruption at the Soufriere Hills Volcano, Montserrat, West Indies, *Geophysical Research Letters*, *25*, 3433–3436.

Nakamura, M (1995), Continuous mixing of crystal mush and replenished magma in the ongoing Unzen eruption, *Geology*, *23*, 807-810.

Namiki, A., and M. Manga (2006) Influence of decompression rate on the expansion velocity and expansion style of bubbly fluids, *Journal of Geophysical Research*, *111*, B11208, doi: 10.1029/2005JB004132.

Nelson, S. T., and A. Montana (1992), Sieve-textured plagioclase in volcanic rocks produced by rapid decompression, *American Mineralogist*, *77*, 1242-1249.

Nitsche, J. M. and G. K. Batchelor (1997), Break-up of a falling drop containing dispersed particles, *Journal of Fluid Mechanics*, *340*, 161-175.

Oldenburg, C. M., F. J. Spera, D. A. Yuen, and G. Sewell (1989), Dynamic Mixing in Magma Bodies: Theory, Simulations and Implications, *Journal of Geophysical Research*, *94*, 9215-9236.

Ottino, J. M. (1990), Mixing, Chaotic Advection, and Turbulence, *Annual Reviews of Fluid Mechanics*, 22, 207-253.

Pallister, J.S., R. P. Hoblitt, and A. G. Reyer (1992), A basalt trigger for the 1991 eruption of Pinatubo volcano?, *Nature*, *356*, 426-428.

Papale, P., A. Neri, and G. Macedonio (1998), The role of magma composition and water content in explosive eruptions: 1. Conduit ascent dynamics, *Journal of Volcanology and Geothermal Research*, *87*, 75-93.

Patankar, S.V. (1980), *Numerical heat transfer and fluid flow*, 210 pp., Hemisphere Publishing Corp., Washington, D. C.

Phillips, J. C., and A. W. Woods (2001), Bubble plumes generated during recharge of basaltic magma reservoirs, *Earth and Planetary Science Letters*, *186*, 297-309.

Pietruszka, A. J., K. H. Rubin, and M. O. Garcia (2001), ^{226}Ra-^{230}Th-^{238}U disequilibrium of historical Kilauea lvas (1790-1982) and the dynamics of mantle melting within the Hawaiian plume, *Earth and Planetary Science Letters*, *186*, 15-21.

Putirka, K. D. (2008), Thermometers and barometers for volcanic systems, *Reviews in Mineralogy and Geochemistry*, *69*, 61-120.

Pyle, D. M., M. Ivanovich, and R. S. J. Sparks (1988), Magma-cumulate mixing identified by U-Th disequilibrium dating. *Nature*, *331*, 157-159.

Ramaprabhu, P., and M. J. Andrews (2004) Experimental investigation of Rayleigh–Taylor mixing at small Atwood numbers, *Journal of Fluid Mechanics*, *502*, 233-271.

Ramberg, H. (1981), *Gravity, deformation, and the earth's crust, in theory, experiments and geological application*, 452 pp., Academic Press, London.

Reagan, M. K., A. M. Volpe, and K. V. Cashman (1992), ^{238}U- and ^{232}Th-series chronology of phonolite fractionation at Mount Erebus, Antarctica. *Geochimica et Cosmochimica Acta*, *56*, 1401-1407.

Reagan, M. K, F. J. Tepley, J. B. Gill, M. Wortel, and J Garrison (2006), Timescales of degassing and crystallization implied by ^{210}Po-^{210}Pb-^{226}Ra disequilibria for andesitic lavas erupted from Arenal Volcano, *Journal of Volcanology and Geothermal Research*, *157*, 135-146.

Reid, M. R., C. D. Coath, T. M. Harrison, and K. D. McKeegan (1997), Prolonged residence times for the youngest rhyolites associated with Long Valley Calderas: ^{230}Th-^{238}U ion microprobe dating of young zircons, *Earth and Planetary Science Letters*, *150*, 27-39.

Reid, M.R. (2003),Timescales of Magma Transfer and Storage in the Crust, *Treatise on Geochemistry*, *3*, 167 - 193.

Rhodes, J., M. A. Dungan, D. P. Blanchard, and P. E. Long (1979), Magma mixing at mid-ocean ridges: Evidence from basalts drilled near 22° N on the Mid-Atlantic Ridge, *Tectonophysics*, *55*, 35-61.

Ruprecht, P., and G. Wörner (2007), Variable regimes in magma systems documented in plagioclase zoning patterns: El Misti Stratovolcano and Andahua monogenetic cones, *Journal of Volcanology and Geothermal Research*, *165*, 142-162.

Ruprecht, P., G. W. Bergantz, and J. Dufek (2008), Modeling of gas-driven magmatic overturn: Tracking of phenocryst dispersal and gathering during magma mixing, *Geochemistry Geophysics Geosystems*, *9*, Q07017.

Ruprecht P. (2009), The Time and Length Scales of Magma Mixing: The Natural Laboratory of Volcán Quizapu, Chile, Ph.D. thesis (unpubl.), Earth and Space Sciences, University of Washington, pp. 283.

Salisbury, M. J., W. A. Bohrson, M. A. Clynne, F. C. Ramos, and P. Hoskin (2008), Multiple Plagioclase Crystal Populations Identified by Crystal Size Distribution and in situ Chemical Data: Implications for Timescales of Magma Chamber Processes Associated with the 1915 Eruption of Lassen Peak, CA, *Journal of Petrology*, *49*, 1755-1780.

Scaillet, B., F. Holtz, and M. Pichavant (1998), Phase equilibrium constraints on the viscosity of silicic magmas: 1. Volcanic-plutonic comparison, *Journal of Geophysical Research*, *103*, 27257-27266.

Shaw, C. S. J. (2006), Effects of melt viscosity and silica activity on the rate and mechanism of quartz dissolution in melts of the CMAS and CAS systems, *Contributions to Mineralogy and Petrology*, *151*, 665-680.

Simon, J. I., P. Renne, and R. Mundil (2008), Implications of pre-eruptive magmatic histories of zircons for U/Pb geochronology of silicic extrusions, *Earth and Planetary Science Letters*, *266*, 182-194.

Singer, B. S., M. A. Dungan, and G. D. Layne (1995), Textures and Sr, Ba, Mg, Fe, K, and Ti compositional profiles in volcanic plagioclase: clues to the dynamics of calc-alkaline magma chambers, *American Mineralogist*, *80*, 776 - 798.

Sinton, J.M., and R. S. Detrick (1992) Mid-Ocean Ridge Magma Chambers. *Journal of Geophysical Research*, *97*, 197-216.

Snyder, D., and S. Tait (1996), Magma mixing by convective entrainment. *Nature*, *379*, 529-531.

Snyder, D. (2000), Thermal effects of the intrusion of basaltic magma into a more silicic magma chamber and implications for eruption triggering, *Earth and Planetary Science Letters*, *175*, 257-273.

Sparks, S. R. J., H. Sigurdsson, and L. Wilson (1977), Magma mixing: a mechanism for triggering acid explosive eruptions, *Nature*, *267*, 315-318.

Spera, F. J. (1984), Some numerical experiments on the withdrawal of magma from crustal reservoirs, *Journal Geophysical Research*, *89*, 8222 – 8236, doi:10.1029/JB089iB10p08222.

Sugawara, T. (2001) Ferric iron partitioning between plagioclase and silicate liquid: thermodynamics and petrological applications, *Contrib. Min. Pet.*, *141*, 659-686.Spera, F. J. (1984), Some numerical experiments on the withdrawal of magma from crustal reservoirs, *Journal of Geophysical Research*, *89*, 8222-8236.

Syamlal, M., W. Rogers, and T. J. O'Brien (1993), MFIX Documentation: Theory Guide, DOE/METC-94/1004, technical note, 49 pp., U.S. Dept. of Energy, Morgantown, W. Va.

Tepley III, F. J., J. P. Davidson, and M. A. Clynne (1999), Magmatic Interactions as Recorded in Plagioclase Phenocrysts of Chaos Crags, Lassen volcanic Center, California, *Journal of Petrology*, *40*, 787-806.

Tepley III, F. J., J. P. Davidson, R. I. Tilling, and J. G. Arth (2000) Magma Mixing, Recharge and Eruption Histories Recorded in Plagioclase Phenocrysts from El Chichon Volcano, Mexico, *Journal of Petrology*, *41*, 1397-1411.

Tepley III, F. J., C. C. Lundstrom, J. B. Gill, and R. W. Williams (2006), U-Th-Ra disequilibria and the time scale of fluid transfer andesite differentiation at Arenal volcano, Costa Rica (1968-2003), *Journal of Volcanology and Geothermal Research*, *157*, 147-165.

Trial, A. F., F. J. Spera, J. Greer, and D. A. Yuen (1992), Simulations of magma withdrawal from compositionally zoned bodies, *Journal of Geophysical Research*, *97*, 6713-6733.

Troll, V., and H. U. Schmincke (2002), Magma Mixing and Crustal Recycling Recorded in Ternary Feldspar from Compositionally Zoned Peralkaline Ignimbrite 'A', Gran Canaria, Canary Islands, *Journal of Petrology*, *43*, 243-270.

Tsuchiyama, A. (1985), Dissolution kinetics of plagioclase in the melt of the system diopside-albite-anorthite, and origin of dusty plagioclase in andesites, *Contributions to Mineralogy and Petrology*, *89*, 1-16.

Turner, S., R. George, D. A. Jerram, N. Carpenter, and C. Hawkesworth (2003), Case studies of plagioclase growth and residence times in island arc lavas from Tonga and the Lesser Antilles, and a model to reconcile discordant age information, *Earth and Planetary Science Letters*, *214*, 279-294.

Vazquez, J. A., and M. R. Reid (2004), Probing the Accumulation History of the Voluminous Toba Magma, *Science*, *305*, 991-994.

Venezky, D, and M. Rutherford (1999), Petrology and Fe-Ti oxide reequilibration of the 1991 Mount Unzen mixed magma, *Journal of Volcanology and Geothermal Research*, *89*, 213-230.

Volpe, A.M., and P. E. Hammond (1991), ^{238}U-^{230}Th-^{226}Ra disequilibria in young Mount St. Helens rocks: time constraint for magma formation and crystallization. *Earth and Planetary Science Letters*, *107*, 475-486.

Von Gruenewaldt, G., D. D. Klemm, J. Henckel, and R. M. Dehm (1985), Exsolution features in titanomagnetites from massive magnetite layers and

their host rocks of the upper zone, eastern Bushveld Complex, *Economic Geology*, *80*, 1049-1061.

Wallace, G. S., and G. W. Bergantz (2005), Reconciling heterogeneity in crystal zoning data: An application of shared characteristic diagrams at Chaos Crags, Lassen Volcanic Center, California, *Contributions to Mineralogy and Petrology*, *149*, 98-112.

Watson, E. B. (1996), Surface enrichment and trace-element uptake during crystal growth, *Geochimica et Cosmochimica Acta*, *60*, 5013-5020.

Watson, E. B., and Y. Liang (1995), A simple model for sector zoning in slowly growth crystals: Implications for growth rate and lattice diffusion, with emphasis on accessory minerals in crustal rocks, *American Mineralogist*, *80*, 1179-1187.

Whitney, J. A. (1988) The origin of granite: The role and source of water in the evolution of granitic magmas, *Geological Society of America Bulletin*, *100*, 1886-1897.

Wilcox, R.E. (1999) The Idea of Magma Mixing: History of a Struggle for Acceptance, *The Journal of Geology*, *107*, 421-432.

Wolf, A., J. B. Swift, H. L. Swinney, and J. A. Vastano (1985), Determining Lyapunov exponents from a time series, *Physics D*, *16*, 285-317, doi:10.1016/0167-2789(85)90011-9.

Wood, B. J., J. D. Blundy (1997) A predictive model for rare earth element partitioning between clinopyroxene and anhydrous silicate melt, *Contributions to Mineralogy and Petrology*, *129*, 166-181.

Youngs, D. L. (1984), Numerical simulation of turbulent mixing by Rayleigh-Taylor instability, *Physica D: Nonlinear Phenomena*, *12*, 32-44.

Zellmer, G. F., S. Blake, D. Vance, C. J. Hawkesworth, and S. Turner (1999), Plagioclase residence times at two island arc volcanoes (Kameni Islands, Santorini, and Soufriere, St. Vincent) determinated by Sr diffusion systematics, *Contributions to Mineralogy and Petrology*, *136*, 345-357.

Zellmer, G., S. Turner, and C. J. Hawkesworth (2000) Timescales of destructive plate margin magmatism: new insights from Santorini, Aegean volcanic arc. *Earth and Planetary Science Letters*, *174*, 265 - 281.

Zellmer, G. F., R. S. J. Sparks, C. J. Hawkesworth, and M. Wiedenbeck (2003), Magma Emplacement and Remobilization Timescales Beneath Montserrat: Insights from Sr and Ba Zonation in Plagioclase Phenocrysts, *Journal of Petrology*, *44*, 1413-1431.

Zellmer, G. F., and S. P. Turner (2007), Arc dacite genesis pathways: Evidence from mafic enclaves and their hosts in Aegean lavas, *Lithos*, *95*, 346-362.

Zhang Y., D. Walker, and C. E. Lesher (1989), Diffusive crystal dissolution, *Contributions to Mineralogy and Petrology*, *102*, 495-513.

Appendix

Appendix A1

Snapshots of the Numerical Simulation Including Lagrangian Particles

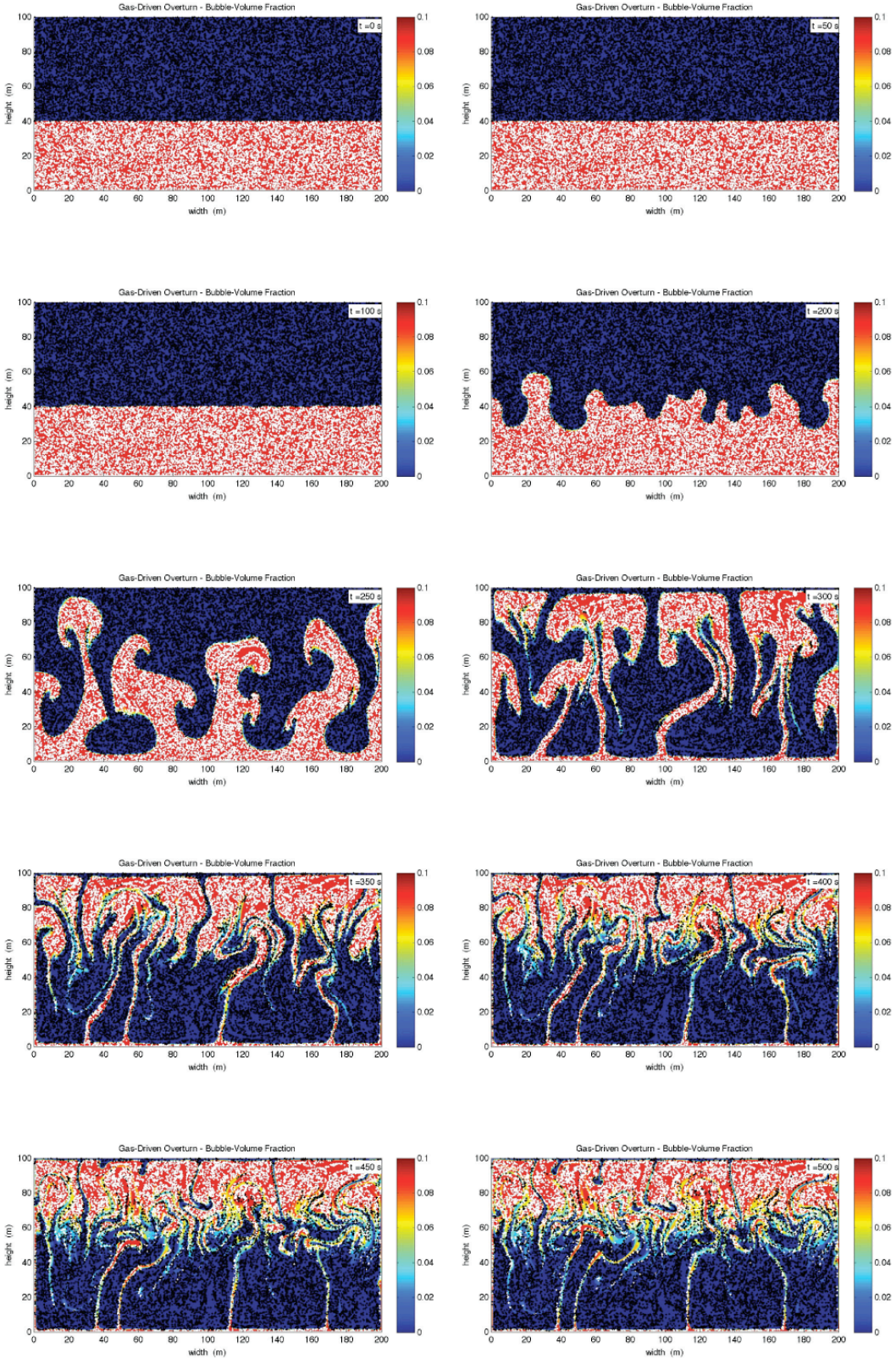
Gas-Driven Overturn - Bubble-Volume Fraction
t =0 s
t =50 s
t =100 s
t =200 s
t =250 s
t =300 s
t =350 s
t =400 s
t =450 s
t =500 s
height (m)
width (m)

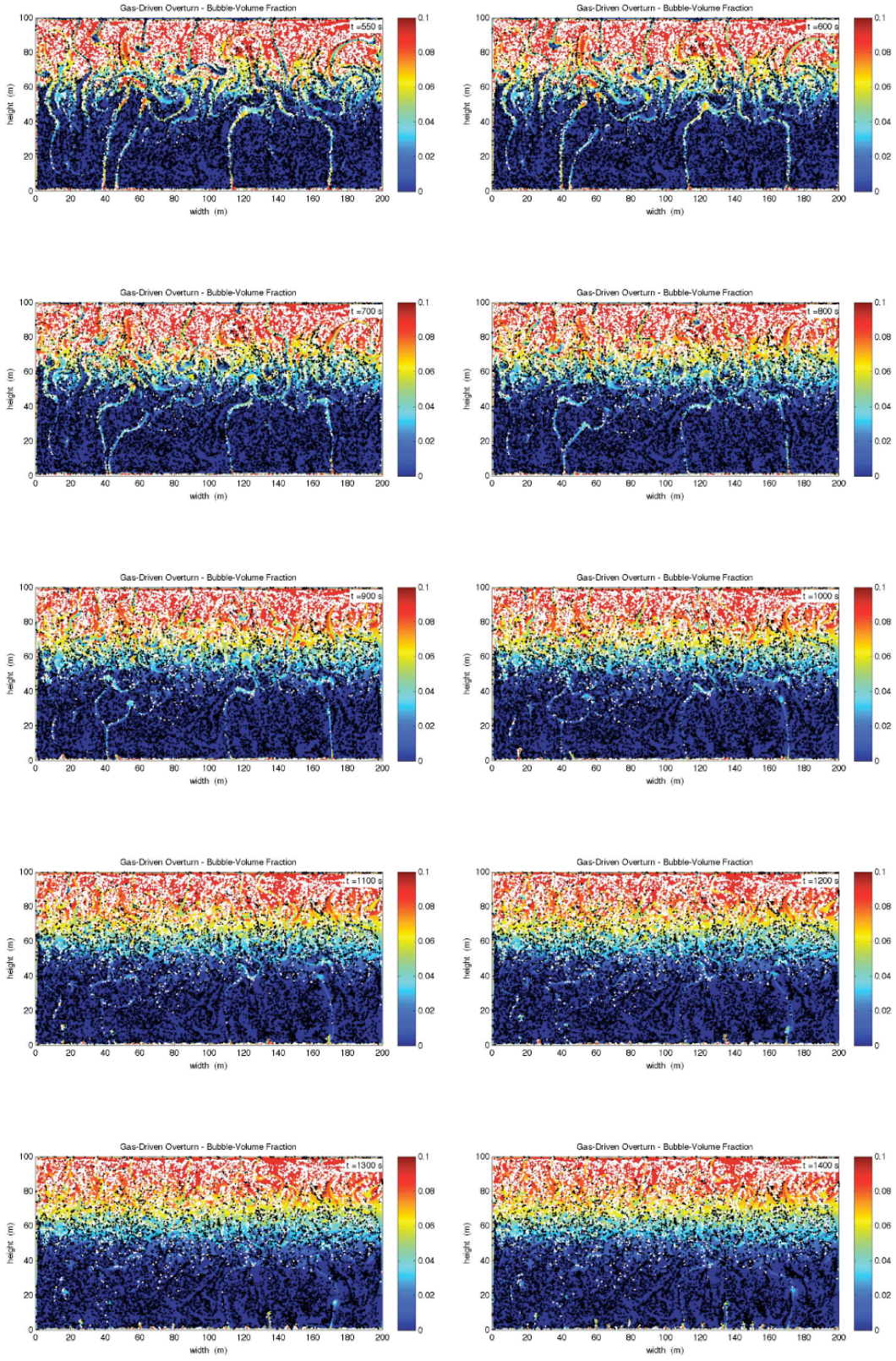
Gas-Driven Overturn - Bubble-Volume Fraction
t =550 s
Gas-Driven Overturn - Bubble-Volume Fraction
t =600 s
Gas-Driven Overturn - Bubble-Volume Fraction
t =700 s
Gas-Driven Overturn - Bubble-Volume Fraction
t =800 s
Gas-Driven Overturn - Bubble-Volume Fraction
t =900 s
Gas-Driven Overturn - Bubble-Volume Fraction
t =1000 s
Gas-Driven Overturn - Bubble-Volume Fraction
t =1100 s
Gas-Driven Overturn - Bubble-Volume Fraction
t =1200 s
Gas-Driven Overturn - Bubble-Volume Fraction
t =1300 s
Gas-Driven Overturn - Bubble-Volume Fraction
t =1400 s
height (m)
width (m)

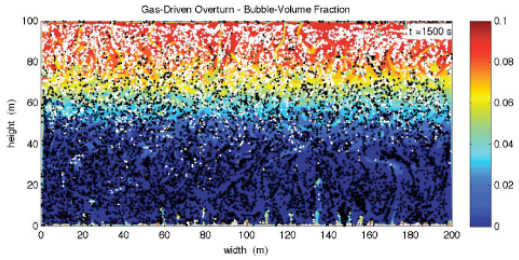
Gas-Driven Overturn - Bubble-Volume Fraction
t =1500 s
height (m)
width (m)

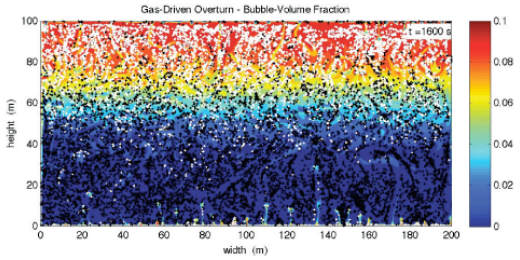
Gas-Driven Overturn - Bubble-Volume Fraction
t =1600 s
height (m)
width (m)

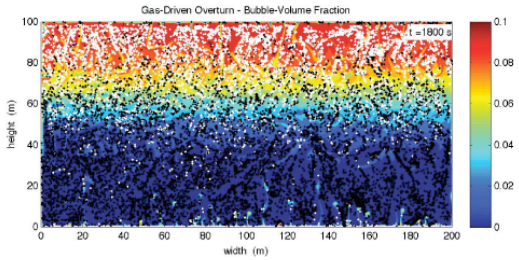
Gas-Driven Overturn - Bubble-Volume Fraction
t =1800 s
height (m)
width (m)

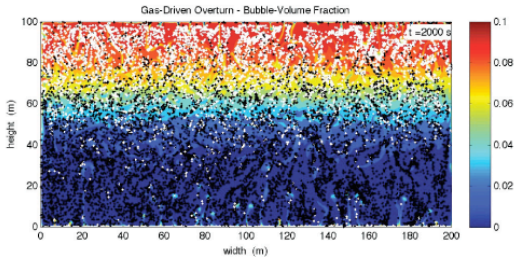
Gas-Driven Overturn - Bubble-Volume Fraction
t =2000 s
height (m)
width (m)

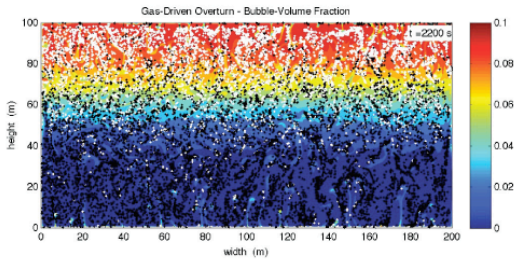
Gas-Driven Overturn - Bubble-Volume Fraction
t =2200 s
height (m)
width (m)

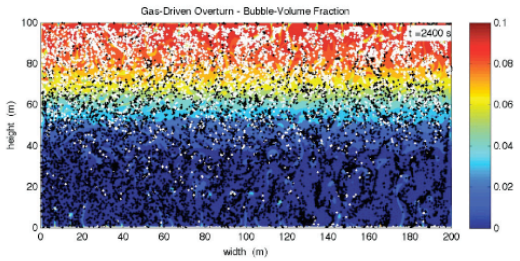
Gas-Driven Overturn - Bubble-Volume Fraction
t =2400 s
height (m)
width (m)

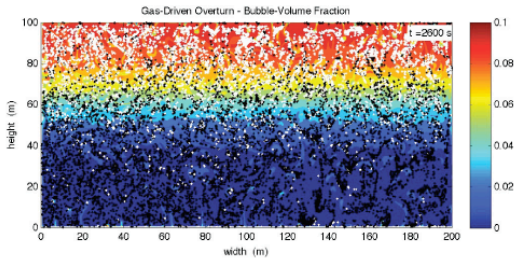
Gas-Driven Overturn - Bubble-Volume Fraction
t =2600 s
height (m)
width (m)

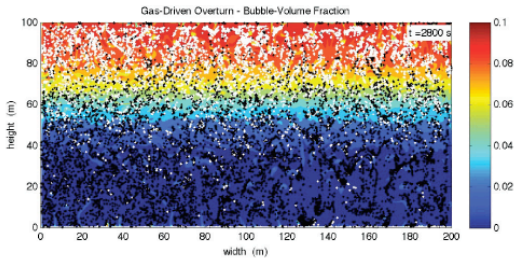
Gas-Driven Overturn - Bubble-Volume Fraction
t =2800 s
height (m)
width (m)

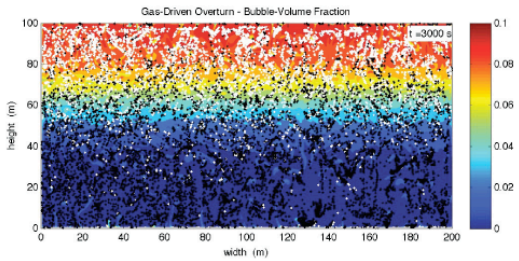
Gas-Driven Overturn - Bubble-Volume Fraction
t =3000 s
height (m)
width (m)

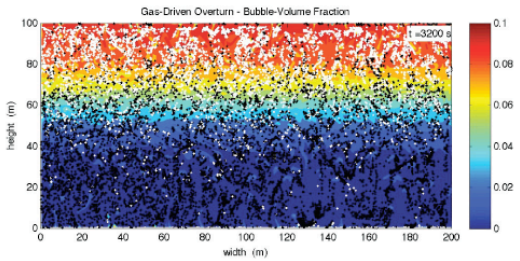
Gas-Driven Overturn - Bubble-Volume Fraction
t =3200 s
height (m)
width (m)

Appendix A2

Snapshots of the Numerical Simulation Without Lagrangian Particles

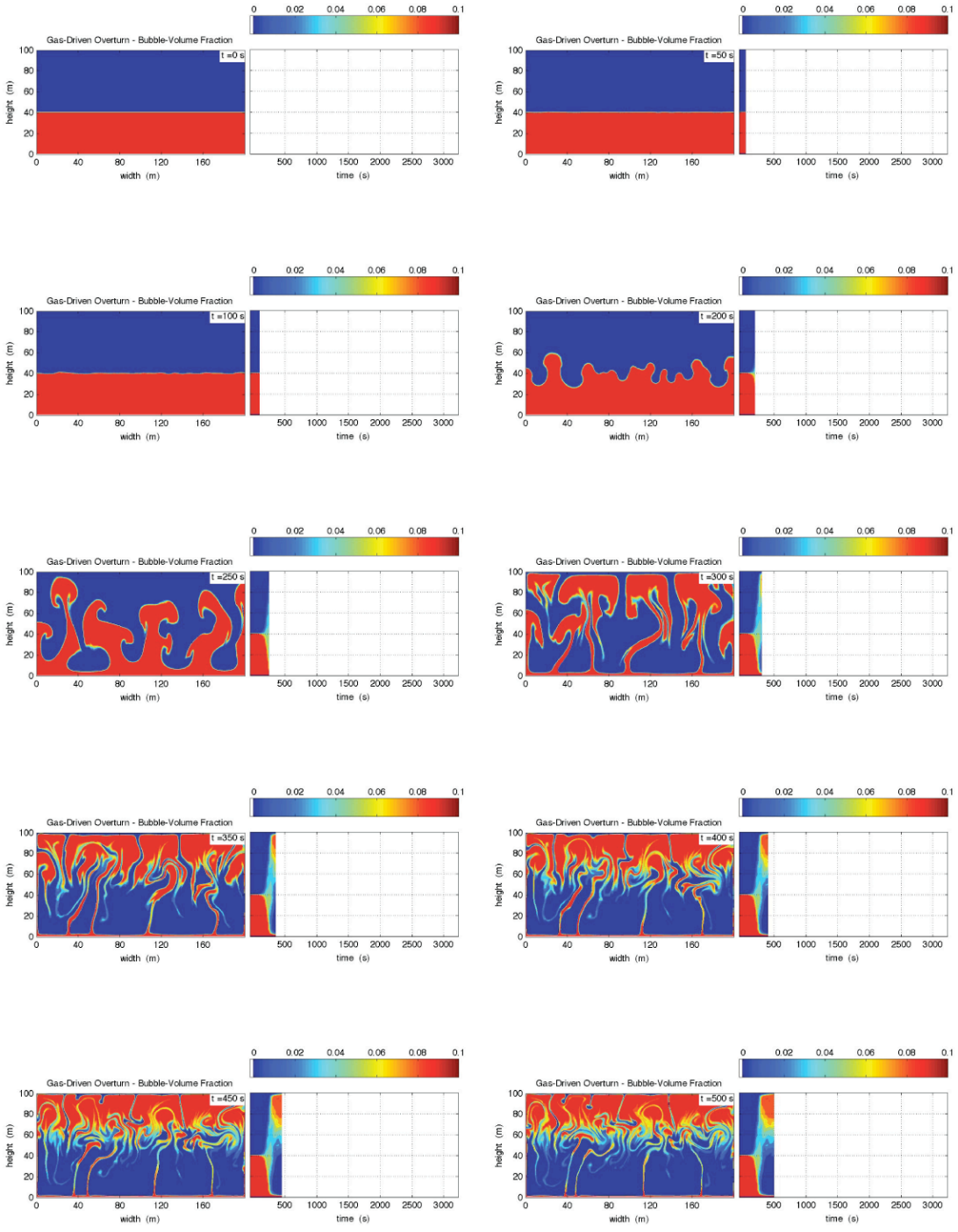
Gas-Driven Overturn - Bubble-Volume Fraction
t =0 s
t =50 s
t =100 s
t =200 s
t =250 s
t =300 s
t =350 s
t =400 s
t =450 s
t =500 s
height (m)
width (m)
time (s)

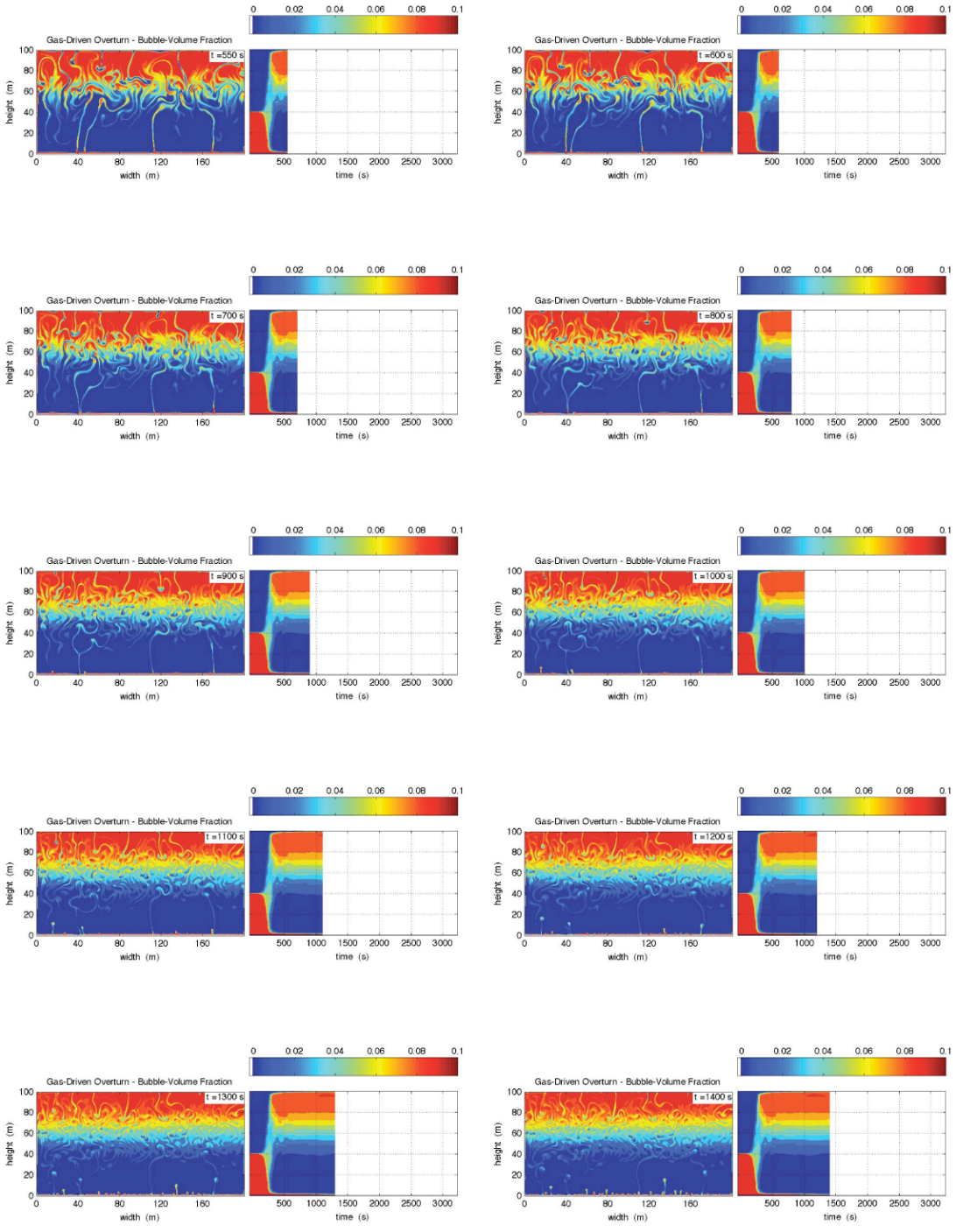
Gas-Driven Overturn - Bubble-Volume Fraction
t =550 s
t =600 s
t =700 s
t =800 s
t =900 s
t =1000 s
t =1100 s
t =1200 s
t =1300 s
t =1400 s
height (m)
width (m)
time (s)

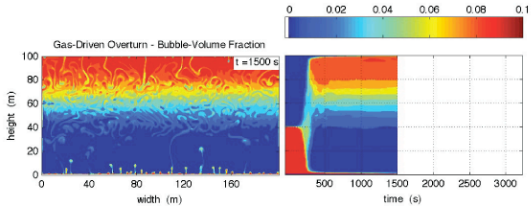
Gas-Driven Overturn - Bubble-Volume Fraction
t =1500 s
height (m)
width (m)
time (s)

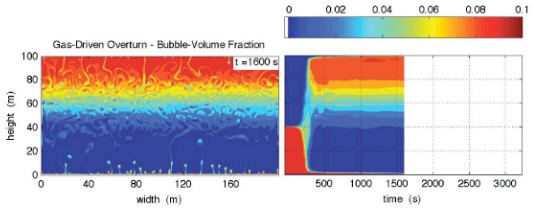
Gas-Driven Overturn - Bubble-Volume Fraction
t =1600 s
height (m)
width (m)
time (s)

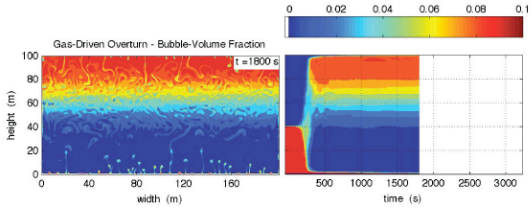
Gas-Driven Overturn - Bubble-Volume Fraction
t =1800 s
height (m)
width (m)
time (s)

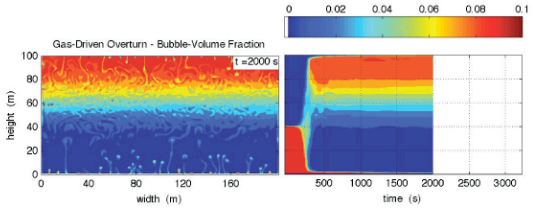
Gas-Driven Overturn - Bubble-Volume Fraction
t =2000 s
height (m)
width (m)
time (s)

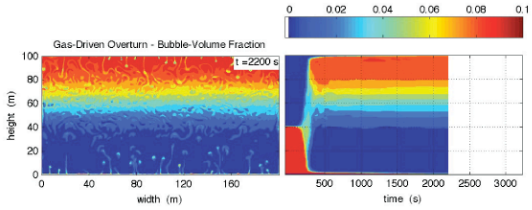
Gas-Driven Overturn - Bubble-Volume Fraction
t =2200 s
height (m)
width (m)
time (s)

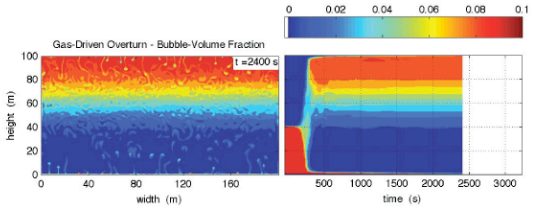
Gas-Driven Overturn - Bubble-Volume Fraction
t =2400 s
height (m)
width (m)
time (s)

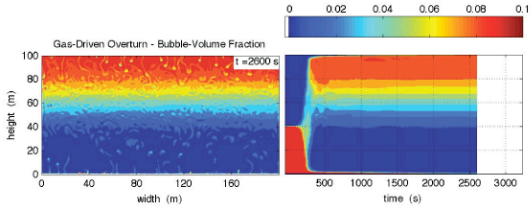
Gas-Driven Overturn - Bubble-Volume Fraction
t =2600 s
height (m)
width (m)
time (s)

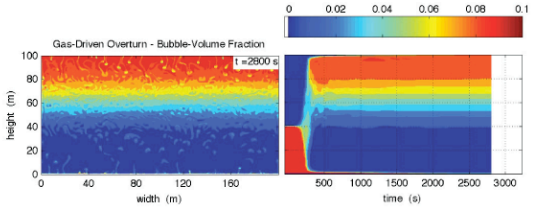
Gas-Driven Overturn - Bubble-Volume Fraction
t =2800 s
height (m)
width (m)
time (s)

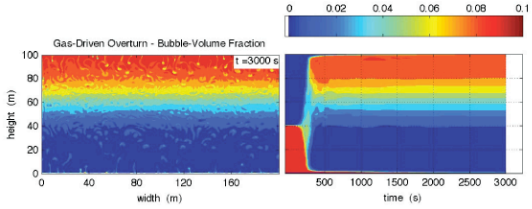
Gas-Driven Overturn - Bubble-Volume Fraction
t =3000 s
height (m)
width (m)
time (s)

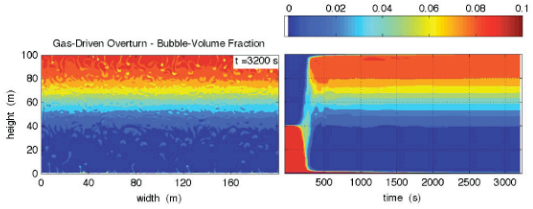
Gas-Driven Overturn - Bubble-Volume Fraction
t =3200 s
height (m)
width (m)
time (s)

Appendix B1 Plagioclase electron microprobe analyses (atomic proportions and weight concentrations)[1]

Label	An[2]	Ab[3]	Or[4]	Si	Al	Fe	Mg	Ca	Sr	Ba	Na	K	Tot[5]	SiO_2	Al_2O_3	FeO	MgO	CaO	SrO	BaO	Na_2O	K_2O	Tot
Q-34 (1846/47)																							
Pl1.1	46.6	51.5	1.9	2.53	1.45	0.016	0.0012	0.47	0.0037	0.0013	0.52	0.019	13.02	55.70	27.15	0.41	0.018	9.70	0.142	b.d.l.	5.92	0.33	99.44
Pl1.2	33.8	63.6	2.6	2.66	1.33	0.012	0.0002	0.34	0.0024	0.0015	0.64	0.026	13.01	59.39	25.21	0.33	b.d.l.	7.07	0.092	b.d.l.	7.35	0.46	99.99
Pl1.3	39.9	57.7	2.5	2.60	1.38	0.014	0.0005	0.40	0.0037	b.d.l.	0.59	0.025	13.02	57.78	26.13	0.38	b.d.l.	8.40	0.141	b.d.l.	6.72	0.44	99.99
Pl1.4	33.0	64.0	3.0	2.68	1.31	0.013	0.0003	0.33	0.0022	0.0013	0.64	0.030	13.00	59.87	24.77	0.34	b.d.l.	6.83	0.084	b.d.l.	7.33	0.53	99.83
Pl1.5	47.9	50.5	1.6	2.53	1.46	0.015	0.0013	0.48	0.0045	0.0008	0.51	0.016	13.01	55.76	27.28	0.41	0.019	9.88	0.170	b.d.l.	5.76	0.28	99.59
Pl1.6	42.9	55.0	2.1	2.57	1.41	0.015	0.0018	0.43	0.0054	0.0013	0.55	0.021	13.01	56.91	26.41	0.40	0.027	8.93	0.206	b.d.l.	6.33	0.36	99.65
Pl1.7	52.5	46.2	1.2	2.47	1.52	0.017	0.0020	0.53	0.0038	b.d.l.	0.46	0.012	13.01	54.19	28.22	0.44	0.029	10.76	0.145	b.d.l.	5.24	0.21	99.24
Pl1.8	47.1	51.1	1.8	2.53	1.45	0.017	0.0016	0.48	0.0051	0.0006	0.52	0.018	13.01	55.92	27.14	0.44	0.024	9.83	0.195	b.d.l.	5.89	0.32	99.79
Pl14.1	35.5	61.6	2.9	2.66	1.33	0.010	b.d.l.	0.35	0.0033	0.0006	0.61	0.028	13.00	59.08	25.10	0.28	b.d.l.	7.34	0.127	b.d.l.	7.03	0.50	99.48
Pl14.2	38.4	59.2	2.4	2.61	1.37	0.010	0.0002	0.39	0.0036	0.0016	0.61	0.025	13.02	57.78	25.81	0.26	b.d.l.	8.15	0.137	b.d.l.	6.93	0.43	99.58
Pl14.3	27.8	68.6	3.6	2.72	1.26	0.011	0.0007	0.28	0.0031	0.0015	0.69	0.036	13.01	60.58	23.83	0.30	b.d.l.	5.81	0.119	b.d.l.	7.94	0.63	99.31
Pl14.4	31.5	65.3	3.2	2.70	1.29	0.011	0.0004	0.31	0.0021	0.0014	0.65	0.032	13.00	60.41	24.53	0.30	b.d.l.	6.55	0.082	b.d.l.	7.51	0.57	100.03
Pl14.5	28.6	67.7	3.7	2.72	1.27	0.011	b.d.l.	0.29	0.0016	0.0008	0.68	0.037	13.00	60.73	23.95	0.30	b.d.l.	5.97	0.060	b.d.l.	7.82	0.65	99.52
Pl17.1	80.2	19.4	0.4	2.19	1.78	0.024	0.0052	0.81	0.0044	0.0004	0.20	0.004	13.02	47.40	32.62	0.63	0.075	16.32	0.165	b.d.l.	2.19	0.06	99.48
Pl17.2	85.2	14.6	0.2	2.14	1.83	0.022	0.0030	0.86	0.0025	0.0012	0.15	0.002	13.02	46.20	33.56	0.58	0.044	17.37	0.093	b.d.l.	1.65	0.04	99.60
Pl17.3	87.4	12.5	0.1	2.12	1.85	0.023	0.0022	0.88	0.0032	b.d.l.	0.13	0.001	13.02	45.69	33.75	0.60	0.032	17.74	0.120	b.d.l.	1.41	b.d.l.	99.35
Pl17.4	52.9	45.9	1.3	2.47	1.49	0.027	0.0053	0.54	0.0049	0.0008	0.47	0.013	13.02	54.52	27.93	0.70	0.079	11.11	0.187	b.d.l.	5.33	0.22	100.13
Pl17.5	51.8	47.0	1.3	2.49	1.48	0.024	0.0035	0.52	0.0043	0.0003	0.47	0.013	13.01	54.71	27.66	0.63	0.051	10.72	0.163	b.d.l.	5.37	0.22	99.55
Pl17.6	33.9	63.1	3.0	2.66	1.32	0.015	0.0009	0.34	0.0034	0.0001	0.64	0.031	13.01	59.31	24.94	0.40	0.014	7.09	0.130	b.d.l.	7.30	0.53	99.72
Pl18.1	78.7	21.0	0.4	2.21	1.76	0.026	0.0032	0.80	0.0040	0.0005	0.21	0.004	13.02	47.69	32.24	0.66	0.047	16.02	0.149	b.d.l.	2.36	0.06	99.25
Pl18.2	79.2	20.4	0.4	2.20	1.77	0.024	0.0025	0.81	0.0043	0.0003	0.21	0.005	13.02	47.60	32.52	0.62	0.037	16.29	0.161	b.d.l.	2.32	0.08	99.64
Pl18.3	80.1	19.6	0.3	2.20	1.77	0.024	0.0044	0.81	0.0037	b.d.l.	0.20	0.003	13.02	47.41	32.46	0.61	0.063	16.33	0.139	b.d.l.	2.21	0.05	99.27
Pl18.4	63.1	36.2	0.7	2.38	1.58	0.026	0.0051	0.65	0.0039	b.d.l.	0.37	0.007	13.02	51.92	29.36	0.69	0.074	13.15	0.145	b.d.l.	4.18	0.12	99.64
Pl19.1	51.0	47.4	1.6	2.47	1.52	0.010	b.d.l.	0.52	0.0034	0.0003	0.48	0.016	13.02	54.86	28.56	0.26	b.d.l.	10.78	0.129	b.d.l.	5.54	0.28	100.42
Pl19.2	32.0	65.0	3.0	2.67	1.32	0.011	b.d.l.	0.32	0.0023	0.0011	0.65	0.030	13.01	59.67	24.97	0.29	b.d.l.	6.68	0.090	b.d.l.	7.50	0.52	99.79
Pl19.3	44.9	53.5	1.6	2.54	1.45	0.010	b.d.l.	0.45	0.0039	0.0006	0.54	0.017	13.02	56.24	27.38	0.27	b.d.l.	9.40	0.149	b.d.l.	6.19	0.29	99.95
Pl19.4	32.3	64.8	3.0	2.68	1.32	0.011	0.0003	0.32	0.0016	0.0010	0.65	0.030	13.00	59.82	24.95	0.30	b.d.l.	6.71	0.062	b.d.l.	7.45	0.52	99.87
Pl2.1	58.3	40.5	1.2	2.43	1.54	0.022	0.0030	0.58	0.0049	b.d.l.	0.40	0.012	13.00	53.32	28.67	0.58	0.044	11.93	0.185	b.d.l.	4.57	0.21	99.50
Pl2.2	48.2	50.1	1.6	2.53	1.45	0.019	0.0028	0.48	0.0042	b.d.l.	0.50	0.016	13.01	56.05	27.24	0.51	0.041	9.98	0.159	b.d.l.	5.73	0.28	99.99

Appendix B1 cotinued

Label	An[2]	Ab[3]	Or[4]	Si	Al	Fe	Mg	Ca	Sr	Ba	Na	K	Tot[5]	SiO_2	Al_2O_3	FeO	MgO	CaO	SrO	BaO	Na_2O	K_2O	Tot
Pl2.3	55.8	43.1	1.1	2.44	1.53	0.021	0.0030	0.57	0.0048	0.0001	0.44	0.011	13.02	53.45	28.53	0.56	0.045	11.60	0.180	b.d.l.	4.95	0.19	99.51
Pl2.4	44.8	53.3	1.9	2.56	1.41	0.020	0.0027	0.45	0.0029	0.0012	0.54	0.019	13.01	56.72	26.49	0.53	0.040	9.32	0.111	b.d.l.	6.12	0.33	99.73
Pl2.5	60.2	38.8	1.0	2.41	1.56	0.024	0.0036	0.61	0.0038	b.d.l.	0.39	0.010	13.01	52.74	29.02	0.62	0.053	12.44	0.142	b.d.l.	4.43	0.18	99.63
Pl3.2	29.0	67.4	3.6	2.72	1.27	0.011	b.d.l.	0.29	0.0021	0.0010	0.68	0.036	13.00	60.71	23.98	0.30	b.d.l.	6.06	0.081	b.d.l.	7.78	0.63	99.60
Pl3.3	35.3	61.8	2.9	2.65	1.34	0.012	b.d.l.	0.35	0.0050	0.0008	0.62	0.029	13.01	58.90	25.19	0.31	b.d.l.	7.32	0.193	b.d.l.	7.09	0.51	99.56
Pl3.4	28.2	68.0	3.8	2.73	1.26	0.012	0.0004	0.28	0.0027	0.0012	0.68	0.038	13.00	60.64	23.71	0.31	b.d.l.	5.86	0.103	b.d.l.	7.81	0.66	99.17
Pl3.5	26.1	69.5	4.4	2.76	1.23	0.011	b.d.l.	0.26	0.0011	0.0010	0.69	0.044	13.00	61.52	23.22	0.28	b.d.l.	5.40	0.044	b.d.l.	7.95	0.77	99.24
Pl3.6	30.6	66.2	3.1	2.69	1.29	0.011	b.d.l.	0.31	0.0030	0.0010	0.67	0.032	13.01	59.93	24.40	0.29	b.d.l.	6.40	0.115	b.d.l.	7.65	0.55	99.39
Pl3.7	29.6	67.2	3.3	2.71	1.28	0.010	b.d.l.	0.30	0.0023	0.0012	0.68	0.033	13.01	60.58	24.20	0.27	b.d.l.	6.20	0.090	b.d.l.	7.79	0.58	99.79
Pl3.8	34.1	62.8	3.0	2.66	1.32	0.011	b.d.l.	0.34	0.0033	0.0007	0.63	0.031	13.01	58.96	24.89	0.30	b.d.l.	7.11	0.125	b.d.l.	7.24	0.53	99.21
Pl4.1	42.1	55.9	2.1	2.57	1.41	0.011	b.d.l.	0.43	0.0028	0.0011	0.57	0.021	13.02	56.92	26.53	0.29	b.d.l.	8.93	0.108	b.d.l.	6.55	0.37	99.76
Pl4.2	52.8	45.8	1.5	2.48	1.51	0.013	b.d.l.	0.53	0.0029	0.0010	0.46	0.015	13.00	54.57	28.13	0.34	b.d.l.	10.84	0.111	b.d.l.	5.19	0.25	99.50
Pl4.3	27.7	68.5	3.8	2.74	1.25	0.012	b.d.l.	0.28	0.0034	0.0014	0.69	0.038	13.00	61.25	23.72	0.32	b.d.l.	5.78	0.132	b.d.l.	7.92	0.67	99.87
Pl4.4	27.2	68.6	4.2	2.74	1.24	0.012	b.d.l.	0.27	0.0028	0.0010	0.69	0.042	13.01	61.22	23.40	0.32	b.d.l.	5.72	0.106	b.d.l.	7.97	0.74	99.53
Pl4.5	36.2	61.3	2.5	2.64	1.34	0.011	0.0004	0.36	0.0038	0.0015	0.62	0.026	13.01	58.36	25.12	0.28	b.d.l.	7.50	0.146	b.d.l.	7.03	0.44	98.97
Pl4.6	29.2	67.2	3.7	2.72	1.26	0.011	0.0003	0.29	0.0030	0.0015	0.67	0.037	13.00	60.62	23.84	0.28	b.d.l.	6.09	0.116	b.d.l.	7.75	0.64	99.43
Pl6.2	33.1	63.9	3.0	2.67	1.32	0.011	b.d.l.	0.33	0.0037	0.0015	0.65	0.030	13.01	59.30	24.86	0.29	b.d.l.	6.93	0.142	b.d.l.	7.40	0.53	99.54
Pl6.3	26.8	69.3	3.9	2.73	1.26	0.012	b.d.l.	0.27	0.0025	0.0013	0.70	0.040	13.01	61.00	23.83	0.32	b.d.l.	5.63	0.096	b.d.l.	8.03	0.69	99.68
Pl6.4	31.8	65.3	2.9	2.68	1.32	0.013	b.d.l.	0.32	0.0022	0.0011	0.65	0.029	13.01	59.42	24.82	0.34	b.d.l.	6.59	0.082	b.d.l.	7.46	0.50	99.28
Pl6.5	28.9	67.9	3.2	2.71	1.28	0.011	0.0005	0.29	0.0028	0.0008	0.68	0.033	13.01	60.33	24.12	0.29	b.d.l.	6.03	0.107	b.d.l.	7.83	0.57	99.34
Pl8.1	29.9	66.5	3.6	2.71	1.27	0.012	b.d.l.	0.30	0.0029	0.0019	0.67	0.036	13.00	60.58	24.11	0.31	b.d.l.	6.26	0.113	b.d.l.	7.69	0.64	99.82
Pl8.2	33.8	63.2	3.0	2.67	1.32	0.011	0.0002	0.34	0.0024	0.0007	0.63	0.030	13.00	59.55	24.91	0.30	b.d.l.	7.06	0.091	b.d.l.	7.30	0.52	99.76
Pl8.3	34.6	62.9	2.5	2.65	1.33	0.012	b.d.l.	0.35	0.0030	0.0015	0.64	0.026	13.02	59.16	25.10	0.32	b.d.l.	7.35	0.116	b.d.l.	7.40	0.45	99.98
Pl8.4	30.5	66.2	3.2	2.69	1.29	0.010	0.0004	0.31	0.0035	0.0013	0.67	0.033	13.01	60.35	24.61	0.27	b.d.l.	6.43	0.134	b.d.l.	7.71	0.57	100.16
Pl8.5	32.1	64.8	3.1	2.69	1.30	0.012	0.0001	0.32	0.0019	0.0011	0.65	0.031	13.00	60.21	24.70	0.32	b.d.l.	6.68	0.073	b.d.l.	7.46	0.54	100.04
Pl8.6	28.4	67.9	3.7	2.73	1.26	0.011	b.d.l.	0.28	0.0033	0.0010	0.67	0.036	12.99	61.22	23.87	0.28	b.d.l.	5.84	0.126	b.d.l.	7.72	0.63	99.73
Q-35 (1846/47)																							
Pl12.1	33.1	62.8	4.0	2.68	1.31	0.012	b.d.l.	0.33	0.0037	0.0011	0.63	0.040	13.00	59.99	24.90	0.32	b.d.l.	6.94	0.142	b.d.l.	7.27	0.71	100.33
Pl12.2	33.6	62.8	3.5	2.67	1.31	0.012	b.d.l.	0.33	0.0039	0.0004	0.62	0.035	13.00	59.67	24.87	0.32	b.d.l.	6.96	0.150	b.d.l.	7.19	0.61	99.79
Pl12.3	24.6	70.5	5.0	2.76	1.22	0.010	b.d.l.	0.24	0.0032	0.0020	0.70	0.050	13.00	61.83	23.25	0.28	b.d.l.	5.11	0.125	0.115	8.10	0.87	99.67

Appendix B1 cotinued

Label	An[2]	Ab[3]	Or[4]	Si	Al	Fe	Mg	Ca	Sr	Ba	Na	K	Tot[5]	SiO_2	Al_2O_3	FeO	MgO	CaO	SrO	BaO	Na_2O	K_2O	Tot
Pl12.4	29.1	66.8	4.1	2.72	1.27	0.011	b.d.l.	0.29	0.0021	0.0012	0.66	0.041	13.00	60.68	24.09	0.28	b.d.l.	6.01	0.082	b.d.l.	7.62	0.71	99.55
Pl13.1	45.3	53.0	1.7	2.55	1.44	0.010	b.d.l.	0.46	0.0037	0.0015	0.53	0.017	13.01	56.57	27.09	0.25	b.d.l.	9.43	0.143	b.d.l.	6.10	0.30	99.97
Pl13.2	33.2	63.9	2.8	2.66	1.33	0.010	b.d.l.	0.33	0.0040	0.0015	0.64	0.029	13.01	59.25	25.18	0.27	b.d.l.	6.95	0.156	b.d.l.	7.39	0.50	99.78
Pl13.3	44.8	53.2	2.0	2.54	1.45	0.011	b.d.l.	0.45	0.0030	0.0011	0.54	0.020	13.02	56.35	27.42	0.29	b.d.l.	9.38	0.115	b.d.l.	6.16	0.34	100.12
Pl13.4	31.8	65.3	2.9	2.68	1.31	0.010	b.d.l.	0.32	0.0029	0.0009	0.66	0.030	13.01	59.86	24.71	0.27	b.d.l.	6.65	0.112	b.d.l.	7.54	0.52	99.72
Pl13.5	29.0	65.8	5.2	2.72	1.27	0.010	b.d.l.	0.29	0.0029	0.0013	0.65	0.052	13.00	60.79	24.03	0.27	b.d.l.	6.01	0.110	b.d.l.	7.53	0.91	99.71
Pl14.1	29.5	67.1	3.4	2.72	1.27	0.012	b.d.l.	0.29	0.0025	0.0011	0.67	0.034	13.00	60.42	23.91	0.31	b.d.l.	6.06	0.096	b.d.l.	7.63	0.59	99.09
Pl14.2	31.4	64.2	4.4	2.69	1.30	0.012	b.d.l.	0.32	0.0029	0.0016	0.65	0.045	13.01	60.31	24.76	0.32	b.d.l.	6.64	0.112	b.d.l.	7.52	0.79	100.54
Pl14.3	27.0	69.0	4.0	2.73	1.26	0.011	b.d.l.	0.27	0.0020	0.0020	0.68	0.040	13.00	61.07	23.89	0.29	b.d.l.	5.57	0.076	0.116	7.85	0.70	99.56
Pl14.4	34.0	63.1	3.0	2.65	1.33	0.011	b.d.l.	0.34	0.0043	0.0012	0.64	0.030	13.01	59.43	25.34	0.30	b.d.l.	7.16	0.166	b.d.l.	7.35	0.53	100.33
Pl14.5	33.7	62.9	3.4	2.67	1.33	0.013	b.d.l.	0.33	0.0035	0.0013	0.62	0.034	13.00	59.57	25.13	0.35	b.d.l.	6.99	0.134	b.d.l.	7.20	0.59	100.04
Pl14.6	34.1	62.4	3.4	2.67	1.32	0.013	b.d.l.	0.34	0.0029	0.0011	0.62	0.034	12.99	59.89	25.06	0.35	b.d.l.	7.03	0.111	b.d.l.	7.11	0.59	100.22
Pl17.1	59.1	39.8	1.0	2.40	1.59	0.012	b.d.l.	0.59	0.0049	0.0001	0.40	0.010	13.01	52.88	29.68	0.33	b.d.l.	12.10	0.185	b.d.l.	4.50	0.18	99.86
Pl17.2	33.3	63.7	3.0	2.68	1.31	0.011	b.d.l.	0.33	0.0029	0.0015	0.64	0.030	13.00	59.86	24.88	0.28	b.d.l.	6.99	0.111	b.d.l.	7.38	0.52	100.11
Pl17.3	29.3	66.2	4.5	2.72	1.27	0.012	b.d.l.	0.29	0.0034	0.0017	0.66	0.045	13.00	60.81	24.13	0.32	b.d.l.	6.10	0.132	b.d.l.	7.63	0.80	100.01
Pl2.1	90.4	9.4	0.3	2.10	1.88	0.024	b.d.l.	0.90	0.0042	0.0004	0.09	0.003	13.01	45.23	34.45	0.61	b.d.l.	18.15	0.155	b.d.l.	1.04	0.04	99.69
Pl2.2	90.1	9.8	0.1	2.09	1.89	0.019	0.0012	0.91	0.0046	b.d.l.	0.10	0.001	13.01	44.90	34.31	0.49	0.018	18.21	0.169	b.d.l.	1.10	b.d.l.	99.20
Pl2.3	72.2	27.3	0.6	2.29	1.68	0.022	0.0035	0.73	0.0043	0.0005	0.27	0.006	13.01	49.77	31.10	0.58	0.051	14.76	0.162	b.d.l.	3.08	0.10	99.63
Pl2.4	82.2	17.5	0.3	2.18	1.79	0.024	0.0015	0.84	0.0048	b.d.l.	0.18	0.003	13.02	47.19	32.79	0.62	0.022	16.98	0.178	b.d.l.	2.00	0.05	99.82
Pl2.5	59.1	39.6	1.2	2.42	1.55	0.023	0.0038	0.60	0.0043	b.d.l.	0.40	0.013	13.02	52.94	28.87	0.61	0.055	12.30	0.161	b.d.l.	4.56	0.22	99.71
Pl3.1	61.5	37.2	1.4	2.40	1.57	0.023	b.d.l.	0.63	0.0048	b.d.l.	0.38	0.014	13.01	52.57	29.12	0.60	b.d.l.	12.81	0.181	b.d.l.	4.28	0.24	99.80
Pl3.2	58.0	40.8	1.2	2.44	1.53	0.026	0.0025	0.58	0.0048	0.0003	0.41	0.012	13.00	53.50	28.51	0.67	0.037	11.88	0.183	b.d.l.	4.61	0.21	99.62
Pl3.3	56.5	42.2	1.3	2.45	1.53	0.023	0.0027	0.57	0.0045	0.0002	0.42	0.013	13.01	53.79	28.55	0.60	0.040	11.65	0.169	b.d.l.	4.81	0.22	99.84
Pl7.1	61.2	37.5	1.4	2.40	1.57	0.024	0.0001	0.63	0.0043	b.d.l.	0.38	0.014	13.02	52.27	29.01	0.62	b.d.l.	12.72	0.163	b.d.l.	4.31	0.24	99.33
Pl7.2	59.9	38.8	1.3	2.43	1.54	0.027	0.0031	0.60	0.0053	b.d.l.	0.39	0.014	13.01	52.72	28.34	0.71	0.045	12.22	0.200	b.d.l.	4.37	0.23	98.82
Pl8.1	32.6	64.2	3.2	2.70	1.29	0.011	b.d.l.	0.32	0.0032	0.0021	0.63	0.032	12.99	60.06	24.39	0.30	b.d.l.	6.69	0.123	0.118	7.28	0.55	99.52
Pl8.2	40.7	56.7	2.6	2.61	1.37	0.015	b.d.l.	0.41	0.0041	0.0004	0.57	0.026	13.00	57.86	25.87	0.41	b.d.l.	8.42	0.156	b.d.l.	6.48	0.45	99.68
Pl8.3	40.2	57.1	2.7	2.62	1.36	0.015	b.d.l.	0.40	0.0043	0.0009	0.57	0.027	12.99	58.15	25.53	0.39	b.d.l.	8.24	0.165	b.d.l.	6.46	0.46	99.46
Pl9.1	49.2	49.3	1.5	2.51	1.47	0.010	b.d.l.	0.50	0.0035	0.0001	0.50	0.015	13.01	55.54	27.69	0.27	b.d.l.	10.32	0.132	b.d.l.	5.72	0.27	99.96
Pl9.2	34.6	62.7	2.8	2.65	1.34	0.010	b.d.l.	0.35	0.0032	0.0019	0.64	0.028	13.02	59.16	25.34	0.26	b.d.l.	7.40	0.122	b.d.l.	7.41	0.50	100.30

Appendix B1 cotinued

Label	An[2]	Ab[3]	Or[4]	Si	Al	Fe	Mg	Ca	Sr	Ba	Na	K	Tot[5]	SiO_2	Al_2O_3	FeO	MgO	CaO	SrO	BaO	Na_2O	K_2O	Tot
Pl9.3	27.7	68.6	3.7	2.73	1.27	0.010	b.d.l.	0.27	0.0031	0.0019	0.68	0.037	13.00	61.20	24.13	0.27	b.d.l.	5.76	0.121	b.d.l.	7.87	0.64	100.11
Pl9.4	30.1	66.5	3.4	2.70	1.29	0.011	b.d.l.	0.30	0.0022	0.0012	0.67	0.034	13.01	60.37	24.39	0.29	b.d.l.	6.35	0.083	b.d.l.	7.76	0.60	99.91
Pl9.5	33.4	63.4	3.2	2.67	1.32	0.011	b.d.l.	0.33	0.0033	0.0001	0.63	0.032	13.00	59.59	25.00	0.29	b.d.l.	6.94	0.126	b.d.l.	7.28	0.55	99.78
Pl9.6	27.9	67.8	4.3	2.74	1.25	0.010	b.d.l.	0.28	0.0018	0.0010	0.67	0.043	12.99	61.49	23.86	0.28	b.d.l.	5.78	0.068	b.d.l.	7.75	0.75	100.03
Pl9.7	34.6	61.8	3.6	2.66	1.33	0.013	b.d.l.	0.34	0.0042	0.0019	0.61	0.036	13.00	59.53	25.37	0.36	b.d.l.	7.20	0.163	b.d.l.	7.10	0.64	100.46
VQ-06-02 (1846/47)																							
Pl14.1	48.0	50.3	1.7	2.54	1.45	0.013	0.0015	0.47	0.0041	0.0005	0.49	0.016	12.99	56.10	27.29	0.35	0.022	9.75	0.157	b.d.l.	5.65	0.28	99.64
Pl14.2?	37.4	59.2	3.4	2.66	1.33	0.011	0.0010	0.37	0.0030	0.0011	0.58	0.034	12.99	59.21	25.04	0.30	0.016	7.65	0.115	b.d.l.	6.70	0.59	99.69
Pl14.2?	37.4	59.2	3.4	2.64	1.34	0.012	0.0014	0.37	0.0041	0.0004	0.59	0.034	13.00	58.81	25.29	0.32	0.021	7.77	0.159	b.d.l.	6.81	0.59	99.80
Pl14.2?	37.0	59.4	3.5	2.65	1.34	0.012	0.0010	0.36	0.0025	0.0009	0.58	0.035	12.99	58.99	25.37	0.33	0.015	7.55	0.094	b.d.l.	6.70	0.61	99.71
Pl2.2	31.5	63.5	5.1	2.71	1.28	0.012	0.0013	0.31	0.0026	0.0012	0.63	0.050	12.99	60.74	24.31	0.33	0.019	6.48	0.099	b.d.l.	7.23	0.88	100.16
Pl21.1	29.6	66.1	4.3	2.73	1.25	0.011	0.0008	0.29	0.0041	0.0015	0.66	0.043	12.99	61.25	23.71	0.29	b.d.l.	6.16	0.158	0.087	7.62	0.76	100.04
Pl22.03	32.1	62.5	5.4	2.72	1.26	0.020	0.0064	0.31	0.0030	0.0014	0.61	0.053	12.99	60.64	23.81	0.53	0.096	6.54	0.117	0.081	7.03	0.93	99.77
Pl22.04	30.2	64.8	5.0	2.73	1.26	0.014	0.0013	0.30	0.0019	0.0012	0.64	0.049	12.99	61.31	23.96	0.38	0.019	6.24	0.074	b.d.l.	7.40	0.86	100.32
Pl22.05	30.0	65.3	4.7	2.73	1.26	0.013	0.0009	0.30	0.0024	0.0016	0.65	0.047	12.99	61.26	23.94	0.34	0.013	6.22	0.095	0.090	7.49	0.82	100.28
Pl22.06	29.8	65.7	4.5	2.72	1.26	0.012	0.0010	0.30	0.0024	0.0010	0.65	0.045	13.00	61.33	24.09	0.33	0.015	6.23	0.092	b.d.l.	7.60	0.79	100.53
Pl22.07	30.0	65.4	4.7	2.73	1.26	0.012	0.0009	0.30	0.0021	0.0013	0.65	0.047	13.00	61.34	23.97	0.33	0.014	6.29	0.082	0.073	7.59	0.82	100.52
Pl22.08	29.8	65.7	4.5	2.73	1.26	0.011	0.0011	0.29	0.0025	0.0015	0.65	0.044	12.99	61.27	23.91	0.31	0.016	6.14	0.095	0.086	7.48	0.78	100.08
Pl22.09	28.9	66.7	4.4	2.74	1.24	0.011	0.0008	0.29	0.0020	0.0006	0.66	0.044	12.99	61.77	23.73	0.30	0.011	6.03	0.079	b.d.l.	7.68	0.77	100.40
Pl22.10	29.6	66.5	3.9	2.72	1.26	0.011	0.0016	0.30	0.0023	0.0013	0.67	0.040	13.00	61.15	23.94	0.30	0.025	6.22	0.088	0.076	7.72	0.70	100.21
Pl22.11	31.3	64.9	3.8	2.71	1.27	0.011	0.0010	0.31	0.0025	0.0014	0.65	0.038	13.00	61.09	24.21	0.29	0.015	6.56	0.099	0.079	7.53	0.67	100.56
Pl22.12	32.7	63.7	3.6	2.69	1.29	0.012	0.0012	0.33	0.0028	0.0007	0.64	0.036	13.00	60.41	24.47	0.32	0.018	6.88	0.110	b.d.l.	7.40	0.63	100.28
Pl22.13	32.5	64.4	3.1	2.69	1.29	0.012	0.0012	0.32	0.0028	0.0012	0.64	0.031	12.99	60.35	24.57	0.33	0.018	6.71	0.108	b.d.l.	7.35	0.54	100.04
Pl22.14	32.4	64.0	3.5	2.69	1.29	0.012	0.0012	0.32	0.0020	0.0013	0.64	0.035	13.00	60.03	24.51	0.31	0.018	6.73	0.076	0.075	7.35	0.62	99.72
Pl22.15	32.6	64.0	3.4	2.70	1.29	0.012	0.0011	0.32	0.0023	0.0010	0.63	0.033	12.99	60.52	24.46	0.32	0.017	6.73	0.089	b.d.l.	7.31	0.59	100.10
Pl22.16	31.6	64.8	3.6	2.71	1.27	0.013	0.0013	0.31	0.0031	0.0014	0.65	0.035	13.00	60.82	24.23	0.36	0.019	6.59	0.120	0.079	7.47	0.62	100.31
Pl22.17	29.2	67.2	3.6	2.73	1.25	0.012	0.0011	0.29	0.0029	0.0012	0.68	0.036	13.00	61.19	23.69	0.32	0.017	6.15	0.114	b.d.l.	7.81	0.63	99.99
Pl22.18	27.5	68.4	4.1	2.74	1.25	0.013	0.0009	0.27	0.0022	0.0015	0.68	0.041	13.00	61.33	23.71	0.34	0.014	5.73	0.083	0.089	7.88	0.72	99.90
Pl22.19	28.0	66.9	5.0	2.74	1.25	0.013	0.0017	0.28	0.0025	0.0014	0.67	0.050	13.00	61.41	23.75	0.35	0.025	5.87	0.096	0.080	7.74	0.88	100.21
Pl22.20	27.5	67.3	5.2	2.74	1.25	0.011	0.0011	0.27	0.0020	0.0014	0.67	0.052	13.00	61.52	23.74	0.28	0.017	5.73	0.078	0.081	7.73	0.91	100.09

Appendix B1 cotinued

Label	An[2]	Ab[3]	Or[4]	Si	Al	Fe	Mg	Ca	Sr	Ba	Na	K	Tot[5]	SiO_2	Al_2O_3	FeO	MgO	CaO	SrO	BaO	Na_2O	K_2O	Tot
Pl22.21	33.0	62.4	4.6	2.69	1.29	0.011	0.0014	0.33	0.0021	0.0008	0.62	0.046	13.00	60.03	24.49	0.29	0.022	6.87	0.082	b.d.l.	7.17	0.81	99.81
Pl22.22	31.0	64.2	4.8	2.71	1.27	0.011	0.0016	0.31	0.0031	0.0018	0.65	0.048	13.01	60.66	24.21	0.30	0.025	6.55	0.120	0.105	7.50	0.85	100.32
Pl22.23	32.7	63.1	4.2	2.69	1.29	0.011	0.0011	0.33	0.0029	0.0011	0.63	0.042	13.00	59.91	24.34	0.28	0.016	6.81	0.111	b.d.l.	7.27	0.73	99.52
Pl22.24	27.0	67.4	5.6	2.75	1.24	0.011	0.0012	0.27	0.0025	0.0010	0.67	0.056	13.00	61.32	23.41	0.30	0.018	5.60	0.098	b.d.l.	7.74	0.97	99.51
Pl22.25	27.3	67.5	5.3	2.75	1.23	0.012	0.0013	0.27	0.0036	0.0021	0.67	0.052	12.99	61.48	23.27	0.31	0.020	5.62	0.140	0.120	7.68	0.91	99.55
Pl22.26	27.6	67.1	5.3	2.74	1.24	0.012	0.0008	0.28	0.0023	0.0016	0.67	0.054	13.00	61.10	23.35	0.32	0.012	5.75	0.089	0.092	7.72	0.93	99.36
Pl22.27	28.0	66.7	5.3	2.74	1.24	0.012	0.0014	0.28	0.0026	0.0012	0.66	0.052	12.99	60.98	23.46	0.31	0.021	5.76	0.101	b.d.l.	7.59	0.91	99.20
Pl22.28	28.3	66.1	5.6	2.74	1.24	0.011	0.0011	0.28	0.0022	0.0020	0.66	0.056	13.00	61.07	23.36	0.30	0.017	5.92	0.086	0.113	7.62	0.97	99.46
Pl22.30	28.9	65.6	5.5	2.74	1.24	0.012	0.0014	0.29	0.0022	0.0010	0.66	0.055	13.00	61.13	23.52	0.31	0.021	6.03	0.086	b.d.l.	7.56	0.96	99.66
Pl22.31	29.2	65.3	5.5	2.74	1.24	0.011	0.0013	0.29	0.0023	0.0016	0.65	0.055	13.00	61.20	23.59	0.30	0.020	6.09	0.087	0.089	7.52	0.96	99.84
Pl22.32	29.4	65.4	5.2	2.73	1.25	0.011	0.0018	0.30	0.0028	0.0013	0.66	0.052	13.00	60.65	23.67	0.30	0.027	6.16	0.107	0.073	7.57	0.91	99.46
Pl22.33	29.7	65.2	5.1	2.73	1.26	0.011	0.0011	0.29	0.0025	0.0015	0.64	0.050	12.99	60.78	23.88	0.29	0.017	6.10	0.094	0.086	7.40	0.88	99.53
Pl22.34	30.1	64.7	5.2	2.72	1.27	0.012	0.0015	0.30	0.0031	0.0014	0.64	0.052	12.99	60.74	24.01	0.31	0.023	6.21	0.121	0.082	7.37	0.91	99.76
Pl22.35	30.6	64.3	5.1	2.72	1.26	0.012	0.0013	0.31	0.0028	0.0011	0.65	0.051	13.00	60.73	23.96	0.33	0.019	6.40	0.109	b.d.l.	7.44	0.89	99.95
Pl22.36	31.7	63.5	4.8	2.71	1.27	0.011	0.0015	0.32	0.0026	0.0008	0.64	0.049	13.00	60.56	24.10	0.30	0.023	6.67	0.102	b.d.l.	7.39	0.86	100.05
Pl22.37	32.2	63.2	4.7	2.70	1.28	0.011	0.0014	0.32	0.0019	0.0018	0.62	0.046	12.99	60.27	24.22	0.30	0.021	6.62	0.073	0.100	7.18	0.81	99.58
Pl22.38	32.6	63.1	4.3	2.70	1.28	0.012	0.0012	0.33	0.0025	0.0013	0.64	0.044	13.00	60.26	24.26	0.32	0.018	6.85	0.097	0.073	7.33	0.77	99.97
Pl22.39	32.4	63.0	4.6	2.69	1.29	0.012	0.0016	0.32	0.0033	0.0011	0.63	0.046	13.00	60.08	24.46	0.33	0.025	6.70	0.128	b.d.l.	7.20	0.80	99.78
Pl22.42	34.0	60.6	5.4	2.73	1.24	0.029	0.0026	0.33	0.0026	0.0016	0.59	0.052	12.98	60.66	23.43	0.77	0.038	6.88	0.100	0.094	6.78	0.91	99.68
Pl25	84.4	15.3	0.3	2.14	1.84	0.026	0.0036	0.85	0.0039	0.0006	0.15	0.003	13.02	45.80	33.49	0.66	0.052	17.05	0.144	b.d.l.	1.70	0.05	98.98
Pl25.1	72.8	26.4	0.8	2.30	1.67	0.029	0.0037	0.73	0.0041	0.0003	0.26	0.008	13.00	50.03	30.93	0.74	0.054	14.81	0.154	b.d.l.	2.97	0.13	99.85
Pl25.1	55.7	40.8	3.6	2.49	1.48	0.033	0.0042	0.54	0.0033	b.d.l.	0.40	0.035	12.98	54.72	27.60	0.87	0.061	11.09	0.126	b.d.l.	4.48	0.60	99.54
Pl27.L1.01	43.6	53.5	2.8	2.58	1.40	0.029	0.0039	0.44	0.0034	0.0011	0.53	0.028	13.01	56.95	26.19	0.75	0.058	8.98	0.129	b.d.l.	6.09	0.49	99.71
Pl27.L1.02	62.7	36.0	1.2	2.36	1.61	0.027	0.0036	0.64	0.0038	0.0003	0.37	0.012	13.02	51.46	29.78	0.69	0.053	12.97	0.143	b.d.l.	4.12	0.21	99.45
Pl27.L1.04	63.3	35.7	1.0	2.35	1.63	0.023	0.0057	0.63	0.0039	0.0001	0.36	0.010	13.02	51.16	30.00	0.61	0.084	12.87	0.145	b.d.l.	4.01	0.18	99.06
Pl27.L1.05	59.5	39.3	1.3	2.41	1.57	0.022	0.0054	0.60	0.0041	0.0001	0.39	0.013	13.01	52.51	28.99	0.57	0.079	12.11	0.155	b.d.l.	4.42	0.22	99.06
Pl27.L1.06	58.2	40.6	1.1	2.41	1.56	0.023	0.0062	0.59	0.0041	0.0005	0.41	0.011	13.02	52.55	28.82	0.59	0.091	11.93	0.155	b.d.l.	4.60	0.19	98.96
Pl27.L1.07	64.4	34.7	1.0	2.36	1.62	0.023	0.0065	0.65	0.0045	0.0003	0.35	0.010	13.01	51.58	29.97	0.61	0.096	13.21	0.169	b.d.l.	3.93	0.16	99.75
Pl27.L1.08	57.7	41.0	1.4	2.43	1.54	0.026	0.0067	0.58	0.0040	0.0007	0.41	0.014	13.01	53.19	28.65	0.67	0.099	11.86	0.152	b.d.l.	4.65	0.23	99.55
Pl27.L1.09	60.9	37.9	1.2	2.40	1.57	0.022	0.0058	0.61	0.0039	0.0006	0.38	0.012	13.01	52.75	29.23	0.58	0.086	12.56	0.147	b.d.l.	4.32	0.20	99.91

Appendix B1 cotinued

Label	An[2]	Ab[3]	Or[4]	Si	Al	Fe	Mg	Ca	Sr	Ba	Na	K	Tot[5]	SiO_2	Al_2O_3	FeO	MgO	CaO	SrO	BaO	Na_2O	K_2O	Tot
Pl27.L1.10	59.8	38.9	1.3	2.40	1.57	0.021	0.0059	0.60	0.0048	0.0005	0.39	0.013	13.02	52.64	29.21	0.56	0.087	12.33	0.183	b.d.l.	4.43	0.23	99.69
Pl27.L1.12	67.0	32.1	0.9	2.34	1.63	0.021	0.0055	0.68	0.0038	b.d.l.	0.33	0.009	13.01	50.87	30.02	0.55	0.080	13.80	0.142	b.d.l.	3.65	0.15	99.27
Pl27.L1.13	63.4	35.7	0.9	2.37	1.60	0.023	0.0058	0.64	0.0043	b.d.l.	0.36	0.009	13.01	51.90	29.68	0.59	0.085	13.09	0.161	b.d.l.	4.08	0.16	99.74
Pl27.L1.14	64.9	34.2	0.9	2.37	1.61	0.022	0.0054	0.65	0.0037	0.0002	0.34	0.009	13.00	51.97	29.94	0.57	0.079	13.24	0.140	b.d.l.	3.86	0.15	99.96
Pl27.L1.15	62.0	36.9	1.0	2.38	1.58	0.027	0.0068	0.63	0.0041	b.d.l.	0.38	0.011	13.02	52.35	29.49	0.72	0.100	12.92	0.154	b.d.l.	4.25	0.18	100.17
Pl27.L1.16	61.4	37.5	1.1	2.38	1.59	0.025	0.0055	0.62	0.0047	0.0002	0.38	0.011	13.02	51.66	29.36	0.65	0.080	12.57	0.178	b.d.l.	4.25	0.19	98.94
Pl27.L1.17	58.5	40.2	1.3	2.41	1.57	0.023	0.0055	0.59	0.0044	b.d.l.	0.40	0.013	13.02	52.80	29.23	0.60	0.081	12.07	0.167	b.d.l.	4.58	0.23	99.76
Pl27.L1.18	64.1	34.8	1.2	2.35	1.62	0.025	0.0045	0.65	0.0038	0.0005	0.35	0.012	13.02	51.50	30.05	0.65	0.067	13.32	0.143	b.d.l.	4.00	0.21	99.96
Pl27.L1.19	60.0	38.7	1.4	2.39	1.58	0.029	0.0049	0.61	0.0036	0.0007	0.39	0.014	13.02	b.d.l.	b.d.l.	b.d.l.	b.d.l.	b.d.l.	b.d.l.	b.d.l.	b.d.l.	b.d.l.	97.23
Pl27.L1.20	60.2	38.1	1.7	2.40	1.57	0.031	0.0044	0.60	0.0041	0.0007	0.38	0.017	13.01	52.56	29.18	0.80	0.064	12.36	0.156	b.d.l.	4.32	0.29	99.77
Pl27.L2.01	35.6	59.6	4.8	2.66	1.31	0.026	0.0031	0.35	0.0032	0.0023	0.59	0.048	13.00	59.53	24.88	0.68	0.047	7.34	0.122	0.130	6.80	0.84	100.37
Pl27.L2.02	49.1	48.6	2.3	2.51	1.46	0.032	0.0043	0.50	0.0040	0.0012	0.49	0.023	13.02	55.22	27.23	0.85	0.063	10.22	0.153	b.d.l.	5.59	0.40	99.79
Pl27.L2.05	66.0	32.8	1.1	2.33	1.64	0.025	0.0049	0.67	0.0037	0.0005	0.33	0.011	13.02	50.91	30.42	0.66	0.072	13.63	0.139	b.d.l.	3.75	0.19	99.81
Pl27.L2.06	65.5	33.3	1.2	2.35	1.62	0.026	0.0044	0.66	0.0040	0.0004	0.34	0.012	13.02	51.51	30.09	0.67	0.064	13.59	0.151	b.d.l.	3.82	0.21	100.13
Pl27.L2.07	60.7	38.2	1.1	2.39	1.58	0.025	0.0054	0.61	0.0042	0.0003	0.38	0.011	13.01	52.52	29.43	0.66	0.079	12.43	0.158	b.d.l.	4.33	0.19	99.82
Pl27.L2.08	64.5	34.5	1.0	2.35	1.62	0.024	0.0057	0.65	0.0040	0.0008	0.35	0.010	13.02	51.49	30.13	0.62	0.085	13.39	0.152	b.d.l.	3.96	0.18	100.06
Pl27.L2.09	64.5	34.5	1.0	2.36	1.61	0.024	0.0058	0.64	0.0045	0.0005	0.34	0.010	13.01	51.92	30.06	0.63	0.085	13.20	0.171	b.d.l.	3.91	0.17	100.17
Pl27.L2.10	63.6	35.6	0.8	2.37	1.61	0.023	0.0056	0.63	0.0039	b.d.l.	0.36	0.008	13.01	51.80	29.88	0.59	0.082	12.95	0.148	b.d.l.	4.01	0.14	99.60
Pl27.L2.11	59.4	39.4	1.2	2.41	1.56	0.022	0.0052	0.60	0.0044	0.0003	0.40	0.012	13.01	52.96	29.08	0.57	0.077	12.30	0.168	b.d.l.	4.51	0.21	99.89
Pl27.L2.12	60.7	38.1	1.2	2.40	1.58	0.021	0.0055	0.61	0.0034	0.0006	0.38	0.012	13.01	52.48	29.38	0.54	0.082	12.43	0.129	b.d.l.	4.31	0.21	99.60
Pl27.L3.01_UL	61.8	36.8	1.4	2.41	1.56	0.029	0.0040	0.61	0.0035	0.0001	0.37	0.014	13.00	52.54	28.77	0.75	0.059	12.49	0.132	b.d.l.	4.11	0.24	99.10
Pl27.L3.02	65.2	33.7	1.2	2.38	1.60	0.027	0.0045	0.64	0.0031	0.0006	0.33	0.012	13.00	51.51	29.38	0.69	0.065	13.04	0.116	b.d.l.	3.72	0.20	98.75
Pl27.L3.03	60.7	38.0	1.3	2.42	1.55	0.024	0.0056	0.60	0.0036	0.0001	0.38	0.013	13.00	52.56	28.56	0.61	0.082	12.17	0.136	b.d.l.	4.21	0.22	98.55
Pl27.L3.04	62.2	36.7	1.1	2.41	1.56	0.022	0.0058	0.61	0.0041	0.0002	0.36	0.011	12.99	b.d.l.	b.d.l.	b.d.l.	b.d.l.	b.d.l.	b.d.l.	b.d.l.	b.d.l.	b.d.l.	97.34
Pl27.L3.05	57.1	41.7	1.3	2.44	1.53	0.023	0.0055	0.57	0.0037	0.0005	0.42	0.013	13.01	b.d.l.	b.d.l.	b.d.l.	b.d.l.	b.d.l.	b.d.l.	b.d.l.	b.d.l.	b.d.l.	97.65
Pl27.L3.06	57.7	41.0	1.3	2.45	1.52	0.025	0.0064	0.57	0.0038	0.0001	0.41	0.013	13.00	53.45	28.03	0.65	0.094	11.67	0.143	b.d.l.	4.58	0.23	98.84
Pl27.L3.07	58.8	40.0	1.3	2.44	1.54	0.023	0.0056	0.58	0.0037	0.0006	0.40	0.013	13.00	53.60	28.65	0.60	0.082	11.98	0.141	b.d.l.	4.50	0.22	99.80
Pl27.L3.08	60.5	38.4	1.1	2.43	1.54	0.021	0.0046	0.59	0.0038	b.d.l.	0.38	0.011	12.99	53.31	28.65	0.54	0.068	12.15	0.144	b.d.l.	4.26	0.19	99.32
Pl27.L3.09	62.0	37.0	1.0	2.40	1.58	0.020	0.0044	0.62	0.0038	0.0001	0.37	0.010	13.00	52.79	29.39	0.52	0.066	12.66	0.144	b.d.l.	4.17	0.17	99.93
Pl27.L3.10	60.0	38.9	1.1	2.41	1.57	0.020	0.0056	0.60	0.0037	0.0005	0.39	0.011	13.00	b.d.l.	b.d.l.	b.d.l.	b.d.l.	b.d.l.	b.d.l.	b.d.l.	b.d.l.	b.d.l.	94.63

Appendix B1 cotinued

Label	An[2]	Ab[3]	Or[4]	Si	Al	Fe	Mg	Ca	Sr	Ba	Na	K	Tot[5]	SiO_2	Al_2O_3	FeO	MgO	CaO	SrO	BaO	Na_2O	K_2O	Tot
Pl27.L3.11	61.2	37.7	1.1	2.41	1.57	0.022	0.0054	0.60	0.0040	0.0001	0.37	0.011	13.00	52.92	29.17	0.57	0.079	12.33	0.150	b.d.l.	4.20	0.19	99.62
Pl27.L3.12	56.9	41.7	1.4	2.46	1.52	0.024	0.0068	0.56	0.0045	0.0001	0.41	0.014	12.99	b.d.l.	b.d.l.	b.d.l.	b.d.l.	b.d.l.	b.d.l.	b.d.l.	b.d.l.	b.d.l.	97.12
Pl27.L3.13	60.3	38.6	1.1	2.40	1.57	0.024	0.0062	0.61	0.0045	0.0003	0.39	0.011	13.02	52.68	29.33	0.62	0.091	12.51	0.169	b.d.l.	4.43	0.19	100.03
Pl27.L3.14	63.1	35.9	1.0	2.39	1.58	0.024	0.0059	0.63	0.0045	0.0003	0.36	0.010	13.00	52.14	29.33	0.63	0.086	12.75	0.169	b.d.l.	4.01	0.17	99.30
Pl27.L3.15	54.1	44.6	1.3	2.48	1.50	0.024	0.0066	0.54	0.0050	0.0002	0.44	0.013	13.00	54.24	27.85	0.62	0.097	10.96	0.189	b.d.l.	5.00	0.22	99.19
Pl27.L3.16	57.5	41.3	1.3	2.44	1.52	0.024	0.0063	0.58	0.0036	0.0003	0.42	0.013	13.01	53.81	28.47	0.62	0.093	11.87	0.138	b.d.l.	4.71	0.22	99.95
Pl27.L3.17	56.4	42.3	1.4	2.48	1.50	0.022	0.0063	0.56	0.0042	0.0007	0.42	0.014	12.99	54.24	27.78	0.59	0.093	11.35	0.160	b.d.l.	4.70	0.23	99.18
Pl27.L3.18	60.5	38.4	1.1	2.42	1.56	0.022	0.0058	0.60	0.0040	0.0001	0.38	0.011	13.00	52.92	28.90	0.57	0.086	12.36	0.153	b.d.l.	4.33	0.19	99.51
Pl27.L3.19	56.6	42.2	1.3	2.46	1.51	0.024	0.0064	0.56	0.0039	0.0011	0.42	0.013	13.00	54.05	28.08	0.62	0.094	11.45	0.149	b.d.l.	4.72	0.22	99.45
Pl27.L3.20	57.7	41.0	1.2	2.45	1.52	0.028	0.0065	0.57	0.0034	0.0004	0.41	0.012	13.00	53.88	28.46	0.73	0.097	11.81	0.127	b.d.l.	4.64	0.21	99.98
Pl27.L3.20_2	58.7	40.1	1.2	2.44	1.53	0.028	0.0069	0.59	0.0040	0.0003	0.40	0.012	13.00	53.49	28.39	0.73	0.101	11.98	0.151	b.d.l.	4.52	0.21	99.59
Pl27.L3.21	64.5	34.5	1.0	2.36	1.62	0.025	0.0064	0.64	0.0038	0.0004	0.34	0.009	13.00	51.47	29.89	0.64	0.093	12.93	0.141	b.d.l.	3.82	0.16	99.17
Pl27.L3.21_2	64.6	34.3	1.1	2.36	1.62	0.026	0.0058	0.64	0.0036	0.0005	0.34	0.011	13.01	51.36	29.91	0.68	0.085	13.07	0.135	b.d.l.	3.84	0.19	99.30
Pl27.L3.22	58.7	39.9	1.4	2.42	1.54	0.029	0.0063	0.59	0.0036	b.d.l.	0.40	0.014	13.01	53.08	28.70	0.76	0.092	12.02	0.136	b.d.l.	4.51	0.24	99.54
Pl27.L3.22_2	59.8	38.9	1.3	2.42	1.55	0.028	0.0061	0.60	0.0032	0.0004	0.39	0.014	13.01	52.97	28.71	0.73	0.089	12.29	0.120	b.d.l.	4.42	0.23	99.58
Pl27.L3.23	63.8	35.0	1.2	2.38	1.59	0.027	0.0045	0.63	0.0035	0.0006	0.35	0.012	13.00	51.80	29.45	0.71	0.066	12.86	0.131	b.d.l.	3.90	0.20	99.15
Pl27.L3.23_2	63.2	35.7	1.1	2.38	1.59	0.028	0.0045	0.63	0.0043	b.d.l.	0.36	0.011	13.01	52.03	29.52	0.72	0.066	12.92	0.161	b.d.l.	4.04	0.19	99.64
Pl27.L3.24	63.4	35.5	1.1	2.38	1.60	0.026	0.0044	0.63	0.0037	b.d.l.	0.35	0.011	13.00	51.54	29.51	0.66	0.064	12.72	0.137	b.d.l.	3.93	0.19	98.76
Pl27.L3.24_2	62.4	36.2	1.4	2.38	1.60	0.026	0.0042	0.62	0.0035	0.0004	0.36	0.014	13.01	51.78	29.47	0.68	0.061	12.67	0.133	b.d.l.	4.07	0.23	99.11
Pl27.L3.25_LR	51.3	46.4	2.3	2.49	1.47	0.033	0.0048	0.52	0.0035	0.0006	0.47	0.023	13.02	54.76	27.42	0.86	0.071	10.60	0.134	b.d.l.	5.30	0.40	99.57
Pl27.L3.25_LR_2	51.0	47.0	2.0	2.50	1.47	0.032	0.0046	0.51	0.0036	b.d.l.	0.47	0.020	13.01	54.98	27.44	0.85	0.068	10.43	0.138	b.d.l.	5.32	0.34	99.56
Pl28.L1.1	76.3	22.8	0.9	2.24	1.73	0.029	0.0031	0.77	0.0031	0.0005	0.23	0.009	13.01	48.42	31.82	0.74	0.045	15.47	0.117	b.d.l.	2.55	0.15	99.35
Pl28.L1.2	88.0	11.8	0.2	2.09	1.89	0.025	0.0029	0.90	0.0039	b.d.l.	0.12	0.002	13.03	45.05	34.54	0.65	0.043	18.22	0.143	b.d.l.	1.35	0.04	100.02
Pl28.L1.3	87.3	12.3	0.4	2.10	1.89	0.025	0.0032	0.88	0.0038	0.0001	0.12	0.004	13.03	44.84	34.23	0.65	0.047	17.66	0.140	b.d.l.	1.38	0.07	99.02
Pl28.L1.4	89.4	10.3	0.3	2.07	1.91	0.026	0.0029	0.92	0.0041	0.0006	0.11	0.003	13.04	b.d.l.	b.d.l.	b.d.l.	b.d.l.	b.d.l.	b.d.l.	b.d.l.	b.d.l.	b.d.l.	98.20
Pl3.01	33.6	63.1	3.3	2.69	1.29	0.011	0.0010	0.33	0.0023	0.0026	0.63	0.033	13.00	60.47	24.71	0.30	0.015	7.03	0.089	0.149	7.30	0.58	100.64
Pl3.02	32.2	62.6	5.2	2.71	1.28	0.014	0.0013	0.32	0.0023	0.0012	0.61	0.051	12.99	b.d.l.	b.d.l.	b.d.l.	b.d.l.	b.d.l.	b.d.l.	b.d.l.	b.d.l.	b.d.l.	96.86
Pl3.04	30.6	64.2	5.2	2.73	1.26	0.012	0.0009	0.30	0.0024	0.0005	0.63	0.051	12.98	61.32	23.98	0.31	0.013	6.30	0.092	b.d.l.	7.29	0.90	100.23
Pl3.05	28.6	66.6	4.9	2.75	1.24	0.011	0.0010	0.28	0.0031	0.0013	0.65	0.048	12.98	61.76	23.58	0.30	0.015	5.86	0.121	b.d.l.	7.56	0.84	100.11
Pl3.06	31.2	64.6	4.2	2.71	1.27	0.011	0.0013	0.31	0.0029	0.0011	0.64	0.042	13.00	60.68	24.19	0.28	0.019	6.50	0.112	b.d.l.	7.44	0.74	100.02

Appendix B1 cotinued

Label	An[2]	Ab[3]	Or[4]	Si	Al	Fe	Mg	Ca	Sr	Ba	Na	K	Tot[5]	SiO_2	Al_2O_3	FeO	MgO	CaO	SrO	BaO	Na_2O	K_2O	Tot
Pl3.07	31.3	64.8	3.9	2.71	1.28	0.012	0.0015	0.31	0.0031	0.0015	0.64	0.039	12.99	60.79	24.42	0.32	0.023	6.50	0.121	0.086	7.43	0.68	100.37
Pl3.08	31.3	64.8	3.9	2.69	1.29	0.012	0.0016	0.32	0.0030	0.0013	0.66	0.040	13.01	60.22	24.59	0.31	0.024	6.63	0.114	b.d.l.	7.57	0.70	100.22
Pl3.09	33.4	63.2	3.5	2.69	1.30	0.011	0.0004	0.33	0.0027	0.0015	0.62	0.034	12.99	60.78	24.85	0.30	b.d.l.	6.95	0.107	0.086	7.27	0.61	100.95
Pl3.10	32.7	64.0	3.3	2.69	1.30	0.011	0.0008	0.33	0.0035	0.0013	0.64	0.033	13.00	60.28	24.69	0.31	b.d.l.	6.83	0.136	b.d.l.	7.38	0.58	100.28
Pl3.11	28.2	67.7	4.0	2.75	1.24	0.012	0.0008	0.28	0.0031	0.0014	0.67	0.040	12.99	61.86	23.66	0.32	0.013	5.87	0.121	b.d.l.	7.79	0.71	100.41
Pl3.12	28.0	68.1	3.9	2.74	1.25	0.012	0.0011	0.28	0.0024	0.0013	0.67	0.038	12.99	61.65	23.85	0.33	0.017	5.78	0.095	b.d.l.	7.78	0.68	100.25
Pl3.13	29.6	66.8	3.6	2.72	1.26	0.012	0.0014	0.29	0.0029	0.0017	0.66	0.036	12.99	61.39	24.17	0.32	0.021	6.16	0.112	0.097	7.69	0.64	100.60
Pl3.14	27.1	69.0	3.9	2.74	1.25	0.011	0.0008	0.27	0.0020	0.0017	0.68	0.039	12.99	61.76	23.94	0.30	b.d.l.	5.60	0.076	0.096	7.91	0.68	100.37
Pl3.15	28.3	67.9	3.8	2.73	1.25	0.013	0.0011	0.29	0.0026	0.0017	0.69	0.039	13.01	60.59	23.61	0.33	0.017	5.98	0.101	0.098	7.94	0.67	99.33
Pl3.16	28.0	68.2	3.9	2.76	1.23	0.012	0.0012	0.28	0.0029	0.0017	0.67	0.038	12.99	61.87	23.34	0.31	0.018	5.77	0.114	0.097	7.77	0.67	99.96
Pl3.17	31.7	64.1	4.2	2.71	1.27	0.011	0.0006	0.31	0.0029	0.0012	0.63	0.041	12.99	60.65	24.16	0.28	b.d.l.	6.52	0.113	b.d.l.	7.28	0.73	99.82
Pl3.18	31.6	64.1	4.3	2.71	1.28	0.011	0.0016	0.31	0.0036	0.0010	0.63	0.042	12.99	60.86	24.28	0.29	0.024	6.49	0.141	b.d.l.	7.28	0.74	100.16
Pl3.19	32.6	63.4	4.1	2.70	1.29	0.012	0.0007	0.32	0.0028	0.0011	0.63	0.041	13.00	60.47	24.48	0.32	b.d.l.	6.79	0.107	b.d.l.	7.30	0.72	100.25
Pl3.20	31.4	63.8	4.8	2.71	1.28	0.012	0.0009	0.31	0.0033	0.0018	0.63	0.047	12.99	60.55	24.15	0.32	0.013	6.41	0.126	0.105	7.20	0.82	99.69
Pl3.21	32.4	63.1	4.5	2.69	1.29	0.010	0.0008	0.32	0.0024	0.0015	0.63	0.044	13.00	60.51	24.64	0.27	0.013	6.75	0.094	b.d.l.	7.26	0.78	100.41
Pl3.22	32.4	62.8	4.8	2.70	1.29	0.011	0.0010	0.32	0.0025	0.0020	0.62	0.048	13.00	60.46	24.51	0.29	0.015	6.74	0.096	0.116	7.23	0.84	100.30
Pl3.23	28.0	66.4	5.6	2.73	1.26	0.011	0.0011	0.28	0.0037	0.0015	0.66	0.056	13.00	61.12	23.92	0.30	0.017	5.84	0.143	b.d.l.	7.65	0.98	100.06
Pl3.25	27.6	66.4	6.0	2.76	1.22	0.014	0.0014	0.27	0.0027	0.0012	0.65	0.059	12.99	62.05	23.33	0.37	0.021	5.70	0.104	b.d.l.	7.58	1.05	100.26
Pl3.26	27.8	66.3	5.8	2.75	1.24	0.011	0.0010	0.28	0.0023	0.0010	0.66	0.058	12.99	61.91	23.63	0.30	0.015	5.78	0.089	b.d.l.	7.62	1.02	100.42
Pl3.27	32.4	62.8	4.8	2.69	1.30	0.010	0.0011	0.33	0.0031	0.0012	0.63	0.048	13.01	60.14	24.64	0.27	0.017	6.80	0.120	b.d.l.	7.30	0.85	100.21
Pl3.28	32.2	63.1	4.8	2.70	1.29	0.012	0.0012	0.32	0.0032	0.0009	0.63	0.048	13.00	60.46	24.47	0.31	0.017	6.72	0.126	b.d.l.	7.28	0.84	100.26
Pl3.29	31.9	63.3	4.8	2.69	1.29	0.012	0.0013	0.32	0.0018	0.0010	0.64	0.048	13.01	60.20	24.52	0.32	0.019	6.71	0.071	b.d.l.	7.35	0.84	100.09
Pl3.30	33.0	62.3	4.7	2.68	1.30	0.011	0.0010	0.33	0.0028	0.0007	0.63	0.047	13.00	60.06	24.65	0.28	0.014	6.92	0.109	b.d.l.	7.22	0.83	100.12
Pl3.31	30.3	56.9	12.8	2.84	1.05	0.079	0.0609	0.28	0.0007	0.0006	0.53	0.118	12.96	b.d.l.	b.d.l.	b.d.l.	b.d.l.	b.d.l.	b.d.l.	b.d.l.	b.d.l.	b.d.l.	92.82
Pl3.31	47.4	49.7	2.9	2.55	1.42	0.027	0.0032	0.48	0.0027	0.0007	0.50	0.029	13.01	56.48	26.75	0.72	0.048	9.88	0.104	b.d.l.	5.72	0.51	100.25
Pl3.32	29.5	58.7	11.8	2.82	1.08	0.073	0.0544	0.28	0.0016	0.0011	0.56	0.111	12.98	b.d.l.	b.d.l.	b.d.l.	b.d.l.	b.d.l.	b.d.l.	b.d.l.	b.d.l.	b.d.l.	93.09
Pl3.32	29.0	66.3	4.7	2.74	1.24	0.011	0.0005	0.29	0.0023	0.0018	0.66	0.047	12.99	61.71	23.72	0.30	b.d.l.	6.03	0.089	0.103	7.61	0.83	100.40
Pl3.33	35.1	59.4	5.5	2.71	1.16	0.085	0.0842	0.35	0.0026	0.0010	0.59	0.055	13.03	b.d.l.	b.d.l.	b.d.l.	b.d.l.	b.d.l.	b.d.l.	b.d.l.	b.d.l.	b.d.l.	93.76
Pl3.33	30.5	64.7	4.7	2.72	1.26	0.012	0.0013	0.30	0.0020	0.0011	0.65	0.047	12.99	61.46	24.08	0.32	0.020	6.41	0.078	b.d.l.	7.51	0.83	100.78
Pl3.34	30.7	64.8	4.5	2.73	1.26	0.011	0.0010	0.30	0.0017	0.0006	0.63	0.044	12.98	61.21	23.89	0.29	0.014	6.27	0.064	b.d.l.	7.33	0.77	99.88

Appendix B1 cotinued

Label	An[2]	Ab[3]	Or[4]	Si	Al	Fe	Mg	Ca	Sr	Ba	Na	K	Tot[5]	SiO_2	Al_2O_3	FeO	MgO	CaO	SrO	BaO	Na_2O	K_2O	Tot
Pl3.35	30.2	65.2	4.5	2.73	1.25	0.012	0.0008	0.30	0.0022	0.0015	0.65	0.045	12.99	61.40	23.82	0.31	b.d.l.	6.33	0.087	0.088	7.56	0.80	100.41
Pl3.36	30.3	65.2	4.5	2.73	1.25	0.012	0.0013	0.30	0.0032	0.0015	0.64	0.044	12.99	61.50	23.93	0.32	0.019	6.27	0.125	0.089	7.44	0.77	100.47
Pl3.37	31.2	64.7	4.1	2.73	1.26	0.012	0.0016	0.31	0.0035	0.0018	0.64	0.040	12.99	60.57	23.71	0.31	0.024	6.37	0.136	0.100	7.30	0.70	99.22
Pl3.38	31.1	65.3	3.7	2.71	1.28	0.011	0.0010	0.31	0.0023	0.0018	0.64	0.036	12.99	61.09	24.38	0.29	0.015	6.42	0.088	0.102	7.46	0.63	100.48
Pl3.39	31.0	65.4	3.7	2.71	1.27	0.011	0.0007	0.31	0.0027	0.0015	0.65	0.037	13.00	61.05	24.34	0.29	b.d.l.	6.52	0.103	b.d.l.	7.60	0.65	100.65
Pl3.40	31.6	64.8	3.6	2.72	1.27	0.011	0.0011	0.31	0.0033	0.0014	0.63	0.036	12.98	61.49	24.29	0.30	0.017	6.53	0.130	b.d.l.	7.40	0.63	100.86
Pl3.41	32.7	64.1	3.2	2.70	1.28	0.012	0.0009	0.33	0.0027	0.0010	0.64	0.032	13.00	60.54	24.29	0.32	0.014	6.86	0.105	b.d.l.	7.43	0.56	100.17
Pl3.42	33.7	62.9	3.4	2.69	1.29	0.011	0.0017	0.33	0.0028	0.0011	0.62	0.034	12.99	60.11	24.54	0.30	0.026	6.95	0.110	b.d.l.	7.17	0.59	99.86
Pl3.43	32.8	64.0	3.2	2.69	1.29	0.012	0.0013	0.33	0.0024	0.0004	0.64	0.032	13.00	60.56	24.67	0.31	0.020	6.88	0.093	b.d.l.	7.41	0.56	100.53
Pl3.44	31.9	64.8	3.3	2.70	1.29	0.012	0.0012	0.31	0.0035	0.0010	0.64	0.032	12.99	60.51	24.52	0.31	0.018	6.55	0.134	b.d.l.	7.37	0.57	100.03
Pl3.45	32.4	64.3	3.3	2.70	1.28	0.012	0.0012	0.32	0.0034	0.0015	0.64	0.033	13.00	60.70	24.41	0.33	0.019	6.77	0.133	b.d.l.	7.42	0.58	100.44
Pl3.46	31.9	64.8	3.3	2.70	1.28	0.010	0.0014	0.32	0.0033	0.0016	0.65	0.032	13.00	60.75	24.36	0.26	0.021	6.66	0.127	0.091	7.48	0.57	100.33
Pl3.47	32.7	64.2	3.1	2.69	1.30	0.011	0.0003	0.33	0.0030	0.0010	0.64	0.031	13.00	60.12	24.62	0.29	b.d.l.	6.85	0.116	b.d.l.	7.44	0.55	100.05
Pl3.48	33.7	63.2	3.1	2.68	1.31	0.011	0.0013	0.34	0.0024	0.0012	0.63	0.031	13.00	60.07	24.92	0.29	0.019	7.08	0.094	b.d.l.	7.34	0.55	100.43
Pl3.49	32.4	64.3	3.3	2.70	1.29	0.010	0.0004	0.32	0.0030	0.0006	0.64	0.032	12.99	60.63	24.55	0.28	b.d.l.	6.73	0.116	b.d.l.	7.39	0.57	100.30
Pl3.50	33.5	63.2	3.2	2.69	1.30	0.011	0.0002	0.33	0.0026	0.0007	0.62	0.032	12.99	60.32	24.84	0.30	b.d.l.	6.92	0.101	b.d.l.	7.21	0.56	100.28
Pl3.51	33.6	63.5	2.9	2.69	1.30	0.012	0.0007	0.33	0.0024	0.0004	0.63	0.029	13.00	60.33	24.70	0.33	b.d.l.	7.01	0.093	b.d.l.	7.32	0.51	100.32
Pl33	62.9	35.5	1.6	2.38	1.60	0.028	0.0042	0.63	0.0037	0.0006	0.35	0.016	13.01	51.88	29.64	0.73	0.061	12.74	0.138	b.d.l.	3.97	0.27	99.46
Pl33	56.8	41.8	1.4	2.44	1.53	0.024	0.0063	0.57	0.0036	b.d.l.	0.42	0.014	13.01	53.76	28.54	0.64	0.093	11.71	0.137	b.d.l.	4.76	0.24	99.88
Pl33.L1.01	54.5	43.5	2.0	2.45	1.52	0.029	0.0034	0.55	0.0037	b.d.l.	0.44	0.020	13.02	53.83	28.36	0.75	0.051	11.38	0.141	b.d.l.	5.01	0.35	99.87
Pl33.L1.02	63.8	34.9	1.3	2.36	1.61	0.026	0.0041	0.65	0.0036	0.0001	0.35	0.013	13.02	51.53	29.71	0.69	0.060	13.16	0.135	b.d.l.	3.97	0.22	99.48
Pl33.L1.03	57.4	40.9	1.7	2.43	1.54	0.031	0.0064	0.58	0.0039	0.0008	0.41	0.017	13.02	53.09	28.62	0.82	0.094	11.82	0.147	b.d.l.	4.66	0.30	99.58
Pl33.L1.04	59.1	39.5	1.3	2.40	1.58	0.029	0.0063	0.60	0.0042	0.0001	0.40	0.014	13.02	52.58	29.32	0.75	0.093	12.24	0.158	b.d.l.	4.52	0.23	99.90
Pl33.L1.05	59.2	39.5	1.3	2.41	1.57	0.027	0.0062	0.60	0.0038	0.0001	0.40	0.013	13.02	52.73	29.16	0.71	0.092	12.20	0.145	b.d.l.	4.49	0.22	99.76
Pl33.L1.06	59.9	38.8	1.2	2.39	1.58	0.025	0.0068	0.61	0.0039	b.d.l.	0.39	0.013	13.02	52.35	29.31	0.65	0.099	12.40	0.149	b.d.l.	4.45	0.21	99.62
Pl33.L1.07	58.0	40.9	1.1	2.42	1.55	0.026	0.0066	0.59	0.0052	0.0003	0.41	0.011	13.02	53.41	28.90	0.68	0.098	12.04	0.197	b.d.l.	4.70	0.19	100.23
Pl33.L1.08	59.7	39.2	1.2	2.42	1.55	0.027	0.0064	0.60	0.0042	0.0004	0.39	0.012	13.01	53.12	28.76	0.72	0.094	12.25	0.160	b.d.l.	4.44	0.20	99.76
Pl33.L1.09	59.1	39.8	1.1	2.40	1.58	0.026	0.0063	0.59	0.0035	0.0002	0.40	0.011	13.02	52.60	29.48	0.69	0.092	12.08	0.133	b.d.l.	4.49	0.19	99.77
Pl33.L1.10	65.8	33.2	1.0	2.33	1.65	0.026	0.0061	0.67	0.0037	0.0005	0.34	0.010	13.02	50.91	30.55	0.67	0.089	13.59	0.139	b.d.l.	3.80	0.17	99.94
Pl33.L1.11	59.7	39.2	1.1	2.38	1.59	0.023	0.0057	0.61	0.0042	b.d.l.	0.40	0.011	13.03	52.17	29.60	0.60	0.084	12.39	0.158	b.d.l.	4.50	0.19	99.70

Appendix B1 cotinued

Label	An[2]	Ab[3]	Or[4]	Si	Al	Fe	Mg	Ca	Sr	Ba	Na	K	Tot[5]	SiO_2	Al_2O_3	FeO	MgO	CaO	SrO	BaO	Na_2O	K_2O	Tot
Pl33.L1.12	57.1	41.7	1.2	2.41	1.56	0.023	0.0056	0.58	0.0035	b.d.l.	0.42	0.013	13.02	52.90	29.11	0.59	0.083	11.83	0.134	b.d.l.	4.78	0.22	99.65
Pl33.L1.13	56.1	42.3	1.5	2.43	1.55	0.023	0.0063	0.57	0.0048	0.0005	0.43	0.015	13.02	53.18	28.78	0.60	0.093	11.62	0.182	b.d.l.	4.85	0.26	99.61
Pl33.L1.14	55.8	42.7	1.5	2.43	1.55	0.022	0.0053	0.56	0.0040	0.0006	0.43	0.015	13.02	53.24	28.87	0.56	0.078	11.47	0.151	b.d.l.	4.86	0.25	99.52
Pl33.L1.15	54.3	44.1	1.6	2.46	1.52	0.022	0.0061	0.55	0.0046	0.0004	0.44	0.016	13.01	54.13	28.36	0.59	0.090	11.21	0.173	b.d.l.	5.04	0.28	99.89
Pl33.L1.16	57.2	41.5	1.3	2.43	1.55	0.026	0.0058	0.57	0.0043	0.0002	0.41	0.013	13.01	53.37	28.79	0.68	0.086	11.72	0.162	b.d.l.	4.69	0.23	99.74
Pl33.L1.17	58.7	40.1	1.2	2.41	1.56	0.024	0.0060	0.59	0.0039	0.0001	0.41	0.012	13.02	53.12	29.07	0.62	0.089	12.20	0.147	b.d.l.	4.62	0.21	100.08
Pl33.L1.18	54.6	43.8	1.6	2.45	1.52	0.027	0.0066	0.55	0.0044	0.0004	0.44	0.016	13.01	53.74	28.21	0.71	0.098	11.18	0.165	b.d.l.	4.95	0.28	99.36
Pl33.L1.19	45.8	48.7	5.5	2.62	1.34	0.045	0.0154	0.43	0.0029	0.0002	0.46	0.052	12.97	57.58	25.01	1.17	0.227	8.89	0.111	b.d.l.	5.22	0.89	99.11
Pl33.L1.20	57.5	40.8	1.7	2.42	1.56	0.028	0.0073	0.58	0.0040	b.d.l.	0.41	0.017	13.02	52.78	28.93	0.72	0.108	11.77	0.149	b.d.l.	4.61	0.29	99.36
Pl33.L1.21	56.1	42.0	1.8	2.48	1.47	0.027	0.0065	0.56	0.0041	0.0002	0.42	0.018	13.00	54.28	27.34	0.70	0.095	11.46	0.154	b.d.l.	4.74	0.31	99.09
Pl33.L1.22	51.3	46.2	2.6	2.49	1.46	0.046	0.0180	0.52	0.0044	0.0006	0.47	0.026	13.03	54.00	26.80	1.18	0.262	10.60	0.163	b.d.l.	5.28	0.45	98.77
Pl33.L1.23	52.0	46.0	1.9	2.47	1.50	0.025	0.0060	0.52	0.0034	0.0008	0.46	0.019	13.02	54.38	28.05	0.65	0.088	10.71	0.129	b.d.l.	5.23	0.34	99.62
Pl33.L1.24	56.7	41.9	1.4	2.42	1.55	0.024	0.0050	0.58	0.0046	0.0002	0.43	0.014	13.02	53.00	28.76	0.63	0.073	11.77	0.175	b.d.l.	4.81	0.25	99.46
Pl33.L1.25	58.8	39.9	1.4	2.40	1.58	0.023	0.0045	0.59	0.0039	0.0002	0.40	0.014	13.02	52.87	29.44	0.61	0.066	12.19	0.148	b.d.l.	4.57	0.24	100.14
Pl33.L1.26	55.3	43.1	1.5	2.44	1.53	0.024	0.0047	0.56	0.0047	0.0006	0.44	0.016	13.02	53.47	28.37	0.64	0.069	11.39	0.179	b.d.l.	4.91	0.27	99.31
Pl33.L1.27	62.6	36.2	1.2	2.36	1.62	0.024	0.0038	0.64	0.0040	0.0003	0.37	0.012	13.03	51.40	29.91	0.63	0.056	13.02	0.151	b.d.l.	4.15	0.21	99.55
Pl33.L1.28	65.5	33.4	1.1	2.34	1.65	0.026	0.0044	0.65	0.0040	0.0001	0.33	0.011	13.01	50.80	30.38	0.67	0.064	13.27	0.151	b.d.l.	3.74	0.19	99.27
Pl33.L1.29	60.4	38.4	1.3	2.39	1.59	0.025	0.0048	0.60	0.0041	0.0007	0.38	0.013	13.01	52.47	29.72	0.66	0.071	12.37	0.154	b.d.l.	4.34	0.22	100.05
Pl33.L1.30	57.8	40.8	1.4	2.41	1.57	0.024	0.0053	0.58	0.0042	b.d.l.	0.41	0.014	13.02	52.83	29.13	0.61	0.078	11.92	0.157	b.d.l.	4.64	0.25	99.63
Pl33.L1.31	55.6	43.0	1.5	2.44	1.53	0.027	0.0064	0.56	0.0037	b.d.l.	0.44	0.015	13.02	53.44	28.56	0.71	0.094	11.54	0.141	b.d.l.	4.93	0.26	99.67
Pl33.L1.32	54.6	43.8	1.6	2.45	1.52	0.028	0.0061	0.55	0.0037	0.0010	0.44	0.016	13.01	53.85	28.33	0.72	0.090	11.17	0.139	b.d.l.	4.95	0.27	99.58
Pl33.L1.33	55.4	43.1	1.5	2.45	1.52	0.026	0.0052	0.56	0.0038	b.d.l.	0.43	0.015	13.01	53.73	28.38	0.69	0.077	11.38	0.144	b.d.l.	4.89	0.25	99.54
Pl33.L1.34	56.0	42.4	1.7	2.43	1.54	0.027	0.0047	0.57	0.0035	0.0008	0.43	0.017	13.02	53.39	28.66	0.70	0.070	11.59	0.134	b.d.l.	4.85	0.29	99.72
Pl33.L1.35	63.8	35.2	1.0	2.35	1.62	0.027	0.0032	0.65	0.0032	0.0003	0.36	0.010	13.02	51.33	30.00	0.69	0.047	13.26	0.119	b.d.l.	4.05	0.18	99.70
Pl33.L2.01_L	38.0	54.4	7.6	2.74	1.23	0.041	0.0039	0.35	0.0023	0.0011	0.50	0.070	12.93	60.82	23.08	1.08	0.059	7.26	0.090	b.d.l.	5.74	1.22	99.41
Pl33.L2.02	63.0	35.8	1.2	2.36	1.61	0.029	0.0038	0.63	0.0039	0.0006	0.36	0.012	13.02	51.40	29.82	0.76	0.056	12.85	0.148	b.d.l.	4.03	0.21	99.31
Pl33.L2.03	56.0	42.3	1.7	2.45	1.52	0.029	0.0050	0.56	0.0043	0.0002	0.42	0.017	13.01	53.82	28.25	0.75	0.074	11.47	0.163	b.d.l.	4.79	0.30	99.62
Pl33.L2.04	62.4	36.5	1.1	2.37	1.60	0.024	0.0051	0.63	0.0045	0.0010	0.37	0.012	13.02	51.99	29.85	0.64	0.075	12.84	0.170	b.d.l.	4.15	0.20	99.96
Pl33.L2.05	59.0	39.9	1.1	2.42	1.55	0.022	0.0056	0.59	0.0034	b.d.l.	0.40	0.012	13.01	53.15	28.77	0.58	0.082	12.13	0.130	b.d.l.	4.53	0.20	99.57
Pl33.L2.06	58.3	40.2	1.4	2.42	1.55	0.021	0.0061	0.59	0.0042	b.d.l.	0.40	0.014	13.01	53.05	28.81	0.56	0.089	11.95	0.158	b.d.l.	4.55	0.24	99.42

Appendix B1 cotinued

Label	An[2]	Ab[3]	Or[4]	Si	Al	Fe	Mg	Ca	Sr	Ba	Na	K	Tot[5]	SiO_2	Al_2O_3	FeO	MgO	CaO	SrO	BaO	Na_2O	K_2O	Tot
Pl33.L2.07	57.3	41.4	1.3	2.43	1.54	0.024	0.0057	0.57	0.0035	0.0003	0.41	0.013	13.01	53.43	28.80	0.63	0.085	11.78	0.131	b.d.l.	4.70	0.23	99.79
Pl33.L2.08	62.8	36.3	0.9	2.37	1.60	0.024	0.0048	0.63	0.0043	0.0006	0.37	0.009	13.02	52.00	29.78	0.64	0.071	12.95	0.164	b.d.l.	4.13	0.16	99.93
Pl33.L2.09	57.6	40.6	1.8	2.43	1.54	0.026	0.0051	0.57	0.0037	b.d.l.	0.40	0.018	13.01	53.26	28.57	0.69	0.075	11.73	0.140	b.d.l.	4.56	0.31	99.33
Pl33.L2.10	56.2	42.2	1.6	2.45	1.52	0.028	0.0058	0.57	0.0042	b.d.l.	0.43	0.016	13.01	53.70	28.28	0.72	0.086	11.60	0.160	b.d.l.	4.81	0.28	99.63
Pl33.L2.11	58.7	40.0	1.3	2.42	1.55	0.028	0.0050	0.59	0.0043	0.0007	0.40	0.013	13.01	52.79	28.61	0.74	0.073	12.05	0.162	b.d.l.	4.53	0.23	99.23
Pl35.L1.01	68.8	30.0	1.1	2.32	1.66	0.027	0.0033	0.69	0.0045	b.d.l.	0.30	0.011	13.01	49.96	30.40	0.70	0.048	13.84	0.169	b.d.l.	3.34	0.19	98.65
Pl35.L1.02	64.7	34.2	1.1	2.35	1.62	0.028	0.0051	0.65	0.0042	0.0001	0.34	0.011	13.01	50.97	29.76	0.73	0.074	13.15	0.158	b.d.l.	3.84	0.18	98.86
Pl35.L1.03	62.1	36.7	1.2	2.38	1.59	0.027	0.0059	0.62	0.0040	0.0002	0.37	0.012	13.01	51.71	29.27	0.70	0.085	12.52	0.149	b.d.l.	4.09	0.21	98.74
Pl35.L1.04	60.6	38.2	1.2	2.40	1.57	0.026	0.0064	0.62	0.0037	0.0013	0.39	0.012	13.02	51.97	28.83	0.68	0.094	12.47	0.138	0.070	4.34	0.20	98.79
Pl35.L1.05	57.5	40.4	2.1	2.43	1.54	0.032	0.0105	0.58	0.0035	0.0005	0.40	0.021	13.02	52.62	28.37	0.83	0.153	11.66	0.132	b.d.l.	4.53	0.36	98.69
Pl35.L1.06	62.4	36.3	1.3	2.37	1.59	0.027	0.0071	0.63	0.0044	b.d.l.	0.37	0.014	13.02	51.51	29.30	0.71	0.103	12.85	0.164	b.d.l.	4.13	0.23	99.00
Pl35.L1.07	56.8	41.5	1.7	2.43	1.54	0.026	0.0078	0.58	0.0042	0.0005	0.42	0.017	13.02	52.62	28.37	0.68	0.113	11.68	0.158	b.d.l.	4.72	0.30	98.67
Pl35.L1.08	66.2	32.7	1.1	2.33	1.64	0.027	0.0056	0.67	0.0043	0.0004	0.33	0.011	13.02	50.53	30.28	0.71	0.081	13.59	0.161	b.d.l.	3.72	0.19	99.29
Pl35.L1.09	65.1	33.7	1.2	2.34	1.64	0.025	0.0062	0.65	0.0040	0.0002	0.34	0.012	13.02	50.75	30.20	0.64	0.090	13.21	0.149	b.d.l.	3.78	0.20	99.03
Pl35.L1.10	84.0	15.6	0.5	2.15	1.83	0.025	0.0037	0.85	0.0034	0.0004	0.16	0.005	13.02	46.33	33.39	0.64	0.053	17.00	0.127	b.d.l.	1.74	0.08	99.39
Pl35.L1.11	83.0	16.5	0.5	2.15	1.83	0.025	0.0035	0.84	0.0035	0.0003	0.17	0.005	13.02	46.23	33.44	0.65	0.051	16.83	0.130	b.d.l.	1.85	0.08	99.27
Pl35.L1.12	76.0	22.3	1.7	2.21	1.76	0.028	0.0049	0.78	0.0038	0.0003	0.23	0.018	13.03	47.60	32.11	0.72	0.071	15.66	0.140	b.d.l.	2.53	0.30	99.16
Pl35.L1.13	67.1	30.7	2.3	2.32	1.65	0.024	0.0038	0.68	0.0034	0.0005	0.31	0.023	13.02	50.42	30.53	0.62	0.056	13.88	0.129	b.d.l.	3.51	0.39	99.57
Pl35.L1.14	82.4	17.0	0.6	2.16	1.82	0.027	0.0033	0.83	0.0038	b.d.l.	0.17	0.006	13.02	46.49	33.35	0.70	0.048	16.72	0.143	b.d.l.	1.90	0.11	99.46
Pl35.L1.15	84.7	14.8	0.4	2.13	1.85	0.026	0.0035	0.85	0.0039	0.0001	0.15	0.005	13.02	45.74	33.76	0.66	0.050	16.99	0.143	b.d.l.	1.64	0.08	99.08
Pl35.L2.01_UR	67.9	30.9	1.2	2.36	1.61	0.032	0.0038	0.66	0.0049	0.0004	0.30	0.012	12.99	51.08	29.49	0.82	0.055	13.41	0.181	b.d.l.	3.37	0.20	98.63
Pl35.L2.02	52.2	45.6	2.2	2.49	1.46	0.042	0.0262	0.52	0.0039	0.0007	0.45	0.022	13.02	54.31	26.98	1.10	0.383	10.51	0.148	b.d.l.	5.07	0.38	98.91
Pl35.L2.03	52.2	45.6	2.2	2.49	1.48	0.032	0.0041	0.52	0.0042	0.0007	0.45	0.022	13.01	54.67	27.62	0.84	0.060	10.67	0.159	b.d.l.	5.15	0.38	99.58
Pl35.L2.04	71.3	27.7	1.0	2.28	1.69	0.031	0.0037	0.72	0.0045	0.0004	0.28	0.010	13.02	49.71	31.16	0.82	0.054	14.54	0.168	b.d.l.	3.12	0.17	99.77
Pl35.L2.05	57.1	39.9	3.0	2.47	1.50	0.033	0.0052	0.56	0.0033	0.0001	0.39	0.030	12.99	54.00	27.90	0.87	0.076	11.47	0.124	b.d.l.	4.43	0.51	99.38
Pl35.L2.06	54.8	42.8	2.4	2.43	1.56	0.026	0.0054	0.55	0.0029	0.0008	0.43	0.024	13.02	b.d.l.	b.d.l.	b.d.l.	b.d.l.	b.d.l.	b.d.l.	b.d.l.	b.d.l.	b.d.l.	88.02
Pl35.L2.07	67.6	31.2	1.1	2.34	1.63	0.030	0.0042	0.68	0.0043	b.d.l.	0.31	0.011	13.01	50.61	30.00	0.76	0.061	13.64	0.160	b.d.l.	3.48	0.19	98.90
Pl35.L2.08	80.8	18.7	0.5	2.19	1.78	0.025	0.0035	0.82	0.0038	0.0001	0.19	0.005	13.02	47.41	32.64	0.64	0.051	16.65	0.141	b.d.l.	2.13	0.09	99.76
Pl35.L2.09	83.2	16.2	0.6	2.18	1.80	0.026	0.0036	0.83	0.0046	0.0001	0.16	0.006	13.01	46.75	32.85	0.68	0.052	16.62	0.171	b.d.l.	1.79	0.09	99.01
Pl35.L2.10	64.9	33.7	1.4	2.36	1.60	0.037	0.0089	0.65	0.0037	b.d.l.	0.34	0.014	13.01	51.21	29.48	0.95	0.130	13.16	0.138	b.d.l.	3.78	0.24	99.08

Appendix B1 cotinued

Label	An[2]	Ab[3]	Or[4]	Si	Al	Fe	Mg	Ca	Sr	Ba	Na	K	Tot[5]	SiO_2	Al_2O_3	FeO	MgO	CaO	SrO	BaO	Na_2O	K_2O	Tot
Pl35.L2.11	67.3	31.5	1.2	2.33	1.64	0.030	0.0057	0.67	0.0043	b.d.l.	0.31	0.012	13.01	50.52	30.20	0.77	0.083	13.56	0.161	b.d.l.	3.51	0.20	99.00
Pl35.L2.12	65.6	33.1	1.3	2.38	1.53	0.069	0.0968	0.63	0.0045	0.0001	0.32	0.012	13.03	51.21	27.90	1.78	1.399	12.58	0.167	b.d.l.	3.51	0.21	98.76
Pl35.L2.13	44.8	50.4	4.8	2.60	1.36	0.034	0.0043	0.44	0.0032	0.0010	0.50	0.047	12.99	57.17	25.47	0.89	0.063	9.03	0.123	b.d.l.	5.62	0.81	99.23
Pl6.2	30.7	64.2	5.2	2.71	1.27	0.012	0.0014	0.31	0.0027	0.0013	0.64	0.052	13.00	60.54	24.07	0.33	0.021	6.39	0.106	0.075	7.39	0.91	99.83
Pl6.3	42.0	55.6	2.4	2.61	1.37	0.016	0.0019	0.42	0.0030	0.0004	0.55	0.024	13.00	57.82	25.82	0.41	0.028	8.65	0.117	b.d.l.	6.33	0.42	99.63
VQ-06-06 (1846/47)																							
Plg2.1	29.2	67.2	3.6	2.71	1.28	0.013	0.0013	0.29	0.0023	0.0017	0.67	0.035	13.00	60.38	24.15	0.34	0.020	6.04	0.089	0.099	7.68	0.62	99.42
Plg2.2	34.9	62.2	2.9	2.65	1.33	0.012	0.0012	0.35	0.0031	0.0015	0.62	0.029	13.01	59.34	25.25	0.32	0.017	7.30	0.118	0.085	7.18	0.50	100.12
Plg2.3	38.5	59.1	2.3	2.60	1.38	0.013	0.0013	0.39	0.0022	0.0008	0.60	0.024	13.02	57.66	25.94	0.35	0.020	8.15	0.083	0.047	6.91	0.41	99.57
Plg3.1	52.9	45.7	1.4	2.48	1.50	0.022	0.0048	0.53	0.0042	0.0004	0.46	0.014	13.01	54.20	27.79	0.58	0.070	10.89	0.160	b.d.l.	5.20	0.24	99.16
Plg3.2	84.4	15.3	0.3	2.15	1.83	0.024	0.0026	0.84	0.0043	0.0003	0.15	0.003	13.01	46.23	33.50	0.62	0.038	16.93	0.159	b.d.l.	1.69	0.06	99.24
Plg3.3	84.9	14.8	0.4	2.14	1.83	0.023	0.0030	0.86	0.0043	0.0001	0.15	0.004	13.02	46.27	33.53	0.60	0.043	17.29	0.159	b.d.l.	1.66	0.06	99.62
Plg4.1	43.3	54.6	2.1	2.57	1.41	0.016	0.0027	0.43	0.0036	0.0006	0.54	0.021	13.01	57.15	26.65	0.42	0.041	8.98	0.137	b.d.l.	6.25	0.37	100.03
Plg4.2	47.1	51.4	1.5	2.52	1.46	0.016	0.0027	0.47	0.0043	0.0007	0.52	0.015	13.01	55.72	27.36	0.43	0.041	9.73	0.163	b.d.l.	5.87	0.27	99.62
Plg4.3	48.0	50.6	1.4	2.51	1.47	0.016	0.0026	0.48	0.0041	0.0002	0.51	0.015	13.01	55.63	27.72	0.42	0.039	9.95	0.157	b.d.l.	5.80	0.25	99.98
Plg4.4	49.2	49.2	1.6	2.50	1.49	0.017	0.0027	0.49	0.0051	0.0007	0.49	0.017	13.01	55.24	27.86	0.45	0.040	10.17	0.193	b.d.l.	5.62	0.29	99.89
Plg4.5	51.0	47.6	1.4	2.48	1.50	0.018	0.0027	0.51	0.0043	0.0005	0.48	0.014	13.01	54.96	28.13	0.47	0.040	10.58	0.162	b.d.l.	5.46	0.24	100.07
Plg4.6	45.8	52.5	1.7	2.53	1.45	0.016	0.0027	0.46	0.0044	0.0005	0.53	0.017	13.01	56.16	27.28	0.41	0.040	9.49	0.167	b.d.l.	6.01	0.29	99.88
Plg4.7	45.7	52.7	1.6	2.53	1.45	0.017	0.0029	0.47	0.0039	0.0007	0.54	0.016	13.02	55.77	27.18	0.44	0.043	9.59	0.149	b.d.l.	6.10	0.28	99.59
Plg5.1	32.1	65.0	2.9	2.68	1.31	0.010	0.0011	0.32	0.0027	0.0010	0.64	0.029	13.00	60.17	24.98	0.26	0.017	6.65	0.104	0.055	7.44	0.50	100.17
Plg5.2	31.5	65.3	3.2	2.68	1.31	0.011	0.0016	0.31	0.0030	0.0008	0.65	0.032	13.01	59.74	24.83	0.30	0.024	6.54	0.114	0.046	7.48	0.55	99.63
Plg5.3	31.1	65.6	3.2	2.70	1.29	0.011	0.0014	0.31	0.0025	0.0012	0.65	0.032	13.00	60.45	24.61	0.30	0.022	6.45	0.098	0.071	7.51	0.56	100.07
Plg5.4	28.7	67.7	3.6	2.70	1.29	0.011	0.0010	0.29	0.0028	0.0012	0.68	0.036	13.01	60.19	24.49	0.29	0.014	6.00	0.109	0.066	7.83	0.63	99.62
Plg5.5	27.9	68.5	3.5	2.70	1.28	0.012	0.0014	0.28	0.0022	0.0009	0.70	0.036	13.02	60.46	24.38	0.31	0.021	5.94	0.085	0.052	8.05	0.63	99.93
Plg5.6	62.6	36.4	1.0	2.35	1.64	0.011	0.0012	0.63	0.0035	0.0006	0.37	0.010	13.02	51.61	30.64	0.29	0.018	12.93	0.131	b.d.l.	4.15	0.18	99.98
Plg5.7	76.1	23.5	0.4	2.22	1.79	0.011	0.0006	0.75	0.0035	0.0002	0.23	0.004	13.01	48.01	32.87	0.29	0.009	15.24	0.131	b.d.l.	2.60	0.06	99.22
Plg5.8	71.9	27.5	0.6	2.25	1.75	0.012	0.0009	0.72	0.0033	0.0001	0.27	0.006	13.01	49.03	32.37	0.32	0.013	14.56	0.124	b.d.l.	3.08	0.10	99.60
VQ-06-10 (1846/47)																							
Pl1.1	27.2	69.0	3.8	2.74	1.24	0.012	0.0014	0.27	0.0026	0.0009	0.69	0.038	13.00	61.79	23.70	0.33	0.021	5.68	0.100	b.d.l.	7.96	0.67	100.30
Pl1.2	31.8	65.1	3.1	2.69	1.30	0.012	0.0010	0.32	0.0031	0.0015	0.65	0.031	13.01	60.27	24.63	0.33	0.015	6.70	0.119	0.085	7.57	0.55	100.27

Appendix B1 cotinued

Label	An[2]	Ab[3]	Or[4]	Si	Al	Fe	Mg	Ca	Sr	Ba	Na	K	Tot[5]	SiO_2	Al_2O_3	FeO	MgO	CaO	SrO	BaO	Na_2O	K_2O	Tot
Pl19.2	34.9	60.8	4.3	2.70	1.29	0.020	0.0039	0.34	0.0030	0.0005	0.58	0.041	12.97	59.84	24.23	0.53	0.058	6.95	0.114	b.d.l.	6.69	0.71	99.15
Pl19.3	33.2	63.7	3.1	2.69	1.29	0.014	0.0008	0.33	0.0033	0.0016	0.64	0.031	13.00	59.97	24.33	0.37	0.012	6.91	0.126	0.092	7.33	0.54	99.67
Pl19.4	31.0	66.0	3.1	2.70	1.28	0.014	0.0012	0.31	0.0031	0.0016	0.66	0.031	13.01	60.26	24.33	0.38	0.018	6.50	0.121	0.092	7.66	0.54	99.90
Pl19.5	31.2	65.9	2.9	2.70	1.28	0.012	0.0011	0.31	0.0031	0.0012	0.66	0.029	13.00	60.50	24.32	0.33	0.017	6.49	0.118	0.070	7.57	0.51	99.93
Pl19.6	33.0	64.1	3.0	2.69	1.30	0.013	0.0012	0.32	0.0025	0.0011	0.63	0.029	12.99	60.10	24.75	0.34	0.018	6.75	0.097	b.d.l.	7.26	0.51	99.89
Pl21.1	59.3	39.6	1.1	2.41	1.57	0.014	0.0019	0.59	0.0046	0.0006	0.40	0.011	13.01	53.13	29.43	0.37	0.028	12.21	0.176	b.d.l.	4.51	0.19	100.08
Pl21.2	52.1	46.7	1.2	2.49	1.49	0.016	0.0017	0.52	0.0048	0.0007	0.47	0.012	13.01	54.98	27.96	0.42	0.025	10.79	0.184	b.d.l.	5.34	0.21	99.94
Pl21.3	27.7	69.0	3.3	2.73	1.25	0.014	0.0010	0.28	0.0032	0.0011	0.70	0.033	13.01	61.25	23.86	0.36	0.015	5.86	0.124	b.d.l.	8.05	0.59	100.18
Pl22.L1.01	53.1	44.6	2.3	2.47	1.50	0.031	0.0061	0.53	0.0034	0.0009	0.45	0.023	13.01	53.95	27.68	0.81	0.089	10.79	0.128	b.d.l.	5.01	0.39	98.88
Pl22.L1.02	80.7	18.7	0.6	2.19	1.79	0.025	0.0066	0.81	0.0034	b.d.l.	0.19	0.006	13.01	b.d.l.	b.d.l.	b.d.l.	b.d.l.	b.d.l.	b.d.l.	b.d.l.	b.d.l.	b.d.l.	91.96
Pl22.L1.03	71.2	28.1	0.7	2.28	1.69	0.024	0.0081	0.72	0.0037	0.0005	0.28	0.007	13.02	49.14	30.79	0.61	0.116	14.46	0.138	b.d.l.	3.15	0.12	98.56
Pl22.L1.04	67.3	31.9	0.8	2.32	1.64	0.026	0.0113	0.68	0.0037	b.d.l.	0.32	0.008	13.02	50.33	30.20	0.67	0.164	13.77	0.140	b.d.l.	3.61	0.14	99.01
Pl22.L1.05	75.4	24.2	0.4	2.22	1.76	0.023	0.0072	0.76	0.0039	b.d.l.	0.24	0.004	13.02	48.20	32.47	0.60	0.105	15.44	0.144	b.d.l.	2.74	0.06	99.76
Pl22.L1.06	68.7	30.8	0.6	2.30	1.68	0.022	0.0087	0.70	0.0030	0.0006	0.31	0.006	13.03	49.66	30.79	0.56	0.127	14.13	0.111	b.d.l.	3.50	0.10	99.01
Pl22.L1.07	71.0	28.4	0.7	2.29	1.68	0.023	0.0088	0.72	0.0034	b.d.l.	0.29	0.007	13.02	49.41	30.86	0.59	0.128	14.57	0.126	b.d.l.	3.22	0.11	99.02
Pl22.L1.08	66.3	33.0	0.8	2.35	1.62	0.024	0.0095	0.66	0.0037	0.0004	0.33	0.008	13.01	50.78	29.72	0.63	0.138	13.36	0.137	b.d.l.	3.67	0.13	98.59
Pl22.L1.09	70.0	29.5	0.5	2.29	1.68	0.024	0.0086	0.71	0.0031	0.0002	0.30	0.006	13.02	49.39	30.64	0.61	0.124	14.36	0.115	b.d.l.	3.34	0.09	98.68
Pl22.L1.10	68.8	30.6	0.6	2.30	1.67	0.023	0.0087	0.70	0.0029	b.d.l.	0.31	0.006	13.02	b.d.l.	b.d.l.	b.d.l.	b.d.l.	b.d.l.	b.d.l.	b.d.l.	b.d.l.	b.d.l.	98.49
Pl22.L1.11	68.5	30.8	0.6	2.31	1.67	0.025	0.0086	0.69	0.0036	0.0006	0.31	0.006	13.02	b.d.l.	b.d.l.	b.d.l.	b.d.l.	b.d.l.	b.d.l.	b.d.l.	b.d.l.	b.d.l.	98.47
Pl22.L1.12	66.5	32.8	0.8	2.32	1.64	0.024	0.0101	0.68	0.0032	0.0001	0.33	0.008	13.02	50.13	30.10	0.62	0.147	13.61	0.118	b.d.l.	3.71	0.13	98.57
Pl22.L1.13	69.9	29.3	0.8	2.28	1.69	0.025	0.0090	0.71	0.0030	0.0005	0.30	0.008	13.03	49.08	30.99	0.64	0.130	14.33	0.113	b.d.l.	3.32	0.14	98.76
Pl22.L1.14	68.1	31.2	0.7	2.30	1.67	0.025	0.0082	0.69	0.0033	0.0002	0.32	0.007	13.03	49.60	30.61	0.63	0.118	13.92	0.124	b.d.l.	3.52	0.12	98.67
Pl22.L1.15	69.2	30.0	0.7	2.30	1.67	0.024	0.0084	0.70	0.0034	0.0002	0.30	0.008	13.02	49.96	30.71	0.62	0.122	14.18	0.127	b.d.l.	3.40	0.13	99.25
Pl22.L1.16	69.7	29.7	0.6	2.31	1.66	0.024	0.0086	0.70	0.0038	0.0001	0.30	0.006	13.01	50.21	30.54	0.63	0.126	14.19	0.143	b.d.l.	3.33	0.10	99.28
Pl22.L1.17	66.8	32.4	0.8	2.33	1.64	0.024	0.0087	0.68	0.0036	b.d.l.	0.33	0.008	13.02	50.92	30.35	0.63	0.128	13.89	0.134	b.d.l.	3.72	0.14	99.92
Pl22.L1.18	66.3	33.0	0.7	2.34	1.63	0.025	0.0091	0.67	0.0035	0.0001	0.33	0.007	13.01	50.99	30.06	0.64	0.133	13.57	0.132	b.d.l.	3.74	0.11	99.39
Pl22.L1.19	67.9	31.3	0.8	2.33	1.64	0.021	0.0081	0.69	0.0028	b.d.l.	0.32	0.008	13.01	50.73	30.33	0.55	0.118	13.93	0.107	b.d.l.	3.55	0.14	99.46
Pl22.L2.01	73.3	26.0	0.7	2.25	1.72	0.024	0.0070	0.74	0.0037	b.d.l.	0.26	0.007	13.02	48.46	31.43	0.61	0.100	14.91	0.136	b.d.l.	2.93	0.12	98.69
Pl22.L2.02	61.3	37.7	1.0	2.38	1.59	0.025	0.0104	0.62	0.0037	0.0007	0.38	0.010	13.02	51.69	29.40	0.65	0.151	12.52	0.140	b.d.l.	4.25	0.17	99.01
Pl22.L2.03	74.2	25.2	0.6	2.24	1.74	0.023	0.0076	0.75	0.0035	0.0002	0.25	0.006	13.02	48.41	31.99	0.60	0.111	15.16	0.132	b.d.l.	2.84	0.10	99.36

Appendix B1 cotinued

Label	An[2]	Ab[3]	Or[4]	Si	Al	Fe	Mg	Ca	Sr	Ba	Na	K	Tot[5]	SiO_2	Al_2O_3	FeO	MgO	CaO	SrO	BaO	Na_2O	K_2O	Tot
Pl22.L2.04	75.3	24.2	0.5	2.23	1.74	0.022	0.0075	0.77	0.0036	0.0003	0.25	0.005	13.02	48.06	31.76	0.56	0.108	15.41	0.132	b.d.l.	2.74	0.08	98.88
Pl22.L2.05	70.3	29.1	0.6	2.28	1.70	0.023	0.0080	0.71	0.0035	b.d.l.	0.29	0.006	13.02	49.37	31.16	0.60	0.117	14.37	0.129	b.d.l.	3.28	0.11	99.15
Pl22.L2.06	71.2	28.1	0.7	2.27	1.70	0.023	0.0079	0.72	0.0033	b.d.l.	0.29	0.007	13.02	48.98	31.17	0.59	0.115	14.58	0.124	b.d.l.	3.17	0.12	98.86
Pl22.L2.07	68.4	30.3	1.3	2.30	1.66	0.031	0.0146	0.69	0.0035	b.d.l.	0.31	0.013	13.03	49.74	30.43	0.80	0.212	13.95	0.132	b.d.l.	3.42	0.23	98.90
Pl22.L2.08	70.4	28.9	0.7	2.29	1.69	0.023	0.0086	0.71	0.0035	b.d.l.	0.29	0.007	13.02	49.47	30.93	0.59	0.124	14.30	0.130	b.d.l.	3.24	0.12	98.92
Pl22.L2.10	72.1	27.2	0.7	2.30	1.67	0.023	0.0079	0.72	0.0032	b.d.l.	0.27	0.007	13.00	50.06	30.90	0.59	0.115	14.52	0.122	b.d.l.	3.03	0.12	99.46
Pl22.L2.11	68.1	31.2	0.6	2.34	1.63	0.023	0.0084	0.69	0.0034	b.d.l.	0.31	0.006	13.01	50.97	30.10	0.60	0.124	13.97	0.127	b.d.l.	3.54	0.11	99.53
Pl22.L2.12	73.0	26.5	0.5	2.29	1.67	0.023	0.0074	0.74	0.0031	b.d.l.	0.27	0.005	13.01	50.02	30.90	0.59	0.109	15.04	0.115	b.d.l.	3.02	0.08	99.87
Pl22.L2.13	70.6	28.7	0.6	2.31	1.66	0.022	0.0073	0.71	0.0032	0.0001	0.29	0.006	13.01	50.44	30.74	0.57	0.106	14.40	0.121	b.d.l.	3.24	0.10	99.73
Pl22.L2.14	61.5	37.1	1.4	2.43	1.52	0.032	0.0161	0.61	0.0038	0.0009	0.37	0.014	13.00	53.22	28.26	0.84	0.236	12.54	0.143	b.d.l.	4.18	0.24	99.70
Pl22.L2.15	71.6	27.8	0.5	2.32	1.65	0.023	0.0080	0.71	0.0036	b.d.l.	0.28	0.005	13.00	50.42	30.52	0.60	0.116	14.44	0.134	b.d.l.	3.10	0.09	99.42
Pl22.L2.16	50.2	46.6	3.2	2.55	1.42	0.028	0.0060	0.49	0.0023	b.d.l.	0.46	0.031	12.98	56.31	26.51	0.74	0.088	10.11	0.088	b.d.l.	5.18	0.54	99.57
Pl23.L1.01_LR	62.6	36.2	1.1	2.41	1.56	0.027	0.0071	0.62	0.0034	0.0001	0.36	0.011	13.00	52.67	28.91	0.69	0.104	12.71	0.130	b.d.l.	4.06	0.19	99.48
Pl23.L1.02	57.3	41.2	1.4	2.46	1.50	0.023	0.0068	0.58	0.0032	0.0003	0.41	0.014	13.00	54.05	28.06	0.60	0.100	11.82	0.123	b.d.l.	4.70	0.24	99.71
Pl23.L1.03	54.1	44.5	1.5	2.50	1.46	0.029	0.0078	0.54	0.0035	0.0003	0.45	0.015	13.00	55.00	27.28	0.75	0.116	11.12	0.131	b.d.l.	5.06	0.25	99.74
Pl23.L1.04	64.4	34.5	1.0	2.39	1.58	0.025	0.0085	0.64	0.0033	b.d.l.	0.34	0.010	13.00	52.30	29.31	0.64	0.124	13.01	0.125	b.d.l.	3.85	0.17	99.53
Pl23.L1.05	62.3	36.8	0.9	2.41	1.55	0.025	0.0095	0.62	0.0032	0.0004	0.37	0.009	13.00	52.97	28.92	0.65	0.140	12.66	0.122	b.d.l.	4.13	0.16	99.78
Pl23.L1.06	60.6	38.3	1.0	2.41	1.55	0.027	0.0097	0.62	0.0034	0.0001	0.39	0.011	13.02	52.75	28.80	0.72	0.143	12.57	0.127	b.d.l.	4.39	0.18	99.69
Pl23.L1.07	66.4	33.1	0.6	2.36	1.60	0.025	0.0086	0.67	0.0035	b.d.l.	0.33	0.006	13.01	51.75	29.84	0.66	0.126	13.66	0.132	b.d.l.	3.76	0.10	100.03
Pl23.L1.08	60.9	38.3	0.8	2.42	1.55	0.028	0.0095	0.61	0.0038	b.d.l.	0.38	0.009	13.01	53.03	28.76	0.73	0.140	12.47	0.142	b.d.l.	4.33	0.15	99.75
Pl23.L1.09	60.8	38.2	0.9	2.42	1.55	0.025	0.0099	0.61	0.0028	0.0002	0.38	0.010	13.00	52.64	28.58	0.66	0.145	12.36	0.107	b.d.l.	4.30	0.16	98.96
Pl23.L1.10	63.5	35.8	0.8	2.39	1.57	0.028	0.0099	0.64	0.0034	0.0005	0.36	0.008	13.01	52.22	29.17	0.72	0.145	13.02	0.129	b.d.l.	4.06	0.13	99.62
Pl23.L1.11	68.9	30.4	0.7	2.34	1.62	0.026	0.0082	0.69	0.0038	0.0002	0.31	0.007	13.01	50.85	29.95	0.66	0.119	14.04	0.143	b.d.l.	3.42	0.11	99.31
Pl23.L1.12	63.5	35.7	0.8	2.40	1.57	0.026	0.0092	0.63	0.0035	0.0001	0.36	0.008	13.00	52.35	28.99	0.67	0.135	12.92	0.133	b.d.l.	4.01	0.14	99.36
Pl23.L1.13	59.9	39.1	1.0	2.43	1.53	0.025	0.0096	0.60	0.0035	0.0001	0.39	0.010	13.00	53.21	28.44	0.66	0.141	12.23	0.131	b.d.l.	4.41	0.18	99.40
Pl23.L1.14	65.7	33.6	0.7	2.37	1.59	0.025	0.0085	0.66	0.0032	0.0005	0.34	0.007	13.01	51.63	29.32	0.66	0.125	13.44	0.118	b.d.l.	3.79	0.12	99.22
Pl23.L1.15	66.8	32.6	0.6	2.34	1.62	0.024	0.0078	0.68	0.0033	0.0006	0.33	0.007	13.02	50.98	29.84	0.63	0.114	13.80	0.125	b.d.l.	3.72	0.11	99.36
Pl23.L1.16	66.9	32.2	0.9	2.35	1.61	0.026	0.0080	0.67	0.0028	b.d.l.	0.32	0.009	13.00	51.23	29.76	0.67	0.117	13.60	0.107	b.d.l.	3.61	0.15	99.24
Pl23.L1.17	65.3	33.8	0.9	2.37	1.60	0.026	0.0085	0.65	0.0037	b.d.l.	0.34	0.009	13.00	51.73	29.55	0.67	0.124	13.19	0.140	b.d.l.	3.78	0.15	99.32
Pl23.L1.18	64.9	34.3	0.9	2.38	1.58	0.026	0.0084	0.65	0.0036	b.d.l.	0.34	0.009	13.00	51.77	29.10	0.68	0.123	13.21	0.136	b.d.l.	3.86	0.15	99.03

Appendix B1 cotinued

Label	An[2]	Ab[3]	Or[4]	Si	Al	Fe	Mg	Ca	Sr	Ba	Na	K	Tot[5]	SiO_2	Al_2O_3	FeO	MgO	CaO	SrO	BaO	Na_2O	K_2O	Tot
Pl23.L1.19	68.4	30.8	0.8	2.35	1.62	0.027	0.0078	0.68	0.0033	0.0004	0.30	0.008	13.00	51.08	29.83	0.70	0.113	13.72	0.123	b.d.l.	3.41	0.13	99.13
Pl23.L1.20	67.8	31.6	0.6	2.35	1.62	0.027	0.0076	0.68	0.0038	b.d.l.	0.32	0.006	13.00	50.91	29.73	0.71	0.111	13.67	0.144	b.d.l.	3.52	0.11	98.90
Pl23.L1.21	66.4	32.7	1.0	2.36	1.60	0.028	0.0077	0.67	0.0024	0.0001	0.33	0.010	13.01	51.20	29.32	0.71	0.113	13.59	0.090	b.d.l.	3.69	0.16	98.88
Pl23.L1.22	59.1	39.9	1.0	2.43	1.53	0.028	0.0085	0.60	0.0025	0.0006	0.40	0.010	13.01	52.93	28.23	0.72	0.124	12.13	0.094	b.d.l.	4.53	0.17	98.97
Pl23.L1.23_UL	63.0	36.1	0.9	2.39	1.57	0.027	0.0078	0.63	0.0029	0.0003	0.36	0.009	13.01	52.02	28.95	0.71	0.114	12.80	0.110	b.d.l.	4.05	0.16	98.92
Pl23.L2.01_L	56.8	41.6	1.5	2.45	1.52	0.030	0.0075	0.57	0.0041	0.0007	0.41	0.015	13.01	54.35	28.57	0.79	0.111	11.71	0.157	b.d.l.	4.74	0.27	100.73
Pl23.L2.02	66.6	32.6	0.8	2.36	1.61	0.025	0.0071	0.67	0.0029	b.d.l.	0.33	0.008	13.01	51.64	29.94	0.66	0.104	13.73	0.109	b.d.l.	3.71	0.13	100.03
Pl23.L2.03	69.7	29.5	0.8	2.35	1.62	0.024	0.0079	0.68	0.0037	0.0002	0.29	0.008	12.99	51.65	30.29	0.64	0.116	13.94	0.142	b.d.l.	3.26	0.14	100.19
Pl23.L2.04	68.5	30.7	0.7	2.34	1.63	0.025	0.0082	0.69	0.0036	b.d.l.	0.31	0.008	13.01	51.45	30.38	0.66	0.121	14.14	0.136	b.d.l.	3.50	0.13	100.53
Pl23.L2.05	66.9	32.2	0.8	2.36	1.61	0.026	0.0087	0.68	0.0034	0.0003	0.33	0.008	13.01	51.59	29.85	0.68	0.128	13.80	0.128	b.d.l.	3.67	0.14	100.02
Pl23.L2.06	69.4	30.1	0.5	2.32	1.64	0.024	0.0083	0.71	0.0032	b.d.l.	0.31	0.005	13.02	50.68	30.30	0.63	0.122	14.42	0.121	b.d.l.	3.46	0.09	99.82
Pl23.L2.07	69.0	30.4	0.6	2.33	1.64	0.025	0.0079	0.69	0.0033	0.0007	0.30	0.006	13.00	50.90	30.30	0.65	0.115	13.97	0.124	b.d.l.	3.40	0.11	99.61
Pl23.L2.08	66.9	32.5	0.7	2.36	1.60	0.026	0.0094	0.67	0.0031	0.0002	0.33	0.007	13.01	51.58	29.79	0.68	0.138	13.77	0.118	b.d.l.	3.70	0.11	99.89
Pl23.L2.09	64.7	34.5	0.8	2.38	1.58	0.024	0.0087	0.66	0.0029	b.d.l.	0.35	0.008	13.01	52.06	29.29	0.64	0.128	13.45	0.110	b.d.l.	3.96	0.13	99.77
Pl23.L2.10	59.2	39.7	1.1	2.43	1.53	0.026	0.0094	0.60	0.0027	0.0002	0.40	0.011	13.01	53.32	28.59	0.69	0.139	12.24	0.102	b.d.l.	4.53	0.18	99.80
Pl23.L2.11	64.0	35.1	0.9	2.38	1.58	0.026	0.0083	0.65	0.0038	0.0003	0.35	0.009	13.01	52.17	29.31	0.68	0.122	13.22	0.143	b.d.l.	4.01	0.15	99.81
Pl23.L2.12	64.5	34.5	0.9	2.39	1.58	0.026	0.0085	0.64	0.0038	b.d.l.	0.34	0.009	13.00	52.03	29.16	0.67	0.124	13.10	0.142	b.d.l.	3.87	0.16	99.27
Pl23.L2.13	52.4	46.2	1.4	2.50	1.47	0.025	0.0073	0.53	0.0035	0.0001	0.46	0.014	13.01	55.16	27.47	0.66	0.108	10.82	0.135	b.d.l.	5.28	0.25	99.88
Pl23.L2.14	61.5	37.3	1.2	2.41	1.56	0.023	0.0060	0.62	0.0032	0.0003	0.37	0.012	13.00	52.67	28.90	0.59	0.088	12.55	0.120	b.d.l.	4.21	0.20	99.34
Pl23.L2.15	59.9	38.7	1.4	2.42	1.54	0.026	0.0069	0.60	0.0034	0.0004	0.39	0.014	13.01	53.07	28.70	0.68	0.102	12.26	0.130	b.d.l.	4.38	0.24	99.58
Pl23.L2.16_U	41.7	54.3	4.0	2.64	1.32	0.030	0.0060	0.41	0.0024	0.0008	0.53	0.039	12.98	58.75	24.89	0.81	0.090	8.44	0.090	b.d.l.	6.07	0.67	99.85
Pl7.2	68.0	31.1	0.9	2.32	1.64	0.024	0.0074	0.69	0.0033	0.0003	0.31	0.009	13.02	50.94	30.58	0.64	0.109	14.06	0.126	b.d.l.	3.55	0.15	100.17
Pl7.3	67.2	32.0	0.8	2.33	1.64	0.024	0.0084	0.67	0.0031	b.d.l.	0.32	0.008	13.01	50.97	30.43	0.63	0.124	13.73	0.117	b.d.l.	3.61	0.14	99.74
Pl7.4	69.4	30.0	0.6	2.32	1.65	0.023	0.0085	0.69	0.0033	0.0001	0.30	0.006	13.01	50.67	30.61	0.59	0.124	14.15	0.125	b.d.l.	3.39	0.10	99.76
Pl7.5	73.2	26.3	0.5	2.28	1.70	0.022	0.0060	0.73	0.0033	b.d.l.	0.26	0.006	13.01	49.39	31.24	0.56	0.087	14.84	0.123	b.d.l.	2.95	0.09	99.29
Pl7.6	68.3	30.9	0.7	2.33	1.65	0.019	0.0041	0.69	0.0046	0.0001	0.31	0.007	13.01	51.02	30.64	0.50	0.060	14.02	0.175	b.d.l.	3.51	0.13	100.06
Pl7.7	69.4	30.0	0.6	2.31	1.68	0.017	0.0025	0.70	0.0037	b.d.l.	0.30	0.006	13.01	50.35	31.03	0.45	0.037	14.19	0.138	b.d.l.	3.40	0.10	99.69
Pl8.1	64.5	34.8	0.7	2.37	1.60	0.026	0.0085	0.65	0.0032	0.0002	0.35	0.007	13.01	51.89	29.73	0.69	0.125	13.26	0.123	b.d.l.	3.95	0.13	99.91
VQ-06-11 (1846/47)																							
Pl1.1	36.7	61.0	2.4	2.64	1.35	0.012	0.0015	0.36	0.0043	0.0009	0.61	0.024	13.00	59.22	25.67	0.31	0.022	7.63	0.167	b.d.l.	7.01	0.41	100.49

Appendix B1 cotinued

Label	An[2]	Ab[3]	Or[4]	Si	Al	Fe	Mg	Ca	Sr	Ba	Na	K	Tot[5]	SiO_2	Al_2O_3	FeO	MgO	CaO	SrO	BaO	Na_2O	K_2O	Tot
Pl1.1 U	32.8	64.0	3.1	2.67	1.31	0.015	0.0024	0.33	0.0035	0.0017	0.65	0.032	13.02	60.11	25.01	0.40	0.036	7.04	0.134	0.100	7.58	0.57	100.96
Pl1.2	62.2	36.9	1.0	2.38	1.60	0.022	0.0035	0.62	0.0043	b.d.l.	0.37	0.010	13.01	52.52	30.08	0.59	0.051	12.82	0.165	b.d.l.	4.20	0.17	100.58
Pl1.3	65.6	33.6	0.8	2.34	1.63	0.024	0.0048	0.67	0.0044	0.0009	0.34	0.008	13.02	51.52	30.40	0.62	0.071	13.66	0.165	b.d.l.	3.86	0.14	100.48
Pl1.4	78.6	21.1	0.3	2.22	1.76	0.023	0.0037	0.79	0.0045	b.d.l.	0.21	0.003	13.01	48.50	32.63	0.60	0.054	16.04	0.171	b.d.l.	2.38	0.05	100.42
Pl1.5	75.5	24.1	0.4	2.25	1.72	0.023	0.0044	0.76	0.0042	b.d.l.	0.24	0.004	13.01	49.01	31.90	0.60	0.065	15.52	0.159	b.d.l.	2.74	0.07	100.05
Pl1.6	81.3	18.4	0.4	2.18	1.80	0.021	0.0039	0.82	0.0033	0.0003	0.18	0.004	13.02	47.61	33.32	0.55	0.057	16.69	0.123	b.d.l.	2.08	0.06	100.52
Pl1.7	78.9	20.8	0.3	2.21	1.76	0.022	0.0043	0.80	0.0052	0.0005	0.21	0.003	13.02	48.13	32.62	0.57	0.063	16.26	0.194	b.d.l.	2.37	0.05	100.29
Pl1.8 C	81.7	18.0	0.4	2.17	1.80	0.022	0.0036	0.82	0.0042	0.0002	0.18	0.004	13.02	47.55	33.46	0.58	0.053	16.81	0.158	b.d.l.	2.05	0.06	100.74
Pl2.1	38.7	58.9	2.3	2.63	1.35	0.011	0.0010	0.39	0.0033	0.0005	0.59	0.024	13.01	58.86	25.73	0.29	0.015	8.17	0.127	b.d.l.	6.87	0.41	100.50
Pl2.2	32.3	64.8	3.0	2.69	1.30	0.010	0.0008	0.32	0.0021	0.0006	0.65	0.030	13.00	60.67	24.88	0.28	0.012	6.78	0.083	b.d.l.	7.52	0.52	100.78
Pl2.3	28.7	67.9	3.4	2.73	1.25	0.011	0.0012	0.28	0.0032	0.0018	0.67	0.034	13.00	62.03	24.15	0.29	0.018	6.03	0.124	0.103	7.89	0.61	101.24
Pl5.1	44.0	54.1	1.9	2.58	1.41	0.009	0.0008	0.44	0.0033	0.0007	0.54	0.019	13.00	57.59	26.65	0.25	0.013	9.13	0.128	b.d.l.	6.21	0.33	100.34
Pl5.2	33.7	63.2	3.0	2.67	1.31	0.013	0.0015	0.34	0.0031	0.0009	0.64	0.031	13.01	60.15	25.03	0.34	0.023	7.22	0.121	b.d.l.	7.47	0.54	100.95
Pl5.3	33.0	63.8	3.2	2.69	1.29	0.012	0.0010	0.33	0.0032	0.0009	0.64	0.032	13.00	60.69	24.57	0.31	0.015	6.94	0.124	b.d.l.	7.40	0.57	100.67
Pl6.1	24.8	69.8	5.4	2.77	1.21	0.017	0.0014	0.24	0.0033	0.0022	0.69	0.053	12.99	62.71	23.21	0.45	0.021	5.13	0.129	0.125	7.99	0.94	100.71
Pl6.2	56.4	42.4	1.2	2.45	1.52	0.022	0.0050	0.57	0.0048	0.0001	0.43	0.012	13.01	54.44	28.78	0.60	0.075	11.77	0.185	b.d.l.	4.89	0.20	100.95
Pl6.3	83.6	16.2	0.2	2.17	1.80	0.025	0.0034	0.84	0.0046	0.0002	0.16	0.002	13.01	47.49	33.51	0.66	0.050	17.11	0.174	b.d.l.	1.84	0.03	100.87
Pl7.1	48.0	50.3	1.6	2.53	1.44	0.012	0.0012	0.49	0.0043	0.0008	0.51	0.017	13.01	56.75	27.34	0.31	0.018	10.26	0.167	b.d.l.	5.94	0.29	101.12
Pl7.2	39.3	58.6	2.1	2.64	1.35	0.012	0.0012	0.39	0.0038	0.0008	0.58	0.021	12.99	59.08	25.64	0.32	0.018	8.10	0.149	b.d.l.	6.69	0.36	100.40
Pl7.3	46.1	52.5	1.4	2.54	1.45	0.011	0.0016	0.46	0.0040	0.0003	0.53	0.014	13.01	56.62	27.32	0.29	0.024	9.62	0.156	b.d.l.	6.05	0.25	100.35
VQ-06-22 (1846/47)																							
Pl1	43.9	54.3	1.8	2.57	1.42	0.015	0.0018	0.44	0.0045	0.0006	0.54	0.018	13.00	57.32	26.82	0.39	0.027	9.11	0.173	b.d.l.	6.22	0.31	100.41
Pl1.3	34.4	62.7	2.9	2.67	1.31	0.012	0.0017	0.35	0.0030	0.0010	0.63	0.029	13.01	59.96	24.98	0.31	0.026	7.25	0.118	b.d.l.	7.32	0.51	100.55
Pl10.1	31.3	65.7	3.0	2.70	1.28	0.013	0.0014	0.32	0.0028	0.0010	0.66	0.031	13.01	60.27	24.33	0.33	0.021	6.59	0.107	b.d.l.	7.64	0.54	99.88
Pl22	52.8	45.9	1.3	2.48	1.50	0.011	0.0015	0.54	0.0036	0.0004	0.47	0.013	13.01	54.67	28.16	0.30	0.022	11.07	0.136	b.d.l.	5.31	0.22	99.91
Pl22.02	30.0	61.7	8.3	2.78	1.18	0.042	0.0145	0.28	0.0014	0.0007	0.58	0.077	12.96	62.12	22.38	1.12	0.217	5.85	0.055	b.d.l.	6.64	1.35	99.77
Pl22.03	59.2	39.2	1.6	2.43	1.53	0.028	0.0079	0.59	0.0040	0.0003	0.39	0.016	13.00	53.32	28.55	0.74	0.116	12.09	0.152	b.d.l.	4.42	0.28	99.68
Pl22.04	74.5	25.0	0.5	2.27	1.70	0.023	0.0077	0.75	0.0035	b.d.l.	0.25	0.005	13.01	49.22	31.30	0.60	0.111	15.13	0.132	b.d.l.	2.80	0.08	99.38
Pl22.05	74.8	24.6	0.6	2.27	1.70	0.023	0.0075	0.76	0.0034	0.0004	0.25	0.006	13.01	49.29	31.33	0.61	0.110	15.37	0.129	b.d.l.	2.80	0.10	99.76
Pl22.06	67.7	31.6	0.7	2.33	1.64	0.025	0.0088	0.69	0.0029	0.0002	0.32	0.007	13.02	50.40	30.11	0.63	0.128	13.87	0.109	b.d.l.	3.58	0.11	98.96

Appendix B1 cotinued

Label	An[2]	Ab[3]	Or[4]	Si	Al	Fe	Mg	Ca	Sr	Ba	Na	K	Tot[5]	SiO_2	Al_2O_3	FeO	MgO	CaO	SrO	BaO	Na_2O	K_2O	Tot
Pl22.07	69.9	29.5	0.6	2.32	1.64	0.022	0.0070	0.71	0.0035	0.0002	0.30	0.006	13.01	50.47	30.33	0.58	0.102	14.46	0.131	b.d.l.	3.37	0.10	99.55
Pl22.08	71.3	28.1	0.5	2.30	1.68	0.023	0.0063	0.72	0.0032	b.d.l.	0.28	0.006	13.01	49.71	30.79	0.60	0.092	14.53	0.119	b.d.l.	3.17	0.09	99.09
Pl22.09	71.2	28.2	0.6	2.29	1.68	0.021	0.0068	0.73	0.0035	0.0001	0.29	0.006	13.02	49.75	30.92	0.56	0.099	14.89	0.130	b.d.l.	3.26	0.11	99.72
Pl22.10	73.8	25.8	0.4	2.27	1.70	0.022	0.0066	0.74	0.0028	0.0004	0.26	0.005	13.01	49.30	31.25	0.58	0.096	14.93	0.103	b.d.l.	2.88	0.08	99.23
Pl22.11	74.6	25.0	0.4	2.27	1.70	0.022	0.0067	0.76	0.0036	0.0002	0.26	0.005	13.02	49.00	31.11	0.57	0.097	15.41	0.133	b.d.l.	2.85	0.08	99.26
Pl22.12	71.8	27.5	0.6	2.29	1.68	0.023	0.0068	0.72	0.0036	0.0001	0.28	0.006	13.01	49.74	30.90	0.59	0.099	14.57	0.135	b.d.l.	3.09	0.11	99.23
VQ-06-22D (1846/47)																							
Plg40	69.0	30.2	0.7	2.32	1.64	0.028	0.0083	0.69	0.0033	0.0004	0.30	0.008	13.01	50.29	30.22	0.72	0.120	14.04	0.124	b.d.l.	3.40	0.13	99.07
Plg40.2	61.1	38.0	0.9	2.40	1.57	0.029	0.0099	0.61	0.0033	0.0004	0.38	0.009	13.01	52.18	29.06	0.76	0.144	12.48	0.123	b.d.l.	4.28	0.16	99.21
Plg40.3	58.9	40.0	1.1	2.42	1.55	0.027	0.0101	0.59	0.0035	0.0001	0.40	0.011	13.01	52.69	28.57	0.71	0.148	12.00	0.132	b.d.l.	4.50	0.19	98.95
VQ-06-22D glomerocrysts (1846/47)																							
Plg1	48.1	50.3	1.6	2.50	1.49	0.010	0.0013	0.48	0.0032	0.0005	0.51	0.016	13.01	54.92	27.67	0.26	0.019	9.90	0.123	b.d.l.	5.72	0.28	98.91
Plg2 center	81.9	17.8	0.3	2.17	1.83	0.011	0.0009	0.81	0.0037	0.0001	0.18	0.003	13.00	46.85	33.48	0.28	0.013	16.31	0.136	b.d.l.	1.96	0.05	99.09
Plg2.1	29.2	67.4	3.3	2.70	1.29	0.012	0.0012	0.29	0.0031	0.0015	0.68	0.033	13.01	60.27	24.55	0.33	0.018	6.11	0.119	0.087	7.78	0.58	99.84
Plg2.10	53.2	45.6	1.3	2.45	1.54	0.010	0.0012	0.53	0.0033	0.0002	0.46	0.013	13.01	53.86	28.72	0.27	0.018	10.97	0.124	b.d.l.	5.19	0.22	99.40
Plg2.11	60.9	38.1	1.0	2.38	1.61	0.011	0.0011	0.61	0.0036	0.0005	0.38	0.010	13.01	52.13	29.92	0.29	0.016	12.55	0.135	b.d.l.	4.34	0.18	99.59
Plg2.12	80.7	19.1	0.2	2.18	1.82	0.014	0.0010	0.80	0.0030	0.0001	0.19	0.002	13.01	47.27	33.43	0.35	0.014	16.23	0.112	b.d.l.	2.13	0.04	99.57
Plg2.2	30.6	66.3	3.1	2.69	1.30	0.011	0.0009	0.30	0.0034	0.0009	0.66	0.031	13.00	60.12	24.65	0.29	0.014	6.35	0.129	0.049	7.59	0.54	99.74
Plg2.3	30.1	66.6	3.3	2.70	1.29	0.012	0.0010	0.30	0.0031	0.0014	0.67	0.033	13.01	60.15	24.42	0.31	0.016	6.27	0.118	0.078	7.65	0.58	99.59
Plg2.4	27.5	69.0	3.5	2.74	1.26	0.012	0.0013	0.27	0.0029	0.0015	0.68	0.034	12.99	61.04	23.80	0.31	0.019	5.64	0.110	0.084	7.81	0.59	99.42
Plg2.5	28.3	68.1	3.6	2.71	1.28	0.011	0.0011	0.29	0.0038	0.0010	0.69	0.036	13.01	60.58	24.35	0.31	0.017	5.96	0.147	0.057	7.91	0.63	99.95
Plg2.6	31.3	65.8	2.9	2.67	1.31	0.010	0.0013	0.32	0.0030	0.0010	0.67	0.030	13.02	59.65	24.87	0.25	0.020	6.59	0.116	0.059	7.66	0.52	99.73
Plg2.7	47.0	51.3	1.7	2.51	1.48	0.010	0.0009	0.47	0.0036	0.0009	0.52	0.017	13.02	55.36	27.57	0.25	0.014	9.75	0.138	0.052	5.88	0.30	99.32
Plg2.8	49.2	49.5	1.4	2.49	1.50	0.010	0.0010	0.49	0.0040	0.0004	0.49	0.014	13.01	54.93	28.11	0.26	0.015	10.08	0.153	b.d.l.	5.61	0.23	99.42
Plg2.9	39.0	58.8	2.1	2.60	1.39	0.010	0.0011	0.39	0.0036	0.0007	0.59	0.021	13.01	57.77	26.17	0.28	0.016	8.10	0.138	b.d.l.	6.75	0.37	99.64
VQ-06-24B (1846/47)																							
Pl13.2	44.9	51.8	3.3	2.57	1.40	0.030	0.0043	0.44	0.0031	0.0006	0.51	0.033	13.00	57.09	26.48	0.79	0.064	9.20	0.119	b.d.l.	5.87	0.57	100.22
Pl13.3	60.9	38.2	0.9	2.39	1.58	0.030	0.0079	0.61	0.0054	0.0009	0.38	0.009	13.02	52.67	29.63	0.79	0.117	12.63	0.207	b.d.l.	4.38	0.15	100.63
Pl13.4	79.2	20.5	0.4	2.20	1.78	0.027	0.0055	0.80	0.0030	b.d.l.	0.21	0.004	13.02	47.65	32.79	0.69	0.080	16.19	0.114	b.d.l.	2.31	0.06	99.89
Pl13.5	76.3	23.2	0.4	2.22	1.75	0.026	0.0059	0.77	0.0034	0.0003	0.24	0.005	13.02	48.26	32.36	0.67	0.086	15.70	0.127	b.d.l.	2.64	0.08	99.95

Appendix B1 cotinued

Label	An[2]	Ab[3]	Or[4]	Si	Al	Fe	Mg	Ca	Sr	Ba	Na	K	Tot[5]	SiO_2	Al_2O_3	FeO	MgO	CaO	SrO	BaO	Na_2O	K_2O	Tot
Pl13.6	79.7	20.0	0.4	2.21	1.77	0.026	0.0055	0.79	0.0039	0.0002	0.20	0.004	13.01	47.97	32.56	0.67	0.080	16.06	0.146	b.d.l.	2.22	0.06	99.78
Pl13.7	79.5	20.2	0.3	2.20	1.77	0.024	0.0055	0.81	0.0039	b.d.l.	0.20	0.004	13.02	47.85	32.66	0.61	0.080	16.38	0.145	b.d.l.	2.30	0.06	100.09
Pl2.1	72.6	26.7	0.6	2.28	1.69	0.024	0.0061	0.73	0.0036	b.d.l.	0.27	0.006	13.01	49.64	31.17	0.64	0.089	14.92	0.135	b.d.l.	3.03	0.11	99.73
Pl2.2	70.2	29.3	0.5	2.32	1.65	0.026	0.0067	0.70	0.0037	b.d.l.	0.29	0.005	13.00	50.69	30.50	0.68	0.098	14.19	0.140	b.d.l.	3.27	0.09	99.66
Pl6.1	32.6	64.4	3.0	2.68	1.30	0.013	0.0020	0.32	0.0026	0.0008	0.64	0.030	13.00	59.86	24.64	0.34	0.029	6.76	0.102	b.d.l.	7.37	0.52	99.66
Pl6.2	48.2	50.1	1.7	2.52	1.46	0.015	0.0016	0.49	0.0034	0.0004	0.51	0.017	13.01	55.73	27.28	0.39	0.023	10.05	0.131	b.d.l.	5.76	0.30	99.69
Pl6.3	59.7	39.5	0.8	2.41	1.58	0.021	0.0039	0.59	0.0037	b.d.l.	0.39	0.008	13.01	52.78	29.33	0.55	0.057	12.17	0.141	b.d.l.	4.44	0.13	99.59
Pl6.4	41.1	56.9	2.0	2.60	1.38	0.013	0.0018	0.41	0.0038	0.0005	0.57	0.020	13.00	57.98	26.17	0.36	0.027	8.56	0.145	b.d.l.	6.54	0.36	100.18
Pl8.01	83.9	16.0	0.1	2.18	1.79	0.023	0.0055	0.86	0.0034	0.0002	0.16	0.002	13.01	47.43	33.01	0.60	0.080	17.40	0.129	b.d.l.	1.83	b.d.l.	100.52
Pl8.01	68.3	31.1	0.6	2.33	1.64	0.026	0.0059	0.69	0.0043	b.d.l.	0.31	0.006	13.01	51.14	30.45	0.69	0.087	14.05	0.164	b.d.l.	3.53	0.10	100.20
Pl8.3	28.3	68.2	3.5	2.73	1.25	0.012	0.0013	0.28	0.0021	0.0008	0.69	0.036	13.01	61.28	23.85	0.33	0.020	5.97	0.083	b.d.l.	7.95	0.63	100.15
Pl8.4	32.0	64.9	3.2	2.69	1.29	0.010	0.0010	0.32	0.0030	0.0015	0.66	0.032	13.01	60.26	24.57	0.28	0.015	6.77	0.115	0.086	7.59	0.57	100.25
Pl8.5	29.9	66.7	3.4	2.71	1.28	0.011	0.0007	0.30	0.0031	0.0010	0.67	0.035	13.01	60.70	24.31	0.29	0.011	6.29	0.119	b.d.l.	7.75	0.61	100.13
Pl8.6	34.0	63.4	2.7	2.67	1.31	0.011	0.0011	0.35	0.0034	0.0008	0.64	0.027	13.01	59.94	25.06	0.29	0.017	7.24	0.134	b.d.l.	7.46	0.48	100.67
Pl8.7	35.9	61.4	2.7	2.65	1.34	0.011	0.0012	0.36	0.0033	0.0009	0.62	0.027	13.00	59.20	25.34	0.29	0.017	7.51	0.127	b.d.l.	7.09	0.47	100.09
Pl8.8	37.1	60.4	2.5	2.64	1.35	0.012	0.0010	0.37	0.0026	0.0010	0.60	0.025	13.00	58.97	25.53	0.31	0.015	7.71	0.101	b.d.l.	6.94	0.44	100.07
Pl8.9	42.7	55.4	1.9	2.58	1.41	0.011	0.0008	0.43	0.0026	0.0012	0.56	0.020	13.01	57.30	26.55	0.29	0.012	8.99	0.102	b.d.l.	6.43	0.34	100.08
VQ-07-44A (1846/47)																							
Pl1.1	52.8	45.5	1.7	2.43	1.56	0.028	0.0053	0.53	0.0037	0.0002	0.46	0.018	13.03	b.d.l.	b.d.l.	b.d.l.	b.d.l.	b.d.l.	b.d.l.	b.d.l.	b.d.l.	b.d.l.	97.61
Pl1.1	77.2	22.5	0.4	2.20	1.79	0.028	0.0052	0.77	0.0038	0.0001	0.22	0.004	13.02	b.d.l.	b.d.l.	b.d.l.	b.d.l.	b.d.l.	b.d.l.	b.d.l.	b.d.l.	b.d.l.	97.16
Pl1.2	83.7	16.0	0.3	2.14	1.85	0.028	0.0050	0.83	0.0038	0.0001	0.16	0.003	13.02	b.d.l.	b.d.l.	b.d.l.	b.d.l.	b.d.l.	b.d.l.	b.d.l.	b.d.l.	b.d.l.	98.37
Pl1.3	82.4	17.3	0.3	2.14	1.85	0.028	0.0041	0.82	0.0041	0.0001	0.17	0.003	13.02	b.d.l.	b.d.l.	b.d.l.	b.d.l.	b.d.l.	b.d.l.	b.d.l.	b.d.l.	b.d.l.	98.33
Pl1.4	83.9	15.9	0.3	2.14	1.86	0.025	0.0045	0.83	0.0036	b.d.l.	0.16	0.003	13.01	45.95	33.88	0.64	0.065	16.61	0.134	b.d.l.	1.74	0.05	99.06
Pl1.5	82.3	17.3	0.3	2.15	1.84	0.027	0.0050	0.82	0.0041	0.0002	0.17	0.003	13.02	46.31	33.56	0.69	0.072	16.47	0.151	b.d.l.	1.92	0.06	99.24
Pl1.6	60.1	38.7	1.2	2.36	1.62	0.031	0.0065	0.60	0.0043	0.0002	0.39	0.012	13.03	b.d.l.	b.d.l.	b.d.l.	b.d.l.	b.d.l.	b.d.l.	b.d.l.	b.d.l.	b.d.l.	97.19
Pl12.1	37.6	57.1	5.3	2.65	1.32	0.023	0.0031	0.38	0.0010	0.0016	0.58	0.054	13.01	b.d.l.	b.d.l.	b.d.l.	b.d.l.	b.d.l.	b.d.l.	b.d.l.	b.d.l.	b.d.l.	97.04
Pl12.2	34.4	62.6	3.0	2.64	1.35	0.013	0.0018	0.34	0.0038	0.0012	0.63	0.030	13.01	b.d.l.	b.d.l.	b.d.l.	b.d.l.	b.d.l.	b.d.l.	b.d.l.	b.d.l.	b.d.l.	98.45
Pl12.3	31.0	65.6	3.4	2.67	1.33	0.013	0.0011	0.31	0.0028	0.0015	0.66	0.035	13.02	b.d.l.	b.d.l.	b.d.l.	b.d.l.	b.d.l.	b.d.l.	b.d.l.	b.d.l.	b.d.l.	97.62
Pl12.4	29.5	66.5	4.0	2.69	1.30	0.012	0.0018	0.30	0.0030	0.0014	0.67	0.040	13.01	b.d.l.	b.d.l.	b.d.l.	b.d.l.	b.d.l.	b.d.l.	b.d.l.	b.d.l.	b.d.l.	94.11
Pl12.5	30.4	66.0	3.6	2.70	1.29	0.011	0.0012	0.30	0.0032	0.0010	0.66	0.036	13.01	59.50	24.13	0.29	0.017	6.27	0.122	0.058	7.52	0.62	98.52

Appendix B1 cotinued

Label	An[2]	Ab[3]	Or[4]	Si	Al	Fe	Mg	Ca	Sr	Ba	Na	K	Tot[5]	SiO_2	Al_2O_3	FeO	MgO	CaO	SrO	BaO	Na_2O	K_2O	Tot
Pl12.6	26.8	69.3	3.8	2.71	1.28	0.011	0.0011	0.27	0.0029	0.0016	0.70	0.039	13.02	b.d.l.	b.d.l.	b.d.l.	b.d.l.	b.d.l.	b.d.l.	b.d.l.	b.d.l.	b.d.l.	97.80
Pl12.7	28.6	67.6	3.8	2.70	1.29	0.011	0.0011	0.28	0.0030	0.0013	0.67	0.038	13.00	b.d.l.	b.d.l.	b.d.l.	b.d.l.	b.d.l.	b.d.l.	b.d.l.	b.d.l.	b.d.l.	97.15
Pl12.8	27.6	68.5	3.9	2.72	1.28	0.013	0.0012	0.27	0.0027	0.0012	0.68	0.039	13.00	b.d.l.	b.d.l.	b.d.l.	b.d.l.	b.d.l.	b.d.l.	b.d.l.	b.d.l.	b.d.l.	97.65
Pl13.1	59.8	39.2	1.1	2.38	1.59	0.031	0.0070	0.60	0.0043	0.0002	0.39	0.011	13.02	b.d.l.	b.d.l.	b.d.l.	b.d.l.	b.d.l.	b.d.l.	b.d.l.	b.d.l.	b.d.l.	96.16
Pl13.2	74.2	25.2	0.7	2.22	1.76	0.026	0.0046	0.75	0.0044	0.0001	0.26	0.007	13.03	b.d.l.	b.d.l.	b.d.l.	b.d.l.	b.d.l.	b.d.l.	b.d.l.	b.d.l.	b.d.l.	96.58
Pl16.1	67.3	31.9	0.8	2.33	1.64	0.026	0.0068	0.67	0.0048	0.0003	0.32	0.008	13.01	50.56	30.29	0.69	0.099	13.64	0.179	b.d.l.	3.57	0.14	99.18
Pl16.2	65.3	34.0	0.7	2.33	1.66	0.019	0.0048	0.66	0.0044	0.0004	0.34	0.007	13.02	b.d.l.	b.d.l.	b.d.l.	b.d.l.	b.d.l.	b.d.l.	b.d.l.	b.d.l.	b.d.l.	98.48
Pl16.3	70.0	29.5	0.5	2.30	1.68	0.021	0.0052	0.70	0.0039	0.0002	0.29	0.005	13.01	49.75	30.92	0.55	0.076	14.08	0.144	b.d.l.	3.28	0.08	98.89
Pl16.4	68.1	31.4	0.5	2.31	1.67	0.022	0.0053	0.68	0.0038	0.0003	0.31	0.005	13.01	b.d.l.	b.d.l.	b.d.l.	b.d.l.	b.d.l.	b.d.l.	b.d.l.	b.d.l.	b.d.l.	98.12
Pl16.5	71.0	28.5	0.5	2.27	1.71	0.020	0.0044	0.71	0.0042	0.0004	0.28	0.005	13.01	49.02	31.31	0.51	0.063	14.27	0.158	b.d.l.	3.17	0.08	98.60
Pl16.6	71.8	27.6	0.6	2.28	1.70	0.020	0.0043	0.72	0.0041	0.0003	0.28	0.006	13.01	49.16	31.00	0.51	0.062	14.56	0.153	b.d.l.	3.10	0.10	98.66
Pl18.1	79.9	19.8	0.3	2.18	1.79	0.033	0.0054	0.81	0.0041	0.0002	0.20	0.003	13.02	b.d.l.	b.d.l.	b.d.l.	b.d.l.	b.d.l.	b.d.l.	b.d.l.	b.d.l.	b.d.l.	97.51
Pl18.2	79.6	20.0	0.4	2.19	1.78	0.035	0.0051	0.80	0.0041	0.0001	0.20	0.004	13.02	b.d.l.	b.d.l.	b.d.l.	b.d.l.	b.d.l.	b.d.l.	b.d.l.	b.d.l.	b.d.l.	97.84
Pl18.3	69.6	29.6	0.8	2.29	1.69	0.033	0.0066	0.70	0.0048	b.d.l.	0.30	0.008	13.02	b.d.l.	b.d.l.	b.d.l.	b.d.l.	b.d.l.	b.d.l.	b.d.l.	b.d.l.	b.d.l.	97.27
Pl18.4	68.8	30.5	0.7	2.28	1.69	0.034	0.0057	0.69	0.0045	0.0002	0.31	0.007	13.03	b.d.l.	b.d.l.	b.d.l.	b.d.l.	b.d.l.	b.d.l.	b.d.l.	b.d.l.	b.d.l.	97.18
Pl18.5	71.4	27.9	0.7	2.27	1.70	0.039	0.0069	0.72	0.0048	b.d.l.	0.28	0.007	13.03	b.d.l.	b.d.l.	b.d.l.	b.d.l.	b.d.l.	b.d.l.	b.d.l.	b.d.l.	b.d.l.	95.03
Pl18.6	68.7	30.5	0.9	2.29	1.68	0.040	0.0074	0.68	0.0044	0.0004	0.30	0.009	13.02	b.d.l.	b.d.l.	b.d.l.	b.d.l.	b.d.l.	b.d.l.	b.d.l.	b.d.l.	b.d.l.	97.13
Pl19.1	28.9	67.6	3.5	2.69	1.30	0.011	0.0008	0.29	0.0030	0.0017	0.69	0.035	13.02	b.d.l.	b.d.l.	b.d.l.	b.d.l.	b.d.l.	b.d.l.	b.d.l.	b.d.l.	b.d.l.	97.44
Pl19.2	30.4	66.4	3.2	2.66	1.33	0.011	0.0011	0.31	0.0030	0.0014	0.67	0.032	13.03	b.d.l.	b.d.l.	b.d.l.	b.d.l.	b.d.l.	b.d.l.	b.d.l.	b.d.l.	b.d.l.	95.98
Pl2.2	30.6	65.4	4.1	2.70	1.29	0.012	0.0015	0.30	0.0027	0.0012	0.64	0.040	13.00	b.d.l.	b.d.l.	b.d.l.	b.d.l.	b.d.l.	b.d.l.	b.d.l.	b.d.l.	b.d.l.	97.79
Pl2.3	28.0	64.8	7.1	2.74	1.24	0.016	0.0054	0.28	0.0021	0.0015	0.64	0.071	13.00	b.d.l.	b.d.l.	b.d.l.	b.d.l.	b.d.l.	b.d.l.	b.d.l.	b.d.l.	b.d.l.	96.84
Pl20.1	80.2	19.4	0.4	2.18	1.80	0.026	0.0052	0.80	0.0041	b.d.l.	0.19	0.004	13.02	b.d.l.	b.d.l.	b.d.l.	b.d.l.	b.d.l.	b.d.l.	b.d.l.	b.d.l.	b.d.l.	98.15
Pl20.2	73.0	26.4	0.6	2.25	1.73	0.025	0.0063	0.73	0.0042	b.d.l.	0.26	0.006	13.02	48.68	31.69	0.64	0.091	14.69	0.155	b.d.l.	2.94	0.09	98.98
Pl20.3	75.3	24.2	0.5	2.22	1.76	0.026	0.0060	0.76	0.0042	0.0004	0.25	0.005	13.03	b.d.l.	b.d.l.	b.d.l.	b.d.l.	b.d.l.	b.d.l.	b.d.l.	b.d.l.	b.d.l.	98.30
Pl20.4	80.7	18.9	0.4	2.19	1.79	0.025	0.0057	0.80	0.0040	0.0001	0.19	0.004	13.01	47.19	32.74	0.65	0.082	16.13	0.149	b.d.l.	2.09	0.06	99.09
Pl20.5	77.1	22.4	0.5	2.23	1.75	0.026	0.0062	0.77	0.0040	b.d.l.	0.22	0.005	13.01	48.08	32.16	0.68	0.090	15.48	0.148	b.d.l.	2.48	0.08	99.20
Pl20.6	84.9	14.8	0.3	2.13	1.86	0.023	0.0042	0.85	0.0038	b.d.l.	0.15	0.003	13.02	b.d.l.	b.d.l.	b.d.l.	b.d.l.	b.d.l.	b.d.l.	b.d.l.	b.d.l.	b.d.l.	98.29
Pl20.7	78.3	19.5	2.2	2.23	1.75	0.028	0.0028	0.76	0.0033	0.0006	0.19	0.022	13.00	47.94	31.96	0.72	0.041	15.28	0.121	b.d.l.	2.10	0.37	98.56
Pl20.8	85.5	14.1	0.3	2.13	1.86	0.026	0.0035	0.85	0.0041	0.0004	0.14	0.003	13.02	45.80	33.97	0.67	0.051	17.18	0.153	b.d.l.	1.57	0.05	99.47
Pl20.9	85.8	14.0	0.2	2.13	1.86	0.027	0.0027	0.85	0.0041	0.0001	0.14	0.002	13.01	45.70	33.95	0.70	0.038	17.05	0.153	b.d.l.	1.54	0.03	99.18

Appendix B1 cotinued

Label	An[2]	Ab[3]	Or[4]	Si	Al	Fe	Mg	Ca	Sr	Ba	Na	K	Tot[5]	SiO_2	Al_2O_3	FeO	MgO	CaO	SrO	BaO	Na_2O	K_2O	Tot
Pl21.1	33.2	63.9	2.9	2.67	1.32	0.011	0.0011	0.33	0.0032	0.0012	0.63	0.029	13.00	59.74	25.08	0.28	0.016	6.83	0.125	0.071	7.27	0.50	99.92
Pl21.2	51.8	46.7	1.5	2.47	1.53	0.010	0.0012	0.51	0.0032	0.0005	0.46	0.015	13.00	b.d.l.	b.d.l.	b.d.l.	b.d.l.	b.d.l.	b.d.l.	b.d.l.	b.d.l.	b.d.l.	98.01
Pl21.3	31.8	64.9	3.3	2.67	1.33	0.011	0.0011	0.31	0.0028	0.0012	0.64	0.032	13.00	b.d.l.	b.d.l.	b.d.l.	b.d.l.	b.d.l.	b.d.l.	b.d.l.	b.d.l.	b.d.l.	97.79
Pl3.1	81.9	17.7	0.4	2.18	1.80	0.027	0.0049	0.82	0.0041	0.0002	0.18	0.004	13.01	47.14	33.17	0.71	0.072	16.51	0.153	b.d.l.	1.97	0.06	99.81
Pl3.2	79.4	20.2	0.4	2.20	1.79	0.027	0.0053	0.79	0.0048	0.0003	0.20	0.004	13.01	47.87	33.01	0.70	0.077	16.04	0.181	b.d.l.	2.25	0.08	100.23
Pl3.3	55.2	39.8	5.0	2.46	1.50	0.040	0.0114	0.56	0.0033	0.0004	0.41	0.051	13.02	b.d.l.	b.d.l.	b.d.l.	b.d.l.	b.d.l.	b.d.l.	b.d.l.	b.d.l.	b.d.l.	97.55
Pl3.4	77.3	22.3	0.4	2.24	1.75	0.026	0.0062	0.76	0.0043	0.0002	0.22	0.004	13.00	48.78	32.31	0.68	0.091	15.46	0.163	b.d.l.	2.46	0.07	100.03
Pl3.5	84.2	15.5	0.3	2.17	1.81	0.025	0.0057	0.83	0.0040	0.0003	0.15	0.003	13.00	46.90	33.28	0.65	0.083	16.66	0.151	b.d.l.	1.70	0.05	99.48
Pl3.6	86.4	13.3	0.3	2.14	1.85	0.023	0.0043	0.86	0.0042	0.0004	0.13	0.003	13.01	46.37	34.00	0.61	0.063	17.33	0.157	b.d.l.	1.47	0.05	100.07
Pl4.1	73.9	25.5	0.6	2.27	1.72	0.025	0.0059	0.73	0.0043	0.0003	0.25	0.006	13.01	49.30	31.70	0.65	0.086	14.82	0.161	b.d.l.	2.83	0.10	99.66
Pl4.2	75.6	23.8	0.5	2.26	1.72	0.024	0.0057	0.75	0.0045	0.0001	0.24	0.005	13.00	49.19	31.78	0.64	0.084	15.15	0.171	b.d.l.	2.64	0.09	99.74
Pl4.3	76.2	23.4	0.4	2.24	1.74	0.023	0.0058	0.75	0.0038	0.0002	0.23	0.004	13.00	48.91	32.22	0.60	0.085	15.25	0.143	b.d.l.	2.59	0.07	99.88
Pl4.4	82.6	17.2	0.3	2.17	1.81	0.025	0.0059	0.82	0.0045	b.d.l.	0.17	0.003	13.01	46.95	33.20	0.66	0.085	16.53	0.169	b.d.l.	1.90	0.04	99.53
Pl5.1	49.3	48.8	1.9	2.49	1.49	0.022	0.0034	0.49	0.0039	0.0008	0.49	0.019	13.01	b.d.l.	b.d.l.	b.d.l.	b.d.l.	b.d.l.	b.d.l.	b.d.l.	b.d.l.	b.d.l.	96.18
Pl5.2	79.0	20.7	0.3	2.16	1.82	0.026	0.0057	0.80	0.0042	0.0005	0.21	0.003	13.03	b.d.l.	b.d.l.	b.d.l.	b.d.l.	b.d.l.	b.d.l.	b.d.l.	b.d.l.	b.d.l.	96.52
Pl5.3	78.9	20.5	0.5	2.18	1.80	0.029	0.0057	0.79	0.0033	b.d.l.	0.21	0.005	13.02	b.d.l.	b.d.l.	b.d.l.	b.d.l.	b.d.l.	b.d.l.	b.d.l.	b.d.l.	b.d.l.	97.30
Pl5.4	76.2	23.4	0.4	2.23	1.76	0.026	0.0063	0.75	0.0040	b.d.l.	0.23	0.004	13.01	b.d.l.	b.d.l.	b.d.l.	b.d.l.	b.d.l.	b.d.l.	b.d.l.	b.d.l.	b.d.l.	97.99
Pl5.5	79.7	19.9	0.4	2.18	1.80	0.027	0.0057	0.79	0.0039	0.0002	0.20	0.004	13.01	b.d.l.	b.d.l.	b.d.l.	b.d.l.	b.d.l.	b.d.l.	b.d.l.	b.d.l.	b.d.l.	97.55
Pl6.2	39.1	58.2	2.6	2.61	1.39	0.016	0.0029	0.39	0.0029	0.0012	0.57	0.026	13.00	57.51	25.97	0.43	0.043	7.94	0.112	0.069	6.53	0.45	99.05
Pl6.3	28.8	67.8	3.4	2.71	1.28	0.011	0.0007	0.28	0.0027	0.0011	0.67	0.033	13.00	60.25	24.13	0.30	0.010	5.87	0.105	0.062	7.64	0.58	98.95
Pl6.4	31.9	64.9	3.2	2.68	1.32	0.011	0.0010	0.32	0.0030	0.0013	0.64	0.032	13.00	59.32	24.80	0.28	0.014	6.57	0.114	0.073	7.37	0.55	99.09
Pl6.5	29.4	67.1	3.5	2.70	1.29	0.011	0.0012	0.29	0.0030	0.0011	0.67	0.035	13.00	59.92	24.31	0.28	0.018	6.04	0.113	0.060	7.62	0.60	98.96
Pl6.6	28.6	67.8	3.6	2.71	1.29	0.011	0.0010	0.28	0.0025	0.0016	0.66	0.035	13.00	60.00	24.25	0.29	0.015	5.79	0.097	0.089	7.59	0.61	98.73
Pl6.7	30.6	66.2	3.2	2.69	1.30	0.011	0.0012	0.31	0.0027	0.0013	0.66	0.032	13.01	59.52	24.49	0.28	0.017	6.31	0.104	0.074	7.55	0.55	98.91
Pl8.1	53.4	45.2	1.4	2.43	1.55	0.030	0.0073	0.53	0.0058	0.0003	0.45	0.014	13.03	b.d.l.	b.d.l.	b.d.l.	b.d.l.	b.d.l.	b.d.l.	b.d.l.	b.d.l.	b.d.l.	93.47
Pl8.2	66.5	33.0	0.6	2.28	1.70	0.026	0.0077	0.67	0.0044	0.0002	0.33	0.006	13.04	b.d.l.	b.d.l.	b.d.l.	b.d.l.	b.d.l.	b.d.l.	b.d.l.	b.d.l.	b.d.l.	95.38
Pl8.3	81.1	18.6	0.4	2.13	1.86	0.027	0.0055	0.82	0.0042	0.0003	0.19	0.004	13.04	b.d.l.	b.d.l.	b.d.l.	b.d.l.	b.d.l.	b.d.l.	b.d.l.	b.d.l.	b.d.l.	95.27
Pl8.4	80.4	19.2	0.4	2.13	1.85	0.029	0.0057	0.81	0.0039	b.d.l.	0.19	0.004	13.04	b.d.l.	b.d.l.	b.d.l.	b.d.l.	b.d.l.	b.d.l.	b.d.l.	b.d.l.	b.d.l.	94.69
Pl9.1	78.1	21.7	0.2	2.19	1.80	0.025	0.0059	0.77	0.0037	0.0004	0.21	0.002	13.02	b.d.l.	b.d.l.	b.d.l.	b.d.l.	b.d.l.	b.d.l.	b.d.l.	b.d.l.	b.d.l.	97.89
Pl9.2	80.3	19.4	0.4	2.17	1.82	0.024	0.0049	0.80	0.0042	0.0002	0.19	0.004	13.02	b.d.l.	b.d.l.	b.d.l.	b.d.l.	b.d.l.	b.d.l.	b.d.l.	b.d.l.	b.d.l.	98.22

Appendix B1 cotinued

Label	An[2]	Ab[3]	Or[4]	Si	Al	Fe	Mg	Ca	Sr	Ba	Na	K	Tot[5]	SiO_2	Al_2O_3	FeO	MgO	CaO	SrO	BaO	Na_2O	K_2O	Tot
Pl9.3	77.6	21.9	0.4	2.18	1.81	0.025	0.0055	0.78	0.0039	0.0001	0.22	0.005	13.03	b.d.l.	b.d.l.	b.d.l.	b.d.l.	b.d.l.	b.d.l.	b.d.l.	b.d.l.	b.d.l.	98.06
Pl9.4	80.2	19.5	0.4	2.18	1.81	0.026	0.0054	0.80	0.0043	b.d.l.	0.19	0.004	13.02	b.d.l.	b.d.l.	b.d.l.	b.d.l.	b.d.l.	b.d.l.	b.d.l.	b.d.l.	b.d.l.	98.37
Pl9.5	80.8	18.9	0.3	2.16	1.83	0.024	0.0053	0.81	0.0043	0.0003	0.19	0.003	13.02	b.d.l.	b.d.l.	b.d.l.	b.d.l.	b.d.l.	b.d.l.	b.d.l.	b.d.l.	b.d.l.	98.39
Pl9.6	82.5	17.2	0.3	2.15	1.84	0.028	0.0046	0.82	0.0044	b.d.l.	0.17	0.003	13.02	45.93	33.38	0.72	0.066	16.33	0.162	b.d.l.	1.88	0.05	98.51
Pl9.7	84.6	14.9	0.5	2.13	1.86	0.028	0.0033	0.83	0.0039	0.0005	0.15	0.005	13.01	b.d.l.	b.d.l.	b.d.l.	b.d.l.	b.d.l.	b.d.l.	b.d.l.	b.d.l.	b.d.l.	97.68
Mount_VQ-06-02 75-125 µm (1846/47)																							
Pl1	29.3	66.0	4.7	2.72	1.27	0.011	0.0010	0.29	0.0023	0.0018	0.65	0.046	12.99	61.15	24.30	0.29	0.014	6.05	0.092	0.102	7.54	0.81	100.35
Pl10	33.1	62.6	4.3	2.68	1.31	0.008	0.0013	0.33	0.0024	0.0010	0.62	0.042	12.99	60.41	24.96	0.22	0.020	6.85	0.094	0.057	7.18	0.74	100.53
Pl11	68.9	30.2	0.8	2.32	1.65	0.025	0.0059	0.69	0.0045	0.0005	0.30	0.008	13.01	50.85	30.76	0.65	0.086	14.02	0.172	b.d.l.	3.40	0.14	100.11
Pl12	31.4	64.8	3.8	2.71	1.29	0.011	0.0011	0.31	0.0028	0.0014	0.63	0.037	12.98	60.84	24.55	0.30	0.017	6.42	0.109	0.079	7.31	0.65	100.27
Pl13	53.3	45.2	1.6	2.48	1.52	0.016	0.0029	0.52	0.0046	0.0004	0.44	0.015	12.99	54.90	28.50	0.42	0.043	10.66	0.179	b.d.l.	5.00	0.26	99.99
Pl14	46.8	51.0	2.1	2.56	1.44	0.011	0.0012	0.45	0.0036	0.0004	0.49	0.021	12.98	57.24	27.38	0.29	0.018	9.42	0.141	b.d.l.	5.67	0.36	100.53
Pl15	41.2	56.0	2.7	2.58	1.42	0.009	0.0014	0.40	0.0034	0.0008	0.55	0.027	12.99	57.43	26.81	0.23	0.020	8.36	0.133	0.046	6.28	0.47	99.77
Pl16	30.9	64.3	4.8	2.69	1.31	0.010	0.0012	0.30	0.0024	0.0012	0.62	0.047	12.99	60.64	24.96	0.27	0.017	6.30	0.093	0.070	7.25	0.82	100.42
Pl17	27.3	68.4	4.3	2.74	1.26	0.013	0.0011	0.26	0.0028	0.0017	0.66	0.042	12.99	61.61	24.15	0.34	0.016	5.55	0.109	0.097	7.70	0.74	100.32
Pl18	51.0	47.5	1.6	2.50	1.49	0.016	0.0030	0.50	0.0052	0.0002	0.47	0.015	13.00	55.39	28.05	0.43	0.044	10.39	0.199	b.d.l.	5.35	0.27	100.12
Pl19	30.2	66.0	3.8	2.71	1.29	0.011	0.0008	0.29	0.0028	0.0014	0.63	0.037	12.98	61.16	24.69	0.29	0.012	6.11	0.108	0.083	7.37	0.65	100.47
Pl2	31.4	64.3	4.4	2.70	1.30	0.011	0.0011	0.31	0.0030	0.0012	0.63	0.043	12.99	60.61	24.72	0.29	0.017	6.43	0.118	0.067	7.27	0.75	100.27
Pl20	32.3	64.1	3.6	2.68	1.31	0.012	0.0010	0.32	0.0030	0.0010	0.63	0.035	13.00	60.30	24.97	0.31	0.015	6.68	0.117	0.059	7.33	0.62	100.40
Pl21	37.1	59.5	3.4	2.62	1.37	0.009	0.0011	0.37	0.0026	0.0010	0.59	0.034	13.01	58.75	26.09	0.24	0.017	7.75	0.103	0.059	6.87	0.59	100.48
Pl22	28.3	67.6	4.1	2.73	1.26	0.010	0.0010	0.27	0.0029	0.0017	0.65	0.040	12.98	61.97	24.29	0.28	0.015	5.81	0.113	0.097	7.65	0.71	100.93
Pl23	28.9	66.0	5.1	2.73	1.26	0.011	0.0009	0.28	0.0028	0.0016	0.64	0.049	12.98	61.60	24.19	0.29	0.013	5.91	0.111	0.092	7.47	0.87	100.55
Pl24	29.1	66.3	4.5	2.72	1.27	0.011	0.0010	0.28	0.0024	0.0013	0.65	0.044	12.99	61.14	24.29	0.28	0.016	5.94	0.094	0.074	7.48	0.78	100.09
Pl25	64.1	35.0	0.9	2.37	1.60	0.024	0.0064	0.64	0.0045	0.0005	0.35	0.009	13.01	52.16	29.87	0.63	0.094	13.12	0.172	b.d.l.	3.95	0.16	100.18
Pl26	29.1	66.4	4.5	2.72	1.28	0.011	0.0010	0.29	0.0026	0.0009	0.65	0.044	12.99	60.52	24.22	0.28	0.014	5.96	0.102	0.053	7.50	0.77	99.41
Pl3	31.5	63.6	4.9	2.70	1.29	0.009	0.0010	0.31	0.0025	0.0015	0.62	0.048	12.99	60.63	24.51	0.25	0.015	6.46	0.097	0.087	7.20	0.85	100.10
Pl4	34.8	61.2	4.0	2.66	1.33	0.012	0.0012	0.34	0.0034	0.0015	0.60	0.039	13.00	59.53	25.29	0.31	0.018	7.16	0.134	0.086	6.96	0.69	100.18
Pl5	30.3	66.1	3.7	2.71	1.29	0.012	0.0009	0.30	0.0026	0.0013	0.64	0.036	12.99	61.00	24.60	0.33	0.013	6.20	0.101	0.074	7.48	0.63	100.43
Pl6	45.8	52.2	2.0	2.53	1.46	0.011	0.0015	0.45	0.0031	0.0008	0.52	0.020	13.00	55.91	27.43	0.28	0.023	9.32	0.119	0.045	5.87	0.34	99.33
Pl7	28.9	67.3	3.8	2.73	1.27	0.011	0.0009	0.28	0.0028	0.0014	0.66	0.038	12.99	61.08	24.12	0.29	0.013	5.92	0.109	0.080	7.62	0.66	99.90

Appendix B1 cotinued

Label	An[2]	Ab[3]	Or[4]	Si	Al	Fe	Mg	Ca	Sr	Ba	Na	K	Tot[5]	SiO_2	Al_2O_3	FeO	MgO	CaO	SrO	BaO	Na_2O	K_2O	Tot
Pl8	38.6	58.5	2.9	2.66	1.34	0.011	0.0010	0.37	0.0029	0.0008	0.56	0.028	12.97	59.26	25.27	0.28	0.016	7.72	0.113	0.049	6.47	0.48	99.66
Pl9	25.7	69.7	4.6	2.79	1.20	0.012	0.0010	0.25	0.0027	0.0018	0.67	0.044	12.97	62.30	22.72	0.31	0.014	5.14	0.105	0.106	7.70	0.77	99.17
Mount_VQ-06-02 125-250 µm (1846/47)																							
Pl1	29.5	65.6	4.8	2.72	1.26	0.013	0.0010	0.29	0.0025	0.0024	0.65	0.048	13.00	61.53	24.20	0.34	0.016	6.19	0.098	0.139	7.60	0.85	100.96
Pl10	31.2	65.0	3.8	2.72	1.27	0.011	0.0015	0.31	0.0023	0.0013	0.64	0.037	12.99	60.96	24.17	0.29	0.022	6.47	0.090	0.074	7.44	0.66	100.17
Pl11	29.5	66.5	3.9	2.72	1.27	0.011	0.0009	0.29	0.0028	0.0014	0.66	0.039	13.00	61.20	24.37	0.30	0.014	6.13	0.109	0.082	7.64	0.68	100.53
Pl12	27.0	68.7	4.2	2.74	1.25	0.013	0.0015	0.26	0.0024	0.0014	0.66	0.041	12.98	62.04	24.07	0.34	0.023	5.52	0.093	0.083	7.76	0.72	100.66
Pl13	45.3	52.3	2.5	2.55	1.44	0.012	0.0006	0.45	0.0035	0.0009	0.52	0.025	13.01	56.41	27.13	0.31	b.d.l.	9.36	0.133	b.d.l.	5.97	0.43	99.81
Pl14	32.2	65.0	2.9	2.70	1.29	0.011	0.0014	0.32	0.0029	0.0009	0.64	0.028	12.99	60.96	24.69	0.30	0.022	6.70	0.115	b.d.l.	7.47	0.50	100.82
Pl15	29.5	66.4	4.1	2.73	1.26	0.011	0.0011	0.29	0.0029	0.0017	0.66	0.041	12.99	60.96	23.95	0.28	0.017	6.10	0.112	0.097	7.58	0.72	99.81
Pl16	30.7	65.8	3.6	2.72	1.27	0.012	0.0019	0.30	0.0017	0.0013	0.65	0.035	12.99	61.37	24.39	0.31	0.029	6.36	0.067	0.077	7.53	0.62	100.75
Pl17	30.8	64.9	4.3	2.73	1.26	0.013	0.0018	0.30	0.0015	0.0014	0.63	0.042	12.98	61.31	23.93	0.34	0.027	6.27	0.058	0.082	7.31	0.74	100.07
Pl18	31.0	65.5	3.5	2.71	1.27	0.012	0.0007	0.31	0.0028	0.0012	0.65	0.034	12.99	61.09	24.32	0.31	b.d.l.	6.45	0.111	0.068	7.52	0.61	100.50
Pl19	51.1	47.5	1.4	2.48	1.51	0.011	0.0001	0.51	0.0028	0.0003	0.48	0.014	13.01	54.95	28.29	0.29	b.d.l.	10.59	0.106	b.d.l.	5.44	0.25	99.93
Pl2	30.4	66.0	3.7	2.70	1.30	0.011	0.0003	0.30	0.0020	0.0007	0.65	0.036	13.00	60.92	24.84	0.30	b.d.l.	6.32	0.080	b.d.l.	7.58	0.64	100.72
Pl20	30.4	65.7	3.9	2.74	1.25	0.012	0.0013	0.29	0.0023	0.0019	0.63	0.037	12.97	61.22	23.59	0.31	0.019	6.06	0.088	0.111	7.25	0.65	99.30
Pl21	46.1	52.1	1.9	2.55	1.44	0.010	0.0018	0.46	0.0035	0.0005	0.52	0.019	13.00	56.29	27.00	0.27	0.027	9.52	0.134	b.d.l.	5.95	0.33	99.56
Pl22	49.2	49.2	1.6	2.52	1.47	0.011	0.0017	0.49	0.0028	0.0011	0.49	0.016	13.00	56.34	27.84	0.29	0.026	10.18	0.107	b.d.l.	5.63	0.28	100.75
Pl23	29.1	66.9	4.0	2.73	1.26	0.011	0.0006	0.29	0.0021	0.0008	0.66	0.040	12.99	61.34	24.12	0.30	b.d.l.	6.04	0.081	b.d.l.	7.68	0.70	100.31
Pl24	26.9	68.3	4.8	2.76	1.23	0.012	0.0012	0.26	0.0021	0.0017	0.66	0.047	12.98	62.09	23.45	0.32	0.018	5.47	0.082	0.096	7.68	0.82	100.03
Pl25	51.5	47.0	1.5	2.48	1.52	0.012	0.0006	0.51	0.0039	0.0001	0.47	0.015	13.01	54.89	28.61	0.33	b.d.l.	10.57	0.149	b.d.l.	5.33	0.26	100.15
Pl26	51.9	46.7	1.5	2.49	1.50	0.013	0.0019	0.51	0.0037	0.0005	0.46	0.014	13.00	55.06	28.28	0.34	0.029	10.63	0.140	b.d.l.	5.28	0.25	100.04
Pl27	25.7	69.9	4.4	2.76	1.23	0.010	0.0013	0.26	0.0025	0.0021	0.69	0.044	13.00	62.34	23.50	0.28	0.019	5.39	0.098	0.120	8.09	0.77	100.61
Pl28	37.1	59.8	3.0	2.63	1.36	0.011	0.0006	0.37	0.0032	0.0007	0.59	0.030	13.00	59.12	25.96	0.29	b.d.l.	7.71	0.122	b.d.l.	6.87	0.53	100.66
Pl29	29.9	65.5	4.7	2.70	1.29	0.010	0.0010	0.30	0.0023	0.0013	0.65	0.047	13.00	60.62	24.49	0.27	0.016	6.24	0.087	0.077	7.56	0.82	100.18
Pl3	31.4	65.2	3.4	2.69	1.30	0.010	0.0012	0.31	0.0036	0.0005	0.64	0.033	12.99	60.52	24.81	0.28	0.018	6.49	0.139	b.d.l.	7.44	0.59	100.31
Pl30	30.4	65.7	3.9	2.72	1.27	0.010	0.0018	0.30	0.0024	0.0009	0.64	0.038	12.98	61.61	24.35	0.28	0.027	6.25	0.096	b.d.l.	7.47	0.67	100.79
Pl4	32.3	63.7	4.1	2.69	1.31	0.012	0.0006	0.32	0.0027	0.0011	0.63	0.040	13.00	60.33	24.89	0.32	b.d.l.	6.69	0.104	b.d.l.	7.29	0.71	100.41
Pl5	38.6	58.3	3.1	2.61	1.39	0.012	0.0024	0.38	0.0027	0.0012	0.57	0.031	13.00	58.52	26.49	0.31	0.036	7.98	0.106	0.066	6.66	0.55	100.72
Pl6	31.8	65.0	3.2	2.67	1.32	0.011	0.0007	0.32	0.0026	0.0011	0.65	0.033	13.01	59.88	25.04	0.29	b.d.l.	6.65	0.100	b.d.l.	7.51	0.57	100.11

Appendix B1 cotinued

Label	An[2]	Ab[3]	Or[4]	Si	Al	Fe	Mg	Ca	Sr	Ba	Na	K	Tot[5]	SiO_2	Al_2O_3	FeO	MgO	CaO	SrO	BaO	Na_2O	K_2O	Tot
Pl7	38.9	59.0	2.1	2.60	1.38	0.011	0.0011	0.39	0.0031	0.0003	0.60	0.021	13.01	57.84	26.09	0.28	0.016	8.16	0.118	b.d.l.	6.84	0.37	99.74
Pl8	32.7	64.0	3.2	2.69	1.31	0.013	0.0007	0.32	0.0028	0.0009	0.63	0.032	12.99	60.43	24.95	0.34	b.d.l.	6.76	0.109	b.d.l.	7.31	0.56	100.52
Pl9	40.7	57.0	2.4	2.59	1.39	0.012	0.0016	0.41	0.0037	0.0003	0.57	0.024	13.01	57.87	26.29	0.32	0.025	8.54	0.141	b.d.l.	6.61	0.42	100.23
Mount_VQ-06-02 250-500 µm (1846/47)																							
Pl1.1	32.9	63.5	3.6	2.68	1.31	0.011	0.0009	0.33	0.0035	0.0011	0.63	0.036	13.00	60.46	25.13	0.29	0.014	6.85	0.139	0.065	7.31	0.63	100.88
Pl1.2	41.5	56.5	2.0	2.57	1.42	0.011	0.0013	0.42	0.0033	0.0004	0.57	0.020	13.01	57.37	26.80	0.29	0.019	8.67	0.129	b.d.l.	6.51	0.35	100.17
Pl10.1	32.3	64.1	3.6	2.68	1.31	0.011	0.0010	0.32	0.0028	0.0015	0.63	0.036	13.00	60.77	25.24	0.28	0.015	6.75	0.109	0.088	7.39	0.63	101.27
Pl11	24.9	70.4	4.7	2.73	1.26	0.010	0.0006	0.25	0.0027	0.0017	0.72	0.049	13.03	61.14	23.89	0.27	0.009	5.32	0.105	0.098	8.31	0.85	99.99
Pl12	29.7	66.6	3.7	2.71	1.29	0.011	0.0007	0.29	0.0027	0.0012	0.65	0.036	12.99	61.32	24.66	0.28	0.011	6.15	0.108	0.068	7.61	0.64	100.85
Pl13	29.1	67.3	3.7	2.72	1.27	0.011	0.0009	0.29	0.0030	0.0015	0.67	0.037	13.00	61.52	24.39	0.29	0.014	6.11	0.118	0.086	7.81	0.65	100.99
Pl14	32.1	64.2	3.7	2.68	1.31	0.010	0.0010	0.31	0.0028	0.0012	0.63	0.036	12.99	60.47	25.11	0.28	0.015	6.62	0.108	0.070	7.31	0.64	100.61
Pl15.1	33.8	62.3	3.9	2.69	1.30	0.011	0.0011	0.33	0.0027	0.0011	0.61	0.038	12.99	60.70	24.94	0.29	0.017	7.00	0.106	0.063	7.14	0.68	100.93
Pl15.2	49.4	49.2	1.4	2.48	1.51	0.012	0.0012	0.50	0.0033	0.0004	0.49	0.014	13.01	55.23	28.49	0.32	0.018	10.28	0.129	b.d.l.	5.65	0.25	100.39
Pl16.1	33.1	63.4	3.5	2.69	1.30	0.012	0.0010	0.33	0.0029	0.0010	0.62	0.034	12.99	60.80	24.93	0.32	0.015	6.86	0.116	0.057	7.26	0.60	100.96
Pl16.2	49.3	49.0	1.7	2.50	1.49	0.010	0.0014	0.49	0.0033	0.0003	0.49	0.017	13.01	56.02	28.36	0.26	0.021	10.31	0.127	b.d.l.	5.66	0.29	101.07
Pl17	27.8	67.9	4.3	2.69	1.29	0.013	0.0010	0.28	0.0024	0.0010	0.69	0.044	13.03	b.d.l.	b.d.l.	b.d.l.	b.d.l.	b.d.l.	b.d.l.	b.d.l.	b.d.l.	b.d.l.	97.34
Pl18	31.5	65.0	3.5	2.68	1.31	0.011	0.0009	0.31	0.0029	0.0010	0.64	0.034	12.99	60.34	25.04	0.29	0.013	6.48	0.115	0.060	7.39	0.61	100.32
Pl19	51.8	46.8	1.4	2.49	1.49	0.012	0.0010	0.52	0.0043	b.d.l.	0.47	0.014	13.00	55.33	28.05	0.32	0.015	10.73	0.165	b.d.l.	5.37	0.25	100.23
Pl2	29.1	66.9	3.9	2.71	1.28	0.013	0.0009	0.29	0.0027	0.0012	0.66	0.039	12.99	61.43	24.65	0.34	0.013	6.03	0.108	0.071	7.65	0.68	100.98
Pl20.1	33.5	62.1	4.3	2.67	1.33	0.011	0.0012	0.33	0.0033	0.0011	0.61	0.043	13.00	59.66	25.15	0.29	0.019	6.92	0.130	0.063	7.09	0.75	100.07
Pl20.2	57.4	41.5	1.1	2.42	1.58	0.008	0.0010	0.58	0.0032	0.0007	0.42	0.011	13.01	53.50	29.66	0.22	0.015	11.89	0.122	b.d.l.	4.75	0.19	100.41
Pl21	27.5	68.0	4.6	2.74	1.25	0.010	0.0009	0.27	0.0029	0.0018	0.67	0.045	12.99	61.51	23.84	0.26	0.014	5.66	0.114	0.103	7.74	0.79	100.04
Pl22	53.3	45.2	1.4	2.48	1.52	0.010	0.0014	0.53	0.0028	0.0007	0.45	0.014	13.00	54.90	28.50	0.27	0.021	10.93	0.107	b.d.l.	5.12	0.25	100.13
Pl23	43.2	54.3	2.5	2.57	1.42	0.011	0.0015	0.43	0.0034	0.0007	0.54	0.025	13.00	57.43	26.86	0.30	0.023	8.93	0.132	b.d.l.	6.21	0.43	100.35
Pl24	27.2	68.6	4.2	2.72	1.27	0.013	0.0008	0.27	0.0029	0.0015	0.68	0.042	13.00	61.29	24.35	0.36	0.013	5.65	0.114	0.090	7.88	0.74	100.48
Pl25	30.8	65.5	3.7	2.68	1.32	0.012	0.0010	0.31	0.0028	0.0013	0.65	0.037	13.01	60.15	25.07	0.32	0.016	6.41	0.111	0.075	7.52	0.65	100.32
Pl26.1	32.9	63.4	3.7	2.68	1.31	0.011	0.0009	0.33	0.0024	0.0014	0.63	0.037	13.00	60.13	24.97	0.28	0.014	6.84	0.092	0.082	7.28	0.65	100.34
Pl26.2	46.4	51.6	1.9	2.52	1.47	0.010	0.0009	0.47	0.0029	0.0011	0.52	0.020	13.01	56.08	27.80	0.27	0.013	9.66	0.113	0.066	5.93	0.34	100.27
Pl27	33.9	63.1	3.0	2.65	1.34	0.012	0.0012	0.34	0.0027	0.0011	0.63	0.030	13.01	59.50	25.52	0.33	0.018	7.08	0.105	0.066	7.30	0.53	100.44
Pl28	39.7	57.8	2.5	2.58	1.42	0.011	0.0013	0.40	0.0033	0.0011	0.58	0.025	13.01	57.66	26.84	0.30	0.020	8.28	0.128	0.061	6.64	0.44	100.37

Appendix B1 cotinued

Label	An[2]	Ab[3]	Or[4]	Si	Al	Fe	Mg	Ca	Sr	Ba	Na	K	Tot[5]	SiO_2	Al_2O_3	FeO	MgO	CaO	SrO	BaO	Na_2O	K_2O	Tot
Pl29	45.2	53.0	1.8	2.53	1.47	0.011	0.0010	0.45	0.0035	0.0006	0.53	0.018	13.01	55.97	27.49	0.29	0.015	9.29	0.133	b.d.l.	6.02	0.31	99.55
Pl3	51.1	47.6	1.3	2.48	1.51	0.011	0.0013	0.51	0.0045	0.0002	0.48	0.014	13.01	55.46	28.63	0.29	0.019	10.70	0.175	b.d.l.	5.50	0.24	101.03
Pl30.1	28.6	67.0	4.4	2.72	1.28	0.013	0.0005	0.28	0.0033	0.0014	0.65	0.043	12.99	61.08	24.34	0.34	0.008	5.85	0.129	0.079	7.58	0.76	100.16
Pl30.2	30.9	64.9	4.2	2.69	1.30	0.010	0.0004	0.31	0.0026	0.0014	0.64	0.042	13.00	60.60	24.84	0.28	0.006	6.43	0.103	0.082	7.47	0.74	100.54
Pl31	33.6	63.1	3.3	2.70	1.29	0.011	0.0013	0.33	0.0026	0.0010	0.62	0.032	12.98	60.79	24.64	0.30	0.020	6.91	0.103	0.060	7.17	0.57	100.57
Pl32	30.8	65.5	3.8	2.70	1.29	0.013	0.0011	0.30	0.0028	0.0015	0.65	0.037	13.00	60.75	24.67	0.34	0.017	6.41	0.111	0.090	7.53	0.66	100.58
Pl33	30.8	65.3	3.9	2.71	1.28	0.011	0.0009	0.30	0.0029	0.0015	0.64	0.038	12.99	60.55	24.30	0.28	0.013	6.30	0.114	0.085	7.38	0.67	99.69
Pl34	41.6	56.0	2.4	2.57	1.43	0.011	0.0012	0.41	0.0031	0.0013	0.55	0.024	13.00	57.08	26.85	0.28	0.018	8.50	0.120	0.073	6.34	0.42	99.68
Pl35	50.8	47.6	1.5	2.48	1.50	0.009	0.0011	0.52	0.0034	0.0009	0.48	0.015	13.02	54.92	28.18	0.24	0.016	10.66	0.130	0.051	5.52	0.27	100.00
Pl36	32.9	63.7	3.3	2.65	1.34	0.010	0.0007	0.33	0.0029	0.0015	0.64	0.033	13.01	59.43	25.52	0.26	0.010	6.88	0.115	0.085	7.36	0.59	100.24
Pl37	30.4	65.5	4.1	2.68	1.32	0.012	0.0010	0.30	0.0028	0.0012	0.65	0.041	13.01	59.66	24.91	0.31	0.015	6.33	0.109	0.068	7.52	0.71	99.64
Pl38	39.8	58.0	2.3	2.59	1.40	0.012	0.0010	0.40	0.0039	0.0006	0.58	0.023	13.01	58.00	26.54	0.31	0.015	8.29	0.150	b.d.l.	6.67	0.40	100.41
Pl39	56.3	42.5	1.2	2.41	1.59	0.011	0.0011	0.56	0.0038	0.0005	0.43	0.012	13.01	53.22	29.72	0.29	0.016	11.59	0.147	b.d.l.	4.84	0.20	100.06
Pl4	34.0	62.8	3.2	2.67	1.31	0.011	0.0012	0.34	0.0029	0.0012	0.62	0.032	13.00	60.28	25.14	0.29	0.017	7.11	0.114	0.072	7.26	0.57	100.85
Pl40	31.4	65.1	3.5	2.67	1.32	0.010	0.0008	0.31	0.0033	0.0017	0.65	0.035	13.01	59.91	25.18	0.27	0.012	6.50	0.129	0.098	7.47	0.62	100.19
Pl41	29.8	65.4	4.8	2.69	1.30	0.011	0.0011	0.30	0.0030	0.0012	0.65	0.048	13.01	60.63	24.94	0.30	0.017	6.27	0.117	0.070	7.61	0.85	100.81
Pl42	30.0	65.1	4.9	2.69	1.30	0.012	0.0012	0.30	0.0027	0.0014	0.65	0.049	13.00	60.53	24.89	0.31	0.018	6.25	0.105	0.082	7.50	0.86	100.55
Pl43.1	30.5	66.5	3.0	2.69	1.31	b.d.l.	0.0012	0.31	0.0025	0.0009	0.67	0.030	13.01	59.89	24.69	b.d.l.	0.019	6.37	0.097	0.052	7.67	0.53	99.32
Pl43.1b	30.9	65.7	3.3	2.74	1.25	0.011	0.0009	0.30	0.0028	0.0012	0.64	0.032	12.97	b.d.l.	b.d.l.	b.d.l.	b.d.l.	b.d.l.	b.d.l.	b.d.l.	b.d.l.	b.d.l.	103.29
Pl43.2	31.9	64.7	3.4	2.69	1.30	0.011	0.0012	0.32	0.0031	0.0012	0.64	0.034	13.00	60.72	24.96	0.29	0.018	6.69	0.123	0.067	7.50	0.61	100.98
Pl43.3	30.3	66.1	3.6	2.69	1.30	0.011	0.0014	0.30	0.0029	0.0013	0.66	0.036	13.01	59.80	24.59	0.29	0.020	6.26	0.112	0.076	7.55	0.63	99.33
Pl5	30.8	64.9	4.2	2.71	1.28	0.011	0.0010	0.30	0.0020	0.0019	0.64	0.042	12.99	61.30	24.49	0.29	0.015	6.43	0.078	0.111	7.48	0.74	100.91
Pl6.1	33.7	62.0	4.3	2.69	1.30	0.010	0.0010	0.33	0.0031	0.0012	0.61	0.043	12.99	60.73	24.81	0.27	0.015	7.02	0.121	0.068	7.15	0.75	100.94
Pl6.2	58.0	40.8	1.3	2.40	1.59	0.012	0.0017	0.58	0.0042	b.d.l.	0.41	0.013	13.02	53.07	29.88	0.31	0.025	12.03	0.164	b.d.l.	4.68	0.22	100.38
Pl7	27.0	69.0	4.0	2.73	1.26	0.009	0.0008	0.27	0.0033	0.0015	0.69	0.040	13.01	61.95	24.34	0.26	0.013	5.70	0.130	0.085	8.08	0.71	101.26
Pl8	32.5	64.1	3.4	2.68	1.32	0.010	0.0008	0.32	0.0029	0.0012	0.62	0.033	12.99	60.89	25.39	0.28	0.013	6.69	0.115	0.068	7.29	0.59	101.33
Pl9	31.5	64.5	3.9	2.69	1.30	0.011	0.0005	0.31	0.0032	0.0012	0.64	0.039	13.00	60.83	24.99	0.30	0.008	6.56	0.125	0.068	7.44	0.69	101.01
Mount_VQ-06-06 125-250 µm (1846/47)																							
Pl1	26.9	69.5	3.6	2.74	1.26	0.009	0.0006	0.27	0.0032	0.0012	0.68	0.035	12.99	61.66	24.09	0.25	b.d.l.	5.57	0.124	0.066	7.95	0.62	100.35
Pl10	44.8	53.2	2.0	2.54	1.44	0.011	0.0009	0.45	0.0030	0.0007	0.54	0.020	13.01	56.53	27.24	0.28	0.013	9.39	0.114	b.d.l.	6.16	0.35	100.11

Appendix B1 cotinued

Label	An[2]	Ab[3]	Or[4]	Si	Al	Fe	Mg	Ca	Sr	Ba	Na	K	Tot[5]	SiO_2	Al_2O_3	FeO	MgO	CaO	SrO	BaO	Na_2O	K_2O	Tot
Pl11	32.1	64.7	3.2	2.69	1.30	0.010	0.0010	0.32	0.0024	0.0017	0.64	0.031	13.00	60.49	24.78	0.26	0.015	6.72	0.094	0.098	7.47	0.55	100.49
Pl13	44.5	53.7	1.9	2.55	1.44	0.010	0.0004	0.45	0.0036	0.0007	0.54	0.019	13.01	56.27	26.94	0.26	b.d.l.	9.28	0.136	b.d.l.	6.19	0.33	99.46
Pl14	56.5	42.4	1.2	2.45	1.54	0.019	0.0036	0.56	0.0047	0.0005	0.42	0.012	13.00	53.60	28.55	0.49	0.053	11.38	0.178	b.d.l.	4.72	0.20	99.20
Pl15	48.3	50.1	1.5	2.52	1.47	0.018	0.0032	0.48	0.0029	0.0003	0.50	0.015	13.00	55.95	27.72	0.48	0.048	9.90	0.112	b.d.l.	5.68	0.27	100.17
Pl16	31.4	65.7	2.9	2.68	1.32	0.010	0.0010	0.31	0.0030	0.0012	0.65	0.029	13.00	59.99	25.01	0.27	0.015	6.53	0.114	0.071	7.54	0.51	100.05
Pl17	39.8	58.0	2.3	2.59	1.40	0.011	0.0018	0.40	0.0041	0.0007	0.58	0.023	13.01	57.72	26.48	0.29	0.027	8.27	0.157	b.d.l.	6.66	0.40	100.04
Pl18	33.2	64.0	2.9	2.68	1.31	0.012	0.0016	0.33	0.0025	0.0010	0.64	0.029	13.00	60.42	25.07	0.31	0.024	6.98	0.097	b.d.l.	7.43	0.50	100.89
Pl19	31.5	65.5	3.0	2.68	1.31	0.011	0.0016	0.31	0.0034	0.0013	0.65	0.030	13.01	60.44	25.02	0.29	0.025	6.61	0.131	0.076	7.60	0.54	100.73
Pl2	25.6	70.4	4.0	2.76	1.23	0.011	0.0002	0.25	0.0029	0.0015	0.70	0.040	13.00	62.06	23.53	0.31	b.d.l.	5.33	0.112	0.084	8.10	0.70	100.23
Pl20	41.3	56.6	2.0	2.59	1.40	0.012	0.0010	0.41	0.0031	0.0011	0.56	0.020	13.00	57.71	26.50	0.32	0.015	8.47	0.119	b.d.l.	6.41	0.35	99.97
Pl21	26.7	69.3	4.0	2.75	1.24	0.010	0.0010	0.26	0.0028	0.0015	0.68	0.040	12.99	62.14	23.75	0.27	0.015	5.51	0.109	0.086	7.91	0.70	100.49
Pl22	34.8	62.4	2.9	2.65	1.34	0.009	0.0008	0.35	0.0025	0.0009	0.62	0.029	13.01	59.05	25.36	0.24	0.013	7.24	0.094	b.d.l.	7.17	0.50	99.71
Pl23	46.8	51.8	1.4	2.53	1.46	0.012	0.0004	0.47	0.0038	0.0004	0.52	0.014	13.00	56.14	27.44	0.31	b.d.l.	9.65	0.144	b.d.l.	5.91	0.25	99.86
Pl24	33.1	64.0	2.9	2.66	1.33	0.012	0.0019	0.33	0.0027	0.0009	0.64	0.029	13.01	59.78	25.24	0.31	0.028	6.92	0.104	b.d.l.	7.39	0.51	100.33
Pl26	28.9	67.5	3.6	2.72	1.28	0.011	0.0012	0.28	0.0023	0.0018	0.66	0.035	12.99	61.28	24.42	0.30	0.019	5.96	0.090	0.106	7.69	0.61	100.48
Pl27	53.8	45.0	1.2	2.45	1.54	0.012	0.0010	0.54	0.0030	0.0010	0.45	0.012	13.01	53.99	28.75	0.31	0.014	10.99	0.113	b.d.l.	5.08	0.20	99.49
Pl28	30.5	66.3	3.2	2.72	1.27	0.012	0.0009	0.30	0.0019	0.0012	0.65	0.032	12.99	61.07	24.27	0.33	0.014	6.30	0.074	0.067	7.56	0.56	100.25
Pl29	31.6	65.3	3.0	2.68	1.31	0.012	0.0015	0.32	0.0032	0.0009	0.65	0.030	13.01	60.02	24.80	0.33	0.022	6.60	0.124	b.d.l.	7.53	0.53	100.02
Pl3	41.0	57.1	1.9	2.58	1.40	0.011	0.0002	0.41	0.0032	0.0014	0.58	0.019	13.01	57.24	26.34	0.29	b.d.l.	8.57	0.122	0.079	6.58	0.34	99.57
Pl30	27.6	68.8	3.6	2.74	1.26	0.011	0.0001	0.27	0.0027	0.0011	0.67	0.035	12.99	61.54	24.05	0.29	b.d.l.	5.67	0.106	b.d.l.	7.81	0.61	100.14
Pl31	45.9	52.3	1.8	2.53	1.46	0.011	0.0010	0.46	0.0041	b.d.l.	0.53	0.018	13.01	56.06	27.35	0.28	0.015	9.54	0.155	b.d.l.	6.01	0.31	99.72
Pl32	29.1	67.5	3.4	2.71	1.28	0.010	0.0012	0.29	0.0030	0.0013	0.66	0.034	12.99	60.98	24.39	0.27	0.019	5.99	0.115	0.076	7.69	0.60	100.13
Pl33.1	28.8	68.0	3.1	2.72	1.27	0.012	0.0011	0.29	0.0028	0.0014	0.68	0.031	13.00	61.34	24.33	0.33	0.016	6.03	0.109	0.082	7.87	0.55	100.66
Pl33.2	29.0	67.7	3.2	2.71	1.28	0.011	0.0005	0.28	0.0029	0.0016	0.66	0.032	12.99	61.20	24.55	0.29	b.d.l.	6.00	0.112	0.094	7.73	0.56	100.53
Pl5	38.4	59.3	2.4	2.62	1.38	0.011	0.0006	0.38	0.0035	0.0011	0.59	0.024	13.00	58.60	26.18	0.28	b.d.l.	7.91	0.136	b.d.l.	6.76	0.41	100.35
Pl6	30.4	66.3	3.3	2.70	1.29	0.010	0.0001	0.30	0.0033	0.0011	0.66	0.032	13.00	60.63	24.66	0.27	b.d.l.	6.31	0.129	0.066	7.59	0.57	100.23
Pl7	31.7	65.1	3.2	2.69	1.30	0.011	0.0002	0.31	0.0028	0.0013	0.64	0.032	13.00	60.33	24.67	0.28	b.d.l.	6.57	0.109	0.075	7.45	0.56	100.05
Pl8	50.0	48.6	1.4	2.52	1.47	0.012	0.0011	0.49	0.0037	0.0002	0.48	0.014	12.99	56.02	27.69	0.31	0.016	10.27	0.141	b.d.l.	5.50	0.24	100.20
Pl9	36.5	60.9	2.6	2.64	1.35	0.011	0.0003	0.37	0.0034	0.0005	0.61	0.026	13.01	58.57	25.45	0.30	b.d.l.	7.62	0.128	b.d.l.	7.02	0.45	99.58

Appendix B1 cotinued

Label	An[2]	Ab[3]	Or[4]	Si	Al	Fe	Mg	Ca	Sr	Ba	Na	K	Tot[5]	SiO_2	Al_2O_3	FeO	MgO	CaO	SrO	BaO	Na_2O	K_2O	Tot
Mount_VQ-06-22A 125-250 µm (1846/47)																							
Pl1	32.7	64.1	3.2	2.68	1.31	0.012	0.0015	0.33	0.0020	0.0013	0.65	0.032	13.01	59.78	24.83	0.32	0.023	6.87	0.078	0.074	7.44	0.56	99.97
Pl10	81.1	18.6	0.3	2.18	1.79	0.019	0.0063	0.83	0.0034	0.0002	0.19	0.003	13.02	47.17	32.90	0.50	0.091	16.67	0.127	b.d.l.	2.12	0.05	99.64
Pl11	67.7	31.4	0.9	2.33	1.64	0.024	0.0088	0.68	0.0035	0.0001	0.32	0.009	13.01	50.55	30.19	0.62	0.128	13.83	0.133	b.d.l.	3.54	0.16	99.15
Pl12	83.6	16.2	0.2	2.17	1.81	0.017	0.0062	0.83	0.0036	0.0006	0.16	0.002	13.01	46.88	33.22	0.45	0.090	16.79	0.133	b.d.l.	1.80	0.04	99.43
Pl13	67.0	32.3	0.7	2.38	1.59	0.028	0.0075	0.66	0.0029	0.0003	0.32	0.007	12.99	52.31	29.77	0.74	0.111	13.53	0.109	b.d.l.	3.61	0.12	100.31
Pl14	68.8	30.6	0.7	2.36	1.61	0.023	0.0082	0.68	0.0021	0.0002	0.30	0.007	12.99	51.27	29.61	0.58	0.120	13.85	0.080	b.d.l.	3.40	0.11	99.04
Pl15	59.5	39.5	1.0	2.42	1.54	0.029	0.0092	0.60	0.0027	0.0003	0.40	0.010	13.02	52.68	28.53	0.75	0.135	12.25	0.103	b.d.l.	4.50	0.18	99.14
Pl16	66.6	32.7	0.7	2.36	1.61	0.025	0.0081	0.67	0.0031	b.d.l.	0.33	0.007	13.01	51.26	29.72	0.65	0.119	13.60	0.118	b.d.l.	3.69	0.12	99.28
Pl17	34.5	62.6	2.9	2.67	1.31	0.013	0.0008	0.34	0.0032	0.0007	0.62	0.029	12.99	59.89	24.94	0.34	b.d.l.	7.15	0.124	b.d.l.	7.16	0.50	100.16
Pl18	61.5	37.5	1.0	2.41	1.57	0.026	0.0095	0.60	0.0029	0.0006	0.37	0.010	13.00	53.23	29.52	0.67	0.141	12.44	0.110	b.d.l.	4.18	0.17	100.50
Pl19	72.1	27.3	0.6	2.33	1.64	0.024	0.0076	0.71	0.0032	0.0002	0.27	0.006	12.99	50.88	30.43	0.61	0.112	14.47	0.120	b.d.l.	3.02	0.10	99.77
Pl2	66.0	33.2	0.8	2.34	1.63	0.026	0.0104	0.67	0.0027	b.d.l.	0.34	0.008	13.02	51.03	30.08	0.68	0.152	13.66	0.103	b.d.l.	3.80	0.14	99.64
Pl20	26.2	70.1	3.7	2.75	1.23	0.011	0.0012	0.26	0.0032	0.0011	0.70	0.037	13.00	61.75	23.43	0.30	0.018	5.50	0.124	b.d.l.	8.14	0.66	99.97
Pl21	83.9	15.8	0.2	2.18	1.79	0.016	0.0066	0.85	0.0031	0.0004	0.16	0.002	13.01	47.23	33.01	0.41	0.096	17.14	0.115	b.d.l.	1.79	0.04	99.85
Pl3	28.7	68.1	3.3	2.73	1.26	0.013	0.0019	0.29	0.0023	0.0010	0.68	0.033	13.00	61.08	23.93	0.35	0.029	5.99	0.089	b.d.l.	7.85	0.57	99.95
Pl4	67.6	31.9	0.6	2.33	1.64	0.024	0.0090	0.68	0.0024	0.0005	0.32	0.006	13.02	50.80	30.33	0.62	0.132	13.93	0.089	b.d.l.	3.63	0.10	99.64
Pl5	84.3	15.5	0.2	2.17	1.81	0.018	0.0057	0.85	0.0019	0.0002	0.16	0.003	13.01	46.91	33.10	0.47	0.083	17.06	0.070	b.d.l.	1.73	0.04	99.49
Pl6	30.4	66.3	3.3	2.68	1.30	0.012	0.0015	0.31	0.0024	0.0008	0.68	0.034	13.03	59.49	24.49	0.32	0.022	6.46	0.092	b.d.l.	7.78	0.59	99.29
Pl8	86.2	13.6	0.2	2.13	1.84	0.015	0.0058	0.88	0.0040	b.d.l.	0.14	0.002	13.02	45.82	33.67	0.39	0.083	17.64	0.149	b.d.l.	1.54	0.03	99.32
Pl9	56.5	41.4	2.1	2.45	1.52	0.028	0.0098	0.57	0.0019	0.0002	0.42	0.021	13.01	54.07	28.48	0.75	0.145	11.74	0.074	b.d.l.	4.75	0.37	100.37
Mount_VQ-06-22D 125-250 µm (1846/47)																							
Pl1	31.1	65.9	3.0	2.66	1.33	0.011	0.0014	0.32	0.0017	0.0014	0.68	0.032	13.04	b.d.l.	b.d.l.	b.d.l.	b.d.l.	b.d.l.	b.d.l.	b.d.l.	b.d.l.	b.d.l.	98.29
Pl10	51.0	47.4	1.6	2.51	1.48	0.011	0.0010	0.51	0.0028	0.0004	0.47	0.016	13.00	b.d.l.	b.d.l.	b.d.l.	b.d.l.	b.d.l.	b.d.l.	b.d.l.	b.d.l.	b.d.l.	102.03
Pl12	32.1	65.0	2.9	2.64	1.34	0.012	0.0014	0.33	0.0034	0.0012	0.67	0.030	13.04	b.d.l.	b.d.l.	b.d.l.	b.d.l.	b.d.l.	b.d.l.	b.d.l.	b.d.l.	b.d.l.	97.42
Pl13	51.5	47.3	1.2	3.31	0.13	0.014	0.0027	0.78	0.0042	0.0015	0.72	0.018	12.99	b.d.l.	b.d.l.	b.d.l.	b.d.l.	b.d.l.	b.d.l.	b.d.l.	b.d.l.	b.d.l.	68.08
Pl13	51.7	46.9	1.4	2.50	1.50	0.010	0.0017	0.51	0.0031	0.0012	0.46	0.014	12.99	b.d.l.	b.d.l.	b.d.l.	b.d.l.	b.d.l.	b.d.l.	b.d.l.	b.d.l.	b.d.l.	98.49
Pl14	31.5	65.4	3.1	2.67	1.32	0.011	0.0011	0.32	0.0031	0.0009	0.66	0.032	13.01	59.08	24.70	0.28	0.016	6.52	0.117	b.d.l.	7.50	0.55	98.81
Pl15	35.4	61.8	2.8	2.67	1.32	0.010	0.0005	0.35	0.0022	0.0007	0.61	0.027	12.99	59.16	24.73	0.26	b.d.l.	7.19	0.082	b.d.l.	6.95	0.48	98.89
Pl16	31.6	65.4	3.0	2.70	1.29	0.011	0.0011	0.31	0.0023	0.0012	0.65	0.030	12.99	59.95	24.19	0.29	0.016	6.47	0.090	0.071	7.41	0.51	98.99

Appendix B1 cotinued

Label	An[2]	Ab[3]	Or[4]	Si	Al	Fe	Mg	Ca	Sr	Ba	Na	K	Tot[5]	SiO_2	Al_2O_3	FeO	MgO	CaO	SrO	BaO	Na_2O	K_2O	Tot
Pl17	48.1	50.5	1.4	2.49	1.50	0.011	0.0004	0.49	0.0031	0.0006	0.52	0.015	13.03	b.d.l.	b.d.l.	b.d.l.	b.d.l.	b.d.l.	b.d.l.	b.d.l.	b.d.l.	b.d.l.	98.26
Pl18	35.5	61.7	2.7	2.62	1.36	0.012	0.0019	0.36	0.0030	0.0012	0.63	0.028	13.02	57.93	25.56	0.32	0.028	7.44	0.115	0.070	7.13	0.48	99.08
Pl19	31.4	65.4	3.3	2.71	1.28	0.010	0.0018	0.31	0.0020	0.0011	0.65	0.032	12.99	61.16	24.42	0.28	0.028	6.53	0.076	b.d.l.	7.53	0.57	100.66
Pl2	28.9	67.4	3.6	2.68	1.31	0.010	0.0008	0.30	0.0038	0.0016	0.69	0.037	13.03	b.d.l.	b.d.l.	b.d.l.	b.d.l.	b.d.l.	b.d.l.	b.d.l.	b.d.l.	b.d.l.	97.37
Pl20	32.5	64.6	2.9	2.68	1.30	0.012	0.0008	0.33	0.0026	0.0014	0.65	0.029	13.01	b.d.l.	b.d.l.	b.d.l.	b.d.l.	b.d.l.	b.d.l.	b.d.l.	b.d.l.	b.d.l.	98.25
Pl21	29.6	67.1	3.3	2.72	1.27	0.012	0.0019	0.29	0.0023	0.0016	0.66	0.033	12.99	61.05	24.30	0.33	0.029	6.09	0.087	0.091	7.63	0.58	100.20
Pl22	33.6	63.9	2.5	2.69	1.30	0.011	0.0018	0.33	0.0025	0.0014	0.63	0.024	12.99	60.59	24.91	0.29	0.027	6.92	0.099	0.079	7.27	0.43	100.61
Pl23	35.6	61.8	2.5	2.66	1.32	0.011	0.0011	0.35	0.0030	0.0011	0.61	0.025	12.99	59.40	25.08	0.28	0.017	7.36	0.116	b.d.l.	7.05	0.44	99.80
Pl24	50.8	47.8	1.4	2.49	1.50	0.010	0.0013	0.51	0.0026	0.0002	0.48	0.014	13.00	b.d.l.	b.d.l.	b.d.l.	b.d.l.	b.d.l.	b.d.l.	b.d.l.	b.d.l.	b.d.l.	101.54
Pl26	31.5	65.2	3.3	2.66	1.34	0.012	0.0007	0.32	0.0021	0.0015	0.66	0.033	13.02	b.d.l.	b.d.l.	b.d.l.	b.d.l.	b.d.l.	b.d.l.	b.d.l.	b.d.l.	b.d.l.	98.05
Pl28	36.5	61.3	2.2	2.65	1.34	0.011	0.0013	0.36	0.0032	0.0013	0.61	0.022	13.00	58.49	25.23	0.28	0.019	7.46	0.124	0.071	6.94	0.37	98.99
Pl29	32.6	64.4	3.0	2.70	1.28	0.011	0.0018	0.32	0.0010	0.0011	0.63	0.030	12.99	b.d.l.	b.d.l.	b.d.l.	b.d.l.	b.d.l.	b.d.l.	b.d.l.	b.d.l.	b.d.l.	101.82
Pl3	54.8	44.1	1.1	2.46	1.53	0.010	0.0009	0.55	0.0033	0.0006	0.45	0.011	13.01	b.d.l.	b.d.l.	b.d.l.	b.d.l.	b.d.l.	b.d.l.	b.d.l.	b.d.l.	b.d.l.	102.16
Pl30	48.1	50.5	1.4	2.55	1.44	0.016	0.0017	0.47	0.0032	0.0006	0.50	0.014	12.99	57.22	27.39	0.43	0.025	9.90	0.125	b.d.l.	5.75	0.24	101.11
Pl31	32.1	64.8	3.1	2.65	1.34	0.011	0.0010	0.33	0.0035	0.0018	0.67	0.032	13.03	b.d.l.	b.d.l.	b.d.l.	b.d.l.	b.d.l.	b.d.l.	b.d.l.	b.d.l.	b.d.l.	97.03
Pl4	33.4	63.9	2.8	2.64	1.34	0.012	0.0012	0.34	0.0025	0.0007	0.65	0.028	13.02	b.d.l.	b.d.l.	b.d.l.	b.d.l.	b.d.l.	b.d.l.	b.d.l.	b.d.l.	b.d.l.	97.25
Pl5	30.1	66.9	3.1	2.66	1.32	0.012	0.0003	0.32	0.0028	0.0008	0.70	0.032	13.05	b.d.l.	b.d.l.	b.d.l.	b.d.l.	b.d.l.	b.d.l.	b.d.l.	b.d.l.	b.d.l.	98.05
Pl6	30.6	66.3	3.1	2.69	1.30	0.011	0.0019	0.31	0.0026	0.0015	0.67	0.031	13.01	59.45	24.35	0.29	0.028	6.36	0.099	0.083	7.60	0.54	98.78
Pl8	34.6	62.8	2.6	2.61	1.38	0.011	0.0017	0.36	0.0034	0.0006	0.65	0.027	13.04	b.d.l.	b.d.l.	b.d.l.	b.d.l.	b.d.l.	b.d.l.	b.d.l.	b.d.l.	b.d.l.	94.87
Pl9	41.9	56.1	2.0	2.59	1.41	0.012	0.0007	0.41	0.0027	0.0012	0.55	0.019	13.00	58.22	26.87	0.31	b.d.l.	8.68	0.105	0.070	6.42	0.34	101.03
Mount_VQ-06-22D 250-500 µm (1846/47)																							
Pl10	29.9	67.0	3.1	2.70	1.30	0.010	0.0019	0.30	0.0024	0.0008	0.67	0.031	13.00	b.d.l.	b.d.l.	b.d.l.	b.d.l.	b.d.l.	b.d.l.	b.d.l.	b.d.l.	b.d.l.	93.50
Pl11	84.4	15.2	0.3	2.16	1.82	0.017	0.0017	0.85	0.0030	b.d.l.	0.15	0.004	13.01	46.64	33.34	0.43	0.024	17.20	0.111	b.d.l.	1.72	0.06	99.51
Pl12	30.6	66.5	2.9	2.69	1.30	0.011	0.0021	0.31	0.0033	0.0014	0.67	0.029	13.01	b.d.l.	b.d.l.	b.d.l.	b.d.l.	b.d.l.	b.d.l.	b.d.l.	b.d.l.	b.d.l.	93.36
Pl13	44.8	53.3	1.9	2.56	1.43	0.010	0.0017	0.45	0.0032	0.0008	0.53	0.019	13.00	56.85	26.93	0.27	0.025	9.23	0.123	b.d.l.	6.08	0.33	99.88
Pl13(??)	32.5	64.5	3.0	2.66	1.32	0.012	0.0011	0.34	0.0032	0.0011	0.66	0.031	13.03	b.d.l.	b.d.l.	b.d.l.	b.d.l.	b.d.l.	b.d.l.	b.d.l.	b.d.l.	b.d.l.	94.27
Pl14	33.8	63.1	3.0	2.67	1.31	0.011	0.0018	0.34	0.0023	0.0010	0.63	0.030	13.00	59.94	25.03	0.29	0.027	7.09	0.088	b.d.l.	7.31	0.53	100.37
Pl15	31.1	65.6	3.3	2.69	1.28	0.013	0.0004	0.32	0.0032	0.0009	0.67	0.034	13.02	59.52	24.07	0.33	b.d.l.	6.52	0.120	b.d.l.	7.62	0.58	98.83
Pl16	30.5	65.9	3.6	2.73	1.26	0.013	0.0019	0.30	0.0027	0.0017	0.65	0.035	12.99	61.05	23.92	0.36	0.028	6.27	0.106	0.097	7.48	0.61	99.92
Pl17	32.2	64.5	3.3	2.68	1.31	0.010	0.0019	0.32	0.0023	0.0011	0.65	0.033	13.01	b.d.l.	b.d.l.	b.d.l.	b.d.l.	b.d.l.	b.d.l.	b.d.l.	b.d.l.	b.d.l.	98.04

Appendix B1 cotinued

Label	An[2]	Ab[3]	Or[4]	Si	Al	Fe	Mg	Ca	Sr	Ba	Na	K	Tot[5]	SiO_2	Al_2O_3	FeO	MgO	CaO	SrO	BaO	Na_2O	K_2O	Tot
Pl19	29.4	67.1	3.5	2.72	1.26	0.013	0.0009	0.30	0.0022	0.0016	0.68	0.035	13.01	60.61	23.92	0.33	b.d.l.	6.19	0.084	0.090	7.82	0.62	99.67
Pl2	53.1	45.6	1.3	2.44	1.55	0.014	0.0023	0.55	0.0029	0.0001	0.47	0.014	13.03	b.d.l.	b.d.l.	b.d.l.	b.d.l.	b.d.l.	b.d.l.	b.d.l.	b.d.l.	b.d.l.	98.37
Pl20	35.8	61.3	2.9	2.66	1.33	0.011	0.0013	0.36	0.0033	0.0007	0.61	0.029	13.00	58.94	24.93	0.29	0.020	7.36	0.125	b.d.l.	6.98	0.50	99.19
Pl21	34.8	62.4	2.9	2.68	1.31	0.012	0.0015	0.34	0.0029	0.0006	0.62	0.029	12.99	59.58	24.67	0.31	0.022	7.16	0.110	b.d.l.	7.10	0.50	99.48
Pl22	32.5	64.4	3.0	2.69	1.30	0.013	0.0015	0.33	0.0024	0.0010	0.65	0.031	13.01	59.47	24.34	0.35	0.023	6.78	0.092	b.d.l.	7.43	0.53	99.07
Pl23	36.5	60.8	2.7	2.65	1.33	0.012	0.0011	0.37	0.0038	0.0013	0.61	0.027	13.00	59.24	25.12	0.31	0.017	7.66	0.146	0.074	7.05	0.48	100.09
Pl24	32.4	64.5	3.1	2.66	1.33	0.010	0.0022	0.33	0.0029	0.0016	0.65	0.031	13.02	b.d.l.	b.d.l.	b.d.l.	b.d.l.	b.d.l.	b.d.l.	b.d.l.	b.d.l.	b.d.l.	95.22
Pl25	34.2	63.1	2.7	2.66	1.32	0.012	0.0017	0.34	0.0024	0.0006	0.63	0.027	13.00	b.d.l.	b.d.l.	b.d.l.	b.d.l.	b.d.l.	b.d.l.	b.d.l.	b.d.l.	b.d.l.	97.19
Pl26	44.8	53.3	1.9	2.53	1.45	0.016	0.0020	0.46	0.0047	0.0005	0.55	0.020	13.03	b.d.l.	b.d.l.	b.d.l.	b.d.l.	b.d.l.	b.d.l.	b.d.l.	b.d.l.	b.d.l.	97.64
Pl28	48.1	50.3	1.5	2.50	1.48	0.017	0.0024	0.49	0.0043	0.0006	0.52	0.016	13.03	b.d.l.	b.d.l.	b.d.l.	b.d.l.	b.d.l.	b.d.l.	b.d.l.	b.d.l.	b.d.l.	97.60
Pl3	40.8	56.9	2.3	2.60	1.38	0.012	0.0017	0.41	0.0039	0.0013	0.57	0.023	13.00	57.79	25.93	0.31	0.025	8.47	0.150	0.071	6.54	0.40	99.69
Pl4	32.7	64.0	3.3	2.63	1.34	0.012	0.0017	0.35	0.0026	0.0007	0.69	0.036	13.07	b.d.l.	b.d.l.	b.d.l.	b.d.l.	b.d.l.	b.d.l.	b.d.l.	b.d.l.	b.d.l.	92.52
Pl5	32.9	64.1	3.0	2.67	1.31	0.011	0.0017	0.33	0.0030	0.0013	0.65	0.031	13.01	59.54	24.70	0.30	0.025	6.92	0.114	0.071	7.46	0.54	99.67
Pl6	30.8	66.1	3.1	2.68	1.30	0.012	0.0020	0.31	0.0024	0.0013	0.67	0.032	13.01	59.24	24.36	0.32	0.030	6.40	0.090	0.073	7.60	0.55	98.65
Pl7	27.8	68.9	3.3	2.72	1.26	0.010	0.0013	0.28	0.0025	0.0010	0.70	0.033	13.01	b.d.l.	b.d.l.	b.d.l.	b.d.l.	b.d.l.	b.d.l.	b.d.l.	b.d.l.	b.d.l.	95.80
Pl8	27.5	69.4	3.0	2.70	1.31	0.008	0.0006	0.27	0.0023	0.0005	0.68	0.030	13.00	b.d.l.	b.d.l.	b.d.l.	b.d.l.	b.d.l.	b.d.l.	b.d.l.	b.d.l.	b.d.l.	88.04
Mount_VQ-07-44A 125-250 µm (1846/47)																							
Pl10	26.3	69.7	4.0	2.74	1.26	0.012	0.0006	0.26	0.0023	0.0013	0.69	0.039	12.99	62.10	24.16	0.31	b.d.l.	5.47	0.088	0.075	8.01	0.69	100.91
Pl11	28.6	68.1	3.3	2.70	1.29	0.012	0.0009	0.28	0.0031	0.0014	0.68	0.033	13.01	61.23	24.87	0.34	0.013	6.01	0.120	0.079	7.91	0.58	101.14
Pl12	40.7	57.4	1.9	2.58	1.43	0.009	0.0007	0.40	0.0025	0.0007	0.56	0.019	13.00	57.35	27.09	0.24	b.d.l.	8.24	0.097	b.d.l.	6.43	0.33	99.83
Pl13	83.9	15.9	0.2	2.16	1.83	0.024	0.0045	0.84	0.0035	0.0004	0.16	0.002	13.01	47.14	33.85	0.61	0.066	17.04	0.131	b.d.l.	1.79	b.d.l.	100.67
Pl15	41.3	56.7	2.1	2.58	1.42	0.011	0.0015	0.41	0.0043	0.0002	0.56	0.020	13.00	57.41	26.77	0.30	0.022	8.48	0.166	b.d.l.	6.44	0.35	99.95
Pl16	84.3	15.5	0.2	2.15	1.83	0.024	0.0053	0.85	0.0037	0.0004	0.16	0.002	13.01	46.80	33.68	0.63	0.077	17.16	0.140	b.d.l.	1.75	b.d.l.	100.28
Pl17	27.4	68.8	3.8	2.72	1.27	0.010	0.0012	0.28	0.0032	0.0012	0.69	0.038	13.01	61.38	24.28	0.28	0.018	5.80	0.124	0.068	8.06	0.67	100.67
Pl18	27.9	68.4	3.7	2.73	1.26	0.011	0.0010	0.27	0.0025	0.0011	0.67	0.036	12.99	61.62	24.14	0.30	0.015	5.72	0.099	b.d.l.	7.76	0.63	100.35
Pl20	83.4	16.4	0.2	2.16	1.83	0.024	0.0039	0.82	0.0042	b.d.l.	0.16	0.002	13.01	47.06	33.96	0.64	0.057	16.81	0.158	b.d.l.	1.83	0.04	100.54
Pl21	40.9	57.2	1.9	2.57	1.42	0.010	0.0010	0.41	0.0037	0.0012	0.58	0.019	13.02	57.58	27.00	0.26	0.015	8.59	0.142	0.068	6.65	0.34	100.64
Pl22	79.5	20.2	0.3	2.22	1.77	0.025	0.0051	0.77	0.0033	0.0002	0.20	0.003	13.00	48.34	32.83	0.65	0.075	15.74	0.125	b.d.l.	2.20	0.05	100.02
Pl24	82.7	17.1	0.3	2.15	1.84	0.025	0.0049	0.81	0.0034	0.0004	0.17	0.003	13.01	47.15	34.21	0.66	0.073	16.50	0.128	b.d.l.	1.88	0.04	100.66
Pl25	31.4	65.7	2.9	2.68	1.32	0.009	0.0010	0.31	0.0039	0.0002	0.65	0.029	13.00	60.51	25.20	0.24	0.015	6.51	0.150	b.d.l.	7.52	0.51	100.66

Appendix B1 cotinued

Label	An[2]	Ab[3]	Or[4]	Si	Al	Fe	Mg	Ca	Sr	Ba	Na	K	Tot[5]	SiO_2	Al_2O_3	FeO	MgO	CaO	SrO	BaO	Na_2O	K_2O	Tot
Pl26	34.9	62.6	2.5	2.63	1.36	0.011	0.0015	0.35	0.0029	0.0007	0.63	0.026	13.02	58.86	25.80	0.29	0.023	7.32	0.110	b.d.l.	7.26	0.45	100.15
Pl27	24.6	71.4	4.1	2.76	1.23	0.012	0.0008	0.24	0.0021	0.0009	0.70	0.040	12.99	62.67	23.78	0.32	0.013	5.12	0.081	b.d.l.	8.22	0.71	100.98
Pl28	28.4	68.3	3.4	2.70	1.28	0.011	0.0003	0.29	0.0029	0.0012	0.69	0.034	13.02	60.48	24.36	0.28	b.d.l.	6.00	0.113	0.070	7.98	0.60	99.87
Pl29	81.5	18.1	0.4	2.18	1.79	0.028	0.0069	0.81	0.0045	0.0004	0.18	0.004	13.01	47.68	33.24	0.74	0.101	16.53	0.169	b.d.l.	2.03	0.06	100.57
Pl3	76.1	23.4	0.4	2.24	1.75	0.026	0.0052	0.74	0.0040	0.0001	0.23	0.004	13.00	49.01	32.64	0.67	0.076	15.22	0.150	b.d.l.	2.59	0.07	100.44
Pl4	82.0	17.8	0.2	2.17	1.83	0.024	0.0051	0.80	0.0044	b.d.l.	0.17	0.002	13.01	47.49	34.04	0.63	0.075	16.42	0.166	b.d.l.	1.97	0.03	100.82
Pl5	36.9	60.5	2.6	2.61	1.38	0.011	0.0006	0.37	0.0030	0.0008	0.61	0.026	13.01	58.68	26.30	0.30	b.d.l.	7.76	0.116	b.d.l.	7.04	0.47	100.71
Pl6	80.3	19.2	0.4	2.19	1.81	0.026	0.0045	0.79	0.0031	b.d.l.	0.19	0.004	13.01	47.59	33.36	0.68	0.066	15.96	0.117	b.d.l.	2.11	0.07	99.96
Pl7	36.0	61.5	2.5	2.64	1.36	0.009	0.0007	0.36	0.0033	0.0013	0.61	0.025	13.00	59.13	25.85	0.25	b.d.l.	7.49	0.130	0.073	7.07	0.43	100.44
Pl8	60.1	39.0	0.9	2.39	1.61	0.014	0.0017	0.59	0.0027	b.d.l.	0.38	0.009	13.00	52.70	30.07	0.37	0.025	12.15	0.103	b.d.l.	4.36	0.16	99.93
Q-16 (1932)																							
Pl1.1	88.0	11.7	0.3	2.10	1.88	0.027	0.0031	0.90	0.0046	0.0008	0.12	0.003	13.03	44.64	33.92	0.67	0.045	17.84	0.170	b.d.l.	1.31	0.05	98.69
Pl1.2	83.6	16.0	0.4	2.13	1.85	0.026	0.0055	0.85	0.0035	b.d.l.	0.16	0.004	13.03	b.d.l.	b.d.l.	b.d.l.	b.d.l.	b.d.l.	b.d.l.	b.d.l.	b.d.l.	b.d.l.	98.18
Pl1.3	68.1	30.8	1.2	2.31	1.66	0.031	0.0055	0.69	0.0042	b.d.l.	0.31	0.012	13.03	49.85	30.45	0.79	0.079	13.96	0.155	b.d.l.	3.48	0.20	98.96
Pl1.4	85.1	14.6	0.3	2.15	1.83	0.030	0.0039	0.85	0.0027	0.0016	0.15	0.003	13.01	46.33	33.46	0.77	0.056	17.01	0.100	b.d.l.	1.61	0.05	99.47
Pl1.5	85.3	14.3	0.4	2.12	1.87	0.023	0.0038	0.85	0.0041	0.0003	0.14	0.004	13.02	b.d.l.	b.d.l.	b.d.l.	b.d.l.	b.d.l.	b.d.l.	b.d.l.	b.d.l.	b.d.l.	97.86
Pl1.6	58.6	39.8	1.5	2.44	1.53	0.032	0.0086	0.58	0.0034	0.0007	0.40	0.015	13.01	53.40	28.37	0.84	0.126	11.96	0.130	b.d.l.	4.49	0.26	99.62
Pl11.1	87.8	12.0	0.1	2.11	1.88	0.021	0.0031	0.87	0.0044	b.d.l.	0.12	0.001	13.01	45.15	34.14	0.53	0.044	17.39	0.161	b.d.l.	1.32	b.d.l.	98.76
Pl11.2	73.0	26.4	0.6	2.25	1.73	0.026	0.0037	0.74	0.0047	b.d.l.	0.27	0.006	13.02	48.78	31.72	0.67	0.054	14.88	0.174	b.d.l.	2.97	0.10	99.35
Pl13.1	55.2	43.2	1.6	2.45	1.53	0.032	0.0079	0.55	0.0035	0.0009	0.43	0.016	13.01	b.d.l.	b.d.l.	b.d.l.	b.d.l.	b.d.l.	b.d.l.	b.d.l.	b.d.l.	b.d.l.	98.39
Pl13.2	57.3	40.9	1.8	2.43	1.55	0.032	0.0082	0.57	0.0028	0.0004	0.41	0.018	13.01	52.75	28.50	0.82	0.120	11.61	0.104	b.d.l.	4.58	0.31	98.81
Pl13.3	56.5	41.9	1.5	2.44	1.53	0.032	0.0082	0.57	0.0037	b.d.l.	0.42	0.016	13.01	53.02	28.26	0.83	0.120	11.49	0.137	b.d.l.	4.71	0.26	98.84
Pl13.4	62.0	36.5	1.5	2.38	1.59	0.029	0.0073	0.63	0.0031	0.0001	0.37	0.015	13.02	51.82	29.45	0.77	0.107	12.82	0.117	b.d.l.	4.18	0.26	99.52
Pl13.5	59.3	39.2	1.4	2.41	1.56	0.033	0.0069	0.60	0.0031	0.0002	0.39	0.014	13.02	52.24	28.59	0.85	0.101	12.05	0.114	b.d.l.	4.41	0.25	98.61
Pl13.6	64.7	34.0	1.3	2.36	1.61	0.034	0.0073	0.65	0.0037	0.0004	0.34	0.013	13.01	51.00	29.61	0.88	0.106	13.04	0.138	b.d.l.	3.79	0.22	98.82
Pl13.7	51.5	46.3	2.2	2.49	1.48	0.035	0.0073	0.51	0.0034	0.0002	0.46	0.022	13.01	54.39	27.43	0.92	0.108	10.47	0.128	b.d.l.	5.20	0.38	99.03
Pl14.1	71.6	27.5	0.9	2.27	1.70	0.025	0.0059	0.72	0.0043	b.d.l.	0.28	0.009	13.02	49.02	31.19	0.64	0.086	14.55	0.159	b.d.l.	3.08	0.16	98.89
Pl14.2	54.7	43.4	2.0	2.45	1.52	0.029	0.0072	0.55	0.0037	0.0006	0.43	0.020	13.01	53.48	28.10	0.76	0.105	11.14	0.141	b.d.l.	4.88	0.33	98.98
Pl14.3	61.3	37.4	1.3	2.39	1.58	0.031	0.0069	0.61	0.0033	0.0008	0.37	0.013	13.01	51.89	29.09	0.79	0.101	12.41	0.122	b.d.l.	4.17	0.22	98.85
Pl15.1	58.9	39.8	1.2	2.41	1.57	0.027	0.0098	0.58	0.0032	0.0010	0.39	0.012	13.01	52.43	29.03	0.70	0.143	11.86	0.121	b.d.l.	4.43	0.21	98.98

Appendix B1 cotinued

Label	An[2]	Ab[3]	Or[4]	Si	Al	Fe	Mg	Ca	Sr	Ba	Na	K	Tot[5]	SiO_2	Al_2O_3	FeO	MgO	CaO	SrO	BaO	Na_2O	K_2O	Tot
Pl15.2	67.2	32.0	0.9	2.33	1.65	0.025	0.0096	0.66	0.0036	0.0005	0.32	0.009	13.01	50.57	30.24	0.65	0.139	13.39	0.134	b.d.l.	3.53	0.14	98.82
Pl15.3	70.9	28.3	0.8	2.29	1.69	0.026	0.0081	0.71	0.0050	0.0004	0.28	0.008	13.01	49.52	31.03	0.66	0.117	14.30	0.186	b.d.l.	3.16	0.13	99.13
Pl15.4	66.7	32.3	0.9	2.33	1.65	0.026	0.0083	0.66	0.0040	0.0001	0.32	0.009	13.01	50.97	30.51	0.68	0.121	13.40	0.150	b.d.l.	3.59	0.16	99.58
Pl15.5	66.3	32.4	1.3	2.34	1.62	0.045	0.0238	0.65	0.0030	0.0004	0.32	0.013	13.01	50.66	29.72	1.15	0.345	13.04	0.113	b.d.l.	3.52	0.21	98.78
Pl15.6	71.8	27.4	0.8	2.28	1.70	0.027	0.0074	0.72	0.0032	b.d.l.	0.27	0.008	13.02	49.52	31.31	0.70	0.109	14.59	0.121	b.d.l.	3.08	0.14	99.57
Pl16.1	30.9	65.0	4.1	2.69	1.31	0.013	0.0006	0.30	0.0027	0.0004	0.63	0.040	12.99	b.d.l.	b.d.l.	b.d.l.	b.d.l.	b.d.l.	b.d.l.	b.d.l.	b.d.l.	b.d.l.	97.96
Pl16.2	45.3	51.7	3.0	2.53	1.44	0.032	0.0064	0.46	0.0027	0.0005	0.52	0.030	13.02	55.24	26.68	0.83	0.093	9.28	0.101	b.d.l.	5.84	0.51	98.59
Pl17.1	58.2	40.1	1.8	2.42	1.56	0.030	0.0065	0.58	0.0038	0.0003	0.40	0.017	13.01	52.78	28.86	0.79	0.095	11.78	0.143	b.d.l.	4.49	0.30	99.24
Pl17.2	86.1	13.5	0.4	2.14	1.85	0.024	0.0034	0.86	0.0031	b.d.l.	0.13	0.004	13.01	45.71	33.51	0.62	0.049	17.13	0.114	b.d.l.	1.49	0.06	98.68
Pl17.3	78.8	20.6	0.6	2.20	1.78	0.025	0.0048	0.78	0.0039	b.d.l.	0.20	0.006	13.01	b.d.l.	b.d.l.	b.d.l.	b.d.l.	b.d.l.	b.d.l.	b.d.l.	b.d.l.	b.d.l.	98.34
Pl17.4	56.7	41.7	1.7	2.44	1.53	0.031	0.0067	0.57	0.0034	0.0005	0.42	0.017	13.02	52.89	28.09	0.80	0.098	11.60	0.126	b.d.l.	4.71	0.28	98.63
Pl18.1	34.3	61.9	3.8	2.67	1.32	0.011	0.0012	0.34	0.0024	0.0009	0.61	0.038	12.99	59.44	24.99	0.30	0.018	7.05	0.091	b.d.l.	7.01	0.65	99.60
Pl18.2	34.2	61.9	3.9	2.67	1.33	0.011	0.0021	0.33	0.0035	0.0015	0.60	0.038	12.99	59.34	24.99	0.29	0.031	6.91	0.135	0.087	6.91	0.65	99.35
Pl18.3	46.9	50.4	2.7	2.54	1.45	0.010	0.0017	0.47	0.0034	0.0014	0.50	0.027	13.00	56.06	27.23	0.27	0.026	9.63	0.129	0.079	5.72	0.46	99.60
Pl18.4	39.3	57.2	3.4	2.63	1.37	0.012	0.0016	0.39	0.0026	0.0010	0.56	0.034	12.99	58.10	25.65	0.31	0.024	7.97	0.099	b.d.l.	6.40	0.59	99.19
Pl18.5	33.9	62.0	4.1	2.67	1.32	0.011	0.0016	0.33	0.0027	0.0015	0.61	0.040	12.99	59.53	25.02	0.29	0.025	6.93	0.105	0.088	7.00	0.70	99.70
Pl18.6	43.8	53.6	2.6	2.56	1.43	0.010	0.0014	0.44	0.0036	0.0013	0.54	0.026	13.01	56.84	26.83	0.26	0.020	9.08	0.136	b.d.l.	6.14	0.45	99.83
Pl18.7	47.2	49.9	2.9	2.55	1.43	0.030	0.0066	0.46	0.0035	0.0006	0.49	0.028	13.00	56.24	26.79	0.80	0.098	9.57	0.134	b.d.l.	5.59	0.49	99.75
Pl2.1	41.9	53.3	4.8	2.62	1.34	0.037	0.0056	0.41	0.0024	0.0012	0.52	0.047	12.99	57.77	25.11	0.99	0.083	8.37	0.091	b.d.l.	5.89	0.81	99.19
Pl2.2	84.1	15.4	0.6	2.14	1.84	0.027	0.0034	0.84	0.0031	b.d.l.	0.15	0.006	13.02	b.d.l.	b.d.l.	b.d.l.	b.d.l.	b.d.l.	b.d.l.	b.d.l.	b.d.l.	b.d.l.	98.09
Pl2.3	84.5	15.1	0.4	2.15	1.84	0.024	0.0036	0.84	0.0045	b.d.l.	0.15	0.004	13.01	45.96	33.42	0.60	0.052	16.74	0.166	b.d.l.	1.65	0.07	98.66
Pl2.4	70.3	28.9	0.8	2.29	1.69	0.029	0.0053	0.70	0.0031	0.0003	0.29	0.008	13.02	49.60	31.06	0.76	0.078	14.26	0.115	b.d.l.	3.23	0.14	99.26
Pl23.1	48.1	50.0	1.9	2.53	1.46	0.018	0.0024	0.48	0.0038	b.d.l.	0.50	0.019	13.00	55.90	27.31	0.46	0.036	9.88	0.146	b.d.l.	5.67	0.32	99.73
Pl23.2	57.5	41.2	1.4	2.43	1.54	0.030	0.0089	0.58	0.0029	0.0004	0.41	0.014	13.01	52.85	28.50	0.79	0.131	11.70	0.108	b.d.l.	4.63	0.23	98.96
Pl23.3	60.7	38.0	1.3	2.39	1.58	0.030	0.0063	0.61	0.0033	0.0006	0.38	0.013	13.02	52.04	29.17	0.79	0.092	12.42	0.125	b.d.l.	4.29	0.23	99.19
Pl5.1	58.4	37.9	3.6	2.43	1.54	0.036	0.0057	0.57	0.0030	0.0001	0.37	0.035	13.00	52.90	28.45	0.92	0.083	11.60	0.111	b.d.l.	4.16	0.60	98.83
Pl5.2	60.1	38.7	1.1	2.39	1.58	0.027	0.0075	0.61	0.0039	0.0001	0.39	0.011	13.02	52.25	29.31	0.69	0.111	12.41	0.146	b.d.l.	4.42	0.19	99.54
Pl5.3	77.0	22.5	0.5	2.23	1.76	0.024	0.0067	0.76	0.0032	0.0001	0.22	0.005	13.01	b.d.l.	b.d.l.	b.d.l.	b.d.l.	b.d.l.	b.d.l.	b.d.l.	b.d.l.	b.d.l.	98.25
Pl7.1	34.7	61.0	4.3	2.66	1.34	0.013	0.0022	0.34	0.0042	0.0005	0.60	0.042	13.00	58.86	25.12	0.34	0.032	7.04	0.159	b.d.l.	6.84	0.74	99.15
Pl7.2	33.0	63.2	3.8	2.68	1.32	0.012	0.0017	0.32	0.0028	0.0009	0.62	0.037	12.99	59.41	24.82	0.31	0.026	6.66	0.107	b.d.l.	7.04	0.65	99.07

Appendix B1 cotinued

Label	An[2]	Ab[3]	Or[4]	Si	Al	Fe	Mg	Ca	Sr	Ba	Na	K	Tot[5]	SiO_2	Al_2O_3	FeO	MgO	CaO	SrO	BaO	Na_2O	K_2O	Tot
Pl7.3	35.3	61.4	3.3	2.64	1.35	0.013	0.0018	0.35	0.0032	0.0004	0.60	0.033	13.00	58.50	25.37	0.34	0.026	7.17	0.121	b.d.l.	6.89	0.57	99.01
Pl7.4	45.1	52.1	2.8	2.54	1.43	0.030	0.0062	0.45	0.0036	0.0011	0.52	0.028	13.02	55.98	26.78	0.78	0.092	9.32	0.136	b.d.l.	5.95	0.48	99.59
Pl8.1	59.8	38.6	1.6	2.42	1.56	0.028	0.0072	0.59	0.0034	0.0004	0.38	0.015	13.00	52.99	28.95	0.73	0.106	12.09	0.128	b.d.l.	4.31	0.26	99.58
Pl8.2	49.7	48.2	2.1	2.51	1.47	0.018	0.0060	0.49	0.0042	0.0006	0.48	0.021	13.00	55.44	27.43	0.48	0.089	10.16	0.160	b.d.l.	5.45	0.37	99.61
Pl8.3	61.6	37.1	1.3	2.39	1.58	0.030	0.0083	0.62	0.0033	0.0005	0.37	0.013	13.01	52.13	29.26	0.78	0.121	12.56	0.123	b.d.l.	4.18	0.22	99.40
Q-21 (1932)																							
Pl1.1	35.8	61.8	2.5	2.64	1.34	0.012	b.d.l.	0.36	0.0042	0.0011	0.62	0.025	13.01	59.08	25.37	0.33	b.d.l.	7.53	0.163	b.d.l.	7.18	0.44	100.15
Pl1.2	49.9	48.6	1.6	2.49	1.49	0.012	b.d.l.	0.51	0.0039	0.0001	0.50	0.016	13.02	54.87	27.96	0.33	b.d.l.	10.46	0.146	b.d.l.	5.63	0.27	99.67
Pl1.3	48.6	49.7	1.7	2.52	1.46	0.017	0.0005	0.49	0.0044	0.0005	0.50	0.017	13.01	55.87	27.51	0.44	b.d.l.	10.10	0.168	b.d.l.	5.70	0.29	100.11
Pl1.4	33.4	63.5	3.1	2.68	1.30	0.012	b.d.l.	0.33	0.0035	0.0016	0.63	0.031	13.00	59.75	24.66	0.32	b.d.l.	6.95	0.136	b.d.l.	7.29	0.54	99.74
Pl10.1	45.3	52.8	1.9	2.57	1.38	0.012	b.d.l.	0.48	0.0047	0.0004	0.56	0.021	13.03	56.50	25.70	0.31	b.d.l.	9.86	0.179	b.d.l.	6.35	0.35	99.27
Pl10.2	73.0	26.4	0.6	2.27	1.70	0.018	b.d.l.	0.74	0.0040	0.0002	0.27	0.006	13.01	49.35	31.34	0.47	b.d.l.	14.95	0.149	b.d.l.	2.99	0.10	99.37
Pl10.3	55.2	43.7	1.1	2.45	1.52	0.017	b.d.l.	0.56	0.0053	0.0004	0.44	0.011	13.01	53.77	28.33	0.46	b.d.l.	11.36	0.201	b.d.l.	4.97	0.20	99.31
Pl10.4	54.6	44.3	1.2	2.45	1.53	0.017	0.0006	0.55	0.0042	b.d.l.	0.44	0.012	13.01	54.00	28.65	0.45	b.d.l.	11.20	0.160	b.d.l.	5.02	0.20	99.69
Pl10.5	32.4	64.6	3.0	2.69	1.30	0.013	b.d.l.	0.32	0.0030	0.0011	0.64	0.030	13.00	60.17	24.67	0.34	b.d.l.	6.74	0.115	b.d.l.	7.43	0.53	100.06
Pl11.1	28.5	68.0	3.5	2.73	1.26	0.012	b.d.l.	0.29	0.0022	0.0012	0.68	0.035	13.00	61.17	23.89	0.32	b.d.l.	5.96	0.087	b.d.l.	7.87	0.62	99.99
Pl11.2	30.7	66.1	3.2	2.72	1.27	0.012	b.d.l.	0.30	0.0014	0.0005	0.66	0.032	12.99	60.65	24.03	0.32	b.d.l.	6.35	0.052	b.d.l.	7.55	0.55	99.53
Pl11.3	31.5	65.4	3.2	2.70	1.29	0.012	b.d.l.	0.32	0.0030	0.0015	0.65	0.032	13.00	60.34	24.41	0.32	b.d.l.	6.58	0.117	b.d.l.	7.55	0.56	99.96
Pl11.4	30.2	66.4	3.4	2.70	1.28	0.012	b.d.l.	0.31	0.0035	0.0014	0.67	0.034	13.01	60.35	24.23	0.31	b.d.l.	6.36	0.136	b.d.l.	7.73	0.59	99.78
Pl11.5	36.2	61.4	2.5	2.65	1.33	0.012	b.d.l.	0.36	0.0049	0.0013	0.61	0.025	13.00	58.99	25.11	0.32	b.d.l.	7.52	0.189	b.d.l.	7.05	0.43	99.69
Pl13.1	41.7	56.4	1.9	2.58	1.41	0.014	b.d.l.	0.42	0.0037	0.0009	0.57	0.019	13.01	57.13	26.45	0.36	b.d.l.	8.67	0.143	b.d.l.	6.48	0.33	99.61
Pl13.2	34.2	63.1	2.7	2.66	1.33	0.012	b.d.l.	0.34	0.0024	0.0005	0.64	0.027	13.01	59.35	25.11	0.31	b.d.l.	7.17	0.094	b.d.l.	7.31	0.47	99.84
Pl13.3	43.2	54.9	1.9	2.57	1.41	0.014	b.d.l.	0.44	0.0041	0.0008	0.56	0.020	13.01	56.98	26.56	0.37	b.d.l.	9.07	0.156	b.d.l.	6.37	0.34	99.91
Pl16.1	61.3	37.7	0.9	2.53	1.35	0.016	b.d.l.	0.67	0.0042	0.0010	0.41	0.010	13.01	b.d.l.	b.d.l.	b.d.l.	b.d.l.	b.d.l.	b.d.l.	b.d.l.	b.d.l.	b.d.l.	92.88
Pl16.2	40.5	57.4	2.1	2.60	1.38	0.015	b.d.l.	0.41	0.0031	0.0004	0.58	0.021	13.00	57.89	26.03	0.40	b.d.l.	8.41	0.119	b.d.l.	6.59	0.37	99.83
Pl2.1	35.9	61.4	2.6	2.65	1.34	0.012	b.d.l.	0.36	0.0042	0.0009	0.61	0.026	13.00	59.16	25.28	0.31	b.d.l.	7.46	0.163	b.d.l.	7.05	0.46	99.93
Pl2.2	29.2	67.5	3.3	2.72	1.27	0.011	b.d.l.	0.29	0.0028	0.0009	0.67	0.033	13.00	61.03	24.18	0.28	b.d.l.	6.10	0.110	b.d.l.	7.79	0.58	100.13
Pl2.3	35.1	62.5	2.4	2.65	1.34	0.012	b.d.l.	0.35	0.0024	0.0016	0.63	0.024	13.01	59.12	25.30	0.31	b.d.l.	7.32	0.094	b.d.l.	7.20	0.43	99.86
Pl5.1	36.3	61.0	2.7	2.65	1.34	0.012	b.d.l.	0.36	0.0030	0.0011	0.61	0.027	13.00	59.13	25.28	0.32	b.d.l.	7.54	0.115	b.d.l.	7.01	0.47	99.93
Pl5.2	34.7	62.7	2.6	2.67	1.32	0.013	b.d.l.	0.35	0.0038	0.0009	0.63	0.026	13.00	59.33	24.83	0.34	b.d.l.	7.24	0.146	b.d.l.	7.22	0.46	99.63

Appendix B1 cotinued

Label	An[2]	Ab[3]	Or[4]	Si	Al	Fe	Mg	Ca	Sr	Ba	Na	K	Tot[5]	SiO_2	Al_2O_3	FeO	MgO	CaO	SrO	BaO	Na_2O	K_2O	Tot
Pl5.3	41.9	55.8	2.2	2.58	1.41	0.013	b.d.l.	0.42	0.0039	0.0012	0.56	0.023	13.01	57.01	26.41	0.34	b.d.l.	8.71	0.149	b.d.l.	6.41	0.39	99.48
Pl5.4	34.7	62.7	2.6	2.66	1.33	0.012	b.d.l.	0.35	0.0043	0.0012	0.63	0.027	13.01	59.06	25.02	0.31	b.d.l.	7.25	0.165	b.d.l.	7.24	0.47	99.58
Pl6.1	34.3	63.0	2.8	2.65	1.33	0.017	b.d.l.	0.35	0.0033	0.0004	0.64	0.028	13.01	59.24	25.18	0.46	b.d.l.	7.21	0.128	b.d.l.	7.32	0.49	100.04
Pl6.2	57.7	41.2	1.1	2.43	1.55	0.018	b.d.l.	0.58	0.0040	b.d.l.	0.42	0.011	13.01	53.27	28.95	0.47	b.d.l.	11.93	0.151	b.d.l.	4.71	0.19	99.67
Pl6.3	36.5	61.2	2.4	2.64	1.34	0.012	b.d.l.	0.37	0.0036	0.0016	0.61	0.024	13.01	58.90	25.38	0.33	b.d.l.	7.61	0.138	b.d.l.	7.06	0.41	99.92
Pl9.1	29.7	67.1	3.2	2.71	1.28	0.011	b.d.l.	0.30	0.0025	0.0009	0.68	0.032	13.01	60.60	24.26	0.29	b.d.l.	6.25	0.098	b.d.l.	7.80	0.56	99.92
Pl9.2	48.5	50.0	1.6	2.51	1.48	0.010	b.d.l.	0.49	0.0030	0.0017	0.50	0.016	13.01	55.74	27.79	0.26	b.d.l.	10.08	0.116	b.d.l.	5.74	0.28	100.10
Q-6 (1932)																							
Pl1.1	35.9	61.7	2.3	2.64	1.35	0.012	b.d.l.	0.36	0.0021	0.0009	0.63	0.024	13.02	58.52	25.43	0.33	b.d.l.	7.55	0.081	b.d.l.	7.18	0.41	99.54
Pl1.2	56.0	43.2	0.8	2.43	1.56	0.016	0.0001	0.56	0.0043	b.d.l.	0.43	0.008	13.00	53.49	29.03	0.41	b.d.l.	11.40	0.162	b.d.l.	4.85	0.14	99.48
Pl1.3	43.7	54.4	1.9	2.55	1.43	0.014	b.d.l.	0.44	0.0041	0.0015	0.55	0.020	13.02	56.48	26.92	0.38	b.d.l.	9.13	0.156	b.d.l.	6.28	0.34	99.75
Pl1.4	33.9	63.5	2.7	2.66	1.33	0.012	b.d.l.	0.34	0.0020	0.0012	0.64	0.027	13.01	59.21	25.17	0.31	b.d.l.	7.06	0.079	b.d.l.	7.32	0.47	99.69
Pl12.1	77.9	21.6	0.4	2.22	1.76	0.020	0.0026	0.78	0.0047	b.d.l.	0.22	0.005	13.01	48.13	32.27	0.52	0.038	15.79	0.177	b.d.l.	2.42	0.08	99.42
Pl12.2	78.0	21.7	0.3	2.22	1.77	0.020	0.0020	0.78	0.0053	b.d.l.	0.22	0.003	13.01	48.02	32.47	0.51	0.029	15.66	0.199	b.d.l.	2.41	0.04	99.33
Pl12.3	24.6	70.5	4.9	2.76	1.22	0.017	b.d.l.	0.25	0.0018	0.0025	0.71	0.049	13.01	61.49	23.04	0.45	b.d.l.	5.12	0.070	0.145	8.11	0.86	99.29
Pl2.1	42.5	54.8	2.6	2.57	1.42	0.015	b.d.l.	0.43	0.0027	0.0008	0.55	0.026	13.01	56.66	26.69	0.38	b.d.l.	8.79	0.102	b.d.l.	6.27	0.45	99.39
Pl2.2	59.2	39.6	1.2	2.41	1.58	0.015	b.d.l.	0.58	0.0046	0.0007	0.39	0.012	13.00	53.01	29.45	0.41	b.d.l.	11.96	0.174	b.d.l.	4.42	0.21	99.67
Pl2.3	59.0	40.0	1.0	2.41	1.57	0.019	0.0002	0.59	0.0034	0.0005	0.40	0.010	13.01	52.90	29.20	0.50	b.d.l.	12.16	0.128	b.d.l.	4.55	0.18	99.65
Pl2.4	44.2	53.9	1.9	2.56	1.43	0.014	b.d.l.	0.44	0.0044	0.0010	0.54	0.019	13.00	56.58	26.77	0.37	b.d.l.	9.08	0.166	b.d.l.	6.12	0.32	99.46
Pl2.5	35.3	62.4	2.4	2.64	1.35	0.013	b.d.l.	0.35	0.0038	0.0011	0.62	0.023	13.00	58.85	25.48	0.34	b.d.l.	7.27	0.146	b.d.l.	7.11	0.41	99.67
Pl3.1	35.6	61.9	2.5	2.63	1.36	0.012	b.d.l.	0.36	0.0030	0.0006	0.62	0.025	13.01	58.55	25.68	0.32	b.d.l.	7.42	0.113	b.d.l.	7.14	0.44	99.70
Pl3.2	31.4	65.8	2.9	2.69	1.30	0.013	b.d.l.	0.31	0.0030	0.0009	0.66	0.029	13.01	59.59	24.46	0.35	b.d.l.	6.50	0.114	b.d.l.	7.54	0.50	99.11
Pl4.4	28.2	68.4	3.4	2.72	1.27	0.012	b.d.l.	0.28	0.0025	0.0016	0.68	0.034	13.00	60.53	23.90	0.32	b.d.l.	5.82	0.094	b.d.l.	7.81	0.59	99.15
Pl4.5	35.6	62.0	2.4	2.63	1.36	0.013	b.d.l.	0.36	0.0025	0.0011	0.62	0.025	13.01	58.64	25.69	0.36	b.d.l.	7.46	0.098	b.d.l.	7.18	0.43	99.91
Pl5.1	26.3	69.7	4.0	2.74	1.24	0.013	b.d.l.	0.26	0.0032	0.0013	0.70	0.040	13.01	61.50	23.58	0.36	b.d.l.	5.51	0.123	b.d.l.	8.08	0.70	99.93
Pl5.2	49.0	49.6	1.4	2.51	1.47	0.014	b.d.l.	0.50	0.0035	0.0003	0.50	0.014	13.01	55.46	27.52	0.37	b.d.l.	10.25	0.133	b.d.l.	5.73	0.25	99.73
Pl5.3	55.8	42.9	1.3	2.43	1.56	0.015	b.d.l.	0.56	0.0041	b.d.l.	0.43	0.013	13.01	53.20	29.01	0.38	b.d.l.	11.43	0.154	b.d.l.	4.86	0.22	99.25
Pl5.4	31.9	65.0	3.1	2.68	1.30	0.012	b.d.l.	0.32	0.0036	0.0013	0.65	0.031	13.01	59.91	24.68	0.33	b.d.l.	6.70	0.138	b.d.l.	7.54	0.55	99.91
Pl5.5	51.3	47.3	1.4	2.48	1.51	0.015	b.d.l.	0.52	0.0050	0.0010	0.48	0.014	13.01	54.66	28.15	0.39	b.d.l.	10.63	0.192	b.d.l.	5.42	0.24	99.73
Pl5.7	31.5	65.6	2.9	2.69	1.30	0.011	b.d.l.	0.32	0.0021	0.0018	0.66	0.030	13.01	59.96	24.55	0.30	b.d.l.	6.57	0.081	b.d.l.	7.56	0.52	99.63

Appendix B1 cotinued

Label	An[2]	Ab[3]	Or[4]	Si	Al	Fe	Mg	Ca	Sr	Ba	Na	K	Tot[5]	SiO_2	Al_2O_3	FeO	MgO	CaO	SrO	BaO	Na_2O	K_2O	Tot
Pl5.8	34.3	63.3	2.4	2.66	1.33	0.011	b.d.l.	0.35	0.0037	0.0012	0.64	0.024	13.01	59.06	25.14	0.28	b.d.l.	7.16	0.144	b.d.l.	7.29	0.42	99.58
Pl5.9	34.2	62.8	2.9	2.66	1.34	0.012	b.d.l.	0.34	0.0028	0.0005	0.62	0.029	13.00	59.16	25.35	0.32	b.d.l.	7.02	0.108	b.d.l.	7.12	0.50	99.60
Pl6.1	32.2	65.0	2.8	2.68	1.32	0.010	b.d.l.	0.32	0.0025	0.0007	0.65	0.028	13.00	59.78	24.98	0.27	b.d.l.	6.67	0.096	b.d.l.	7.45	0.49	99.77
Pl6.2	51.8	46.8	1.4	2.48	1.51	0.010	b.d.l.	0.52	0.0044	0.0001	0.47	0.014	13.01	54.53	28.27	0.25	b.d.l.	10.67	0.166	b.d.l.	5.33	0.24	99.46
Pl6.3	30.4	66.6	3.0	2.70	1.29	0.012	b.d.l.	0.30	0.0029	0.0006	0.66	0.030	13.00	60.16	24.45	0.33	b.d.l.	6.29	0.111	b.d.l.	7.62	0.52	99.51
Pl6.4	36.9	60.9	2.2	2.62	1.36	0.016	b.d.l.	0.37	0.0038	0.0006	0.62	0.022	13.02	58.10	25.65	0.42	b.d.l.	7.72	0.143	b.d.l.	7.03	0.38	99.48
Pl8.1	29.6	67.0	3.3	2.71	1.28	0.011	b.d.l.	0.30	0.0028	0.0019	0.67	0.033	13.00	60.23	24.17	0.29	b.d.l.	6.15	0.107	b.d.l.	7.69	0.58	99.33
Pl8.2	49.5	49.2	1.3	2.51	1.48	0.010	b.d.l.	0.50	0.0039	0.0008	0.49	0.013	13.01	55.14	27.72	0.25	b.d.l.	10.20	0.148	b.d.l.	5.60	0.22	99.33
Pl8.3	26.7	69.7	3.6	2.74	1.26	0.012	b.d.l.	0.27	0.0030	0.0015	0.69	0.035	13.00	61.11	23.80	0.32	b.d.l.	5.54	0.116	b.d.l.	7.98	0.62	99.57
Pl8.4	34.1	63.3	2.6	2.66	1.32	0.013	b.d.l.	0.34	0.0043	0.0002	0.63	0.026	13.01	59.32	25.00	0.34	b.d.l.	7.10	0.166	b.d.l.	7.29	0.46	99.68
Pl9.1	28.1	68.3	3.6	2.72	1.27	0.011	b.d.l.	0.28	0.0029	0.0016	0.68	0.036	13.00	60.81	24.02	0.30	b.d.l.	5.83	0.111	b.d.l.	7.84	0.64	99.64
Pl9.2	33.6	63.6	2.7	2.66	1.33	0.012	b.d.l.	0.34	0.0035	0.0007	0.64	0.028	13.01	58.76	24.86	0.30	b.d.l.	7.01	0.132	b.d.l.	7.32	0.48	98.90
Pl9.3	31.6	65.4	3.0	2.67	1.31	0.012	b.d.l.	0.32	0.0048	0.0012	0.66	0.030	13.01	59.48	24.80	0.32	b.d.l.	6.61	0.185	b.d.l.	7.55	0.53	99.54
Pl9.4	35.7	61.7	2.6	2.64	1.35	0.013	b.d.l.	0.36	0.0032	0.0006	0.62	0.026	13.01	58.42	25.30	0.34	b.d.l.	7.40	0.121	b.d.l.	7.06	0.45	99.12
Pl9.5	36.7	61.0	2.3	2.62	1.37	0.015	0.0002	0.37	0.0029	0.0015	0.62	0.023	13.02	57.73	25.64	0.39	b.d.l.	7.63	0.112	b.d.l.	7.00	0.40	98.97
Pl9.6	32.6	64.5	2.9	2.66	1.33	0.011	b.d.l.	0.33	0.0038	0.0005	0.66	0.029	13.02	58.66	24.96	0.30	b.d.l.	6.85	0.144	b.d.l.	7.48	0.51	98.93
VQ-06-17 (1932)																							
Pl1.10	80.2	19.5	0.3	2.19	1.77	0.022	0.0020	0.83	0.0041	b.d.l.	0.20	0.003	13.03	47.55	32.61	0.57	0.030	16.82	0.152	b.d.l.	2.26	0.05	100.03
Pl1.11	81.6	18.1	0.3	2.19	1.78	0.022	0.0021	0.83	0.0044	0.0001	0.19	0.003	13.02	47.64	32.87	0.57	0.030	16.97	0.166	b.d.l.	2.08	0.05	100.39
Pl1.12	80.3	19.3	0.4	2.20	1.77	0.020	0.0019	0.81	0.0039	0.0004	0.20	0.004	13.01	47.74	32.49	0.51	0.027	16.45	0.146	b.d.l.	2.19	0.06	99.63
Pl1.13	81.4	18.2	0.4	2.19	1.78	0.024	0.0019	0.83	0.0041	0.0002	0.19	0.004	13.02	47.41	32.76	0.62	0.028	16.87	0.153	b.d.l.	2.08	0.06	100.00
Pl1.14	77.1	22.4	0.5	2.24	1.72	0.025	0.0035	0.78	0.0048	b.d.l.	0.23	0.005	13.01	48.78	31.80	0.66	0.051	15.84	0.181	b.d.l.	2.54	0.08	99.93
Pl1.15	77.1	22.5	0.4	2.25	1.72	0.023	0.0037	0.78	0.0040	0.0004	0.23	0.004	13.01	48.81	31.59	0.59	0.054	15.88	0.148	b.d.l.	2.56	0.07	99.72
Pl1.16	79.1	20.6	0.3	2.21	1.76	0.024	0.0042	0.81	0.0038	0.0004	0.21	0.004	13.02	48.09	32.41	0.61	0.061	16.42	0.142	b.d.l.	2.36	0.06	100.18
Pl1.17	78.0	21.6	0.4	2.23	1.73	0.024	0.0050	0.79	0.0036	b.d.l.	0.22	0.004	13.01	48.62	31.92	0.62	0.073	16.11	0.134	b.d.l.	2.47	0.06	100.01
Pl1.18	76.4	23.0	0.5	2.24	1.73	0.024	0.0052	0.78	0.0034	b.d.l.	0.23	0.005	13.02	48.48	31.81	0.61	0.076	15.74	0.128	b.d.l.	2.62	0.09	99.56
Pl1.1L1	34.1	63.0	2.9	2.68	1.30	0.013	0.0013	0.34	0.0032	0.0011	0.63	0.029	13.00	60.18	24.77	0.35	0.020	7.12	0.125	0.064	7.26	0.51	100.39
Pl1.2	34.6	62.7	2.7	2.66	1.32	0.012	0.0013	0.35	0.0034	0.0011	0.63	0.027	13.00	59.72	25.14	0.32	0.019	7.24	0.133	0.065	7.25	0.48	100.36
Pl1.3	51.6	46.9	1.5	2.49	1.49	0.014	0.0017	0.52	0.0042	0.0004	0.47	0.015	13.01	55.48	28.15	0.38	0.025	10.75	0.162	b.d.l.	5.40	0.26	100.62
Pl1.4	55.9	43.0	1.1	2.44	1.53	0.015	0.0016	0.56	0.0046	0.0007	0.43	0.011	13.01	54.12	28.81	0.40	0.024	11.67	0.174	b.d.l.	4.96	0.19	100.40

Appendix B1 cotinued

Label	An[2]	Ab[3]	Or[4]	Si	Al	Fe	Mg	Ca	Sr	Ba	Na	K	Tot[5]	SiO_2	Al_2O_3	FeO	MgO	CaO	SrO	BaO	Na_2O	K_2O	Tot
Pl1.5	52.2	46.5	1.3	2.49	1.49	0.016	0.0020	0.53	0.0042	0.0003	0.47	0.013	13.01	55.17	27.97	0.43	0.029	11.00	0.161	b.d.l.	5.41	0.22	100.42
Pl1.6	50.4	48.2	1.4	2.50	1.47	0.015	0.0020	0.52	0.0042	0.0006	0.49	0.015	13.02	55.40	27.59	0.39	0.030	10.67	0.162	b.d.l.	5.63	0.25	100.16
Pl1.7	79.3	20.4	0.4	2.21	1.77	0.020	0.0017	0.80	0.0041	0.0004	0.21	0.004	13.01	48.02	32.60	0.51	0.024	16.28	0.153	b.d.l.	2.31	0.06	99.99
Pl1.8	85.2	14.5	0.3	2.15	1.82	0.021	0.0016	0.86	0.0042	0.0003	0.15	0.003	13.01	46.73	33.64	0.55	0.023	17.52	0.157	b.d.l.	1.65	0.05	100.34
Pl1.9 L2	56.4	42.5	1.2	2.45	1.53	0.016	0.0051	0.57	0.0043	0.0001	0.43	0.012	13.01	54.06	28.62	0.43	0.076	11.72	0.166	b.d.l.	4.88	0.20	100.15
Pl10.1	35.3	62.0	2.7	2.66	1.31	0.011	0.0014	0.36	0.0037	0.0007	0.63	0.027	13.01	59.46	24.89	0.30	0.022	7.42	0.141	b.d.l.	7.21	0.48	99.96
Pl10.2	33.3	63.9	2.8	2.68	1.31	0.011	0.0011	0.33	0.0028	0.0007	0.64	0.028	13.00	60.00	24.80	0.29	0.016	6.98	0.109	b.d.l.	7.40	0.50	100.13
Pl10.3	47.6	51.0	1.4	2.54	1.44	0.012	0.0013	0.48	0.0038	0.0010	0.52	0.015	13.01	56.40	27.26	0.31	0.020	9.99	0.147	0.059	5.91	0.26	100.36
Pl11.10	80.6	19.0	0.4	2.21	1.76	0.020	0.0013	0.82	0.0039	b.d.l.	0.19	0.004	13.01	47.98	32.38	0.52	0.018	16.63	0.148	b.d.l.	2.17	0.07	99.92
Pl11.11	80.8	18.8	0.4	2.21	1.76	0.020	0.0016	0.82	0.0033	0.0002	0.19	0.004	13.01	47.81	32.35	0.53	0.023	16.68	0.124	b.d.l.	2.14	0.07	99.73
Pl11.12	66.0	33.3	0.8	2.37	1.60	0.019	0.0017	0.67	0.0042	0.0003	0.34	0.008	13.01	52.09	29.91	0.49	0.024	13.73	0.159	b.d.l.	3.83	0.14	100.38
Pl11.1L1	34.1	63.1	2.8	2.67	1.30	0.013	0.0010	0.34	0.0032	0.0012	0.64	0.028	13.01	59.78	24.73	0.34	0.015	7.18	0.122	0.070	7.35	0.49	100.08
Pl11.2	36.8	60.8	2.5	2.65	1.34	0.013	0.0013	0.37	0.0039	0.0010	0.61	0.025	13.00	59.31	25.40	0.36	0.019	7.72	0.149	0.058	7.06	0.43	100.51
Pl11.3	40.4	57.3	2.3	2.61	1.37	0.013	0.0016	0.41	0.0039	0.0007	0.58	0.023	13.01	58.35	26.13	0.34	0.024	8.53	0.152	b.d.l.	6.69	0.41	100.67
Pl11.4	46.2	51.9	1.9	2.54	1.44	0.014	0.0015	0.46	0.0050	0.0005	0.52	0.019	13.01	56.53	27.13	0.36	0.023	9.62	0.193	b.d.l.	5.97	0.33	100.18
Pl11.5	51.1	47.5	1.4	2.50	1.48	0.014	0.0016	0.51	0.0044	0.0005	0.48	0.014	13.01	55.43	27.95	0.36	0.023	10.60	0.167	b.d.l.	5.45	0.25	100.25
Pl11.6	46.8	51.6	1.6	2.54	1.43	0.014	0.0013	0.47	0.0045	0.0007	0.52	0.016	13.01	56.52	26.99	0.37	0.020	9.80	0.172	b.d.l.	5.97	0.28	100.17
Pl11.7	51.6	46.9	1.5	2.49	1.48	0.016	0.0017	0.53	0.0052	0.0004	0.48	0.015	13.02	55.24	27.90	0.43	0.025	10.92	0.199	b.d.l.	5.48	0.27	100.47
Pl11.8	52.9	45.6	1.4	2.48	1.49	0.015	0.0016	0.54	0.0042	0.0004	0.47	0.015	13.02	54.74	28.00	0.40	0.023	11.15	0.162	b.d.l.	5.31	0.25	100.07
Pl11.9	70.8	28.6	0.6	2.31	1.66	0.017	0.0018	0.73	0.0046	0.0003	0.29	0.007	13.02	50.50	30.80	0.44	0.027	14.87	0.174	b.d.l.	3.32	0.11	100.26
Pl112.1	68.0	31.4	0.6	2.33	1.64	0.024	0.0095	0.69	0.0046	0.0005	0.32	0.006	13.02	50.95	30.40	0.64	0.139	14.07	0.172	b.d.l.	3.59	0.11	100.10
Pl12.1	34.8	62.4	2.8	2.67	1.30	0.012	0.0013	0.35	0.0032	0.0013	0.63	0.029	13.01	59.68	24.66	0.32	0.019	7.33	0.122	0.075	7.27	0.50	99.98
Pl12.2	34.6	62.6	2.8	2.67	1.31	0.013	0.0015	0.35	0.0028	0.0009	0.62	0.028	13.00	59.64	24.75	0.34	0.023	7.18	0.106	0.051	7.19	0.49	99.76
Pl12.3	28.4	68.1	3.5	2.74	1.23	0.011	0.0012	0.29	0.0026	0.0013	0.69	0.036	13.00	61.60	23.49	0.28	0.018	5.99	0.102	0.075	7.94	0.62	100.12
Pl12.4	27.5	68.6	3.8	2.75	1.23	0.013	0.0012	0.28	0.0028	0.0015	0.69	0.038	13.00	61.81	23.39	0.34	0.018	5.78	0.110	0.086	7.96	0.68	100.17
Pl12.5	34.6	62.7	2.7	2.67	1.32	0.011	0.0013	0.35	0.0017	0.0014	0.63	0.027	13.00	59.89	25.05	0.30	0.020	7.25	0.067	0.081	7.27	0.48	100.41
Pl12.6	39.1	58.8	2.1	2.64	1.35	0.010	0.0012	0.39	0.0022	0.0012	0.59	0.021	12.99	58.74	25.42	0.27	0.018	8.10	0.086	0.066	6.74	0.37	99.81
Pl12.7	38.4	59.3	2.2	2.63	1.35	0.011	0.0012	0.39	0.0026	0.0009	0.60	0.023	13.00	58.48	25.38	0.28	0.017	8.02	0.099	0.053	6.84	0.39	99.56
Pl12.8	43.0	55.0	2.0	2.58	1.40	0.011	0.0014	0.43	0.0028	0.0009	0.55	0.020	13.00	57.46	26.37	0.28	0.022	8.97	0.106	0.052	6.35	0.34	99.96
Pl14.1	42.5	55.5	2.1	2.58	1.40	0.013	0.0015	0.43	0.0038	0.0002	0.56	0.021	13.01	57.54	26.50	0.36	0.022	8.97	0.146	b.d.l.	6.47	0.37	100.38

Appendix B1 cotinued

Label	An[2]	Ab[3]	Or[4]	Si	Al	Fe	Mg	Ca	Sr	Ba	Na	K	Tot[5]	SiO_2	Al_2O_3	FeO	MgO	CaO	SrO	BaO	Na_2O	K_2O	Tot
Pl14.2	54.8	44.0	1.2	2.46	1.52	0.017	0.0017	0.55	0.0040	0.0002	0.44	0.012	13.01	54.37	28.51	0.44	0.025	11.40	0.154	b.d.l.	5.06	0.21	100.19
Pl14.3	43.4	54.5	2.1	2.58	1.40	0.018	0.0022	0.44	0.0042	0.0002	0.55	0.021	13.01	57.35	26.38	0.48	0.033	9.12	0.162	b.d.l.	6.33	0.36	100.23
Pl15.1	34.0	63.2	2.8	2.66	1.32	0.013	0.0013	0.34	0.0024	0.0011	0.64	0.028	13.01	59.57	25.07	0.33	0.020	7.19	0.093	0.062	7.37	0.50	100.21
Pl15.2	28.3	68.0	3.7	2.73	1.25	0.011	0.0014	0.28	0.0028	0.0015	0.67	0.036	13.00	61.71	23.99	0.30	0.022	5.91	0.110	0.086	7.86	0.64	100.64
Pl16.1	34.0	63.3	2.7	2.66	1.32	0.012	0.0018	0.35	0.0033	0.0009	0.64	0.027	13.01	59.69	25.06	0.31	0.027	7.23	0.126	0.054	7.43	0.48	100.39
Pl16.2	30.7	66.0	3.2	2.71	1.27	0.012	0.0012	0.31	0.0029	0.0012	0.66	0.033	13.00	61.01	24.30	0.32	0.019	6.47	0.113	0.071	7.69	0.58	100.57
Pl16.3	32.1	64.9	3.0	2.69	1.30	0.012	0.0014	0.32	0.0025	0.0012	0.65	0.030	13.00	60.44	24.73	0.31	0.021	6.75	0.097	0.069	7.55	0.53	100.49
Pl17.1	34.2	63.2	2.6	2.67	1.31	0.012	0.0013	0.34	0.0032	0.0008	0.63	0.026	13.00	60.26	25.06	0.32	0.020	7.21	0.123	b.d.l.	7.36	0.46	100.86
Pl17.2	32.2	64.8	2.9	2.69	1.29	0.013	0.0011	0.32	0.0034	0.0006	0.65	0.030	13.01	60.48	24.53	0.35	0.016	6.81	0.131	b.d.l.	7.56	0.52	100.44
Pl17.3	45.7	52.5	1.8	2.55	1.43	0.011	0.0013	0.46	0.0039	0.0006	0.52	0.018	13.00	56.85	27.02	0.30	0.019	9.49	0.150	b.d.l.	6.02	0.32	100.20
Pl18.10	59.3	39.7	1.0	2.40	1.57	0.015	0.0015	0.60	0.0039	0.0004	0.40	0.010	13.02	53.02	29.45	0.39	0.022	12.40	0.150	b.d.l.	4.59	0.17	100.21
Pl18.11	59.3	39.7	1.0	2.41	1.57	0.015	0.0011	0.61	0.0042	0.0001	0.41	0.010	13.02	52.86	29.19	0.38	0.016	12.42	0.158	b.d.l.	4.59	0.18	99.80
Pl18.12	61.1	38.2	0.8	2.39	1.59	0.017	0.0014	0.62	0.0038	0.0004	0.39	0.008	13.01	52.51	29.57	0.44	0.021	12.70	0.144	b.d.l.	4.38	0.13	99.92
Pl18.1L1	34.3	62.9	2.8	2.67	1.32	0.011	0.0014	0.34	0.0034	0.0009	0.63	0.028	13.00	59.79	25.02	0.30	0.021	7.20	0.132	0.052	7.30	0.49	100.31
Pl18.2	43.1	55.0	1.9	2.58	1.40	0.013	0.0015	0.43	0.0037	0.0007	0.55	0.019	13.00	57.69	26.51	0.35	0.022	9.00	0.142	b.d.l.	6.35	0.33	100.44
Pl18.3	48.6	49.9	1.5	2.51	1.47	0.014	0.0016	0.50	0.0045	0.0007	0.51	0.015	13.02	55.36	27.56	0.37	0.023	10.25	0.173	b.d.l.	5.82	0.26	99.85
Pl18.4	52.8	45.9	1.3	2.47	1.51	0.017	0.0018	0.54	0.0038	0.0003	0.47	0.013	13.02	54.66	28.34	0.44	0.027	11.12	0.147	b.d.l.	5.35	0.23	100.33
Pl18.5	54.8	43.9	1.2	2.46	1.52	0.015	0.0015	0.56	0.0044	0.0005	0.45	0.013	13.02	54.18	28.37	0.39	0.022	11.53	0.169	b.d.l.	5.10	0.22	100.01
Pl18.6	58.2	40.7	1.1	2.43	1.54	0.015	0.0015	0.59	0.0036	b.d.l.	0.41	0.011	13.01	53.42	28.80	0.40	0.023	12.16	0.136	b.d.l.	4.70	0.20	99.84
Pl18.7	59.3	39.7	0.9	2.41	1.56	0.015	0.0016	0.60	0.0036	0.0003	0.40	0.010	13.01	53.13	29.22	0.39	0.024	12.36	0.138	b.d.l.	4.58	0.17	100.03
Pl18.8	58.7	40.4	0.9	2.42	1.56	0.017	0.0016	0.59	0.0042	0.0003	0.41	0.009	13.01	53.40	29.13	0.44	0.024	12.20	0.161	b.d.l.	4.64	0.16	100.18
Pl18.9	58.2	40.8	1.1	2.41	1.56	0.017	0.0016	0.59	0.0042	0.0005	0.41	0.011	13.02	53.12	29.19	0.44	0.024	12.14	0.161	b.d.l.	4.70	0.19	99.98
Pl19.1L1	36.3	61.2	2.5	2.65	1.33	0.013	0.0014	0.36	0.0033	0.0007	0.61	0.025	13.00	59.52	25.39	0.36	0.021	7.59	0.127	b.d.l.	7.07	0.44	100.55
Pl19.2	38.5	59.5	2.0	2.62	1.36	0.013	0.0015	0.39	0.0036	0.0008	0.60	0.021	13.01	58.70	25.80	0.35	0.022	8.10	0.140	0.044	6.92	0.36	100.44
Pl19.3	49.2	49.3	1.5	2.51	1.47	0.016	0.0017	0.50	0.0041	0.0006	0.50	0.015	13.02	55.61	27.65	0.44	0.026	10.43	0.157	b.d.l.	5.77	0.26	100.37
Pl19.4	52.1	46.6	1.3	2.49	1.50	0.016	0.0015	0.52	0.0043	0.0002	0.46	0.013	13.00	55.28	28.19	0.42	0.023	10.75	0.167	b.d.l.	5.32	0.23	100.40
Pl19.5	52.0	46.5	1.5	2.48	1.50	0.017	0.0018	0.53	0.0041	0.0005	0.47	0.015	13.01	55.19	28.23	0.45	0.027	10.90	0.157	b.d.l.	5.39	0.26	100.64
Pl19.6	53.6	45.0	1.4	2.47	1.51	0.015	0.0019	0.54	0.0046	0.0003	0.45	0.014	13.01	54.77	28.39	0.40	0.029	11.19	0.176	b.d.l.	5.19	0.25	100.42
Pl19.7	60.1	39.0	0.9	2.40	1.58	0.017	0.0021	0.61	0.0043	0.0005	0.40	0.009	13.02	52.85	29.60	0.44	0.031	12.61	0.162	b.d.l.	4.52	0.16	100.39
Pl19.8	56.5	42.3	1.2	2.44	1.54	0.016	0.0018	0.57	0.0048	b.d.l.	0.43	0.012	13.01	54.03	28.82	0.43	0.026	11.75	0.182	b.d.l.	4.86	0.21	100.31

Appendix B1 cotinued

Label	An[2]	Ab[3]	Or[4]	Si	Al	Fe	Mg	Ca	Sr	Ba	Na	K	Tot[5]	SiO_2	Al_2O_3	FeO	MgO	CaO	SrO	BaO	Na_2O	K_2O	Tot
Pl2.1L1	33.1	64.0	2.9	2.67	1.31	0.012	0.0012	0.33	0.0036	0.0008	0.65	0.030	13.01	59.88	24.95	0.33	0.018	7.01	0.140	0.047	7.49	0.52	100.39
Pl2.2	33.6	63.7	2.7	2.66	1.32	0.014	0.0013	0.34	0.0035	0.0008	0.64	0.027	13.01	59.83	25.20	0.39	0.019	7.08	0.136	0.045	7.42	0.47	100.59
Pl2.3	36.9	60.6	2.4	2.65	1.34	0.015	0.0015	0.37	0.0039	0.0005	0.60	0.024	13.00	59.34	25.39	0.39	0.023	7.69	0.152	b.d.l.	6.97	0.42	100.40
Pl2.4	38.3	59.3	2.4	2.63	1.35	0.015	0.0017	0.39	0.0041	0.0007	0.60	0.024	13.01	58.69	25.55	0.39	0.026	8.08	0.156	b.d.l.	6.91	0.42	100.27
Pl2.5	45.3	53.0	1.8	2.56	1.42	0.016	0.0022	0.46	0.0046	0.0006	0.54	0.018	13.01	56.74	26.74	0.43	0.032	9.53	0.176	b.d.l.	6.16	0.31	100.15
Pl2.6	42.0	56.0	2.0	2.59	1.39	0.016	0.0020	0.43	0.0042	0.0003	0.57	0.021	13.01	57.79	26.35	0.42	0.030	8.89	0.164	b.d.l.	6.56	0.36	100.58
Pl2.7	42.8	55.3	1.9	2.57	1.41	0.015	0.0017	0.43	0.0038	0.0007	0.56	0.019	13.01	57.49	26.71	0.39	0.025	9.04	0.147	b.d.l.	6.45	0.34	100.63
Pl2.8	42.4	55.6	1.9	2.58	1.40	0.018	0.0023	0.43	0.0045	0.0005	0.56	0.020	13.01	57.57	26.41	0.47	0.034	8.88	0.175	b.d.l.	6.43	0.34	100.34
Pl20.2	75.0	24.5	0.4	2.27	1.69	0.025	0.0088	0.76	0.0038	0.0005	0.25	0.005	13.02	49.07	31.10	0.66	0.128	15.46	0.140	b.d.l.	2.79	0.08	99.44
Pl20.3	62.8	36.3	1.0	2.39	1.57	0.019	0.0036	0.63	0.0046	0.0005	0.37	0.010	13.01	52.37	29.22	0.50	0.053	12.94	0.174	b.d.l.	4.14	0.17	99.59
Pl20.4	59.0	40.1	0.9	2.44	1.53	0.019	0.0037	0.60	0.0040	0.0004	0.41	0.010	13.01	53.10	28.21	0.50	0.055	12.10	0.149	b.d.l.	4.55	0.16	98.85
Pl21.1	33.3	63.8	2.9	2.70	1.28	0.013	0.0013	0.33	0.0030	0.0012	0.64	0.030	13.00	59.59	23.98	0.34	0.019	6.87	0.114	0.067	7.28	0.51	98.78
Pl21.2	37.2	60.3	2.5	2.65	1.32	0.012	0.0014	0.38	0.0028	0.0011	0.61	0.025	13.01	58.27	24.73	0.31	0.020	7.78	0.107	0.060	6.98	0.44	98.70
Pl21.3	87.6	12.2	0.2	2.13	1.83	0.012	0.0007	0.92	0.0027	0.0006	0.13	0.002	13.02	45.49	33.12	0.30	0.011	18.26	0.099	b.d.l.	1.41	0.03	98.75
Pl21.4	85.2	14.6	0.2	2.18	1.78	0.014	0.0013	0.89	0.0024	0.0004	0.15	0.002	13.01	b.d.l.	b.d.l.	b.d.l.	b.d.l.	b.d.l.	b.d.l.	b.d.l.	b.d.l.	b.d.l.	96.05
Pl3.1L1	29.9	67.0	3.1	2.71	1.27	0.012	0.0016	0.30	0.0027	0.0009	0.67	0.031	13.00	61.05	24.25	0.33	0.024	6.26	0.105	0.051	7.76	0.54	100.36
Pl3.2	30.0	66.8	3.2	2.72	1.26	0.011	0.0011	0.30	0.0032	0.0013	0.68	0.032	13.01	61.12	24.05	0.29	0.017	6.38	0.122	0.074	7.83	0.56	100.45
Pl3.3	31.9	64.9	3.2	2.71	1.27	0.012	0.0014	0.32	0.0037	0.0007	0.65	0.032	13.00	60.81	24.18	0.32	0.021	6.65	0.145	b.d.l.	7.49	0.56	100.23
Pl3.4	29.2	67.5	3.4	2.73	1.26	0.012	0.0014	0.29	0.0026	0.0012	0.68	0.034	13.00	61.25	23.99	0.32	0.021	6.12	0.102	0.070	7.83	0.59	100.29
Pl3.5	59.7	39.1	1.1	2.41	1.58	0.011	0.0012	0.60	0.0033	0.0004	0.39	0.011	13.01	53.31	29.60	0.29	0.018	12.44	0.125	b.d.l.	4.50	0.20	100.50
Pl3.6	56.9	41.9	1.2	2.43	1.55	0.011	0.0010	0.58	0.0034	0.0006	0.42	0.012	13.01	53.97	29.13	0.28	0.016	11.93	0.128	b.d.l.	4.86	0.20	100.56
Pl4.1	34.7	62.7	2.7	2.67	1.31	0.013	0.0014	0.35	0.0037	0.0011	0.63	0.027	13.00	59.68	24.87	0.35	0.021	7.27	0.144	0.066	7.25	0.47	100.11
Pl4.2	30.8	66.2	3.0	2.71	1.27	0.011	0.0012	0.31	0.0024	0.0012	0.67	0.031	13.01	61.20	24.36	0.30	0.018	6.58	0.094	0.067	7.80	0.54	100.95
Pl4.3	32.7	64.3	3.0	2.70	1.28	0.012	0.0012	0.33	0.0029	0.0012	0.65	0.030	13.00	60.56	24.38	0.31	0.018	6.95	0.111	0.068	7.54	0.53	100.47
Pl4.4	31.0	65.6	3.4	2.71	1.27	0.011	0.0013	0.31	0.0029	0.0014	0.65	0.034	13.00	60.89	24.27	0.31	0.020	6.47	0.113	0.079	7.56	0.59	100.30
Pl5.1	35.2	62.2	2.6	2.66	1.33	0.012	0.0015	0.35	0.0035	0.0010	0.62	0.026	13.00	59.52	25.20	0.33	0.022	7.37	0.134	0.058	7.20	0.45	100.28
Pl5.2	44.5	53.6	1.9	2.57	1.42	0.011	0.0012	0.44	0.0034	0.0006	0.54	0.019	13.00	57.18	26.79	0.28	0.018	9.23	0.130	b.d.l.	6.16	0.33	100.15
Pl5.3	47.3	51.2	1.5	2.54	1.45	0.011	0.0013	0.47	0.0041	0.0007	0.51	0.015	13.00	56.68	27.51	0.31	0.019	9.83	0.156	b.d.l.	5.87	0.26	100.67
Pl5.4	42.3	55.5	2.2	2.60	1.39	0.010	0.0012	0.42	0.0037	0.0009	0.55	0.021	12.99	57.98	26.36	0.28	0.018	8.68	0.143	0.051	6.29	0.37	100.17
Pl5.5	36.3	61.2	2.5	2.65	1.33	0.012	0.0014	0.37	0.0034	0.0006	0.62	0.026	13.01	59.58	25.44	0.32	0.021	7.68	0.130	b.d.l.	7.16	0.45	100.81

Appendix B1 cotinued

Label	An[2]	Ab[3]	Or[4]	Si	Al	Fe	Mg	Ca	Sr	Ba	Na	K	Tot[5]	SiO_2	Al_2O_3	FeO	MgO	CaO	SrO	BaO	Na_2O	K_2O	Tot
Pl6.1	35.7	61.6	2.7	2.66	1.33	0.013	0.0015	0.36	0.0036	0.0007	0.61	0.027	13.00	59.83	25.32	0.36	0.023	7.48	0.139	b.d.l.	7.13	0.48	100.80
Pl6.2	37.7	59.9	2.3	2.63	1.35	0.012	0.0016	0.38	0.0043	0.0011	0.60	0.024	13.00	59.05	25.62	0.33	0.025	7.91	0.168	0.064	6.94	0.41	100.52
Pl6.3	47.2	51.1	1.7	2.54	1.44	0.018	0.0021	0.48	0.0048	0.0008	0.52	0.017	13.01	56.51	27.11	0.47	0.031	9.91	0.185	0.046	5.93	0.29	100.48
Pl6.4	53.2	45.5	1.3	2.46	1.51	0.016	0.0020	0.54	0.0044	b.d.l.	0.47	0.014	13.02	54.63	28.42	0.42	0.030	11.27	0.169	b.d.l.	5.32	0.24	100.49
Pl7.1	34.5	62.6	2.8	2.67	1.31	0.012	0.0015	0.35	0.0033	0.0011	0.63	0.029	13.01	59.60	24.91	0.33	0.022	7.28	0.126	0.061	7.30	0.50	100.13
Pl7.2	49.5	48.9	1.6	2.52	1.46	0.012	0.0015	0.50	0.0048	0.0007	0.50	0.016	13.01	55.86	27.51	0.31	0.022	10.45	0.185	b.d.l.	5.71	0.28	100.36
Pl8.1	36.3	61.1	2.6	2.65	1.33	0.014	0.0016	0.37	0.0037	0.0007	0.62	0.026	13.01	59.02	25.18	0.36	0.024	7.63	0.141	b.d.l.	7.09	0.45	99.95
Pl8.2	52.3	46.3	1.4	2.48	1.49	0.017	0.0022	0.53	0.0040	0.0006	0.47	0.014	13.01	55.21	28.21	0.45	0.033	11.01	0.153	b.d.l.	5.38	0.24	100.72
Pl9.1	37.0	60.7	2.4	2.65	1.34	0.013	0.0013	0.37	0.0030	0.0010	0.60	0.024	13.00	59.23	25.43	0.34	0.020	7.66	0.115	0.055	6.95	0.41	100.21
Pl9.2	31.2	65.6	3.2	2.71	1.28	0.013	0.0011	0.31	0.0032	0.0014	0.65	0.032	13.00	60.68	24.25	0.35	0.016	6.50	0.125	0.079	7.56	0.56	100.13
Pl9.3	36.1	61.6	2.4	2.65	1.33	0.013	0.0013	0.36	0.0030	0.0012	0.62	0.024	13.01	59.25	25.11	0.34	0.020	7.56	0.116	0.069	7.14	0.41	100.02
Pl1.19	50.7	47.9	1.4	2.51	1.46	0.017	0.0027	0.51	0.0035	0.0008	0.48	0.014	13.01	55.68	27.54	0.45	0.040	10.57	0.135	0.046	5.52	0.25	100.23
Pl1.20	57.5	41.5	1.0	2.43	1.55	0.018	0.0028	0.58	0.0042	0.0006	0.42	0.010	13.01	53.53	29.01	0.48	0.042	11.97	0.159	b.d.l.	4.77	0.18	100.17
Pl1.21	79.2	20.5	0.4	2.21	1.76	0.021	0.0021	0.81	0.0040	0.0003	0.21	0.004	13.02	47.97	32.31	0.54	0.030	16.41	0.149	b.d.l.	2.35	0.06	99.83
Pl1.ctr	78.6	21.0	0.4	2.21	1.77	0.023	0.0044	0.79	0.0043	0.0004	0.21	0.004	13.02	b.d.l.	b.d.l.	b.d.l.	b.d.l.	b.d.l.	b.d.l.	b.d.l.	b.d.l.	b.d.l.	98.08
Pl22.1	77.7	21.9	0.4	2.23	1.75	0.022	0.0080	0.78	0.0039	0.0001	0.22	0.004	13.01	48.43	32.19	0.56	0.117	15.82	0.145	b.d.l.	2.46	0.06	99.79
Pl24.1	68.6	30.8	0.6	2.33	1.63	0.025	0.0093	0.70	0.0038	b.d.l.	0.31	0.006	13.01	50.99	30.32	0.66	0.137	14.22	0.145	b.d.l.	3.53	0.11	100.10
Pl3.7	64.9	34.3	0.8	2.36	1.63	0.011	0.0010	0.65	0.0031	0.0001	0.34	0.008	13.00	51.72	30.23	0.29	0.015	13.32	0.117	b.d.l.	3.89	0.13	99.72
Pl1.1-glom	70.6	28.7	0.7	2.30	1.68	0.011	0.0018	0.72	0.0035	0.0003	0.29	0.007	13.01	50.26	31.23	0.29	0.026	14.69	0.130	b.d.l.	3.30	0.13	100.06
VQ-07-37D (1932)																							
Pl1.1	33.7	63.6	2.6	2.65	1.34	0.012	0.0013	0.34	0.0036	0.0008	0.65	0.027	13.02	58.60	25.21	0.31	0.019	7.09	0.138	0.046	7.40	0.47	99.28
Pl1.2	35.6	61.9	2.5	2.65	1.34	0.014	0.0014	0.36	0.0039	0.0013	0.62	0.025	13.01	58.83	25.25	0.38	0.021	7.41	0.151	0.075	7.13	0.43	99.68
Pl1.3	46.6	51.8	1.6	2.54	1.44	0.015	0.0016	0.47	0.0045	0.0004	0.52	0.016	13.01	56.32	27.07	0.41	0.024	9.69	0.173	b.d.l.	5.95	0.28	99.93
Pl1.4	45.2	53.1	1.8	2.55	1.43	0.012	0.0016	0.46	0.0041	0.0005	0.54	0.018	13.01	56.65	26.98	0.32	0.023	9.52	0.156	b.d.l.	6.18	0.31	100.16
Pl1.5	35.8	61.8	2.5	2.64	1.34	0.013	0.0011	0.36	0.0032	0.0007	0.63	0.025	13.01	58.97	25.30	0.34	0.017	7.57	0.123	b.d.l.	7.22	0.44	100.01
Pl10.1	35.1	62.1	2.8	2.63	1.35	0.014	0.0014	0.36	0.0037	0.0011	0.64	0.029	13.03	57.74	25.23	0.37	0.021	7.36	0.141	0.060	7.21	0.50	98.62
Pl10.2	29.8	66.8	3.4	2.72	1.27	0.012	0.0013	0.30	0.0028	0.0014	0.67	0.034	13.00	60.48	24.01	0.32	0.019	6.16	0.107	0.079	7.64	0.59	99.41
Pl10.3	31.9	65.0	3.1	2.69	1.30	0.011	0.0011	0.32	0.0029	0.0014	0.65	0.031	13.00	59.85	24.47	0.28	0.017	6.62	0.110	0.079	7.44	0.53	99.39
Pl11.1	26.2	69.7	4.1	2.76	1.22	0.012	0.0015	0.26	0.0024	0.0012	0.69	0.041	12.99	61.91	23.19	0.32	0.022	5.42	0.091	0.069	7.97	0.71	99.69
Pl11.2	40.5	57.3	2.2	2.59	1.39	0.011	0.0010	0.41	0.0027	0.0012	0.58	0.022	13.01	57.70	26.25	0.30	0.014	8.51	0.102	0.071	6.66	0.39	100.00

Appendix B1 cotinued

Label	An[2]	Ab[3]	Or[4]	Si	Al	Fe	Mg	Ca	Sr	Ba	Na	K	Tot[5]	SiO_2	Al_2O_3	FeO	MgO	CaO	SrO	BaO	Na_2O	K_2O	Tot
Pl11.3	38.1	59.5	2.4	2.61	1.37	0.011	0.0011	0.39	0.0033	0.0008	0.61	0.024	13.02	57.64	25.60	0.30	0.016	8.02	0.124	0.045	6.92	0.42	99.07
Pl12.1	62.4	36.4	1.2	2.38	1.59	0.030	0.0078	0.63	0.0032	0.0002	0.37	0.012	13.02	51.51	29.25	0.77	0.114	12.77	0.121	b.d.l.	4.11	0.20	98.86
Pl12.2	56.2	42.3	1.4	2.43	1.54	0.027	0.0070	0.58	0.0037	0.0001	0.44	0.015	13.03	52.82	28.39	0.71	0.102	11.74	0.138	b.d.l.	4.89	0.25	99.04
Pl12.3	69.7	29.4	0.9	2.31	1.66	0.024	0.0059	0.71	0.0038	0.0002	0.30	0.009	13.02	b.d.l.	b.d.l.	b.d.l.	b.d.l.	b.d.l.	b.d.l.	b.d.l.	b.d.l.	b.d.l.	98.12
Pl13.1	31.9	65.2	2.8	2.67	1.31	0.012	0.0009	0.33	0.0032	0.0010	0.68	0.030	13.03	59.53	24.82	0.33	0.014	6.91	0.125	0.059	7.80	0.52	100.10
Pl13.2	31.4	65.5	3.0	2.69	1.29	0.014	0.0014	0.32	0.0035	0.0011	0.66	0.030	13.01	59.89	24.46	0.37	0.020	6.55	0.133	0.064	7.55	0.53	99.58
Pl14.1	34.2	63.2	2.6	2.66	1.32	0.013	0.0012	0.34	0.0038	0.0009	0.64	0.026	13.01	58.85	24.87	0.35	0.018	7.11	0.145	0.050	7.25	0.46	99.10
Pl14.2	29.1	67.5	3.4	2.70	1.28	0.011	0.0012	0.30	0.0035	0.0012	0.69	0.034	13.02	59.78	24.00	0.29	0.018	6.10	0.134	0.070	7.81	0.59	98.79
Pl15.1	32.8	64.0	3.2	2.67	1.31	0.012	0.0010	0.33	0.0039	0.0010	0.65	0.032	13.01	59.06	24.51	0.31	0.014	6.85	0.149	0.055	7.40	0.56	98.91
Pl15.2	41.3	56.8	2.0	2.60	1.39	0.011	0.0014	0.42	0.0034	0.0009	0.57	0.020	13.01	57.48	26.08	0.29	0.021	8.58	0.129	0.053	6.53	0.35	99.51
Pl2.1	55.8	43.0	1.2	2.44	1.53	0.023	0.0024	0.57	0.0045	0.0006	0.44	0.012	13.02	54.08	28.72	0.60	0.035	11.75	0.172	b.d.l.	5.00	0.21	100.60
Pl2.2	44.5	53.7	1.8	2.58	1.40	0.014	0.0019	0.45	0.0045	0.0005	0.54	0.019	13.00	57.54	26.56	0.38	0.028	9.29	0.173	b.d.l.	6.19	0.32	100.52
Pl3.1	33.9	63.4	2.7	2.65	1.33	0.012	0.0012	0.34	0.0034	0.0007	0.64	0.027	13.01	59.39	25.33	0.32	0.017	7.14	0.129	b.d.l.	7.39	0.48	100.24
Pl3.2	31.2	65.7	3.1	2.68	1.31	0.012	0.0014	0.32	0.0032	0.0012	0.66	0.031	13.02	59.62	24.78	0.32	0.022	6.55	0.122	0.067	7.62	0.54	99.64
Pl3.3	27.7	68.6	3.7	2.72	1.26	0.012	0.0012	0.28	0.0034	0.0014	0.69	0.037	13.01	60.86	23.97	0.32	0.018	5.79	0.129	0.081	7.91	0.65	99.73
Pl4.1	35.8	61.6	2.6	2.65	1.34	0.013	0.0015	0.36	0.0039	0.0009	0.62	0.026	13.01	59.10	25.30	0.34	0.023	7.53	0.152	0.051	7.17	0.46	100.12
Pl4.2	32.4	64.8	2.7	2.67	1.31	0.012	0.0014	0.33	0.0036	0.0009	0.66	0.028	13.02	59.48	24.73	0.32	0.020	6.83	0.140	0.050	7.55	0.49	99.62
Pl4.3	30.1	66.7	3.2	2.70	1.28	0.013	0.0015	0.31	0.0037	0.0013	0.68	0.033	13.02	59.85	24.09	0.34	0.022	6.33	0.142	0.074	7.74	0.57	99.16
Pl5.1	46.4	51.8	1.8	2.55	1.43	0.013	0.0016	0.47	0.0040	0.0007	0.52	0.018	13.01	56.41	26.95	0.35	0.023	9.68	0.152	b.d.l.	5.97	0.31	99.89
Pl5.2	56.7	42.1	1.2	2.43	1.55	0.015	0.0014	0.58	0.0044	0.0004	0.43	0.012	13.02	53.18	28.80	0.39	0.021	11.93	0.168	b.d.l.	4.89	0.21	99.62
Pl5.3	32.1	64.7	3.1	2.68	1.30	0.012	0.0012	0.33	0.0035	0.0012	0.66	0.032	13.01	59.55	24.42	0.32	0.018	6.74	0.132	0.067	7.51	0.55	99.32
Pl5.4	34.9	62.3	2.8	2.65	1.33	0.013	0.0013	0.36	0.0032	0.0008	0.63	0.028	13.02	59.06	25.02	0.34	0.020	7.39	0.124	0.044	7.28	0.49	99.78
Pl5.5	47.7	50.5	1.8	2.52	1.47	0.012	0.0015	0.48	0.0036	0.0005	0.50	0.018	13.01	55.54	27.39	0.31	0.022	9.79	0.137	b.d.l.	5.73	0.31	99.26
Pl6.1	32.5	64.7	2.9	2.67	1.31	0.012	0.0012	0.33	0.0035	0.0006	0.66	0.029	13.02	59.73	24.89	0.33	0.018	6.88	0.135	b.d.l.	7.57	0.51	100.09
Pl6.2	38.1	59.5	2.4	2.60	1.39	0.013	0.0013	0.39	0.0036	0.0011	0.61	0.025	13.03	57.50	26.10	0.34	0.019	8.10	0.136	0.060	6.98	0.43	99.66
Pl6.3	41.8	56.2	2.0	2.58	1.40	0.012	0.0014	0.42	0.0042	0.0004	0.57	0.021	13.01	57.16	26.27	0.32	0.021	8.73	0.159	b.d.l.	6.50	0.36	99.54
Pl7.1	55.5	43.1	1.4	2.44	1.53	0.028	0.0049	0.56	0.0038	0.0005	0.44	0.014	13.02	53.32	28.25	0.73	0.072	11.47	0.142	b.d.l.	4.92	0.24	99.18
Pl7.2	62.3	36.6	1.1	2.39	1.58	0.029	0.0060	0.63	0.0035	0.0004	0.37	0.011	13.01	52.02	29.10	0.75	0.088	12.79	0.133	b.d.l.	4.16	0.19	99.25
Pl7.3	67.7	31.3	1.0	2.32	1.64	0.024	0.0042	0.69	0.0041	0.0003	0.32	0.010	13.02	50.79	30.45	0.62	0.062	14.08	0.154	b.d.l.	3.60	0.17	99.95

Appendix B1 cotinued

Label	An[2]	Ab[3]	Or[4]	Si	Al	Fe	Mg	Ca	Sr	Ba	Na	K	Tot[5]	SiO_2	Al_2O_3	FeO	MgO	CaO	SrO	BaO	Na_2O	K_2O	Tot
Pl8.1	58.1	40.5	1.4	2.44	1.52	0.028	0.0069	0.58	0.0030	b.d.l.	0.40	0.014	13.00	53.32	28.17	0.72	0.100	11.81	0.113	b.d.l.	4.55	0.24	99.02
Pl9.1	65.1	34.0	0.9	2.36	1.61	0.026	0.0050	0.66	0.0040	0.0008	0.34	0.009	13.01	51.13	29.64	0.68	0.072	13.30	0.149	0.045	3.84	0.15	99.00
Mount_Q-4 HF (1932)																							
Pl1.1	57.4	41.3	1.2	2.45	1.53	0.018	0.0026	0.57	0.0046	b.d.l.	0.41	0.012	13.00	53.51	28.45	0.47	0.038	11.57	0.175	b.d.l.	4.60	0.21	99.03
Pl10.1	34.6	62.5	2.8	2.67	1.32	0.013	0.0012	0.34	0.0036	0.0007	0.62	0.028	13.00	59.42	24.89	0.34	0.018	7.12	0.139	b.d.l.	7.11	0.49	99.56
Pl11.1	44.8	53.4	1.9	2.55	1.43	0.015	0.0016	0.45	0.0033	0.0006	0.54	0.019	13.01	56.07	26.66	0.38	0.023	9.27	0.126	b.d.l.	6.11	0.33	99.02
Pl11.2	47.0	51.2	1.7	2.52	1.46	0.016	0.0019	0.47	0.0054	0.0005	0.51	0.017	13.01	b.d.l.	b.d.l.	b.d.l.	b.d.l.	b.d.l.	b.d.l.	b.d.l.	b.d.l.	b.d.l.	98.41
Pl11.3	30.4	62.7	6.9	2.75	1.22	0.019	0.0049	0.29	0.0028	0.0009	0.60	0.067	12.97	b.d.l.	b.d.l.	b.d.l.	b.d.l.	b.d.l.	b.d.l.	b.d.l.	b.d.l.	b.d.l.	98.07
Pl12.1	36.2	61.2	2.6	2.64	1.35	0.013	0.0013	0.36	0.0036	0.0011	0.61	0.026	13.01	58.08	25.17	0.33	0.020	7.44	0.136	0.063	6.94	0.44	98.61
Pl13.1	27.1	69.2	3.7	2.72	1.28	0.010	0.0012	0.27	0.0029	0.0017	0.69	0.038	13.01	60.19	24.01	0.27	0.018	5.62	0.110	0.095	7.93	0.65	98.89
Pl14.1	47.3	51.0	1.7	2.52	1.47	0.011	0.0009	0.47	0.0038	0.0002	0.51	0.017	13.01	55.52	27.42	0.29	0.013	9.68	0.142	b.d.l.	5.78	0.29	99.15
Pl14.2	32.1	65.0	2.9	2.68	1.31	0.012	0.0014	0.32	0.0036	0.0015	0.64	0.029	13.00	59.94	24.78	0.31	0.021	6.58	0.138	0.086	7.36	0.50	99.72
Pl2.1	56.6	42.1	1.3	2.43	1.55	0.011	0.0010	0.57	0.0035	0.0005	0.42	0.013	13.01	53.06	28.76	0.29	0.014	11.60	0.131	b.d.l.	4.76	0.22	98.86
Pl2.2	31.9	64.8	3.3	2.69	1.30	0.011	0.0013	0.32	0.0032	0.0011	0.64	0.033	13.00	60.01	24.51	0.29	0.019	6.58	0.121	0.060	7.37	0.57	99.54
Pl3.1	30.1	66.7	3.2	2.71	1.28	0.012	0.0013	0.30	0.0026	0.0013	0.66	0.032	13.00	60.43	24.26	0.31	0.019	6.20	0.100	0.077	7.60	0.56	99.56
Pl4.1	32.3	64.7	3.0	2.68	1.31	0.012	0.0014	0.32	0.0033	0.0011	0.64	0.030	13.00	59.64	24.71	0.31	0.021	6.69	0.125	0.060	7.40	0.52	99.47
Pl5.1	32.5	64.5	3.0	2.68	1.30	0.012	0.0011	0.33	0.0033	0.0011	0.65	0.030	13.01	59.61	24.49	0.31	0.016	6.78	0.128	0.064	7.45	0.52	99.37
Pl6.1	42.1	55.9	2.0	2.59	1.40	0.014	0.0018	0.42	0.0040	0.0006	0.55	0.019	12.99	57.75	26.35	0.36	0.028	8.63	0.152	b.d.l.	6.33	0.34	99.97
Pl7.1	26.6	69.5	3.9	2.75	1.24	0.012	0.0013	0.26	0.0026	0.0012	0.69	0.038	13.00	61.17	23.31	0.33	0.019	5.47	0.100	0.068	7.90	0.67	99.02
Pl8.1	26.6	69.7	3.7	2.75	1.24	0.012	0.0011	0.26	0.0028	0.0012	0.68	0.036	12.99	61.46	23.49	0.31	0.017	5.45	0.109	0.069	7.89	0.64	99.43
Pl8.2	30.8	65.9	3.2	2.70	1.28	0.010	0.0013	0.31	0.0029	0.0014	0.66	0.032	13.00	60.19	24.17	0.28	0.019	6.40	0.110	0.082	7.57	0.56	99.37
Pl9.1	26.0	69.8	4.2	2.75	1.23	0.010	0.0010	0.27	0.0026	0.0016	0.71	0.043	13.02	b.d.l.	b.d.l.	b.d.l.	b.d.l.	b.d.l.	b.d.l.	b.d.l.	b.d.l.	b.d.l.	98.31
Mount_Q-4 (1932)																							
Pl1.1	31.7	65.2	3.1	2.68	1.31	0.013	0.0013	0.32	0.0031	0.0012	0.66	0.031	13.01	59.45	24.75	0.34	0.019	6.62	0.119	0.067	7.53	0.54	99.42
Pl10.1	74.7	24.9	0.4	2.22	1.77	0.016	0.0014	0.76	0.0036	b.d.l.	0.25	0.005	13.02	48.00	32.49	0.42	0.020	15.30	0.136	b.d.l.	2.81	0.08	99.25
Pl10.2	51.3	47.3	1.4	2.46	1.53	0.012	0.0017	0.52	0.0037	0.0002	0.48	0.014	13.02	53.73	28.29	0.31	0.026	10.52	0.141	b.d.l.	5.36	0.24	98.63
Pl11.1	51.3	47.3	1.4	2.46	1.53	0.010	0.0012	0.52	0.0042	0.0004	0.48	0.014	13.02	53.65	28.32	0.27	0.017	10.59	0.158	b.d.l.	5.40	0.24	98.67
Pl11.2	31.5	65.6	3.0	2.67	1.33	0.012	0.0015	0.31	0.0031	0.0012	0.65	0.030	13.01	b.d.l.	b.d.l.	b.d.l.	b.d.l.	b.d.l.	b.d.l.	b.d.l.	b.d.l.	b.d.l.	98.29
Pl2.1	54.4	44.4	1.2	2.44	1.54	0.015	0.0018	0.55	0.0042	0.0003	0.45	0.012	13.02	53.57	28.57	0.39	0.027	11.30	0.160	b.d.l.	5.09	0.21	99.35
Pl3.1	34.9	62.5	2.5	2.64	1.35	0.013	0.0015	0.35	0.0040	0.0008	0.62	0.025	13.01	b.d.l.	b.d.l.	b.d.l.	b.d.l.	b.d.l.	b.d.l.	b.d.l.	b.d.l.	b.d.l.	98.22

Appendix B1 cotinued

Label	An[2]	Ab[3]	Or[4]	Si	Al	Fe	Mg	Ca	Sr	Ba	Na	K	Tot[5]	SiO_2	Al_2O_3	FeO	MgO	CaO	SrO	BaO	Na_2O	K_2O	Tot
Pl4.1	47.3	51.0	1.7	2.50	1.49	0.012	0.0013	0.48	0.0037	0.0003	0.52	0.017	13.02	54.92	27.66	0.31	0.020	9.82	0.139	b.d.l.	5.85	0.29	99.03
Pl4.2	49.5	49.0	1.5	2.47	1.52	0.013	0.0017	0.50	0.0042	0.0004	0.50	0.016	13.02	b.d.l.	b.d.l.	b.d.l.	b.d.l.	b.d.l.	b.d.l.	b.d.l.	b.d.l.	b.d.l.	98.16
Pl5.1	31.6	65.3	3.1	2.66	1.33	0.010	0.0015	0.32	0.0029	0.0017	0.66	0.032	13.02	b.d.l.	b.d.l.	b.d.l.	b.d.l.	b.d.l.	b.d.l.	b.d.l.	b.d.l.	b.d.l.	98.49
Pl6.1	78.0	21.5	0.5	2.16	1.83	0.015	0.0011	0.80	0.0046	0.0002	0.22	0.005	13.04	b.d.l.	b.d.l.	b.d.l.	b.d.l.	b.d.l.	b.d.l.	b.d.l.	b.d.l.	b.d.l.	97.36
Pl6.2	36.2	61.3	2.5	2.61	1.38	0.012	0.0013	0.36	0.0038	0.0006	0.62	0.025	13.02	b.d.l.	b.d.l.	b.d.l.	b.d.l.	b.d.l.	b.d.l.	b.d.l.	b.d.l.	b.d.l.	98.35
Pl6.3	78.6	20.9	0.4	2.17	1.83	0.015	0.0009	0.79	0.0038	0.0005	0.21	0.004	13.03	b.d.l.	b.d.l.	b.d.l.	b.d.l.	b.d.l.	b.d.l.	b.d.l.	b.d.l.	b.d.l.	98.03
Pl7.1	28.8	67.5	3.7	2.72	1.27	0.011	0.0010	0.29	0.0029	0.0013	0.67	0.037	13.00	60.17	23.87	0.30	0.015	5.90	0.112	0.071	7.66	0.63	98.74
Pl8.1	29.3	67.5	3.2	2.69	1.31	0.011	0.0016	0.29	0.0031	0.0013	0.67	0.032	13.01	b.d.l.	b.d.l.	b.d.l.	b.d.l.	b.d.l.	b.d.l.	b.d.l.	b.d.l.	b.d.l.	98.10
Pl9.1	50.8	47.9	1.4	2.46	1.53	0.018	0.0025	0.52	0.0051	0.0002	0.49	0.014	13.03	b.d.l.	b.d.l.	b.d.l.	b.d.l.	b.d.l.	b.d.l.	b.d.l.	b.d.l.	b.d.l.	97.81
Mount_Q-6 (1932)																							
Pl1.1	50.4	48.3	1.3	2.48	1.51	0.016	0.0016	0.51	0.0035	0.0007	0.49	0.013	13.02	54.30	28.02	0.42	0.023	10.43	0.134	b.d.l.	5.52	0.23	99.12
Pl1.2	34.3	63.1	2.5	2.63	1.35	0.012	0.0013	0.35	0.0028	0.0007	0.65	0.026	13.03	59.25	25.81	0.32	0.020	7.38	0.108	b.d.l.	7.51	0.46	100.90
Pl10.1	45.5	52.8	1.7	2.52	1.47	0.016	0.0019	0.46	0.0042	0.0006	0.54	0.017	13.03	55.13	27.33	0.41	0.027	9.49	0.158	b.d.l.	6.09	0.29	98.96
Pl10.2	33.3	64.1	2.6	2.63	1.36	0.012	0.0017	0.34	0.0038	0.0011	0.65	0.027	13.03	57.89	25.37	0.31	0.025	6.98	0.145	0.059	7.42	0.46	98.65
Pl11.1	36.2	61.4	2.5	2.61	1.38	0.012	0.0011	0.37	0.0034	0.0013	0.62	0.025	13.02	57.83	25.96	0.31	0.016	7.55	0.129	0.075	7.08	0.43	99.39
Pl12.1	34.9	62.6	2.5	2.63	1.36	0.011	0.0012	0.35	0.0035	0.0006	0.63	0.026	13.02	58.18	25.51	0.29	0.017	7.29	0.135	b.d.l.	7.23	0.44	99.14
Pl13.1	29.3	67.7	3.0	2.68	1.31	0.012	0.0012	0.30	0.0022	0.0014	0.69	0.031	13.02	59.84	24.77	0.32	0.018	6.16	0.086	0.078	7.88	0.53	99.68
Pl14.1	34.4	63.0	2.6	2.62	1.36	0.012	0.0013	0.36	0.0033	0.0006	0.65	0.027	13.04	58.24	25.72	0.33	0.019	7.37	0.126	b.d.l.	7.47	0.47	99.77
Pl14.2	28.5	68.2	3.3	2.69	1.30	0.011	0.0012	0.29	0.0029	0.0013	0.70	0.033	13.03	59.56	24.48	0.30	0.017	6.00	0.110	0.076	7.95	0.58	99.07
Pl2.1	44.8	53.6	1.7	2.53	1.46	0.014	0.0016	0.45	0.0039	0.0006	0.54	0.017	13.02	55.78	27.31	0.36	0.023	9.28	0.149	b.d.l.	6.14	0.29	99.36
Pl3.1	31.3	65.7	3.0	2.67	1.32	0.012	0.0012	0.32	0.0028	0.0012	0.67	0.031	13.02	59.90	25.09	0.32	0.017	6.67	0.107	0.071	7.75	0.54	100.46
Pl4.1	53.7	45.2	1.1	2.42	1.57	0.010	0.0014	0.55	0.0035	0.0005	0.46	0.012	13.03	53.10	29.09	0.27	0.021	11.27	0.134	b.d.l.	5.23	0.20	99.34
Pl5.1	40.5	57.4	2.1	2.56	1.42	0.009	0.0012	0.42	0.0033	0.0010	0.59	0.021	13.03	56.69	26.74	0.24	0.018	8.59	0.127	0.057	6.72	0.37	99.55
Pl6.1	33.1	64.4	2.5	2.64	1.36	0.011	0.0010	0.34	0.0023	0.0006	0.66	0.026	13.03	58.52	25.55	0.30	0.016	7.00	0.089	b.d.l.	7.53	0.45	99.49
Pl7.1	26.3	70.0	3.6	2.71	1.28	0.012	0.0013	0.27	0.0033	0.0015	0.71	0.037	13.02	60.49	24.19	0.31	0.019	5.57	0.127	0.085	8.20	0.65	99.64
Pl7.2	31.4	65.5	3.1	2.65	1.34	0.012	0.0013	0.32	0.0029	0.0013	0.67	0.032	13.03	58.44	25.03	0.31	0.019	6.62	0.110	0.074	7.64	0.55	98.79
Pl8.1	52.3	46.5	1.2	2.44	1.55	0.010	0.0012	0.54	0.0033	0.0006	0.48	0.012	13.03	53.12	28.62	0.26	0.018	10.88	0.122	b.d.l.	5.36	0.21	98.63
Pl8.2	54.1	44.8	1.1	2.41	1.58	0.010	0.0013	0.55	0.0031	0.0009	0.46	0.011	13.03	52.74	29.30	0.26	0.019	11.26	0.115	0.048	5.15	0.19	99.08
Pl9.1	45.3	53.0	1.7	2.50	1.49	0.011	0.0009	0.46	0.0034	0.0001	0.54	0.017	13.03	54.89	27.75	0.28	0.014	9.46	0.127	b.d.l.	6.12	0.30	98.95

Appendix B1 cotinued

Label	An[2]	Ab[3]	Or[4]	Si	Al	Fe	Mg	Ca	Sr	Ba	Na	K	Tot[5]	SiO_2	Al_2O_3	FeO	MgO	CaO	SrO	BaO	Na_2O	K_2O	Tot
Mount_VQ-06-17 125-250 µm (1932)																							
Pl1.1	29.5	67.2	3.3	2.68	1.31	0.013	0.0012	0.30	0.0027	0.0016	0.69	0.033	13.03	b.d.l.	b.d.l.	b.d.l.	b.d.l.	b.d.l.	b.d.l.	b.d.l.	b.d.l.	b.d.l.	98.03
Pl10.1	29.8	66.7	3.5	2.70	1.29	0.011	0.0011	0.30	0.0032	0.0014	0.67	0.035	13.00	60.14	24.39	0.29	0.017	6.17	0.125	0.082	7.64	0.61	99.47
Pl11.1	29.3	67.3	3.4	2.71	1.28	0.012	0.0012	0.29	0.0029	0.0012	0.67	0.034	13.01	60.43	24.19	0.31	0.018	6.11	0.110	0.071	7.75	0.59	99.57
Pl12.1	30.5	66.3	3.3	2.69	1.30	0.011	0.0007	0.31	0.0035	0.0014	0.66	0.033	13.01	59.76	24.55	0.28	0.011	6.34	0.133	0.078	7.61	0.57	99.33
Pl12.2	46.0	52.1	1.9	2.53	1.46	0.010	0.0013	0.46	0.0033	0.0008	0.52	0.019	13.01	55.88	27.38	0.27	0.019	9.49	0.125	b.d.l.	5.94	0.32	99.48
Pl12.3	79.0	20.5	0.4	2.19	1.80	0.012	0.0013	0.80	0.0032	b.d.l.	0.21	0.004	13.02	47.77	33.28	0.31	0.019	16.21	0.120	b.d.l.	2.33	0.07	100.11
Pl13.1	37.7	59.9	2.4	2.62	1.36	0.011	0.0012	0.38	0.0035	0.0014	0.61	0.024	13.01	58.17	25.62	0.29	0.018	7.92	0.133	0.079	6.95	0.42	99.60
Pl13.2	27.4	69.2	3.4	2.73	1.26	0.013	0.0011	0.27	0.0027	0.0015	0.69	0.034	13.01	61.08	23.87	0.35	0.017	5.71	0.103	0.087	7.99	0.60	99.81
Pl14.1	28.7	68.0	3.3	2.72	1.28	0.008	0.0008	0.28	0.0025	0.0014	0.67	0.033	13.00	60.67	24.17	0.21	0.013	5.89	0.095	0.082	7.73	0.57	99.45
Pl15.1	45.4	52.9	1.7	2.53	1.46	0.009	0.0013	0.46	0.0036	0.0006	0.53	0.017	13.01	56.50	27.75	0.25	0.019	9.50	0.137	b.d.l.	6.12	0.30	100.60
Pl15.2	32.0	65.0	3.0	2.68	1.31	0.011	0.0010	0.32	0.0029	0.0013	0.65	0.030	13.01	59.63	24.82	0.28	0.015	6.71	0.110	0.071	7.52	0.52	99.66
Pl16.1	78.6	20.9	0.5	2.19	1.79	0.013	0.0008	0.80	0.0042	0.0002	0.21	0.005	13.02	47.58	33.00	0.32	0.012	16.16	0.159	b.d.l.	2.37	0.08	99.70
Pl16.2	65.7	33.4	0.9	2.32	1.67	0.011	0.0010	0.66	0.0041	b.d.l.	0.34	0.009	13.02	50.82	30.90	0.29	0.014	13.52	0.154	b.d.l.	3.80	0.16	99.65
Pl17.1	24.8	70.8	4.4	2.75	1.24	0.010	0.0007	0.25	0.0027	0.0015	0.71	0.044	13.01	61.25	23.51	0.28	0.010	5.20	0.104	0.086	8.20	0.77	99.41
Pl2.1	29.0	67.7	3.3	2.70	1.29	0.012	0.0008	0.29	0.0025	0.0013	0.68	0.033	13.01	b.d.l.	b.d.l.	b.d.l.	b.d.l.	b.d.l.	b.d.l.	b.d.l.	b.d.l.	b.d.l.	98.34
Pl2.2	39.9	57.9	2.1	2.58	1.40	0.013	0.0009	0.40	0.0039	0.0008	0.59	0.022	13.02	57.35	26.39	0.34	0.014	8.39	0.150	0.046	6.72	0.38	99.77
Pl3.1	26.6	69.6	3.8	2.73	1.26	0.011	0.0012	0.27	0.0026	0.0014	0.70	0.038	13.01	60.76	23.77	0.30	0.019	5.53	0.101	0.078	7.99	0.65	99.20
Pl3.2	32.3	65.0	2.8	2.66	1.33	0.011	0.0013	0.33	0.0030	0.0013	0.66	0.028	13.02	58.79	25.04	0.28	0.020	6.78	0.113	0.074	7.54	0.49	99.12
Pl4.1	54.0	44.7	1.3	2.45	1.53	0.011	0.0013	0.55	0.0034	0.0008	0.45	0.013	13.02	54.21	28.72	0.28	0.019	11.31	0.129	b.d.l.	5.17	0.22	100.10
Pl5.1	35.1	62.2	2.7	2.65	1.33	0.012	0.0013	0.35	0.0034	0.0008	0.62	0.027	13.01	59.71	25.51	0.31	0.020	7.40	0.130	0.049	7.26	0.47	100.87
Pl5.2	46.4	52.1	1.5	2.52	1.47	0.010	0.0014	0.47	0.0036	0.0010	0.53	0.016	13.02	55.91	27.59	0.27	0.021	9.69	0.137	0.056	6.02	0.27	99.96
Pl6.1	32.5	64.5	3.0	2.68	1.30	0.012	0.0015	0.33	0.0020	0.0013	0.66	0.031	13.02	b.d.l.	b.d.l.	b.d.l.	b.d.l.	b.d.l.	b.d.l.	b.d.l.	b.d.l.	b.d.l.	97.97
Pl7.1	32.2	64.8	3.0	2.67	1.32	0.011	0.0012	0.32	0.0025	0.0010	0.65	0.030	13.01	60.05	25.09	0.30	0.019	6.80	0.098	0.057	7.56	0.53	100.52
Pl8.1	84.7	15.1	0.2	2.13	1.85	0.011	0.0006	0.87	0.0034	0.0001	0.15	0.002	13.02	45.81	33.73	0.28	0.008	17.36	0.126	b.d.l.	1.71	0.03	99.06
Pl9.1	50.1	48.3	1.5	2.49	1.50	0.016	0.0023	0.50	0.0053	0.0002	0.48	0.016	13.01	54.49	27.80	0.42	0.034	10.26	0.199	b.d.l.	5.46	0.27	98.94
Pl9.2	35.9	61.7	2.4	2.64	1.35	0.013	0.0013	0.36	0.0043	0.0009	0.62	0.024	13.01	58.41	25.31	0.35	0.020	7.40	0.164	0.053	7.04	0.42	99.17
Mount_VQ-07-37D 125-250 µm (1932)																							
Pl1.2	31.5	65.5	2.9	2.68	1.31	0.011	0.0013	0.31	0.0033	0.0013	0.65	0.029	13.01	59.83	24.80	0.30	0.019	6.55	0.128	0.077	7.52	0.51	99.74
Pl10.1	31.1	66.0	2.9	2.69	1.30	0.012	0.0010	0.31	0.0031	0.0009	0.66	0.029	13.01	60.07	24.64	0.31	0.015	6.47	0.120	0.054	7.60	0.51	99.79

Appendix B1 cotinued

Label	An[2]	Ab[3]	Or[4]	Si	Al	Fe	Mg	Ca	Sr	Ba	Na	K	Tot[5]	SiO_2	Al_2O_3	FeO	MgO	CaO	SrO	BaO	Na_2O	K_2O	Tot
Pl11.1	34.2	62.8	3.0	2.66	1.32	0.014	0.0019	0.34	0.0034	0.0010	0.63	0.030	13.01	59.10	24.92	0.37	0.028	7.09	0.130	0.056	7.19	0.52	99.39
Pl12.1	25.0	71.9	3.0	2.75	1.25	0.004	b.d.l.	0.25	0.0023	0.0004	0.72	0.031	13.01	61.11	23.59	0.11	b.d.l.	5.22	0.087	b.d.l.	8.29	0.53	98.96
Pl12.2	49.2	49.6	1.1	2.49	1.49	0.011	0.0006	0.50	0.0037	0.0011	0.51	0.012	13.02	54.86	27.77	0.30	0.009	10.33	0.140	0.063	5.75	0.20	99.43
Pl13.1	32.2	64.6	3.1	2.68	1.30	0.013	0.0013	0.32	0.0028	0.0010	0.65	0.031	13.01	59.44	24.49	0.34	0.019	6.67	0.105	0.059	7.39	0.55	99.06
Pl13.2	36.4	61.3	2.3	2.63	1.35	0.014	0.0013	0.37	0.0029	0.0010	0.62	0.023	13.02	58.52	25.54	0.37	0.019	7.65	0.113	0.058	7.12	0.40	99.80
Pl14.1	25.1	70.5	4.4	2.74	1.25	0.009	0.0006	0.25	0.0019	0.0014	0.71	0.045	13.02	60.63	23.51	0.24	0.009	5.24	0.074	0.076	8.15	0.78	98.71
Pl15.1	35.5	61.9	2.6	2.64	1.35	0.012	0.0011	0.36	0.0034	0.0012	0.62	0.026	13.01	58.16	25.16	0.31	0.016	7.30	0.129	0.069	7.04	0.45	98.63
Pl16.1	34.3	63.2	2.5	2.64	1.35	0.011	0.0015	0.35	0.0024	0.0008	0.64	0.026	13.02	58.46	25.42	0.29	0.023	7.18	0.092	0.046	7.31	0.44	99.27
Pl16.2	75.0	24.6	0.4	2.23	1.76	0.011	0.0010	0.76	0.0021	0.0003	0.25	0.004	13.01	48.48	32.33	0.29	0.014	15.30	0.079	b.d.l.	2.78	0.07	99.35
Pl17.1	36.2	61.4	2.4	2.62	1.36	0.013	0.0014	0.37	0.0035	0.0006	0.62	0.025	13.02	57.75	25.49	0.34	0.021	7.55	0.134	b.d.l.	7.07	0.42	98.81
Pl18.1	32.3	64.6	3.0	2.69	1.30	0.011	0.0011	0.32	0.0030	0.0012	0.64	0.030	12.99	59.46	24.35	0.29	0.017	6.56	0.116	0.069	7.24	0.52	98.62
Pl19.1	33.3	63.8	2.9	2.67	1.32	0.013	0.0013	0.34	0.0031	0.0011	0.65	0.029	13.01	58.99	24.73	0.33	0.020	6.97	0.120	0.061	7.39	0.50	99.11
Pl2.1	45.2	53.0	1.8	2.55	1.44	0.010	0.0012	0.45	0.0033	0.0010	0.53	0.018	13.01	56.15	26.98	0.26	0.018	9.32	0.127	0.054	6.03	0.31	99.25
Pl20.1	54.0	44.8	1.2	2.46	1.53	0.010	0.0013	0.54	0.0032	0.0007	0.45	0.012	13.01	53.71	28.42	0.27	0.019	11.10	0.119	b.d.l.	5.09	0.20	98.96
Pl21.1	32.7	64.2	3.1	2.67	1.32	0.012	0.0011	0.33	0.0025	0.0016	0.65	0.031	13.01	b.d.l.	b.d.l.	b.d.l.	b.d.l.	b.d.l.	b.d.l.	b.d.l.	b.d.l.	b.d.l.	98.41
Pl22.1	34.8	62.7	2.6	2.64	1.35	0.012	0.0014	0.35	0.0037	0.0009	0.63	0.026	13.02	58.52	25.41	0.31	0.021	7.29	0.143	0.051	7.26	0.45	99.46
Pl23.1	30.0	66.5	3.4	2.69	1.30	0.011	0.0011	0.30	0.0026	0.0010	0.67	0.035	13.01	b.d.l.	b.d.l.	b.d.l.	b.d.l.	b.d.l.	b.d.l.	b.d.l.	b.d.l.	b.d.l.	98.33
Pl24.1	38.4	59.3	2.3	2.61	1.37	0.013	0.0013	0.39	0.0028	0.0007	0.60	0.023	13.02	57.39	25.65	0.35	0.020	7.99	0.108	b.d.l.	6.82	0.40	98.77
Pl24.2	57.7	41.3	1.0	2.41	1.58	0.013	0.0016	0.58	0.0036	0.0004	0.42	0.010	13.01	53.06	29.41	0.34	0.023	11.94	0.136	b.d.l.	4.72	0.17	99.83
Pl25.1	31.8	65.2	3.0	2.68	1.31	0.013	0.0008	0.32	0.0032	0.0009	0.66	0.030	13.01	59.49	24.73	0.33	0.013	6.66	0.123	0.053	7.54	0.53	99.46
Pl26.1	33.4	63.6	3.0	2.66	1.33	0.012	0.0015	0.34	0.0031	0.0009	0.64	0.030	13.01	59.14	25.07	0.31	0.022	6.99	0.121	0.050	7.34	0.52	99.57
Pl27.1	36.1	61.3	2.6	2.64	1.34	0.013	0.0013	0.37	0.0027	0.0011	0.62	0.027	13.01	58.22	25.06	0.33	0.019	7.53	0.101	0.061	7.06	0.46	98.85
Pl28.1	35.4	62.0	2.6	2.64	1.34	0.012	0.0013	0.36	0.0034	0.0007	0.62	0.026	13.01	58.50	25.20	0.32	0.020	7.33	0.130	b.d.l.	7.09	0.45	99.09
Pl29.1	34.5	63.0	2.5	2.65	1.33	0.012	0.0015	0.35	0.0032	0.0012	0.64	0.025	13.01	58.98	25.17	0.32	0.022	7.24	0.122	0.070	7.29	0.44	99.65
Pl3.1	33.3	63.9	2.8	2.67	1.32	0.012	0.0011	0.33	0.0028	0.0009	0.64	0.028	13.01	59.38	24.93	0.32	0.017	6.91	0.109	0.051	7.34	0.49	99.54
Pl30.1	30.9	66.1	3.0	2.69	1.30	0.011	0.0013	0.31	0.0035	0.0013	0.66	0.030	13.01	59.84	24.66	0.30	0.020	6.44	0.133	0.073	7.60	0.52	99.59
Pl30.2	38.7	59.0	2.3	2.61	1.38	0.012	0.0013	0.39	0.0035	0.0011	0.59	0.023	13.01	57.55	25.89	0.31	0.020	8.02	0.132	0.061	6.77	0.40	99.14
Pl31.1	32.9	64.3	2.8	2.66	1.32	0.013	0.0010	0.33	0.0031	0.0014	0.65	0.029	13.01	59.06	24.84	0.36	0.015	6.87	0.118	0.077	7.42	0.50	99.24
Pl32.1	46.1	51.9	2.0	2.52	1.46	0.012	0.0009	0.47	0.0029	0.0012	0.53	0.020	13.02	b.d.l.	b.d.l.	b.d.l.	b.d.l.	b.d.l.	b.d.l.	b.d.l.	b.d.l.	b.d.l.	97.41
Pl32.2	31.8	65.3	2.9	2.68	1.31	0.012	0.0010	0.32	0.0030	0.0008	0.66	0.029	13.01	59.14	24.55	0.32	0.015	6.62	0.116	0.046	7.51	0.50	98.82

Appendix B1 cotinued

Label	An[2]	Ab[3]	Or[4]	Si	Al	Fe	Mg	Ca	Sr	Ba	Na	K	Tot[5]	SiO_2	Al_2O_3	FeO	MgO	CaO	SrO	BaO	Na_2O	K_2O	Tot
Pl33.1	49.9	48.5	1.5	2.48	1.51	0.014	0.0019	0.51	0.0040	0.0002	0.50	0.016	13.02	b.d.l.	b.d.l.	b.d.l.	b.d.l.	b.d.l.	b.d.l.	b.d.l.	b.d.l.	b.d.l.	97.23
Pl4.1	55.7	43.0	1.2	2.43	1.55	0.016	0.0017	0.57	0.0045	0.0005	0.44	0.012	13.02	53.62	28.92	0.43	0.026	11.63	0.172	b.d.l.	4.96	0.21	99.98
Pl5.1	47.3	51.1	1.6	2.52	1.46	0.015	0.0014	0.48	0.0044	0.0004	0.51	0.016	13.01	55.45	27.22	0.39	0.021	9.75	0.166	b.d.l.	5.82	0.28	99.11
Pl6.1	64.3	34.9	0.8	2.35	1.62	0.022	0.0024	0.65	0.0041	0.0001	0.35	0.008	13.02	51.14	29.86	0.57	0.034	13.22	0.155	b.d.l.	3.96	0.13	99.08
Pl7.1	49.3	49.1	1.6	2.49	1.49	0.010	0.0010	0.50	0.0028	0.0008	0.50	0.016	13.02	55.16	27.93	0.28	0.015	10.39	0.108	0.046	5.72	0.28	99.92
Pl8.1	30.4	66.4	3.2	2.70	1.29	0.011	0.0012	0.30	0.0030	0.0011	0.66	0.032	13.00	59.93	24.25	0.30	0.018	6.29	0.116	0.061	7.58	0.56	99.10
Pl9.1	51.8	46.7	1.4	2.46	1.52	0.018	0.0028	0.52	0.0052	0.0006	0.47	0.015	13.02	53.89	28.25	0.47	0.041	10.65	0.197	b.d.l.	5.30	0.25	99.09
Mount_VQ-07-37D 250-500 µm (1932)																							
Pl1.1	33.1	64.1	2.8	2.68	1.31	0.011	0.0011	0.33	0.0027	0.0010	0.64	0.028	13.01	58.97	24.43	0.30	0.016	6.85	0.101	0.055	7.32	0.49	98.53
Pl1.2	47.4	50.8	1.7	2.52	1.46	0.012	0.0010	0.48	0.0031	0.0006	0.52	0.018	13.02	b.d.l.	b.d.l.	b.d.l.	b.d.l.	b.d.l.	b.d.l.	b.d.l.	b.d.l.	b.d.l.	98.35
Pl10.1	45.6	52.7	1.7	2.54	1.44	0.015	0.0021	0.46	0.0037	0.0005	0.53	0.017	13.01	55.86	26.73	0.39	0.031	9.47	0.139	b.d.l.	6.04	0.30	98.99
Pl11.1	27.5	68.4	4.1	2.73	1.25	0.010	0.0008	0.27	0.0024	0.0015	0.68	0.041	13.00	b.d.l.	b.d.l.	b.d.l.	b.d.l.	b.d.l.	b.d.l.	b.d.l.	b.d.l.	b.d.l.	97.96
Pl12.1	45.2	53.0	1.8	2.55	1.44	0.011	0.0011	0.46	0.0026	0.0008	0.54	0.018	13.02	b.d.l.	b.d.l.	b.d.l.	b.d.l.	b.d.l.	b.d.l.	b.d.l.	b.d.l.	b.d.l.	97.55
Pl13.1	30.4	66.3	3.3	2.71	1.28	0.013	0.0013	0.30	0.0025	0.0015	0.66	0.034	13.01	59.74	23.96	0.33	0.019	6.29	0.094	0.084	7.57	0.58	98.67
Pl14.1	34.2	63.1	2.7	2.66	1.32	0.013	0.0010	0.34	0.0033	0.0009	0.63	0.027	13.00	59.48	25.04	0.34	0.015	7.11	0.129	0.054	7.25	0.48	99.89
Pl15.1	52.0	46.7	1.3	2.49	1.50	0.010	0.0011	0.52	0.0038	0.0003	0.46	0.013	13.00	54.71	28.06	0.27	0.016	10.60	0.143	b.d.l.	5.25	0.23	99.29
Pl16.1	33.0	63.9	3.1	2.69	1.30	0.011	0.0013	0.33	0.0026	0.0009	0.64	0.031	13.00	59.21	24.29	0.30	0.020	6.79	0.101	0.048	7.26	0.54	98.56
Pl17.1	33.6	63.6	2.7	2.68	1.31	0.012	0.0014	0.33	0.0036	0.0011	0.63	0.027	12.99	59.23	24.58	0.32	0.020	6.85	0.138	0.063	7.16	0.47	98.82
Pl17.2	51.6	47.0	1.4	2.49	1.49	0.011	0.0011	0.52	0.0032	0.0004	0.47	0.014	13.00	54.40	27.62	0.29	0.016	10.54	0.120	b.d.l.	5.31	0.24	98.56
Pl18.1	30.9	65.5	3.6	2.69	1.29	0.011	0.0009	0.31	0.0029	0.0011	0.66	0.036	13.01	59.66	24.31	0.29	0.013	6.46	0.112	0.060	7.56	0.63	99.10
Pl19.1	46.9	51.5	1.6	2.54	1.44	0.010	0.0010	0.47	0.0035	0.0006	0.52	0.017	13.00	55.99	26.89	0.26	0.014	9.67	0.134	b.d.l.	5.87	0.28	99.14
Pl2.1	29.2	67.2	3.6	2.72	1.27	0.013	0.0013	0.29	0.0029	0.0016	0.67	0.036	13.00	b.d.l.	b.d.l.	b.d.l.	b.d.l.	b.d.l.	b.d.l.	b.d.l.	b.d.l.	b.d.l.	97.84
Pl20.1	24.5	70.8	4.7	2.78	1.21	0.009	0.0011	0.24	0.0023	0.0016	0.71	0.047	13.00	62.01	22.94	0.23	0.016	5.09	0.090	0.093	8.12	0.81	99.40
Pl21.1	31.5	65.5	3.0	2.70	1.28	0.011	0.0013	0.31	0.0027	0.0014	0.65	0.030	13.00	60.56	24.34	0.30	0.019	6.54	0.105	0.083	7.51	0.52	99.97
Pl22.1	47.3	50.3	2.4	2.54	1.44	0.012	0.0018	0.47	0.0025	0.0008	0.50	0.024	13.00	55.94	26.94	0.31	0.027	9.65	0.095	0.046	5.66	0.41	99.08
Pl23.1	34.8	62.2	3.0	2.68	1.30	0.011	0.0015	0.35	0.0035	0.0014	0.62	0.030	12.99	59.77	24.57	0.30	0.022	7.19	0.136	0.081	7.11	0.52	99.71
Pl24.1	30.2	66.6	3.2	2.72	1.27	0.012	0.0008	0.30	0.0024	0.0011	0.66	0.032	12.99	60.67	23.95	0.32	0.013	6.21	0.094	0.062	7.56	0.55	99.44
Pl25.1	57.0	41.7	1.3	2.43	1.55	0.010	0.0010	0.58	0.0030	b.d.l.	0.42	0.013	13.01	b.d.l.	b.d.l.	b.d.l.	b.d.l.	b.d.l.	b.d.l.	b.d.l.	b.d.l.	b.d.l.	98.46
Pl25.2	59.6	39.3	1.1	2.40	1.59	0.012	0.0012	0.60	0.0032	0.0006	0.39	0.011	13.01	52.31	29.54	0.30	0.018	12.19	0.119	b.d.l.	4.44	0.18	99.14
Pl26.1	31.2	65.5	3.4	2.70	1.28	0.011	0.0011	0.31	0.0027	0.0010	0.65	0.034	13.00	b.d.l.	b.d.l.	b.d.l.	b.d.l.	b.d.l.	b.d.l.	b.d.l.	b.d.l.	b.d.l.	98.40

Appendix B1 cotinued

Label	An[2]	Ab[3]	Or[4]	Si	Al	Fe	Mg	Ca	Sr	Ba	Na	K	Tot[5]	SiO_2	Al_2O_3	FeO	MgO	CaO	SrO	BaO	Na_2O	K_2O	Tot
Pl26.2	45.5	52.7	1.8	2.52	1.46	0.012	0.0010	0.47	0.0040	0.0003	0.54	0.019	13.03	b.d.l.	b.d.l.	b.d.l.	b.d.l.	b.d.l.	b.d.l.	b.d.l.	b.d.l.	b.d.l.	97.98
Pl27.1	35.6	61.9	2.5	2.66	1.33	0.013	0.0016	0.35	0.0039	0.0009	0.62	0.025	13.00	59.04	25.04	0.35	0.024	7.34	0.148	0.050	7.05	0.43	99.48
Pl28.1	39.4	58.2	2.4	2.62	1.36	0.011	0.0012	0.40	0.0032	0.0006	0.59	0.024	13.01	b.d.l.	b.d.l.	b.d.l.	b.d.l.	b.d.l.	b.d.l.	b.d.l.	b.d.l.	b.d.l.	98.01
Pl28.2	36.7	60.6	2.7	2.65	1.33	0.013	0.0014	0.37	0.0037	0.0009	0.61	0.027	13.00	b.d.l.	b.d.l.	b.d.l.	b.d.l.	b.d.l.	b.d.l.	b.d.l.	b.d.l.	b.d.l.	98.21
Pl29.1	42.8	55.2	2.0	2.59	1.39	0.011	0.0014	0.43	0.0028	0.0009	0.56	0.020	13.00	56.76	25.88	0.28	0.020	8.80	0.107	0.048	6.28	0.34	98.51
Pl3.1	31.6	65.1	3.3	2.70	1.29	0.013	0.0012	0.32	0.0026	0.0018	0.65	0.033	13.01	b.d.l.	b.d.l.	b.d.l.	b.d.l.	b.d.l.	b.d.l.	b.d.l.	b.d.l.	b.d.l.	98.45
Pl30.1	31.2	65.4	3.4	2.71	1.27	0.011	0.0015	0.31	0.0026	0.0015	0.65	0.034	12.99	60.22	23.88	0.28	0.023	6.41	0.100	0.086	7.41	0.59	98.99
Pl31.1	32.1	64.6	3.3	2.70	1.28	0.012	0.0013	0.32	0.0025	0.0015	0.65	0.033	13.00	b.d.l.	b.d.l.	b.d.l.	b.d.l.	b.d.l.	b.d.l.	b.d.l.	b.d.l.	b.d.l.	97.22
Pl31.2	39.6	58.1	2.3	2.62	1.36	0.012	0.0013	0.40	0.0029	0.0013	0.58	0.023	13.00	b.d.l.	b.d.l.	b.d.l.	b.d.l.	b.d.l.	b.d.l.	b.d.l.	b.d.l.	b.d.l.	97.51
Pl32.1	28.7	67.5	3.7	2.72	1.27	0.009	0.0009	0.29	0.0021	0.0016	0.68	0.038	13.00	b.d.l.	b.d.l.	b.d.l.	b.d.l.	b.d.l.	b.d.l.	b.d.l.	b.d.l.	b.d.l.	96.99
Pl32.2	23.2	71.7	5.1	2.76	1.22	0.012	0.0008	0.24	0.0027	0.0021	0.73	0.051	13.01	b.d.l.	b.d.l.	b.d.l.	b.d.l.	b.d.l.	b.d.l.	b.d.l.	b.d.l.	b.d.l.	96.42
Pl33.1	24.5	70.5	5.0	2.77	1.21	0.009	0.0006	0.25	0.0021	0.0017	0.72	0.051	13.01	b.d.l.	b.d.l.	b.d.l.	b.d.l.	b.d.l.	b.d.l.	b.d.l.	b.d.l.	b.d.l.	96.04
Pl4.1	29.5	66.9	3.5	2.72	1.26	0.011	0.0012	0.29	0.0028	0.0012	0.66	0.035	12.99	60.43	23.78	0.30	0.018	6.05	0.108	0.067	7.57	0.60	98.92
Pl4.2	39.9	57.6	2.5	2.61	1.37	0.011	0.0009	0.40	0.0029	0.0006	0.58	0.025	13.00	57.75	25.77	0.29	0.013	8.27	0.110	b.d.l.	6.60	0.43	99.27
Pl5.1	35.1	62.3	2.6	2.67	1.31	0.012	0.0014	0.35	0.0033	0.0013	0.62	0.026	13.00	58.79	24.56	0.31	0.021	7.16	0.126	0.072	7.02	0.45	98.51
Pl6.1	30.3	66.2	3.5	2.71	1.27	0.013	0.0013	0.31	0.0033	0.0016	0.67	0.036	13.01	60.26	24.01	0.34	0.020	6.38	0.125	0.090	7.69	0.62	99.53
Pl6.2	54.2	44.4	1.4	2.45	1.53	0.011	0.0012	0.55	0.0028	0.0003	0.45	0.015	13.01	53.40	28.23	0.29	0.018	11.16	0.106	b.d.l.	5.06	0.25	98.53
Pl7.1	28.0	67.7	4.2	2.74	1.24	0.010	0.0006	0.28	0.0025	0.0016	0.68	0.043	13.00	b.d.l.	b.d.l.	b.d.l.	b.d.l.	b.d.l.	b.d.l.	b.d.l.	b.d.l.	b.d.l.	98.06
Pl8.1	38.1	59.4	2.4	2.62	1.36	0.013	0.0013	0.38	0.0036	0.0006	0.60	0.025	13.01	b.d.l.	b.d.l.	b.d.l.	b.d.l.	b.d.l.	b.d.l.	b.d.l.	b.d.l.	b.d.l.	98.31
Pl9.1	32.3	64.6	3.1	2.69	1.29	0.012	0.0016	0.32	0.0031	0.0013	0.65	0.031	13.00	b.d.l.	b.d.l.	b.d.l.	b.d.l.	b.d.l.	b.d.l.	b.d.l.	b.d.l.	b.d.l.	97.59

[1] analyses taken at University of Washington; b.d.l. = below detection limit

[2] An = anorthite content (100xCa/(Ca+Na+K)

[3] Ab = albite content (100xNa/(Ca+Na+K)

[4] Or = orthoclase content (100xK/(Ca+Na+K)

[5] Tot = atomic proportions total calculated assuming 8 oxygen cations

Appendix B2 Amphibole electron microprobe analyses (atomic proportions and weight concentrations)[1]

Label	Si	Ti	Al	Fe	Mn	Mg	Ca	Na	K	Cl	O	Tot	SiO_2	TiO_2	Al_2O_3	FeO	MnO	MgO	CaO	Na_2O	K_2O	Cl	Tot
Q-34 (1846/47)																							
Amph1.1	6.29	0.34	1.95	1.43	0.024	3.11	1.84	0.70	0.106	0.011	22.99	38.79	42.53	3.09	11.22	11.58	0.19	14.09	11.62	2.43	0.56	0.04	97.34
Amph1.2	6.32	0.29	1.94	1.53	0.026	3.09	1.82	0.71	0.096	0.015	22.99	38.82	42.98	2.64	11.17	12.44	0.21	14.11	11.56	2.49	0.51	0.06	98.16
Amph1.3	6.37	0.32	1.85	1.79	0.034	2.83	1.78	0.69	0.094	0.016	22.98	38.77	42.87	2.85	10.59	14.42	0.27	12.80	11.21	2.40	0.50	0.06	97.95
Amph1.4	6.52	0.33	1.68	1.47	0.054	3.05	1.78	0.70	0.110	0.026	22.97	38.70	44.37	2.99	9.70	11.96	0.44	13.92	11.31	2.45	0.59	0.10	97.81
Amph2.1	6.48	0.36	1.63	1.72	0.055	2.87	1.79	0.73	0.132	0.038	22.96	38.76	43.77	3.20	9.35	13.87	0.44	12.99	11.28	2.54	0.70	0.15	98.26
Amph2.2	6.44	0.36	1.69	1.53	0.045	3.07	1.77	0.76	0.103	0.024	22.98	38.77	43.90	3.25	9.80	12.44	0.36	14.06	11.26	2.67	0.55	0.10	98.36
Amph2.3	6.43	0.35	1.69	1.62	0.047	2.99	1.80	0.76	0.116	0.021	22.98	38.80	43.47	3.14	9.69	13.08	0.37	13.54	11.35	2.66	0.61	0.08	97.97
Amph2.4	6.44	0.35	1.70	1.56	0.049	3.08	1.77	0.73	0.102	0.029	22.97	38.77	43.46	3.11	9.72	12.56	0.39	13.95	11.14	2.56	0.54	0.12	97.52
Amph3.1	6.66	0.31	1.42	1.77	0.050	2.96	1.75	0.66	0.121	0.035	22.97	38.69	44.93	2.74	8.15	14.26	0.40	13.38	11.01	2.29	0.64	0.14	97.89
Amph3.2	6.69	0.29	1.40	1.78	0.052	2.95	1.73	0.67	0.136	0.044	22.96	38.69	45.31	2.64	8.03	14.41	0.42	13.38	10.94	2.32	0.72	0.18	98.30
Amph3.3	6.74	0.29	1.39	1.70	0.053	2.99	1.71	0.63	0.129	0.038	22.96	38.64	45.58	2.63	8.00	13.75	0.42	13.56	10.82	2.20	0.69	0.15	97.76
Amph3.4	6.70	0.30	1.43	1.66	0.050	2.99	1.76	0.68	0.109	0.038	22.96	38.67	45.57	2.68	8.28	13.49	0.40	13.63	11.16	2.38	0.58	0.15	98.29
Amph4.1	6.67	0.30	1.47	1.58	0.044	3.04	1.78	0.67	0.129	0.037	22.96	38.68	44.96	2.66	8.42	12.74	0.35	13.76	11.18	2.32	0.68	0.15	97.19
Amph4.2	6.70	0.29	1.38	1.71	0.064	2.96	1.77	0.66	0.123	0.048	22.95	38.68	44.92	2.62	7.86	13.74	0.51	13.30	11.10	2.28	0.65	0.19	97.13
Amph4.3	6.69	0.30	1.43	1.71	0.052	2.97	1.74	0.66	0.128	0.053	22.95	38.67	45.02	2.67	8.16	13.78	0.42	13.40	10.94	2.28	0.67	0.21	97.50
Amph5.1	6.39	0.34	1.80	1.49	0.048	3.06	1.81	0.72	0.105	0.023	22.98	38.77	43.40	3.08	10.39	12.08	0.38	13.91	11.47	2.53	0.56	0.09	97.86
Amph5.2	6.41	0.33	1.79	1.46	0.039	3.10	1.80	0.73	0.099	0.021	22.98	38.76	43.42	3.01	10.29	11.79	0.31	14.08	11.39	2.55	0.53	0.08	97.42
Amph6.1	6.62	0.32	1.44	1.64	0.040	3.11	1.74	0.68	0.123	0.040	22.96	38.72	44.62	2.88	8.25	13.21	0.32	14.04	10.96	2.38	0.65	0.16	97.43
Amph6.2	6.34	0.35	1.83	1.75	0.047	2.84	1.79	0.80	0.101	0.013	22.99	38.84	42.60	3.14	10.45	14.03	0.37	12.79	11.20	2.76	0.53	0.05	97.92
Amph6.3	6.35	0.34	1.82	1.74	0.051	2.86	1.79	0.79	0.089	0.013	22.99	38.83	42.51	3.07	10.35	13.95	0.40	12.84	11.19	2.72	0.47	0.05	97.54
Amph6.4	6.62	0.31	1.46	1.74	0.041	2.98	1.76	0.69	0.127	0.044	22.96	38.73	44.44	2.74	8.32	13.94	0.33	13.43	11.05	2.38	0.67	0.17	97.41
Amph6.5	6.57	0.30	1.53	1.62	0.044	3.11	1.75	0.71	0.109	0.037	22.96	38.75	44.29	2.73	8.78	13.02	0.35	14.06	11.02	2.46	0.58	0.15	97.40
Q-35 (1846/47)																							
Amph1.1	6.28	0.36	1.90	1.56	0.022	3.08	1.81	0.70	0.107	0.014	22.99	38.81	42.51	3.22	10.93	12.60	0.18	13.99	11.46	2.45	0.57	0.05	97.94
Amph1.2	6.32	0.37	1.85	1.48	0.025	3.09	1.83	0.75	0.104	0.014	22.99	38.81	43.14	3.35	10.71	12.08	0.20	14.17	11.65	2.64	0.56	0.06	98.54
Amph1.3	6.30	0.37	1.86	1.50	0.029	3.07	1.84	0.73	0.099	0.021	22.98	38.80	42.89	3.35	10.75	12.24	0.24	14.04	11.66	2.56	0.53	0.08	98.31
Amph1.4	6.32	0.39	1.80	1.55	0.037	3.02	1.80	0.79	0.107	0.025	22.98	38.82	43.00	3.56	10.39	12.63	0.30	13.78	11.42	2.75	0.57	0.10	98.47
Amph2.1	6.60	0.32	1.49	1.73	0.044	2.97	1.75	0.73	0.121	0.037	22.96	38.75	44.66	2.86	8.53	14.03	0.35	13.49	11.04	2.53	0.64	0.15	98.24
Amph2.2	6.61	0.33	1.47	1.72	0.053	2.96	1.75	0.70	0.129	0.027	22.97	38.73	44.57	2.94	8.41	13.89	0.42	13.41	11.01	2.44	0.68	0.11	97.86

Appendix B2 continued

Label	Si	Ti	Al	Fe	Mn	Mg	Ca	Na	K	Cl	O	Tot	SiO_2	TiO_2	Al_2O_3	FeO	MnO	MgO	CaO	Na_2O	K_2O	Cl	Tot
Amph2.3	6.67	0.29	1.40	1.78	0.052	3.00	1.75	0.69	0.119	0.018	22.98	38.74	44.95	2.63	7.98	14.32	0.41	13.57	10.98	2.39	0.63	0.07	97.91
Amph3.1	6.32	0.30	2.00	1.29	0.017	3.26	1.81	0.69	0.096	0.016	22.98	38.77	43.10	2.71	11.56	10.51	0.14	14.94	11.51	2.42	0.52	0.07	97.45
Amph3.4	6.30	0.32	1.94	1.45	0.029	3.16	1.83	0.66	0.092	0.012	22.99	38.78	42.70	2.91	11.17	11.77	0.23	14.40	11.56	2.31	0.49	0.05	97.58
Amph3.5	6.39	0.33	1.84	1.49	0.024	3.06	1.82	0.73	0.096	0.014	22.99	38.77	43.50	2.95	10.63	12.17	0.20	14.00	11.56	2.55	0.51	0.06	98.13
Amph4.1	6.66	0.30	1.42	1.78	0.043	2.92	1.75	0.75	0.125	0.044	22.96	38.75	45.05	2.70	8.15	14.40	0.34	13.27	11.08	2.62	0.66	0.18	98.41
Amph4.2	6.64	0.30	1.43	1.77	0.056	2.98	1.73	0.72	0.123	0.036	22.96	38.75	44.63	2.68	8.13	14.26	0.44	13.41	10.84	2.48	0.65	0.14	97.63
Amph4.3	6.67	0.30	1.41	1.76	0.047	2.95	1.74	0.71	0.121	0.053	22.95	38.71	45.23	2.73	8.09	14.27	0.38	13.41	11.00	2.46	0.64	0.21	98.38
Amph5.1	6.67	0.29	1.39	1.80	0.057	2.95	1.75	0.67	0.128	0.046	22.95	38.72	44.78	2.59	7.93	14.45	0.45	13.28	10.98	2.33	0.67	0.18	97.61
Amph5.2	6.66	0.29	1.38	1.83	0.058	2.99	1.73	0.66	0.134	0.049	22.95	38.73	45.04	2.59	7.92	14.80	0.47	13.55	10.94	2.30	0.71	0.19	98.46
Amph5.3	6.68	0.29	1.39	1.81	0.062	2.95	1.76	0.65	0.131	0.039	22.96	38.72	45.35	2.59	8.00	14.74	0.49	13.44	11.13	2.29	0.70	0.16	98.87
Amph5.4	6.67	0.30	1.39	1.77	0.047	2.98	1.74	0.70	0.127	0.048	22.95	38.72	45.25	2.73	7.97	14.33	0.38	13.56	11.02	2.45	0.68	0.19	98.51
Amph5.5	6.68	0.29	1.39	1.82	0.056	2.93	1.74	0.69	0.135	0.042	22.96	38.73	45.15	2.61	7.96	14.74	0.45	13.29	10.96	2.42	0.71	0.17	98.42
Amph5.6	6.69	0.30	1.38	1.80	0.059	2.96	1.73	0.67	0.132	0.043	22.96	38.70	45.43	2.70	7.93	14.62	0.48	13.48	10.95	2.33	0.70	0.17	98.74
Amph5.7	6.64	0.31	1.43	1.79	0.060	2.91	1.76	0.69	0.127	0.047	22.95	38.72	44.94	2.78	8.24	14.47	0.48	13.23	11.12	2.41	0.67	0.19	98.50
Amph5.8	6.64	0.30	1.41	1.79	0.054	2.99	1.73	0.69	0.119	0.036	22.96	38.73	44.38	2.70	8.02	14.29	0.43	13.42	10.79	2.36	0.62	0.14	97.11
VQ-06-06 (1846/47)																							
Amph1 L1.7	6.65	0.33	1.51	1.56	0.041	3.09	1.65	0.71	0.125	0.038	22.96	38.67	45.00	2.95	8.70	12.63	0.33	14.04	10.44	2.47	0.67	0.15	97.34
Amph1 L1.8	6.57	0.34	1.50	1.64	0.044	3.08	1.76	0.68	0.129	0.042	22.96	38.73	44.29	3.01	8.57	13.26	0.35	13.92	11.07	2.37	0.68	0.17	97.65
Amph1 L1.9	6.62	0.32	1.48	1.67	0.046	3.05	1.70	0.69	0.122	0.036	22.96	38.71	44.89	2.91	8.52	13.53	0.37	13.89	10.74	2.43	0.65	0.14	98.05
Amph1 L1.10	6.63	0.31	1.44	1.69	0.049	3.04	1.74	0.69	0.126	0.056	22.94	38.72	44.31	2.76	8.18	13.53	0.39	13.62	10.83	2.38	0.66	0.22	96.82
Amph1 L1.11	6.72	0.31	1.41	1.71	0.052	2.98	1.69	0.67	0.115	0.023	22.98	38.66	45.22	2.74	8.02	13.79	0.42	13.47	10.62	2.34	0.61	0.09	97.30
Amph1 L1.12	6.65	0.32	1.43	1.75	0.050	2.99	1.71	0.67	0.132	0.035	22.97	38.70	45.33	2.87	8.26	14.22	0.40	13.67	10.88	2.34	0.70	0.14	98.77
Amph1 L1.13	6.76	0.30	1.37	1.69	0.054	3.01	1.66	0.68	0.119	0.039	22.96	38.64	45.82	2.69	7.87	13.72	0.43	13.68	10.52	2.36	0.63	0.15	97.85
Amph1 L1.15	6.70	0.30	1.40	1.69	0.051	3.09	1.67	0.68	0.117	0.034	22.97	38.69	45.58	2.68	8.07	13.76	0.41	14.08	10.58	2.39	0.62	0.14	98.28
Amph1 L1.16	6.64	0.29	1.38	1.73	0.050	3.12	1.73	0.70	0.118	0.038	22.96	38.77	44.47	2.61	7.82	13.85	0.40	14.02	10.80	2.43	0.62	0.15	97.13
Amph1 L1.17	6.72	0.29	1.37	1.69	0.053	3.09	1.67	0.68	0.112	0.044	22.96	38.68	45.43	2.65	7.85	13.70	0.42	14.01	10.54	2.37	0.59	0.17	97.70
Amph1 L1.18	6.70	0.30	1.38	1.71	0.050	3.07	1.70	0.68	0.113	0.052	22.95	38.69	45.05	2.69	7.85	13.72	0.40	13.85	10.65	2.36	0.60	0.21	97.34
Amph1 L1.19	6.72	0.29	1.36	1.70	0.050	3.10	1.66	0.70	0.117	0.039	22.96	38.70	45.24	2.60	7.76	13.71	0.40	13.98	10.44	2.41	0.62	0.16	97.28
Amph1 L1.20	6.65	0.31	1.42	1.73	0.048	3.02	1.72	0.71	0.124	0.034	22.97	38.73	44.63	2.80	8.10	13.87	0.38	13.60	10.75	2.45	0.65	0.13	97.33
Amph1 L1.21	6.67	0.32	1.42	1.73	0.048	3.01	1.68	0.71	0.115	0.046	22.95	38.70	44.75	2.85	8.08	13.86	0.38	13.53	10.53	2.47	0.60	0.18	97.20

Appendix B2 continued

Label	Si	Ti	Al	Fe	Mn	Mg	Ca	Na	K	Cl	O	Tot	SiO_2	TiO_2	Al_2O_3	FeO	MnO	MgO	CaO	Na_2O	K_2O	Cl	Tot
Amph1 L1.22	6.61	0.32	1.46	1.72	0.044	3.06	1.72	0.70	0.124	0.043	22.96	38.75	44.30	2.81	8.28	13.80	0.35	13.77	10.75	2.44	0.65	0.17	97.27
Amph1 L1.23	6.66	0.31	1.44	1.71	0.052	3.04	1.68	0.71	0.117	0.034	22.97	38.71	44.88	2.78	8.23	13.79	0.41	13.73	10.60	2.47	0.62	0.14	97.62
Amph1 L1.24 core	6.66	0.32	1.44	1.71	0.048	3.00	1.71	0.69	0.123	0.039	22.96	38.70	44.81	2.82	8.22	13.73	0.38	13.55	10.77	2.41	0.65	0.16	97.47
Amph2 L1.2	6.48	0.34	1.67	1.59	0.045	3.08	1.70	0.70	0.134	0.045	22.96	38.74	43.83	3.04	9.61	12.83	0.36	14.00	10.72	2.43	0.71	0.18	97.67
Amph2 L1.3	6.54	0.32	1.56	1.63	0.042	3.13	1.70	0.71	0.124	0.036	22.96	38.76	43.85	2.90	8.85	13.12	0.33	14.09	10.67	2.46	0.65	0.14	97.04
Amph2 L1.4	6.58	0.34	1.52	1.64	0.039	3.05	1.72	0.71	0.129	0.035	22.97	38.72	44.55	3.03	8.74	13.24	0.31	13.84	10.88	2.46	0.68	0.14	97.85
Amph2 L1.5	6.51	0.33	1.57	1.67	0.046	3.11	1.69	0.72	0.128	0.045	22.96	38.78	43.47	2.91	8.92	13.32	0.36	13.93	10.52	2.48	0.67	0.18	96.72
Amph2 L1.6	6.47	0.33	1.59	1.68	0.040	3.14	1.73	0.70	0.126	0.040	22.96	38.80	43.32	2.94	9.03	13.47	0.32	14.11	10.81	2.42	0.66	0.16	97.20
Amph2 L1.9	6.45	0.25	1.76	1.58	0.036	3.19	1.72	0.76	0.091	0.021	22.98	38.84	43.40	2.21	10.06	12.73	0.29	14.42	10.82	2.65	0.48	0.08	97.12
Amph2 L1.12	6.27	0.23	1.97	1.66	0.027	3.10	1.81	0.79	0.094	0.003	23.00	38.95	41.72	2.04	11.11	13.17	0.21	13.84	11.24	2.70	0.49	0.01	96.52
Amph2 L1.13	6.62	0.25	1.53	1.59	0.032	3.26	1.67	0.69	0.108	0.021	22.98	38.75	44.38	2.26	8.71	12.78	0.25	14.66	10.46	2.38	0.57	0.08	96.51
Amph2 L1.15	6.59	0.30	1.45	1.68	0.039	3.23	1.67	0.71	0.123	0.045	22.96	38.78	44.20	2.66	8.24	13.50	0.31	14.52	10.43	2.44	0.64	0.18	97.07
Amph2 L1.16	6.57	0.31	1.58	1.65	0.045	3.05	1.70	0.69	0.126	0.042	22.96	38.72	43.98	2.78	8.96	13.20	0.36	13.70	10.64	2.37	0.66	0.17	96.79
Amph2 L1.19	6.67	0.30	1.45	1.67	0.046	3.07	1.65	0.71	0.120	0.029	22.97	38.70	45.00	2.73	8.32	13.48	0.36	13.89	10.39	2.48	0.63	0.12	97.38
Amph2 L1.20	6.55	0.32	1.49	1.71	0.044	3.14	1.71	0.69	0.127	0.047	22.95	38.78	43.67	2.85	8.43	13.61	0.35	14.04	10.67	2.38	0.67	0.19	96.82
Amph2 L1.22	6.55	0.32	1.47	1.72	0.046	3.13	1.73	0.71	0.127	0.040	22.96	38.79	44.01	2.86	8.41	13.83	0.36	14.10	10.83	2.45	0.67	0.16	97.64
Amph2 L1.24	6.56	0.32	1.46	1.74	0.054	3.13	1.70	0.70	0.128	0.051	22.95	38.78	43.59	2.83	8.22	13.82	0.42	13.94	10.57	2.40	0.67	0.20	96.63
Amph2 L1.26	6.49	0.31	1.50	1.71	0.051	3.21	1.73	0.71	0.132	0.043	22.96	38.85	43.24	2.79	8.48	13.67	0.40	14.35	10.75	2.44	0.69	0.17	96.94
Amph3 L1.6	6.76	0.29	1.36	1.71	0.051	3.03	1.68	0.62	0.133	0.047	22.95	38.62	45.78	2.59	7.80	13.85	0.41	13.75	10.60	2.15	0.70	0.19	97.77
Amph3 L1.7	6.81	0.28	1.33	1.73	0.057	2.98	1.65	0.63	0.122	0.034	22.97	38.60	45.69	2.53	7.57	13.91	0.45	13.40	10.35	2.18	0.64	0.13	96.82
Amph3 L1.8	6.75	0.29	1.35	1.76	0.054	2.97	1.70	0.63	0.130	0.053	22.95	38.64	45.54	2.64	7.73	14.22	0.43	13.46	10.72	2.20	0.69	0.21	97.79
Amph3 L1.9	6.86	0.30	1.35	1.77	0.056	2.77	1.67	0.61	0.130	0.053	22.95	38.51	45.96	2.63	7.65	14.15	0.44	12.47	10.45	2.10	0.68	0.21	96.70
Amph3 L1.10	6.55	0.30	1.54	1.74	0.052	3.08	1.67	0.71	0.124	0.056	22.94	38.77	44.27	2.66	8.85	14.09	0.42	13.95	10.56	2.48	0.66	0.22	98.09
Amph3 L1.11	6.72	0.30	1.40	1.76	0.050	2.97	1.67	0.67	0.118	0.046	22.95	38.65	45.39	2.66	8.02	14.25	0.40	13.48	10.51	2.32	0.62	0.18	97.78
Amph3 L1.12	6.66	0.31	1.43	1.77	0.048	2.97	1.72	0.68	0.122	0.038	22.96	38.70	44.89	2.77	8.21	14.27	0.38	13.42	10.81	2.35	0.65	0.15	97.86
Amph3 L1.13	6.67	0.29	1.43	1.76	0.048	3.00	1.69	0.68	0.120	0.047	22.95	38.70	44.99	2.60	8.20	14.22	0.38	13.55	10.66	2.35	0.63	0.19	97.72
Amph3 L1.15	6.65	0.30	1.45	1.74	0.052	3.01	1.68	0.70	0.124	0.049	22.95	38.71	45.33	2.73	8.36	14.19	0.42	13.77	10.67	2.46	0.66	0.20	98.74
Amph3 L1.16	6.67	0.30	1.43	1.73	0.052	2.99	1.73	0.69	0.125	0.051	22.95	38.70	45.29	2.71	8.22	14.05	0.42	13.62	10.98	2.41	0.66	0.20	98.51
Amph3 L1.17	6.69	0.30	1.40	1.75	0.045	3.02	1.69	0.67	0.124	0.031	22.97	38.69	45.37	2.71	8.07	14.18	0.36	13.76	10.67	2.33	0.66	0.13	98.22
Amph3 L1.18	6.71	0.30	1.40	1.71	0.049	2.99	1.72	0.67	0.131	0.053	22.95	38.67	45.82	2.69	8.09	13.96	0.39	13.71	10.97	2.37	0.70	0.22	98.88

Appendix B2 continued

Label	Si	Ti	Al	Fe	Mn	Mg	Ca	Na	K	Cl	O	Tot	SiO_2	TiO_2	Al_2O_3	FeO	MnO	MgO	CaO	Na_2O	K_2O	Cl	Tot
VQ-06-22 (1846/47)																							
Amph1	6.66	0.32	1.47	1.57	0.048	3.14	1.71	0.65	0.055	0.040	22.96	38.62	45.28	2.85	8.45	12.77	0.38	14.31	10.85	2.28	0.29	0.16	97.60
Amph1 L1.1 rim	6.56	0.33	1.55	1.55	0.046	3.15	1.71	0.72	0.116	0.036	22.96	38.73	44.31	2.99	8.88	12.49	0.36	14.24	10.76	2.49	0.62	0.14	97.24
Amph1 L1.2	6.49	0.35	1.60	1.56	0.055	3.15	1.72	0.72	0.116	0.023	22.98	38.77	44.15	3.18	9.23	12.73	0.44	14.38	10.94	2.53	0.62	0.09	98.28
Amph1 L1.3	6.56	0.33	1.56	1.54	0.047	3.12	1.73	0.70	0.123	0.035	22.97	38.72	44.37	2.98	8.98	12.49	0.37	14.18	10.95	2.43	0.65	0.14	97.53
Amph1 L1.4	6.59	0.32	1.52	1.53	0.047	3.17	1.75	0.67	0.124	0.039	22.96	38.71	44.63	2.92	8.72	12.38	0.37	14.40	11.06	2.34	0.66	0.16	97.60
Amph1 L1.5	6.57	0.32	1.55	1.57	0.052	3.14	1.71	0.69	0.118	0.038	22.96	38.72	44.60	2.91	8.94	12.74	0.42	14.31	10.87	2.41	0.63	0.15	97.94
Amph1 L1.6	6.54	0.34	1.57	1.59	0.051	3.09	1.74	0.71	0.123	0.039	22.96	38.74	44.26	3.03	9.00	12.90	0.40	14.02	11.01	2.48	0.65	0.16	97.88
Amph1 L1.7	6.59	0.32	1.53	1.59	0.048	3.12	1.71	0.68	0.111	0.038	22.96	38.70	44.63	2.89	8.81	12.90	0.38	14.18	10.78	2.39	0.59	0.15	97.66
Amph1 L1.8	6.62	0.32	1.47	1.57	0.050	3.16	1.73	0.67	0.113	0.035	22.97	38.70	45.53	2.94	8.56	12.95	0.41	14.60	11.12	2.38	0.61	0.14	99.21
Amph1 L1.9	6.66	0.31	1.46	1.59	0.058	3.14	1.69	0.68	0.120	0.042	22.96	38.69	45.13	2.76	8.37	12.91	0.46	14.27	10.69	2.38	0.64	0.17	97.73
Amph1 L1.10	6.64	0.31	1.46	1.60	0.044	3.13	1.72	0.66	0.130	0.050	22.95	38.68	45.25	2.85	8.45	13.00	0.36	14.29	10.91	2.30	0.70	0.20	98.25
Amph1 L1.11	6.65	0.31	1.46	1.61	0.049	3.11	1.71	0.66	0.121	0.035	22.97	38.68	44.94	2.80	8.39	12.99	0.39	14.12	10.78	2.30	0.64	0.14	97.46
Amph1 L1.12	6.64	0.31	1.46	1.60	0.047	3.14	1.71	0.66	0.121	0.041	22.96	38.69	44.88	2.82	8.37	12.95	0.38	14.23	10.77	2.31	0.64	0.16	97.48
Amph1 L1.13	6.63	0.31	1.47	1.63	0.043	3.13	1.71	0.66	0.121	0.042	22.96	38.69	45.14	2.81	8.47	13.23	0.34	14.28	10.83	2.32	0.65	0.17	98.19
Amph1 L1.14	6.67	0.31	1.45	1.61	0.043	3.06	1.72	0.66	0.126	0.044	22.96	38.66	45.26	2.80	8.36	13.05	0.34	13.94	10.91	2.32	0.67	0.18	97.80
Amph1 L1.15	6.65	0.31	1.46	1.62	0.047	3.11	1.72	0.65	0.120	0.030	22.97	38.69	44.95	2.79	8.40	13.12	0.37	14.10	10.83	2.28	0.64	0.12	97.57
Amph1 L1.16	6.64	0.31	1.46	1.60	0.053	3.11	1.73	0.67	0.128	0.020	22.98	38.70	45.65	2.84	8.52	13.12	0.43	14.35	11.08	2.37	0.69	0.08	99.11
Amph1 L1.17	6.67	0.31	1.45	1.58	0.048	3.10	1.72	0.67	0.128	0.031	22.97	38.68	45.01	2.74	8.32	12.75	0.38	14.03	10.82	2.32	0.68	0.12	97.13
Amph1 L1.18	6.65	0.32	1.46	1.59	0.044	3.10	1.72	0.65	0.128	0.044	22.96	38.67	45.26	2.87	8.43	12.93	0.36	14.16	10.92	2.28	0.68	0.18	98.02
Amph1 L1.19	6.66	0.31	1.46	1.58	0.053	3.10	1.72	0.67	0.121	0.043	22.96	38.67	44.96	2.78	8.35	12.78	0.42	14.01	10.82	2.32	0.64	0.17	97.23
Amph1 L1.20	6.63	0.32	1.44	1.61	0.047	3.13	1.73	0.66	0.133	0.037	22.96	38.70	45.05	2.86	8.32	13.09	0.38	14.24	10.99	2.29	0.71	0.15	98.04
Amph1 L1.21	6.62	0.32	1.47	1.61	0.044	3.14	1.72	0.67	0.119	0.036	22.96	38.71	44.84	2.85	8.45	13.03	0.35	14.29	10.87	2.35	0.63	0.14	97.77
Amph1 L1.22	6.64	0.32	1.46	1.58	0.049	3.12	1.72	0.65	0.133	0.032	22.97	38.68	45.08	2.90	8.42	12.85	0.39	14.21	10.90	2.28	0.71	0.13	97.85
Amph1 L1.23	6.64	0.32	1.46	1.59	0.049	3.14	1.71	0.67	0.124	0.036	22.96	38.69	45.19	2.85	8.45	12.92	0.40	14.33	10.85	2.34	0.66	0.15	98.09
Amph1 L1.24	6.63	0.31	1.47	1.64	0.054	3.12	1.70	0.66	0.123	0.036	22.96	38.70	44.72	2.78	8.38	13.21	0.43	14.10	10.68	2.31	0.65	0.14	97.36
Amph1 L1.25	6.68	0.31	1.45	1.61	0.052	3.11	1.67	0.67	0.123	0.043	22.96	38.67	45.43	2.79	8.38	13.07	0.42	14.19	10.58	2.36	0.66	0.17	98.01
Amph1 L1.27	6.70	0.31	1.44	1.61	0.052	3.08	1.68	0.66	0.123	0.042	22.96	38.64	45.41	2.79	8.31	13.04	0.41	14.03	10.61	2.29	0.65	0.17	97.67
Amph1 L1.28	6.66	0.31	1.45	1.61	0.048	3.11	1.72	0.64	0.120	0.040	22.96	38.66	45.03	2.81	8.29	13.00	0.38	14.08	10.83	2.22	0.63	0.16	97.39
Amph1 L1.31	6.68	0.31	1.45	1.65	0.047	3.06	1.69	0.64	0.126	0.045	22.96	38.65	45.45	2.78	8.35	13.40	0.38	13.96	10.71	2.25	0.67	0.18	98.09

Appendix B2 continued

Label	Si	Ti	Al	Fe	Mn	Mg	Ca	Na	K	Cl	O	Tot	SiO_2	TiO_2	Al_2O_3	FeO	MnO	MgO	CaO	Na_2O	K_2O	Cl	Tot
Amph1 L1.32	6.67	0.30	1.45	1.64	0.053	3.08	1.69	0.68	0.124	0.041	22.96	38.68	45.17	2.75	8.34	13.26	0.42	13.99	10.69	2.37	0.66	0.17	97.77
Amph1 L1.33	6.68	0.31	1.45	1.66	0.050	3.07	1.68	0.66	0.118	0.036	22.96	38.66	45.04	2.77	8.27	13.42	0.40	13.88	10.56	2.29	0.63	0.14	97.36
Amph1 L1.34	6.63	0.32	1.44	1.68	0.053	3.09	1.72	0.66	0.124	0.030	22.97	38.71	44.92	2.86	8.31	13.61	0.42	14.05	10.89	2.31	0.66	0.12	98.12
Amph1 L1.35	6.63	0.31	1.47	1.66	0.049	3.13	1.68	0.67	0.114	0.034	22.97	38.70	44.44	2.74	8.34	13.26	0.39	14.07	10.50	2.32	0.60	0.13	96.76
Amph1 L1.36	6.63	0.32	1.44	1.66	0.042	3.10	1.72	0.67	0.130	0.037	22.96	38.71	44.77	2.83	8.26	13.44	0.33	14.06	10.82	2.33	0.69	0.15	97.64
Amph1 L1.37	6.63	0.30	1.47	1.70	0.052	3.10	1.67	0.67	0.120	0.042	22.96	38.71	44.62	2.72	8.39	13.65	0.42	13.98	10.51	2.32	0.63	0.17	97.37
Amph1 L1.38	6.63	0.32	1.46	1.67	0.050	3.09	1.69	0.68	0.130	0.032	22.97	38.71	44.73	2.85	8.34	13.48	0.40	14.00	10.65	2.36	0.69	0.13	97.59
Amph1 L1.39	6.68	0.32	1.45	1.64	0.051	3.07	1.67	0.67	0.113	0.031	22.97	38.66	45.07	2.83	8.28	13.20	0.41	13.88	10.51	2.33	0.60	0.12	97.20
Amph1 L1.40	6.63	0.31	1.45	1.65	0.046	3.11	1.71	0.68	0.126	0.040	22.96	38.71	44.57	2.81	8.28	13.22	0.37	14.00	10.73	2.34	0.66	0.16	97.11
Amph1 L1.41	6.62	0.32	1.47	1.66	0.049	3.11	1.68	0.68	0.122	0.038	22.96	38.71	44.59	2.85	8.39	13.39	0.39	14.05	10.53	2.35	0.64	0.15	97.31
Amph1 L1.42	6.64	0.31	1.45	1.68	0.052	3.08	1.71	0.67	0.121	0.034	22.97	38.70	44.97	2.81	8.33	13.57	0.41	13.98	10.79	2.33	0.64	0.14	97.93
Amph1 L1.43	6.63	0.31	1.46	1.66	0.047	3.11	1.68	0.68	0.120	0.039	22.96	38.70	44.78	2.82	8.37	13.38	0.37	14.10	10.56	2.36	0.63	0.15	97.50
Amph1 L1.44	6.62	0.31	1.48	1.63	0.051	3.10	1.72	0.64	0.117	0.033	22.97	38.69	45.08	2.81	8.57	13.29	0.41	14.17	10.94	2.26	0.63	0.13	98.26
Amph1 L1.45	6.63	0.31	1.48	1.65	0.057	3.13	1.66	0.68	0.117	0.037	22.96	38.71	44.69	2.75	8.45	13.33	0.45	14.15	10.47	2.35	0.62	0.15	97.37
Amph1 L1.46	6.61	0.31	1.47	1.69	0.043	3.08	1.73	0.67	0.123	0.036	22.96	38.72	44.58	2.79	8.42	13.61	0.34	13.96	10.92	2.32	0.65	0.14	97.71
Amph1 L1.47	6.59	0.33	1.50	1.69	0.042	3.08	1.70	0.69	0.126	0.038	22.96	38.73	44.62	2.95	8.60	13.67	0.34	13.99	10.72	2.40	0.67	0.15	98.07
Amph1 L1.48	6.58	0.32	1.50	1.68	0.051	3.08	1.73	0.67	0.126	0.043	22.96	38.73	44.34	2.85	8.58	13.50	0.41	13.93	10.85	2.34	0.67	0.17	97.60
Amph1 L1.49	6.55	0.32	1.56	1.68	0.054	3.10	1.67	0.69	0.118	0.028	22.97	38.74	44.28	2.83	8.97	13.57	0.43	14.03	10.54	2.41	0.63	0.11	97.79
Amph1 L1.50 core	6.50	0.33	1.57	1.67	0.053	3.08	1.74	0.69	0.134	0.044	22.96	38.77	43.72	2.99	8.93	13.44	0.42	13.87	10.94	2.39	0.71	0.17	97.54
Amph2 L1.2	6.56	0.32	1.52	1.61	0.054	3.17	1.71	0.69	0.115	0.031	22.97	38.75	44.41	2.92	8.70	13.03	0.43	14.38	10.83	2.40	0.61	0.12	97.81
Amph2 L1.4	6.57	0.32	1.51	1.58	0.046	3.17	1.73	0.70	0.108	0.028	22.97	38.74	44.38	2.90	8.67	12.76	0.37	14.35	10.92	2.43	0.57	0.11	97.44
Amph2 L1.5	6.57	0.32	1.53	1.59	0.047	3.17	1.68	0.70	0.117	0.031	22.97	38.73	44.17	2.90	8.75	12.77	0.37	14.30	10.53	2.42	0.62	0.12	96.94
Amph2 L1.6	6.58	0.33	1.53	1.55	0.050	3.14	1.73	0.69	0.112	0.034	22.97	38.71	44.15	2.94	8.68	12.43	0.40	14.14	10.85	2.37	0.59	0.13	96.66
Amph2 L1.7	6.54	0.32	1.62	1.57	0.050	3.14	1.68	0.68	0.119	0.043	22.96	38.71	44.04	2.86	9.24	12.63	0.40	14.19	10.56	2.37	0.63	0.17	97.05
Amph2 L1.8	6.50	0.30	1.61	1.61	0.047	3.16	1.73	0.73	0.117	0.036	22.96	38.80	43.91	2.72	9.25	13.02	0.38	14.32	10.89	2.55	0.62	0.14	97.77
Amph2 L1.9	6.42	0.30	1.72	1.64	0.052	3.14	1.72	0.74	0.108	0.029	22.97	38.84	42.95	2.63	9.78	13.16	0.41	14.10	10.76	2.57	0.57	0.11	97.01
Amph2 L1.11	6.52	0.32	1.57	1.55	0.049	3.22	1.71	0.70	0.116	0.031	22.97	38.76	43.98	2.89	8.96	12.50	0.39	14.57	10.78	2.44	0.61	0.12	97.21
Amph2 L1.12	6.42	0.30	1.69	1.58	0.044	3.18	1.76	0.73	0.107	0.043	22.96	38.83	43.34	2.72	9.69	12.79	0.35	14.42	11.10	2.55	0.57	0.17	97.67
Amph2 L1.13	6.44	0.30	1.72	1.55	0.047	3.20	1.71	0.75	0.095	0.022	22.98	38.81	43.13	2.69	9.81	12.43	0.37	14.39	10.68	2.59	0.50	0.09	96.64
Amph2 L1.14	6.40	0.30	1.73	1.56	0.046	3.19	1.76	0.77	0.097	0.029	22.97	38.85	42.95	2.68	9.82	12.52	0.36	14.38	11.03	2.65	0.51	0.11	96.99

Appendix B2 continued

Label	Si	Ti	Al	Fe	Mn	Mg	Ca	Na	K	Cl	O	Tot	SiO_2	TiO_2	Al_2O_3	FeO	MnO	MgO	CaO	Na_2O	K_2O	Cl	Tot
Amph2 L1.15	6.44	0.30	1.72	1.51	0.045	3.24	1.72	0.73	0.092	0.015	22.99	38.80	43.66	2.73	9.93	12.28	0.36	14.73	10.89	2.56	0.49	0.06	97.67
Amph2 L1.16	6.44	0.32	1.70	1.51	0.049	3.21	1.73	0.75	0.102	0.024	22.98	38.81	43.31	2.83	9.70	12.14	0.39	14.49	10.87	2.59	0.54	0.09	96.93
Amph2 L1.17	6.42	0.32	1.73	1.50	0.040	3.23	1.72	0.75	0.101	0.019	22.98	38.81	43.19	2.91	9.89	12.07	0.31	14.58	10.79	2.60	0.53	0.08	96.92
Amph2 L1.18	6.37	0.33	1.72	1.55	0.043	3.20	1.76	0.76	0.103	0.025	22.98	38.85	42.65	2.97	9.77	12.42	0.34	14.38	11.02	2.62	0.54	0.10	96.80
Amph2 L1.19	6.49	0.32	1.64	1.47	0.038	3.28	1.71	0.73	0.094	0.033	22.97	38.77	43.79	2.85	9.40	11.85	0.30	14.86	10.79	2.56	0.50	0.13	97.00
Amph2 L1.20	6.46	0.31	1.62	1.51	0.044	3.31	1.73	0.72	0.096	0.023	22.98	38.81	44.12	2.85	9.38	12.36	0.35	15.15	11.04	2.52	0.52	0.09	98.35
Amph2 L1.21	6.52	0.31	1.63	1.46	0.041	3.29	1.69	0.71	0.105	0.019	22.98	38.76	43.86	2.81	9.30	11.75	0.33	14.85	10.64	2.47	0.55	0.07	96.61
Amph2 L1.22	6.49	0.32	1.64	1.48	0.042	3.26	1.73	0.72	0.103	0.025	22.98	38.78	43.53	2.82	9.33	11.89	0.33	14.68	10.86	2.49	0.54	0.10	96.56
Amph2 L1.26	6.48	0.32	1.63	1.49	0.042	3.25	1.74	0.73	0.110	0.023	22.98	38.79	44.26	2.94	9.43	12.13	0.34	14.89	11.11	2.56	0.59	0.09	98.32
Amph2 L1.28	6.44	0.33	1.64	1.50	0.043	3.28	1.74	0.74	0.100	0.024	22.98	38.82	43.50	2.98	9.43	12.14	0.34	14.85	10.99	2.57	0.53	0.10	97.40
Amph2 L1.29	6.53	0.31	1.63	1.47	0.043	3.24	1.69	0.73	0.104	0.019	22.98	38.75	44.28	2.83	9.40	11.94	0.34	14.72	10.72	2.54	0.55	0.07	97.38
Amph2 L1.30	6.48	0.32	1.64	1.49	0.050	3.26	1.73	0.72	0.097	0.025	22.98	38.78	43.65	2.83	9.38	11.99	0.40	14.74	10.89	2.49	0.51	0.10	96.97
Amph2 L1.31	6.51	0.32	1.66	1.49	0.041	3.21	1.67	0.72	0.102	0.029	22.97	38.73	44.02	2.91	9.50	12.03	0.33	14.57	10.53	2.52	0.54	0.11	97.04
Amph2 L1.33	6.51	0.31	1.65	1.48	0.044	3.23	1.70	0.73	0.099	0.026	22.97	38.75	43.95	2.82	9.42	11.92	0.35	14.63	10.68	2.54	0.52	0.10	96.93
Amph2 L1.34	6.41	0.31	1.69	1.49	0.045	3.33	1.72	0.73	0.109	0.034	22.97	38.83	43.52	2.83	9.72	12.09	0.36	15.19	10.92	2.54	0.58	0.14	97.86
Amph2 L1.36	6.44	0.32	1.68	1.50	0.045	3.26	1.72	0.75	0.104	0.031	22.97	38.81	43.50	2.87	9.60	12.11	0.36	14.77	10.82	2.60	0.55	0.13	97.27
Amph2 L1.38	6.45	0.33	1.65	1.50	0.048	3.26	1.74	0.72	0.106	0.036	22.96	38.79	43.45	2.92	9.41	12.07	0.38	14.73	10.93	2.50	0.56	0.14	97.06
Amph2 L1.39	6.51	0.31	1.64	1.47	0.046	3.28	1.70	0.72	0.100	0.012	22.99	38.77	44.25	2.76	9.43	11.96	0.37	14.95	10.75	2.52	0.53	0.05	97.57
Q-6 (1932)																							
Amph1.1	6.57	0.34	1.57	1.56	0.052	3.04	1.77	0.70	0.124	0.030	22.97	38.71	44.47	3.03	9.00	12.63	0.42	13.83	11.18	2.45	0.66	0.12	97.74
Amph1.2	6.42	0.27	1.84	1.58	0.035	3.08	1.77	0.74	0.089	0.025	22.98	38.80	43.75	2.41	10.62	12.85	0.28	14.07	11.24	2.59	0.47	0.10	98.36
Amph1.3	6.58	0.33	1.54	1.58	0.047	3.08	1.76	0.68	0.115	0.033	22.97	38.70	44.47	2.97	8.86	12.74	0.37	13.95	11.11	2.36	0.61	0.13	97.53
Amph2.1	6.63	0.31	1.47	1.68	0.046	3.00	1.77	0.67	0.124	0.034	22.97	38.70	44.88	2.77	8.46	13.64	0.37	13.61	11.19	2.34	0.66	0.14	98.02
Amph2.2	6.73	0.29	1.38	1.80	0.042	2.91	1.73	0.64	0.120	0.039	22.96	38.65	45.13	2.59	7.87	14.40	0.34	13.10	10.84	2.21	0.63	0.15	97.23
Amph2.3	6.64	0.32	1.45	1.59	0.052	3.13	1.75	0.65	0.123	0.043	22.96	38.69	44.81	2.86	8.29	12.82	0.41	14.19	11.04	2.25	0.65	0.17	97.44
Amph3.1	6.79	0.27	1.29	1.85	0.057	2.93	1.72	0.61	0.125	0.041	22.96	38.64	45.80	2.43	7.36	14.92	0.45	13.26	10.81	2.13	0.66	0.16	97.95
Amph3.2	6.79	0.27	1.31	1.61	0.059	3.15	1.72	0.61	0.128	0.048	22.95	38.64	45.91	2.41	7.51	13.00	0.47	14.27	10.88	2.14	0.68	0.19	97.42
Amph4.1	6.28	0.34	1.89	1.61	0.044	2.99	1.83	0.79	0.099	0.017	22.98	38.87	42.04	3.01	10.74	12.87	0.34	13.43	11.45	2.73	0.52	0.07	97.18
Amph5.1	6.69	0.29	1.40	1.74	0.053	3.00	1.74	0.65	0.127	0.027	22.97	38.69	45.02	2.62	7.98	14.04	0.42	13.54	10.93	2.26	0.67	0.11	97.56
Amph5.2	6.60	0.32	1.51	1.61	0.056	3.06	1.75	0.67	0.118	0.036	22.96	38.70	44.47	2.88	8.65	12.99	0.45	13.85	10.98	2.32	0.62	0.14	97.32

Appendix B2 continued

Label	Si	Ti	Al	Fe	Mn	Mg	Ca	Na	K	Cl	O	Tot	SiO_2	TiO_2	Al_2O_3	FeO	MnO	MgO	CaO	Na_2O	K_2O	Cl	Tot
Q-21 (1932)																							
Amph1.1	6.43	0.34	1.73	1.80	0.048	2.82	1.78	0.73	0.102	0.031	22.97	38.77	42.94	3.06	9.79	14.37	0.38	12.63	11.07	2.52	0.53	0.12	97.37
Amph1.2	6.76	0.33	1.44	1.59	0.053	2.86	1.76	0.63	0.116	0.044	22.96	38.54	45.79	2.98	8.27	12.92	0.42	13.02	11.11	2.19	0.61	0.18	97.45
Amph3.1	6.26	0.35	1.90	1.46	0.028	3.20	1.82	0.75	0.094	0.018	22.98	38.86	42.23	3.15	10.87	11.79	0.22	14.48	11.47	2.61	0.49	0.07	97.37
Amph3.2	6.51	0.34	1.58	1.58	0.049	3.12	1.76	0.72	0.116	0.036	22.96	38.77	43.71	3.01	8.98	12.68	0.39	14.05	11.03	2.51	0.61	0.14	97.09
Amph4.1	6.51	0.35	1.60	1.68	0.050	2.96	1.77	0.71	0.121	0.030	22.97	38.75	43.90	3.12	9.13	13.54	0.40	13.40	11.14	2.48	0.64	0.12	97.84
Amph4.2	6.58	0.33	1.56	1.55	0.050	3.05	1.77	0.70	0.117	0.037	22.96	38.70	44.41	2.96	8.95	12.55	0.40	13.79	11.12	2.43	0.62	0.15	97.34
Amph6.1	6.27	0.36	1.89	1.54	0.026	3.07	1.83	0.75	0.087	0.015	22.99	38.83	42.47	3.25	10.88	12.49	0.20	13.93	11.56	2.61	0.46	0.06	97.90
Amph6.2	6.28	0.38	1.90	1.50	0.028	3.03	1.82	0.78	0.083	0.017	22.98	38.81	42.09	3.40	10.82	12.05	0.22	13.61	11.36	2.70	0.43	0.07	96.74
Amph6.3	6.34	0.35	1.83	1.52	0.038	3.07	1.82	0.77	0.089	0.014	22.99	38.82	42.76	3.09	10.46	12.24	0.30	13.86	11.44	2.69	0.47	0.06	97.36
Amph6.4	6.44	0.34	1.70	1.58	0.052	3.06	1.78	0.73	0.103	0.012	22.99	38.78	43.61	3.03	9.78	12.78	0.41	13.90	11.26	2.54	0.55	0.05	97.89
VQ-06-17 (1932)																							
Amph1 L1.2	6.58	0.32	1.52	1.57	0.060	3.14	1.73	0.69	0.118	0.029	22.97	38.73	44.15	2.84	8.66	12.61	0.48	14.12	10.82	2.39	0.62	0.12	96.77
Amph1 L1.3	6.60	0.32	1.52	1.58	0.051	3.14	1.69	0.70	0.114	0.022	22.98	38.72	44.48	2.88	8.72	12.73	0.41	14.18	10.60	2.45	0.60	0.09	97.12
Amph1 L1.4	6.60	0.33	1.51	1.56	0.048	3.14	1.72	0.69	0.118	0.033	22.97	38.71	45.19	2.96	8.77	12.77	0.39	14.42	11.00	2.44	0.63	0.13	98.69
Amph1 L1.6	6.58	0.33	1.54	1.56	0.053	3.10	1.71	0.69	0.126	0.043	22.96	38.70	44.66	2.99	8.88	12.67	0.43	14.13	10.86	2.41	0.67	0.17	97.84
Amph1 L1.7	6.60	0.33	1.51	1.57	0.051	3.17	1.68	0.66	0.117	0.026	22.97	38.70	45.28	3.00	8.82	12.90	0.41	14.61	10.76	2.35	0.63	0.11	98.85
Amph1 L1.8	6.55	0.33	1.55	1.59	0.048	3.15	1.73	0.69	0.118	0.022	22.98	38.74	44.16	2.99	8.85	12.81	0.38	14.24	10.87	2.40	0.63	0.09	97.40
Amph1 L1.9	6.58	0.33	1.54	1.58	0.049	3.15	1.68	0.70	0.114	0.025	22.98	38.72	44.22	2.93	8.78	12.70	0.39	14.21	10.53	2.42	0.60	0.10	96.85
Amph1 L1.10	6.53	0.34	1.57	1.59	0.050	3.09	1.73	0.70	0.129	0.042	22.96	38.73	44.34	3.09	9.02	12.88	0.40	14.08	10.94	2.45	0.69	0.17	98.04
Amph1 L1.11	6.55	0.34	1.58	1.60	0.042	3.07	1.70	0.72	0.114	0.020	22.98	38.73	44.00	3.02	9.02	12.84	0.33	13.85	10.68	2.51	0.60	0.08	96.90
Amph1 L1.12	6.51	0.35	1.57	1.61	0.051	3.07	1.75	0.72	0.124	0.041	22.96	38.75	44.16	3.19	9.01	13.09	0.41	13.95	11.08	2.50	0.66	0.16	98.19
Amph1 L1.13	6.55	0.34	1.56	1.63	0.053	3.08	1.69	0.72	0.121	0.035	22.97	38.74	44.26	3.02	8.97	13.21	0.43	13.97	10.64	2.51	0.64	0.14	97.75
Amph1 L1.14	6.66	0.31	1.42	1.61	0.053	3.15	1.70	0.68	0.119	0.043	22.96	38.70	45.25	2.82	8.22	13.05	0.42	14.36	10.79	2.37	0.64	0.17	98.05
Amph1 L1.15	6.73	0.29	1.37	1.57	0.047	3.19	1.67	0.68	0.112	0.039	22.96	38.67	45.91	2.65	7.93	12.82	0.38	14.60	10.63	2.38	0.60	0.16	98.03
Amph1 L1.16	6.73	0.29	1.38	1.60	0.047	3.18	1.70	0.62	0.126	0.042	22.96	38.65	45.77	2.58	7.95	13.02	0.37	14.52	10.78	2.17	0.67	0.17	97.97
Amph1 L1.19	6.73	0.29	1.42	1.62	0.053	3.12	1.64	0.65	0.120	0.048	22.95	38.64	45.99	2.60	8.21	13.26	0.42	14.32	10.49	2.30	0.64	0.19	98.38
Amph1 L1.20	6.70	0.28	1.39	1.65	0.057	3.15	1.70	0.64	0.131	0.045	22.96	38.69	45.46	2.57	7.98	13.38	0.46	14.34	10.74	2.23	0.70	0.18	98.00
Amph1 L1.22	6.71	0.30	1.39	1.69	0.052	3.08	1.69	0.64	0.128	0.053	22.95	38.66	45.45	2.66	7.97	13.65	0.41	13.99	10.70	2.22	0.68	0.21	97.90
Amph1 L1.23	6.73	0.29	1.37	1.70	0.050	3.08	1.66	0.65	0.117	0.046	22.96	38.65	45.89	2.66	7.95	13.83	0.40	14.10	10.56	2.30	0.63	0.18	98.45

Appendix B2 continued

Label	Si	Ti	Al	Fe	Mn	Mg	Ca	Na	K	Cl	O	Tot	SiO_2	TiO_2	Al_2O_3	FeO	MnO	MgO	CaO	Na_2O	K_2O	Cl	Tot
Amph1 L1.24	6.71	0.29	1.38	1.71	0.053	3.06	1.70	0.64	0.120	0.035	22.97	38.67	45.53	2.64	7.96	13.88	0.43	13.95	10.79	2.24	0.64	0.14	98.17
Amph1 L1.25	6.73	0.29	1.39	1.71	0.050	3.07	1.65	0.64	0.123	0.048	22.95	38.64	45.62	2.62	7.96	13.82	0.40	13.93	10.41	2.25	0.65	0.19	97.82
Amph1 L1.26	6.70	0.30	1.40	1.71	0.048	3.05	1.68	0.65	0.127	0.043	22.96	38.67	45.35	2.66	8.04	13.85	0.39	13.85	10.58	2.28	0.67	0.17	97.80
Amph1 L1.27	6.70	0.29	1.38	1.72	0.056	3.08	1.68	0.65	0.119	0.035	22.97	38.68	45.09	2.59	7.89	13.85	0.44	13.90	10.54	2.26	0.63	0.14	97.29
Amph1 L1.28	6.69	0.29	1.40	1.72	0.053	3.07	1.70	0.64	0.121	0.056	22.95	38.67	45.64	2.66	8.10	14.07	0.43	14.05	10.80	2.24	0.65	0.22	98.81
Amph1 L1.29	6.73	0.29	1.40	1.72	0.052	3.05	1.65	0.65	0.123	0.031	22.97	38.66	45.38	2.58	7.99	13.90	0.42	13.78	10.40	2.27	0.65	0.12	97.46
Amph1 L1.30	6.68	0.29	1.40	1.73	0.058	3.06	1.69	0.65	0.131	0.054	22.95	38.70	45.59	2.67	8.08	14.13	0.46	14.03	10.79	2.31	0.70	0.22	98.94
Amph1 L1.31	6.72	0.29	1.39	1.75	0.051	3.02	1.67	0.65	0.113	0.048	22.95	38.65	45.42	2.60	7.98	14.12	0.41	13.71	10.51	2.26	0.60	0.19	97.74
Amph1 L1.32	6.70	0.30	1.38	1.76	0.052	3.04	1.69	0.65	0.118	0.041	22.96	38.68	45.29	2.69	7.93	14.22	0.42	13.78	10.66	2.26	0.63	0.16	97.99
Amph1 L1.33	6.71	0.29	1.38	1.75	0.058	3.05	1.66	0.64	0.115	0.063	22.94	38.65	45.32	2.64	7.94	14.12	0.46	13.81	10.47	2.23	0.61	0.25	97.80
Amph1 L1.34	6.67	0.30	1.40	1.76	0.052	3.05	1.71	0.63	0.130	0.046	22.95	38.69	44.96	2.69	7.99	14.18	0.41	13.79	10.74	2.20	0.69	0.18	97.78
Amph1 L1.35	6.71	0.30	1.40	1.76	0.052	3.03	1.64	0.64	0.124	0.043	22.96	38.66	45.20	2.64	7.99	14.15	0.41	13.71	10.32	2.22	0.66	0.17	97.45
Amph1 L1.36	6.70	0.30	1.41	1.73	0.051	3.00	1.70	0.64	0.124	0.050	22.95	38.66	45.41	2.71	8.12	14.06	0.41	13.63	10.76	2.24	0.66	0.20	98.16
Amph1 L1.37	6.68	0.30	1.41	1.78	0.055	3.00	1.67	0.66	0.126	0.048	22.95	38.69	45.11	2.73	8.06	14.38	0.44	13.60	10.51	2.31	0.67	0.19	97.96
Amph1 L1.38	6.67	0.30	1.40	1.78	0.056	3.00	1.71	0.63	0.126	0.049	22.95	38.68	45.07	2.73	8.05	14.34	0.45	13.59	10.79	2.19	0.67	0.20	98.02
Amph1 L1.39	6.70	0.30	1.40	1.77	0.057	3.01	1.65	0.65	0.127	0.053	22.95	38.66	45.16	2.67	8.02	14.24	0.45	13.59	10.40	2.24	0.67	0.21	97.61
Amph1 L1.42	6.63	0.28	1.61	1.73	0.048	2.91	1.67	0.66	0.132	0.051	22.95	38.66	45.22	2.54	9.31	14.10	0.38	13.32	10.64	2.31	0.70	0.20	98.68
Amph1 L1.44	6.66	0.30	1.43	1.77	0.050	3.00	1.70	0.65	0.126	0.059	22.94	38.69	45.24	2.69	8.22	14.38	0.40	13.68	10.79	2.27	0.67	0.24	98.52
Amph1 L1.45	6.72	0.29	1.39	1.79	0.056	3.00	1.65	0.65	0.125	0.037	22.96	38.67	45.90	2.62	8.07	14.60	0.46	13.74	10.54	2.30	0.67	0.15	99.01
Amph1 L1.46	6.71	0.29	1.39	1.74	0.047	3.00	1.71	0.64	0.130	0.051	22.95	38.66	45.32	2.65	7.95	14.07	0.37	13.60	10.76	2.21	0.69	0.20	97.77
Amph1 L1.47	6.73	0.30	1.38	1.74	0.059	3.00	1.67	0.67	0.115	0.049	22.95	38.65	45.40	2.66	7.88	14.01	0.47	13.58	10.51	2.33	0.61	0.19	97.59
Amph1 L1.48	6.67	0.30	1.40	1.74	0.054	3.00	1.74	0.65	0.132	0.041	22.96	38.70	45.69	2.75	8.14	14.29	0.44	13.80	11.15	2.31	0.71	0.16	99.40
Amph1 L1.49	6.69	0.30	1.38	1.77	0.053	3.02	1.70	0.64	0.124	0.040	22.96	38.68	45.08	2.68	7.89	14.28	0.42	13.65	10.67	2.23	0.66	0.16	97.69
Amph1 L1.50	6.67	0.30	1.40	1.74	0.056	3.03	1.71	0.66	0.127	0.041	22.96	38.69	45.18	2.74	8.05	14.06	0.45	13.75	10.79	2.30	0.67	0.16	98.13
Amph1 L1.51	6.67	0.30	1.41	1.78	0.048	3.02	1.69	0.66	0.122	0.040	22.96	38.70	44.96	2.71	8.09	14.34	0.38	13.66	10.61	2.30	0.64	0.16	97.82
Amph1 L1.52	6.69	0.30	1.40	1.76	0.053	3.02	1.70	0.64	0.125	0.045	22.96	38.67	45.05	2.67	8.00	14.18	0.42	13.63	10.69	2.21	0.66	0.18	97.66
Amph1 L1.53	6.69	0.29	1.40	1.75	0.050	3.04	1.67	0.66	0.123	0.049	22.95	38.69	45.39	2.65	8.05	14.22	0.40	13.85	10.61	2.31	0.66	0.20	98.29
Amph1 L1.54	6.69	0.30	1.38	1.74	0.049	3.02	1.71	0.67	0.125	0.044	22.96	38.69	45.42	2.74	7.98	14.16	0.40	13.78	10.83	2.34	0.66	0.18	98.44
Amph1 L1.55	6.68	0.30	1.39	1.76	0.048	3.06	1.67	0.68	0.124	0.035	22.97	38.71	44.71	2.63	7.87	14.08	0.38	13.73	10.46	2.35	0.65	0.14	96.96
Amph1 L1.56	6.62	0.30	1.41	1.79	0.048	3.10	1.71	0.66	0.134	0.032	22.97	38.77	44.48	2.66	8.02	14.37	0.38	14.00	10.72	2.30	0.71	0.13	97.73

Appendix B2 continued

Label	Si	Ti	Al	Fe	Mn	Mg	Ca	Na	K	Cl	O	Tot	SiO_2	TiO_2	Al_2O_3	FeO	MnO	MgO	CaO	Na_2O	K_2O	Cl	Tot
Amph1 L1.57	6.68	0.30	1.39	1.75	0.050	3.09	1.67	0.65	0.119	0.037	22.96	38.70	44.54	2.65	7.85	13.96	0.39	13.84	10.39	2.24	0.62	0.15	96.60
Amph1 L1.58	6.62	0.29	1.40	1.78	0.050	3.14	1.69	0.67	0.118	0.040	22.96	38.76	44.20	2.60	7.92	14.22	0.39	14.07	10.55	2.31	0.62	0.16	97.00
Amph1 L1.59	6.65	0.29	1.39	1.75	0.058	3.14	1.65	0.67	0.121	0.061	22.94	38.73	44.33	2.56	7.87	13.97	0.45	14.02	10.29	2.30	0.63	0.24	96.61
Amph1 L1.82	6.59	0.32	1.46	1.72	0.047	3.09	1.73	0.67	0.125	0.041	22.96	38.74	43.94	2.85	8.24	13.74	0.37	13.82	10.79	2.30	0.65	0.16	96.84
Amph1 L1.83	6.60	0.32	1.47	1.71	0.050	3.09	1.68	0.69	0.119	0.041	22.96	38.72	44.61	2.88	8.42	13.81	0.40	13.99	10.57	2.40	0.63	0.16	97.84
Amph1 L1.84	6.58	0.33	1.47	1.73	0.042	3.06	1.74	0.68	0.121	0.036	22.96	38.75	44.14	2.92	8.37	13.88	0.33	13.80	10.91	2.36	0.64	0.14	97.45
Amph1 L1.85	6.61	0.32	1.46	1.75	0.053	3.08	1.64	0.68	0.115	0.050	22.95	38.72	44.33	2.84	8.33	14.03	0.42	13.86	10.29	2.37	0.60	0.20	97.21
Amph1 L1.87	6.59	0.32	1.50	1.71	0.047	3.07	1.68	0.70	0.120	0.052	22.95	38.73	44.15	2.83	8.51	13.69	0.38	13.81	10.48	2.41	0.63	0.21	97.04
Amph1 L1.88 core	6.58	0.31	1.48	1.71	0.050	3.12	1.70	0.68	0.118	0.037	22.96	38.75	44.10	2.80	8.42	13.69	0.39	14.03	10.65	2.34	0.62	0.15	97.15
Amph2 core	6.22	0.39	1.97	1.73	0.047	2.89	1.73	0.76	0.122	0.027	22.97	38.84	41.63	3.45	11.18	13.85	0.37	12.97	10.79	2.64	0.64	0.11	97.59
Amph2 rim	6.52	0.32	1.54	1.60	0.049	3.20	1.72	0.72	0.121	0.041	22.96	38.78	43.90	2.88	8.80	12.84	0.39	14.44	10.80	2.49	0.64	0.16	97.31
Amph3 L1.2	6.55	0.32	1.55	1.56	0.053	3.18	1.72	0.70	0.118	0.036	22.96	38.75	44.15	2.84	8.85	12.59	0.42	14.40	10.79	2.42	0.62	0.14	97.19
Amph3 L1.4	6.54	0.32	1.53	1.57	0.057	3.21	1.70	0.71	0.119	0.046	22.95	38.76	44.09	2.87	8.77	12.68	0.45	14.52	10.67	2.48	0.63	0.18	97.30
Amph3 L1.5	6.58	0.32	1.52	1.55	0.051	3.20	1.69	0.69	0.113	0.039	22.96	38.72	44.26	2.82	8.69	12.49	0.40	14.45	10.57	2.41	0.60	0.15	96.80
Amph3 L1.6	6.53	0.33	1.53	1.57	0.052	3.23	1.72	0.71	0.112	0.044	22.96	38.77	44.03	2.93	8.78	12.66	0.41	14.61	10.81	2.47	0.59	0.18	97.44
Amph3 L1.7	6.56	0.32	1.54	1.60	0.054	3.17	1.67	0.71	0.110	0.045	22.96	38.74	44.38	2.87	8.86	12.90	0.43	14.39	10.52	2.49	0.58	0.18	97.56
Amph3 L1.8	6.51	0.33	1.57	1.55	0.051	3.22	1.72	0.71	0.117	0.038	22.96	38.77	43.94	2.97	8.96	12.47	0.41	14.57	10.87	2.46	0.62	0.15	97.38
Amph3 L1.9	6.53	0.33	1.54	1.61	0.046	3.22	1.65	0.71	0.117	0.050	22.95	38.76	43.97	2.95	8.81	12.97	0.37	14.57	10.38	2.46	0.62	0.20	97.25
Amph3 L1.10	6.53	0.32	1.51	1.56	0.052	3.28	1.71	0.71	0.114	0.044	22.96	38.79	44.33	2.86	8.67	12.65	0.42	14.95	10.81	2.49	0.60	0.17	97.93
Amph3 L1.11	6.56	0.32	1.48	1.60	0.045	3.30	1.67	0.70	0.103	0.049	22.95	38.77	44.03	2.82	8.44	12.83	0.35	14.86	10.50	2.42	0.54	0.19	96.94
Amph3 L1.12	6.52	0.34	1.54	1.58	0.048	3.22	1.71	0.70	0.116	0.035	22.97	38.77	43.67	3.00	8.78	12.64	0.38	14.50	10.68	2.42	0.61	0.14	96.78
Amph3 L1.13	6.52	0.32	1.55	1.59	0.051	3.23	1.68	0.71	0.116	0.025	22.98	38.78	43.76	2.89	8.82	12.78	0.41	14.54	10.51	2.45	0.61	0.10	96.84
Amph3 L1.14	6.49	0.35	1.55	1.61	0.048	3.16	1.74	0.72	0.121	0.028	22.97	38.79	43.53	3.11	8.81	12.90	0.38	14.23	10.86	2.48	0.64	0.11	97.03
Amph3 L1.15	6.52	0.34	1.57	1.61	0.049	3.17	1.67	0.71	0.120	0.035	22.97	38.76	44.01	3.02	8.99	12.97	0.39	14.34	10.53	2.49	0.64	0.14	97.50
Amph3 L1.16	6.51	0.34	1.63	1.59	0.042	3.07	1.72	0.70	0.127	0.042	22.96	38.72	43.71	3.06	9.26	12.73	0.33	13.82	10.75	2.42	0.67	0.17	96.87
Amph3 L1.17	6.51	0.34	1.58	1.58	0.046	3.18	1.69	0.71	0.117	0.041	22.96	38.75	44.10	3.07	9.05	12.83	0.36	14.45	10.69	2.48	0.62	0.16	97.77
Amph3 L1.18	6.46	0.32	1.64	1.60	0.042	3.16	1.73	0.73	0.114	0.037	22.96	38.80	43.69	2.85	9.43	12.94	0.34	14.33	10.91	2.54	0.60	0.15	97.74
Amph3 L1.19	6.46	0.32	1.71	1.58	0.037	3.11	1.71	0.72	0.108	0.035	22.97	38.76	43.39	2.87	9.72	12.65	0.29	14.03	10.72	2.50	0.57	0.14	96.85
Amph3 L1.20	6.35	0.33	1.77	1.59	0.049	3.17	1.75	0.75	0.115	0.030	22.97	38.86	42.98	2.95	10.16	12.88	0.39	14.40	11.05	2.62	0.61	0.12	98.13
Amph3 L1.21	6.39	0.31	1.73	1.51	0.039	3.31	1.69	0.79	0.108	0.026	22.97	38.87	43.66	2.82	10.00	12.31	0.31	15.14	10.76	2.77	0.58	0.10	98.45

Appendix B2 continued

Label	Si	Ti	Al	Fe	Mn	Mg	Ca	Na	K	Cl	O	Tot	SiO_2	TiO_2	Al_2O_3	FeO	MnO	MgO	CaO	Na_2O	K_2O	Cl	Tot
Amph3 L1.23	6.35	0.33	1.83	1.58	0.032	3.10	1.73	0.76	0.103	0.025	22.98	38.82	42.96	2.97	10.52	12.76	0.25	14.05	10.92	2.64	0.55	0.10	97.70
Amph3 L1.24	6.29	0.34	1.85	1.56	0.037	3.12	1.79	0.76	0.112	0.031	22.97	38.87	42.15	3.01	10.54	12.53	0.29	14.05	11.21	2.62	0.59	0.12	97.09
Amph3 L1.25	6.36	0.33	1.84	1.54	0.030	3.13	1.72	0.79	0.098	0.020	22.98	38.83	42.74	2.97	10.49	12.41	0.24	14.10	10.79	2.73	0.52	0.08	97.04
Amph3 L1.26	6.36	0.32	1.82	1.50	0.031	3.15	1.78	0.77	0.102	0.020	22.98	38.83	42.88	2.89	10.44	12.13	0.24	14.23	11.18	2.68	0.54	0.08	97.26
Amph3 L1.27	6.36	0.33	1.85	1.54	0.027	3.10	1.72	0.77	0.098	0.030	22.97	38.80	43.04	2.97	10.63	12.47	0.22	14.08	10.86	2.69	0.52	0.12	97.57
Amph3 L1.29	6.35	0.33	1.88	1.52	0.031	3.11	1.72	0.77	0.106	0.015	22.99	38.81	43.11	2.94	10.81	12.29	0.25	14.16	10.92	2.69	0.56	0.06	97.78
Amph3 L1.31	6.32	0.34	1.88	1.49	0.027	3.18	1.72	0.78	0.096	0.027	22.97	38.83	42.62	3.03	10.78	12.02	0.21	14.38	10.83	2.70	0.51	0.11	97.16
Amph3 L1.33	6.27	0.36	1.95	1.50	0.021	3.11	1.74	0.79	0.086	0.028	22.97	38.82	42.61	3.24	11.27	12.18	0.17	14.19	11.03	2.76	0.46	0.11	97.99
Amph3 L1.34	6.18	0.35	2.03	1.49	0.024	3.12	1.80	0.82	0.087	0.012	22.99	38.90	41.89	3.16	11.68	12.09	0.19	14.20	11.40	2.86	0.46	0.05	97.97
Amph3 L1.35	6.21	0.34	2.04	1.47	0.024	3.17	1.73	0.82	0.086	0.007	22.99	38.88	41.62	3.02	11.59	11.77	0.19	14.23	10.83	2.82	0.45	0.03	96.56
Amph3 L1.36	6.21	0.33	2.02	1.47	0.022	3.16	1.78	0.78	0.101	0.011	22.99	38.88	42.26	3.01	11.66	11.93	0.18	14.44	11.33	2.75	0.54	0.04	98.13
Amph3 L1.37	6.29	0.32	1.95	1.44	0.020	3.20	1.74	0.78	0.098	0.020	22.98	38.84	42.40	2.87	11.18	11.62	0.16	14.46	10.96	2.70	0.52	0.08	96.93
Amph3 L1.38	6.17	0.34	2.00	1.46	0.016	3.23	1.81	0.82	0.093	0.022	22.98	38.94	41.52	3.02	11.39	11.77	0.13	14.56	11.38	2.85	0.49	0.09	97.18
Amph3 L1.39	6.21	0.34	2.03	1.47	0.021	3.19	1.74	0.78	0.086	0.019	22.98	38.86	42.32	3.09	11.72	11.95	0.17	14.58	11.04	2.74	0.46	0.08	98.12
Amph3 L1.40	6.17	0.34	2.05	1.48	0.022	3.16	1.80	0.80	0.082	0.003	23.00	38.90	41.93	3.08	11.84	11.99	0.18	14.38	11.39	2.82	0.44	0.01	98.06
Amph3 L1.41	6.19	0.34	2.06	1.50	0.022	3.12	1.76	0.81	0.087	0.011	22.99	38.88	41.79	3.05	11.79	12.08	0.18	14.16	11.12	2.81	0.46	0.04	97.45
Amph3 L1.42	6.21	0.35	2.02	1.49	0.013	3.12	1.80	0.80	0.087	0.010	22.99	38.87	42.37	3.13	11.68	12.12	0.11	14.29	11.47	2.80	0.47	0.04	98.46
Amph4 L1.2	6.64	0.32	1.49	1.57	0.046	3.16	1.65	0.69	0.113	0.039	22.96	38.68	45.34	2.89	8.66	12.82	0.37	14.50	10.55	2.44	0.60	0.16	98.29
Amph4 L1.3	6.58	0.34	1.52	1.56	0.048	3.15	1.71	0.72	0.114	0.030	22.97	38.73	44.70	3.04	8.77	12.65	0.39	14.36	10.84	2.52	0.61	0.12	97.97
Amph4 L1.4	6.62	0.33	1.52	1.56	0.046	3.10	1.70	0.67	0.112	0.032	22.97	38.66	45.12	2.99	8.80	12.70	0.37	14.15	10.80	2.37	0.60	0.13	97.99
Amph4 L1.5	6.61	0.32	1.50	1.56	0.049	3.15	1.72	0.69	0.114	0.028	22.97	38.71	45.39	2.93	8.77	12.81	0.40	14.53	11.01	2.46	0.61	0.11	99.00
Amph4 L1.6	6.60	0.32	1.53	1.57	0.051	3.13	1.69	0.70	0.114	0.033	22.97	38.70	45.01	2.93	8.85	12.78	0.41	14.30	10.75	2.47	0.61	0.13	98.20
Amph4 L1.7	6.56	0.35	1.55	1.58	0.050	3.08	1.74	0.68	0.120	0.028	22.97	38.70	44.62	3.20	8.93	12.84	0.40	14.07	11.02	2.39	0.64	0.11	98.18
Amph4 L1.8	6.63	0.33	1.52	1.54	0.046	3.13	1.68	0.69	0.115	0.029	22.97	38.67	45.53	3.02	8.87	12.65	0.38	14.41	10.75	2.44	0.62	0.12	98.76
Amph4 L1.9	6.61	0.33	1.52	1.54	0.053	3.11	1.73	0.68	0.111	0.034	22.97	38.69	45.24	2.96	8.85	12.61	0.43	14.30	11.08	2.41	0.59	0.14	98.58
Amph4 L1.10	6.58	0.35	1.55	1.60	0.054	3.05	1.68	0.71	0.119	0.044	22.96	38.69	44.88	3.15	8.97	13.01	0.43	13.94	10.71	2.49	0.63	0.18	98.34
Amph4 L1.11	6.50	0.34	1.59	1.61	0.054	3.11	1.74	0.72	0.128	0.026	22.97	38.78	44.41	3.07	9.21	13.13	0.43	14.26	11.08	2.53	0.69	0.10	98.90
Amph4 L1.12	6.66	0.31	1.46	1.63	0.047	3.10	1.68	0.67	0.124	0.043	22.96	38.67	45.17	2.82	8.38	13.24	0.37	14.10	10.60	2.33	0.66	0.17	97.81
Amph4 L1.13	6.64	0.32	1.43	1.68	0.049	3.07	1.71	0.65	0.123	0.049	22.95	38.68	45.21	2.90	8.28	13.66	0.40	14.02	10.84	2.29	0.66	0.20	98.41
Amph4 L1.14	6.67	0.32	1.45	1.67	0.053	3.03	1.67	0.66	0.121	0.042	22.96	38.65	45.38	2.88	8.39	13.60	0.42	13.81	10.58	2.33	0.64	0.17	98.16

Appendix B2 continued

Label	Si	Ti	Al	Fe	Mn	Mg	Ca	Na	K	Cl	O	Tot	SiO_2	TiO_2	Al_2O_3	FeO	MnO	MgO	CaO	Na_2O	K_2O	Cl	Tot
Amph4 L1.15	6.64	0.32	1.50	1.72	0.052	2.95	1.69	0.67	0.125	0.046	22.95	38.66	44.64	2.84	8.55	13.80	0.42	13.31	10.58	2.32	0.66	0.18	97.25
Amph4 L1.16	6.67	0.33	1.47	1.74	0.046	2.91	1.69	0.69	0.119	0.043	22.96	38.65	45.41	2.99	8.50	14.13	0.37	13.29	10.72	2.41	0.64	0.17	98.58
Amph4 L1.17	6.60	0.33	1.52	1.74	0.047	2.97	1.70	0.69	0.121	0.036	22.96	38.71	45.47	3.00	8.86	14.34	0.38	13.73	10.95	2.45	0.66	0.15	99.95
Amph4 L1.18	6.66	0.32	1.50	1.72	0.047	2.94	1.68	0.71	0.108	0.027	22.97	38.67	45.31	2.92	8.64	14.00	0.37	13.41	10.65	2.48	0.58	0.11	98.44
Amph4 L1.20	6.58	0.34	1.55	1.74	0.053	2.95	1.67	0.70	0.110	0.030	22.97	38.69	44.60	3.04	8.94	14.08	0.43	13.41	10.53	2.44	0.58	0.12	98.14
Amph4 L1.21	6.54	0.33	1.57	1.73	0.051	2.97	1.72	0.71	0.108	0.034	22.97	38.73	44.37	3.02	9.06	14.01	0.41	13.52	10.91	2.47	0.57	0.14	98.46
Amph4 L1.22	6.57	0.33	1.57	1.70	0.051	3.01	1.68	0.71	0.104	0.025	22.98	38.72	44.53	2.95	9.00	13.79	0.41	13.67	10.63	2.49	0.55	0.10	98.09
Amph4 L1.26	6.48	0.34	1.61	1.69	0.049	3.06	1.69	0.75	0.118	0.036	22.96	38.79	43.68	3.07	9.23	13.60	0.39	13.82	10.65	2.62	0.62	0.14	97.80
Amph4 L1.27	6.49	0.35	1.62	1.65	0.049	3.02	1.72	0.72	0.117	0.023	22.98	38.75	43.86	3.17	9.31	13.36	0.39	13.69	10.87	2.52	0.62	0.09	97.84
Amph4 L1.28	6.52	0.35	1.60	1.65	0.047	3.00	1.73	0.73	0.115	0.029	22.97	38.74	44.54	3.21	9.29	13.47	0.38	13.74	11.01	2.58	0.62	0.12	98.92
Amph4 L1.30	6.49	0.36	1.63	1.66	0.044	3.00	1.71	0.73	0.120	0.030	22.97	38.75	44.04	3.22	9.39	13.45	0.35	13.67	10.81	2.56	0.64	0.12	98.22
Amph4 L1.31	6.43	0.36	1.65	1.66	0.046	3.05	1.75	0.72	0.125	0.036	22.96	38.79	43.48	3.25	9.49	13.40	0.36	13.83	11.05	2.50	0.66	0.14	98.14
Amph4 L1.32	6.48	0.36	1.65	1.64	0.050	3.04	1.67	0.73	0.115	0.035	22.97	38.74	43.89	3.27	9.45	13.29	0.40	13.78	10.55	2.55	0.61	0.14	97.89
Amph4 L1.33	6.48	0.37	1.63	1.61	0.041	3.01	1.77	0.72	0.123	0.027	22.97	38.75	44.28	3.34	9.47	13.13	0.33	13.83	11.32	2.54	0.66	0.11	98.97
Amph4 L1.34	6.53	0.34	1.64	1.59	0.040	3.04	1.70	0.73	0.113	0.017	22.98	38.72	44.16	3.10	9.40	12.85	0.32	13.78	10.77	2.55	0.60	0.07	97.58
Amph4 L1.35	6.49	0.35	1.62	1.60	0.045	3.04	1.77	0.70	0.114	0.028	22.97	38.74	44.44	3.20	9.42	13.12	0.37	13.95	11.33	2.49	0.61	0.11	99.00
Amph4 L1.36	6.54	0.35	1.62	1.59	0.042	3.04	1.69	0.71	0.114	0.027	22.97	38.70	44.40	3.17	9.32	12.91	0.33	13.84	10.71	2.50	0.60	0.11	97.88
Amph4 L1.37	6.47	0.37	1.65	1.60	0.041	3.03	1.76	0.73	0.112	0.033	22.97	38.75	43.84	3.30	9.50	12.95	0.33	13.77	11.13	2.54	0.60	0.13	98.06
Amph4 L1.38	6.51	0.37	1.65	1.58	0.044	3.01	1.70	0.74	0.117	0.026	22.97	38.72	44.61	3.34	9.59	12.96	0.36	13.86	10.88	2.60	0.63	0.10	98.92
Amph4 L1.39	6.39	0.38	1.70	1.61	0.041	3.06	1.76	0.75	0.112	0.027	22.97	38.80	43.42	3.44	9.79	13.05	0.33	13.93	11.15	2.64	0.60	0.11	98.43
Amph4 L1.40	6.46	0.37	1.68	1.60	0.039	3.03	1.72	0.73	0.114	0.032	22.97	38.74	43.87	3.34	9.67	12.96	0.31	13.81	10.89	2.56	0.61	0.13	98.12
Amph4 L1.41	6.49	0.35	1.61	1.58	0.041	3.14	1.73	0.72	0.121	0.018	22.98	38.77	44.52	3.18	9.39	12.96	0.33	14.45	11.10	2.54	0.65	0.07	99.16
Amph4 L1.42	6.49	0.36	1.65	1.57	0.031	3.11	1.68	0.73	0.116	0.023	22.98	38.74	43.93	3.26	9.46	12.72	0.25	14.10	10.64	2.54	0.62	0.09	97.59
Amph4 L1.43 core	6.48	0.36	1.63	1.55	0.046	3.11	1.73	0.74	0.106	0.021	22.98	38.76	44.19	3.24	9.43	12.62	0.37	14.22	11.00	2.61	0.57	0.08	98.32

[1] analyses taken at University of Washington

Appendix B3a Fe-Ti oxide electron microprobe analyses (atomic proportions)[1]

Label	Si	Ti	Al	Cr	Fe	Mn	Ni	Mg	Zn	Nb	V	Tot
VQ-06-02 (1846/47)												
Mt1	0.0027	0.27	0.055	0.0014	1.66	0.014	b.d.l.	0.09	0.0009	0.0001	n.m.	5.09
Mt1	0.0024	0.30	0.052	0.0016	1.66	0.015	b.d.l.	0.09	0.0009	0.0001	n.m.	5.12
Il1	b.d.l.	0.79	0.007	0.0005	1.00	0.012	b.d.l.	0.12	0.0008	0.0001	n.m.	4.94
Mt2	0.0024	0.31	0.054	0.0006	1.68	0.014	b.d.l.	0.11	0.0009	0.0001	n.m.	5.17
Il2	0.0007	0.81	0.007	0.0003	1.01	0.014	b.d.l.	0.13	0.0008	0.0001	n.m.	4.97
Mt3	0.0029	0.29	0.048	0.0009	1.63	0.015	0.0002	0.08	0.0009	0.0001	n.m.	5.06
Il3	0.0010	0.79	0.006	0.0002	0.98	0.014	b.d.l.	0.11	0.0008	0.0001	n.m.	4.89
Mount_VQ-06-02 (1846/47)												
Mt1	0.0019	0.21	0.069	0.0014	1.81	0.021	b.d.l.	0.09	0.0009	b.d.l.	0.02	5.23
Il1	b.d.l.	0.86	0.009	b.d.l.	1.00	0.019	b.d.l.	0.16	0.0009	b.d.l.	0.02	5.06
Mt1	0.0010	0.31	0.079	0.0012	1.70	0.022	b.d.l.	0.13	0.0009	b.d.l.	0.03	5.27
Il2	b.d.l.	0.83	0.006	b.d.l.	1.07	0.021	b.d.l.	0.12	0.0009	b.d.l.	0.01	5.06
Mt2	0.0025	0.31	0.050	0.0010	1.74	0.024	b.d.l.	0.09	0.0009	b.d.l.	0.02	5.24
Il3	b.d.l.	0.81	0.005	b.d.l.	1.01	0.021	b.d.l.	0.11	0.0008	b.d.l.	0.02	4.97
Mt3	0.0014	0.30	0.048	0.0010	1.72	0.024	b.d.l.	0.09	0.0009	b.d.l.	0.02	5.21
Il4	b.d.l.	0.83	0.005	0.0002	1.02	0.020	b.d.l.	0.12	0.0008	b.d.l.	0.02	5.01
Mt4	0.0014	0.32	0.048	0.0011	1.67	0.024	b.d.l.	0.09	0.0009	b.d.l.	0.02	5.17
Il5	b.d.l.	0.81	0.005	0.0002	1.04	0.021	b.d.l.	0.12	0.0008	b.d.l.	0.01	5.01
Mt5	0.0017	0.31	0.049	0.0013	1.73	0.024	b.d.l.	0.09	0.0009	b.d.l.	0.02	5.24
Il6	b.d.l.	0.86	0.006	b.d.l.	1.09	0.022	b.d.l.	0.13	0.0009	b.d.l.	0.02	5.12
Mt6	0.0009	0.33	0.051	0.0008	1.76	0.024	b.d.l.	0.09	0.0009	b.d.l.	0.03	5.29
Il7	b.d.l.	0.83	0.006	0.0002	1.07	0.021	b.d.l.	0.11	0.0009	b.d.l.	0.02	5.05
Mt7	0.0086	0.35	0.046	0.0009	1.62	0.023	b.d.l.	0.09	0.0009	b.d.l.	0.02	5.16
Il8	b.d.l.	0.81	0.005	b.d.l.	1.01	0.019	b.d.l.	0.12	0.0008	b.d.l.	0.01	4.98
Mt8	0.0029	0.30	0.054	0.0012	1.69	0.022	b.d.l.	0.10	0.0009	b.d.l.	0.02	5.20
Il9	b.d.l.	0.82	0.005	b.d.l.	1.05	0.021	b.d.l.	0.11	0.0009	b.d.l.	0.01	5.02
Mt9	0.0011	0.31	0.049	0.0011	1.75	0.024	b.d.l.	0.09	0.0009	b.d.l.	0.02	5.25
VQ-06-06 (1846/47)												
Il1	b.d.l.	0.83	0.005	b.d.l.	1.08	0.027	b.d.l.	0.12	0.0009	b.d.l.	0.01	5.08

Appendix B3a continued

Label	Si	Ti	Al	Cr	Fe	Mn	Ni	Mg	Zn	Nb	V	Tot
Mt1	0.0010	0.22	0.066	0.0012	1.94	0.028	b.d.l.	0.09	0.0010	b.d.l.	0.02	5.37
Il2	b.d.l.	0.84	0.005	0.0003	1.09	0.028	b.d.l.	0.12	0.0009	b.d.l.	0.01	5.10
Mt2	0.0044	0.24	0.013	0.0010	1.99	0.014	b.d.l.	0.06	0.0010	b.d.l.	0.00	5.33
Il3	b.d.l.	0.77	0.010	0.0001	1.14	0.020	b.d.l.	0.13	0.0009	b.d.l.	0.02	5.09
Mt3	0.0010	0.20	0.092	0.0011	1.92	0.026	b.d.l.	0.09	0.0010	b.d.l.	0.03	5.36
Il4	b.d.l.	0.84	0.005	b.d.l.	1.08	0.028	b.d.l.	0.12	0.0009	b.d.l.	0.01	5.09
Mt4	0.0004	0.23	0.064	0.0008	1.90	0.029	b.d.l.	0.08	0.0010	b.d.l.	0.02	5.32
Mount_VQ-06-22A (1846/47)												
Mt1	0.0007	0.38	0.027	0.0020	1.43	0.019	b.d.l.	0.04	0.0009	b.d.l.	0.04	4.94
Mt2	0.0034	0.30	0.160	0.0029	1.49	0.017	0.0001	0.15	0.0009	b.d.l.	0.04	5.16
Mt3	0.0038	0.29	0.026	0.0058	1.59	0.018	b.d.l.	0.05	0.0009	b.d.l.	0.06	5.04
Cr-sp1	0.0003	0.13	0.296	0.2428	1.20	0.016	b.d.l.	0.16	0.0008	0.0001	0.04	5.09
Mt4	0.0015	0.31	0.046	0.0144	1.62	0.017	b.d.l.	0.06	0.0009	b.d.l.	0.07	5.14
Cr-Sp2	0.0007	0.25	0.152	0.2248	1.20	0.018	b.d.l.	0.13	0.0009	b.d.l.	0.06	5.04
VQ-06-22 (1846/47)												
Il1	b.d.l.	0.87	0.005	b.d.l.	1.06	0.025	b.d.l.	0.10	0.0009	b.d.l.	0.02	5.08
Mt1	0.0023	0.35	0.067	0.0016	1.72	0.026	b.d.l.	0.07	0.0009	b.d.l.	0.02	5.26
Il2	b.d.l.	0.85	0.005	b.d.l.	1.01	0.024	b.d.l.	0.11	0.0009	b.d.l.	0.02	5.02
Mt2	0.0013	0.35	0.074	0.0026	1.74	0.027	b.d.l.	0.09	0.0010	b.d.l.	0.04	5.32
Il3	b.d.l.	0.87	0.008	0.0002	1.09	0.025	b.d.l.	0.11	0.0009	b.d.l.	0.02	5.12
Mt3	0.0013	0.36	0.068	0.0018	1.74	0.028	b.d.l.	0.09	0.0010	b.d.l.	0.03	5.32
Il4	b.d.l.	0.86	0.008	0.0005	1.10	0.023	b.d.l.	0.09	0.0009	b.d.l.	0.02	5.10
Mt4	0.0015	0.36	0.063	0.0009	1.66	0.027	b.d.l.	0.08	0.0009	b.d.l.	0.03	5.22
Il5	b.d.l.	0.85	0.009	b.d.l.	1.06	0.020	b.d.l.	0.13	0.0009	b.d.l.	0.01	5.08
Mt5	0.0024	0.36	0.077	0.0012	1.70	0.025	b.d.l.	0.10	0.0009	b.d.l.	0.02	5.29
Mt6	0.0036	0.31	0.062	0.0014	1.70	0.023	b.d.l.	0.10	0.0009	b.d.l.	0.02	5.22
Il6	0.0021	0.85	0.014	b.d.l.	1.04	0.021	b.d.l.	0.13	0.0009	b.d.l.	0.01	5.07
Mount_VQ-07-44A (1846/47)												
Il1	b.d.l.	0.82	0.005	0.0002	1.01	0.023	b.d.l.	0.13	0.0008	b.d.l.	0.01	5.00
Mt1	0.0007	0.36	0.065	0.0012	1.68	0.022	b.d.l.	0.07	0.0009	b.d.l.	0.03	5.23

Appendix B3a continued

Label	Si	Ti	Al	Cr	Fe	Mn	Ni	Mg	Zn	Nb	V	Tot
Il2	b.d.l.	0.83	0.007	b.d.l.	1.00	0.020	b.d.l.	0.17	0.0008	b.d.l.	0.01	5.04
Mt2	0.0005	0.15	0.101	0.0019	1.88	0.022	b.d.l.	0.10	0.0009	b.d.l.	0.03	5.28
Il3	b.d.l.	0.81	0.006	b.d.l.	1.01	0.020	b.d.l.	0.13	0.0008	b.d.l.	0.01	5.00
Mt3	0.0011	0.11	0.111	0.0014	2.10	0.019	b.d.l.	0.06	0.0010	b.d.l.	0.03	5.42
Il4	b.d.l.	0.81	0.004	b.d.l.	1.05	0.021	b.d.l.	0.12	0.0009	b.d.l.	0.01	5.02
Mt4	0.0004	0.09	0.077	0.0010	2.03	0.019	b.d.l.	0.05	0.0010	b.d.l.	0.02	5.29
Il5	b.d.l.	0.82	0.004	b.d.l.	1.12	0.021	b.d.l.	0.09	0.0009	b.d.l.	0.01	5.07
Mt5	0.0217	0.01	0.003	0.0006	1.89	0.021	b.d.l.	0.00	0.0009	b.d.l.	0.00	4.95
Mount_VQ-06-17 (1932)												
Il1	b.d.l.	0.83	0.004	0.0001	1.04	0.030	b.d.l.	0.12	0.0009	b.d.l.	0.01	5.03
Mt1	b.d.l.	0.20	0.061	0.0010	1.83	0.029	b.d.l.	0.07	0.0009	0.0002	0.02	5.22
Il2	b.d.l.	0.83	0.004	b.d.l.	1.03	0.030	b.d.l.	0.12	0.0009	b.d.l.	0.01	5.02
Mt2	0.0001	0.21	0.061	0.0013	1.84	0.030	b.d.l.	0.07	0.0009	b.d.l.	0.02	5.23
Il3	b.d.l.	0.83	0.004	b.d.l.	1.03	0.031	b.d.l.	0.11	0.0009	b.d.l.	0.01	5.02
Mt3	b.d.l.	0.21	0.063	0.0013	1.86	0.030	b.d.l.	0.07	0.0009	b.d.l.	0.02	5.25
Il4	b.d.l.	0.82	0.004	b.d.l.	1.03	0.030	b.d.l.	0.12	0.0009	b.d.l.	0.01	5.02
Il4	b.d.l.	0.21	0.062	0.0010	1.87	0.030	b.d.l.	0.07	0.0009	b.d.l.	0.02	5.26
Il5	b.d.l.	0.84	0.004	0.0001	1.04	0.031	b.d.l.	0.11	0.0009	b.d.l.	0.01	5.04
Mt5	0.0003	0.21	0.063	0.0016	1.91	0.030	b.d.l.	0.08	0.0010	b.d.l.	0.02	5.30
Il6	b.d.l.	0.84	0.004	0.0001	1.05	0.031	b.d.l.	0.11	0.0009	b.d.l.	0.01	5.05
Mt6	0.0001	0.21	0.063	0.0010	1.89	0.030	b.d.l.	0.07	0.0010	b.d.l.	0.02	5.29
Mount_VQ-07-37D (1932)												
Il1	b.d.l.	0.84	0.003	b.d.l.	1.05	0.030	b.d.l.	0.10	0.0009	b.d.l.	0.01	5.04
Mt1	0.0002	0.21	0.062	0.0013	1.88	0.029	b.d.l.	0.08	0.0010	b.d.l.	0.02	5.29
Il2	0.0011	0.26	0.130	0.0083	1.73	0.018	b.d.l.	0.15	0.0009	b.d.l.	0.06	5.35
Mt2	0.0006	0.21	0.062	0.0011	1.88	0.030	b.d.l.	0.07	0.0010	b.d.l.	0.02	5.28
Il3	b.d.l.	0.83	0.004	b.d.l.	1.04	0.031	b.d.l.	0.12	0.0009	b.d.l.	0.01	5.04
Mt3	0.0006	0.21	0.062	0.0014	1.90	0.030	b.d.l.	0.07	0.0010	b.d.l.	0.02	5.30

[1] analyses taken at University of Washington; b.d.l. = below detection limit; n.m. = not measured

Appendix B3b Fe-Ti oxide electron microprobe analyses (weight concentrations)[1]

Label	SiO_2	TiO_2	Al_2O_3	Cr_2O_3	FeO	MnO	NiO	MgO	ZnO	Nb_2O_5	V_2O_5	O
VQ-06-02 (1846/47)												
Mt1	0.10	13.48	1.76	0.07	75.38	0.62	b.d.l.	2.31	0.046	0.007	n.m.	6.2
Mt1	0.09	15.06	1.67	0.08	74.52	0.65	b.d.l.	2.38	0.046	0.007	n.m.	5.5
Il1	0.00	43.49	0.23	0.03	49.30	0.60	b.d.l.	3.36	0.046	0.007	n.m.	2.9
Mt2	0.09	15.18	1.71	0.03	74.76	0.63	b.d.l.	2.66	0.046	0.007	n.m.	4.9
Il2	0.03	43.83	0.23	0.01	49.29	0.67	b.d.l.	3.58	0.046	0.007	n.m.	2.3
Mt3	0.11	14.68	1.55	0.05	74.52	0.67	0.008	2.02	0.046	0.007	n.m.	6.3
Il3	0.04	43.66	0.19	0.01	48.77	0.67	b.d.l.	3.08	0.046	0.007	n.m.	3.5
Mount_VQ-06-02 (1846/47)												
Mt1	0.07	10.20	2.11	0.06	78.50	0.91	b.d.l.	2.08	0.046	b.d.l.	1.28	4.8
Il1	b.d.l.	45.27	0.29	b.d.l.	47.62	0.88	b.d.l.	4.34	0.046	b.d.l.	1.02	0.5
Mt1	0.04	15.02	2.44	0.06	73.55	0.92	b.d.l.	3.13	0.046	b.d.l.	1.53	3.3
Il2	b.d.l.	43.40	0.19	b.d.l.	50.48	0.97	b.d.l.	3.18	0.046	b.d.l.	0.81	0.9
Mt2	0.09	15.00	1.53	0.05	75.18	1.03	b.d.l.	2.21	0.046	b.d.l.	1.12	3.8
Il3	b.d.l.	43.56	0.18	b.d.l.	49.11	0.98	b.d.l.	3.04	0.046	b.d.l.	0.95	2.1
Mt3	0.05	14.78	1.47	0.05	75.07	1.02	b.d.l.	2.18	0.046	b.d.l.	1.24	4.1
Il4	b.d.l.	44.08	0.18	0.01	49.14	0.95	b.d.l.	3.23	0.046	b.d.l.	0.92	1.5
Mt4	0.05	15.59	1.50	0.05	73.78	1.03	b.d.l.	2.30	0.046	b.d.l.	1.22	4.4
Il5	b.d.l.	43.35	0.16	0.01	49.70	0.97	b.d.l.	3.20	0.046	b.d.l.	0.88	1.7
Mt5	0.06	15.04	1.52	0.06	74.96	1.04	b.d.l.	2.30	0.046	b.d.l.	1.28	3.7
Il6	b.d.l.	44.26	0.18	b.d.l.	50.21	1.01	b.d.l.	3.28	0.046	b.d.l.	1.14	-0.1
Mt6	0.03	15.53	1.55	0.04	75.08	1.02	b.d.l.	2.20	0.046	b.d.l.	1.50	3.0
Il7	b.d.l.	43.47	0.20	0.01	50.43	0.98	b.d.l.	2.90	0.046	b.d.l.	0.99	1.0
Mt7	0.32	17.53	1.46	0.04	72.06	1.01	b.d.l.	2.24	0.046	b.d.l.	1.07	4.2
Il8	b.d.l.	43.53	0.19	b.d.l.	49.01	0.92	b.d.l.	3.39	0.046	b.d.l.	0.91	2.0
Mt8	0.11	14.72	1.70	0.06	74.46	0.96	b.d.l.	2.45	0.046	b.d.l.	1.21	4.3
Il9	b.d.l.	43.37	0.17	b.d.l.	50.02	1.00	b.d.l.	3.03	0.046	b.d.l.	0.90	1.5
Mt9	0.04	14.89	1.50	0.05	75.56	1.03	b.d.l.	2.10	0.046	b.d.l.	1.10	3.7
VQ-06-06 (1846/47)												
Il1	b.d.l.	43.34	0.18	b.d.l.	50.53	1.26	b.d.l.	3.11	0.046	b.d.l.	0.85	0.7

Appendix B3b continued

Label	SiO_2	TiO_2	Al_2O_3	Cr_2O_3	FeO	MnO	NiO	MgO	ZnO	Nb_2O_5	V_2O_5	O
Mt1	0.04	10.01	1.93	0.05	80.47	1.16	b.d.l.	2.01	0.046	b.d.l.	1.04	3.3
Il2	b.d.l.	43.32	0.17	0.01	50.84	1.27	b.d.l.	3.14	0.046	b.d.l.	0.74	0.4
Mt2	0.15	11.03	0.37	0.05	82.40	0.55	b.d.l.	1.42	0.046	b.d.l.	0.22	3.8
Il3	b.d.l.	39.83	0.32	0.00	53.31	0.93	b.d.l.	3.37	0.046	b.d.l.	1.02	1.2
Mt3	0.03	9.11	2.72	0.05	80.07	1.07	b.d.l.	2.18	0.046	b.d.l.	1.34	3.4
Il4	b.d.l.	43.60	0.16	b.d.l.	50.33	1.29	b.d.l.	3.23	0.046	b.d.l.	0.88	0.5
Mt4	0.02	10.56	1.92	0.04	79.58	1.20	b.d.l.	2.00	0.046	b.d.l.	1.01	3.6
Mount_VQ-06-22A (1846/47)												
Mt1	0.03	20.10	0.92	0.10	67.99	0.89	b.d.l.	1.01	0.046	b.d.l.	2.65	6.3
Mt2	0.13	15.14	5.19	0.14	68.28	0.76	0.007	3.85	0.046	b.d.l.	2.49	4.0
Mt3	0.14	14.85	0.84	0.28	72.56	0.79	b.d.l.	1.18	0.046	b.d.l.	3.65	5.7
Cr-sp1	0.01	7.20	10.15	12.40	57.88	0.75	b.d.l.	4.38	0.046	0.012	2.36	4.8
Mt4	0.06	15.52	1.44	0.68	72.27	0.73	b.d.l.	1.40	0.046	b.d.l.	3.72	4.2
Cr-Sp2	0.03	13.21	5.15	11.37	57.58	0.83	b.d.l.	3.48	0.046	b.d.l.	3.71	4.6
VQ-06-22 (1846/47)												
Il1	b.d.l.	45.36	0.18	b.d.l.	49.37	1.14	b.d.l.	2.68	0.046	b.d.l.	1.03	0.2
Mt1	0.08	16.72	2.05	0.07	73.81	1.11	b.d.l.	1.76	0.046	b.d.l.	1.35	3.0
Il2	b.d.l.	45.39	0.16	b.d.l.	48.25	1.11	b.d.l.	3.07	0.046	b.d.l.	0.95	1.0
Mt2	0.05	16.29	2.21	0.12	73.75	1.11	b.d.l.	2.06	0.046	b.d.l.	2.08	2.3
Il3	b.d.l.	44.80	0.26	0.01	50.15	1.13	b.d.l.	2.88	0.046	b.d.l.	0.99	-0.3
Mt3	0.04	17.13	2.04	0.08	73.52	1.18	b.d.l.	2.13	0.046	b.d.l.	1.61	2.2
Il4	b.d.l.	44.06	0.26	0.02	50.85	1.05	b.d.l.	2.46	0.046	b.d.l.	1.13	0.1
Mt4	0.06	17.58	1.94	0.04	72.55	1.18	b.d.l.	1.85	0.046	b.d.l.	1.38	3.4
Il5	b.d.l.	44.19	0.31	b.d.l.	49.90	0.94	b.d.l.	3.37	0.046	b.d.l.	0.78	0.5
Mt5	0.09	17.15	2.34	0.05	72.97	1.04	b.d.l.	2.48	0.046	b.d.l.	1.19	2.7
Mt6	0.13	15.10	1.93	0.06	74.29	1.01	b.d.l.	2.45	0.046	b.d.l.	1.09	3.9
Il6	0.08	44.49	0.45	b.d.l.	49.31	0.97	b.d.l.	3.33	0.046	b.d.l.	0.67	0.6
Mount_VQ-07-44A (1846/47)												
Il1	b.d.l.	43.98	0.17	0.01	48.68	1.08	b.d.l.	3.59	0.046	b.d.l.	0.77	1.7
Mt1	0.02	17.21	2.00	0.06	73.23	0.93	b.d.l.	1.82	0.046	b.d.l.	1.38	3.3

Appendix B3b continued

Label	SiO_2	TiO_2	Al_2O_3	Cr_2O_3	FeO	MnO	NiO	MgO	ZnO	Nb_2O_5	V_2O_5	O
Il2	b.d.l.	44.28	0.23	b.d.l.	47.94	0.93	b.d.l.	4.59	0.046	b.d.l.	0.80	1.2
Mt2	0.02	7.26	3.06	0.09	80.26	0.94	b.d.l.	2.32	0.046	b.d.l.	1.55	4.5
Il3	b.d.l.	43.79	0.19	b.d.l.	48.72	0.97	b.d.l.	3.65	0.046	b.d.l.	0.86	1.8
Mt3	0.04	4.82	3.18	0.06	84.99	0.75	b.d.l.	1.32	0.046	b.d.l.	1.45	3.4
Il4	b.d.l.	43.19	0.14	b.d.l.	50.03	1.01	b.d.l.	3.25	0.046	b.d.l.	0.83	1.5
Mt4	0.01	4.21	2.29	0.04	85.17	0.79	b.d.l.	1.27	0.046	b.d.l.	0.96	5.2
Il5	b.d.l.	42.55	0.13	0.00	52.23	0.98	b.d.l.	2.28	0.046	b.d.l.	0.82	1.0
Mt5	0.84	0.54	0.09	0.03	87.05	0.95	b.d.l.	0.02	0.046	b.d.l.	0.08	10.4
Mount_VQ-06-17 (1932)												
Il1	b.d.l.	43.78	0.14	0.00	49.51	1.43	b.d.l.	3.11	0.046	b.d.l.	0.73	1.2
Mt1	b.d.l.	9.82	1.86	0.05	79.23	1.24	b.d.l.	1.76	0.046	0.016	0.95	5.0
Il2	b.d.l.	44.06	0.14	0.00	49.17	1.42	b.d.l.	3.08	0.046	b.d.l.	0.72	1.4
Mt2	0.01	9.84	1.86	0.06	79.22	1.27	b.d.l.	1.80	0.046	b.d.l.	1.01	4.9
Il3	b.d.l.	43.84	0.14	b.d.l.	49.36	1.44	b.d.l.	3.07	0.046	b.d.l.	0.68	1.4
Mt3	b.d.l.	9.88	1.91	0.06	79.58	1.24	b.d.l.	1.75	0.046	b.d.l.	0.93	4.6
Il4	b.d.l.	43.87	0.15	0.00	49.14	1.44	b.d.l.	3.09	0.046	b.d.l.	0.78	1.5
Il4	b.d.l.	9.90	1.86	0.04	79.73	1.26	b.d.l.	1.78	0.046	b.d.l.	0.88	4.5
Il5	b.d.l.	44.12	0.14	0.01	49.41	1.44	b.d.l.	3.05	0.046	b.d.l.	0.76	1.0
Mt5	0.01	9.62	1.88	0.07	80.34	1.25	b.d.l.	1.78	0.046	b.d.l.	0.94	4.1
Il6	b.d.l.	44.07	0.14	0.00	49.66	1.44	b.d.l.	2.95	0.046	b.d.l.	0.66	1.0
Mt6	0.00	9.80	1.90	0.05	79.99	1.23	b.d.l.	1.77	0.046	b.d.l.	1.00	4.2
Mount_VQ-07-37D (1932)												
Il1	b.d.l.	44.04	0.10	b.d.l.	49.76	1.39	b.d.l.	2.75	0.046	b.d.l.	0.83	1.1
Mt1	0.01	10.08	1.88	0.06	79.71	1.23	b.d.l.	1.83	0.046	b.d.l.	1.01	4.2
Il2	0.04	12.28	3.92	0.38	73.69	0.77	b.d.l.	3.61	0.046	b.d.l.	3.07	2.2
Mt2	0.02	10.00	1.87	0.05	79.74	1.24	b.d.l.	1.78	0.046	b.d.l.	0.94	4.3
Il3	b.d.l.	43.65	0.13	b.d.l.	49.62	1.44	b.d.l.	3.09	0.046	b.d.l.	0.80	1.2
Mt3	0.02	9.98	1.85	0.06	80.06	1.23	b.d.l.	1.74	0.046	b.d.l.	1.00	4.0

[1] analyses taken at University of Washington; oxygen calculated from 100% sums; b.d.l. = below detection limit; n.m. = not measured

Appendix B4a Pyroxene electron microprobe analyses (atomic proportions)[1]

Label	Mg#[2]	Wo[3]	En[4]	Fs[5]	Si	Ti	Al	Cr	Fe	Mn	Mg	Ca	Na	Tot[6]
VQ-06-02 (1846/47)														
Px1	64.7	2.2	63.2	34.5	1.99	0.006	0.020	b.d.l.	0.67	0.04	1.22	0.04	0.003	9.99
Px10	65.7	2.3	64.3	33.7	1.99	0.006	0.028	b.d.l.	0.65	0.03	1.25	0.05	0.004	10.00
Px11	65.9	2.4	64.2	33.2	1.99	0.007	0.024	0.0001	0.64	0.04	1.24	0.05	0.006	9.99
Px12	74.5	3.3	72.2	24.7	1.94	0.010	0.102	b.d.l.	0.48	0.01	1.40	0.06	0.006	10.01
Px13	64.4	2.3	62.9	34.8	1.98	0.008	0.033	0.0005	0.67	0.04	1.22	0.04	0.009	10.00
Px14	70.1	41.3	38.4	16.4	1.99	0.012	0.056	b.d.l.	0.32	0.02	0.74	0.80	0.044	9.99
Px15	76.8	42.1	44.1	13.3	1.93	0.015	0.109	0.0003	0.26	0.01	0.85	0.81	0.027	10.01
Px16	65.1	2.7	62.8	33.7	2.00	0.006	0.021	0.0002	0.65	0.04	1.22	0.05	0.007	9.99
Px17	81.7	45.0	43.4	9.7	1.89	0.016	0.171	0.0136	0.19	0.00	0.84	0.87	0.025	10.02
Px18	77.6	43.0	43.2	12.5	1.98	0.005	0.050	0.0064	0.24	0.02	0.84	0.83	0.036	10.00
Px19	73.4	39.0	44.0	15.9	1.85	0.030	0.205	0.0014	0.31	0.01	0.85	0.75	0.030	10.04
Px2	64.5	2.3	63.1	34.7	1.99	0.006	0.019	b.d.l.	0.67	0.04	1.22	0.05	0.014	10.00
Px20	64.2	2.3	62.4	34.8	2.00	0.005	0.015	b.d.l.	0.67	0.04	1.21	0.04	0.004	9.99
Px21	64.5	2.5	62.8	34.6	2.00	0.004	0.016	b.d.l.	0.67	0.04	1.21	0.05	0.004	9.99
Px22	65.0	2.5	63.2	34.1	2.00	0.005	0.018	b.d.l.	0.66	0.04	1.22	0.05	0.002	9.99
Px23	64.4	2.2	63.5	35.1	1.99	0.005	0.013	b.d.l.	0.68	0.04	1.23	0.04	0.010	10.01
Px25	74.8	6.9	68.1	22.9	1.98	0.009	0.076	b.d.l.	0.44	0.01	1.32	0.13	0.019	9.99
Px26	76.9	39.1	44.8	13.5	1.97	0.012	0.083	0.0002	0.26	0.01	0.87	0.76	0.025	9.99
Px27	74.3	40.6	41.9	14.5	1.90	0.027	0.168	0.0003	0.28	0.01	0.81	0.79	0.030	10.01
Px28	65.3	2.5	62.8	33.4	2.01	0.005	0.017	0.0001	0.65	0.04	1.22	0.05	0.006	9.98
Px29	64.5	2.5	62.3	34.3	1.99	0.006	0.025	0.0002	0.66	0.04	1.21	0.05	0.012	9.99
Px3	64.4	2.5	62.5	34.6	2.00	0.005	0.016	0.0001	0.67	0.04	1.21	0.05	0.006	9.99
Px30	63.4	2.6	61.4	35.4	1.99	0.007	0.019	0.0001	0.69	0.04	1.19	0.05	0.010	10.00
Px31	65.0	2.5	62.8	33.8	2.00	0.006	0.033	b.d.l.	0.65	0.02	1.21	0.05	0.005	9.98
Px32	77.1	42.5	43.2	12.8	1.89	0.021	0.171	0.0021	0.25	0.01	0.84	0.82	0.026	10.02
Px33	76.1	3.7	74.1	23.3	1.97	0.008	0.048	b.d.l.	0.45	0.01	1.43	0.07	0.006	10.00
Px34	76.7	43.2	42.6	12.9	1.92	0.018	0.128	0.0005	0.25	0.01	0.83	0.84	0.024	10.01
Px35	76.4	42.2	41.1	12.7	1.85	0.029	0.233	0.0076	0.25	0.01	0.80	0.82	0.024	10.01
Px36	72.7	42.0	41.2	15.5	1.98	0.008	0.044	b.d.l.	0.30	0.02	0.80	0.81	0.039	10.00

Appendix B4a continued

Label	Mg#[2]	Wo[3]	En[4]	Fs[5]	Si	Ti	Al	Cr	Fe	Mn	Mg	Ca	Na	Tot[6]
Px4	75.3	3.3	73.1	24.0	1.96	0.008	0.069	0.0007	0.46	0.02	1.41	0.06	0.005	10.00
Px5	64.0	2.3	62.9	35.3	1.99	0.005	0.016	b.d.l.	0.68	0.04	1.22	0.04	0.015	10.01
Px6	75.4	2.9	73.9	24.2	1.97	0.007	0.057	0.0004	0.47	0.02	1.43	0.06	0.003	10.00
Px7	76.6	39.7	44.4	13.6	1.92	0.018	0.130	0.0005	0.26	0.01	0.86	0.77	0.083	10.04
Px8	65.6	2.7	63.5	33.3	1.99	0.007	0.022	b.d.l.	0.64	0.04	1.23	0.05	0.007	9.99
Px9	74.2	2.6	72.3	25.1	1.97	0.008	0.053	b.d.l.	0.49	0.02	1.40	0.05	0.007	10.00
VQ-06-06 (1846/47)														
Px10	65.9	2.5	64.4	33.4	1.99	0.005	0.018	0.0005	0.65	0.04	1.25	0.05	0.004	10.00
Px1-gc	73.6	43.2	42.0	15.1	1.98	0.006	0.038	b.d.l.	0.29	0.02	0.81	0.84	0.032	10.02
Px2-gc	75.6	43.1	42.5	13.7	1.98	0.009	0.051	b.d.l.	0.27	0.02	0.82	0.83	0.029	10.00
Px3-gc	68.0	2.5	66.7	31.3	1.98	0.006	0.033	b.d.l.	0.61	0.03	1.29	0.05	0.004	10.00
Px4	66.9	2.3	65.1	32.2	2.00	0.005	0.019	b.d.l.	0.62	0.04	1.26	0.05	0.002	9.99
Px5	76.3	43.9	42.4	13.1	1.96	0.010	0.071	0.0027	0.25	0.02	0.82	0.85	0.029	10.01
Px6	66.1	2.3	64.8	33.2	1.99	0.006	0.022	b.d.l.	0.64	0.04	1.25	0.04	0.002	10.00
Px7	65.3	2.6	63.9	34.0	1.97	0.008	0.041	b.d.l.	0.66	0.04	1.24	0.05	0.006	10.01
Px8	65.7	2.7	63.9	33.3	1.99	0.007	0.024	0.0001	0.64	0.04	1.24	0.05	0.002	10.00
Px9	67.3	2.2	67.0	32.5	1.98	0.005	0.023	b.d.l.	0.63	0.04	1.30	0.04	0.002	10.01
VQ-06-22A (1846/47)														
Px1	74.1	40.1	43.8	15.3	1.95	0.015	0.078	b.d.l.	0.30	0.01	0.85	0.78	0.024	10.00
Px10	69.5	3.3	67.3	29.5	1.95	0.009	0.080	0.0007	0.57	0.02	1.30	0.06	0.002	10.00
Px11	63.6	8.2	61.3	35.1	1.94	0.008	0.047	b.d.l.	0.68	0.02	1.19	0.16	0.003	10.04
Px12	68.5	3.1	66.2	30.4	1.96	0.009	0.078	b.d.l.	0.59	0.02	1.28	0.06	0.003	10.00
Px14	73.5	36.6	42.3	15.2	1.99	0.014	0.093	0.0007	0.30	0.01	0.82	0.71	0.028	9.96
Px15	59.4	34.0	37.2	25.4	2.00	0.015	0.041	0.0005	0.49	0.02	0.72	0.66	0.028	9.97
Px16	70.4	3.2	68.9	29.0	1.96	0.010	0.061	0.0002	0.56	0.02	1.33	0.06	0.004	10.01
Px17	60.2	34.6	39.2	26.0	1.98	0.013	0.036	b.d.l.	0.50	0.02	0.76	0.67	0.028	10.00
Px18	70.0	3.6	68.7	29.4	1.96	0.008	0.045	0.0001	0.57	0.02	1.33	0.07	0.002	10.01
Px19	70.7	3.2	68.2	28.3	1.97	0.010	0.066	b.d.l.	0.55	0.02	1.32	0.06	0.003	9.99
Px2	71.7	40.2	41.7	16.4	1.94	0.020	0.094	0.0013	0.32	0.01	0.81	0.78	0.027	10.00
Px20	69.5	3.3	67.6	29.7	1.97	0.009	0.052	b.d.l.	0.58	0.02	1.31	0.06	0.002	10.00

Appendix B4a continued

Label	Mg#[2]	Wo[3]	En[4]	Fs[5]	Si	Ti	Al	Cr	Fe	Mn	Mg	Ca	Na	Tot[6]
Px21	69.1	3.7	67.1	30.0	1.96	0.011	0.056	0.0013	0.58	0.02	1.30	0.07	0.002	10.00
Px23	62.5	37.7	35.8	21.5	1.74	0.067	0.347	0.0017	0.42	0.01	0.69	0.73	0.030	10.03
Px24_rim	58.6	4.2	55.7	39.3	2.00	0.009	0.027	b.d.l.	0.76	0.02	1.08	0.08	0.004	9.98
Px3	69.4	5.1	63.7	28.1	2.00	0.010	0.053	0.0007	0.54	0.02	1.23	0.10	0.009	9.97
Px6	68.8	4.2	67.0	30.4	1.96	0.007	0.046	b.d.l.	0.59	0.02	1.30	0.08	0.007	10.01
Px7	70.5	2.6	69.4	29.1	1.96	0.009	0.061	0.0004	0.56	0.02	1.34	0.05	0.002	10.01
Px8	58.7	6.3	56.1	39.5	1.98	0.009	0.014	0.0001	0.76	0.02	1.09	0.12	0.005	10.00
VQ-06-22D (1846/47)														
Px25-gc	67.3	2.6	66.3	32.2	1.97	0.007	0.035	b.d.l.	0.62	0.04	1.28	0.05	0.002	10.01
Px26	72.4	39.9	44.9	17.1	1.86	0.026	0.150	0.0007	0.33	0.01	0.87	0.77	0.026	10.05
Px27	76.4	41.8	46.3	14.3	1.87	0.022	0.136	0.0057	0.28	0.01	0.90	0.81	0.021	10.05
Px28	75.8	38.5	48.5	15.5	1.93	0.013	0.071	0.0008	0.30	0.01	0.94	0.75	0.016	10.03
Px29	70.7	3.5	68.6	28.5	1.96	0.010	0.057	b.d.l.	0.55	0.02	1.33	0.07	0.002	10.00
Px30	72.2	3.6	70.8	27.2	1.94	0.011	0.073	0.0003	0.53	0.02	1.37	0.07	0.003	10.01
Px31	71.7	39.8	42.7	16.8	1.90	0.025	0.137	0.0007	0.33	0.01	0.83	0.77	0.028	10.02
Px32	74.0	3.2	75.0	26.3	1.95	0.006	0.035	b.d.l.	0.51	0.02	1.45	0.06	0.002	10.03
Px33	67.5	4.2	66.9	32.2	1.94	0.011	0.047	b.d.l.	0.62	0.03	1.29	0.08	0.002	10.03
Px35	73.4	4.1	72.7	26.4	1.94	0.008	0.057	0.0004	0.51	0.02	1.41	0.08	0.002	10.02
Px36	69.5	2.3	67.4	29.6	1.99	0.005	0.027	b.d.l.	0.57	0.04	1.30	0.04	0.004	9.99
Px38	69.9	39.9	40.5	17.5	1.82	0.046	0.234	0.0017	0.34	0.01	0.78	0.77	0.033	10.04
VQ-06-44a (1846/47)														
Px1	62.1	2.2	61.1	37.3	1.99	0.004	0.013	b.d.l.	0.72	0.05	1.18	0.04	0.003	10.00
Px11	76.6	37.1	49.4	15.1	1.93	0.013	0.085	0.0003	0.29	0.01	0.95	0.72	0.012	10.02
Px12	64.5	2.7	63.0	34.7	1.99	0.006	0.019	b.d.l.	0.67	0.04	1.22	0.05	0.003	10.00
Px13	65.1	2.5	64.9	34.8	1.97	0.006	0.026	b.d.l.	0.67	0.04	1.26	0.05	0.002	10.02
Px14	64.2	2.5	63.5	35.5	1.96	0.008	0.034	0.0001	0.69	0.04	1.23	0.05	0.003	10.01
Px15	74.9	42.3	41.9	14.1	1.86	0.025	0.202	0.0008	0.27	0.01	0.81	0.82	0.022	10.02
Px2	63.6	2.6	62.6	35.8	1.98	0.006	0.023	b.d.l.	0.69	0.04	1.21	0.05	0.001	10.01
Px3	77.4	40.6	48.0	14.0	1.92	0.012	0.086	b.d.l.	0.27	0.01	0.93	0.79	0.017	10.03
Px5	81.5	43.9	46.3	10.5	1.92	0.011	0.112	0.0052	0.20	0.01	0.90	0.85	0.018	10.02

Appendix B4a continued

Label	Mg#[2]	Wo[3]	En[4]	Fs[5]	Si	Ti	Al	Cr	Fe	Mn	Mg	Ca	Na	Tot[6]
Px6	78.5	44.0	44.4	12.1	1.89	0.017	0.141	0.0018	0.23	0.01	0.86	0.85	0.021	10.03
Px8	67.1	2.7	65.8	32.3	1.99	0.008	0.017	b.d.l.	0.63	0.04	1.27	0.05	0.001	10.00
VQ-06-17 (1932)														
Px1	69.0	2.2	68.7	30.9	1.98	0.005	0.022	b.d.l.	0.60	0.04	1.33	0.04	0.003	10.01
Px10	69.9	12.1	61.9	26.6	1.98	0.008	0.030	b.d.l.	0.51	0.03	1.20	0.23	0.011	10.01
Px11	68.3	2.5	66.6	31.0	1.98	0.007	0.026	b.d.l.	0.60	0.04	1.29	0.05	0.002	10.00
Px12	67.9	2.4	67.0	31.6	1.98	0.005	0.021	b.d.l.	0.61	0.04	1.30	0.05	0.003	10.01
Px13	69.6	2.2	67.9	29.6	1.99	0.005	0.025	b.d.l.	0.57	0.04	1.31	0.04	0.004	9.99
Px14	66.5	2.9	65.7	33.1	1.98	0.005	0.017	0.0002	0.64	0.04	1.27	0.06	0.003	10.01
Px15	70.9	1.8	70.9	29.1	1.96	0.005	0.036	b.d.l.	0.56	0.04	1.37	0.03	0.003	10.01
Px16	67.3	2.2	65.5	31.8	1.99	0.007	0.017	0.0006	0.62	0.04	1.27	0.04	0.003	9.99
Px2	66.0	2.4	65.4	33.7	1.97	0.006	0.030	b.d.l.	0.65	0.04	1.27	0.05	0.003	10.01
Px3	68.8	2.5	67.9	30.8	1.97	0.008	0.029	b.d.l.	0.60	0.04	1.31	0.05	0.005	10.01
Px4	67.6	2.7	67.3	32.2	1.97	0.007	0.025	b.d.l.	0.62	0.04	1.30	0.05	0.003	10.02
Px5	65.9	2.4	64.9	33.6	1.98	0.006	0.029	0.0001	0.65	0.04	1.26	0.05	0.004	10.01
Px6	66.1	2.5	64.7	33.2	1.98	0.006	0.026	0.0002	0.64	0.04	1.25	0.05	0.021	10.01
Px7	68.9	2.3	68.7	31.1	1.97	0.006	0.020	0.0004	0.60	0.04	1.33	0.05	0.003	10.02
Px9	69.3	2.2	68.8	30.4	1.97	0.006	0.029	0.0001	0.59	0.04	1.33	0.04	0.004	10.01
VQ-07-37D (1932)														
Px1	67.9	2.5	67.3	31.9	1.97	0.007	0.022	0.0004	0.62	0.04	1.30	0.05	0.004	10.01
Px10	68.9	2.6	67.8	30.7	1.98	0.007	0.020	b.d.l.	0.59	0.04	1.31	0.05	0.002	10.00
Px11	66.2	2.5	63.7	32.6	1.97	0.007	0.056	0.0002	0.63	0.04	1.23	0.05	0.002	9.99
Px12	70.3	2.2	70.0	29.6	1.97	0.005	0.033	0.0004	0.57	0.04	1.35	0.04	0.002	10.01
Px13	69.9	2.3	69.7	30.0	1.98	0.005	0.017	b.d.l.	0.58	0.04	1.35	0.05	0.001	10.01
Px14	68.6	2.4	67.6	31.0	1.98	0.005	0.020	0.0006	0.60	0.04	1.31	0.05	0.002	10.00
Px15	65.8	2.4	64.8	33.7	1.97	0.007	0.044	b.d.l.	0.65	0.04	1.25	0.05	0.002	10.01
Px16	67.5	2.7	67.0	32.2	1.98	0.005	0.019	0.0003	0.62	0.04	1.30	0.05	0.002	10.01
Px17	69.4	2.5	70.0	30.8	1.96	0.005	0.018	b.d.l.	0.60	0.04	1.35	0.05	0.002	10.03
Px18	69.3	2.3	68.8	30.6	1.97	0.005	0.026	b.d.l.	0.59	0.04	1.33	0.04	0.002	10.01
Px19	72.3	3.7	71.2	27.2	1.97	0.007	0.033	b.d.l.	0.53	0.02	1.38	0.07	0.006	10.01

Appendix B4a continued

Label	Mg#[2]	Wo[3]	En[4]	Fs[5]	Si	Ti	Al	Cr	Fe	Mn	Mg	Ca	Na	Tot[6]
Px2	67.2	2.6	66.1	32.2	1.98	0.005	0.026	0.0002	0.62	0.04	1.28	0.05	0.003	10.00
Px21	65.5	2.6	65.3	34.3	1.97	0.006	0.021	0.0001	0.66	0.04	1.26	0.05	0.002	10.02
Px22	65.1	2.7	63.6	34.1	1.99	0.006	0.017	b.d.l.	0.66	0.04	1.23	0.05	0.003	10.00
Px23	69.8	2.7	68.5	29.7	1.95	0.010	0.062	b.d.l.	0.57	0.03	1.33	0.05	0.002	10.01
Px24	67.9	2.1	67.3	31.8	1.98	0.005	0.021	0.0002	0.61	0.04	1.30	0.04	0.003	10.01
Px5	67.0	2.2	67.0	33.0	1.98	0.004	0.013	0.0004	0.64	0.04	1.30	0.04	0.002	10.02
Px6	66.1	2.6	65.1	33.4	1.96	0.008	0.048	b.d.l.	0.65	0.03	1.26	0.05	0.003	10.01
Px7	69.0	2.1	68.2	30.6	1.98	0.005	0.021	0.0003	0.59	0.04	1.32	0.04	0.002	10.00
Px8	69.3	2.2	68.5	30.3	1.98	0.006	0.023	b.d.l.	0.59	0.04	1.33	0.04	0.003	10.00
Px9	71.7	3.7	70.4	27.8	1.97	0.009	0.040	0.0007	0.54	0.02	1.36	0.07	0.004	10.01

[1]analyses taken at University of Washington; b.d.l. = below detection limit

[2]Mg# = Magnesium number (100xMg/(Mg+Fe)

[3]Wo = wollastonite content (100xCa/(Ca+Mg+Fe)

[4]En = enstatite content (100xMg/(Ca+Mg+Fe)

[5]Fs = ferrosillite content (100xFe/(Ca+Mg+Fe)

[6]Tot = atomic proportions total calculated assuming 6 oxygen cations

Appendix B4b Pyroxene electron microprobe analyses (weight concentrations)[1]

Label	SiO_2	TiO_2	Al_2O_3	Cr_2O_3	FeO	MnO	MgO	CaO	Na_2O	Tot
VQ-06-02 (1846/47)										
Px1	53.39	0.20	0.46	b.d.l.	21.41	1.18	22.00	1.07	0.04	99.73
Px10	53.42	0.21	0.63	b.d.l.	20.95	1.04	22.48	1.14	0.06	99.92
Px11	53.44	0.25	0.54	0.003	20.62	1.16	22.37	1.19	0.08	99.64
Px12	54.02	0.37	2.41	b.d.l.	15.96	0.49	26.16	1.68	0.08	101.17
Px13	52.64	0.28	0.75	0.018	21.40	1.23	21.73	1.11	0.13	99.28
Px14	52.13	0.41	1.24	b.d.l.	9.94	0.60	13.04	19.51	0.60	97.47
Px15	52.26	0.54	2.50	0.010	8.32	0.25	15.50	20.56	0.37	100.32
Px16	54.02	0.21	0.49	0.007	21.07	1.30	22.07	1.31	0.09	100.57
Px17	51.21	0.56	3.92	0.468	6.11	0.13	15.29	22.07	0.35	100.12
Px18	53.58	0.18	1.16	0.220	7.79	0.52	15.17	21.02	0.50	100.14
Px19	49.65	1.07	4.67	0.047	9.90	0.30	15.37	18.95	0.42	100.39
Px2	53.57	0.22	0.43	b.d.l.	21.65	1.30	22.09	1.13	0.19	100.58
Px20	53.91	0.17	0.34	b.d.l.	21.71	1.30	21.83	1.10	0.05	100.42
Px21	53.63	0.14	0.37	b.d.l.	21.47	1.25	21.87	1.19	0.05	99.97
Px22	53.43	0.17	0.42	b.d.l.	21.08	1.19	21.97	1.19	0.03	99.47
Px23	51.59	0.16	0.29	b.d.l.	21.11	1.35	21.41	1.05	0.14	97.10
Px25	54.69	0.34	1.78	b.d.l.	14.66	0.42	24.47	3.47	0.27	100.10
Px26	53.04	0.44	1.89	0.006	8.39	0.31	15.66	18.99	0.34	99.07
Px27	51.14	0.97	3.83	0.010	9.05	0.30	14.66	19.78	0.42	100.16
Px28	54.02	0.19	0.38	0.004	20.77	1.18	21.96	1.23	0.09	99.84
Px29	53.55	0.21	0.57	0.005	21.28	1.26	21.71	1.20	0.16	99.95
Px3	53.91	0.17	0.36	0.003	21.57	1.29	21.87	1.24	0.08	100.49
Px30	53.12	0.23	0.44	0.005	21.85	1.28	21.25	1.27	0.14	99.59
Px31	53.49	0.22	0.74	b.d.l.	20.94	0.56	21.80	1.22	0.06	99.04
Px32	50.99	0.74	3.93	0.073	8.03	0.19	15.17	20.72	0.37	100.22
Px33	54.31	0.28	1.12	b.d.l.	14.84	0.48	26.52	1.83	0.09	99.45
Px34	49.00	0.62	2.77	0.015	7.64	0.25	14.13	19.93	0.32	94.68
Px35	50.38	1.04	5.38	0.260	7.99	0.18	14.52	20.70	0.34	100.80
Px36	53.33	0.30	1.01	b.d.l.	9.61	0.59	14.36	20.39	0.53	100.13

Appendix B4b continued

Label	SiO_2	TiO_2	Al_2O_3	Cr_2O_3	FeO	MnO	MgO	CaO	Na_2O	Tot
Px4	53.96	0.29	1.62	0.023	15.31	0.53	26.15	1.66	0.07	99.61
Px5	52.80	0.16	0.36	b.d.l.	21.75	1.34	21.72	1.11	0.20	99.43
Px6	54.57	0.26	1.34	0.015	15.52	0.53	26.63	1.44	0.05	100.35
Px7	51.24	0.63	2.95	0.016	8.39	0.24	15.44	19.17	1.15	99.23
Px8	53.39	0.24	0.49	b.d.l.	20.62	1.27	22.08	1.30	0.09	99.49
Px9	55.17	0.30	1.27	b.d.l.	16.23	0.61	26.23	1.33	0.10	101.23
VQ-06-06 (1846/47)										
Px10	54.07	0.18	0.42	0.019	20.96	1.16	22.69	1.25	0.06	100.81
Px1-gc	52.91	0.23	0.87	b.d.l.	9.35	0.62	14.61	20.91	0.45	99.93
Px2-gc	53.42	0.33	1.17	b.d.l.	8.59	0.56	14.93	21.03	0.41	100.44
Px3-gc	54.03	0.23	0.77	b.d.l.	19.81	1.11	23.64	1.25	0.06	100.90
Px4	54.54	0.17	0.45	b.d.l.	20.32	1.21	23.09	1.16	0.03	100.97
Px5	53.65	0.35	1.66	0.095	8.32	0.52	15.06	21.73	0.40	101.79
Px6	54.15	0.22	0.50	b.d.l.	20.93	1.25	22.91	1.12	0.02	101.10
Px7	52.77	0.28	0.93	b.d.l.	21.13	1.27	22.27	1.27	0.09	100.00
Px8	54.18	0.24	0.56	0.004	21.02	1.34	22.60	1.33	0.03	101.31
Px9	53.53	0.16	0.54	b.d.l.	20.37	1.13	23.55	1.08	0.03	100.40
VQ-06-22A (1846/47)										
Px1	52.57	0.55	1.79	b.d.l.	9.54	0.40	15.30	19.48	0.33	99.97
Px10	53.48	0.33	1.86	0.024	18.70	0.53	23.92	1.63	0.03	100.50
Px11	51.29	0.29	1.05	b.d.l.	21.51	0.60	21.09	3.91	0.04	99.78
Px12	53.25	0.32	1.80	0.000	19.14	0.57	23.37	1.53	0.04	100.02
Px14	54.71	0.53	2.16	0.025	9.69	0.41	15.08	18.16	0.39	101.16
Px15	53.08	0.54	0.91	0.016	15.56	0.53	12.77	16.24	0.38	100.04
Px16	53.05	0.35	1.40	0.005	18.20	0.64	24.27	1.59	0.05	99.55
Px17	51.85	0.45	0.81	b.d.l.	15.74	0.59	13.34	16.38	0.37	99.53
Px18	53.68	0.29	1.05	0.002	18.60	0.63	24.37	1.77	0.03	100.42
Px19	53.56	0.34	1.53	b.d.l.	17.85	0.63	24.14	1.58	0.04	99.67
Px2	52.34	0.73	2.15	0.046	10.24	0.41	14.57	19.56	0.37	100.40
Px20	53.62	0.34	1.20	b.d.l.	18.74	0.61	23.92	1.61	0.02	100.08

Appendix B4b continued

Label	SiO_2	TiO_2	Al_2O_3	Cr_2O_3	FeO	MnO	MgO	CaO	Na_2O	Tot
Px21	53.68	0.41	1.30	0.046	19.04	0.60	23.85	1.83	0.03	100.78
Px23	45.52	2.33	7.70	0.056	12.99	0.24	12.14	17.82	0.41	99.22
Px24_rim	53.23	0.32	0.60	b.d.l.	24.21	0.75	19.24	2.04	0.05	100.43
Px3	52.96	0.34	1.19	0.024	17.19	0.57	21.88	2.42	0.12	96.69
Px6	52.57	0.24	1.05	0.002	18.83	0.70	23.27	2.01	0.10	98.77
Px7	53.26	0.31	1.40	0.014	18.30	0.66	24.51	1.27	0.03	99.76
Px8	52.83	0.31	0.31	0.003	24.36	0.63	19.40	3.04	0.07	100.94
VQ-06-22D (1846/47)										
Px25-gc	53.56	0.26	0.80	b.d.l.	20.26	1.34	23.41	1.30	0.02	100.95
Px26	49.28	0.93	3.36	0.023	10.47	0.38	15.41	19.04	0.35	99.25
Px27	49.67	0.78	3.06	0.193	8.76	0.28	15.93	20.02	0.28	98.98
Px28	52.23	0.46	1.62	0.027	9.67	0.31	17.03	18.79	0.23	100.37
Px29	53.64	0.36	1.31	b.d.l.	17.98	0.64	24.33	1.74	0.02	100.02
Px30	53.09	0.41	1.69	0.011	17.23	0.49	25.11	1.76	0.04	99.83
Px31	50.64	0.87	3.10	0.023	10.39	0.38	14.79	19.15	0.38	99.72
Px32	52.98	0.21	0.81	0.001	16.58	0.60	26.52	1.58	0.03	99.32
Px33	50.47	0.39	1.04	b.d.l.	19.36	0.84	22.58	2.00	0.03	96.70
Px35	52.50	0.28	1.30	0.012	16.50	0.49	25.50	2.01	0.03	98.61
Px36	54.15	0.19	0.61	b.d.l.	18.62	1.20	23.77	1.14	0.05	99.73
Px38	48.08	1.62	5.26	0.058	10.69	0.33	13.91	19.07	0.45	99.48
VQ-06-44a (1846/47)										
Px1	52.26	0.13	0.29	b.d.l.	22.65	1.46	20.85	1.04	0.04	98.73
Px11	51.88	0.45	1.94	0.009	9.37	0.35	17.20	17.99	0.17	99.35
Px12	52.94	0.20	0.43	b.d.l.	21.39	1.27	21.77	1.29	0.04	99.34
Px13	50.74	0.21	0.56	b.d.l.	20.76	1.21	21.75	1.16	0.02	96.41
Px14	51.69	0.28	0.75	0.004	21.62	1.35	21.71	1.19	0.03	98.62
Px15	50.05	0.90	4.61	0.027	8.76	0.21	14.63	20.51	0.31	99.99
Px2	51.54	0.21	0.51	b.d.l.	21.59	1.27	21.18	1.24	0.02	97.55
Px3	50.91	0.44	1.93	b.d.l.	8.58	0.29	16.50	19.44	0.23	98.32
Px5	51.25	0.40	2.54	0.175	6.49	0.19	16.06	21.15	0.24	98.52

Appendix B4b continued

Label	SiO_2	TiO_2	Al_2O_3	Cr_2O_3	FeO	MnO	MgO	CaO	Na_2O	Tot
Px6	50.92	0.61	3.22	0.062	7.55	0.16	15.49	21.37	0.29	99.66
Px8	53.27	0.27	0.39	0.001	20.08	1.17	22.94	1.31	0.01	99.43
VQ-06-17 (1932)										
Px1	52.23	0.16	0.49	0.001	18.89	1.17	23.57	1.05	0.04	97.59
Px10	52.07	0.27	0.67	b.d.l.	16.20	1.08	21.15	5.76	0.15	97.35
Px11	53.25	0.26	0.60	b.d.l.	19.23	1.33	23.20	1.21	0.03	99.10
Px12	52.76	0.19	0.47	b.d.l.	19.48	1.29	23.17	1.17	0.04	98.58
Px13	53.98	0.18	0.57	b.d.l.	18.58	1.23	23.90	1.07	0.05	99.57
Px14	52.94	0.18	0.39	0.007	20.49	1.29	22.83	1.41	0.04	99.56
Px15	52.93	0.17	0.82	b.d.l.	18.13	1.20	24.79	0.85	0.04	98.93
Px16	53.56	0.26	0.39	0.020	19.77	1.38	22.82	1.06	0.04	99.31
Px2	51.68	0.20	0.66	b.d.l.	20.45	1.27	22.28	1.14	0.03	97.72
Px3	52.24	0.27	0.66	0.000	18.92	1.34	23.38	1.18	0.07	98.06
Px4	51.47	0.24	0.56	b.d.l.	19.51	1.21	22.88	1.27	0.04	97.19
Px5	52.54	0.22	0.65	0.004	20.67	1.16	22.41	1.14	0.05	98.86
Px6	52.48	0.23	0.58	0.007	20.42	1.26	22.29	1.21	0.29	98.77
Px7	52.08	0.21	0.45	0.012	19.02	1.28	23.59	1.12	0.04	97.80
Px9	52.18	0.22	0.64	0.004	18.64	1.22	23.65	1.07	0.05	97.68
VQ-07-37D (1932)										
Px1	52.81	0.24	0.50	0.012	19.77	1.27	23.42	1.19	0.06	99.28
Px10	53.90	0.25	0.47	b.d.l.	19.32	1.30	23.97	1.28	0.02	100.50
Px11	52.73	0.24	1.27	0.006	20.14	1.28	22.10	1.20	0.02	99.00
Px12	53.61	0.19	0.76	0.014	18.64	1.14	24.77	1.10	0.03	100.25
Px13	53.95	0.18	0.39	b.d.l.	18.95	1.24	24.72	1.15	0.02	100.60
Px14	53.75	0.18	0.45	0.019	19.43	1.38	23.79	1.16	0.03	100.19
Px15	53.16	0.27	1.01	b.d.l.	21.08	1.16	22.74	1.15	0.03	100.60
Px16	53.33	0.18	0.44	0.010	20.12	1.19	23.47	1.32	0.03	100.08
Px17	52.31	0.18	0.42	0.001	19.01	1.29	24.23	1.22	0.03	98.70
Px18	53.07	0.18	0.59	b.d.l.	19.02	1.29	24.04	1.10	0.02	99.31
Px19	54.08	0.26	0.77	b.d.l.	17.31	0.56	25.39	1.85	0.09	100.31

Appendix B4b continued

Label	SiO_2	TiO_2	Al_2O_3	Cr_2O_3	FeO	MnO	MgO	CaO	Na_2O	Tot
Px2	53.28	0.18	0.60	0.005	20.05	1.12	23.08	1.27	0.04	99.62
Px21	52.61	0.20	0.48	0.004	21.20	1.24	22.63	1.26	0.03	99.65
Px22	52.90	0.22	0.39	b.d.l.	20.95	1.23	21.97	1.28	0.04	98.99
Px23	52.94	0.35	1.43	b.d.l.	18.63	0.96	24.13	1.33	0.03	99.80
Px24	53.37	0.18	0.48	0.005	19.81	1.30	23.54	1.03	0.04	99.76
Px5	53.23	0.13	0.31	0.014	20.56	1.41	23.43	1.06	0.03	100.16
Px6	52.79	0.27	1.09	b.d.l.	20.82	1.00	22.74	1.26	0.05	100.02
Px7	54.26	0.20	0.49	0.010	19.36	1.32	24.22	1.05	0.02	100.92
Px8	54.11	0.20	0.53	b.d.l.	19.18	1.20	24.30	1.07	0.04	100.63
Px9	53.94	0.32	0.93	0.025	17.66	0.53	25.05	1.84	0.05	100.34

[1]analyses taken at University of Washington; b.d.l. = below detection limit

Appendix B5 Olivine electron microprobe analyses (atomic proportions and weight concentrations)[1]

Label	Fo[2]	Si	Ti	Al	Cr	Fe	Mn	Mg	Ca	Na	Tot[3]	SiO_2	TiO_2	Al_2O_3	Cr_2O_3	FeO	MnO	MgO	CaO	Na_2O	Tot
VQ-06-22A (1846/47)																					
Ol1	76.6	1.00	0.0002	0.0003	0.0001	0.46	0.009	1.52	0.005	0.0002	7.00	38.74	0.009	0.008	0.007	21.46	0.40	39.32	0.19	0.004	100.1
Ol2	76.2	1.00	0.0006	0.0004	0.0003	0.48	0.007	1.52	0.005	0.0005	7.00	38.64	0.031	0.014	0.014	22.06	0.32	39.57	0.19	0.010	100.9
Ol4	75.7	1.00	0.0002	0.0006	b.d.l.	0.48	0.007	1.51	0.005	0.0012	7.00	38.62	0.012	0.019	b.d.l.	22.48	0.34	39.27	0.18	0.023	101.0
Ol5	76.5	1.00	0.0003	0.0007	0.0004	0.47	0.007	1.52	0.005	0.0003	7.00	38.64	0.015	0.022	0.018	21.53	0.30	39.38	0.20	0.006	100.1
Ol9	74.6	1.00	b.d.l.	0.0002	b.d.l.	0.50	0.009	1.48	0.004	0.0003	7.00	38.60	b.d.l.	0.007	b.d.l.	23.22	0.40	38.28	0.15	0.005	100.7
Mount_VQ-06-22A (1846/47)																					
Ol1	76.0	0.99	0.0005	0.0009	b.d.l.	0.48	0.007	1.52	0.005	0.0006	7.01	38.42	0.023	0.030	b.d.l.	22.23	0.31	39.46	0.18	0.012	100.7
Ol2	76.0	1.00	0.0005	0.0011	b.d.l.	0.48	0.009	1.51	0.006	0.0001	7.00	38.85	0.025	0.038	b.d.l.	22.28	0.40	39.60	0.21	0.001	101.4
Ol3	76.2	0.98	0.0002	0.0002	0.0007	0.48	0.008	1.55	0.005	0.0004	7.02	37.51	0.010	0.006	0.032	22.11	0.35	39.73	0.19	0.007	99.9
Ol4	75.5	1.00	0.0004	0.0007	0.0004	0.49	0.008	1.50	0.005	0.0008	7.00	38.47	0.020	0.023	0.021	22.55	0.38	38.92	0.19	0.016	100.6
Ol5	75.5	1.00	b.d.l.	0.0005	0.0003	0.49	0.007	1.50	0.005	0.0023	7.00	38.84	b.d.l.	0.018	0.013	22.70	0.30	39.22	0.19	0.047	101.3
Ol6	75.8	1.00	0.0001	0.0008	0.0001	0.48	0.007	1.51	0.005	0.0013	7.00	38.52	0.008	0.026	0.006	22.28	0.34	39.06	0.19	0.025	100.5
Ol7	75.4	0.99	b.d.l.	0.0007	0.0001	0.49	0.007	1.51	0.006	0.0025	7.01	38.27	b.d.l.	0.023	0.004	22.71	0.32	39.02	0.22	0.049	100.6
Ol8	76.2	1.00	0.0001	0.0010	0.0003	0.47	0.007	1.51	0.005	0.0110	7.01	38.63	0.006	0.033	0.013	21.95	0.32	39.33	0.18	0.220	100.7
Ol9	74.7	0.99	0.0001	0.0009	0.0005	0.50	0.007	1.49	0.004	0.0010	7.00	38.36	0.002	0.028	0.022	23.25	0.34	38.62	0.13	0.020	100.8
Mount_VQ-07-44A (1846/47)																					
Ol4	76.6	0.97	0.0005	0.0003	0.0001	0.48	0.008	1.57	0.005	b.d.l.	7.03	35.55	0.023	0.010	0.007	20.96	0.33	38.49	0.16	b.d.l.	95.5
Mount_VQ-06-17 (1932)																					
Ol8	71.4	0.99	b.d.l.	b.d.l.	0.0001	0.57	0.020	1.43	0.002	0.0009	7.01	36.77	0.001	b.d.l.	0.007	25.52	0.89	35.71	0.06	0.019	99.0
Mount_VQ-07-37D (1932)																					
Ol20	70.2	1.00	0.0001	0.0008	0.0001	0.59	0.009	1.39	0.006	0.0013	7.00	37.72	0.005	0.026	0.007	26.69	0.42	35.21	0.20	0.026	100.3
Ol4	71.7	1.00	0.0001	0.0007	b.d.l.	0.56	0.011	1.43	0.004	0.0007	7.00	37.99	0.006	0.021	b.d.l.	25.74	0.51	36.61	0.15	0.015	101.0

[1] analyses taken at University of Washington; b.d.l. = below detection limit

[2] Fo = forsterite content (100xMg/(Mg+Fe)

[3] Tot = atomic proportions total calculated assuming 4 oxygen cations

Appendix B6a Glass electron microprobe analyses (atomic concentrations)[1]

Label	Si	Ti	Al	Fe	Mn	Mg	Ca	Na	K	Ba	Sr	P	Cl	O	Tot
VQ-06-02 (1846/47)															
Pl25-Gl	4.08	0.030	0.80	0.108	0.003	0.014	0.036	0.40	0.37	0.000	b.d.l.	0.007	0.03	9.97	15.85
Pl25-Gl	4.03	0.026	0.85	0.103	0.001	0.021	0.053	0.44	0.35	0.002	b.d.l.	0.005	0.03	9.97	15.89
Pl27-Gl	3.87	0.023	1.03	0.085	0.000	0.009	0.145	0.54	0.27	0.000	0.001	0.003	0.02	9.99	15.98
Pl27-Gl	4.09	0.029	0.80	0.102	0.003	0.013	0.036	0.40	0.37	0.001	b.d.l.	0.005	0.02	9.98	15.85
Pl27-Gl	4.07	0.029	0.81	0.105	0.002	0.016	0.036	0.40	0.39	0.001	b.d.l.	0.006	0.03	9.97	15.86
Pl35-Gl	4.07	0.031	0.81	0.108	0.003	0.017	0.034	0.39	0.38	0.001	b.d.l.	0.004	0.03	9.97	15.86
Pl35-Gl	4.05	0.031	0.82	0.110	0.003	0.041	0.035	0.41	0.37	0.000	b.d.l.	0.006	0.03	9.97	15.87
VQ-06-10 (1846/47)															
Pl23-Gl	3.81	0.024	1.03	0.125	0.003	0.070	0.172	0.52	0.24	0.002	b.d.l.	0.008	0.02	9.98	16.01
Pl23-Gl	3.59	0.014	1.31	0.083	0.002	0.027	0.290	0.66	0.16	0.003	0.001	0.007	0.01	10.00	16.14
Pl22-Gl	3.78	0.020	1.15	0.063	0.002	0.008	0.187	0.61	0.21	0.002	b.d.l.	0.006	0.01	9.99	16.02
Pl22-Gl	3.62	0.014	1.30	0.075	0.001	0.024	0.267	0.65	0.16	0.002	0.001	0.007	0.00	10.00	16.12
Pl21-Gl	3.63	0.017	1.28	0.066	0.001	0.017	0.266	0.63	0.16	0.002	0.002	0.005	0.01	9.99	16.09
Pl21-Gl	3.62	0.015	1.31	0.063	0.000	0.014	0.276	0.63	0.17	0.001	0.001	0.004	0.01	9.99	16.10
VQ-06-11 (1846/47)															
Pl6-Gl	3.97	0.020	0.94	0.095	0.004	0.034	0.065	0.53	0.29	0.003	b.d.l.	0.002	0.01	9.99	15.95
Pl6-Gl	4.02	0.018	0.90	0.074	0.002	0.023	0.057	0.50	0.31	0.000	b.d.l.	0.003	0.02	9.99	15.90
Pl1-Gl	4.01	0.019	0.91	0.071	0.001	0.018	0.045	0.50	0.35	0.002	b.d.l.	0.003	0.03	9.97	15.92
Pl1-Gl	3.99	0.016	0.95	0.062	0.001	0.017	0.054	0.54	0.31	0.001	b.d.l.	0.003	0.02	9.98	15.93
Pl4-Gl	4.01	0.018	0.92	0.068	0.003	0.020	0.057	0.52	0.32	0.001	b.d.l.	0.003	0.01	9.99	15.92
Pl4-Gl	3.78	0.011	1.16	0.053	0.001	0.019	0.142	0.70	0.21	0.001	b.d.l.	0.004	0.01	9.99	16.08
Pl4-Gl	3.90	0.013	1.04	0.048	0.001	0.012	0.083	0.67	0.25	0.002	b.d.l.	0.002	0.01	9.99	16.02
Pl4-Gl	3.97	0.016	0.97	0.056	0.001	0.014	0.065	0.58	0.30	0.001	b.d.l.	0.003	0.01	9.99	15.96

[1] analyses taken at University of Washington; b.d.l. = below detection limit

Appendix B6b Glass electron microprobe analyses (weight concentrations)[1]

Label	SiO_2	TiO_2	Al_2O_3	FeO	MnO	MgO	CaO	Na_2O	K_2O	BaO	SrO	P_2O_5	Cl	Tot
VQ-06-02 (1846/47)														
Pl25-Gl	74.76	0.72	12.42	2.36	0.063	0.17	0.62	3.75	5.36	0.01	b.d.l.	0.16	0.29	100.6
Pl25-Gl	73.07	0.63	13.11	2.24	0.010	0.26	0.90	4.14	5.00	0.08	b.d.l.	0.10	0.35	99.8
Pl27-Gl	69.37	0.54	15.70	1.83	0.000	0.11	2.42	5.00	3.79	0.02	0.018	0.07	0.16	99.0
Pl27-Gl	74.57	0.69	12.34	2.22	0.070	0.16	0.62	3.77	5.23	0.06	b.d.l.	0.11	0.20	100.0
Pl27-Gl	73.89	0.71	12.47	2.27	0.034	0.19	0.60	3.71	5.48	0.06	b.d.l.	0.12	0.34	99.8
Pl35-Gl	74.07	0.75	12.48	2.35	0.061	0.21	0.57	3.65	5.47	0.06	b.d.l.	0.09	0.33	100.0
Pl35-Gl	73.60	0.74	12.56	2.38	0.065	0.50	0.59	3.82	5.26	0.02	b.d.l.	0.12	0.33	99.9
VQ-06-10 (1846/47)														
Pl23-Gl	68.96	0.57	15.81	2.70	0.064	0.84	2.90	4.89	3.45	0.08	b.d.l.	0.16	0.18	100.6
Pl23-Gl	64.08	0.34	19.87	1.77	0.034	0.32	4.83	6.09	2.20	0.11	0.027	0.16	0.06	99.9
Pl22-Gl	68.71	0.49	17.70	1.36	0.037	0.09	3.17	5.68	2.96	0.08	b.d.l.	0.13	0.12	100.5
Pl22-Gl	65.10	0.33	19.77	1.61	0.019	0.29	4.48	6.03	2.27	0.09	0.039	0.15	0.03	100.2
Pl21-Gl	65.48	0.41	19.63	1.41	0.012	0.21	4.47	5.89	2.33	0.11	0.052	0.11	0.15	100.2
Pl21-Gl	65.21	0.36	19.97	1.36	0.002	0.16	4.64	5.84	2.39	0.03	0.014	0.09	0.11	100.1
VQ-06-11 (1846/47)														
Pl6-Gl	72.71	0.48	14.56	2.09	0.081	0.41	1.11	5.05	4.17	0.13	b.d.l.	0.05	0.15	101.0
Pl6-Gl	73.65	0.43	14.04	1.62	0.044	0.28	0.97	4.69	4.46	0.02	b.d.l.	0.06	0.16	100.4
Pl1-Gl	72.85	0.45	14.08	1.55	0.029	0.22	0.77	4.66	4.96	0.09	b.d.l.	0.07	0.34	100.0
Pl1-Gl	72.50	0.40	14.61	1.35	0.012	0.20	0.92	5.05	4.43	0.06	b.d.l.	0.07	0.25	99.8
Pl4-Gl	73.46	0.43	14.25	1.50	0.059	0.25	0.97	4.88	4.55	0.04	b.d.l.	0.06	0.16	100.6
Pl4-Gl	68.23	0.25	17.76	1.14	0.024	0.23	2.39	6.53	2.96	0.04	b.d.l.	0.08	0.10	99.7
Pl4-Gl	71.11	0.32	16.16	1.04	0.027	0.14	1.42	6.29	3.53	0.08	b.d.l.	0.05	0.14	100.3
Pl4-Gl	72.28	0.39	14.96	1.22	0.031	0.16	1.10	5.43	4.23	0.06	b.d.l.	0.06	0.15	100.0

[1] analyses taken at University of Washington; b.d.l. = below detection limit

Appendix B7 LA-ICP MS data for plagioclase separates of grain mounts from the 1846/47 eruption[1]

Sample	02-250 Pl30	02-250 Pl29	02-250 Pl28	02-250 Pl27	02-250 Pl26	02-250 Pl25	02-250 Pl24	02-250 Pl23	02-250 Pl22	02-250 Pl20	02-250 Pl21	02-250 Pl19	02-250 Pl18	02-250 Pl14	02-250 Pl15	02-250 Pl16	02-250 Pl17
An	30.41	29.88	37.10	25.72	51.87	51.51	26.89	29.08	49.16	30.38	46.06	51.10	31.04	32.17	29.50	30.67	30.79
Conc. (µg/g)																	
Li	12.3	13.5	13.1	12.4	10.1	11.7	11.4	11.9	11.4	10.6	10.2	11.7	11.9	12.1	10.1	12.7	12.0
Mg	104	122	132	97	109	126	110	97	125	115	115	112	100	119	103	116	133
Si	301255	358467	323188	338321	265127	261234	323081	315019	274073	287920	318397	281218	351559	325841	287861	305151	277646
Ca	44668	44597	55103	38522	75972	75543	39094	43168	72756	43310	68039	75686	46098	47885	43596	45455	44811
Ti	192	179	201	130	224	368	262	143	264	204	239	356	191	165	186	149	174
Fe	2858	3164	3184	2942	2675	3057	3197	2780	2619	2846	2986	2752	3186	2985	2665	2864	2803
Cu	28.5	72.6	40.8	51.1	3.6	4.0	5.5	5.5	12.2	1.3	2.5	2.6	3.4	1.6	3.7	2.6	3.5
Zn	10.1	10.0	9.1	9.1	6.2	3.7	5.1	7.0	8.0	5.4	6.4	5.7	5.2	5.8	6.1	5.1	4.0
Sr	891	929	1018	798	1117	1251	860	848	1182	860	1251	1029	919	952	818	937	862
Y	0.22	0.36	0.29	0.25	0.28	0.22	0.21	0.12	0.57	0.29	0.26	0.32	0.25	0.20	0.27	0.25	0.18
Ba	585	740	411	808	158	138	759	645	213	620	306	243	846	682	594	620	575
La	6.7	8.6	6.2	8.0	2.9	2.6	7.4	7.8	4.1	7.9	4.0	2.8	8.7	8.4	7.0	7.6	7.2
Ce	10.5	13.1	9.5	11.2	5.4	4.4	11.2	10.8	6.5	11.2	6.8	5.1	12.9	11.6	11.2	12.3	10.6
Pr	0.85	1.05	0.83	0.90	0.53	0.39	0.86	0.86	0.68	1.00	0.57	0.62	1.05	1.04	0.95	0.92	0.77
Nd	2.8	2.9	2.5	2.5	1.9	1.7	2.4	2.9	2.3	3.2	1.6	2.1	2.9	2.9	2.8	2.6	2.6
Sm	0.44	0.42	0.24	0.12	0.30	b.d.l.	0.13	0.24	0.40	0.44	b.d.l.	b.d.l.	0.14	0.43	0.14	b.d.l.	b.d.l.
Eu	1.82	2.20	1.83	2.06	0.99	0.78	2.12	2.17	1.26	1.98	1.50	1.55	2.32	2.33	1.93	1.95	2.04
Pb	8.4	9.3	7.7	9.6	5.4	2.2	7.8	8.9	6.3	6.9	7.9	6.3	10.8	8.9	8.4	7.8	7.1
1SE (µg/g)																	
Li	1.4	1.6	1.6	1.4	1.2	1.4	1.3	1.3	1.3	1.3	1.4	1.4	1.3	1.5	1.2	1.5	1.5
Mg	3.9	4.9	4.7	4.7	4.2	4.7	3.8	3.6	3.8	4.7	4.2	4.5	4.3	4.4	3.5	5.5	6.4
Si	8080	6501	7804	6587	4341	4502	5192	9292	5631	6892	5619	9943	8281	6798	7970	6281	7153
Ca	827	826	1020	713	1407	1399	724	799	1347	802	1260	1401	853	887	807	842	830
Ti	16	14	17	10	16	28	19	11	20	16	19	27	15	12	14	12	14
Fe	97	85	89	82	82	89	100	128	76	95	90	115	101	82	82	99	94
Cu	1618	886	17	46	24	1	3	381	4	1	1	2	1	1	1	2	3
Zn	4.0	3.5	0.7	1.4	1.1	0.5	0.3	0.8	6.0	0.5	0.4	0.5	0.4	0.4	0.3	0.6	0.7
Sr	22	18	26	17	27	24	17	21	24	19	25	23	20	19	17	20	18
Y	0.06	0.06	0.03	0.04	0.04	0.04	0.04	0.05	0.06	0.04	0.03	0.05	0.05	0.04	0.03	0.04	0.10
Ba	16	13	9	14	3	3	15	16	4	14	6	6	16	13	11	12	16
La	0.32	0.29	0.33	0.21	0.15	0.11	0.27	0.27	0.13	0.29	0.13	0.11	0.31	0.30	0.20	0.49	0.23
Ce	0.31	0.26	0.26	0.25	0.16	0.18	0.37	0.28	0.15	0.39	0.24	0.13	0.33	0.31	0.30	0.37	0.37
Pr	0.10	0.07	0.08	0.06	0.06	0.03	0.09	0.10	0.06	0.08	0.08	0.07	0.11	0.08	0.07	0.12	0.10
Nd	0.19	0.29	0.42	0.11	0.18	0.24	0.22	0.06	0.12	0.31	0.18	0.09	0.26	0.24	0.20	0.43	0.25
Sm	0.10	0.11	0.05	0.10	0.06	b.d.l.	0.12	0.03	0.12	0.11	b.d.l.	b.d.l.	0.05	0.10	0.06	b.d.l.	b.d.l.
Eu	0.11	0.16	0.07	0.20	0.08	0.10	0.11	0.13	0.09	0.12	0.09	0.15	0.13	0.14	0.13	0.08	0.19
Pb	0.83	0.90	0.73	1.00	0.54	0.22	0.74	0.88	1.70	0.71	0.82	0.62	1.15	0.86	0.82	0.80	0.76

Appendix B7 continued

Sample	02-250 Pl12	02-250 Pl13	02-250 Pl10	02-250 Pl11	02-250 Pl9	02-250 Pl7	02-250 Pl8	02-250 Pl5	02-250 Pl6	02-250 Pl4	02-250 Pl3	02-250 Pl1	02-250 Pl2	06-250 Pl18	06-250 Pl17	06-250 Pl16	06-250 Pl15
An	27.05	45.26	31.22	29.53	40.66	38.91	32.75	38.61	31.79	32.25	31.43	29.55	30.36	33.19	39.77	31.43	48.31
Conc. (µg/g)																	
Li	9.9	9.4	11.9	11.3	11.2	12.8	11.3	9.3	9.1	9.3	9.9	8.2	9.8	5.4	7.1	5.6	6.2
Mg	107	138	104	92	139	123	113	117	108	122	97	119	114	91	97	118	283
Si	288633	301858	305172	308217	290453	318254	316020	248162	266362	291833	252669	316950	312840	292878	293067	284502	274474
Ca	39451	66895	46241	43811	61035	58319	48313	57033	47527	47813	46384	44240	45169	49886	59105	46670	70755
Ti	184	249	184	196	202	261	173	199	181	175	199	185	163	177	224	159	304
Fe	2733	3070	2784	2839	3104	2961	2929	2667	2541	2694	2280	2847	2715	2806	2586	2531	4554
Cu	4.2	1.7	1.7	7.7	13.4	4.6	7.8	2.1	2.9	3.6	1.4	23.8	3.0	1.4	1.7	2.3	36.0
Zn	2.3	5.0	5.2	5.1	7.7	7.1	6.5	4.7	4.3	5.2	4.9	5.7	5.5	5.2	4.5	4.8	7.7
Sr	862	1119	922	926	1114	1143	931	950	902	897	864	901	899	952	1180	899	951
Y	0.25	0.51	0.28	0.29	0.22	0.25	0.31	0.32	0.27	0.30	0.35	0.36	0.16	0.34	0.31	0.33	0.47
Ba	676	404	636	661	375	465	582	330	394	536	396	715	620	497	355	531	249
La	8.2	7.2	7.5	8.0	7.7	6.9	8.4	4.8	5.7	6.8	4.9	8.0	7.6	7.2	5.9	7.3	4.9
Ce	10.3	13.1	11.0	10.6	10.2	9.9	11.1	7.6	8.7	10.3	7.7	11.3	10.9	10.5	8.7	10.3	8.3
Pr	0.80	1.06	0.82	0.96	0.96	0.80	1.08	0.70	0.66	0.83	0.81	1.02	1.01	0.86	0.78	1.01	0.76
Nd	3.0	4.0	3.3	2.7	2.9	3.0	2.6	2.4	2.5	2.7	2.2	2.7	2.9	3.0	2.6	3.2	3.2
Sm	0.13	0.58	0.07	0.25	0.40	0.35	0.28	0.33	0.33	0.20	0.18	0.42	0.37	0.44	0.12	0.31	0.12
Eu	1.87	1.83	1.97	1.99	1.71	1.75	2.17	1.63	1.66	1.94	1.42	2.11	1.99	1.96	1.97	2.10	1.31
Pb	7.0	7.5	8.2	7.5	6.5	8.1	8.4	6.3	6.8	7.2	6.7	7.6	8.2	7.3	6.5	7.1	4.1
1SE (µg/g)																	
Li	1.2	1.1	1.5	1.3	1.3	1.5	1.3	1.1	1.0	1.1	1.2	1.0	1.1	0.8	0.9	0.7	0.8
Mg	7.9	5.1	4.2	4.9	4.5	5.2	4.3	4.3	4.2	3.6	3.1	5.5	4.3	3.9	3.7	5.2	10.6
Si	6428	5850	9451	7826	5776	6287	5518	4449	4758	4894	6612	6321	6571	5582	5490	3914	4212
Ca	730	1238	856	811	1130	1080	894	1056	880	885	859	819	836	924	1094	864	1310
Ti	14	19	15	15	15	20	13	15	13	13	15	14	13	13	17	12	23
Fe	86	85	95	96	88	86	87	73	82	83	69	109	80	124	79	79	212
Cu	3	6	1	3	8	10	4	3	1	34	3	29	11	17	0	2	20
Zn	0.7	0.3	0.4	0.3	1.1	1.0	1.5	0.7	0.4	1.3	0.4	2.5	0.6	0.5	0.4	0.5	1.3
Sr	20	23	26	21	23	24	18	19	19	21	19	19	20	18	24	16	17
Y	0.04	0.09	0.04	0.06	0.06	0.04	0.07	0.05	0.06	0.04	0.05	0.37	0.02	0.06	0.03	0.04	0.07
Ba	18	7	15	14	7	9	10	7	11	11	8	13	12	9	11	10	5
La	0.40	0.32	0.25	0.21	0.25	0.28	0.30	0.12	0.27	0.28	0.17	0.40	0.20	0.28	0.27	0.20	0.11
Ce	0.26	0.39	0.27	0.37	0.28	0.22	0.24	0.16	0.24	0.25	0.36	0.88	0.35	0.23	0.19	0.22	0.16
Pr	0.08	0.09	0.07	0.08	0.08	0.06	0.07	0.06	0.06	0.07	0.09	0.16	0.09	0.08	0.05	0.07	0.05
Nd	0.22	0.35	0.22	0.12	0.20	0.35	0.10	0.21	0.16	0.29	0.28	0.47	0.24	0.38	0.20	0.36	0.18
Sm	0.03	0.09	0.09	0.06	0.08	0.09	0.04	0.05	0.09	0.07	0.09	0.20	0.12	0.16	0.06	0.04	0.11
Eu	0.10	0.11	0.18	0.13	0.12	0.08	0.11	0.11	0.07	0.12	0.10	0.09	0.10	0.16	0.17	0.16	0.12
Pb	0.68	0.82	0.86	0.74	0.68	0.79	0.81	0.63	0.65	0.77	0.69	0.75	0.82	0.72	0.72	0.68	0.45

Appendix B7 continued

Sample	06-250 Pl14	06-250 Pl13	06-250 Pl32	06-250 Pl11	06-250 Pl10	06-250 Pl9	06-250 Pl8	06-250 Pl7	06-250 Pl6	06-250 Pl5	06-250 Pl3	06-250 Pl2	06-250 Pl1	06-250 Pl30	06-250 Pl29	06-250 Pl28	06-250 Pl27
An	56.45	44.45	29.05	32.15	44.84	36.53	50.05	31.70	30.42	38.35	41.04	25.58	26.93	27.63	31.65	30.50	53.83
Conc. (µg/g)																	
Li	5.2	7.1	6.4	7.1	7.6	5.9	6.1	6.5	6.3	6.2	6.6	7.6	6.6	7.3	6.2	8.2	6.6
Mg	251	105	99	104	109	94	101	98	104	94	119	85	78	105	128	100	111
Si	257373	283271	299992	304613	331107	281447	287867	306349	306949	303338	351995	320450	304407	311098	295824	286854	296724
Ca	81332	66324	42810	48027	67110	54460	73399	46955	45097	56532	61249	38093	39808	40523	47170	45026	78545
Ti	214	189	154	185	210	251	170	206	179	181	244	146	132	250	233	176	250
Fe	4526	2723	2651	2630	2873	2529	2881	2803	2706	2414	3093	2574	2426	2867	2895	2726	2712
Cu	31.9	65.2	14.3	2.3	1.4	2.6	6.7	b.d.l.	1.2	2.4	2.0	0.6	6.2	0.9	1.0	3.4	14.9
Zn	4.8	6.2	5.9	5.3	6.6	4.5	5.7	5.1	4.7	4.6	5.8	5.0	4.5	6.1	5.6	4.8	5.6
Sr	1434	1237	898	960	1125	994	1131	917	933	937	1231	820	829	872	1003	846	978
Y	0.21	0.25	0.32	0.34	0.37	0.36	0.33	0.24	0.16	0.23	0.41	0.16	0.18	0.28	0.22	0.24	0.72
Ba	122	241	631	578	480	403	238	607	691	456	630	823	687	751	443	559	337
La	2.9	3.4	8.0	7.7	8.2	7.0	5.8	7.4	8.3	5.0	8.5	8.2	7.3	7.0	5.2	7.6	4.2
Ce	4.6	5.5	11.2	11.0	11.9	9.4	9.1	11.1	12.8	7.8	12.8	11.9	11.7	11.2	8.0	10.5	7.3
Pr	0.44	0.50	1.04	0.94	1.15	0.96	0.90	0.95	0.97	0.58	1.05	0.88	1.12	0.91	0.64	0.92	0.68
Nd	1.4	1.5	3.1	3.8	3.3	3.5	2.4	3.0	3.4	1.9	3.8	3.3	3.1	2.7	2.2	3.5	3.4
Sm	0.14	b.d.l.	0.21	0.38	0.50	b.d.l.	0.10	0.30	0.35	0.26	0.43	0.24	0.43	0.29	0.15	0.28	0.36
Eu	0.57	1.33	2.08	2.09	2.02	1.81	1.16	2.28	1.99	2.34	2.30	2.56	2.37	2.21	1.66	2.27	1.77
Pb	2.2	6.4	8.1	7.9	8.6	6.9	6.4	8.3	8.7	9.0	9.0	8.9	8.1	7.7	6.4	6.9	8.0
1SE (µg/g)																	
Li	0.8	0.8	0.8	0.9	0.9	0.9	0.7	0.8	0.8	0.8	0.9	0.9	0.8	1.0	0.8	1.0	0.8
Mg	8.7	5.2	3.1	4.8	3.4	3.5	3.5	4.0	4.0	3.5	5.9	3.3	3.4	3.9	4.3	4.1	4.5
Si	3582	5355	10491	4418	5770	4373	4259	6687	6849	5164	11597	4638	5138	4551	7277	6115	7273
Ca	1506	1228	793	889	1242	1008	1359	869	835	1047	1134	705	737	750	873	834	1454
Ti	17	14	11	14	15	19	12	16	17	13	19	13	11	18	17	13	18
Fe	135	87	88	83	95	83	87	86	103	85	121	97	73	89	85	95	84
Cu	17	56	14	1	1	1	3	b.d.l.	1	1	2	1	20	0	0	1	12
Zn	0.4	1.1	0.6	0.6	0.8	0.3	0.3	0.3	0.3	0.3	0.4	0.3	0.8	0.4	0.4	0.7	0.6
Sr	27	28	21	18	25	19	25	17	20	20	29	18	19	17	20	20	19
Y	0.04	0.03	0.06	0.03	0.07	0.04	0.04	0.06	0.04	0.03	0.05	0.04	0.03	0.04	0.03	0.06	0.07
Ba	3	5	16	11	11	9	5	12	18	13	25	18	16	14	8	13	8
La	0.12	0.17	0.24	0.23	0.21	0.19	0.22	0.18	0.24	0.19	0.30	0.38	0.25	0.19	0.17	0.20	0.19
Ce	0.20	0.11	0.41	0.45	0.45	0.21	0.42	0.31	0.35	0.22	0.36	0.38	0.28	0.34	0.19	0.29	0.23
Pr	0.04	0.06	0.08	0.10	0.08	0.06	0.07	0.10	0.09	0.08	0.10	0.08	0.11	0.08	0.05	0.09	0.08
Nd	0.12	0.16	0.33	0.38	0.24	0.30	0.31	0.24	0.29	0.27	0.22	0.24	0.24	0.12	0.22	0.30	0.18
Sm	0.06	b.d.l.	0.08	0.08	0.06	b.d.l.	0.08	0.12	0.10	0.07	0.16	0.11	0.07	0.05	0.04	0.09	0.14
Eu	0.04	0.11	0.20	0.25	0.18	0.18	0.12	0.19	0.22	0.18	0.22	0.23	0.19	0.18	0.13	0.28	0.16
Pb	0.22	0.62	0.82	0.75	0.88	0.68	0.64	0.80	0.94	0.87	0.87	0.87	0.78	0.79	0.63	0.66	0.76

Appendix B7 continued

Sample	06-250 Pl31	06-250 Pl26	06-250 Pl24	06-250 Pl33	06-250 Pl19	06-250 Pl20	06-250 Pl21	06-250 Pl22	06-250 Pl23	22A-250 Pl3	22A-250 Pl2	22A-250 Pl1	22A-250 Pl19	22A-250 Pl20	22A-250 Pl4	22A-250 Pl5	22A-250 Pl18
An	45.88	28.94	33.09	28.83	31.49	41.33	26.69	34.78	46.79	28.68	65.96	32.73	72.11	26.18	67.57	84.25	61.53
Conc. (µg/g)																	
Li	6.5	6.0	5.7	6.9	6.5	7.2	6.3	8.5	5.8	13.8	9.2	12.9	10.4	11.2	14.4	5.6	17.2
Mg	105	91	115	101	105	109	84	102	108	113	894	138	872	118	929	584	894
Si	296481	295520	284527	312146	323838	294340	307862	346324	297798	294994	274915	295435	280642	255814	289710	247725	263022
Ca	68182	42596	49457	43096	47241	60535	39380	51744	68968	42810	97627	49099	103416	39308	99557	121927	88908
Ti	355	219	147	159	177	234	227	235	279	195	331	197	309	168	351	129	391
Fe	2546	2739	2751	2671	2646	2733	2697	2874	2780	2854	7069	2920	6306	2725	7068	4900	6799
Cu	4.0	14.4	42.0	6.7	98.1	9.2	7.5	3.0	38.1	44.2	2.2	2.2	16.9	77.4	6.3	5.5	8.6
Zn	6.4	5.7	9.9	6.6	10.4	6.1	5.0	5.6	9.2	11.7	6.4	4.8	6.3	5.2	5.5	1.7	5.3
Sr	1040	858	977	898	908	1090	828	999	1206	844	1045	1004	1076	851	1091	999	993
Y	0.53	0.22	0.28	0.28	0.25	0.30	0.24	0.14	0.23	0.21	0.07	0.39	0.10	0.19	0.21	0.10	0.23
Ba	336	667	436	597	643	341	684	575	233	560	86	571	76	476	92	38	93
La	4.5	7.0	7.1	7.4	7.9	4.4	6.5	6.7	3.2	6.5	1.3	7.5	1.3	6.3	1.2	0.8	1.2
Ce	7.7	9.5	9.8	10.6	11.7	7.7	11.0	10.6	5.8	10.4	2.2	10.9	2.1	9.2	2.2	1.7	2.3
Pr	0.87	0.83	0.99	1.03	1.10	0.72	0.98	0.93	0.56	0.94	0.27	0.99	0.27	0.80	0.25	0.22	0.26
Nd	2.6	3.3	2.9	2.9	2.7	2.2	3.2	2.9	1.6	2.3	0.9	3.0	1.0	2.9	0.5	0.6	1.0
Sm	0.21	0.16	0.33	0.35	0.11	0.11	0.18	0.16	0.25	0.40	b.d.l.	0.27	b.d.l.	0.18	b.d.l.	b.d.l.	0.15
Eu	1.74	2.47	2.08	2.43	2.28	1.86	1.93	2.18	1.44	1.89	0.31	1.73	0.34	1.53	0.24	0.23	0.44
Pb	7.9	7.4	6.8	8.5	8.7	6.7	8.8	8.7	6.8	8.0	1.1	8.1	1.1	6.5	1.0	0.7	1.0
1SE (µg/g)																	
Li	0.8	0.7	0.8	0.8	0.8	0.8	0.8	1.1	0.7	1.7	1.2	1.6	1.4	1.4	1.9	0.7	2.2
Mg	3.5	2.9	5.2	3.8	4.2	3.8	3.4	5.4	4.7	5.1	31.0	5.1	25.4	6.0	27.1	17.7	44.5
Si	7252	4725	3978	5059	7268	5179	5668	9271	5041	5467	4695	4542	5524	6221	5408	4749	7404
Ca	1262	789	916	798	875	1121	729	958	1277	793	1807	909	1915	728	1843	2257	1646
Ti	28	16	11	12	14	17	17	19	21	15	24	14	25	13	27	9	34
Fe	90	81	79	78	89	82	80	109	103	78	216	96	220	87	211	145	213
Cu	6	8	50	23	58	9	44	4	267	365	47	1	39	76	4	26	24
Zn	0.9	0.5	3.6	1.6	3.7	0.8	0.9	0.3	3.2	8.6	1.8	0.5	1.2	1.8	0.5	0.2	0.4
Sr	19	16	17	17	18	21	16	26	24	15	22	19	20	19	19	18	17
Y	0.06	0.02	0.03	0.04	0.03	0.05	0.02	0.04	0.04	0.04	0.03	0.06	0.04	0.04	0.04	0.01	0.05
Ba	7	14	8	12	15	8	13	15	5	12	2	12	2	12	2	1	2
La	0.15	0.22	0.30	0.27	0.22	0.18	0.32	0.23	0.16	0.21	0.08	0.21	0.11	0.20	0.07	0.05	0.05
Ce	0.22	0.32	0.29	0.34	0.26	0.19	0.35	0.45	0.19	0.38	0.11	0.29	0.12	0.27	0.11	0.13	0.10
Pr	0.06	0.06	0.09	0.07	0.08	0.07	0.07	0.07	0.04	0.08	0.04	0.07	0.03	0.07	0.03	0.03	0.03
Nd	0.24	0.11	0.32	0.22	0.16	0.16	0.24	0.44	0.15	0.25	0.08	0.29	0.11	0.21	0.10	0.07	0.17
Sm	0.05	0.13	0.03	0.09	0.08	0.09	0.08	0.09	0.06	0.08	b.d.l.	0.05	b.d.l.	0.02	b.d.l.	b.d.l.	0.02
Eu	0.16	0.24	0.15	0.23	0.26	0.17	0.18	0.17	0.14	0.16	0.04	0.10	0.03	0.08	0.03	0.04	0.05
Pb	0.77	0.72	0.65	0.88	0.92	0.72	0.91	0.87	0.67	0.81	0.14	0.83	0.11	0.62	0.12	0.09	0.17

Appendix B7 continued

Sample	22A-250 Pl17	22A-250 Pl16	22A-250 Pl15	22A-250 Pl14	22A-250 Pl13	22A-250 Pl12	22A-250 Pl11	22A-250 Pl10	22A-250 Pl8	22A-250 Pl9	22A-250 Pl6	22D-250 Pl14	22D-250 Pl15	22D-250 Pl16	22D-250 Pl17	22D-250 Pl19	22D-250 Pl18
An	34.55	66.63	59.47	68.77	66.98	83.56	67.73	81.05	86.21	56.51	30.43	31.45	35.37	31.58	48.07	31.36	35.55
Conc. (µg/g)																	
Li	9.8	15.0	7.2	6.3	13.1	5.5	8.8	7.8	8.1	11.5	11.5	14.5	14.1	11.4	14.2	16.0	15.2
Mg	182	893	776	613	955	643	867	740	619	985	129	134	99	103	130	127	198
Si	295783	284989	232920	219772	266096	257171	265513	262605	244632	241694	272749	321904	291453	240261	308240	324244	322929
Ca	51101	97198	87550	98985	96698	119997	98842	119140	126072	83905	46169	46598	51387	46241	71184	46670	53173
Ti	206	361	268	174	351	145	293	213	124	391	171	175	271	201	366	187	186
Fe	3398	7002	5607	4660	6763	4663	6517	5006	4343	6740	2648	3044	2519	2082	2704	3026	3404
Cu	0.0	1.4	2.0	3.8	10.8	3.1	0.0	3.9	4.9	16.3	1.2	17.5	25.4	853.0	64.1	1.3	8.9
Zn	6.0	4.8	4.0	3.1	5.6	3.4	3.7	2.6	2.3	4.7	4.8	5.6	5.9	9.1	7.5	6.0	12.0
Sr	1027	1063	877	922	1036	1033	1052	1102	1047	915	851	945	880	784	1030	973	1072
Y	5.62	0.11	0.21	0.12	0.18	0.15	0.18	0.14	0.12	0.35	0.27	0.19	0.41	0.37	0.64	0.23	0.30
Ba	504	94	59	46	87	39	84	48	35	88	494	617	521	303	335	580	520
La	13.4	1.3	1.1	0.9	1.1	0.8	1.2	0.9	0.7	1.2	6.3	7.5	6.8	4.1	4.1	7.5	7.6
Ce	26.0	2.5	1.8	1.5	2.1	1.4	2.2	1.7	1.4	2.3	9.9	11.4	11.7	8.2	7.0	11.4	11.6
Pr	2.92	0.18	0.20	0.12	0.25	0.22	0.24	0.16	0.16	0.20	0.98	0.74	1.31	0.67	0.78	0.85	0.92
Nd	11.5	0.9	0.7	0.5	0.9	0.4	1.0	0.4	0.6	0.9	2.4	2.7	3.4	2.0	2.2	2.9	3.0
Sm	1.97	b.d.l.	0.20	b.d.l.	0.15	0.22	0.28	b.d.l.	0.11	b.d.l.	0.48	b.d.l.	0.36	0.24	0.05	0.31	0.23
Eu	1.53	0.42	0.24	0.22	0.37	0.14	0.33	0.29	0.23	0.24	1.64	1.80	2.12	1.23	2.06	1.80	1.89
Pb	7.4	1.2	0.7	0.6	1.2	0.7	1.0	0.6	0.7	1.0	6.8	8.8	8.0	6.9	8.8	7.5	8.1
1SE (µg/g)																	
Li	1.2	1.8	1.0	0.8	1.7	0.8	1.3	1.1	1.0	1.5	1.4	1.9	1.7	1.4	1.8	2.1	1.9
Mg	8.5	25.9	22.1	25.0	30.4	17.8	32.5	26.7	17.9	65.6	4.1	4.4	4.3	4.2	4.4	4.4	7.5
Si	6404	4749	3992	4399	4218	4681	6469	8729	3995	3843	4125	8203	5527	4903	5273	8426	7171
Ca	946	1800	1621	1833	1790	2222	1830	2206	2334	1553	855	863	951	856	1318	864	984
Ti	17	27	21	14	26	11	22	18	9	38	12	13	23	15	27	14	16
Fe	136	196	154	147	190	156	235	160	127	237	102	113	91	77	102	116	150
Cu	0	1	1	4	4	5	1	2	1	7	2	41	113	997	1038	4	60
Zn	0.6	0.6	0.4	0.8	1.2	0.7	1.0	0.4	0.5	0.4	0.3	2.0	1.9	3.3	4.8	0.8	5.9
Sr	22	19	15	18	17	17	27	22	19	19	15	20	18	18	19	21	21
Y	0.50	0.05	0.03	0.03	0.02	0.03	0.05	0.02	0.02	0.10	0.05	0.04	0.06	0.04	0.10	0.03	0.06
Ba	19	2	1	2	2	1	6	1	1	2	10	13	9	6	5	13	15
La	0.63	0.12	0.04	0.02	0.06	0.09	0.13	0.07	0.06	0.07	0.14	0.16	0.24	0.11	0.13	0.27	0.25
Ce	0.91	0.17	0.11	0.06	0.08	0.06	0.17	0.06	0.11	0.12	0.29	0.32	0.28	0.23	0.24	0.50	0.33
Pr	0.39	0.02	0.02	0.02	0.02	0.03	0.05	0.02	0.02	0.03	0.07	0.08	0.13	0.05	0.09	0.06	0.07
Nd	0.81	0.10	0.06	0.04	0.06	0.08	0.11	0.13	0.09	0.12	0.21	0.26	0.25	0.21	0.44	0.16	0.20
Sm	0.35	b.d.l.	0.09	b.d.l.	0.04	0.04	0.05	b.d.l.	0.04	b.d.l.	0.13	b.d.l.	0.14	0.08	0.12	0.04	0.08
Eu	0.11	0.05	0.03	0.05	0.07	0.04	0.02	0.02	0.04	0.04	0.13	0.17	0.21	0.10	0.13	0.12	0.10
Pb	0.78	0.14	0.13	0.07	0.19	0.08	0.13	0.09	0.08	0.14	0.65	0.90	0.80	0.64	0.89	0.75	0.80

Appendix B7 continued

Sample	22D-250 Pl28	22D-250 Pl27	22D-250 Pl26	22D-250 Pl24	22D-250 Pl23	22D-250 Pl22	22D-250 Pl20	22D-250 Pl21	22D-250 Pl29	22D-250 Pl30	22D-250 Pl31	22D-250 Pl13	22D-250 Pl12	22D-250 Pl10	22D-250 Pl5	22D-250 Pl1	22D-250 Pl4
An	36.47	0.00	31.50	50.77	35.64	33.62	32.50	29.58	32.55	48.06	32.11	51.69	32.13	50.97	30.06	31.06	33.37
Conc. (µg/g)																	
Li	14.3	0.2	14.8	14.4	13.3	15.1	16.0	13.1	15.1	14.7	14.2	13.0	15.1	14.7	16.0	14.5	13.4
Mg	127	2	157	130	120	126	168	128	130	182	136	129	139	130	118	176	133
Si	291484	5142	348414	285902	293084	308865	339232	291608	326700	300635	303949	258082	303859	296206	328042	321743	331010
Ca	53316	715	46598	75829	52601	49457	48170	43525	48671	70755	47742	74257	48170	76544	46169	47170	49242
Ti	179	3	212	262	276	173	285	187	193	157	177	277	181	269	221	259	178
Fe	2688	50	3123	2655	2709	2826	3375	2796	3144	3786	2939	2373	2988	3009	3101	3390	3108
Cu	80.3	0.1	23.4	150.0	0.8	4.0	3.8	0.8	22.3	7.3	22.2	3.9	0.7	4.5	5.9	22.6	7.9
Zn	5.5	0.3	11.2	5.1	5.7	5.0	6.7	5.7	7.4	5.6	5.9	4.6	5.1	5.3	6.8	6.2	8.2
Sr	999	15	999	1163	957	995	996	944	955	1446	926	900	1006	1260	949	996	1010
Y	0.32	0.00	0.31	0.25	0.47	0.19	0.55	0.25	0.34	0.18	0.27	0.73	0.19	0.31	0.31	0.88	0.19
Ba	513	10	732	205	458	542	769	571	653	246	603	320	566	233	708	597	647
La	8.4	0.1	8.3	3.1	6.6	7.0	9.2	7.2	8.7	5.8	7.5	4.1	7.7	3.9	8.1	7.6	8.5
Ce	11.9	0.2	11.9	5.4	9.7	10.7	15.4	9.8	12.5	8.6	11.6	7.9	11.0	6.8	12.7	13.5	12.9
Pr	1.14	0.01	0.90	0.59	0.95	0.82	1.22	0.85	1.08	0.68	0.85	0.83	0.98	0.64	1.05	1.11	1.15
Nd	3.3	0.0	3.0	1.5	2.8	2.3	3.6	3.0	3.3	2.5	3.0	2.8	3.2	2.1	3.3	3.0	3.2
Sm	0.41	0.01	0.22	0.05	0.41	0.16	0.44	0.28	0.30	0.29	0.06	0.40	0.34	0.12	0.38	0.28	0.44
Eu	1.53	0.03	2.60	1.38	1.75	1.72	1.87	1.79	2.19	0.89	2.11	1.95	1.76	1.45	2.32	1.74	2.09
Pb	8.0	0.1	8.6	7.4	7.3	7.8	9.2	6.6	8.4	4.8	8.1	7.5	7.5	6.5	7.5	8.2	8.0
1SE (µg/g)																	
Li	1.7	0.0	1.8	1.8	1.7	1.9	1.9	1.6	1.8	1.8	1.7	1.6	1.9	1.9	2.1	1.7	1.7
Mg	5.5	0.1	7.3	4.8	5.2	4.7	12.9	4.4	5.6	7.6	6.1	4.2	5.9	4.2	5.6	14.6	6.3
Si	7713	80	6778	4314	4474	9552	5289	5905	5968	4796	5772	4165	4501	5356	8747	6454	6415
Ca	987	13	863	1404	974	916	892	806	901	1310	884	1375	892	1417	855	873	912
Ti	13	0	17	19	20	13	23	15	14	14	14	20	14	20	18	32	14
Fe	106	2	105	97	106	105	135	99	112	153	97	85	102	99	103	144	131
Cu	70	0	17	118	1	1	7	1	12	15	14	2	1	2	14	30	12
Zn	0.5	0.1	1.9	1.8	0.4	0.4	0.8	0.5	1.9	1.0	0.4	0.2	0.4	0.3	0.8	0.4	1.1
Sr	21	0	20	22	17	20	18	19	22	27	19	17	19	24	21	19	19
Y	0.05	0.00	0.06	0.06	0.05	0.04	0.12	0.03	0.05	0.07	0.05	0.07	0.02	0.04	0.04	0.27	0.03
Ba	9	0	13	4	8	9	15	11	11	4	11	6	11	4	14	14	13
La	0.22	0.00	0.23	0.12	0.25	0.30	0.64	0.23	0.20	0.16	0.13	0.28	0.19	0.12	0.37	0.28	0.23
Ce	0.42	0.00	0.41	0.26	0.30	0.41	0.50	0.33	0.42	0.23	0.52	0.31	0.36	0.19	0.44	0.51	0.29
Pr	0.08	0.00	0.11	0.05	0.08	0.05	0.08	0.07	0.11	0.06	0.06	0.09	0.06	0.05	0.09	0.07	0.08
Nd	0.42	0.01	0.35	0.18	0.30	0.39	0.29	0.40	0.19	0.11	0.14	0.33	0.27	0.09	0.12	0.32	0.25
Sm	0.06	0.00	0.10	0.12	0.06	0.03	0.14	0.12	0.08	0.12	0.13	0.07	0.04	0.07	0.07	0.09	0.13
Eu	0.15	0.00	0.18	0.14	0.09	0.07	0.12	0.16	0.19	0.13	0.16	0.07	0.14	0.13	0.09	0.14	0.12
Pb	0.81	0.02	0.83	0.76	0.71	0.78	0.92	0.67	0.80	0.47	0.87	0.72	0.73	0.60	0.88	0.86	0.78

Appendix B7 continued

Sample	22D-250 Pl3	22D-250 Pl2	22D-250 Pl6	22D-250 Pl8	22D-250 Pl9	22D-500 Pl22	22D-500 Pl21	22D-500 Pl19	22D-500 Pl20	22D-500 Pl28	22D-500 Pl23	22D-500 Pl2	22D-500 Pl3	22D-500 Pl5	22D-500 Pl26	22D-500 Pl6	22D-500 Pl24
An	54.76	28.91	30.64	34.64	41.91	32.50	34.80	29.40	35.80	48.10	36.50	53.10	40.80	32.90	44.80	30.80	32.40
Conc. (µg/g)																	
Li	13.2	15.0	15.1	14.8	15.2	14.8	13.4	18.4	12.2	17.1	15.1	19.1	15.3	16.0	17.7	17.0	12.6
Mg	129	134	134	151	223	137	157	124	196	232	168	272	165	144	189	153	158
Si	291886	310147	325918	291442	329988	332046	300648	351606	292156	346447	328368	356505	328710	336668	380997	354651	318070
Ca	83405	43096	45455	50672	62035	48456	51172	44240	52601	70969	54746	79260	60535	49457	66181	45740	46455
Ti	368	175	160	165	277	170	158	236	253	212	170	306	221	201	207	239	178
Fe	2873	2799	2918	3147	4030	3095	3090	3297	3513	4290	3416	4390	3690	3477	4289	3620	3151
Cu	1.8	40.4	4.1	94.2	111.0	3.2	21.9	0.7	1.7	1.2	29.6	1.4	1.8	0.9	b.d.l.	0.8	10.7
Zn	5.1	5.7	5.4	16.5	17.8	6.8	5.4	5.5	7.7	7.3	8.4	7.5	8.1	8.1	8.6	6.9	4.6
Sr	1326	977	958	1029	1056	951	1060	878	928	1402	1145	1307	1088	969	1399	911	961
Y	0.34	0.14	0.29	0.26	0.38	0.23	0.24	0.27	0.74	0.26	0.37	0.43	0.20	0.24	0.25	0.26	0.26
Ba	173	549	671	414	579	549	452	739	354	243	503	291	369	508	365	653	616
La	3.1	6.8	7.8	6.3	8.8	7.4	6.9	7.5	6.1	5.1	8.0	4.4	5.5	6.5	6.2	7.1	7.6
Ce	5.8	9.6	12.1	10.2	14.9	11.6	10.9	11.2	10.3	8.5	10.6	8.5	9.9	11.3	10.9	11.7	10.4
Pr	0.47	0.82	1.04	0.97	1.36	0.96	0.95	1.01	0.95	0.70	1.13	0.87	0.84	0.97	0.75	1.01	1.01
Nd	2.3	1.9	3.3	2.3	4.2	2.4	2.6	3.1	3.0	2.4	3.1	2.1	2.4	3.1	2.1	2.4	3.1
Sm	0.19	0.28	0.22	0.27	0.21	0.56	0.18	0.29	0.21	0.31	0.40	0.31	0.24	0.22	b.d.l.	0.16	0.21
Eu	1.03	1.58	2.21	1.35	2.56	1.79	1.44	2.50	1.35	1.47	1.47	1.45	1.33	1.80	1.29	1.63	1.83
Pb	5.0	7.3	8.0	6.9	8.4	8.2	8.2	9.9	7.8	5.3	8.2	6.4	7.6	9.2	7.8	9.2	8.4
1SE (µg/g)																	
Li	1.8	2.0	1.8	1.8	2.0	1.8	1.6	2.2	1.5	2.1	1.9	2.5	2.0	2.0	2.2	2.1	1.6
Mg	4.3	4.4	5.6	4.7	20.0	4.2	5.5	3.9	16.7	7.0	6.9	8.6	5.2	5.2	7.0	5.8	5.6
Si	4871	8066	5640	6117	8176	8504	8919	9399	7637	10391	8553	9779	11766	14487	12834	7781	7869
Ca	1544	798	842	938	1149	897	947	819	974	1314	1014	1467	1121	916	1225	847	860
Ti	27	13	12	13	32	13	13	17	28	16	20	22	17	15	15	19	14
Fe	106	110	96	106	426	97	99	122	155	135	162	157	165	151	140	118	100
Cu	23	64	18	114	100	2	18	0	1	1	16	1	2	4	b.d.l.	0	4
Zn	0.2	0.5	0.3	6.7	3.7	0.6	2.5	0.5	0.7	0.5	3.8	0.4	0.7	0.7	0.8	0.7	0.4
Sr	27	18	17	20	27	16	19	14	15	23	21	28	17	19	28	17	19
Y	0.06	0.04	0.05	0.03	0.05	0.02	0.04	0.04	0.16	0.04	0.05	0.05	0.02	0.04	0.03	0.06	0.04
Ba	3	10	13	7	13	12	11	16	12	5	12	7	9	13	12	18	15
La	0.12	0.17	0.30	0.19	0.22	0.27	0.24	0.22	0.26	0.12	0.20	0.24	0.18	0.16	0.29	0.18	0.23
Ce	0.22	0.31	0.41	0.43	0.53	0.30	0.34	0.25	0.40	0.16	0.47	0.19	0.31	0.28	0.29	0.33	0.30
Pr	0.04	0.07	0.10	0.07	0.13	0.14	0.08	0.07	0.09	0.07	0.09	0.09	0.06	0.08	0.05	0.10	0.10
Nd	0.14	0.12	0.27	0.17	0.35	0.36	0.22	0.26	0.23	0.13	0.18	0.46	0.17	0.20	0.22	0.19	0.42
Sm	0.04	0.04	0.08	0.09	0.07	0.17	0.06	0.12	0.07	0.08	0.11	0.03	0.06	0.10	b.d.l.	0.05	0.09
Eu	0.05	0.11	0.12	0.10	0.21	0.09	0.09	0.15	0.09	0.10	0.12	0.06	0.12	0.17	0.08	0.14	0.08
Pb	0.46	0.69	0.77	0.67	0.85	0.83	0.85	1.02	0.79	0.54	0.86	0.65	0.85	0.97	0.88	0.99	0.84

Appendix B7 continued

Sample	22D-500 Pl25	22D-500 Pl10	22D-500 Pl8	22D-500 Pl7	22D-500 Pl11	22D-500 Pl13	22D-500 Pl14	22D-500 Pl15	22D-500 Pl16	22D-500 Pl17	22D-500 Pl18	22D-500 Pl12	44A-250 Pl1	44A-250 Pl3	44A-250 Pl4	44A-250 Pl5	44A-250 Pl6
An	34.20	29.90	27.50	27.80	84.40	44.80	33.80	31.10	30.50	32.20	32.50	30.60	29.20	76.10	82.00	36.90	80.30
Conc. (µg/g)																	
Li	15.6	13.0	14.9	13.5	4.4	15.8	15.3	16.2	14.6	16.2	20.1	12.5	14.3	9.1	8.2	11.9	9.9
Mg	145	122	119	119	123	146	148	132	129	138	410	121	101	541	487	96	519
Si	347556	289042	303070	305616	283803	340280	319814	352885	323704	356316	400481	267273	324950	265123	251375	295083	250298
Ca	49528	41524	35806	40237	122927	65966	50672	46598	44811	47170	47027	42596	43525	108776	117353	55460	114065
Ti	170	183	221	167	120	231	196	252	241	217	545	128	199	178	128	286	129
Fe	3489	2933	2958	2843	4456	3211	2825	3296	3309	3193	5325	2647	2959	6434	6110	3269	6589
Cu	3.6	6.9	1.9	1.8	70.9	34.7	1.3	58.6	7.8	56.8	17.0	2.8	1539.9	5.7	107.8	38.3	38.9
Zn	6.6	5.8	4.9	5.0	8.1	8.7	6.2	8.5	7.2	9.1	13.6	5.3	10.2	11.3	6.0	20.4	3.5
Sr	1011	799	763	818	1061	1163	983	938	934	974	987	868	905	1253	1181	1063	1187
Y	0.21	0.19	0.14	0.07	0.32	0.26	0.40	0.16	0.15	0.16	2.93	0.18	0.22	0.16	0.11	0.38	0.08
Ba	505	504	617	484	65	384	477	725	676	685	766	492	693	58	34	396	47
La	6.3	6.0	6.0	5.8	1.2	6.6	6.9	8.0	6.5	7.2	11.4	6.5	7.1	1.2	0.7	6.5	1.0
Ce	10.2	9.8	8.8	9.1	2.6	10.6	10.6	12.2	9.6	11.8	19.2	9.3	10.8	2.4	1.4	11.2	1.8
Pr	0.90	0.83	0.76	0.84	0.19	1.00	0.94	1.08	0.84	0.97	1.94	0.80	0.85	0.29	0.13	1.12	0.16
Nd	2.7	2.9	2.0	2.3	0.9	3.2	3.4	3.2	2.2	3.3	6.1	2.7	3.1	0.9	0.6	3.2	0.7
Sm	0.26	0.27	0.09	0.25	b.d.l.	0.35	0.34	0.32	0.31	0.36	1.03	0.42	b.d.l.	b.d.l.	b.d.l.	0.40	0.19
Eu	1.63	1.70	1.85	1.48	0.36	1.73	1.70	2.09	1.75	1.93	2.33	1.52	1.95	0.25	0.30	1.51	0.25
Pb	9.1	8.4	8.5	8.2	4.2	8.0	8.7	9.8	8.7	9.6	13.8	6.4	8.8	1.3	0.6	7.4	0.7
1SE (µg/g)																	
Li	1.9	1.6	1.8	1.7	0.6	1.9	1.9	2.0	1.7	2.0	2.4	1.5	1.8	1.1	1.1	1.6	1.2
Mg	4.6	4.4	4.5	4.2	4.9	5.2	6.6	5.1	5.2	6.5	19.4	3.8	4.3	18.9	19.1	13.7	18.2
Si	13786	6958	8743	9207	7029	7998	9653	8313	7087	12154	9268	5707	5888	5386	6632	5815	7588
Ca	917	769	663	745	2276	1221	938	863	830	873	871	789	806	2014	2173	1027	2112
Ti	14	14	16	12	10	17	14	19	18	18	45	10	15	14	9	23	9
Fe	108	95	92	114	140	105	89	142	98	132	175	85	93	183	209	91	245
Cu	1	2	1	1	177	55	1	67	26	67	47	64	920	7	147	23	47
Zn	0.5	0.9	0.5	0.3	3.0	1.6	0.5	1.4	1.0	1.0	1.7	0.5	4.7	2.4	2.9	8.3	0.4
Sr	19	13	14	13	18	23	19	15	18	18	16	16	19	21	19	20	20
Y	0.03	0.03	0.04	0.02	0.04	0.03	0.04	0.02	0.02	0.03	0.31	0.02	0.03	0.05	0.03	0.09	0.03
Ba	12	12	15	10	2	10	10	17	16	20	17	12	13	1	1	7	1
La	0.22	0.17	0.26	0.15	0.10	0.26	0.19	0.23	0.23	0.31	0.34	0.17	0.15	0.07	0.04	0.14	0.04
Ce	0.22	0.26	0.19	0.20	0.09	0.39	0.29	0.21	0.39	0.27	0.71	0.25	0.25	0.14	0.08	0.25	0.08
Pr	0.06	0.07	0.06	0.07	0.03	0.08	0.06	0.08	0.06	0.07	0.15	0.06	0.08	0.04	0.03	0.09	0.03
Nd	0.14	0.12	0.23	0.20	0.06	0.24	0.28	0.28	0.22	0.16	0.21	0.25	0.27	0.18	0.06	0.25	0.18
Sm	0.06	0.06	0.06	0.06	b.d.l.	0.12	0.04	0.05	0.13	0.05	0.10	0.09	b.d.l.	b.d.l.	b.d.l.	0.08	0.08
Eu	0.16	0.09	0.09	0.09	0.03	0.06	0.11	0.07	0.10	0.17	0.07	0.11	0.13	0.05	0.04	0.09	0.03
Pb	0.94	0.85	0.87	0.87	0.49	0.80	0.94	1.02	0.88	1.08	1.39	0.65	0.89	0.16	0.10	0.74	0.11

Appendix B7 continued

Sample	44A-250 Pl7	44A-250 Pl8	44A-250 Pl10	44A-250 Pl11	44A-250 Pl12	44A-250 Pl13	44A-250 Pl15	44A-250 Pl16	44A-250 Pl17	44A-250 Pl18	44A-250 Pl20	44A-250 Pl21	44A-250 Pl22	44A-250 Pl24	44A-250 Pl25	44A-250 Pl26	44A-250 Pl27
An	36.00	60.10	26.30	28.60	40.70	83.90	41.30	84.30	27.40	27.90	83.40	40.90	79.50	82.70	31.40	34.90	24.60
Conc. (µg/g)																	
Li	14.9	14.4	12.2	12.0	13.2	6.8	11.5	6.9	13.8	10.0	7.5	11.4	8.9	6.0	12.8	14.3	11.8
Mg	100	154	83	94	90	509	113	509	83	87	478	93	473	464	86	109	94
Si	347597	265327	277868	270215	260806	258362	299535	251429	301669	307982	243236	286984	245288	239681	283927	306108	281372
Ca	53531	86835	39094	42953	58891	121784	60606	122642	41452	40881	120140	61392	112493	117925	46527	52316	36592
Ti	294	307	192	162	311	128	203	129	231	140	110	225	138	117	193	216	178
Fe	3266	3472	2485	2463	2311	6714	2764	6152	2791	2640	6113	2488	6342	6158	2580	2813	2650
Cu	3.1	3.5	1.4	8.0	6.6	40.0	6.3	1.5	1.7	0.9	8.5	b.d.l.	1.3	1.0	2.5	2.2	46.4
Zn	5.7	4.0	5.0	5.9	4.7	5.1	9.8	3.1	4.7	3.7	2.5	4.8	3.3	3.7	5.2	5.8	6.5
Sr	1155	1068	779	825	872	1240	1097	1229	886	848	1179	1031	1221	1194	885	1037	821
Y	0.21	0.21	0.20	0.25	0.37	0.20	0.27	0.18	0.22	0.20	0.07	0.42	0.09	0.12	0.20	0.31	0.15
Ba	683	96	565	520	344	34	425	33	711	666	31	335	49	34	552	520	630
La	7.1	0.9	6.4	6.7	4.7	0.8	6.3	0.7	7.7	7.3	0.9	5.0	1.0	0.7	7.3	6.9	6.8
Ce	11.3	2.0	9.8	10.2	8.1	1.4	8.8	1.3	10.3	10.3	1.5	8.4	2.1	1.3	10.6	10.3	9.8
Pr	0.97	0.14	0.77	0.81	0.87	0.20	0.81	0.15	0.99	0.81	0.14	0.67	0.22	0.13	0.97	0.88	0.85
Nd	2.8	0.7	2.6	3.1	2.0	0.6	2.3	0.7	3.2	2.6	0.6	2.3	0.9	0.5	3.2	2.5	2.2
Sm	0.34	b.d.l.	0.34	0.40	0.29	b.d.l.	0.43	b.d.l.	0.28	0.32	b.d.l.	0.43	b.d.l.	b.d.l.	0.11	0.39	0.21
Eu	2.26	0.40	1.61	1.78	1.40	0.23	1.95	0.16	2.23	1.89	0.22	1.45	0.35	0.10	1.71	1.75	1.76
Pb	10.0	2.1	6.9	7.2	7.0	0.7	8.2	0.7	8.3	8.2	0.7	7.2	0.9	0.8	7.9	8.4	7.0
1SE (µg/g)																	
Li	1.9	1.9	1.5	1.6	1.6	0.9	1.6	0.9	1.7	1.2	1.0	1.4	1.2	0.7	1.8	1.8	1.5
Mg	3.5	6.3	3.5	4.6	3.8	16.9	4.6	17.4	3.2	3.2	16.7	5.9	16.2	16.0	3.5	5.1	4.1
Si	6825	5998	6701	5668	6501	6937	8287	5400	9119	6745	5415	5249	6471	4653	6476	5698	5002
Ca	991	1608	724	795	1090	2255	1122	2271	767	757	2224	1137	2083	2183	861	969	677
Ti	22	22	14	13	23	10	17	10	18	11	8	18	12	9	15	16	14
Fe	111	117	72	72	65	211	94	181	107	84	182	73	173	195	73	83	75
Cu	14	6	7	10	6	45	24	9	1	13	4	b.d.l.	1	1	7	4	49
Zn	0.4	0.5	0.3	0.9	0.6	1.5	1.1	0.6	0.3	0.5	0.2	0.3	0.3	2.3	0.3	0.8	0.9
Sr	21	21	15	16	16	20	22	22	21	16	19	17	20	20	15	20	15
Y	0.03	0.05	0.03	0.04	0.05	0.04	0.06	0.05	0.03	0.04	0.02	0.05	0.01	0.05	0.03	0.03	0.04
Ba	12	2	11	9	8	1	9	1	18	13	1	6	1	1	10	9	12
La	0.36	0.09	0.21	0.18	0.19	0.07	0.26	0.06	0.28	0.28	0.03	0.13	0.05	0.02	0.29	0.25	0.15
Ce	0.52	0.08	0.26	0.36	0.24	0.07	0.31	0.07	0.26	0.24	0.09	0.30	0.12	0.13	0.33	0.21	0.28
Pr	0.07	0.03	0.06	0.06	0.06	0.03	0.06	0.02	0.08	0.08	0.02	0.08	0.03	0.02	0.08	0.09	0.09
Nd	0.15	0.15	0.36	0.17	0.12	0.20	0.29	0.11	0.28	0.26	0.06	0.15	0.17	0.20	0.21	0.35	0.36
Sm	0.08	b.d.l.	0.10	0.05	0.04	b.d.l.	0.12	b.d.l.	0.08	0.11	b.d.l.	0.16	b.d.l.	b.d.l.	0.06	0.06	0.07
Eu	0.10	0.04	0.16	0.09	0.09	0.03	0.16	0.05	0.21	0.10	0.03	0.12	0.04	0.05	0.13	0.10	0.12
Pb	1.03	0.23	0.70	0.73	0.67	0.11	0.84	0.10	0.79	0.81	0.11	0.69	0.09	0.09	0.76	0.84	0.70

Appendix B7 continued

Sample	44A-250 Pl28	44A-250 Pl29
An	28.40	81.50
Conc. (µg/g)		
Li	14.2	6.9
Mg	87	501
Si	327617	251205
Ca	42882	118139
Ti	219	137
Fe	2849	6516
Cu	4.3	2.1
Zn	6.9	3.6
Sr	935	1247
Y	0.29	0.09
Ba	708	45
La	7.8	1.1
Ce	11.6	2.0
Pr	0.91	0.26
Nd	2.7	0.8
Sm	0.32	b.d.l.
Eu	2.30	0.27
Pb	9.0	0.9
1SE (µg/g)		
Li	1.8	0.9
Mg	3.1	17.0
Si	7245	8979
Ca	794	2187
Ti	17	11
Fe	106	191
Cu	9	3
Zn	1.4	0.9
Sr	18	21
Y	0.04	0.03
Ba	14	1
La	0.23	0.06
Ce	0.23	0.12
Pr	0.09	0.04
Nd	0.26	0.10
Sm	0.10	b.d.l.
Eu	0.16	0.04
Pb	0.87	0.15

[1] analyses taken at Oregon State University; b.d.l. = below detection limit

Appendix B8 LA-ICP MS data for plagioclase separates of grain mounts from the 1932 eruption[1]

Sample	Q-4 Pl1.1	Q-4 Pl2.1	Q-4 Pl3.1	Q-4 Pl4.1	Q-4 Pl4.2	Q-4 Pl5.1	Q-4 Pl6.1	Q-4 Pl6.2	Q-4 Pl6.3	Q-4 Pl7.1	Q-4 Pl8.1	Q-4 Pl9.1	Q-4 Pl10.1	Q-4 Pl11.1	Q-4 Pl11.2
An	31.68	54.44	34.93	47.33	49.52	31.57	77.97	36.22	78.61	28.77	29.31	50.78	74.69	51.27	31.49
Conc. (µg/g)															
Li	9.9	7.1	9.1	8.4	6.4	8.1	3.7	6.3	8.2	7.3	7.5	7.2	3.5	7.0	7.4
Mg	150	178	154	176	152	158	148	180	201	132	128	203	220	132	133
Si	374320	291404	328817	345551	283391	343711	260392	255964	396402	298597	293810	278667	257742	289798	314694
Ca	47313	80760	51029	70183	72541	46741	112421	53245	112779	42167	42596	74400	109348	75686	45955
Ti	179	223	168	207	206	198	216	167	257	158	185	201	200	254	217
Fe	3012	3513	2929	3282	2899	2888	3931	2620	4298	2576	2565	3906	4996	2445	2755
Cu	1.2	1.2	2.9	1.2	1.1	2.1	2.1	0.9	2.0	1.1	0.4	1.0	1.6	0.5	0.6
Zn	8.1	6.5	6.0	6.8	6.2	6.8	5.2	3.3	7.3	5.9	5.2	7.5	15.8	5.7	6.6
Sr	936	1394	1085	1330	1243	979	1275	1072	1654	862	865	1513	1392	1245	930
Y	0.24	0.22	0.21	0.42	0.41	0.35	0.81	0.80	1.52	0.17	0.19	0.20	0.42	0.22	0.22
Ba	675	151	464	426	237	708	162	390	401	606	598	160	98	189	566
La	7.7	3.0	6.9	7.6	4.2	7.5	4.0	7.6	8.5	6.8	6.3	3.4	2.1	3.3	6.6
Ce	13.0	6.0	11.4	11.1	8.2	11.6	8.7	10.0	15.0	11.4	10.5	6.3	5.3	5.8	10.9
Pr	0.89	0.55	0.95	1.00	0.77	0.93	1.04	0.85	1.40	0.92	0.94	0.53	0.49	0.57	0.82
Nd	2.7	2.0	3.0	3.6	2.4	2.2	3.1	3.3	4.4	2.9	2.2	1.6	2.3	1.5	2.4
Sm	b.d.l.	b.d.l.	b.d.l.	b.d.l.	b.d.l.	b.d.l.	0.38	b.d.l.	0.75	b.d.l.	b.d.l.	b.d.l.	b.d.l.	b.d.l.	b.d.l.
Eu	2.10	0.82	1.70	1.52	1.35	2.00	1.16	1.48	1.55	1.76	1.67	0.68	0.41	1.07	1.76
Pb	10.7	4.1	8.8	8.0	6.1	8.4	6.3	6.3	8.9	8.3	7.6	3.4	4.7	6.5	8.1
1SE (µg/g)															
Li	1.1	0.8	1.1	1.1	0.7	1.0	0.6	0.8	1.1	0.9	1.0	0.9	0.4	0.9	0.9
Mg	5.1	5.7	6.1	5.9	4.8	6.1	4.6	8.2	8.1	4.8	4.7	7.8	10.3	4.2	4.1
Si	7799	5307	7952	7438	4867	8679	7359	7224	15430	10209	5081	9382	7222	7424	7140
Ca	876	1495	945	1299	1343	865	2081	986	2088	781	789	1377	2024	1401	851
Ti	13.3	16.7	12.7	16.1	15.5	14.9	27.4	13.2	20.4	11.5	13.8	15.2	15.5	18.6	15.9
Fe	81.1	97.1	88.4	105.6	80.1	86.6	149.3	104.5	150.9	84.9	86.2	127.0	327.6	77.2	80.0
Cu	6.5	3.0	7.6	0.9	0.9	3.8	3.0	1.1	1.3	2.6	2.5	0.7	4.6	0.5	1.1
Zn	3.7	1.1	0.6	1.3	0.6	3.8	1.1	0.2	0.6	1.1	0.7	0.4	3.8	0.4	0.4
Sr	18	27	22	26	24	24	24	21	52	17	17	32	26	25	17
Y	0.03	0.05	0.04	0.05	0.05	0.05	0.13	0.11	0.32	0.03	0.03	0.03	0.05	0.04	0.04
Ba	13	3	9	13	5	16	3	11	19	12	21	3	2	4	12
La	0.30	0.08	0.18	0.17	0.15	0.18	0.23	0.21	0.28	0.19	0.13	0.09	0.05	0.18	0.18
Ce	0.44	0.16	0.38	0.49	0.15	0.24	0.27	0.33	0.36	0.19	0.27	0.19	0.21	0.23	0.29
Pr	0.06	0.06	0.07	0.10	0.06	0.09	0.10	0.10	0.11	0.06	0.08	0.05	0.05	0.04	0.08
Nd	0.24	0.22	0.36	0.27	0.17	0.29	0.27	0.29	0.43	0.15	0.15	0.16	0.15	0.13	0.22
Sm	b.d.l.	b.d.l.	b.d.l.	b.d.l.	b.d.l.	b.d.l.	0.13	b.d.l.	0.13	b.d.l.	b.d.l.	b.d.l.	b.d.l.	b.d.l.	b.d.l.
Eu	0.12	0.06	0.11	0.04	0.08	0.07	0.11	0.07	0.21	0.09	0.08	0.05	0.09	0.06	0.10
Pb	1.02	0.41	0.90	0.78	0.64	0.86	0.62	0.70	0.87	0.86	0.75	0.33	0.48	0.63	0.77

Appendix B8 continued

Sample	Q-4HF Pl1.1	Q-4HF Pl2.1	Q-4HF Pl2.2	Q-4HF Pl3.1	Q-4HF Pl4.1	Q-4HF Pl5.1	Q-4HF Pl6.1	Q-4HF Pl7.1	Q-4HF Pl8.1	Q-4HF Pl8.2	Q-4HF Pl9.1	Q-4HF Pl10.1	Q-4HF Pl11.1	Q-4HF Pl11.2	Q-4HF Pl12.1
An	57.42	56.64	31.94	30.06	32.33	32.47	42.11	26.60	26.62	30.82	26.03	34.61	44.75	47.04	36.24
Conc. (µg/g)															
Li	6.0	6.4	6.5	7.4	7.7	8.2	9.3	7.4	6.0	8.3	9.9	7.8	8.0	6.8	10.4
Mg	271	125	129	133	147	138	169	123	106	133	128	152	199	193	152
Si	273439	278382	291721	294011	324862	314957	283063	286966	259139	321467	326490	307987	324469	304571	314282
Ca	82690	82905	47027	44311	47813	48456	61678	39094	38951	45740	39094	50886	66252	68253	53173
Ti	189	336	176	183	190	202	146	236	195	212	172	172	264	188	185
Fe	4217	2405	2627	2615	2669	2682	3124	2562	2351	2740	2768	2995	3683	3833	3021
Cu	0.4	1.1	b.d.l.	0.0	0.4	0.9	0.8	0.8	1.4	b.d.l.	1.3	1.8	2.6	1.0	b.d.l.
Zn	7.5	6.2	6.3	6.5	6.0	6.5	8.7	5.6	6.8	6.9	8.8	5.7	9.2	8.7	6.3
Sr	1539	1117	927	856	984	972	1187	791	738	881	771	1096	1243	1484	1050
Y	0.10	0.42	0.34	0.24	0.30	0.22	0.17	0.21	0.20	0.26	0.66	0.29	0.32	0.17	0.25
Ba	128	161	562	608	571	599	278	680	510	651	759	508	324	224	438
La	3.0	2.5	7.7	7.1	7.4	6.9	5.6	6.5	6.2	6.9	7.9	7.1	5.9	4.6	6.5
Ce	4.9	4.9	11.4	11.6	12.3	12.2	9.1	10.0	10.3	11.3	12.8	11.9	10.7	8.0	11.5
Pr	0.49	0.48	0.87	1.01	0.91	0.89	0.61	0.78	0.76	0.90	1.02	0.87	1.02	0.67	0.75
Nd	1.8	1.8	2.5	3.1	3.0	3.2	2.1	2.2	2.5	3.4	2.8	2.8	2.9	2.6	2.3
Sm	b.d.l.	b.d.l.	0.39	b.d.l.	0.33	0.38	b.d.l.	b.d.l.	0.29	0.37	b.d.l.	b.d.l.	b.d.l.	b.d.l.	b.d.l.
Eu	0.49	1.26	2.12	1.84	1.77	1.92	1.06	1.78	1.54	1.96	1.82	1.51	1.21	0.81	1.40
Pb	2.4	6.8	8.1	7.9	8.5	8.2	5.4	7.4	7.4	8.6	11.4	8.7	6.2	4.8	7.7
1SE (µg/g)															
Li	0.8	0.8	0.9	0.9	1.0	1.0	1.2	0.9	0.9	1.0	1.4	1.0	1.0	0.9	1.4
Mg	13.2	4.4	4.9	5.1	5.8	5.0	6.1	4.7	4.6	5.5	7.8	5.9	7.1	7.0	5.4
Si	8769	6601	10561	7568	9441	7658	6257	9609	14082	8888	8753	10215	8509	10879	7398
Ca	1531	1535	871	820	885	897	1142	724	721	847	724	942	1227	1264	984
Ti	14.2	24.6	13.2	13.4	14.1	15.3	11.8	17.2	16.6	16.7	15.9	12.6	20.0	14.4	14.7
Fe	138.8	90.4	97.0	93.2	98.9	84.5	115.2	91.1	116.3	100.6	116.9	115.7	136.5	144.5	112.3
Cu	1.0	0.4	b.d.l.	1.3	0.6	1.8	0.8	3.2	0.4	b.d.l.	0.7	0.8	0.9	0.5	b.d.l.
Zn	4.6	0.5	0.9	0.9	0.8	1.2	0.9	0.7	3.0	0.6	1.1	0.3	1.5	0.7	0.7
Sr	29	22	19	19	19	19	26	15	25	17	17	23	27	29	22
Y	0.02	0.06	0.08	0.03	0.05	0.05	0.04	0.03	0.02	0.05	0.11	0.05	0.19	0.03	0.04
Ba	3	4	13	14	13	13	6	16	35	18	22	12	8	7	11
La	0.12	0.14	0.26	0.17	0.19	0.18	0.22	0.15	0.22	0.19	0.18	0.23	0.24	0.18	0.32
Ce	0.15	0.16	0.30	0.34	0.32	0.39	0.26	0.32	0.37	0.33	0.46	0.36	0.68	0.23	0.33
Pr	0.04	0.04	0.07	0.08	0.07	0.08	0.07	0.07	0.06	0.09	0.08	0.08	0.18	0.05	0.07
Nd	0.13	0.18	0.28	0.16	0.15	0.23	0.19	0.22	0.22	0.25	0.24	0.27	0.39	0.26	0.23
Sm	b.d.l.	b.d.l.	0.08	b.d.l.	0.09	0.14	b.d.l.	b.d.l.	0.05	0.07	b.d.l.	b.d.l.	b.d.l.	b.d.l.	b.d.l.
Eu	0.04	0.09	0.10	0.09	0.11	0.08	0.08	0.11	0.07	0.10	0.14	0.07	0.09	0.07	0.10
Pb	0.26	0.74	0.78	0.82	0.82	0.79	0.57	0.71	0.76	0.82	1.12	0.85	0.60	0.54	0.75

Appendix B8 continued

Sample	Q-4HF Pl13.1	Q-4HF Pl14.1	Q-4HF Pl14.2	Q-6 Pl1.1	Q-6 Pl1.2	Q-6 Pl2.1	Q-6 Pl3.1	Q-6 Pl4.1	Q-6 Pl5.1	Q-6 Pl6.1	Q-6 Pl7.1	Q-6 Pl7.2	Q-6 Pl8.2	Q-6 Pl9.1	Q-6 Pl10.1
An	27.10	47.26	32.10	50.41	34.31	44.75	31.26	53.72	40.53	33.10	26.31	31.37	54.13	45.27	45.52
Conc. (µg/g)															
Li	8.1	7.3	8.8	39.8	37.5	21.9	20.6	20.2	22.2	32.3	32.7	20.8	16.0	23.8	40.2
Mg	123	138	138	189	148	204	158	135	159	139	132	141	131	119	190
Si	330019	322235	333734	241577	280868	383728	355056	281527	343150	337652	322446	264332	288397	270089	299446
Ca	40166	69182	47027	74543	52744	66324	47670	80546	61392	50029	39808	47313	80475	67610	67824
Ti	212	222	192	188	164	234	219	364	301	200	146	154	249	355	196
Fe	2600	2955	2975	3049	2868	3417	2974	2517	2700	2891	2577	2405	2304	2362	3527
Cu	1.6	1.0	1.4	1.0	1.0	2.0	3.3	0.5	1.0	1.3	0.7	2.2	1.1	0.3	0.8
Zn	8.3	14.8	12.5	7.4	7.3	8.4	9.4	5.0	10.3	6.8	6.6	3.8	5.5	5.3	8.8
Sr	763	1251	938	1332	1002	1252	927	1021	1038	973	815	928	1055	1035	1425
Y	0.15	0.18	0.24	0.26	0.23	0.29	0.14	0.53	0.21	0.28	0.21	0.32	0.61	0.18	0.24
Ba	631	207	558	184	316	398	581	300	487	569	700	591	276	196	257
La	5.7	3.5	6.4	4.1	5.3	6.3	6.3	3.7	4.4	6.2	6.9	7.8	4.4	2.5	5.2
Ce	11.0	7.2	11.6	6.1	9.0	11.7	11.2	8.0	8.2	10.4	11.9	10.6	9.4	4.5	8.8
Pr	0.82	0.62	0.97	0.64	0.74	0.87	0.85	0.87	0.71	0.90	0.90	0.96	1.03	0.35	0.77
Nd	2.2	2.3	2.7	2.0	2.0	3.1	2.7	2.7	1.9	2.4	2.8	3.3	3.2	1.8	2.7
Sm	b.d.l.	b.d.l.	b.d.l.	b.d.l.	b.d.l.	b.d.l.	b.d.l.	b.d.l.	b.d.l.	b.d.l.	b.d.l.	0.40	0.56	b.d.l.	b.d.l.
Eu	1.81	1.10	1.50	0.92	0.98	1.48	1.58	1.64	1.82	1.80	1.85	2.15	1.59	1.17	0.99
Pb	10.8	5.9	9.1	3.7	5.9	9.2	9.6	8.2	10.3	9.0	8.7	7.6	8.9	6.1	6.7
1SE (µg/g)															
Li	1.2	1.0	1.1	4.6	4.5	2.6	2.4	2.4	2.5	3.8	3.9	2.4	1.9	2.9	4.7
Mg	4.9	5.1	4.7	5.8	5.5	8.2	5.9	5.1	5.0	4.5	4.7	4.4	5.4	4.5	6.2
Si	9957	8883	9127	5801	6574	16132	6942	8660	11221	7682	10652	7620	7888	10402	8182
Ca	744	1281	871	1380	976	1228	883	1491	1137	926	737	876	1490	1252	1256
Ti	16.1	17.0	14.2	14.0	12.0	17.8	16.2	26.5	22.1	14.8	11.7	11.5	18.2	25.8	14.3
Fe	98.2	102.5	105.7	110.7	95.2	102.3	123.5	92.4	95.8	86.9	82.1	75.5	82.8	82.0	109.1
Cu	2.3	3.1	11.5	3.3	1.0	5.0	95.1	12.5	11.6	3.6	3.1	1.9	2.3	0.8	5.1
Zn	2.8	6.0	7.7	3.4	4.7	3.0	11.3	2.4	3.6	0.9	4.2	0.3	0.5	0.5	0.6
Sr	17	27	19	25	19	25	18	17	18	21	14	18	19	19	27
Y	0.03	0.03	0.03	0.03	0.03	0.10	0.07	0.07	0.03	0.04	0.05	0.04	0.07	0.05	0.04
Ba	20	5	14	4	5	9	8	5	12	10	11	12	6	4	4
La	0.16	0.30	0.15	0.12	0.15	0.15	0.20	0.15	0.23	0.34	0.15	0.24	0.13	0.13	0.20
Ce	0.28	0.25	0.31	0.25	0.29	0.29	0.28	0.26	0.34	0.37	0.35	0.38	0.37	0.22	0.33
Pr	0.07	0.05	0.12	0.07	0.06	0.07	0.08	0.06	0.06	0.09	0.08	0.07	0.08	0.04	0.08
Nd	0.23	0.27	0.29	0.11	0.24	0.25	0.28	0.24	0.33	0.25	0.27	0.07	0.15	0.10	0.23
Sm	b.d.l.	b.d.l.	b.d.l.	b.d.l.	b.d.l.	b.d.l.	b.d.l.	b.d.l.	b.d.l.	b.d.l.	b.d.l.	0.09	0.09	b.d.l.	b.d.l.
Eu	0.17	0.07	0.08	0.09	0.07	0.10	0.14	0.13	0.15	0.15	0.14	0.16	0.16	0.08	0.08
Pb	1.03	0.62	1.03	0.39	0.57	0.87	0.97	0.81	1.04	0.90	0.81	0.71	0.84	0.61	0.63

Appendix B8 continued

Sample	Q-6 Pl10.2	Q-6 Pl11.1	Q-6 Pl12.1	Q-6 Pl13.1	Q-6 Pl14.1	Q-6 Pl14.2	VQ17-250 Pl1.1	VQ17-250 Pl2.1	VQ17-250 Pl2.2	VQ17-250 Pl3.1	VQ17-250 Pl3.2	VQ17-250 Pl4.1	VQ17-250 Pl5.1	VQ17-250 Pl5.2	VQ17-250 Pl6.1
An	33.31	36.18	34.87	29.25	34.36	28.50	29.53	29.02	39.95	26.63	32.28	54.03	35.09	46.36	32.53
Conc. (µg/g)															
Li	31.6	35.6	16.7	31.6	9.6	14.2	13.1	7.6	7.0	20.6	18.2	27.3	25.1	35.2	29.7
Mg	157	153	149	134	274	124	126	118	123	123	143	148	153	171	140
Si	244578	337875	334594	323641	316614	322078	300009	308012	276787	282439	300119	284059	293315	342832	289183
Ca	49886	53959	52101	44025	52673	42882	44025	42810	59963	39523	48456	80832	52887	69254	48385
Ti	145	213	217	210	311	148	209	223	258	187	194	286	167	257	195
Fe	2258	3047	3065	2831	3852	2545	2693	2835	2599	2543	2719	2560	2761	2940	2657
Cu	3.7	2.5	0.9	0.9	2.3	1.5	1.5	2.0	b.d.l.	0.4	1.3	7.2	3.5	0.8	1.1
Zn	2.5	6.9	7.1	6.3	8.2	5.5	7.3	7.5	5.7	7.1	6.6	54.4	19.2	12.5	6.7
Sr	1075	1031	1041	911	1089	919	821	892	1194	789	951	1184	1080	1161	924
Y	0.18	0.19	0.30	0.24	1.45	0.25	0.21	0.17	0.22	0.12	0.26	0.61	0.21	0.28	0.29
Ba	361	602	654	667	533	689	667	666	376	584	592	263	458	561	555
La	7.3	7.5	8.5	7.1	8.2	7.6	6.2	7.2	5.5	6.8	7.4	3.4	7.0	7.6	7.1
Ce	8.8	12.6	13.3	11.7	14.8	12.6	10.1	11.1	8.6	10.9	11.3	7.4	11.1	12.3	11.1
Pr	0.81	0.95	1.06	0.87	1.06	0.96	0.88	0.92	0.82	0.79	0.95	0.77	1.04	1.12	0.91
Nd	2.2	3.5	3.3	3.1	3.8	3.0	3.0	3.3	2.6	2.2	2.5	3.2	2.9	2.6	3.1
Sm	b.d.l.	0.60	0.26	b.d.l.	0.61	b.d.l.	b.d.l.	0.47	b.d.l.	b.d.l.	b.d.l.	b.d.l.	b.d.l.	b.d.l.	b.d.l.
Eu	1.46	2.07	2.20	1.92	1.70	1.93	2.26	2.18	1.84	1.74	1.65	1.75	1.22	2.22	2.07
Pb	5.3	10.2	9.2	8.4	10.0	8.9	9.2	7.5	7.2	8.2	8.5	9.0	8.5	10.3	8.0
1SE (µg/g)															
Li	3.7	4.3	2.1	3.7	1.3	1.7	1.5	1.0	0.8	2.4	2.1	3.2	2.8	4.0	3.3
Mg	5.6	6.2	4.9	4.6	27.4	4.0	4.8	4.7	5.2	4.5	5.5	6.0	5.6	6.2	5.4
Si	5289	9947	8666	8447	9581	7582	5813	9083	5200	4432	4671	5530	8799	8557	11254
Ca	924	999	965	815	975	794	815	793	1110	732	897	1497	979	1282	896
Ti	10.9	15.7	16.4	15.2	40.1	11.7	16.4	17.1	18.8	14.1	14.1	20.7	12.4	19.8	14.2
Fe	85.0	101.9	105.4	102.0	267.9	89.4	120.1	87.1	71.4	83.1	79.5	75.0	78.0	94.9	79.6
Cu	6.2	1.4	1.3	1.5	2.6	3.7	0.5	0.6	b.d.l.	1.5	1.1	8.1	2.6	1.1	0.3
Zn	0.4	0.4	0.5	0.5	0.8	0.5	0.7	1.1	0.4	5.6	0.7	53.0	26.8	8.0	0.3
Sr	21	19	20	17	21	19	17	16	22	15	17	22	21	21	19
Y	0.09	0.04	0.03	0.06	0.29	0.05	0.03	0.03	0.03	0.05	0.06	0.07	0.03	0.06	0.08
Ba	7	10	11	11	13	11	10	12	6	11	10	4	7	13	9
La	0.33	0.17	0.23	0.17	0.31	0.20	0.16	0.15	0.15	0.15	0.26	0.15	0.24	0.23	0.21
Ce	0.29	0.45	0.29	0.38	0.97	0.35	0.33	0.49	0.23	0.32	0.29	0.28	0.27	0.33	0.25
Pr	0.11	0.08	0.09	0.07	0.11	0.06	0.06	0.08	0.06	0.07	0.07	0.06	0.08	0.11	0.08
Nd	0.45	0.28	0.15	0.35	0.36	0.23	0.32	0.29	0.11	0.39	0.27	0.34	0.29	0.22	0.19
Sm	b.d.l.	0.08	0.14	b.d.l.	0.08	b.d.l.	b.d.l.	0.05	b.d.l.	b.d.l.	b.d.l.	b.d.l.	b.d.l.	b.d.l.	b.d.l.
Eu	0.16	0.13	0.15	0.19	0.12	0.14	0.13	0.11	0.11	0.18	0.12	0.18	0.14	0.11	0.11
Pb	0.53	1.00	0.96	0.83	1.11	0.88	0.92	0.77	0.73	0.81	0.82	0.86	0.84	0.99	0.79

Appendix B8 continued

Sample	VQ17-250 Pl7.1	VQ17-250 Pl8.1	VQ17-250 Pl9.1	VQ17-250 Pl9.2	VQ17-250 Pl10.1	VQ17-250 Pl11.1	VQ17-250 Pl12.12	VQ17-250 Pl12.23	VQ17-250 Pl13.1	VQ17-250 Pl13.2	VQ17-250 Pl14.1	VQ17-250 Pl15.1	VQ17-250 Pl15.2	VQ17-250 Pl16.1	VQ17-250 Pl16.2
An	32.19	84.72	50.13	35.87	29.77	29.33	38.24	62.51	37.74	27.36	28.66	45.36	32.05	78.62	65.66
Conc. (µg/g)															
Li	21.8	8.5	28.9	22.2	21.0	21.9	20.8	10.4	10.3	8.4	23.8	21.7	11.4	14.2	11.2
Mg	136	85	200	153	133	133	159	121	129	120	105	129	124	110	79
Si	303217	244216	285890	263469	305111	324184	347628	271911	331146	304960	290479	286654	269432	254065	198518
Ca	48599	124071	73328	52887	44097	43668	56568	91838	56604	40809	42095	67896	47956	115495	96627
Ti	190	131	165	149	225	252	245	198	272	230	157	298	237	157	114
Fe	2786	2798	3482	2740	2549	2823	3145	2399	2729	2785	2067	2406	2283	3064	2311
Cu	1.4	0.6	0.2	b.d.l.	1.0	0.8	1.2	0.6	0.6	0.8	1.8	1.5	0.5	b.d.l.	0.9
Zn	5.8	4.2	6.6	5.1	6.1	5.3	6.8	3.8	7.1	5.9	12.3	6.6	5.2	2.0	2.2
Sr	929	1014	1564	1196	869	900	1110	1049	985	840	935	1076	843	1087	865
Y	0.22	0.71	0.69	0.21	0.31	0.23	0.25	0.35	0.44	0.20	0.21	0.35	0.30	0.36	0.19
Ba	593	135	237	319	713	654	585	146	541	671	487	271	436	49	60
La	8.0	2.5	6.7	6.0	7.1	6.8	7.6	2.0	6.4	6.6	8.3	4.2	5.4	0.8	0.9
Ce	11.3	6.6	10.3	8.8	11.3	11.0	11.4	3.9	11.5	10.7	11.8	7.5	9.0	1.3	1.8
Pr	1.04	0.66	1.07	0.77	0.94	0.89	1.07	0.40	0.82	0.91	0.83	0.80	0.86	0.12	0.24
Nd	3.6	2.1	2.9	2.2	2.6	2.5	2.6	1.2	3.0	2.8	2.9	2.5	2.4	0.7	0.8
Sm	b.d.l.	0.49	0.20	b.d.l.	b.d.l.	0.54	b.d.l.	0.23	b.d.l.	0.32	0.51	0.39	0.50	b.d.l.	b.d.l.
Eu	2.20	1.03	0.95	1.19	1.73	2.21	1.82	0.62	2.39	2.11	1.50	1.37	1.57	0.46	0.70
Pb	9.6	6.7	5.5	5.2	8.4	7.8	8.9	5.0	9.6	8.5	7.9	7.9	6.8	4.3	4.8
1SE (µg/g)															
Li	2.5	1.0	3.3	2.5	2.4	2.5	2.6	1.2	1.2	1.0	2.8	2.4	1.3	1.8	1.3
Mg	5.0	3.8	7.3	5.8	5.1	5.1	6.3	5.2	5.1	4.8	4.0	4.7	5.0	8.1	3.2
Si	10817	6516	5448	5679	6995	12857	7114	9752	9656	8147	6634	7256	4056	18992	7530
Ca	900	2297	1358	979	816	808	1047	1700	1048	756	779	1257	888	2138	1789
Ti	14.0	9.8	12.0	11.3	16.8	19.6	18.7	15.1	20.3	18.0	11.8	22.3	17.4	12.8	8.4
Fe	91.6	103.9	105.7	96.7	85.5	100.4	103.6	79.9	97.7	119.2	78.4	75.0	64.6	127.4	70.5
Cu	0.5	2.0	0.4	b.d.l.	0.4	0.3	0.3	0.2	0.2	0.6	11.6	0.5	0.3	b.d.l.	0.4
Zn	0.4	2.2	0.6	0.2	0.5	0.4	0.4	0.2	0.4	0.4	9.5	1.1	0.4	3.6	0.1
Sr	20	19	31	23	17	20	22	24	18	18	18	24	15	22	16
Y	0.04	0.08	0.12	0.04	0.05	0.06	0.17	0.04	0.05	0.04	0.04	0.05	0.06	0.07	0.04
Ba	11	4	4	8	13	16	11	5	8	12	11	5	7	1	1
La	0.34	0.08	0.29	0.24	0.34	0.17	0.33	0.08	0.14	0.24	0.34	0.13	0.18	0.07	0.06
Ce	0.44	0.30	0.24	0.20	0.23	0.40	0.35	0.19	0.27	0.26	0.24	0.24	0.27	0.12	0.07
Pr	0.09	0.07	0.09	0.07	0.08	0.08	0.08	0.04	0.07	0.08	0.07	0.08	0.08	0.04	0.03
Nd	0.27	0.25	0.31	0.27	0.32	0.22	0.25	0.18	0.23	0.30	0.26	0.25	0.27	0.09	0.12
Sm	b.d.l.	0.16	0.22	b.d.l.	b.d.l.	0.13	b.d.l.	0.17	b.d.l.	0.09	0.09	0.07	0.11	b.d.l.	b.d.l.
Eu	0.20	0.10	0.06	0.08	0.11	0.20	0.12	0.04	0.11	0.13	0.10	0.09	0.10	0.06	0.08
Pb	1.01	2.29	0.52	0.54	0.85	0.77	0.90	0.48	0.94	0.90	0.76	0.80	0.66	0.55	0.56

Appendix B8 continued

Sample	VQ17-250 Pl17.1	VQ37D-250 Pl1.2	VQ37D-250 Pl2.1	VQ37D-250 Pl3.1	VQ37D-250 Pl4.1	VQ37D-250 Pl5.1	VQ37D-250 Pl6.1	VQ37D-250 Pl7.1	VQ37D-250 Pl8.1	VQ37D-250 Pl9.1	VQ37D-250 Pl10.1	VQ37D-250 Pl11.1	VQ37D-250 Pl12.2	VQ37D-250 Pl13.1	VQ37D-250 Pl13.2
An	24.80	31.54	45.23	33.25	55.74	47.28	64.33	49.29	30.40	51.84	31.06	34.20	49.25	32.22	36.40
Conc. (µg/g)															
Li	13.7	8.0	10.8	7.7	6.5	7.6	5.5	8.5	8.7	8.1	9.2	10.6	5.5	7.5	8.4
Mg	99	142	155	132	199	175	217	135	140	259	132	138	1707	130	149
Si	284144	308590	247866	287397	281131	265987	235601	266842	346899	282980	311258	252840	310428	287789	325521
Ca	37164	46812	66609	49385	83119	69683	94483	74257	44954	76115	46241	50672	73828	47670	54674
Ti	127	209	232	159	195	180	217	262	229	191	196	165	353	148	181
Fe	2336	2752	2279	2717	3960	3171	4650	2380	2939	4044	2789	2662	4380	2626	2920
Cu	0.5	1.4	1.6	1.8	1.8	1.1	3.2	2.9	0.9	1.6	b.d.l.	2.1	38.7	0.9	1.0
Zn	5.6	7.0	4.3	31.9	46.1	7.0	7.4	4.5	7.3	7.3	5.8	8.5	21.1	5.3	6.3
Sr	789	1028	1096	1061	1588	1355	1071	1130	929	1559	912	956	1098	911	1144
Y	0.23	0.44	0.41	0.20	0.20	0.14	0.16	0.47	0.25	0.15	0.35	0.30	1.44	0.18	0.15
Ba	746	579	250	448	168	243	68	261	702	175	586	340	304	436	502
La	7.7	8.0	4.2	6.6	3.9	5.1	1.2	3.7	7.4	3.5	6.9	5.8	5.4	6.4	7.8
Ce	11.1	11.9	6.3	10.7	6.5	8.1	2.3	6.6	12.4	6.4	11.6	9.2	10.6	9.9	11.5
Pr	0.88	1.07	0.58	0.87	0.67	0.67	0.26	0.68	0.97	0.62	0.91	0.64	1.26	0.69	0.95
Nd	2.3	3.2	2.3	2.5	1.9	2.5	1.0	2.0	3.0	1.3	3.0	2.4	4.3	2.6	2.8
Sm	b.d.l.	0.53	0.21	b.d.l.	b.d.l.	0.30	b.d.l.	b.d.l.	b.d.l.	b.d.l.	0.42	b.d.l.	0.85	0.28	b.d.l.
Eu	1.69	1.55	1.60	1.57	0.73	1.08	0.31	1.39	1.98	0.81	1.67	1.39	1.25	1.13	1.56
Pb	8.6	8.4	6.8	7.8	4.4	6.4	2.1	7.4	9.0	3.1	7.7	7.1	11.5	7.5	7.8
1SE (µg/g)															
Li	1.7	1.0	1.5	1.0	0.8	1.0	0.7	1.2	1.1	1.0	1.4	1.3	0.7	0.9	1.0
Mg	3.5	7.2	5.9	4.1	6.7	6.7	29.5	4.1	5.1	9.6	4.6	4.6	218.9	4.4	4.6
Si	10207	7443	5784	5519	7010	7698	6891	4435	8619	8494	12936	3841	7643	4621	5519
Ca	688	867	1233	914	1539	1290	1749	1375	832	1409	856	938	1367	883	1012
Ti	9.4	19.1	17.2	11.8	14.7	13.6	17.1	20.5	16.7	14.1	14.7	13.3	28.3	11.2	13.3
Fe	65.9	88.8	82.7	94.6	140.0	135.7	149.6	83.9	95.4	140.2	87.2	82.1	257.9	92.5	93.1
Cu	0.6	3.3	1.3	3.3	11.7	11.7	2.1	1.7	1.0	1.6	b.d.l.	0.8	11.0	0.5	0.3
Zn	0.5	1.6	0.7	15.8	19.4	4.9	1.2	0.3	1.4	1.2	0.4	2.9	2.7	0.4	0.3
Sr	15	19	19	21	31	36	19	23	19	30	17	19	20	17	24
Y	0.03	0.11	0.09	0.04	0.06	0.05	0.02	0.08	0.04	0.04	0.05	0.05	0.18	0.03	0.03
Ba	12	11	6	9	3	6	2	5	16	4	11	7	6	9	11
La	0.40	0.21	0.19	0.16	0.12	0.22	0.13	0.13	0.26	0.24	0.34	0.20	0.29	0.18	0.30
Ce	0.28	0.42	0.17	0.34	0.29	0.27	0.09	0.21	0.34	0.16	0.45	0.24	0.76	0.32	0.29
Pr	0.07	0.08	0.08	0.07	0.06	0.07	0.04	0.06	0.07	0.07	0.10	0.06	0.18	0.08	0.08
Nd	0.15	0.22	0.08	0.24	0.11	0.16	0.13	0.18	0.19	0.19	0.32	0.18	0.47	0.14	0.25
Sm	b.d.l.	0.13	0.11	b.d.l.	b.d.l.	0.06	b.d.l.	b.d.l.	b.d.l.	b.d.l.	0.07	b.d.l.	0.15	0.11	b.d.l.
Eu	0.12	0.10	0.15	0.12	0.06	0.10	0.05	0.16	0.12	0.05	0.18	0.13	0.08	0.14	0.15
Pb	0.81	0.85	0.69	0.77	0.60	0.77	0.28	0.74	0.90	0.34	0.84	0.71	1.12	0.72	0.80

Appendix B8 continued

Sample	VQ37D-250 Pl14.1	VQ37D-250 Pl15.1	VQ37D-250 Pl16.2	VQ37D-250 Pl17.1	VQ37D-250 Pl18.1	VQ37D-250 Pl19.1	VQ37D-250 Pl20.1	VQ37D-250 Pl21.1	VQ37D-250 Pl22.1	VQ37D-250 Pl23.1	VQ37D-250 Pl24.1	VQ37D-250 Pl24.2	VQ37D-250 Pl25.1	VQ37D-250 Pl26.1	VQ37D-250 Pl27.1
An	25.05	35.47	74.99	36.22	32.34	33.29	53.99	32.66	34.75	30.04	38.39	57.68	31.81	33.45	36.11
Conc. (µg/g)															
Li	10.6	8.5	16.7	8.4	8.6	9.4	6.7	6.9	8.1	6.5	6.8	8.5	9.4	10.8	12.1
Mg	90	157	147	148	124	138	136	135	153	128	132	165	143	150	142
Si	324101	324085	347999	308999	353517	346170	290672	328056	338801	304174	260794	306672	318008	311756	286385
Ca	37450	52173	109348	53959	46884	49814	79331	48313	52101	44240	57104	85334	47599	49957	53816
Ti	117	165	237	166	167	199	355	197	177	158	159	188	160	192	171
Fe	2389	3148	3053	2895	2574	2840	2644	2910	3030	2590	2613	3039	2817	2972	2705
Cu	1.5	0.5	1.3	0.8	1.9	b.d.l.	0.2	0.5	0.6	1.9	0.6	b.d.l.	1.4	b.d.l.	b.d.l.
Zn	6.1	9.3	6.6	7.0	4.7	8.1	5.8	6.3	7.6	6.7	6.4	6.9	6.4	7.1	5.4
Sr	712	1090	1166	1097	984	984	1120	924	1079	896	970	1304	986	1048	1099
Y	0.21	0.20	0.80	0.27	0.21	0.25	0.59	0.18	0.22	0.17	0.33	0.31	0.20	0.34	0.23
Ba	837	516	273	451	699	614	218	606	526	555	302	207	573	504	453
La	8.1	7.4	5.1	7.0	8.5	7.5	3.6	7.7	7.3	6.6	5.3	3.6	6.8	7.0	7.2
Ce	12.1	11.3	12.7	11.4	12.2	12.0	6.9	11.8	11.5	11.0	9.9	7.0	11.6	12.0	10.8
Pr	0.92	0.96	1.40	0.79	0.97	0.88	0.57	0.96	0.87	0.88	0.86	0.68	0.92	0.87	0.94
Nd	3.3	2.7	4.2	2.5	2.9	2.6	2.1	2.4	3.0	2.5	2.8	2.1	2.5	2.6	3.2
Sm	b.d.l.	b.d.l.	0.58	b.d.l.	b.d.l.	b.d.l.	b.d.l.	b.d.l.	b.d.l.	b.d.l.	b.d.l.	b.d.l.	b.d.l.	b.d.l.	0.16
Eu	1.76	1.62	2.10	1.62	2.14	1.89	1.17	2.21	1.56	1.94	1.22	1.29	1.56	1.60	1.29
Pb	11.4	8.2	9.0	7.7	10.0	9.3	7.4	9.3	8.4	8.3	8.0	7.0	9.0	8.6	6.9
1SE (µg/g)															
Li	1.3	1.1	2.1	1.1	1.1	1.1	0.8	0.9	1.0	0.9	0.9	1.1	1.2	1.3	1.5
Mg	5.0	5.3	5.4	4.5	3.9	4.7	4.8	4.3	4.7	4.0	5.2	5.5	4.9	4.7	4.7
Si	7903	5433	12138	4245	10247	8297	5621	8381	9604	4477	10976	11968	6352	9097	6141
Ca	693	966	2024	999	868	922	1469	894	965	819	1057	1580	881	925	996
Ti	10.6	12.5	17.8	13.1	12.8	15.8	27.6	14.4	13.5	11.9	12.7	14.5	12.8	14.1	13.5
Fe	119.5	105.4	102.5	97.8	78.5	99.2	91.8	104.4	109.2	81.1	98.9	111.2	92.8	100.3	83.1
Cu	0.6	0.3	0.5	0.4	0.6	b.d.l.	0.6	0.1	0.3	1.0	0.2	b.d.l.	1.9	b.d.l.	b.d.l.
Zn	0.5	2.3	0.4	0.5	0.6	0.6	0.4	0.3	0.5	0.6	0.4	0.5	0.4	0.4	0.4
Sr	14	19	21	25	18	18	23	18	21	16	26	29	19	20	20
Y	0.05	0.06	0.10	0.04	0.04	0.03	0.05	0.04	0.07	0.04	0.07	0.05	0.03	0.06	0.04
Ba	19	10	8	10	14	12	5	13	12	14	16	6	13	11	9
La	0.28	0.38	0.51	0.31	0.27	0.23	0.12	0.22	0.20	0.14	0.32	0.17	0.16	0.25	0.17
Ce	0.44	0.39	0.87	0.36	0.34	0.32	0.24	0.30	0.37	0.29	0.34	0.19	0.30	0.40	0.29
Pr	0.08	0.08	0.14	0.08	0.08	0.07	0.05	0.07	0.06	0.07	0.07	0.08	0.11	0.07	0.07
Nd	0.26	0.21	0.44	0.23	0.31	0.32	0.20	0.36	0.12	0.12	0.12	0.24	0.36	0.25	0.30
Sm	b.d.l.	b.d.l.	0.06	b.d.l.	b.d.l.	b.d.l.	b.d.l.	b.d.l.	b.d.l.	b.d.l.	b.d.l.	b.d.l.	b.d.l.	b.d.l.	0.06
Eu	0.17	0.16	0.17	0.11	0.13	0.11	0.11	0.13	0.10	0.11	0.09	0.11	0.14	0.12	0.17
Pb	1.06	0.84	0.87	0.85	1.04	1.07	0.70	0.93	0.78	0.81	0.77	0.72	0.88	0.81	0.69

Appendix B8 continued

Sample	VQ37D-250 Pl28.1	VQ37D-250 Pl29.1	VQ37D-250 Pl30.1	VQ37D-250 Pl30.2	VQ37D-250 Pl31.1	VQ37D-250 Pl32.2	VQ37D-250 Pl33.1	VQ37D-500 Pl1.1	VQ37D-500 Pl1.2	VQ37D-500 Pl2.1	VQ37D-500 Pl3.1	VQ37D-500 Pl4.1	VQ37D-500 Pl4.2	VQ37D-500 Pl5.1	VQ37D-500 Pl6.1
An	35.40	34.53	30.94	38.67	32.89	31.83	49.93	33.13	47.43	29.18	31.61	29.55	39.89	35.07	30.32
Conc. (µg/g)															
Li	9.1	7.3	10.6	8.7	9.6	8.3	16.7	9.4	7.6	7.6	8.6	8.2	8.2	7.3	6.8
Mg	156	142	126	140	133	137	365	132	121	134	138	125	121	138	135
Si	322415	276680	286277	314896	302675	339896	389838	341501	297458	324088	341725	327090	324704	282360	301986
Ca	52387	51744	46026	57318	49099	47313	72970	48957	70183	42453	46670	43239	59105	51172	45597
Ti	180	168	196	228	173	200	375	192	274	214	231	299	289	160	214
Fe	2901	2702	2408	2502	2588	2774	4555	2779	2583	2765	2931	2832	2718	2660	2726
Cu	2.2	3.2	0.7	0.4	0.5	b.d.l.	1.1	0.7	b.d.l.	1.7	1.3	1.0	b.d.l.	1.4	2.6
Zn	11.6	8.9	6.4	6.5	5.5	6.5	11.3	10.3	7.3	7.1	8.3	6.2	6.5	6.6	5.4
Sr	1045	1005	916	1046	1010	943	1429	914	1092	834	853	862	937	1026	981
Y	0.28	0.14	0.21	0.30	0.41	0.13	1.22	0.15	0.36	0.24	0.19	0.11	0.19	0.20	0.24
Ba	503	347	464	443	503	574	550	548	260	625	700	585	443	425	584
La	7.2	5.1	5.8	6.4	7.4	6.7	10.7	6.9	3.9	6.1	6.1	5.6	4.8	6.5	7.0
Ce	11.0	9.1	9.0	10.2	11.6	10.8	16.1	11.2	7.5	11.1	11.7	9.8	8.6	11.2	10.8
Pr	1.00	0.71	0.80	0.87	0.92	0.95	1.61	0.78	0.64	0.87	0.96	0.74	0.68	0.71	0.92
Nd	2.6	2.1	2.7	2.5	2.9	2.8	3.7	2.2	2.7	3.1	2.7	2.3	2.5	2.6	2.4
Sm	b.d.l.	b.d.l.	b.d.l.	b.d.l.	b.d.l.	b.d.l.	0.34	b.d.l.	b.d.l.	b.d.l.	b.d.l.	b.d.l.	0.27	b.d.l.	b.d.l.
Eu	1.39	1.18	1.50	1.88	1.76	1.82	1.71	1.73	1.22	1.61	2.21	1.80	1.84	1.43	2.04
Pb	8.0	6.7	7.7	9.5	7.8	9.2	10.5	8.3	7.6	8.0	9.2	8.6	9.3	7.1	8.0
1SE (µg/g)															
Li	1.1	1.0	1.5	1.1	1.3	1.1	2.1	1.1	0.9	1.0	1.1	1.1	1.0	0.9	0.9
Mg	5.9	4.3	4.5	4.3	4.6	5.1	53.6	4.7	4.3	4.9	4.9	4.3	5.4	5.4	6.2
Si	5140	11177	6187	4642	8535	5175	13105	13693	11149	11696	13455	11644	13109	13066	10973
Ca	970	958	852	1061	909	876	1351	906	1299	786	864	801	1094	947	844
Ti	13.6	13.3	14.7	16.7	12.9	15.3	52.4	14.4	20.4	16.3	17.7	22.2	21.5	12.0	15.6
Fe	88.1	99.0	88.1	82.9	78.9	91.4	332.3	83.6	72.0	84.7	111.0	79.4	85.5	85.2	77.3
Cu	1.7	7.4	531.4	0.4	0.3	b.d.l.	7.6	0.8	b.d.l.	1.7	0.9	0.6	b.d.l.	0.5	5.8
Zn	2.3	3.6	0.3	0.6	0.3	0.5	1.7	1.4	0.5	1.4	1.2	0.6	0.5	0.6	0.8
Sr	22	21	18	19	19	21	32	18	22	16	17	18	20	21	18
Y	0.11	0.02	0.03	0.04	0.07	0.04	0.52	0.05	0.06	0.03	0.04	0.02	0.03	0.04	0.02
Ba	11	7	10	10	12	12	24	9	6	10	12	9	8	7	9
La	0.30	0.24	0.30	0.17	0.16	0.25	0.95	0.19	0.18	0.26	0.39	0.18	0.21	0.18	0.21
Ce	0.38	0.27	0.32	0.33	0.36	0.40	1.31	0.19	0.21	0.25	0.26	0.40	0.13	0.24	0.24
Pr	0.09	0.07	0.07	0.08	0.08	0.07	0.21	0.09	0.06	0.07	0.07	0.08	0.07	0.06	0.07
Nd	0.19	0.19	0.35	0.40	0.37	0.18	0.31	0.23	0.11	0.14	0.10	0.21	0.29	0.22	0.26
Sm	b.d.l.	b.d.l.	b.d.l.	b.d.l.	b.d.l.	b.d.l.	0.35	b.d.l.	b.d.l.	b.d.l.	b.d.l.	b.d.l.	0.14	b.d.l.	b.d.l.
Eu	0.10	0.12	0.10	0.17	0.11	0.21	0.10	0.06	0.13	0.11	0.18	0.12	0.17	0.09	0.17
Pb	0.87	0.75	0.85	0.93	0.73	1.06	1.10	0.83	0.75	0.84	0.92	0.87	0.87	0.70	0.76

Appendix B8 continued

Sample	VQ37D-500 Pl6.2	VQ37D-500 Pl7.1	VQ37D-500 Pl8.1	VQ37D-500 Pl9.1	VQ37D-500 Pl10.1	VQ37D-500 Pl11.1	VQ37D-500 Pl12.1	VQ37D-500 Pl13.1	VQ37D-500 Pl14.1	VQ37D-500 Pl15.1	VQ37D-500 Pl16.1	VQ37D-500 Pl17.1	VQ37D-500 Pl17.2	VQ37D-500 Pl18.1	VQ37D-500 Pl19.1
An	54.15	28.01	38.15	32.29	45.65	27.52	45.22	30.39	34.18	52.00	33.02	33.64	51.59	30.90	46.87
Conc. (µg/g)															
Li	6.5	7.5	7.8	8.4	6.8	9.6	7.3	8.0	8.9	6.2	8.1	13.3	11.0	10.0	8.3
Mg	129	90	145	135	217	98	115	128	135	116	141	276	196	122	138
Si	295630	309591	288076	316010	294502	340062	294701	327175	333299	280417	341691	338317	478960	348126	298567
Ca	79760	41238	56175	47027	67682	40237	66467	44954	50815	75758	48528	48957	75329	46169	69111
Ti	337	145	177	190	205	155	305	222	226	192	212	328	319	239	268
Fe	2566	2283	2785	2725	3477	2686	2526	2919	2941	2540	2951	3791	3993	2911	2506
Cu	1.0	1.4	1.0	0.4	1.1	2.6	1.4	1.1	0.8	0.7	b.d.l.	3.4	1.2	1.0	0.8
Zn	5.4	3.9	9.8	8.7	12.1	16.1	6.7	6.3	7.3	6.6	6.5	9.8	9.2	6.6	4.0
Sr	1381	831	1292	935	1377	813	1018	872	1028	1142	966	1020	1450	939	1184
Y	0.18	0.21	0.17	0.26	0.22	0.21	0.34	0.26	0.24	0.38	0.23	0.88	0.19	0.34	0.32
Ba	192	771	346	600	213	750	290	684	516	187	663	528	702	727	352
La	3.4	8.2	6.4	6.8	4.1	8.1	4.5	6.7	6.1	3.5	7.4	7.7	7.9	7.5	4.7
Ce	5.9	11.0	9.6	10.8	8.1	12.0	8.9	11.4	10.8	6.5	12.9	14.6	13.3	12.7	7.8
Pr	0.52	0.91	0.60	0.80	0.70	0.80	0.67	0.95	0.80	0.62	0.89	1.18	0.91	0.84	0.73
Nd	2.2	2.4	2.5	2.6	1.9	2.3	2.0	2.7	2.5	2.4	3.2	3.3	3.2	3.1	2.2
Sm	b.d.l.	b.d.l.	b.d.l.	b.d.l.	b.d.l.	b.d.l.	b.d.l.	0.51	b.d.l.	b.d.l.	b.d.l.	b.d.l.	b.d.l.	0.19	b.d.l.
Eu	1.00	2.22	1.17	1.84	1.02	1.68	1.32	2.05	1.71	1.15	1.83	1.39	2.93	2.04	1.80
Pb	5.7	9.4	6.1	8.3	3.8	10.6	6.7	8.1	7.7	7.1	9.1	10.4	12.7	10.2	8.4
1SE (µg/g)															
Li	0.8	0.9	0.9	1.1	1.0	1.1	0.9	1.1	1.1	0.9	1.0	1.5	1.4	1.3	1.0
Mg	4.5	3.9	5.0	5.0	8.0	5.4	4.6	5.9	5.3	4.3	4.9	13.6	7.0	4.7	5.0
Si	15006	11525	10131	11147	10213	12661	12683	12774	11663	11004	11898	11907	16124	15109	12215
Ca	1477	763	1040	871	1253	745	1231	832	941	1403	898	906	1395	855	1280
Ti	24.5	11.1	13.2	14.7	14.8	11.9	22.5	16.0	16.5	14.7	16.2	26.4	23.7	18.5	19.7
Fe	76.3	67.4	82.3	88.3	108.6	94.1	78.9	95.8	83.5	79.4	99.8	129.6	109.3	106.7	74.2
Cu	3.6	0.5	12.0	0.7	1.2	12.3	0.5	0.5	0.4	0.6	b.d.l.	2.7	0.3	0.3	2.5
Zn	0.5	1.0	8.2	1.3	3.9	7.2	0.5	0.6	0.5	0.5	0.5	1.3	1.0	0.6	0.5
Sr	28	18	24	20	28	21	22	17	20	22	18	23	26	22	25
Y	0.05	0.04	0.05	0.03	0.04	0.03	0.05	0.04	0.03	0.06	0.03	0.15	0.03	0.06	0.05
Ba	4	16	6	13	4	19	6	13	10	3	12	11	12	17	10
La	0.20	0.23	0.21	0.28	0.15	0.24	0.18	0.20	0.19	0.14	0.30	0.25	0.29	0.36	0.17
Ce	0.20	0.29	0.23	0.21	0.24	0.22	0.16	0.32	0.34	0.23	0.39	0.54	0.28	0.29	0.17
Pr	0.06	0.08	0.08	0.06	0.07	0.06	0.07	0.08	0.06	0.04	0.09	0.10	0.08	0.08	0.07
Nd	0.25	0.19	0.17	0.14	0.26	0.22	0.29	0.15	0.37	0.25	0.29	0.20	0.14	0.23	0.31
Sm	b.d.l.	b.d.l.	b.d.l.	b.d.l.	b.d.l.	b.d.l.	b.d.l.	0.07	b.d.l.	b.d.l.	b.d.l.	b.d.l.	b.d.l.	0.11	b.d.l.
Eu	0.12	0.16	0.08	0.21	0.11	0.16	0.09	0.17	0.16	0.08	0.11	0.12	0.14	0.26	0.12
Pb	0.63	0.89	0.61	0.77	0.41	1.02	0.64	0.81	0.72	0.71	0.85	1.06	1.23	1.01	0.80

Appendix B8 continued

Sample	VQ37D-500 Pl20.1	VQ37D-500 Pl21.1	VQ37D-500 Pl22.1	VQ37D-500 Pl23.1	VQ37D-500 Pl24.1	VQ37D-500 Pl25.1	VQ37D-500 Pl26.1	VQ37D-500 Pl26.2	VQ37D-500 Pl27.1	VQ37D-500 Pl28.1	VQ37D-500 Pl28.2	VQ37D-500 Pl29.1	VQ37D-500 Pl30.1	VQ37D-500 Pl31.1	VQ37D-500 Pl31.2
An	24.52	31.54	47.34	34.79	30.23	57.02	31.17	45.46	35.62	39.40	36.69	42.79	31.22	32.08	39.58
Conc. (µg/g)															
Li	7.2	7.7	7.1	7.3	7.2	7.1	6.8	6.5	6.8	9.4	8.9	7.3	8.5	8.8	9.5
Mg	77	132	232	136	112	115	120	130	148	166	143	135	142	138	159
Si	257830	320426	301604	288563	292328	234395	287561	303671	296254	348421	320107	292849	357259	340866	368854
Ca	36378	46741	68968	51387	44383	84048	45740	67539	52459	57890	53674	62893	45812	46598	57676
Ti	114	219	570	157	210	243	169	198	168	216	190	231	206	230	246
Fe	1867	2635	2849	2742	2660	2333	2693	2614	2945	3369	2907	2563	3078	3056	3304
Cu	1.2	1.2	0.4	1.1	0.7	0.2	0.5	b.d.l.	0.4	b.d.l.	b.d.l.	1.4	b.d.l.	b.d.l.	0.9
Zn	2.3	6.6	5.1	6.1	4.9	3.7	5.6	5.6	5.9	6.8	6.2	6.0	7.0	7.5	8.7
Sr	757	908	841	1020	841	1095	929	1255	1062	1143	1068	1058	905	896	1083
Y	0.26	0.15	0.40	0.17	0.26	0.36	0.21	0.35	0.23	0.24	0.13	0.42	0.30	0.28	0.28
Ba	706	646	410	471	720	143	482	266	404	531	438	411	764	652	637
La	8.4	7.2	5.4	7.6	7.2	1.8	6.6	4.9	5.7	7.4	6.8	5.6	7.7	6.8	7.7
Ce	9.8	11.3	9.3	11.0	10.9	3.3	10.5	8.2	10.3	12.6	11.3	10.5	13.0	11.5	12.7
Pr	0.91	0.96	0.89	0.86	0.92	0.35	0.81	0.65	0.82	1.19	0.91	0.94	0.88	0.88	0.98
Nd	2.6	3.1	2.4	2.4	2.7	1.0	2.2	1.8	2.0	3.1	3.0	3.6	2.6	2.7	2.5
Sm	b.d.l.	0.35	0.37	b.d.l.	0.32	b.d.l.	0.25	0.42	b.d.l.	0.28	0.34	b.d.l.	b.d.l.	b.d.l.	b.d.l.
Eu	2.43	1.82	1.51	1.62	1.96	0.89	1.60	1.46	1.28	1.99	1.74	1.69	1.84	2.10	2.46
Pb	9.2	9.1	11.3	7.9	8.2	5.8	7.3	7.1	7.6	8.7	7.6	10.0	9.7	10.3	11.0
1SE (µg/g)															
Li	0.8	1.0	1.0	0.9	0.9	0.8	0.8	0.9	0.9	1.1	1.2	1.0	1.0	1.1	1.3
Mg	3.0	6.3	21.0	5.2	5.0	3.9	4.3	4.9	5.5	6.2	5.4	6.6	5.2	5.4	5.6
Si	9268	12818	10870	10252	10460	8783	12162	11287	11760	13196	11667	15454	17385	12667	15323
Ca	673	865	1277	951	822	1556	847	1250	971	1072	994	1164	848	863	1068
Ti	8.3	17.1	51.2	12.0	15.2	17.7	12.9	14.7	12.4	17.0	14.3	17.6	15.0	17.2	18.3
Fe	60.3	79.5	83.5	84.6	80.3	69.4	83.2	82.2	80.5	149.3	88.4	109.4	109.6	106.5	96.1
Cu	0.7	0.6	0.4	0.4	0.3	0.7	18.3	b.d.l.	0.3	b.d.l.	b.d.l.	0.5	b.d.l.	b.d.l.	0.2
Zn	0.2	1.0	7.6	0.5	0.5	0.4	0.4	0.4	0.5	0.5	0.4	0.4	0.5	1.6	0.7
Sr	20	19	19	23	19	21	17	23	20	26	22	25	17	18	23
Y	0.04	0.02	0.07	0.03	0.05	0.04	0.03	0.05	0.03	0.05	0.03	0.05	0.05	0.04	0.07
Ba	21	11	9	9	17	2	8	4	8	15	7	15	22	11	11
La	0.34	0.19	0.16	0.18	0.27	0.08	0.16	0.19	0.33	0.24	0.17	0.31	0.27	0.23	0.29
Ce	0.36	0.27	0.27	0.26	0.29	0.08	0.25	0.25	0.35	0.30	0.27	0.46	0.25	0.18	0.57
Pr	0.06	0.07	0.07	0.08	0.07	0.04	0.07	0.04	0.07	0.11	0.06	0.07	0.08	0.08	0.06
Nd	0.28	0.46	0.28	0.55	0.29	0.22	0.13	0.28	0.27	0.31	0.29	0.26	0.19	0.28	0.35
Sm	b.d.l.	0.07	0.10	b.d.l.	0.07	b.d.l.	0.09	0.11	b.d.l.	0.11	0.11	b.d.l.	b.d.l.	b.d.l.	b.d.l.
Eu	0.18	0.16	0.13	0.14	0.16	0.11	0.11	0.11	0.07	0.14	0.11	0.13	0.10	0.13	0.18
Pb	0.94	0.87	1.17	0.82	0.78	0.59	0.75	0.67	0.74	0.82	0.74	1.22	1.02	1.00	1.09

Appendix B8 continued

Sample	VQ37D-500 Pl32.1	VQ37D-500 Pl33.1
An	28.72	24.50
Conc. (µg/g)		
Li	10.5	10.1
Mg	94	82
Si	343889	366121
Ca	41667	35878
Ti	149	140
Fe	2590	2616
Cu	0.3	b.d.l.
Zn	6.8	6.9
Sr	764	767
Y	0.15	0.15
Ba	768	903
La	7.5	8.4
Ce	12.3	13.4
Pr	0.83	0.97
Nd	2.6	2.7
Sm	b.d.l.	b.d.l.
Eu	2.02	1.68
Pb	13.0	14.4
1SE (µg/g)		
Li	1.2	1.2
Mg	3.4	3.6
Si	12766	15543
Ca	771	664
Ti	12.8	11.5
Fe	79.7	73.3
Cu	0.3	b.d.l.
Zn	0.5	0.6
Sr	14	17
Y	0.03	0.02
Ba	13	18
La	0.35	0.24
Ce	0.25	0.28
Pr	0.09	0.10
Nd	0.24	0.30
Sm	b.d.l.	b.d.l.
Eu	0.20	0.15
Pb	1.23	1.46

[1] analyses taken at Oregon State University; b.d.l. = below detection limit

Appendix C1

Plagioclase Separation – Changing the Fractions of Different Populations in the Analyzed Sample

Analyzing bulk mineral separates introduces the potential complication of measuring mixed crystal populations. U-series ages on mixed crystal populations may have no geologically meaningful age implications unless detailed crystal-chemical and textural information on the crystal cargo is integrated with the U-series results. A detailed characterization of potentially mixed crystal populations and their implications for residence ages using uranium-series is necessary.

In contrast to systems with complex crystal population assemblages and distinct crystal growth histories, systems with limited evidence for magma mixing and incorporation of distinct phenocrysts populations may be straightforward when using bulk mineral separates for uranium-series analysis. *Cooper et al.* [2001] however have shown that for geologically meaningful ages even in the case of a simple single crystal population under equilibrium growth conditions the effects of Ra and Ba fractionation need to be taken into account. Unfortunately, systems of such simple assembly are rare, instead most magmatic systems show complex evolutionary paths of mixing, assimilation, and differentiation.

Quantitative microprobe analyses provide a valuable overview of the phenocryst assemblage, however using electron microprobe spot analyses to infer volume fractions of the different types of plagioclase in any given sample can lead to erroneous results. Emphasis is given to all types of crystals present in thin section and crystals with anomalous zoning patterns are likely being overrepresented. A better representation of the different plagioclase populations and their volume

fractions in different samples can be obtained by mapping via microprobe large areas on individual thin sections. Using BSE maps with long counting times provide the textural framework and all phases in the thin section.

We have analyzed plagioclase grain mounts to identify variations of plagioclase compositions between the thin sections and the corresponding mineral separates used for U-series analysis. From microprobe work on the grain mounts we conclude that except for quartz, which was found as rare crystals in the grain mounts, no other inidividual crystals were part of the mineral separates. Any other phase, such as zircon, must have entered the mineral separate as small mineral inclusions. Figure C1 shows the frequency and the associated volume for varying plagioclase compositions in samples that have been analyzed for uranium series isotopes. Samples show prominent peaks for sodic plagioclases of An < 40 mol-%. More calcic plagioclase is variable among the different samples, but almost absent in dacitic samples (VQ-22D, VQ-06). Even the basaltic andesites, like VQ-22A, that have a very homogenous plagioclase populations based on analyses of the thin sections have large fractions of sodic plagioclase (An30) in the mineral separates. VQ-22A contains only andesite-derived plagioclase, based on grayscale-interpreted BSE maps of a thin section (Figure 4.2). Most likely the sodic plagioclase that is observed in a plagioclase grain mount of VQ-22A originates from the rinds of dacitic magma sticking to andesitic inclusions that could not be completely removed during the mineral separate preparation. During the separation procedure the sodic plagioclase is enriched with respect to calcic plagioclase.

Both rock crushing and magnetic separation cause the enrichment of sodic plagioclase in all mineral separates. The sodic plagioclase crystals are typically the largest plagioclase crystals in the rock (e.g., Figure 4.2). During crushing the largest crystals are most likely to break into pure plagioclase fragments, while other smaller sizes may preferentially remain attached to adhering glass. In the following magnetic

separation any plagioclase fragment with substantial volume of adhering glass is removed from the separate. Additionally, plagioclase fragments clean of adhering glass but varying in Fe content may also be separated during magnetic separation.

Sodic plagioclase has a constant low Fe content, while more calcic plagioclase has on average higher Fe content consistent with magmatic differentiation [*Ruprecht*, 2009; Chapter 3]. During magnetic separation the low Fe sodic plagioclase is preferentially concentrated for a clean separate for U-series analyses. This effect may be only minor, since most Fe may occur in plagioclase as ferric iron. The most common site in the plagioclase lattice for Fe is the tetrahedral position during the substitution for Al [*Bindeman et al.*, 1998]. Thus, this affect is most likely minor compared to adhering glass causing the separation of specific plagioclase components.

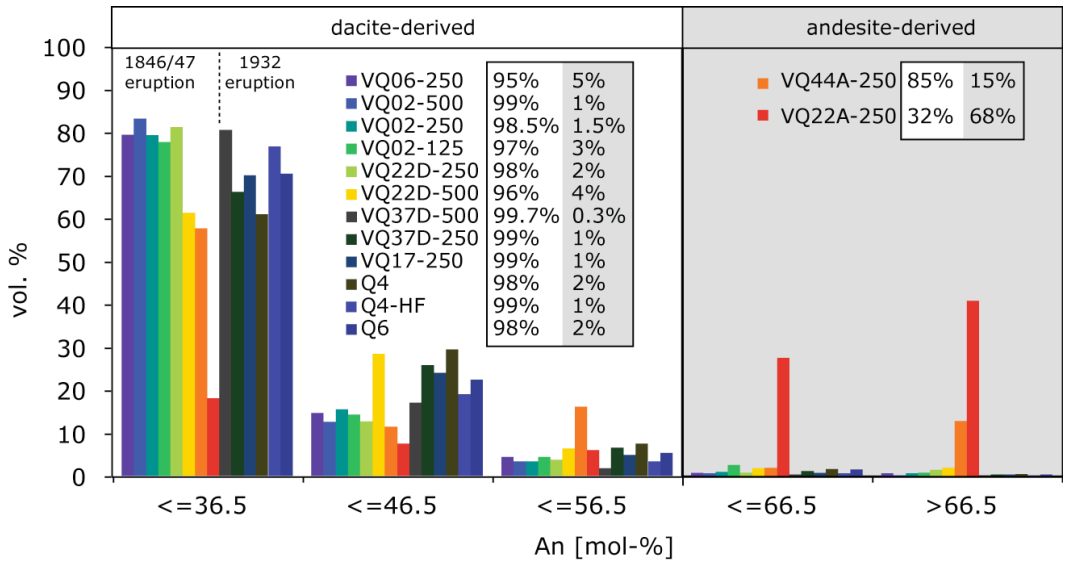

Figure C1 Fractions of Andesite- and Dacite-Derived Plagioclase in Grain Mounts from Mineral Separates used in U-series Isotope Analysis. Fractions estimated from gray-scale interpreted back-scattered maps of the grain mount obtained via microprobe. Note that with the exception of samples Q2 and Q34 all plagioclase separates have been characterized via grain mounts by electron microprobe.

Curriculum Vitae

Philipp Ruprecht

Education

Georg-August Universität Göttingen, Germany 1998-2004
B.Sc. in Geowissenschaften (Geo-sciences), 7/2001
Diplom in Geowissenschaften (Geo-sciences), 5/2004

University of Washington, Seattle, WA 2004-2009
Ph.D. in Geological Sciences, 2009

Philipp Ruprecht was born in Hannover, Germany. He grew up in Celle, Germany and graduated from Kaiser Auguste-Viktoria Gymnasium, Celle. He attended the Georg-August Universität Göttingen, Germany, and majored in Geo-sciences. At the Georg-August Universität Göttingen he had the opportunity to work with Prof. Gerhard Wörner on magma evolution in the Andes. While at the Georg-August Universität Göttingen he received an Education Abroad Program scholarship from the University of California. During his stay at the University of California, Los Angeles, he developed his interest in the time scales of magmatic processes while working with Prof. Mary Reid. After his return to Germany, he continued his work on magmatic processes in the Andes with Prof. Gerhard Wörner. In 2004 he started his doctoral work at the University of Washington working with Prof. George Bergantz and Prof. Kari Cooper. His doctoral research has since focused on magma mixing in the shallow crust. He has accepted a postdoctoral research scientist position at Columbia University's Lamont-Doherty Earth Observatory, New York, where he will continue to examine the physical and chemical interaction of magmas in the crust.

Awards and Scholarships

- Johnston Award for academic excellence recognizing graduate student reseach (University of Washington), 2004
- Received Education Abroad Program Scholarship of the University of California, 2001-2002

Publications

Ruprecht P., Bergantz G., Dufek J. (2008). Modeling of Gas-Driven Magmatic Overturn: Tracking of Phenocryst Dispersal and Gathering During Magma Mixing. Geochem. Geophys. Geosyst. 9, Q07017, doi:10.1029/2008GC002022.

Ruprecht P., Wörner G. (2007). Variable regimes in magma systems documented in plagioclase zoning patterns: El Misti stratovolcano and Andahua monogenetic cones. Journal of Volcanology and Geothermal Research 165: 142-162.

Meeting presentations

Ruprecht P., Cooper K.M., Bergantz G.W. (2008). Prolonged Storage of Andesitic Recharge Magmas Inferred From 238U-230Th-226Ra Mineral Separate Data. AGU Fall Meet. Suppl., Abstract V11D-06

Wörner G., Ruprecht P., Hora J., Ginibre C. (2008). Variable Regimes in Central Andean Magma Systems. Geological Congress of Peru, Lima

Ruprecht P., Cooper K.M., Bergantz G.W. (2007). Modeling Magma Mixing: Evidence from U-series age dating and Numerical Simulations. AGU Fall Meet. Suppl., Abstract V41F-03

Ruprecht P., Cooper K.M., Bergantz G.W. (2007). ^{238}U-^{230}Th and ^{226}Ra-^{230}Th crystal ages at Volcán Quizapu: A prime location for studying magma mixing processes on short time scales. Goldschmidt Conference 2007, Geochimica et Cosmochimica Acta 71 (15), Suppl. 1: A860

Ruprecht P., Cooper K.M., Bergantz G.W. (2005). U-series Crystal Ages in Historic Eruptions of Volcán Quizapu, Chile. AGU Fall Meet. Suppl., Abstract V13B-0529

Ruprecht P., Bergantz G.W., Cooper K.M. (2005). Magmatic Processes in the Crust Revealed from Modeling Magma Dynamics Combined with U-series Disequilibria: A Progress Report on Volcán Quizapu. 6th International Symposium on Andean Geodynamics, Barcelona, Sep 12-14.

Ruprecht P., Wörner G., Kronz A. (2004). Variable regimes in the El Misti stratovolcano and Andagua monogenetic magma systems documented in plagioclase zoning patterns. IAVCEI (Int. Assoc. Vol. Chem. Earth's Interior) General Assembly, Pucon, Nov 15-19.

Ruprecht P., Wörner G. (2003). Trace Element Variations in Volcanic Rocks of the Central Andes from 15°S to 27°S – a Statistical Approach –, Geochem 2003, Oldenburg

Wörner G., Mamani M., Ruprecht P., Mercier R., Hartmann G., Simon K., Thouret J.C. (2003). Crustal control on Central Andean Magmatism in time and space: implications from geochemical data of igneous rocks between 16°S and 27°S from Cretaceous to Recent times, 10th Congreso Geologico Chileno, Concepción

Ruprecht P., Wörner G., Martin A., Kronz A. (2003). Feldspar Zonation in Andesites from Monogenetic Cones and Long-lived Stratovolcanos (Andagua and El Misti, S. Peru): Constraints for Eruption Triggers. Eos Trans. AGU, 84(46), Fall Meet. Suppl., Abstract V11F-07